



Proceedings of CIGRE Colloquium on

# New Development of Rotating Electrical Machines

Beijing, China Sep 11–13, 2011

*Enter*



# Committees

## Steering committee

### Chairmen:

Erli F Figueiredo	Chairman of SC A1, Brazil
Lu Yanchang	Chairman of CIGRE National Committee of China, China

### Member:

Robert Fenton	Generation Technology Consultants, Inc, USA
Tortello Enzo	Ansaldo Energia, Italy
Tang Renyuan	Shenyang University of Technology, China
Liang Weiyang	Harbin Electric Corporation (Group), China
Rémi Tremblay	Hydro - Québec, Canada
Qu Dazhuang	State Nuclear Power Technology Corporation Ltd, China
Miao Lijie	Harbin Electric Corporation (Group), China
Zhu Yuanchao	Dongfang Electric Corporation (Group), China
Yuan Jianhua	Shanghai Electric Corporation (Group), China
Sam Salem	GE Energy - Renewable, US
Yang Qing	China Three Gorges Corporation, China
Qiu Xiliang	Harbin Electrical Machinery Company Limited, China
Zhang Cheng	China Yangtse Power Company Ltd, China
Zhou Jianxiong	Xiangtan Electric Manufacturing Corporation Ltd, China

## Technical committee

### Chairmen:

Erli F Figueiredo	Chairman of SC A1, Brazil
Sun Yutian	Harbin Research Institute of Large Electrical Machinery, China

### Member:

Wang Xiangheng	Tsinghua University, China
Trevor Stokes	Consultant Independent, UK
Shen Liangwei	Harbin Research Institute of Large Electrical Machinery, China
Dan Zlatanovici	Energy Research and Modernisation Institute, Romania
Zou Jibin	Harbin Institute of Technology, China
Liu Gongzhi	Harbin Electric Machinery Company Limited, China
Ge Baojun	Harbin University of Science and Technology, China
Bai Yamin	North China Electric Power Research Institute, China
Sun Shumin	Shandong Electric Power Research Institute, China
Zhuge Wenbing	Beijing BEIZHONG Steam Turbine Generator Co, Ltd, China

## **Organization committee**

### **Chairmen**

Wang Guohai Harbin Electrical Machinery Company Limited, China  
Li Ruomei Secretary of CIGRE National Committee of China, China

### **Member**

Sun Yutian Harbin Research Institute of Large Electrical Machinery, China  
Zhao Jianjun CIGRE National Committee of China, China  
Chi Su Harbin Research Institute of Large Electrical Machinery, China  
Hu Weiming China Three Gorges Corporation, China  
Guo Dengta Xiangtan Electric Manufacturing Corporation Ltd, China  
Wang Gui Harbin Electric Machinery AC-DC Motor Company Limited,  
China

## **Secretariat**

### **Secretary-general**

Sun Yutian, Zhao Jianjun

### **Secretary**

Shen Liangwei, Fan Jisong, Luan Qingwei, Zhang Qianqian, Ren Taolin  
Li Jing, Ai Zhifei

# Contents

## I Insulation

Generator Stator Bar Deterioration Due to Vibration Sparking and Partial Discharge . . . . .	001
	W.G. Moore
The Development of Insulation Materials in Harbin Electric Machinery Company Limited . . . . .	010
	Lu Chunlian, Man Yuguang
Comprehensive Risk Evaluation for Chemical Materials Applied to a Turbine Generator, and the Comprehensive Chemical Risk Comparison between Different Generators. . . . .	018
	Hiroshi Hatano, Hiromichi Ito, Hisakazu Matsumoto, et al
Detect and Evaluation of Corona Defects on Generator Stator Winding Overhangs . . . . .	024
	Wang Jinsong, Bai Kai, Guo Jiayang, Zen Fang, et al
Design and Acceptance Test of 23kV Stator Bars for the Largest Air Cooled Hydro Generator in Xiang Jia Ba Right Bank. . . . .	032
	Thomas Klamt, Yang Zhongguo
Thermal Cycle Testing for Large Air-Cooled Hydrogenerator Stator Bars . . . . .	041
	Chen Yang, Wei Wei
Key Points of On-site Operation and Interpretation of Off-line Partial Discharge Test on Generator Stator Windings. . . . .	048
	Mei Zhigang, Bai Kai, Wang Jinsong, et al

Environment Simulation Test on Stator Coil for 1000MW Hydro-Generator ..... 053

Fu Qiang, Man Yuguang, Lu Chunlian, et al

## II Hydroelectric Generators

Recent Technologies for Hydro Generators and Generator-Motors ..... 061

Toru Kubo, Hideyuki Hachiya, Wu Jinshui

Development of Air-cooled Hydrogenerators for 700MW Level Capacity ..... 069

Sun Yutian, Gao Qingfei

Optimization and Improvement on Vibration & Noise Performance of Unit 15~18 for the Right Bank

Power Station of TGP..... 077

He Jianhua, Chen Changlin, Duo Lin, et al

Methods for Fixation of the Rotor Winding Overhang of Large Asynchronous Hydrogenerators..... 086

F.Neumayer, F.Ramsauer, M.Himmelreich, et al

Inter-turn Short Circuit of Field Winding in Synchronous Machines..... 093

Sun Yuguang, Hao Liangliang, Wang Xiangheng, et al

Simulation Test and Research on Evaporative Cooling of Hydraulic Generator for TGP Underground

Power Plant..... 101

Liao Yigang, Hou Xiaoquan, Zhou Guanghou

Thermal Analysis of Large Hydro-Generator Based on a Multi-physic Approach ..... 109

Chaaban M., Leduc J., Hudon C., et al

Selection of Cooling Mode for Giant Hydro-generator ..... 117

Li Dingzhong

Research on Transposition Methods of the Stator Bars for Huge Hydro-generator ..... 125

Sun Yang, Liang Yanping, Sun Yutian

### III Turbogenerators

Experience with Turbine Generator Life Cycle Management Process .....	132
G.C. Stone, J. Kapler, J. Stein	
Temperature of Turbo-generator Stator Strands .....	140
Y.Satake, K.Hattori, K.Takahashi	
The Developing Road of HEC Turbine Generator .....	148
Shen Liangwei, Jiao Xiaoxia	
Calculation of Electric Field and Structure Design of Semi-conduction Layer for Stator Bar of 1000MW Turbo-generator.....	157
Sun Liang, Hu Haitao, Yuan Xiaohong, et al	
Nonlinearity of Torsional Damping and its Effect on SSR Characteristics of Turbine Generators .....	163
Xie Xiaorong, Zhang Xiaojin, Dong Xiaoliang, et al	
Sensitive Analysis on Electrical Parameters of Generators to Sub-synchronous Resonance.....	171
Song Peng, Xie Xiaorong, Zeng Fang, et al	
Resistance Analysis on the Gap-pickup Diagonal Flow Passage in Turbine Generator Rotors .....	178
Hu Lei , Yuan jianhua , Hu xiaohong, et al	
Negative Sequence Eddy Current Field Analysis and Temperature Calculations of 1100MW Turbo-generator with 3D Finite Element Methods.....	185
Zhong Houhong, Xian Zhelong, Zhao Wei, et al	
Study and Application of Mitigation and Protection Technology To SSR/SSO .....	192
Zheng Wei, Chang Fujie, Ji Han, et al	
Test Analysis of 600MW Generator Stator Bar Temperature Measure .....	201
Xing Xuhui, Wang Yunshan, Zhuge Wenbing, et al	
Study on Internal Cooling Water Quality and Coils Corrosion of Large Generators .....	209
Cui Yibo, Ruan Ling	

Technical Characteristics of 1100MW Nuclear Power Generator Designed by Shanghai Generator Works.....	216
---	-----

Wang Tingshan, Hu Jianbo, Wei Yanfei

Refurbishment Model of Turbine Generator in Nuclear Power Plant .....	223
---	-----

A.Semba, M.Sugiyama, T.Sano, et al

## IV Large Motors

Study on Electromagnetic Design of Special Brushless Exciter Used for Synchronous Motors .....	230
--	-----

Sun Yutian, Zhang Chunli

Asymmetry of Windings Inductance in High-Torque Low-Speed Multi-Unit Permanent Magnet Synchronous Motor.....	238
--	-----

Zou Jibin, Zhao Bo

## V Wind Generators

Overview of Permanent Magnet Wind Generators in China .....	246
---	-----

Tang Renyuan, An Zhongliang, Tong Wenming

2G HTS Wind Turbin Generators .....	255
-------------------------------------	-----

Yu.F. Antonov, Ya.B. Danilevich, Li Weili

Brushless Excitation System 2G HTS Wind Turbine Generator Based on Topological Generator (Flux PUPM).....	264
---	-----

Yu.F. Antonov

The Development of 5MW Off-shore Direct-drive Wind Turbine Generator .....	272
--	-----

Lei Xiangfu, Yang Guowei, Li Chunlin, et al

Development of Permanent Magnet Wind Generators with Fractional Slot Concentrated Winding. ....	279
---	-----

Tang Renyuan, Tong Wenming, An Zhongliang

Modelling and Simulation of Direct-coupled Permanent Magnet Wind Generators System with Maximum Power Point Tracking Control Using Simplorer. ....	287
Yan Cheng, Sun Shumin , Du jinhua, Liang Deliang	
Research on Low-voltage Ride-through Technology of grid-connected Doubly-Fed Wind Power Generation System. ....	294
Chen Fujia, Wang Hongyu, Tang Jianeng	
Study on Maximum Power Point Tracking Control for Switched Reluctance Generator Used in Wind Power Generation. ....	300
Sun Shumin, Wen Ding, Liang Deliang	
Design and Research of 10MW Large Wind Turbine Generator .....	308
Ning Yuquan	

## **VI Operation and Monitoring**

Guide for On-line Monitoring of Turbo-generators .....	315
D. Zlatanovici	
Detailed On-Site Measurements to Validate Generator Numerical Modeling .....	324
Hudon C., Chaaban M., Belanger, S., et al	
Study of Quasi-synchronization Grid Connected 1000MW Hydro-generator .....	332
Yang Mo, Ge Baojun	
Experience with Acoustic Emission Monitoring of Stator Winding Delaminations During Thermal Cycling Testing. ....	339
H. Zhu, D. Kung, M. Colwell, et al	
A Novel Online Diagnosing Technique of Turn-to-Turn Short Circuit of Large Turbine Generator ...	347
Zhang Zhengping	

Online PD Monitoring System with Microstrip Antenna for Rotating Machines .....	355
H.Sako, Y.Kaneda, S.Tomita, et al	
Necessity and Impendency of Online Monitoring the Vibration of 800MW Generator Stator End Winding in Suizhong Power Plant.....	364
Ni Zhiying	
Impact of Auxiliaries Response on the Voltage Ride Through Capability of Synchronous Generator Power Plants .....	373
L. Díez-Maroto, F. Fernández-Bernal, L. Rouco, et al	
The Conditional Diagrams Between the Electric Generator and the Electric Grid to Which it is Connected.....	382
R.Zlatanovici, D.Zlatanovici, C.Cicirone, et al	
Study on Asynchronous Self-excitation and Its Protection Measures in Generator .....	390
Zheng Wei, Wang Xiaofeng, Wang Yingying, et al	
The Simulation and Discussion on SSR of TCSC Transmission System in a Power Station .....	398
Li Guifen, Sun Yutian, Fan Jisong	
Effect of Automatic Reclosing on the Torsional Fatigue Life Expenditure of Turbine-Generator Shafts.....	407
Wang Xitian, Yang Xue, Chen Chen	
Methods for Inter Coil Short Circuit Detection in Excitation Winding Coils of Turbo Generator in Operation and in Standstill Condition.....	415
J. Polak, A. Elez, J. Študir, et al	

**Generator Stator Bar Deterioration  
Due to  
Vibration Sparking and Partial Discharge**

**W.G. Moore  
National Electric Coil  
U.S.A.**

**SUMMARY**

This paper will present findings on observable generator stator winding deterioration due to vibration sparking and partial discharge. (Vibration Sparking is also referred to as Spark Erosion). Actual visual evidence (based on removed stator bars) of both deterioration mechanisms will be presented. The root cause of each deterioration mechanism will be discussed, along with the distinct differences between each. The most severe and damaging stator bar insulation damage mechanism is Vibration Sparking, but evidence of partial discharge is often present also. Both of these deterioration mechanisms are common on large, high voltage, modern, air-cooled generators. There are distinct visual pattern differences between each failure mechanism. Borescope inspection of the windings provides an indication of the degree of damage. Bars removed from these generators were closely examined for insulation damage and correlated with the borescope inspections. The deterioration mechanisms will be described through visual observation, high magnification photography, dissection and evaluation. Insulation damage can be correlated with the amount of service hours of the unit. Multiple inspections have enabled a regression curve to be formulated indicating a time line for failure. Of these large, air-cooled generators, the majority are failing or are having to be rewound prior to failure within their first ten years of service life. Typical generator stator winding insulation systems last an average of thirty years or more. These modern, epoxy mica based insulation systems are failing prematurely due to vibration sparking and partial discharge. Root causes of the insulation degradation are presented, along with readily available solutions that can be implemented to present this problem as part of a rewind.

**KEYWORDS**

Vibration sparking, Partial discharge, Spark erosion, Generator, Stator, Winding, Bar.

## 1 INTRODUCTION

Spark Erosion damage to the stator bar ground insulation is occurring on many large air-cooled generators, causing premature failures and rewinds. Many of these machines have less than ten years of service time. Spark erosion occurs primarily on stator bars that are loose in the slot, in combination with very low surface resistivity of the bars' semi-conductive coating. Bars become loose over time in the slot, due to the type of side packing system originally installed. This side packing system does not keep the bars tight, allowing gaps to open up between the bar and the core iron. With steady state slot pounding forces, repeated opening and closing of these gaps create the vibration-related sparking and spark erosion damage. The intermittent contact, combined with the voltage presence on the surface of the bar, creates sparking.

## 2 CHARACTERISTICS OF SPARK EROSION

Spark erosion damage is very fast acting. The first industry reported failure in the U.S. occurred shortly after 33,000 service hours – about 4.5 years of operation after initial commercialization. Fig. 1 shows a close-up photograph of stator bar spark erosion from a bar removed from the generator. Arc strikes, working their way first through the semi-conductive outer layers, then through the mica tape, are clearly visible. Some correlation exists with service hours and deterioration level as indicated in Fig. 2. The data in this graph represents service hour and damage correlations from over 40 generator inspections. The inspection range covers those units with very little service hours (< 2,000 hours) to those with significantly more (> 50,000 hours), including units that have failed or had to be rewound.



Fig. 1 Vibration sparking damage on stator insulation.

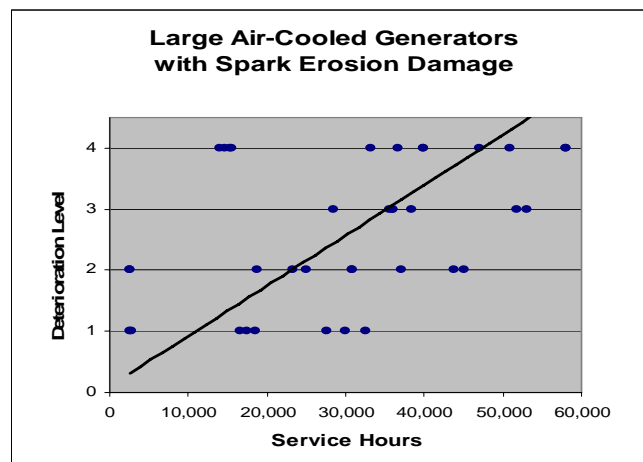


Fig.2 Spark Erosion deterioration level versus service hours on inspected stator windings

### 3 VISUAL INDICATIONS OF VIBRATION SPARKING

Since these generators typically need to be rewound in less than ten years of service, in most cases, the generator rotors have never been removed. To assess the condition of the stator winding with the rotor in place, a borescope inspection through the vent duct openings in the back of the core may be possible.

There are clear visual differences between evidence of spark erosion, and that of partial discharge. Spark erosion damage starts off as dark pitted areas in its initial stages (Fig.3), rapidly forming larger craters as the spark progresses into the ground insulation.



**Fig.3 Initial stages of spark erosion.**

It is important to realize, however, that a borescope inspection, while valuable, has limitations. The graphic below in Fig. 4 illustrates what might be seen through a borescope examination. With only the core vent duct access visible, much of the damage may be hidden as illustrated.

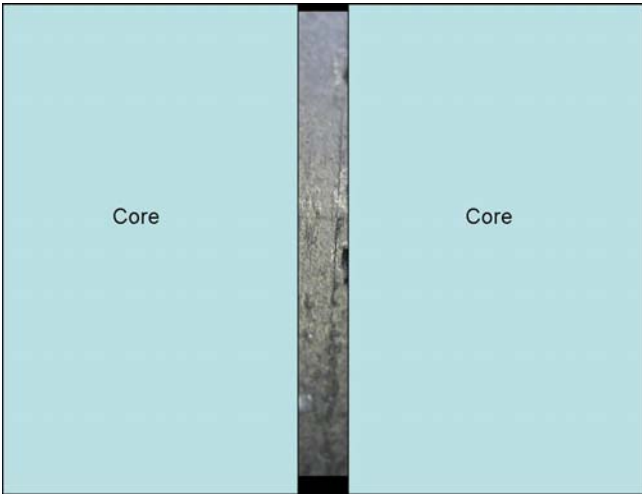


**Fig .4 Initial stages of vibration sparking, illustrated as if viewing through a borescope. Only the one dark spot at the edge of the vent duct provides an indication that spark erosion activity exists.**

In a similar manner, even higher levels of vibration sparking can be less visible, until the damage spreads all the way across the vent duct. The figures that follows illustrates this point. Fig. 5 shows level 2 damage, as evidenced by the increasing depth and rough areas next to the stator core. But as shown in Fig. 6, with the core “pulled away,” the photo of the same bar shows that the majority of the damage was hidden from view behind the stator core. The vent duct areas, where significant damage has yet to occur, can be clearly seen in Fig. 6.

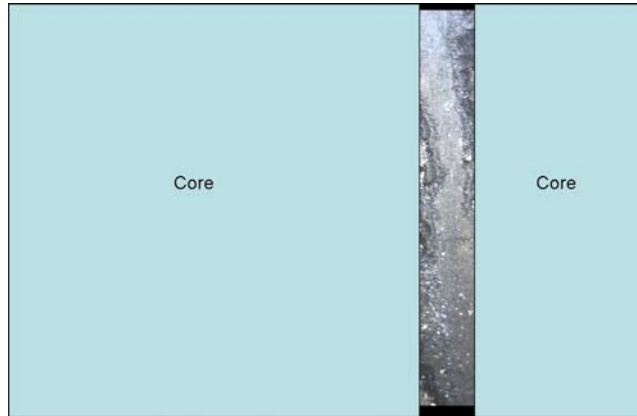


**Fig.5 Illustration of Level 2 damage as seen through a borescope examination.**



**Fig. 6 Level 2 damage with core obstruction "pulled away."**

This is mentioned not to discourage the use of borescope examinations for spark erosion detection, but to indicate a word of caution when performing this type of inspection. Experienced, trained inspectors, who are knowledgeable in both borescope inspection techniques, including lens angles, magnifications, etc., along with individuals who are skilled in what to look for, should perform this inspection. Finally, in the advanced, Level 3 damage stage, the vibration sparking damage spreads across the vent duct and is clearly visible with the borescope inspection, as illustrated in the actual bar photos and graphics below in Fig. 7 and 8.

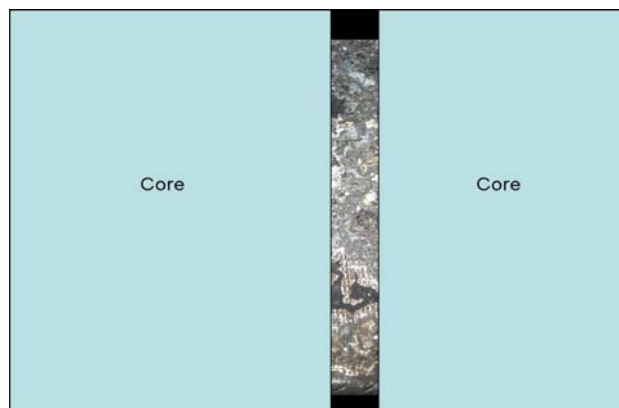


**Fig. 7 In this advanced stage of vibration sparking damage, visual evidence of damage is clearly seen across the entire vent duct.**



**Fig. 8 This bar photo and graphic illustrates that in this case, even with the core fully pulled back, no evidence of the vent duct “undamaged areas” exist. The damage has progressed fully across the vent duct.**

Vibration sparking damage can occur on a stator bar of any voltage, since it is primarily dependent upon the looseness of the stator bar in the slot, and to a lesser extent, the surface resistivity of the semi-conductive coating. Spark erosion initially occurs between the core iron and the coil surface. The graph below documents the lack of correlation between each bar’s voltage (shown in the blue pyramid shape) and the degree of spark erosion damage (shown in the magenta colored curve with various peaks independent of the blue voltage line). On the other hand, the yellow trapezoidal shape, which represents visual observations of bleaching indications – a sign of partial discharge, does correlate well with stator bar voltage. These observations were made on a removed stator winding in which each bar was laid out and visually inspected for signs of spark erosion and partial discharge.

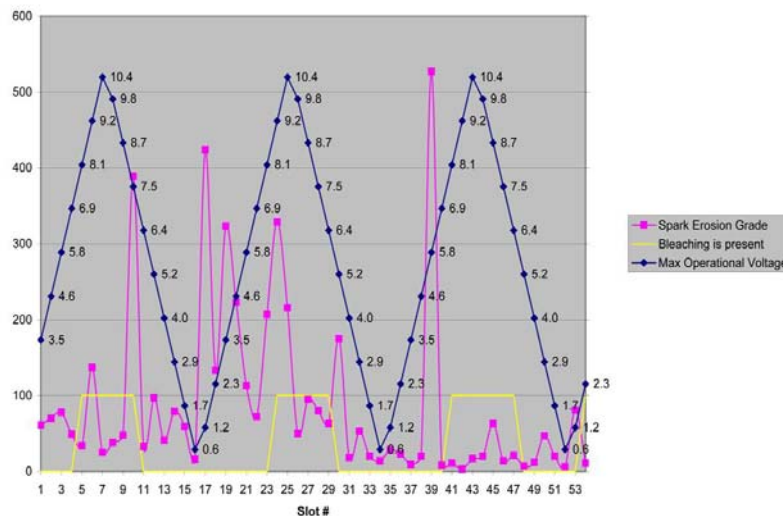


**Fig.9 Inspection of full stator winding with bars removed show no correlation between bar voltage and spark erosion damage but good correlation between bar voltage and bleaching partial discharge.**

Most of these units that are inspected and found with spark erosion damage are being rewound. Some in as little as 15,000 service hours, and all before 55,000 service hours. The rewind should include a significant change in the design approach to assure the stator bars are kept tight in the slot. It is also known that the surface resistivity can decrease with age, so levels of surface resistivity high enough to anticipate this reduction should be incorporated during the initial bar manufacture.

Original designs for these large air-cooled machines have used a flat semi-conductive side packing material or an alternate design that includes a compressible material that fills the gap during bar installation. Proper fitting of the flat side packing during initial bar installation can result in relatively small gaps between the bar and the core, but as the unit goes through its repeated thermal cycles

during operation, the existing insulation will shrink, move and wear, opening up larger gaps and allowing the bars to vibrate. Likewise, with the compressible packing, initial installation appears tight, but over time without any follow-up loading, gaps open up and spark erosion damage can occur.

Semi-conductive side ripple springs, however, allow the bar to be fitted tight against the core iron, down the entire length of the slot, initially, and more importantly, these springs keep the stator bar tight against the slot for many years. The spring action loading of the ripple maintains a constant force pushing the bar tight against the core. Although side ripple springs are more costly, the resulting improved performance justifies their installation.

Lower values of surface resistivity will create higher levels of sparking current, more rapidly damaging the bar ground insulation, if gaps and bar vibration exist. Surface resistivity values will decrease over time as the insulation ages, so a minimum value is needed.

If the bar is solidly pressed to the core and the surface properly grounded, lower values of surface resistivity are not detrimental. This is evidenced when looking at the situation of the bottom bars in one failed unit. Even with low values of surface resistivity, no spark erosion damage was found on the bottom bars (see case history below). If low surface resistivity was the primary contributor to spark erosion, damage would have been observed on these bottom bars, also.

For a rewind, the new design should incorporate (as the primary mechanism to guard against spark erosion) both top and bottom semi-conductive side ripple springs to keep the bars tight in the slot. Flat side fillers or other systems with no follow-up loading capability should not be installed, since these systems will not maintain loading for a long period of time. In addition, top ripple springs should also be incorporated to keep the bars tight. A semi-conductive coating, in combination with a semi-conductive side ripple spring, is an excellent combination that will keep the bar tightly pressed against the core, and provide an aid to ground the surface appropriately at the same time.

**4 PARTIAL DISCHARGE DAMAGE TO THE STATOR WINDING**

Spark erosion damage is not the only problem plaguing these modern air-cooled generators. Insulation deterioration due to partial discharge activity, particularly in the slot, have been observed on many machines. Although partial discharge is not a fast acting damage mechanism like spark erosion, it is often more widespread, deteriorating the surface layers of the semi-conductive coating in the slot along with the initial layers of the ground insulation system. Extensive bleaching on large portions of the stator bar in the slot straight section are also associated with this problem. Bleaching of the outer insulation layers of a winding removed for a rewind is shown in Fig. 10.



**Fig. 10 Stator bar bleaching and deterioration from partial discharge and ozone.**

The partial discharge activity in the slots of some of these machines is so severe; the side packing system is completely eaten away, leaving only the white colored glass fiber material.

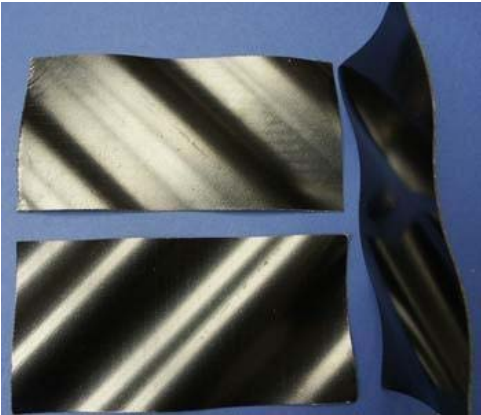
Inspections for partial discharge deterioration in the slot are possible on those units with vent ducts that can be accessed from the core outer diameter. The appearance of the partial discharge damage in the vent duct is typically round in appearance in the early stage of deterioration. Often the outer semi-conductive layer is eaten or torn away with clear visual evidence of a woven material. The borescope

photo in Fig. 11 provides such an example. Stator bars removed from units affected with these issues show a correlation of partial discharge deterioration with bar voltage.



**Fig. 11 Borescope inspection showing partial discharge deterioration on the side of the coil.**

Many of these machines that are suffering from spark erosion damage and partial discharge damage in the stator slots have had windings installed with a flat semi-conductive side packing material. Proper fitting of the flat side packing during initial bar installation can result in relatively small gaps between the bar and the core. But as the unit goes through its repeated thermal cycles during operation, the existing insulation will shrink, move and wear, opening up larger gaps and allowing the bars to vibrate leading to vibration sparking damage. One major coil manufacturer, along with one OEM, has recommended and used semi-conductive side ripple springs for many years. Side ripple springs, as shown in Fig. 12 allow the bar to be fitted tight against the core iron, down the entire length of the slot.



**Fig. 12 Semi-conductive side ripple spring.**

More importantly, the side ripple springs keep the stator bar tight against the slot for many years, due to the spring action loading of the ripple, maintaining a constant force pushing the bar tight against the core. Typically, on those units that have been rewound, more spark erosion damage was found on the top bars. Vibration of top bars is more likely since the radial forces affecting the top bar are three times higher than the bottom bar. The bottom bar also has more rigid constraints with the core at the bottom and the hard top bar at the top. Vibration of bottom bars is less likely, and therefore the probability of spark erosion on the bottom bars is less likely.

Surface resistivity on the outer semi-conductive layer measured on failed windings removed from stators have measured as low as 150 ohms/square. These values are considered too low for new installations, although no industry standard is in place. Lower values of surface resistivity will create higher levels of sparking current (inductive model), more rapidly damaging the bar ground insulation, if gaps and bar vibration exist.

If the bar is solidly pressed to the core, properly grounded, without vibration, the low values of surface resistivity are not detrimental. This is evidenced when looking at the situation of the bottom bars of one winding removed. Even with low values of surface resistivity (300 to 400 ohms/square); no spark erosion damage was found. If low surface resistivity was the primary contributor to spark erosion, damage would have been observed on these bottom bars.

## **5 CONCLUSION**

Spark erosion (vibration sparking) is a failure mechanism recognized decades ago. It has made resurgence of late with the installation of larger, higher voltage air-cooled generators. Many of these machines are failing or have to be rewound before even a full ten years of in-service operation. These machines in almost all cases have insufficient side packing to hold the bars tight in the slot. Lower surface resistivity of the semi-conductive coating, contributing to the spark erosion damage mechanism when bars are loose, have been observed as well. On certain styles of machines, spark erosion damage to the stator bar insulation system can be inspected and evaluated by with a borescope visual inspection. There is some correlation with deterioration level due to spark erosion with the amount of service hours the unit has experienced. Inspections and deterioration level classification on over 40 generators indicate a failure or a rewind will be necessary before 55,000 hours of service life. Some machines are being rewound due to spark erosion at a much lower value of service hours. Partial discharge deterioration can also be observed via the borescope inspection. It has a distinct pattern that is different than the spark erosion damage. It is generally recognized in the industry that visual evidence of deterioration due to partial discharge is not as severe as spark erosion, in terms of causing a ground fault. A case history of one machine failure due to spark erosion damage documented spark erosion damage on bars of all voltage. In addition, only top bars showed spark erosion damage.

## **6 RECOMMENDATIONS**

The use of semi-conductive side ripple springs should be utilized as part of the side packing arrangement on all large, high voltage generators. Flat side fillers and RTV compressible type compounds provide evidence of initial tightness during installation. However, they provide no follow up loading and do not maintain tightness in the slot over a long period of time. The ripple spring provides a continuous force on the coil, pushing it against the grounded core. With the proper surface resistivity of the semi-conductive treatment on the stator bar and proper grounding of the coil surface to the core, damaging sparking currents will likely not occur and spark erosion damage is minimized.

## **7 BIBLIOGRAPHY**

- [1] Moore B. Borescope Inspection Findings on Air-Cooled Generators with Spark Erosion and Partial Discharge[C]// EPRI Winter 2010 Turbine Generator Users Group Meeting, January 18, 2010, Williamsburg, VA.
- [2] Maughan C, Stone G. Electrical Failure Mechanisms on Large Generator Stator Windings[C]//75th Annual Doble Client Conference, Boston, 2008
- [3] Moore B, Khazanov A, Moudy H. Stator Winding Failure due to Spark Erosion[C]// EPRI 5th Generator Technology Transfer Workshop, Concord, NC, August 11, 2008
- [4] Moore B. Refurbishment of Large, Air – Cooled Generators[C]// Iris Rotating Machinery Conference, Toronto, Canada, 2006
- [5] Moore, B, Timperley J. Optimizing Your New Generator Stator Winding for Maximum Output and Reliability[C]// Electric Power, Chicago, IL, 2005
- [6] Nindra B, Khazanov A, Timperley J. Physical Processes in Corona Suppression Systems Under Electrical and Thermal Stresses in High Voltage Rotating Machines[C]// Iris Rotating Machinery Conference, Scottsdale, AZ, 2005
- [7] Schultz, R. Premature Failure of a 18kV Air – Cooled Generator[C]// Iris Rotating Machinery Conference, Long Beach, California, 2008
- [8] Schwieger, R. Air-Cooled Generators. Combined Cycle Journal, Second Quarter, 2007: 123
- [9] Stone G, Warren V. Trends in Stator Winding Partial Discharge in Modern Air-Cooled Generators and Motors, 2005

## **BIOGRAPHY**



Bill Moore, P.E., is Director, Technical Services with National Electric Coil. He has been with NEC for 14 years and prior to this position has been manager of engineering. Previously, he worked for FPL at three different power plants and started his 30+ career in the Power Industry as a generator design engineer with Westinghouse. He has published over 70 industry technical papers and is a frequent short course instructor on generator failures. He holds two M.S. degrees, one from the University of Pittsburgh and one from Florida Institute of Technology. His undergraduate engineering degree is from the University of Notre Dame. Bill can be reached at [bmoore@national-electric-coil.com](mailto:bmoore@national-electric-coil.com).

**The Development of Insulation Materials in Harbin Electric Machinery Company Limited**

**Lu Chunlian<sup>1,2,3</sup>, Man Yuguang<sup>1,2,3</sup>**

**<sup>1</sup> State Key Laboratory of Hydropower Equipment**

**<sup>2</sup> National Engineering Research Center-Hydropower Equipment**

**<sup>3</sup> Harbin Research Institute of Large Electrical Machinery  
Harbin, China**

**SUMMARY**

This paper introduces the progress of insulation technology for Harbin Electric Machinery Company Limited (HEC) from four aspects including the stator coil insulation system, anticorona technology, rotor insulation technology and supplementary insulation system. Rich-resin mica tapes molded insulation system is the key technology of HEC. The stator coils made by rich-resin molded technics reaches the advanced level in the world. “once mold cure technic of the corona and insulation materials” is another HEC key technology. The anti-corona technology of more than 20 kV generators, which is always improved and innovated by learning from foreign advanced experience, has been the special anti-corona technology system for HEC. HEC have study a series of new products by using these two key technologies. The generator rotor insulation technology and supplementary insulation materials are developed and innovated all the time with researching new products and improving insulation materials.

**KEYWORDS**

Harbin electric machinery company limited, Insulation, Class F, Rich resin mica tape molded sulation system, Progress

# 1 THE DEVELOPMENT OF THE MAIN INSULATION TECHNOLOGY FOR THE LARGE GENERATOR STATE COILS

## 1.1 Exploitation of class F insulation system

In the early 1970s, Harbin Electric Machinery Company Limited (HEC) took on the important task on developing national electric machinery industry and researched the new class F main insulation for high voltage generators. Harbin Institute of Large Generator and Harbin Insulation Materials Factory exploited and applied the epoxy powder mica tapes. In the period of exploiting, HEC researched early or late naphthenic acid lead insulation system, rich-mica paper insulation system and class F Tong Ma epoxy powder mica insulation (FTMI) system. HEC finally chose FTMI as the main research direction for the main insulations of the large generators. HEC used FTMI materials in 15.75 kV/210 MW turbine-generators in 1988 and late in Tian Sheng Qiao hydro-generators. Hereafter, HEC used the FTMI materials as the stator coil main insulation of the class F generators, for example, the 300MW and 600MW turbine-generators and all the large hydro-generators. Other internal enterprises of the same occupation also used the FTMI materials one after another. The application of the FTMI materials improved the thermal resistance from the class B to the class F for the large generator stator coil main insulation, and reduced the main insulation thickness of the stator coils at a certain extent, especially saved up the fabrication costs of the generators.

## 1.2 Development of hydro-generator class F main insulation system

The HEC generator fabrication technology developed rapidly in the 1990s. The power of hydro-generators increased from original 6.8MW to Er Tan 550MW and Three Gorge 700MW, the voltage class increased to more than 20kV. HEC cooperated with Canadian GE to fabricate Er Tan 550MW, 18kV air-cool hydro-generator in 1996. HEC improved the form pressing technology and sent the stator coils, which were made of the advance materials and technology, to the Canadian GE to generally evaluate the electrical properties. Canadian GE really approbated HEC insulation technology by the favourable results of electric and heat ageing test (as shown in Table I ). HEC fabricated the first domestic air-cooling 550MW, 18kV hydro-generator by independent insulation technology.

**Table I HEC Stator Coils Main Insulation Aging Assessed by Canada GE .**

GE standard	120°C, 41.5kV ≥400h	After heat and cold cycle tests ≥250h
HEC stator coils tests result	≥1300h	≥370h

**Table II : The Property of High Voltage FTMI Tape.**

Items	Property	Units	Index	The entry tests
1	Mica content	%	≥40	41.5
2	Resin Content	%	37~40	40.0
3	Volatile content	%	0.7~1.1	1.1
4	Gel time	min	10~14	13min20s
5	Average thickness	mm	0.14±0.01	0.14
6	Electrical strength	MV/m	≥40	54.14

**Table III Three Gorge 20kV Stator Coils Electrical Aging Assessed by Swiss BIRR .**

Assessment site	Swiss BIRR		Harbin in china	
Coil types	No hollow conductor in the coils		Hollow conductor in the coils	
ALSTOM standards	32kV ≥4000h	40kV ≥1000h	32kV ≥4000h	40kV 1000h
Assessment results of HEC coils	>7880h	2080h	>4438h	≥1251h

The Three Gorges Dam left bank generators were the cooperative production project of HEC and the Swiss ABB. HEC must produce the standard coils, which would conform to the ABB standards, according to the ABB blueprint. Because ABB stator coils insulation was the resin-less VPI system, its insulation thickness is only 4.6mm, the withstand voltage of the stator coils are 4 times of rated voltage (80kV/min), the other electrical performances standards are also the highest levels in the world. Whether HEC RRFP insulation system could satisfy the requests of ABB, this was also one stern

challenge for HEC. HEC improved the electrical and mechanical properties of the insulation tapes from the powder mica paper, the mica pastern. HEC, Harbin Insulation Factory and Hang Zhou Mica Factory successfully developed together the new high field intensity mica tapes (as shown in Table II) and improved the internal shield structure of the coil conductors based on that of the Er Tan coils. In 1998, HEC fabricated the stator coils of the Three Gorges Dam left bank with the RRFP insulation system. The electrical aging and other electrical properties of these coils generally evaluated in the Swiss ABB laboratory (as shown in Table III) were obtained the approval and affirmation from the ABB. In 2002, HEC at last obtained the qualifications to manufacture the stator coils of the Three Gorges Dam left bank with itself insulation system, and attained the manufactory compact of the stator coils of three hydro-generators.



**Fig. 1 The Stator Windings of Three Gorge Dam Left Bank Hydro-Generator.**

In 2006, HEC started to research the technology of 700 MW whole air-cooled hydro-generator. The stator coils of the Three Gorges Dam right bank converted the water-cooled structure into the air-cooled one (as shown in Fig.1). The ratio of the highness and the width of the stator coil conductors increased greatly ((87.91mm/14.42mm)>6.0), which made more difficult for the control of the RRFP. Therefore, HEC improved the technologies of the conductor pressing and the pressing process of the RRFP equipments, especially researched deeply the improvement of the corner field intensity of the conductors.

**Table IV The Main Insulation Property of Three Gorge Dam Right Bank Hydro-Generator of HEC.**

Items	Standards	Test results
Starting value of dielectric loss (%)	≤1.0	0.78
Corona voltage (kV)	≥30	46
Power frequency breakdown voltage (kV)	≥110	129

**Table V The Insulation Properties of 1000 MW Hydro-Generator Stator Coil.**

Items	Test results
Normal dielectric loss (0.2 U <sub>N</sub> )	≤0.85%
Thermal dielectric loss (0.6 U <sub>N</sub> )	≤4%
Partial discharge (1.0 U <sub>N</sub> )	≤400pC
Corona voltage	≥55kV
Breakdown voltage	≥160kV
The cold and heat circulations	Pass
The environment simulation experiments	Pass

According to HEC actual situation, the Three Gorges Dam right bank generators adopted painting semiconductor coating. Finally the maximal power air-cooled generators in the world were manufactured and the property of coils was outstanding (as shown in Table IV).

China Three Gorges Corporation requested the domestic generator Manufacturer (HEC and DEC, DongFang Electrical Machinery Company Limited) developed 24kV and 26kV voltage class 1000 MW air-cooled hydro-generators in 2009. At present, no manufacturers had fabricated so high rated voltage and power hydro-generator in the world. HEC researched the stator coils of the 24kV, 26kV voltage class 1000MW hydro-generators using the conventional RRF technology which was HEC independent technology. The stator coil properties were excellent by a series of experimental verifications, such as the electric heating aging, the cold and heat circulations, and the environment simulation experiments (as shown in Table V and Fig. 2).

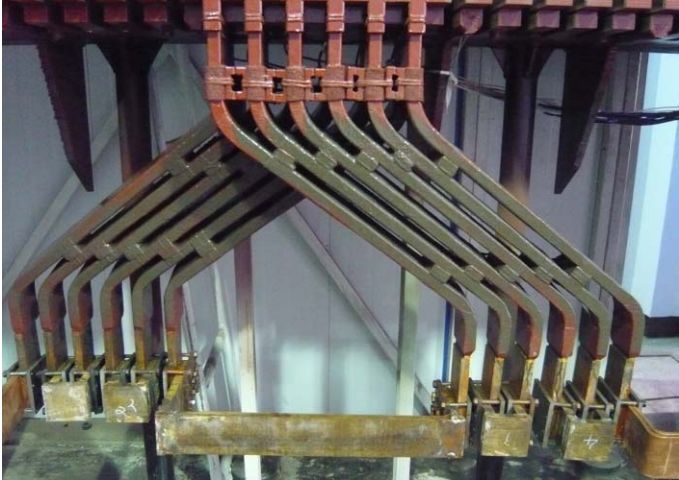


**Fig. 2 The Environment Simulation Experiments of 1000 MW Hydro-Generator Form Pressing Stator Coil.**

**1.3 Development of the F class main insulation of turbo-generator**

With the fierce competition of the generator market, HEC continuously cooperated with the foreign companies with excellent technology to manufacture turbo-generator. For example, 390H (470 MW/19 kV) gas turbo-generator cooperated with American GE Corporation, one million kW (1000 MW/27 kV) the ultra supercritical turbo-generator and air-cooled (200 MW/18kV) turbo-generator with Toshiba Corporation. But no including the stator coil technique of manufacture when introducing the foreign generator technology. The unit cost of the generator would increase greatly when HEC purchased their stator coils.

**Table VI The electrical Properties of 390H Gas Turbo-Generator Stator Coil Main Insulation.**

Items	GE stator coils	HEC stator coils
Normal dielectric loss (0.2 U <sub>N</sub> )	≤1.6%	≤0.8%
Partial discharge (1.0 U <sub>N</sub> )	≤190pC	≤180pC
Corona voltage	≥50kV	≥54kV
Breakdown voltage	127kV	120kV

**Table VII The Electrical Properties of 1000MW Turbo-Generator Stator Coil Main Insulation.**

Items	Stator coils of Toshiba	Stator coils of HEC
Normal dielectric loss (0.2 U <sub>N</sub> )	≤0.58%	≤0.74%
Thermal dielectric loss (0.6 U <sub>N</sub> )	≤2.7%	≤1.3%
Partial discharge (1.0 U <sub>N</sub> )	≤180pC	≤150pC
Corona voltage	-	≥81kV
Breakdown voltage	182kV	175kV

Under these circumstances, HEC strived for developing independent innovation technique and improved the conventional RRF insulation system and the fabrication technology. At last, HEC succeeded to manufacture 390H gas turbo-generator stator coils (as shown in Fig. 3), 1000MW/27kV ultra supercritical turbo-generator (as shown in Fig. 4) and air-cooled 200 MW/18kV turbo generators. The property of the coils had been up to the level of foreign same product (as shown in Table VI, Table VII and Table VIII) and the coils could completely substitute the import coils.



**Fig. 3 390H Gas Turbo-Generator Stator Coils of HEC.**



**Fig. 4 1000MW Turbo-Generator Stator Coil of HEC.**

**Table VIII 200MW/18kV Air-Cooled Turbo-Generator Stator Coil Main Insulation of HEC.**

Items	Stator coils of Toshiba	Form pressing stator coils of HEC	VPI stator coils of HEC
Normal dielectric loss ( $0.2 U_N$ )	0.75%	0.81%	0.83%
Thermal dielectric loss ( $0.6 U_N$ )	0.87%	1.2%	1.2%
Partial discharge ( $1.0 U_N$ )	$\leq 180\text{pC}$	$\leq 150\text{pC}$	$\leq 150\text{pC}$
Breakdown voltage	113kV	110kV	120kV
Thermal stability ( $180^\circ\text{C}/48\text{h}$ )	Delamination, discoloration, resin flow	Little gap, little discoloration	Partial gap, little discoloration

#### **1.4 Development of F class resin-less VPI insulation system**

In 2008, HEC started to research the resin-less single coil vacuum pressure impregnation (SVPI) insulation system. Although foreign firms had the mature technology and advanced equipments, HEC relied on independent research and development cooperated with the domestic VPI equipment factory, and successfully manufactured the domestic maximum horizontal type vacuum pressure impregnation (VPI) equipment. The VPI equipment could satisfy the technology requests of the stator coils for the large-scale hydro-generators and turbo-generators. Now HEC had got the batch production of the VPI stator coils for 200MW turbo-generator, as shown in Fig. 5. The VPI coil properties were not inferior to the foreign same products, as shown in Table VIII.



**Fig. 5 The VPI Stator Coils for 200MW Turbo-Generator.**

## **2 DEVELOPMENT OF THE STATOR WINDINGS ANTI-CORONA TECHNOLOGY**

The anti-corona technology of the high voltage stator windings is the generator's another key technology, which is continually improved along with the main insulation material development and the voltage class elevation. In the 1960s, the anti-corona coating of the stator coils adopted the painting structure. The anti-corona material was the semiconductor lacquer which contained organic solvent. In order to avoid the solvent being harmful to people and polluting the environment, in 1971, Harbin Institute of Large Electrical Machinery succeeded in developing “once-solidification-molding” (OSM) anti-corona structure, which involved wrapping up multi-layers main insulation and then directly wrapping up the anti-corona tapes. The coils with the OSM technology need not second anti-corona painting treatment so that the OSM reduced pollution and also greatly improved the production efficiency. The OSM technology was firstly applied to the Huang Longtan water power plant 13.8kV hydro-generator, which has operated for over 30 years. The OSM anti-corona structure was a domestic anti-corona technology revolution and pioneering technology in china. It was quickly used in the national electrical machinery factories.

Since the 1980s, with the aim of keeping up with the world advanced level, HEC has started to develop new anti-corona material. The reinforced material of anti-corona tape had be replaced the asbestos tape by the glassfiber one. The anti-corona structure was developed to be used in more high voltage class. And now, the research works of 18kV~26kV anti-corona structures had been made the breakthrough progress.

In the 1990s, with the rapid development of large-scale high voltage generators, anti-corona technology must satisfy the further requirements. Especially the stator coils of the Three Gorges Dam left bank were requested to pass the test of 80kV, 1 minute withstand voltage test, which was stern test for the main insulation and anti-corona systems. In order to solve such difficulty, HEC researched the new anti-corona material with the cooperation of anti-corona material factories. The suitable anti-corona structure was finally confirmed by the series experiments. 1084 coils of Three Gorges left bank once passed the withstand voltage tests of 80kV, 1 minute by using the new anti-corona material. HEC keeps ahead in stator coil anti-corona technology in the world. This technology is adopted in these water power stations of Three Gorges Dam right bank, Three Gorges underground, LongTan and XiaoWan, and so on.

In recent years, HEC continued to research anti-corona technology. The new anti-corona materials have the characters of stable resistance value, humidity resistance and greasy dirt resistance. These achievements have successfully been applied to the stator coils of million kilo-Watt hydro-generator (1000MW/26kV) and ultra supercritical generator (1000MW/27kV), and also have laid the foundation for the anti-corona technology research on million kilo-Watt nuclear power generator.

### **3 ROTOR INSULATION TECHNOLOGY DEVELOPMENTS FOR HIGH VOLTAGE GENERATOR**

#### **3.1 Rotor insulation technology of hydro-generator**

F class interturn insulation of hydro-generator pole coils was the resorcinol epoxy glass greige cloth in the 80s. In the 90s, with the increasing of the products, HEC introduced foreign polyaryl amide fibre sized paper (Nomex sized paper impregnated with adhesive varnish) to enhance hydro-generator rotor insulation level. Nomex paper could reduction 20% thickness of interturn insulation and has good thermal resistance and adhibition strength. But the imported Nomex paper was confined to the transportation and storage; sometime they were difficulty to satisfy HEC production needs. Therefore, HEC began to research the adhesive varnish to Nomex paper. Nowadays, HEC pole coil interturn insulation had arrived at the world advanced level.

The rotor winding insulations basically used the combination insulations of the epoxy phenol aldehyde woven glass fabric sheet and the phenol aldehyde glass fiber laminate before the 90s. After the 90s, the “L” type Nomex papers were used in the corner side of pole coil to lengthen the creepage distance of the combined insulations. The pole body insulation structure, which was comprised of the multi-layered Nomex paper coated with adhesive, inserting epoxy board and glue-in polyester felt, had the very high electric strength, the mechanical strength and leakage current resistance. At present, HEC pole body insulation technology is also mature and advanced one in the world.

#### **3.2 Rotor insulation technology of turbo-generator**

The interturn insulation generally used the melamine laminated sheet and the epoxy glass fabric laminated sheet with one-sided grinding, the copper wire was adhibited and then cured by thermo-compression. For the introduction of foreign technology and the application of the Nomex paper as the interturn insulation, the interturn insulation thickness had lessened from traditional 0.4mm to 0.25mm, and rotor slot insulation thickness from 1.4mm to 1.2mm. In addition, the composite slot liner comprised with the epoxy glass fabric /NHN/ epoxy glass fabric greatly improved the electrical property, the mechanical property and the thermal stability of rotor slot insulation.

The rotor slip-ring sleeve insulation was made of the multi-layer filament glass cloth in which the layers were agglutinated by the thermosetting epoxy resin. The shrink fit technology required that the rotor spindle insulation must have enough linear thermal-expansion coefficient and smooth surface, so it could closely contact with the rotor spindle. The rotor retaining ring insulation was fabricated by hot-pressing the multi-layer glass cloth, which was the soft thin flake after being cured and had the high mechanical property, the electrical property and the thermo-stability. The compressive strength of the rotor retaining ring insulation is more than 289MPa at 145°C.

The insulating strips under the wedges, end sleeve insulations and the interelectrode blocks in rotor winding slot were made of the high strength epoxy laminated material. HEC designed the structure that the slippage cloth was pasted on the bottom side of insulating strips and the sleeve insulations. Such ingenuity structure had some advantages for rotor windings. Firstly, the rotor windings could be close fixed, simultaneously could endure the very high mechanical force and the overvoltage function. Secondly, the copper wire of the coils would be caused expand or shrink when the coils were in hot or cold environments, and the coils could slip freely due to the slippage cloth. Lastly, the winding insulation may be prevented from the damage by reducing the friction during they were deformed.

### **4 DEVELOPMENT OF STATOR AUXILIARY INSULATION**

#### **4.1 Fixed insulation in stator slot and end winding of hydro-generator**

The preferable fixed method was adopted in stator slots in order to overcome the electromagnetic vibration force of the stator winding. The fixed method in stator slots was that the semiconductor boards were inserted in the sides of slots before the 90s. After the 90s, the new fixed method was that the “U” type semiconductor slot liners were wrapped up the coils to fix them (ABB Corporation technology). The “U” type material was the three-in-one structure constituted with two layers semiconductor non-woven fabric and silica rubber in the middle of them. The slot liners were sparsely

wrapped up the coil slot parts and then the coils were pushed into stator slots and fixed them. The new fixed method improved the contact area of the coils and the iron core and reduced the slot electric potential. Adaptive impregnation polyester felt used in the bottom of slot and among the layers of coils was in favour of the stator slots fixed

The ordinary end hoop was made of stainless steel wrapped with epoxy powder mica tape, which was used to immobilise the end windings. Moreover the soft end hoop was composed of glass fibre rope and injection resin. The  $\Phi 50$  glass fibre rope used as the soft end hoop was immobilised with the end windings, then the resin was gradually injected into different subsections of the entire end hoop respectively. The resin could cure at the room temperature. The glass fibre rope injected resin can expand to fill up the gap between the end hoop and windings (including partial gaps among windings). The end windings may also freely expand and shrink to obtain optimum matching states between the end hoop and the end windings.

#### **4.2 Fixed insulation in stator slot and end winding of turbo-generator**

The fixed method in stator slots was that the semiconductor sheets or corrugated plates were inserted into the sides of slots; the elastic corrugated sheet was used under the slot wedge; the slot wedges were made of high strength glass fibre phenolics with the slipping function; the axial fixed between winding layers was used the high strength laminated sheet. These new materials not only caused the more stable fixed windings in the slots but also avoided damaging stator coils.

End winding fixed structures of 200MW, 300MW turbo-generator comprised of supports rings (glass reinforced plastic), the clamping plates (epoxy phenol aldehyde glass pressing workpiece), the insulation support (glass reinforced plastic). That of the 600MW-650MW unit comprised of the big cone (glass reinforced plastic), the insulating ring with slipping surface (glass reinforced plastic, Teflon cloth), adjustable banding ring (glass reinforced plastic), inner support ring (glass reinforced plastic), the insulation support (epoxy glass cloth laminated sheet). The big cone forms a whole insulating layer in the end winding which isolates the end windings and the metal, apart from support and the fixed action. Adaptive material Terylene woven hollow strip impregnated adhesive was laid in the contact place between the end windings of the bottom coils and the big cone. The adaptive material was modified according to the end turn shape which is the involutes shape, which could ensure the close contact between the coils and big cone. The soft tube being the special rotary hose was laid in the middle of top and bottom end turn. The soft tube injected epoxy resin curing at the middle temperature ensured firm adhesiveness between the coils and supported them to suitable shape. End winding fixed structures of 1000MW unit was comprised of the insulation support (epoxy glass cloth laminated sheet), the insulation banding ring (glass fiber reinforced resin banding ring), the end winding tautness rope (polyester fiber sleeve and impregnated polyester glue glass fiber bundle) and the end adaptive intestines structure.

### **5 CONCLUSIONS**

HEC has developed the generator insulation technology for 50years and made great progresses; especially the main insulation RRFP technology of generator stator winding has achieved the world advanced level. HEC resin-less VPI technology obtains the rapid development and the volume production ability, which may satisfy the demands of different customers. HEC have achieved the foreign company advanced level for the generator rotor insulation and the auxiliary insulation by successful assimilation of foreign technology to achieve indigenous technological development. In the future, during insulation technology development, HEC will Hold on to independent research and development, and the introduction and absorption of the advanced foreign technology. HEC will improve the RRFP and resin-less VPI main insulation technology to satisfy the technology demands of more than 27KV voltage class generators. At the same time, HEC will cooperate with other generator manufacturers in the world to develop the turbo-generator and hydro-generator for all the human beings.



Beijing, China

SC A1

**COLLOQUIUM ON NEW DEVELOPMENT IN MACHINE DESIGN  
AND INSULATION MATERIALS**

11~13 September, 2011

---

## **Comprehensive Risk Evaluation for Chemical Materials Applied to a Turbine Generator, and the Comprehensive Chemical Risk Comparison between Different Generators**

**Hiroshi Hatano, Hiromichi Ito, Hisakazu Matsumoto, Hideyuki Shimada  
Toshiba Corporation  
Japan**

### **SUMMARY**

Organic chemical materials and their complexes are applied to a turbine generator as insulation material. Epoxy resins compose of stator bar insulation and several kinds of solvent are used for washing and diluting varnish. Generally, utilization of these chemical materials is controlled by national laws with respect to human health and environment, and chemical supplier obligated to furnish Safety Data Sheet (SDS) to users. SDS shows lots of information prescribed by national standards.

However, all the hazardous data are subdivided to each hazardous item at each chemical material. Thus, the total chemical risk, to human health and environment, of all chemical materials applied to turbine generator could not be evaluated comprehensively. Generator designers, production engineers and safety manager, who are not specialists in organic chemical materials, need a simple method for determining the potential chemical and environmental risk in the material selection process and manufacturing line construction process. Regretfully, there are no indices for expressing the potential chemical risks to human health comprehensively.

So, in this paper, we propose chemical risk evaluation method and index to express comprehensively by using hazardous information described in SDS and the hazardous classifications according to Globally Harmonized System of Classification and Labeling of Chemicals (GHS).

Furthermore, we applied this evaluation method to several turbine generator adopted with different stator bar insulation systems.

### **KEYWORDS**

Turbine generator, Insulation, Chemical material, Hazardous index

## 1 INTRODUCTION

We proposed comprehensive hazardous evaluation method based on SDS\* in 2006<sup>[1]</sup>. Comprehensive hazardous index was calculated based on each hazardous items, weighting between hazardous items, level classification in each hazardous item and the amount of chemical materials applied for turbine generator. The weighting and the level classification is tentatively decided. According to GHS\*\*, the level classification is defined in this paper. As a result, the definition of the comprehensive hazardous index is clarified, the legitimacy of comprehensive hazardous index is improved. So we re-evaluate the chemical hazardous risks of our turbine generators. Especially, comprehensive hazardous indices of both turbine generator applied with VPI\*\*\* and RR\*\*\*\* insulation are compared.

SDS\* : Safty Data Sheet  
GHS\*\* : Globally Harmonized System of Classification and Labeling of Chemicals  
VPI\*\*\* : Vacuum Pressure Impregnation  
RR\*\*\*\* : Resin Rich

## 2 OBJECTIVES

The objective of this work is to create an evaluation method of comprehensive chemical potential risk in a turbine generator according to GHS and to compare both turbine generators applied with different insulation systems, VPI and RR insulation system. Fig.1 shows major insulation parts applied for a turbine generator.

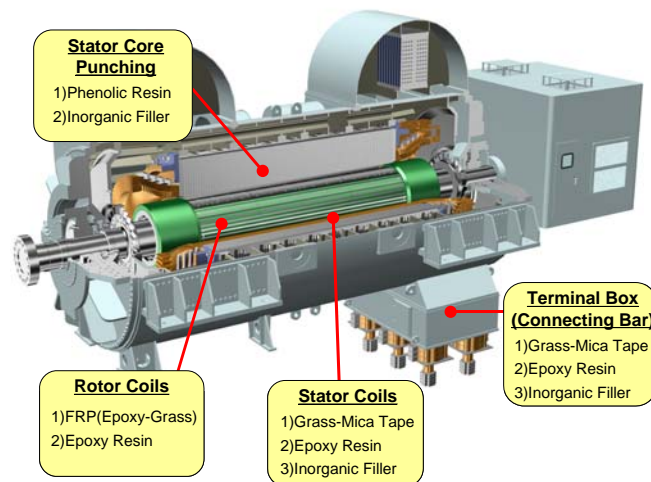


Fig.1 Major insulation parts applied for a turbine generator

Here, after completing turbine generator, several kinds of chemical material described in SDS will be changed. For example, curing epoxy resin and hadener, both materials will be changed to different material including the same basic function. In other case, drying solvent type resin, the solvent will be volatilized. Despite that, we consider chemical material described in SDS will remain after completing turbine generator in this paper.

## 3 COMPREHENSIVE RISK EVALUATION OF CHEMICAL MATERIALS

We propose comprehensive chemical risk evaluation method and index to express comprehensively by using hazardous information described in SDS. Firstly, we select hazardous items, ex. irritation to skin, corrosion to skin, sensitization, oral toxicity and carcinogenicity, mutagenicity, and then weighted and scored for integrating these hazardous items. As a result, we obtain comprehensive chemical hazardous index at every chemical materials. Secondly, we investigate the chemical materials applied to turbine generator and the quantity. Finally, multiplying the quantity of each chemical material and

the hazardous index at every chemical material, and summing multiplied data, we obtain the comprehensive chemical hazardous index to human health in hole of turbine generator.

### 3.1 Classification of each hazardous item based on GHS

Classification of each hazardous item, irritation to skin, corrosion to skin, sensitization, oral toxicity and carcinogenicity, mutagenicity is shown in Table I.

**Table I Classification of each hazardous item**

Acute toxicity	Classification based on GHS	Class 1		Class 2		Class 3		Class 4		Class 5		Class 6	
		Min. (<)	Max (≤)	Min. (<)	Max (≤)	Min. (<)	Max (≤)	Min. (<)	Max (≤)	Min. (<)	Max (≤)	Min. (<)	Max (≤)
Via oral (mg/kg)	LD 50	0	5	5	50	50	300	300	2000	2000	5000	5000	---
	LD 50	0	50	50	200	200	1000	1000	2000	2000	5000	5000	---
Irritation/corrosion to skin	Classification based on GHS	Class 1		Class 2		Class 3		Class 4					
	Hazardous information	heavy damage to skin		irritation to skin		slight irritation to skin		not applicable					
Sensitization to skin	Classification based on GHS	Class 1		Class 2									
	Hazardous information	Suspicion of allergic skin activity		not applicable									
Mutagenicity	Classification based on GHS	Class 1		Class 2		Class 3							
	Hazardous information	possibility of hereditary disease		Suspicion of hereditary disease possibility		not applicable							
Carcinogenicity	Classification based on GHS	Class 1A		Class 1B		Class 2		--		--			
	Classification based on IARC	Gr.1		Gr.2A		Gr.2B		Gr.3		Gr.4			
	Hazardous information	Calcinogenicity to human		possibility of carcinogenicity to human		Suspicion of Carcinogenic possibility to human		Can not classify to carcinogenicity to human		Perhaps not show carcinogenicity to human			

### 3.2 Scoring and weighting of each hazardous item based on GHS

The scoring and weighting of above-mentioned hazardous items are shown in Fig.2. Here, indicating highest hazardousness, the score is assigned to 1 point. Indicating lowest hazardousness, the score is assigned to 0 point. The weight coefficients are decided tentatively and the scores are decided according to Table 1.

Toxicity	Tentative Weight Coefficient	score
<b>Skin Contact</b>	0.6	Corrosion : → 1 points
-Irritation to Skin		Irritation : → 0.66 points
-Corrosion to Skin		Irritation Light : → 0.33 points
		Not Observed : → 0 points
-Sensitization	0.4	Applicable : 1 point, not applicable : 0 point
<b>Ingestion</b>	1.5	LD50 0~5mg/kg → 1 points
-Oral Toxicity		LD50 5~50mg/kg → 0.8 point
		LD50 50~300mg/kg → 0.6 point
		LD50 300~2000mg/kg → 0.4 point
		LD50 2000~5000mg/kg → 0.2 point
		LD50 5000mg/kg~ → 0 point
<b>Carcinogenicity</b>	1	IARC Gr.1 → 1 points
-Carcinogenicity		IARC Gr.2A → 0.75 point
		IARC Gr.2B → 0.5 point
		IARC Gr.3 → 0.25 point
		IARC Gr.4 → 0 point
-Mutagenicity	0.18	Applicable : 1 point, under suspicion : 0.5 point, not applicable : 0 point
<b>Degradability</b>	0.1	Well degradable : 0 point
-Degradability in Vivo		Hard to degrade : 1 point

**Fig.2 Scoring and weighting of hazardous items based on GHS**

**3.3 Hazardous index in each chemical material**

Hazardous index, integrating hazardous items, of each chemical material is calculated by summing above-mentioned parameters as shown below.

$$\begin{aligned}
 \text{Hazardous Index} = & \left( \begin{array}{l} 0.6 \times \text{score} \\ \text{Irritation to Skin} \\ \text{Corrosion to Skin} \end{array} \right) + \left( \begin{array}{l} 0.4 \times \text{score} \\ \text{Sensitization} \end{array} \right) + \left( \begin{array}{l} 1.5 \times \text{score} \\ \text{Oral Toxicity} \end{array} \right) \\
 & + \left( \begin{array}{l} 1.0 \times \text{score} \\ \text{Carcinogenicity} \end{array} \right) + \left( \begin{array}{l} 0.18 \times \text{score} \\ \text{Mutagenicity} \end{array} \right) + \left( \begin{array}{l} 0.1 \times \text{score} \\ \text{Biodegradability} \end{array} \right)
 \end{aligned}$$

We selected six major chemical materials applying turbine generators and calculated hazardous indices from above-shown formula and the updated hazardous information from SDS. The results are shown in Fig.3. Almost of all materials show the equivalent hazardous indices except for Non bis A/F epoxy. Since the sensitization of non bis A/F epoxy is smaller than the other materials, the hazardous index shows low value.

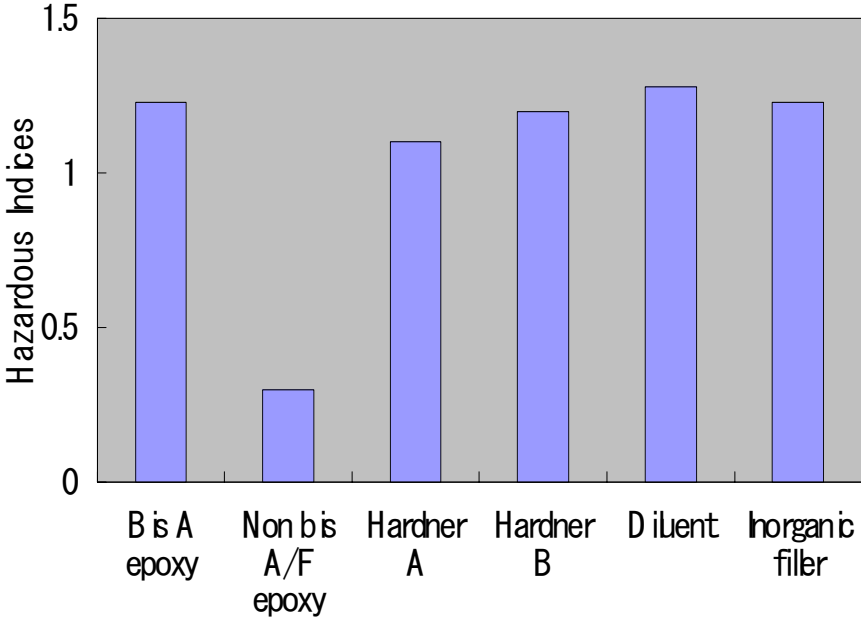


**Fig.3 Hazardous indices of chemical materials**

**3.4 Comprehensive hazardous indices of generators applied with different insulation system**

**3.4.1 Amounts of chemical materials applied for turbine generators with VPI and RR insulation**

We investigate the amounts of above-mentioned six major chemical materials applied to our both turbine generators (220MVA class) with different insulation system, VPI/RR. For reference, the relative amounts (Total amount of VPI: 100) of the six major chemical materials are shown in Table II.

Table II Relative amounts of organic chemical materials in two types of generator

	VPI	RR
B is A epoxy	6	22
Non bis A/F epoxy	41	10
Hardener A	36	17
Hardener B	3	1
Diluent	13	0
Inorganic filler	1	1
Total amount	100	52

### 3.4.2 Comprehensive hazardous evaluation of turbine generators with VPI and RR insulation

The comprehensive hazardous indices calculated from the above-mentioned data are shown in Fig.4. As a result, the comprehensive hazardous index of our turbine generator with RR insulation is smaller than our generator with VPI insulation by more than 30%.

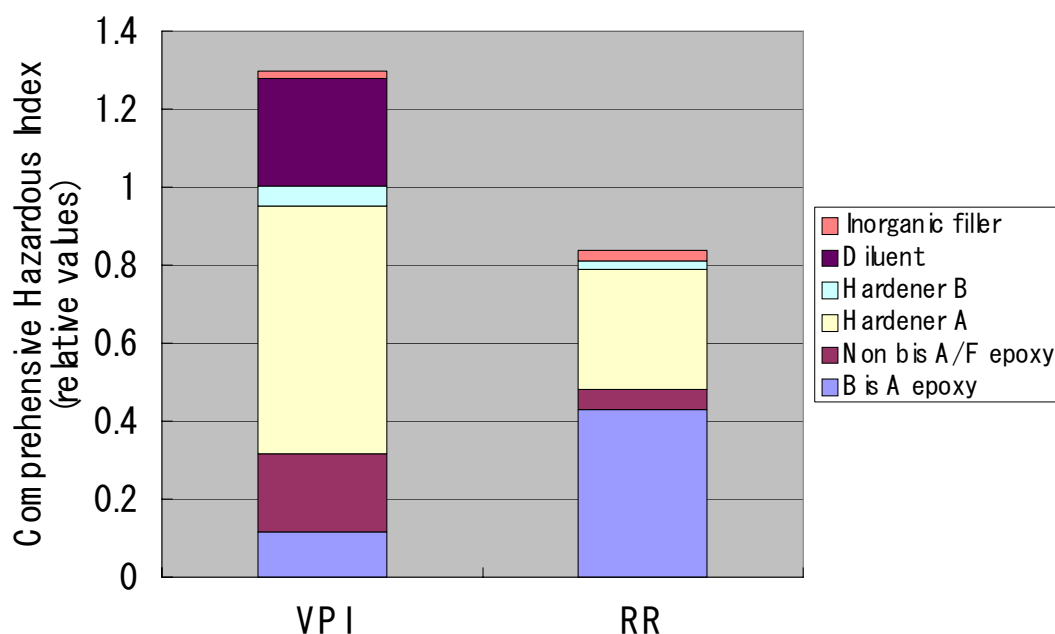


Fig.4 Calculation results of risk indices multiplied by organic chemical amounts

## 4 CONCLUSION

- 1) We proposed the comprehensive hazardous evaluation method and index of chemical materials applied for turbine generator.
- 2) Classifying the level of hazardous items according to GHS, the definition of comprehensive hazardous index is clarified. As a result, the legitimacy of comprehensive hazardous index is improved
- 3) Calculating the hazardous indices of our both turbine generators applied with VPI and RR insulation system, the hazardous index of the turbine generator with RR shows smaller value than the generator with VPI by more than 30%.

## **BIBLIOGRAPHY**

- [1] H.Hatano, R.Takahashi, H.Noda, T.Teijima, T.Murakami, R. Carson, K.Flemstroem, S.Haeggstroem “Risk Evaluation of Organic Chemicals Utilized in Turbine Generators”, (The Seventh International Conference on Eco Balance, 2006, Tsukuba, Japan)

**Detect and Evaluation of Corona Defects on Generator  
Stator Winding Overhangs**

**Wang Jinsong, Bai Kai, Guo Jiayang  
Mei Zhigang, Song Peng  
Wu Yuhui, Bai Yamin  
North China Electric Power  
Research Institute  
China**

**Zen Fang, Sun Weiben  
  
Datang Power Corporation  
China**

**SUMMARY**

The defects of corona or discharge are important factors to result maybe in failures on stator winding. It is meaningful to detect the corona defects at the early stage of faulty coming on. This paper presents a new method to detect and evaluate the corona defects on stator winding overhangs. A test bench that consists of real stator bar spare, ultraviolet radiation detector and partial discharge measurement instrument has been developed in the laboratory. Corona would be brought on at selected areas of spare stator bars under the controllable test situation. Ultraviolet radiation and partial discharge of the corona are measured simultaneously. Test environment and distance between ultraviolet radiation detector and corona defect should also be important parameters. The statistical relation between partial discharge and ultraviolet radiation is analyzed based on tests. The parameters of saturation intensity of corona are developed to describe the corona area and corona intensity.

Under the basis of data relation, the ultraviolet radiation of corona is able to corresponding to the partial discharge. It is a way to evaluate the crisis of corona. Because ultraviolet radiation imaging and measurement system can take on the advantage of visualization, it is convenience to locate the corona areas accurately.

The paper also presents the principle of evaluating the failure risk of stator winding in the next 5~6 years based on above measurement. Difference repair and maintenance schemes can be adopted according to the risk level of corona defects. Up to date, over 20 large Generators have been inspected and evaluated.

**KEYWORDS**

Generator, Stator winding insulation, Corona, Partial discharge, Ultraviolet radiation detector

## **1 INTRODUCTION**

Recently, more and more power generators had corona defects on surface of stator winding overhangs. For example, 9 generators had been found corona problems in a Power Group Corporation [1].

The defects arose from damage of resistance grading. The common reasons are mechanical abrasion or resistance grading design defect.

At the early stage of corona defect, the insulation is not damaged very much. It can be repaired by restore local insulation or only restore local surface resistance grading. But if it is not repaired at the early stage, it might result failure during operation. At that situation, local repair is not possible because ground insulation was damaged and the damaged stator bar must be replaced. Under the worst situation, the damage caused failures during operation. These kinds of failures can prove costly both from a repair or replacement standpoint and from lost production or downtime.

The interval of overhaul for generator is about 5~6years. During the time period, corona defect can deteriorate dramatically, so it is meaningful to early detect the discharge or corona on the winding overhangs.

But at the early stage of defect, it is more difficult to detect. Therefore, it is necessary to develop efficient test methods that are truly capable of indicating the deterioration condition of resistance grading and finding the sensitive parameters to assess the resistance grading or insulation defect of stator winding overhangs. Moreover this is of great significance in planning an effective overhaul and maintenance.

This paper presents a method to detect and quantity evaluates the corona defects on stator winding overhangs.

## **2 CORONA MECHANISMS OF POWER GENERATOR STATOR WINDING OVERHANGS**

In the introduction, it was stated that there are two common reasons arose corona defect. They are mechanical abrasion or resistance grading design defect.

Power generators stator winding overhangs operate in a more severe electric and larger mechanical loading than those parts of winding in the slots. Stator windings in the slot are supported by stator core and tightened by wedges, it is reliable mechanically. But stator winding overhangs are tightened by winding overhang supports such as banding and pressing plate. It is weak compared to those parts in slots. It vibrates like over hanging beam and effect significantly by the manufacturing quality of tightening and electric transient process during operation.

When there is mechanical erosion caused by vibration, it will damage corona shielding first and then ground insulation. Wherever the corona shielding and ground insulation is damaged on the stator winding overhangs, the electric stress will be changed dramatically. This is why defects are more likely to occur at this parts of power generators.

Other factors that can led to damage corona shielding including improper design and poor manufacturing quality.

All those factors can lead to the significant variation on the potential gradient. If the electric stress increased to 3kV/mm (varies with air pressure and humidity) in air, there will be ionization in the air, this activity will continue and cause partial discharge or corona. Wherever corona occurs, there will be hot pot and erode gas. Those factors can damage insulation. Consequently, the time to failure will be reduced.

If allowed to continue, corona will eventually cause a complete breakdown or failure of the insulation.

## **3 METHODS OF DETECT CORONA DEFECT**

Wherever corona occurs, there will be impulse current accompanying with emission of light, acoustic radiation, ultrasonic and electromagnetic radiation. By detect the variations of those parameters, corona defects can be found out. Every method correspond to difference parameters detections.

The methods are currently employed to detect defects including:

- Partial discharge measurement
- Ultrasonic emission detection
- Black out test (Visual observation of visible light)
- Daytime ultraviolet radiation detection with UV camera.

Partial discharge measurement is widely used in detection of insulation defect and surface corona defect. The method is standardized for many years. By compare to the history measurement results, the deterioration of defect can be known. The pC reading shows the condition of most serious part of insulation. But for partial discharge measurement, it is very difficult to locate the corona defect exactly.

Blackout test is visual inspection of visible light caused by surface corona defects. It needs energize winding and eliminate ambient light. The test method can locate the defect. But it is difficult to rating the defects according to stand. The judgement of defect depends on the experience of tester to a large extent. For example, some defects might be considered to be acceptable and need not repair. But after four years' operation, the defects proved to be damageable.

Ultraviolet radiation detection with solar blind UV camera can locate the corona defect exactly. Solar blind UV camera produces a video image of ultraviolet radiation and imagine of the visible test object. By combining the two related images and presented as one image to the user, it is easy to locate the position of corona. Due to the ozone layer surrounding the earth, the wavelength between 240-280nm are absorb. There are some kinds of corona detection cameras only detect wavelength falls into the solar-blind spectrum, and can be used in daytime. So it can be called daytime UV camera.

Daytime UV camera has unique advantages because of a weak background interference, reliability and convenience.

The main advantage of corona detection camera is that the measurements result can not assess the serious of corona defects in term of qualification. No practicable normalizing method has been developed by now. Consequently limit the use of the device.

So it is very important to develop a normalizing method for daytime UV camera.

#### **4 NORMALIZING PRINCIPLE OF ULTRAVIOLET RADIATION DETECTOR**

In some case, the corona is under the acceptable intensity. The defect can be considered minor and will not damage the surface resistance grading and other insulation system during the next overhaul interval. This kind of defects has small failure probability during operation. So it can be inspected and evaluated during the next overhaul to determine the further treat measures. There are many experiences that some slight corona areas have no significant deterioration during several overhaul periods. Excessive maintenance is not necessary and not economy. But definitely those corona areas need reliable evaluated for the next overhaul. It is very necessary to normalizing the photon counting of ultraviolet radiation detector to enable the quantity assessment of corona risk level.

The result of daytime UV camera measurements is affected significant by several factors. They are distance, air pressure, humidity, observation angle and the gain of device. Nevertheless some researches indicated that quantity of PD, the corona impulse current and ultraviolet radiation of corona have the corresponding relationship with the statistical regularity under the circumstance of almost the same atmosphere, as shows in fig.1[2]. So in order to quantify the intensity of the corona discharge detected by corona camera, partial discharge measurement is introduced as a comparing parameter.

Since the partial discharge measurement can detect the discharge both in the insulation and on the surface, it is essential to control the discharge mainly on the surface. Only in this way, the relationship between the partial discharge and the UV camera photon counting readings can be established. Then eliminate the influence of the discharge in the insulation that can not be detected by UV camera.

So the idea is to measure a single certain corona area, then introduce the relationship between the partial discharge and the corona camera numerical readings statistically under the same circumstance in the laboratory. After normalizing the UV camera photon counting, it is possible to evaluate the corona according to the counting.

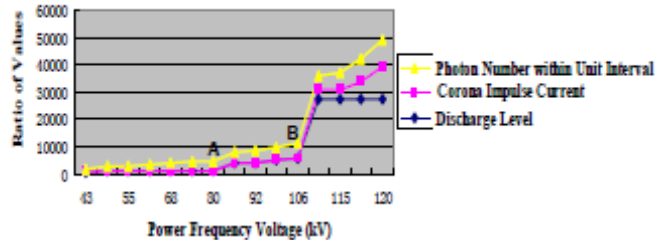


Fig.1 Tendency chart of the discharge lever, the peak value of corona impulse current, and the photon counting with voltage.

## 5 NORMALIZING METHOD OF CORONA INTENSITY

The processing of normalizing is in the laboratory in order to eliminate the environment electromagnetic noise. The partial discharge background of the laboratory is not above 10pC. The humidity is not above 80%RH, and the temperature is between 5°C~40°C. The background of the UV camera photon counting is 0.

### 5.1 Arrangement of test bench

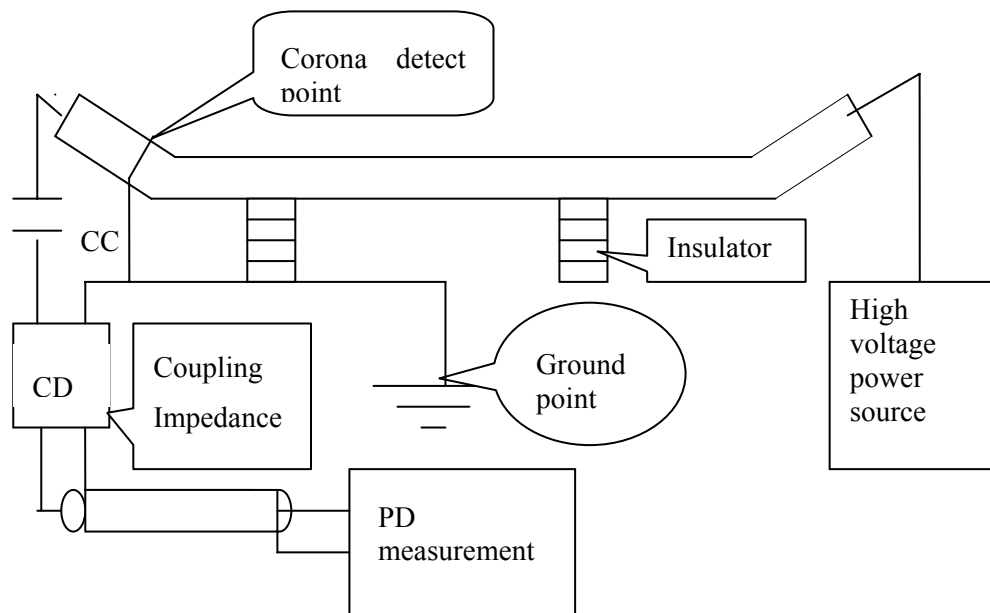


Fig.2 setup of the test bench

The arrangement of test bench shows in fig.2. It consists of 6 parts:

- The first part is a real spare bar. The spare bar is in a good insulation and surface resistance grading is in good condition
- The second part is high voltage power source. The PD from the power source should below 100pC
- The third part is PD measurement device
- The fourth part is daytime UV camera
- The fifth part is ground cooper wire. The spare bar is as the test sample, and is grounded on a single surface of four by a thin cooper wire
- The sixth part is insulators. The insulators can bear five times rate voltage of the test bar

In this arrangement, since no other part of bar is grounded, the corona only can occur at grounding surface of the bar.

In this way, the measurement of PD has a good corresponding with the UV camera that observed. On the other words, corona would be brought on at selected areas of spare stator bars under the controllable test situation. Ultraviolet radiation and partial discharge of the corona are measured simultaneously.

**5.2 Test data processing method**

In the laboratory, nine real spare stator bars are selected for test, two of them rate voltage are 18kV and 7 of them are 6kV. All of the spare bars have integrated resistance grading. Every spare bar is grounded at a single point to assure that the ground point is the only point discharge can happen. So there is a unique PD point and can be detect by corona detection camera and PD measurement device simultaneously. The PD readings and corona detection camera photon readings are recorded at the same voltage. Considered that the test voltage is far below the rate voltage, so the PD in the insulation is minor and so can be neglected. It should remain that all the coronas are observed at 2m distance from ground point by UV camera.

The measurement procedure is as following. First ground 7cm away from the conductor and then energize the stator bar. When the reading of the PD about  $1000\text{pC} \pm 100\text{pC}$ , hold on the voltage and then record the photo counting 2m away from the ground point. After record the readings and shut down the power that applied on the stator bar, shift the ground point 2cm more away form the previous ground point. Until the voltage is about rated voltage and the PD is still not reach  $1000\text{pC} \pm 100\text{pC}$ . At the other end of bar, the measurement is repeated in the same way.

By doing the measurements at both ends of 9 stator bars, the total test units are 18 and available data is about 100 groups. The test is done under  $6^{\circ}\text{C}$ , the humidity is 26%RH.

75 test data groups are chosen from all data, which PD is between  $900\text{pC}$  and  $1100\text{pC}$ . The photo counting is recorded by UV camera at the 100% gain situation. Fig.3 shows the photo counting distribution that gain is 100%.

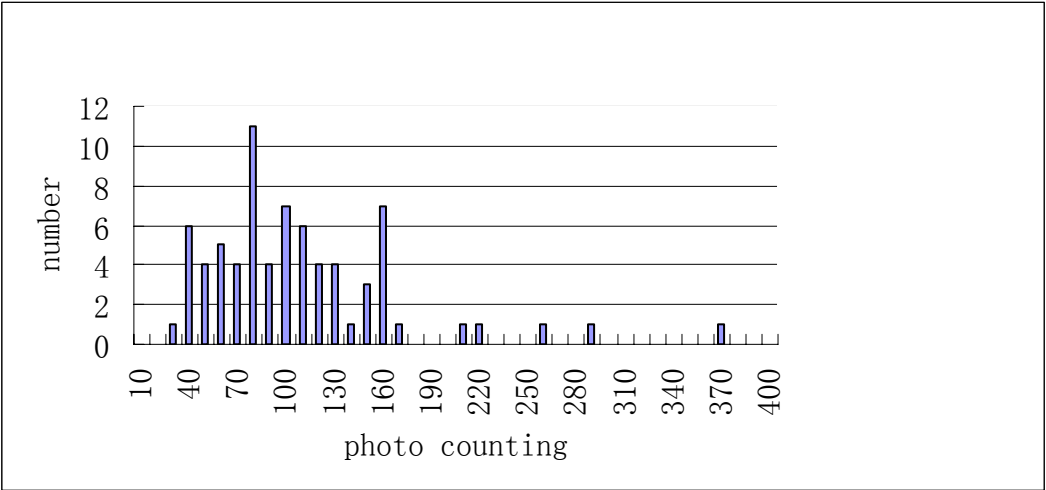


**Fig.3 photon counting distribution**

According to the test data, the average photon counting can be calculated, that is 108.

According to the photon counting distribution from fig.3, photon counting probability distribution can be conducted. The confidence limit is set to be 95%, and then the confidence upper limit is 220. The confidence upper limit is symbolized as **Nc**.

For different UV camera, the result will be different. So the normalizing process should be done to every UV camera device.

### 5.3 Corona density

In the measurement process, the gain  $K$  is adjusted to obtain the maximum photon counting  $P_{max}$ . Normally speaking, the photon counting will decrease with the decrease of the gain. That is the maximum photon counting  $P_{max}$  corresponding to the 100% gain. In some situation, the corona is focus on a very small area. When decrease the gain of UV camera at the situation, the photon counting will increase. There is a gain number  $K_{max}$  corresponding to the maximum photon counting.

In order to describe the corona, the saturation intensity of corona  $D$  is introduced, defined as the reciprocal of  $K_{max}$ . That is  $D=1/ K_{max}$ .

## 6 FIELD TEST OF GENERATOR

For different UV camera, the photon counting is different. After normalizing the UV camera as described in sector 5, the measurement and locate of corona can be done in field.

### 6.1 Stage of field test and test voltage

Since the different parts of generator have the different maximum electrical stress, the voltage applied should be difference according to the part of corona. To locate the corona between winding and ground, the energized voltage is about phase to ground. To those coronas between phase windings, the test voltage should be nominal voltage of generator.

So in field test, the test is carried out in two stages. The first stage is to check the phase to ground part of winding overhangs; the second stage is to check the phase to phase parts. According to above principle, the voltage applied on the stator windings list in table I, where  $U_n$  is the nominal voltage rating of test generator. It is should remained that the voltage applied on test generator must be modified according to the altitude as the stand JB/T 8439 specified.

**Table I Test Voltage Applied on Winding.**

Cooling Type of Winding	Applied Voltage	
	First Stage	Second Stage
Air cooled	$1.1U_n/\sqrt{3}$	$1.1U_n$
Hydrogen cooled	$U_n/\sqrt{3}$	$U_n$

### 6.2 Observe distance and background photon counting

The Observe distance from UV camera to the winding overhangs should be 2m (according to the device normalizing distance). If it is not 2m or the distance of normalizing in laboratory, the photon counting need be modified with the conduced photon counting-distance relationship.

The photon counting-distance relationship can be conduced as follow.

At a certain corona density, record the photon counting in 3-4 different distance. And then a curve of photon counting-distance relationship can be conduced. Fig.4 shows the photon counting-distance relation at difference gains for a daytime UV camera. By curve fitting, the photon counting of different distance can be calculated at a certain gain. Because for the generator test, the distance is between 2-4m, so the straight line fitting can be used in an engineering opinion.

The background photo counting should be very small. Sine daytime UV camera is daytime, it can be used in natural light. Before test, scan and record the background photon counting  $N_e$  is absolutely necessary. If compare to  $N_e$  that described in section 5, it means the background photon counting  $N_e$  can not be neglected, tester should shut down all the lamps that might bring in background ultraviolet radiation.

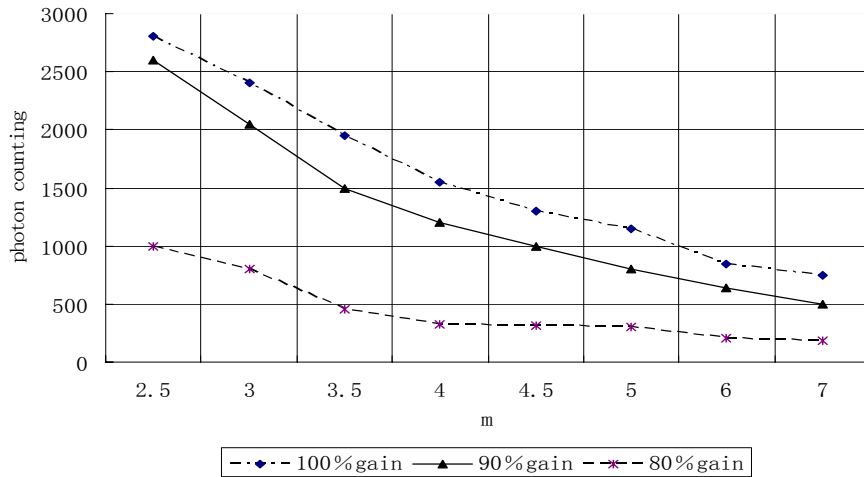


Fig.3 relationship between photon counting and distance at difference gains

### 7 QUANTIFY EVALUATION OF WINDING OVERHANGS CORONA RISK

Before the generator of field test, background ultraviolet radiation is measured by UV camera and the photon counting  $N_e$  should be recorded.

For the first stage, the recorded photon counting  $N$  should not exceed twice time of background photon counting, that is  $2 * N_e$ . Otherwise the generator need be repaired.

For the second stage, the recorded photon counting  $N$  and the repair and maintenance scheme shows in table II. It should remind that corona density should be considered.

Table II Photon counting and repair schemes at second stage (phase to phase corona)

Voltage applied	Photon counting	Corona density D	repair and maintenance scheme
1.1Un (air cooled) or Un (Hydrogen cooled)	$(N - N_e) < N_c$	—	Need not repair
	$N_c \leq (N - N_e) \leq 4N_c$	1~1.09	Other factors should be considered to determin if repair or not in the overhaul. If not repair, should check in the next overhaul
	$N_c \leq (N - N_e) \leq 4N_c$	>1.1	Need repair in the overhaul
	$(N - N_e) > 4N_c$	—	Need repair in the overhaul

$N_c$  : the photo counting in normalizing stage that descibe in section 5  
 $N_e$  : the test background photo counting that descibe in section 6.2

### 8 RESULTS AND DISCUSSION

According to the above evaluation principle, over 20 large generators that suspect corona defects have been inspected and evaluated. All of the generators were inspected during overhauls. Among the 20 generators, 10 generators were restored stressing control coat, 2 other units were not repaired because of the photon counting not exceed the number in table II, so can be neglected. After repaired, the inspections were conducted to evaluate the rapier result. Until the corona level were acceptable.

In June 2007, an air cooled generator was checked during the overhaul. 12 corona defects were located, and 8 of them need to be repaired. After repair and 3 years' operation, inspection was done during overhaul. The inspection shows that no new corona was found. It also shows that 8 repaired areas do not deteriorate during the operation. For 4 not repaired areas, inspection shows that the photon counting is not increase.

That shows the repair and maintenance scheme is reasonable and practicable.

We found that early detect and evaluation of corona can reduce the risk of failure dramatically. We also think that the experimental study of the influence factors to measurement is essential for future establishment of repair and maintenance scheme of the generator and further work in this field is necessary.

## **BIBLIOGRAPHY**

Wang Jinsong was born in Hebei, China, on January 1972. He received his Master degree from Department of Electric Power Engineering, Huazhong University of Science and Technology in 1997. He is now a senior engineer in North China Electric Power Research Institute.

## **REFERENCE**

- [1] Qiu M .Cause Analysis of Bar terminal Insulation of 600MW Generator and Precaution//North China Power Technology, December 2007
- [2] MA B, ZHOU W, WANG T, DING Y.Study on Corona Discharge Test under the Power Frequency Voltage of the Severe Non-uniform Electric field based on the UV-light Imaging Technology// CEEM'2006



Beijing, China

SC A1  
COLLOQUIUM ON NEW DEVELOPMENT OF ROTATING  
ELECTRICAL MACHINES

11~13 September, 2011

---

**Design and Acceptance Test of 23kV Stator Bars for the  
Largest Air Cooled Hydro Generator in Xiang Jia Ba Right Bank**

**Thomas Klamt**  
ALSTOM Hydro (Switzerland) Ltd  
Zentralstrasse Birr  
Switzerland

**Yang Zhongguo**  
Tianjin ALSTOM Hydro Power Co., Ltd.  
Gaofeng road, Beichen district  
Tianjin, China

**SUMMARY**

For Xiang Jia Ba hydro power plant, the biggest air-cooled hydro generator with an output of 890 MVA will be installed. The machine, within the scope of supply for ALSTOM at Right Bank, is designed with a 23 kV stator winding which finally allows an optimized electrical design of the entire machine considering the project specific speed and output.

This paper will introduce the design, the manufacturing and the acceptance test of the air-cooled 23kV stator bars. The complete acceptance tests of the bars show that the insulation system has good properties on thermal-electric aging, breakdown capability, dielectric losses and corona protection. This is a quite valuable reference to design stator winding at higher voltage level for in large machine up to 1000MW for example.

**KEYWORDS**

Large hydro generator, 23kV voltage, Stator bar, Design, Manufacturing, Acceptance test

## 1 INTRODUCTION

For the future the worldwide electrical energy consumption will on average continue to increase. According to the American Energy Information Administration (EIA) and to the International Energy Agency (IEA), this increase will be by 2% per year in the next two(2) decades till 2030. The highest annual growth of energy consumption is predicted for Asia (3.7%) and Central and South America (2.8%). Being one of the fast developing countries in the world, China is expected to increase its total capacity of power generation by 4.6% per year in the next decade till 2020, while 5.5% increase per year for hydro, according to the report from China Hydro Power Development Overview in 21st Century.

China has a lot of hydro power plant potential. Several new huge power plants are planned and some are in the phase of pre-studying the potential. By the end of installation of Three Gorges (32×700MW), huge power plants like Xian Jia Ba (8×800MW) and Xi Luo Du (18×770MW) are being built. To optimize such power plants bigger machines in size, higher power output and higher voltages are under investigation.

## 2 XIANG JIABA RIGHT BANK HYDRO POWER PLANT PROJECT

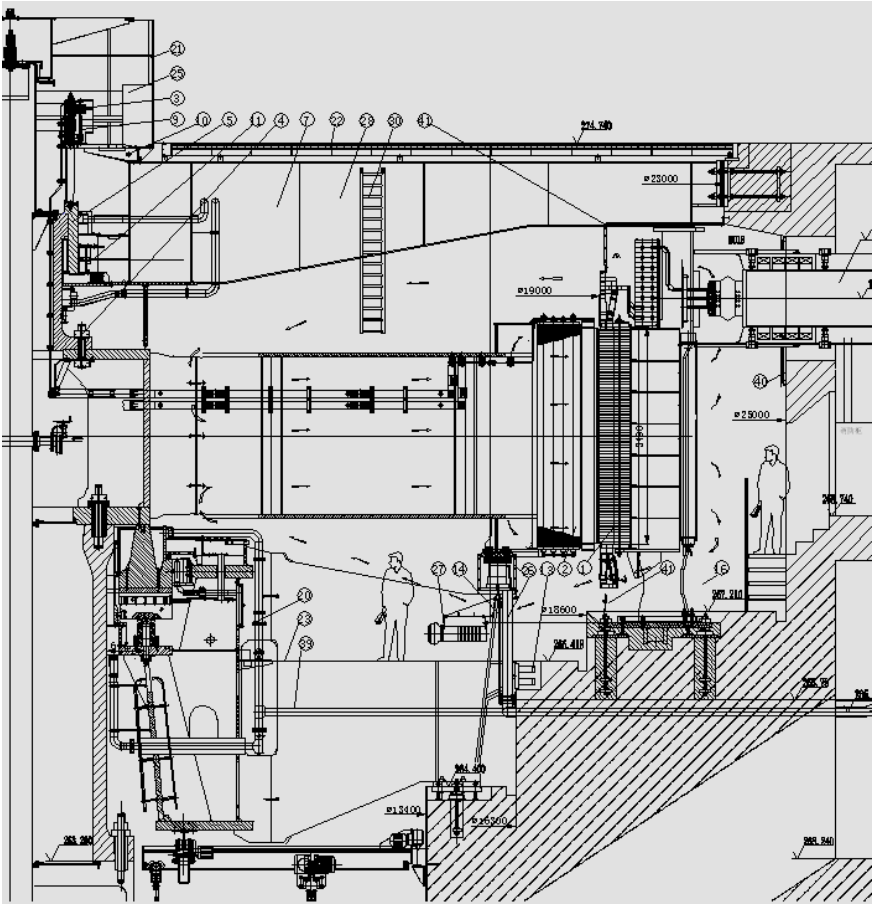
For Xiang Jiaba Right Bank hydro power plant, the biggest air-cooled hydro generator with an output of 890 MVA will be installed. The project data in table I show the comparison with the data from Three Gorges project (Left bank, Right bank and Underground).

Table I Technical data of Xiang Jia Ba and Three Gorges

Power station	Unit	Xiang Jia Ba (RB)	Three Gorges (LB)	Three Gorges (RB+UG)
Number of ALSTOM units		4	8	6
Rated Output	(MVA)	888.9	777.8	777.8
Max. continuous output	(MVA)	888.9	840	840
Rated voltage	(kV)	23	20	20
Rated power factor		0.9	0.9	0.9
Rated frequency	(Hz)	50	50	50
Rated speed	(rpm)	71.4	75	71.4
Runaway speed	(rpm)	134	150	143
Flywheel effect	(tm <sup>2</sup> )	490'000	450'000	450'000
Rated efficiency (contract)	(%)	98.8	98.77	98.83
Stator winding		air cooled	water cooled	water cooled
Stator bore diameter	(mm)	19'000	18'800	18'800
Stator stacking height	(mm)	3'490	2'950	3'150
Pit diameter	(mm)	25'000	25'000	25'000
Rotor mass	(t)	2'059	2'000	2'027
Stator mass	(t)	958	795	851
Generator mass	(t)	3'790	3'380	3'540

The cross section of the machine is shown in fig.1. The machine is designed with a 23 kV stator winding which finally allows an optimized electrical design of the entire machine considering the

project specific speed and output. In general, rated voltages above 20 kV offer a new potential for the overall optimization of very large hydro units.



**Fig. 1 Cross section of Xian Jia Ba Right Bank generator**

The application of such a high voltage requires specific attention during the design, the manufacturing, the testing and the installation phases. ALSTOM has continuously developed the stator winding technology towards increased field strength and also increased voltages.

The used unique installation method of ALSTOM gives the confidence of a safe and long time operation. This method is used as standard for all hydro projects with stator bars in the last years and is approved up to the highest voltages.

Based on the feedback from installed generators with the same insulation system called Micadur® the stator winding design for Xiang Jiaba Right Bank project was done. With the continuous improvements in the insulation system generators with rated voltages up to 27kV for turbo generators and 23 kV for hydro generators are running. All these experiences were very useful for the final design of the stator bars.

Before acceptance test and mass production of the stator bars for Xiang Jia Ba Right Bank project several improvements were done in the workshop based on the experiences of the manufacturing of large stator bars for turbo generators within our company. Also the experiences of other manufacturing locations for large hydro stator bars are implemented as best praxis. The stator bars will be manufactured with the standard materials used for the insulation system Micadur®.

For the approval of the design several test bars were manufactured in advance. These pre – manufactured test bars are used for the extensive lab tests. Different tests were done either in a mock-up to simulate the stator core or as single stator bars to check the manufacturing processes and the used materials. The test results are very important and will be used for further improvements and optimizations.

In addition to the standard manufacturing tests and the tests in the mock-up several lab tests were done with the single stator bars, such as Voltage Endurance Tests (VET), measuring of the corona inception and corona extinguish voltage, Dissipation factor ( $\text{tg}\delta$ ) measurement with real screen and break down tests.

These test results give a good indication for necessary and possible improvements for Xiang Jia Ba Right Bank stator bars in design and manufacturing and confirm the insulation quality of the bars. The results of the tests can also be used for further projects of hydro generators with increased voltages, higher field strength or larger size of the bars.

**3 STATOR WINDING WITH 23KV RATED VOLTAGE**

Stator windings with rated voltage above 20 kV are very seldom. For the Turbo machinery there are several machines with UN = 21 kV as air-cooled machines. Higher rated voltages are mostly water-cooled or gas (hydrogen) cooled. Generators up to UN = 27 kV are running with the ALSTOM VPI system Micadur®.

**3.1 Design of the stator winding**

Improvements on materials and effective process control during manufacturing enable higher field strength in the main insulation system and as a consequence higher voltages for large units. High voltage applications require special attention on the stator winding overhang design and the corona protection system.

ALSTOM has qualified its Micadur® VPI insulation system for machine voltage up to 30 kV, whereas ALSTOM Hydro generators up to 23 kV are in operation. Table II shows the reference of ALSTOM hydro generators for high voltage equal to or more than 20kV.

**Table II Reference of ALSTOM hydro generators for high voltage projects**

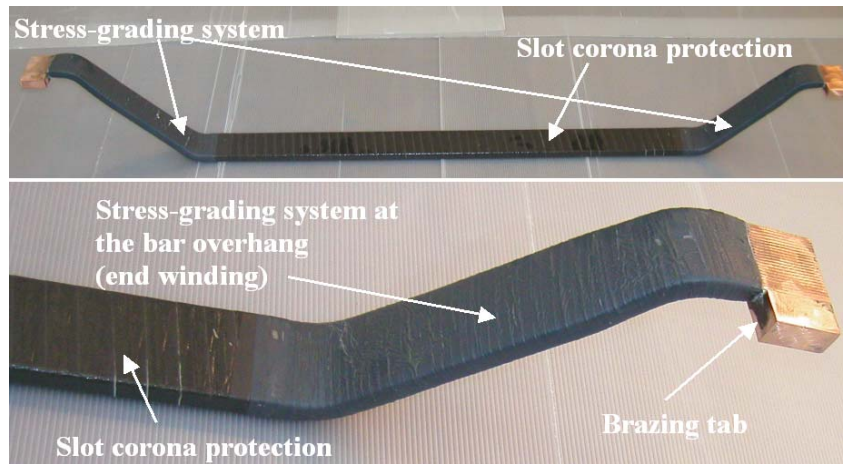
Plant name	Rated power MVA	Rated voltage kV	Cooling of Stator winding	Stage
Raccoon Mountain (US)	476	23	Water	operation
Bieudron (Switzerland)	465	21	Water	operation
Three Gorges (China)	778	20	Water	operation
Xiang Jia Ba(China)	889	23	Air	installation
Jin Ping II (China)	667	20	Air	installation
Guan Yin Yan(China)	667	20	Air	installation

**3.1.1 Corona protection system**

For the corona protection at a stator bar there are two(2) different materials. In the slot part a conductive outer surface is required to suppress slot corona discharges. Such discharges can lead to degradation of the main insulation. The result can be a ground fault. The outer conductive surface can be realized with tapes or with varnish.

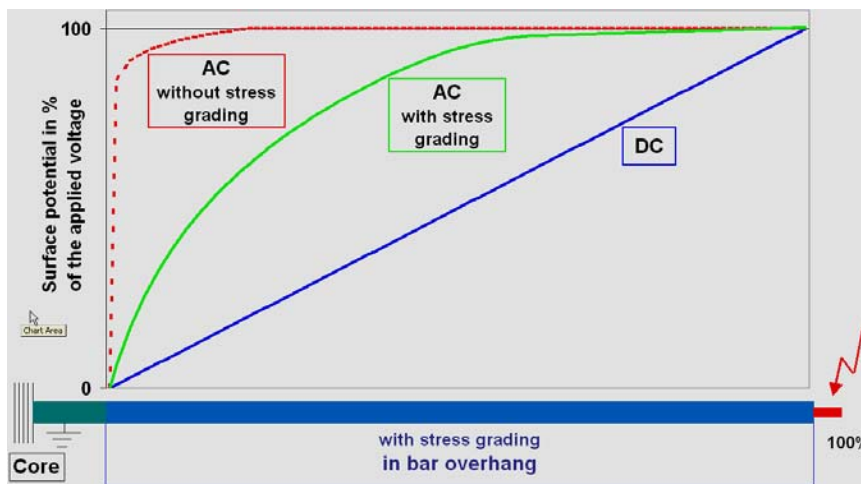
The ALSTOM corona protection system is approved for voltages up to 30kV. It is used in turbo and hydro generators and machines up to 27kV are in service. Particularly for rated voltages above 16kV, the grading system needs well-defined and stable characteristics. The interface between the slot corona protection and the grading system, as well as in the phase separations, the grading system are the most critical areas for the application.

The surface resistance of grading materials depends on the electrical field. In general, a high electrical field requires a lower surface resistance, in order to protect the winding from corona effects. Tests have shown that the application of the stress grading system on the entire winding overhang increases the corona inception voltage to values above typical customer requirements. In fig.2, a stator bar with such an applied grading system is shown.



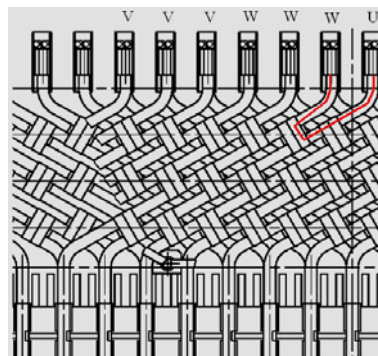
**Fig. 2 Stator bar with Corona protection system**

Fig.3 shows the function of the stress grading system along the stator bar surface in the winding overhang. The maximum electrical field strength ( $=dv/dx$ ) is reduced.



**Fig. 3 Function of the stress grading system**

In fig.4 the section of a typical stator winding overhang including a part of the support system is presented. It is visible that the grading system applied over the total length of the overhang controls the voltage distribution and reduces the risk of corona in phase separations. Especially during high-voltage tests of the stator winding, the voltage difference between bar ends in phase separations can be higher than the corona inception voltage. The length of the path along the surfaces from one bar end to the next bar end, between two phases, can be too short and therefore, the electrical field strength can be locally too high with the risk of corona activity. All these potential risks have been considered during the winding design.



**Fig. 4 Typical section of the winding overhang of a hydro generator**

### 3.1.2 Stator bar design

With an increase of the electrical field strength, the insulation thickness of the main insulation is reduced, compared to traditional systems, in order to increase the slot filling factor and finally, the efficiency of the generator.

In addition to the slot filling factor, the total length of the stator winding can be minimized with optimizing the winding overhang geometry. These optimizations in the winding overhang can be done with the consideration of the necessary air distances, in combination with the used grading system. Also, with the customer requirements of the blackout tests, it is possible to optimize the length of the winding overhang. In figure 4 a typical section of the winding overhang is shown. There are several phase separations with the critical air distances to suppress the corona activities during operation.

Other criteria for the design are the support system of the winding to ensure a safe operation and withstand short circuit failure modes. In addition, the cooling of the stator bars in the winding overhang and the connections between the bars and the terminals has to be considered and confirmed with the ventilation calculation.

### 3.2 Stator bar manufacturing

Due to the size of the stator bar, a specific knowledge in material science and manufacturing processes of HV-insulation is required. All the processes of different manufacturing steps, especially the VPI process and the curing process, are very strict and are based on best practice from the production and testing of large hydro and turbo generator bars. Sharing the experiences between factories, as well as the definition of the common processes, is done under the responsibility of Alstom global manufacturing organization with a strong support from the Global Technology Centre.

The ALSTOM Hydro factory in Tianjin is used to manufacture stator bars up to the rated voltage of  $UN = 20$  kV. For the Xiang Jia Ba Right Bank project with the rated voltage of  $UN = 23$  kV tests for the approval of the manufacturing were necessary. The acceptance tests and mass production were taken place only after a series of tests in advance for approval to guarantee the high quality standard for ALSTOM stator windings with the trade name Micadur® and to fulfill the customer requirements according contract.

## 4 ACCEPTANCE TEST

Acceptance tests on 16 stator bars were performed on April 13 to May 7, 2010. The tests included a voltage endurance test (VET) in accordance with IEEE Std 1043-1996 and IEEE Std 1553-2002, schedule A (400 hrs @ 2,17 UN (49.9 kV) on four(4) bars. Six(6) bars were subjected for a breakdown voltage test and two(2) bars for a loss factor measured at 155 °C. The remaining four(4) bars are spare bars. The results of all performed tests on the bars fulfill the specified requirements.

### 4.1 Corona Test

The corona test was performed on all test bars. The bars were connected in parallel to the ground (see fig.5). The light was switched off and the voltage was increased in the rate of 1~2 kV/s to 1.5 UN = 34.5 kV (criterion value). No corona lights or surface discharges could be detected. Additionally the voltage was increased up to 2UN = 46 kV, also no corona lights could be detected on the corona protection. Only at the bar ends (brazing lugs) coronal lights could visibly. The test passed the criterion, no visible corona by eye.



Fig. 5 Set up corona test

## 4.2 Loss factor measurement

All measured bars within the incoming test were in the expected and normal range. The loss factor measurement after Voltage Endurance Test showed no significant changes, generally the loss-factor is lower after the VET test (see table III). This is typical for a good insulation system, during the endurance test a post-curing of the resin occurred. All tested bars fulfilled the requirements of the required criteria before and after VET test.

**Table III Loss factor measurement results**

Bar No.	Testing time (hours)	tg $\delta$ 0.2UN	tg $\delta$ 0.6UN - tg $\delta$ 0.2UN	Max. $\Delta$ tg $\delta$ 0.2UN-step
		%o	%o	%o
A1	0	5.306	0.90	0.50
	400	3.375	0.60	0.70
A2	0	6.276	1.04	0.60
	400	3.975	0.90	0.70
A4	0	5.476	0.70	0.46
A5	0	5.616	0.83	0.57
A7	0	5.946	1.16	0.58
A10	0	4.816	1.06	0.60
B1	0	5.376	0.74	0.44
	400	3.076	1.10	0.80
B3	0	6.336	0.49	0.37
	400	2.976	0.60	0.90
B4	0	5.436	0.83	0.50
B5	0	5.116	0.96	0.48
B7	0	5.436	0.72	0.48
B10	0	5.616	0.76	0.47
Maximum value		15%o	5%o	3.0%o

## 4.3 Loss factor measurement at 155 °C

The measurement was carried out after reach stable state of all surface temperature (see fig.6). The two test bars fulfilled the customer requirements (see table IV).

**Table IV Thermal loss factor measurement results**

Bar No.	tg $\delta$ 0.6UN
A10	69.73 %o
B10	93.14 %o
Required value	$\leq$ 100 %o



**Fig. 6 Set up loss factor measurement at 155°C**

#### 4.4 Thermal electrical endurance test

The long-term voltage endurance test on four(4) bars with  $2.17U_n = 49.9 \text{ kV/50 Hz}$  at  $110^\circ\text{C}$  was carried in a thermal box, which was heated up by hot air. The test was started on 20th April and stopped on 7th May 2010, after a total duration of 400 hours. Due to big size of the bars, it was agreed to carry out the test only on the straight part (see fig.7), according to IEEE 1043-1996.



Fig. 7 Set-up voltage endurance test

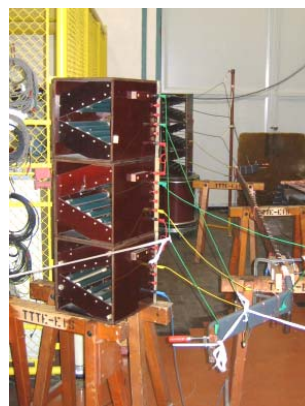


Fig. 8 Set-up breakdown voltage test

#### 4.5 Breakdown voltage test

The breakdown tests were carried out with an external stress release system (see fig.8), to avoid a thermal overstress of the end-winding corona protection. The 50 Hz AC – test voltage was applied between the copper conductor and the earthed slot corona protection of each bar. The test voltage was increased on each bar until breakdown. The rate of rise of the test voltage was chosen, so that most breakdowns occurred in the range between 10 and 20 seconds (IEC 60243-1). The rate of the increasing of the bar A5 is too fast, because of an error in the adjustment of the increase speed.

All six(6) tested bars passed the criterion  $\geq 6U_n = 138 \text{ kV}$ . The breakdown values were in the range of 6.00 UN and 6.91 UN (see table 5).

Table V Test results of breakdown voltage

Bar No.	Breakdown voltage (kV)	UBD/ $U_n$	Rate of Increasing (kV/s)	Breakdown location
A4	152	6.61	10.1	End-winding on non No. Side
A5	159	6.91	26.5	Straight part, 82.5cm from Non No. Side
A7	155	6.74	10.1	Straight part, 129cm from Non No. Side
B4	138	6.00	10.1	Transposition area on No. Side
B5	150	6.52	9.86	Straight part, 155cm from Non No. Side
B7	152	6.61	10.0	Straight part, 127cm from Non No. Side

#### 5 CONCLUSION

All tested bars passed the performed investigation without problems.

The manufacturing of stator bars for rated voltages up to 27 kV is common praxis within ALSTOM for hydrogen-cooled generators in thermal power plants. With the experiences and the Know How of the different manufacturing locations and the exchange of experiences between turbo and hydro generator units the manufacturing of stator bars for an air cooled generator with  $U_n = 23 \text{ kV}$  is reliable.

Also higher rated voltages than  $U_n = 23 \text{ kV}$  seems possible. With such tests done for the Xiang Jia Ba Right Bank project it could be shown that the limit for the air-cooled generators is not reached. All the

experiences show that regarding the voltage level, stator windings with voltages up to 25 kV or even higher are realistic.

## **BIBLIOGRAPHY**

- [1] Wendel C, Stephan C E, Kunz T. Life Time Prediction on Active Components of Hydro Generators - a Way to Optimise Condition-Based Maintenance// *Hydropower & Dams*, 2009
- [2] Klamt T, Noel S. Influence of Stress-Grading Systems on Insulation Resistance and Polarization Index// International Symposium on Electrical Insulation ISEI, Vancouver 2008
- [3] Klamt T, Kunz Ts. High-Voltage Stator Windings, Comparison of Factory Measurements for Quality Control with Measurements in Lab Scale// International Electric Machines and Drives Conference, Miami Florida
- [4] Klamt T, Yang Z. Design and Performance Test of 23kV Stator Bars for the Largest Air Cooled Hydro Generator in Xiang Jia Ba// Water Resources and Renewable Energy Development in Asia, Malaysia, March 2010



Beijing, China

SC A1

**COLLOQUIUM ON NEW DEVELOPMENT OF ROTATING  
ELECTRICAL MACHINES**

11~13 September, 2011

---

**Thermal Cycle Testing for Large Air-Cooled Hydrogenerator Stator Bars**

**Chen Yang, Wei Wei  
Harbin Research Institute of Large Electrical Machinery  
China**

**SUMMARY**

In order to verify the ability of large air-cooled hydrogenerator stator bars to withstand load cycle and to examine the extent of resulted fatigue crack, HEC has developed a thermal cycle testing device with advanced function, based on relevant specifications in IEEE 1310-1996. Thermal cycle testing equipment is consisted of heating device, cooling device, temperature control system and testing chamber. It takes inner heating manner and outer cooling manner.

Testing is performed on stator bars of large air-cooled hydrogenerator. To simulate at most the thermal cycle process during starts and stops of air-cooled hydrogenerator and temperature gradient, a testing bar is selected randomly among all the specimens for temperature control. Copper hard linking block with suitable size, soft link between magnetic voltage regulator and specimens are designed and stator bars are bound to ensure that no other forces would affect the bars during the thermal cycle testing except inner mechanical stress, thus testing accuracy can be increased. It is one of the best characteristic to increase and reduce temperature uniformly. After setting the time of increasing and reducing temperature, the system can automatically calculate the rate of temperature rise and drop, and thus generate an ideal temperature curve. In the heating stage, copper conductor resistance keep changing with temperature rise, which is under real-time comparison with idea temperature curve, and the output of magnetic voltage regulator is accordingly adjusted by the control system, thus uniform temperature rise can be ensured. In the cooling stage, the control system adjusts the frequency of the converter and operating condition of the refrigerating compressor according to real-time comparison with the ideal temperature curve, thus linear temperature curve is obtained.

The cycle temperature is 40°C~150°C. In order to examine the fatigue crack and delamination of the testing bars during and after thermal cycle testing, tap testing, dielectric dissipation factor measurement and partial discharge measurement are performed on the specimens after 0, 50, 100, 250, 500 cycle. Moreover, to further observe the deterioration of the insulation, three specimens are selected randomly and destructive voltage endurance testing at 120°C is performed on them.

The results of diagnosis procedure show that the performance of the specimens changes little after the thermal cycle testing and no evident degradation is observed.

**KEYWORDS**

Air-cooled hydrogenerator stator bars, Thermal cycle testing, Diagnosis procedure

## **1 PURPOSE AND SIGNIFICANCE OF THE TESTING**

Large air-cooled hydrogenerator and pumped storage generator/motor often change suddenly between no-load and load condition when they are used for peak load adjusting with frequent starts/stops. As a result, the temperature of the stator bars and ground-wall insulation also change rapidly. The mechanical stress between copper conductor and ground-wall insulation, as well as between the insulation layers likely result in fatigue crack and affect the insulation life, even threaten the safe operation of the unit in worse situation.

Therefore, it's very significant and impendent to develop a suitable device and verify the ability of large air-cooled hydrogenerator stator bars to withstand load cycle.

## **2 PRINCIPLE AND DEVICE OF THE TESTING**

Based on IEEE 1310-1996, an advanced thermal cycle testing device is developed and stator bars of large air-cooled hydrogenerator are considered. Testing parameters are determined as following:

Cycle temperature: 40°C~150°C.

Time of temperature rise/drop: within 45min.

### **2.1 Heating device**

In the actual process of heating cycle in air-cooled hydrogenerator stator bars, heat of copper conductor is conducted from inner to the outer. So it's an inner heating manner. With this set of device, the specimens are heated by magnetic voltage regulator including silicon rectifier. The capability of the voltage regulator is 120kVA, which can well meet the demands required by thermal cycle testing of various size of hydrogenerator stator bars. The two outputs of the regulator are connected with the specimens in series, to achieve heating by large current.

### **2.2 Cooling device**

In the actual cooling process of air-cooled hydrogenerator, heat is dissipated from ground-wall insulation to the iron and ventilation ducts, i.e. heat of copper conductor is transferred outside through the ground-wall insulation. So it's an outer cooling manner. This set of device employs screw type refrigerating compressor with air discharging volume of 165m<sup>3</sup>/h and 4 groups of high power three phase asynchronous motor (with axial flow fan) to perform forced cooling from outside.

### **2.3 Temperature control system**

The whole progress (heating and cooling) of thermal cycle testing is controlled automatically by PLC computer with touch screen.

### **2.4 Testing chamber**

#### **2.4.1 Material of the chamber**

The required cycle temperature of copper conductor is 40°C~150°C, and in the end of the heating cycle, copper temperature should be 150°C. In order to reduce the copper temperature to 40°C within 45 minutes, forced cooling has to be performed. It can be seen from the temperature curve in Fig.9, that the ambient temperature of the chamber is even lower than 0°C in the cooling stage. Large variation rang of the ambient temperature leads to a high demand for the heat preserving performance and thermal expanding performance of the chamber material. Therefore, polyurethane form (PUF, with good flexibility and elasticity in molecule linkage) with thickness of 100mm is selected as the heating preserving material in this set of testing device.

#### **2.4.2 Special design of the testing chamber**

##### **(1) rail vehicle**

To facilitate placement and moving of the specimens, a rail vehicle with bracket is developed specially (Fig.1). Two separate rail vehicles are combined and fixed with guide rails. The vehicles have extending rails that can be joined and locked with the testing chamber. The specimens are put into the chamber through the guide rails.

(2) lead holes

Wire holes are arranged on the left of the chamber. The copper lead plates are connected to the magnetic voltage regulator through the lead holes (Fig.2).

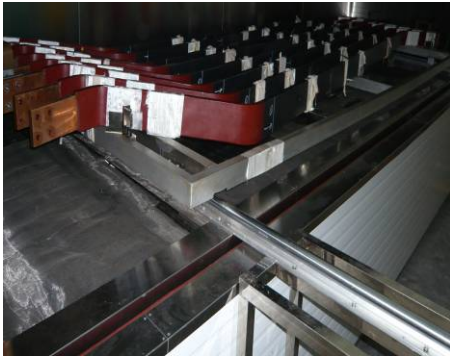


**Fig.1 Rail Vehicle.**

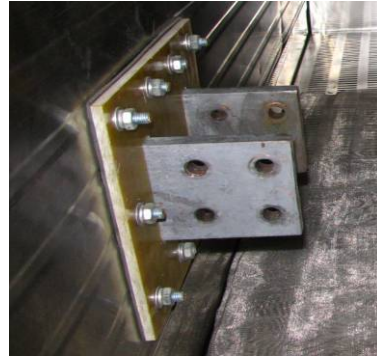


**Fig.2 Copper Lead Plates.**

(3) silicon rubber curtain

In order to preserve the temperature inside the chamber, a silicon rubber curtain is put between the door and the chamber (Fig.3).



**Fig.3 Silicon Rubber Curtain.**

### 3 TESTING PROCEDURE

Thermal cycle testing is performed on total 6 specimens, one of which is temperature control bar.

#### 3.1 Preparation of specimen for temperature control

To simulate at most the thermal cycle process during starts and stops of air-cooled hydrogenerator and temperature gradient, a testing bar is selected randomly among all the specimens for temperature control. Along the narrow side of the bar axially, five holes are drilled uniformly into the insulation (three at slot portion and two at end portion), with diameter of  $\phi 6$  and depth onto the surface of copper conductor (Fig.4). Temperature is measured by inserting temperature sensors (Pt100), and one of the sensors at slot portion is chosen as temperature controlling point (Fig.5).

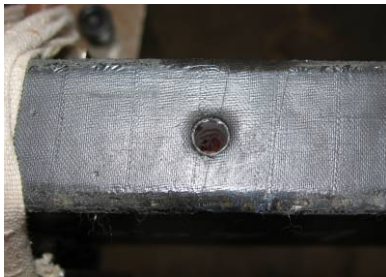


**Fig.4 A hole of  $\Phi 6$  in the ground-wall insulation of the temperature control bar at slot portion, deep onto the surface of the copper conductor.**



**Fig.5 Temperature Sensor Is Inserted Into The Hole.**

### 3.2 Testing Steps

Place the 6 specimens in parallel with equal clearance in the testing chamber. Connect the bars in serial with copper connecting blocks, join the beginning and the end with the copper lead plates of the magnetic voltage regulator. Close the door of the chamber and get ready to start the testing. Press the power supply button of the panel ant to set operating parameters (setting values of low temperature limit, high temperature limit, temperature lifting time, temperature reducing time, number of cycle, etc.). Put on the heating system of the magnetic voltage regulator and keep it in service. Start heating cycle. When the temperature of the copper conductor rises to 150°C, heating cycle will be stop and cooling cycle will start immediately. When the copper temperature drops to 40°C, cooling cycle will stop and heating cycle will start immediately. On this analogy, Thermal cycle testing can go on automatically according to the given settings. There is no delay between heating cycle and cooling cycle. During the whole testing process, temperature gradient always exists in all the layers along the radial direction of the test bars, from copper conductor to the surface of ground-wall insulation, and thus the real operating condition during the starts and stops of air-cooled hydrogenerators is reproduced.

### 3.3 Actions taken to ensure the accuracy of the testing

#### 3.3.1 Eliminating outside affecting forces

In order to eliminate the effect of outside forces except inner mechanical stress leading to fatigue crack, copper hard linking block with suitable size (Fig.6), soft link between magnetic voltage regulator and specimens (Fig.7) are specially designed. Also special clamp is designed and the supported position is bound (Fig.8).



Fig.6 Hard link.



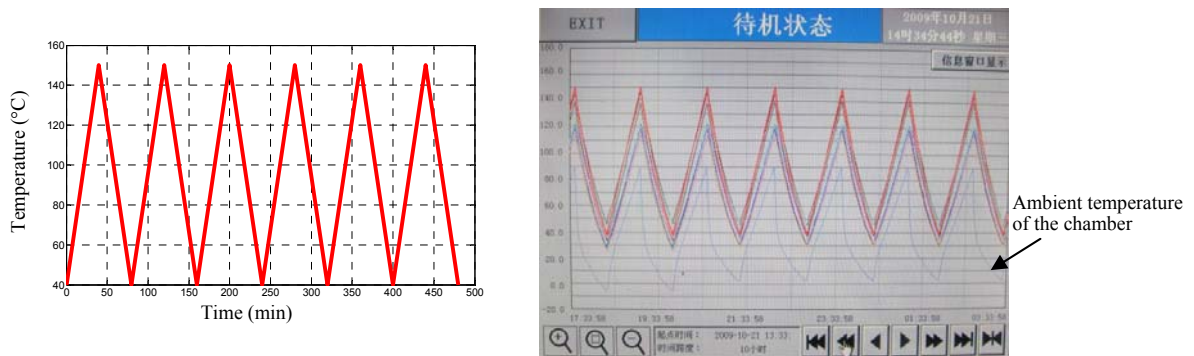
Fig.7 Soft link.



Fig.8 Special clamp and binding.

### 3.3.2 Temperature curve

In thermal cycle testing, insulation quality is evaluated based on changing temperature, and the changing process will directly affect the diagnosis result. Therefore, it's very important to increase and reduce the temperature uniformly and in the specified time.



**Fig.9 Ideal temperature curve and actual operation curve.**

One of the features of this set of equipment is that it can increase and reduce temperature uniformly. After setting the time of increasing and reducing temperature, the system can automatically calculate the rate of temperature rise and drop and thus generate an ideal temperature curve. In the heating stage, copper conductor resistance keep changing with temperature rise, which is under real-time comparison with ideal temperature curve, and the output of magnetic voltage regulator is accordingly adjusted by the control system, thus uniform temperature rise can be ensured. On the other hand, in the cooling stage, based on the different refrigerating amount and air velocity required by different temperature, the control system adjusts the frequency of the converter (controlling the motor and the fan) and operating condition of the refrigerating compressor according to real-time comparison with the ideal temperature cure, thus uniform temperature drop can be ensured (Fig.9).

## 4 DIAGNOSIS PROCEDURE

In order to examine the fatigue crack and delamination of the testing bars during and after thermal cycle testing, tap testing, dielectric dissipation factor ( $\tan\delta$ ) measurement and partial discharge measurement are performed on the specimens after 0, 50, 100, 250 and 500 cycle, respectively. Moreover, to further observe the deterioration of the insulation, three specimens are selected randomly and destructive voltage endurance testing at 120°C is performed on them according to IEEE 1043-1996.

### 4.1 Tap testing

Knocking on the ground-wall insulation surface with solid hammer does not show evidence of large void. Tap testing gives good result.

### 4.2 Dissipation factor ( $\tan\delta$ ) and partial discharge measurement

Dissipation factor and its increment as well as partial discharge magnitude ( $Q_{\max}$ ) are measured at normal state, and their relationship with the number of thermal cycle is shown in Fig.10.

### 4.3 Voltage endurance testing at 120°C

Voltage endurance testing equipment consists of test transformer units, heating mould, and temperature control unit (Fig.11). It's double contact regulation manner to reduce wave distortion of the output voltage and to improve the accuracy of test results. Advanced compensating voltage stabilizer is used to eliminate the influence of power swing to the testing by adjusting input voltage. Both test transformer and voltage regulator adapt oil-cooled manner to ensure their long term operation under rated capacity and rated voltage.

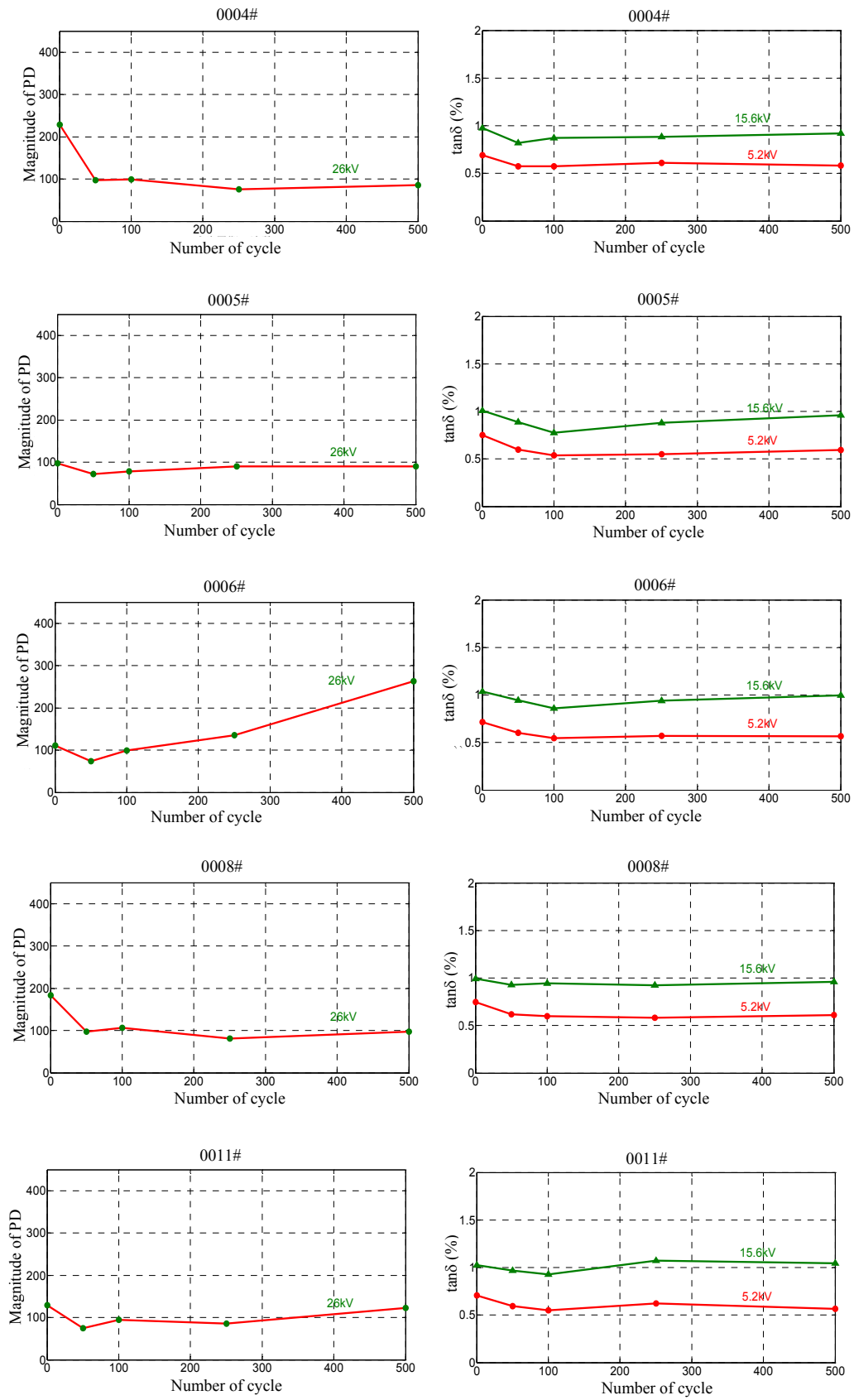


**Fig.10** Variation of PD ( $Q_{max}$ ) and  $\tan \delta$  of the specimens with the number of thermal cycle



**Fig.11 Arrangement of voltage endurance testing**

High-intensity aluminum material is selected to make heating mould. Advanced control manner of the temperature control system is realized by a circuit of mechanical overheat alarm and a circuit of PID. Testing results are shown in Table I.

**Table I: Results of voltage endurance testing of specimens for large hydrogenerator stator bars after thermal cycle**

Bar number	Electric stress	Duration (h)
0005	8.47kV/mm	1623.5 (breakdown)
0006		>1959.5
0008		>1959.5

## 5 CONCLUSION

The thermal cycle testing equipment has advanced functions, can fully meet the requirement of IEEE1310-1996. The testing method is scientific and reasonable. The ability of insulation to withstand load change can be truly verified.

Diagnosis procedure shows that the performance of air-cooled hydrogenerator stator bars change little after thermal cycle, no evident deterioration is observed.

## BIBLIOGRAPHY

- [1] IEEE Std 1310-1996 IEEE Trial Use Recommended Practice for Thermal Cycle Testing of Form-Wound Stator Bars and Coils for Large Generators.
- [2] IEEE Std 1043-1996 IEEE Recommended Practice for Voltage-Endurance Testing of Form-Wound Bars and Coils.
- [3] Sumereder C, Weiers T. Significance of Defects Inside In-Service Aged Winding Insulations// IEEE Trans. On Energy Conversion, 2008,23(1):9-14

**Key Points of On-site Operation and Interpretation of Off-line  
Partial Discharge Test on Generator Stator Windings**

**Mei Zhigang, Bai Kai, Wang Jinsong, Wu Yuhui, Bai Yamin**  
**North China Electric Power Research Institute Co. Ltd., Beijing**  
**China**

**SUMMARY**

Partial Discharge (PD) testing is employed to detect deterioration in generator stator windings. Key Points of the on-site operation and interpretation, which are often neglected, enable a practical test that could be done by non-specialists. Off-line PD test requires an external PD free power supply, which energizes the stator to a desired voltage, and the detection system measures partial discharge signals through one or more PD sensors and detection impedances. Some technical advisers intend the test to be done just after the generator is shut down and still hot. This is a wrong way; off-line PD test should be performed after the stator being cleaned. Due to the winding characteristic and the measurement bandwidth of coupling unit, the PD magnitudes from the measured results by different detectors are completely different. The method being applied should have a good anti-interference performance. The general method of Off-line PD test Interpretation is comparison analysis. Data under comparison should be gained by an identical method. Through the analysis of the PD pulse repetition rate and the polarity domination of PD magnitude we can approximately determine how widespread the PD is and the location of the deterioration within the stator groundwall.

**KEYWORDS**

Generator, Stator windings, Ageing, Diagnosis, Partial discharge

## **1 INTRODUCTION**

Partial Discharge (PD) testing has been used to measure the quality of generator stator windings insulation. The goal of on-site off-line PD measurement is to detect if insulation deterioration has occurred. Now, a practical off-line PD test is often carried out by average testers who are not specialists majoring in PD. Although PD test circuits and procedures have been clearly given in IEC 60034-27, there are still some wrong ideas and misunderstandings. Some technical advisers in electric utilities and industry insist that the test be done shortly after generator is shut down when it is still hot. A few testers even believe that A PD magnitude value from one kind of detector approximates that from another kind of detector. Almost all average testers expect absolute PD measurement criteria to be set in order to simplify the analysis of PD results.

The reasons why those points are wrong are presented in this article through analysis of some on-site measurement data. Some key points of on-site operation and interpretation of off-line PD test is emphasized after a brief discussion of test procedures.

## **2 ON-SITE PD TEST PROCEDURES**

On-site off-line PD test is always done on a complete stator winding. The measuring method is shown in figure 1. Each of the three windings is tested separately with the other two windings shorted to ground.

Generally, only one coupling unit is used to detect PD signals from line terminals, which is connected to point C in figure 1. A coupling unit is made up of a PD sensor (coupling capacitor) and detection impedance, which blocks the power frequency voltage and conducts the high frequency voltage pulse that accompanies PD. Sometimes an additional coupling unit is used to detect PD signals from neutral point terminals, which is connected to point A.

During an on-site PD test, a PD free AC power frequency supply is often connected between the star point side of the winding and the ground, while the unique coupling unit is connected to the high voltage phase terminals, in order to utilize the advantage of damping effect of the winding to suppress conducted interference from the power supply. The reason why we should connect the coupling unit to line terminal is that line end bars are exposed to full rated voltage during on-line operation and PD in those parts is generally more severely. The coupling unit should be installed as close to the terminals as possible in order to get a higher sensitivity.

A new technology has been developed to reduce the noise from power supply, which uses an additional coupling unit connected to point B in fig.1, that is, two coupling units are used to detect PD signals from line terminals. This method separates PD from power supply on the bases of pulse characteristic and time-of-arrival [1]. Test in this connection can reliably account for power supply noise and ensure there is no impact on PD measurements.

The power supply is adjustable over the desired voltage range of the test. After a conditioning period for about 5 min at the maximum test voltage, the test voltage are set at a starting voltage of 3 kV Vrms, and increased on 3 kV steps up to the phase-to-ground voltage of the winding. The number, magnitude and AC phase position of the PD pulses are recorded at various levels during test voltage increase and decrease.

## **3 DO THE TEST AFTER CLEANING**

Some technical advisers in electric utilities and industry insist that the test be done shortly after generator is shut down when it is still hot. The given reason is that the hot standstill condition is analogous to its normal on-line condition. In fact, if identical detectors and measurement systems are used, there are still many differences between on-line and off-line test. A characteristic comparison is listed in Table I [II].

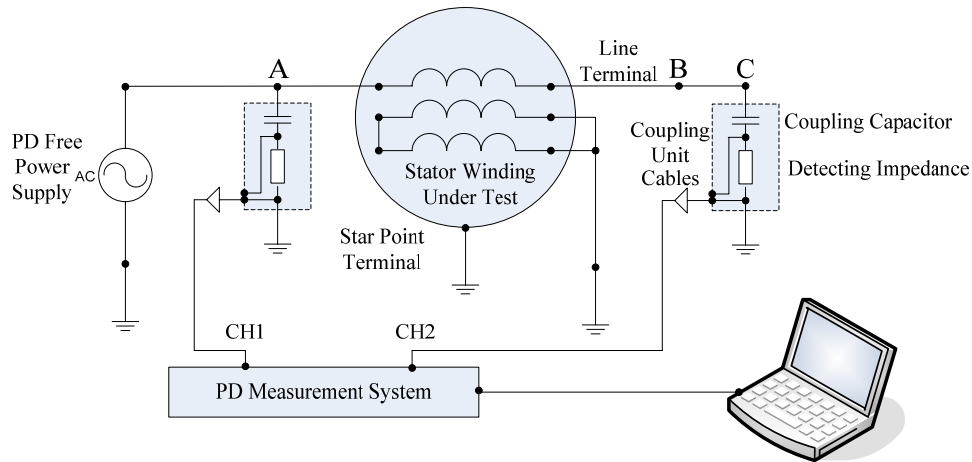


**Fig.1 On-site PD test setup on a complete stator winding**

**Table I A comparison of on-line and off-line PD testing**

On-line PD testing	Off-line PD testing
Normal electrical, mechanical, thermal and electromagnetic stresses on generators are present under test. The inception voltage in high pressure hydrogen is much higher than that in atmosphere.	Electrical stress is present only and hence off-line PD testing is not sensitive to slot discharge/loose winding due to no electromagnetic forces.
Heavy noise environment. The noise cannot be eliminated.	Most of noise sources can be eliminated, since the generator is at the standstill and isolated from other electrical equipment.
Only line end bars are exposed to full rated voltage.	Voltage is applied to entire stator winding.

From table 1, we can see that it is a wrong way to do off-line PD test at hot standstill state only because we need an analogy. And there are more important reasons.

Under a hot standstill condition, the winding has not been cleaned yet. So conductive contamination (Carbon, oily dust, abrasion, etc.) does exist. It causes surface discharge and corona. Though the surface PD maybe ten or hundred times higher than internal PD or PD from delamination, it does not indicate ageing phenomena that lead to premature insulation failure. Whereas, the presence of delamination processes, independent of measured PD amplitudes, indicate rapid degradation that needs to be repaired promptly. That is to say, the risk associated with surface discharge is low, and most of PD sources of these two kinds can be eliminated by cleaning the winding, which will make the test results more interpretable.

A comparison of test results before and after cleaning the winding is shown in figure 2. It indicate that the value of PD magnitude after cleaning is a lot smaller than that before cleaning, which will lead to a more reasonable conclusion.

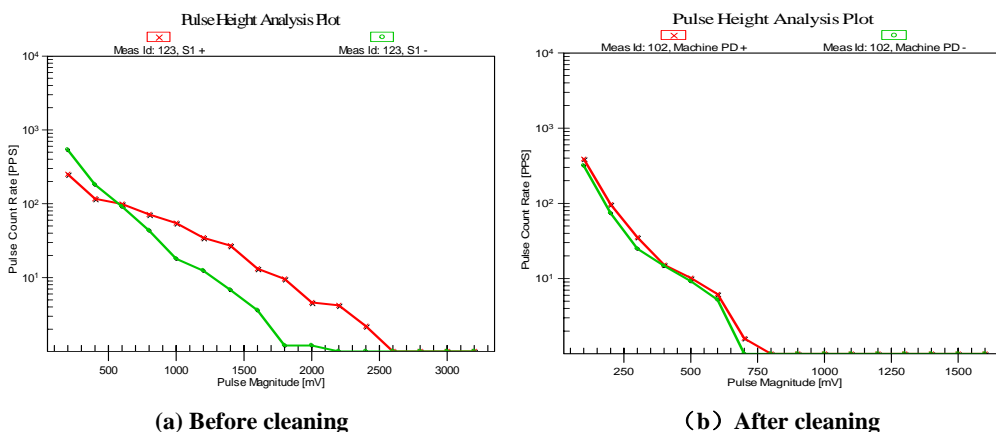


**Fig.2 A comparison of test results before and after cleaning the winding**

### 3 INFLUENCES OF WINDING CHARACTERISTICS AND COUPLING UNITS ON PD MAGNITUDES

When we perform a on-site off-line PD test on a certain generator stator winding, we use a certain detector with a coupling unit. As a PD event occur, a certain amount of charge is injected into the measurement circuit in a few nanoseconds. It will generate a current pulse.

The current pulse excites a wide range of resonant frequencies because the stator winding is modelled as a LC ladder network. Since most PD detectors (coupling units) work in a rather limited frequency range, the detected PD magnitude depends on whether the resonant frequencies are contained in the measurement bandwidth. If they are, the detector indicates large PD activity; If they are not, the detector detects little PD.

When PD pulses travel through stator winding, they are attenuated and modified in frequency content by the LC ladder network. And higher frequencies are attenuated more. So a measurement in the lower frequency range will detect more energy of the PD signals, which will ensures good sensitivity not only for PD in bars/coils close to the coupling unit, but also for those that originate from further away in the winding; While a measurement in the very high frequency range may acquire a very small proportion of the total PD energy, which results in sensitivity to signals originating only very close to the coupling unit [3]. However, the latter has a better anti-interference performance than the former.

Influence of winding characteristics and coupling units determine that different detectors give completely different results (table II and fig.2), which sets up an obstacle to the interpretation of PD test.

**Table II Detected PD magnitudes on the same 300MW generator stator winding with 3 different detectors**

Detector	Number of Coupling Unit	Capacitance of Coupling Sensor	Bandwidth	PD Magnitude
A	1	1000 pF	40k~300kHz	1087pC
B	1	80 pF	50k~5 MHz	$Q_{m+}$ : 6735mV, $Q_{m-}$ : 2080mV
C	2	80 pF	40~350MHz	$Q_{m+}$ : 418mV, $Q_{m-}$ : 250mV

Notes:  $Q_{m+}$  is the peak magnitude of PD that occurs in the negative half of the AC cycle, while  $Q_{m-}$  is the peak magnitude of PD that occurs in the positive half of the AC cycle.

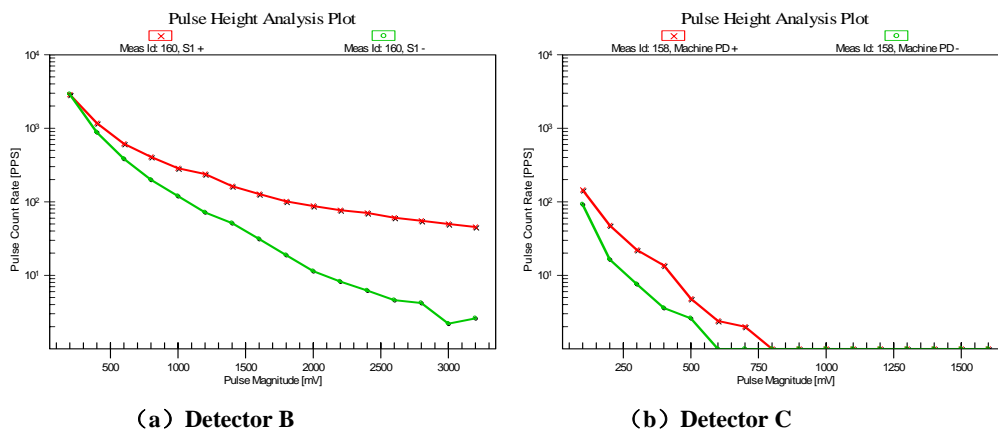


**Fig.2 A comparison of test results with two different detectors**

### 4 INTERPRETATION OF OFF-LINE PD TEST--- A COMPARATIVE PROCESS

Among several results given by PD tests, the peak PD magnitude  $Q_m$ , i.e., the magnitude of the highest PD pulse is the key measure. As discussed in previous section, the detected  $Q_m$  is influenced by capacitance of the winding and the inductance between the PD site and the PD detector. Besides, it is still affected by the size of defect [4]. So the detected  $Q_m$  depends approximately on these three

factors. On the one hand, these plus other effects make it difficult to define an absolute PD magnitude that indicated that winding has seriously deteriorated [5]. On the other hand, it enables comparisons among tests using an identical method. Thus off-line PD test is a comparison test, and interpretation of PD results from generator stator windings is essentially a comparative process.

One can determine which phase has the highest  $Q_m$  and, thus, which phase has the greatest deterioration. One can also compare several similar machines to see which has the highest PD. Finally, one can compare the PD from the same generator stator over time, i.e., trend the data. If the PD increases dramatically, then the stator winding insulation is aging rapidly. During these comparative processes, identical instrument and test setup should be applied.

Furthermore, from the comparison of positive and negative PD pulses, to see which one is predominant, the PD test can sometimes give approximate location of deterioration within groundwall [4]. As shown in figure 1 and 2, if the positive PD pulses (which, by definition, occur in approximately the negative half of the AC cycle) are larger than negative PD pulses, then it is likely that the PD originate most from the surface of the coil. If the negative PD is predominant, the PD is most likely occurring at the surface of the copper. If there is no polarity predominance, then PD is likely to arise within the groundwall.

PD pulse repetition rate (PD pulse count rate) is another important parameter. It enables testers to measure how widespread the PD is [4]. It is said that as many as 10,000 PD pulses may be generated per second in a stator winding. It seems that a single defect only produces at most one or two PD pulses per half AC cycle. So, if only a few hundred PD pulses are occurring per second, there only a few PD sites in the winding and the aging process is limited to small parts. If there are 10,000 PD pulses per second, then there are thousands of PD sites and the deterioration is widespread.

## 5 CONCLUSION

(1) Off-line PD test should be done after the winding being cleaned. For a PD test on generator stator winding, Analogy between hot standstill state and normal operation state is incorrect.

(2) The influence of winding characteristic and coupling units determine that different detectors give completely different results. Methods which have better anti-interference performance should be applied during an off-line PD test.

(3) The interpretation of PD results is essentially a comparative process. The comparison can be done between phases, or among similar machines. PD activity within a given winding can be trended over time. Through the analysis of the PD pulse repetition rate and the polarity domination of PD magnitude we can approximately determine how widespread the PD is and the location of the deterioration within the stator groundwall.

## BIBLIOGRAPHY

- [1] Campbell S R , et al. Practical on-line partial discharge tests for turbine generators and motors.IEEE Transactions on Energy Conversion, June 1994, 9 : 281 – 287
- [2] Zhu H, Green V, Huynh D. Application of on-line versus off-line PD testing for stator insulation monitoring//Electrical Insulation Conference and Electrical Manufacturing & Coil Winding Conference, 1999 :175-178
- [3] IEC TS 60034-27-2006.Off-line partial discharge measurements on the stator winding insulation of rotating electrical machines
- [4] Stone G C, Boulter E A, Culbert I, Dhirani H. Electrical Insulation for Rotating Machines - Design, Evaluation, Aging, Testing and Repair:John Wiley and Sons, Inc., 2004
- [5] Stone G C.Partial discharge. XXV. Calibration of PD measurements for motor and generator windings-why it can't be done.Electrical Insulation Magazine, IEEE, Jan 1998 ,14 : 9 – 12

**Environment Simulation Test on Stator Coil for 1000MW Hydro-Generator**

**Fu Qiang, Man Yuguang, Lu Chunlian, He Xin**  
**State Key Laboratory of Hydropower Equipment;**  
**National Engineering Research Center Hydropower Equipment;**  
**Harbin Research Institute of Large Electrical Machinery**  
**Harbin, China**

**SUMMARY**

The purpose of this paper was to introduce a new way to assess the stator coil insulation property of 1000MW hydro-generator through environment simulation test, which included four factors, such as the humidity, oil filth, powder and thermal aging. The dust and grease contamination was coated on the surface of the stator coils, and then these coils were in store in the humid and thermal environment for 14 days. The stator coils could pass the property test after 14 days; these stator coils would be given access to next cycle of 14 days. There were three cycles in the environment simulation test. The property test included insulation resistance, dielectric losses, party discharge and withstand voltage test. The test results showed that 1000MW hydro-generator stator coils had favourable property after three cycles in the environment simulation test.

**KEYWORDS**

1000MW hydro-generator, Stator coil, Insulation property, Environment simulation test.

## 1 INTRODUCTION

When 1000MW hydro-generator operates long-time, it is unknown that how the environment factors such as dust, grease contamination, humidity, have an influence on the insulation property of stator winding. So far, there are no test methods and judgment standards on three factors of dust, grease contamination and humidity influencing the performances of the stator winding. Thus, this paper involved the three environmental factors influence using the environment simulation test. The partial discharge and dielectric loss of the stator windings were measured in each cycle of the experimental process. If the partial discharge (PD) and the dielectric loss have no obvious changes, the stator winding insulation could be little affected by the operation environment of hydro-generator. And the insulation can satisfy the request of the large hydro-generator long-term safety operation. The class F Tong Ma epoxy powder mica insulation (FTMI) system adopted by HEC is of the safe and reliable operation experience in the high-voltage generator winding, but the 24kV, 26kV million kilowatt hydro-generators have not such operation experience; especially for the winding environmental resistance has no definite conclusion in published papers. Therefore, this paper involved the environment simulation tests of the million kilowatts hydro-generator windings.

## 2 EXPERIMENTS

### 2.1 Device of simulation stator slots

Simulation stator slot was laminated with silicon steel sheets, with the same length as the actual generator. The slot size (as shown in Table I) and the distance between the end windings were designed according to rated voltage 24kV, 26kV respectively. Simulation stator slots was equipped with heating device, which could increase the temperature of stator windings to  $120^{\circ}\text{C}\pm 5^{\circ}\text{C}$  (temperature-control reference point was the highest temperature point of the stator windings). PT100 temperature detectors were put into the space between the top and bottom of stator windings in each slot (from the eighth to the third slot as shown in Fig. 1). Temperature and time could be controlled and noted automatically. Simulation stator slot was also equipped with humidifying device, which could increase the relative humidity to more than 90% at room temperature (control reference point was at bottom of test box).

The 24kV, 26kV actual stator coils of HEC 1000WM hydro-generators were 6 top coils and 6 bottom coils respectively (as shown in Fig. 1). The slot parts of these coils lapped over in the slots, and the high, low anti-corona layers were also overlapped. No less than 5 coils were overlapped in the high anti-corona area. 12 stator coils were connected in series by copper bus bar in which contact surfaces needed to be grinded by the sand paper and be coated with conductive putty. Then the coils were connected to transformer which was used to do large electrical current test. The direct current from the transformer was used to heat up the stator windings. The measure temperature device was to monitor every measure temperature points (as shown in Fig. 2).

### 2.2 Environment simulation test chamber

Two group stator windings (one group of 12 coils) could be tested at the same time in the test chamber which size was  $6\text{m} \times 2\text{m} \times 6.3\text{m}$ . The chamber was equipped with the large electrical current heating device, air blast and exhaust equipment. The stator windings' temperature could reach  $120^{\circ}\text{C}\pm 5^{\circ}\text{C}$  in the chamber. The temperature control and measure was subjected to the temperature of the space between the top and bottom of stator windings in each slot. The humidity was not less than 90% in the chamber so that the humidity aging test could carry out at the room temperature. The test chamber could connect high voltage test circuitry and measure circuitry. The high voltage test circuitry was not influenced by grease contamination.

### 2.3 Environment simulation test

The properties of the test coils should be measured such as the appearance, insulation resistance, dielectric loss and partial discharge before embedding them into the simulation stator slots. And should they be measured, after the test coils were embedded and the end winding surface insulations were cured. Then the coils carried out  $2U_N+1\text{kV}$ , 1min withstand voltage. Observed whether the coils had corona at  $1.05U_N$  test voltage or not. ( $U_N$  was the stator winding rated voltage, the same below).

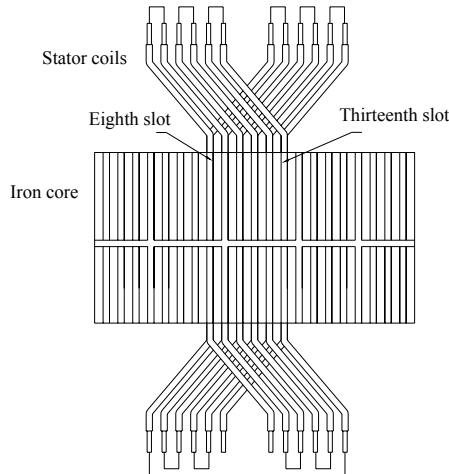


**Fig.1 Sketch Map of the End Windings Connecting in the Simulation Iron Core.**



**Fig. 2 Measuring Temperature Device.**

The simulation stator windings' temperature could be heated up to  $120^{\circ}\text{C}\pm 5^{\circ}\text{C}$  and kept 14 days in the heating aging. Then the temperature was dropped to the room temperature. At the same time, the relative humidity of the test chamber was regulated more than 90% to carry out the humidity test, in which the test time was kept for 14 days. The humidity of test chamber should keep in the stated scope in the whole test cycle. One cycle of the heating aging and humidity was 28 days, and three continuous cycle tests should be carried out in the environment simulation test. The stator winding insulation resistance was measured with 5000V megohm meter before and after every test cycle.

**Table I The Simulation Iron Core Slot Sizes for 1000MW Hydro-Generator Test Stator Coils.**

Slot marks		8th	9th	10th	11th	12th	13th
Top sizes (mm)	Width	26.3	26.2	26.4	26.4	26.2	26.2
	Depth	255.7	255.5	255.7	255.6	255.4	255.4
Middle sizes (mm)	Width	26.2	26.3	26.2	26.3	26.3	26.4
	Depth	255.5	255.3	255.2	255.3	255.4	255.3
Bottom sizes (mm)	Width	26.36	26.38	26.38	26.40	26.31	26.18
	Depth	255.2	255.3	255.3	255.1	255.1	255.4

Note: stator lamination size:  $26.4\text{mm} (+0/-0.4\text{mm})\times 255.46\text{mm} (+0/-0.4\text{mm})$ .

The dielectric loss and partial discharge were also measured before and after every test cycle. The simulation stator windings should be dried out after the last humidity test. The dryness process was that stator windings were heated up to  $60^{\circ}\text{C}\sim 70^{\circ}\text{C}$  for 48h and then dropped to room temperature to measure their insulation resistance, dielectric loss and partial discharge. The test voltage of insulation resistance was 5000V, the maximum test voltage of the dielectric loss was  $1.0U_N$ , the maximum test voltage of partial discharge was  $1.2U_N/\sqrt{3}$ . The 1 min withstand voltage test was measured after

finishing three cycle tests. The withstand voltage test was measured as following order:  $1.3U_{\phi}$  ( $U_{\phi}$  为 stator windings rated phase voltage ),  $0.5U_N$  ,  $1.5U_N$  ,  $2.0U_N$  . Observing and noting the test situation of the stator winding corona and discharge.

### 3 RESULTS AND DISCUSSIONS

#### 3.1 Dust and grease contamination

The surface and volume resistance of bearing lubricating oil, dust and grease contamination on the surface of coils and confected cement and grease contamination were measured by three electrode system and the insulation support board. The test results were shown in Table II and Table III.

In Table II, the insulation support board as the test baseplate was epoxy laminated sheet. The lubricating oil was pure bearing lubricating oil. Three Gorge sample and Ge Zhouba sample were the dust and grease contamination collected from the stator coils. The cement and grease contamination sample was the mixture with Qin Ling P.C 32.5 composite silicate cement and bearing lubricating oil. Two components mass ratio was 1:1 in the mixture. The composite silicate cement was sifted from 400grit and the particle size was less than  $38\mu\text{m}$ .

**Table II Surface Resistivity of Dust and Grease Contamination. unit:  $\Omega$**

Lubricating oil	Three gorge sample	Ge Zhouba sample	Cement and grease contamination sample
$7.5\pm 0.71\times 10^{13}$	$9.51\pm 12.75\times 10^{12}$	$1.70\pm 1.09\times 10^{11}$	$9.76\pm 11.82\times 10^{12}$

In Table III, the lubricating oil was pure bearing lubricating oil. Three Gorge sample and Ge Zhouba sample, whose dust and grease contamination were collected from the stator coils, were calcined at  $450\text{ }^{\circ}\text{C}$  to burn off the grease. The cement sample was Qin Ling P.C 32.5 composite silicate cement, which had been sifted from 400grit and the particle size was less than  $38\mu\text{m}$ .

**Table III: Volume Resistivity of the Dust and Grease Contamination. Unit:  $\Omega\cdot\text{m}$ .**

Lubricating oil	Three Gorge sample	Ge Zhouba sample	Cement sample
$1.91\pm 2.01\times 10^{12}$	$9.71\pm 5.67\times 10^5$	$2.11\pm 0.77\times 10^5$	$4.38\pm 0.43\times 10^6$

The test results showed that the dust and grease contamination collected from the stator coils had large surface resistivity, it was belonged to semiconductivity medium; the surface resistivity of the cement sample were similar to that of the dust and grease contamination collected from the stator coils, so the cement sample could be served as the dust sample in the environment simulation test.

#### 3.2 Insulation resistance

When the stator coils were embedded into the slots, the end windings were painted with cold curing adhesive, and then painted with high resistance anti-corona lacquer and red enamel paint, which should be heated up 24h at  $90^{\circ}\text{C}$ . The insulation resistance was measured to calculate absorptance and polarization index (as shown in Table IV). After the withstand voltage test, the confected dust and grease contamination was sprayed on to the surface of the end windings and the iron core (as shown in Fig. 3).

9.3.18 section of the national standard GB/T 8564-2003 ‘‘Specification installation of hydraulic turbine generator units’’ requests that when temperature is below  $40\text{ }^{\circ}\text{C}$ , the insulation resistance absorptance R60s/R15s of epoxy powder mica insulation is no less than 1.6, or the polarization index R600s/R60s is no less than 2.0.

The insulation resistance of the stator windings was relative to the measure temperature. Therefore, in order to compare and analyze the change of the stator windings insulation resistance in different circumstances of the environment simulation test, the resistance  $R_t$  at  $t\text{ }^{\circ}\text{C}$  measured at different temperatures needed to be dealt with the normalization approach, by which the resistance was converted into equivalent value R100 at  $100\text{ }^{\circ}\text{C}$ . The normalization results could reduce temperature to affect the measure resistance.

The insulation resistance  $R_t$  could be converted into equivalent value R100 by using the formula (1).

$$R_{100} = R_t \cdot 1.6^{(100-t)/10} \quad (1)$$

$$\text{Absorptance} = R_{60}/R_{15} \quad (2)$$

$$\text{Polarization index} = R_{600}/R_{60} \quad (3)$$

In the formula (2), (3), R15, R60 and R600 are the insulation resistances at 15s, 60s and 600s respectively.



**Fig. 3 The Stator Windings Before (a) and After (b) Spraying the Dust and Grease Contamination.**

**Table IV The Insulation Resistance and Absorptance of the Stator Windings.**

Tests and dates	Temperature °C	Insulation resistance (GΩ)			Absorptance	
		15 s	60 s	600 s	standards	results
Before spraying*, 09-08-11	28.0	10.4	29.8	98.0	≥1.6	2.87
After spraying**, 09-08-18	24.5	12.1	32.6	114	≥1.6	2.69
After 1st test cycle, 09-10-08	21.0	6.95	17.8	81.0	≥1.6	2.56
After 2nd test cycle, 09-11-13	13.5	5.15	16.1	116.0	≥1.6	3.13
After 3rd test cycle, 09-11-18	12.0	5.05	16.5	117.0	≥1.6	3.27

Note: \*before spraying the dust and grease contamination; \*\*after spraying the dust and grease contamination.

**Table V The Insulation Resistance and Polarization Index of the Stator Windings.**

Tests and dates	Temperature °C	Insulation resistance (GΩ)			Polarization index	
		15 s	60 s	600 s	standards	results
Before spraying, 09-08-11	28.0	10.4	29.8	98.0	≥2.0	3.29
After spraying, 09-08-18	24.5	12.1	32.6	114	≥2.0	3.49
After 1st test cycle, 09-10-08	21.0	6.95	17.8	81.0	≥2.0	4.55
After 2nd test cycle, 09-11-13	13.5	5.15	16.1	116.0	≥2.0	7.20
After 3rd test cycle, 09-11-18	12.0	5.05	16.5	117.0	≥2.0	7.09

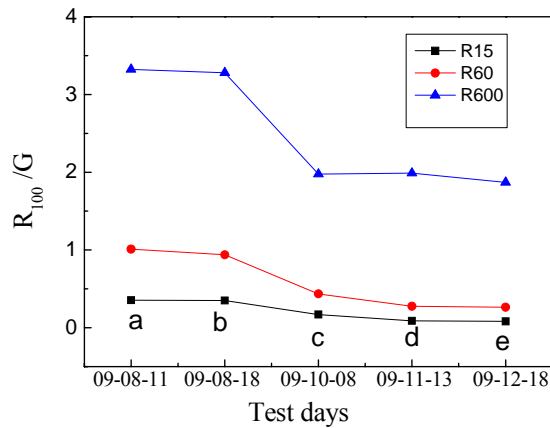


**Fig. 4 The 100 °C Insulation Resistance Measured at Different Times.**

The Table IV and V showed that the stator winding absorptances were more than 1.6 and the polarization indexes were more than 2.0. The absorptances and polarization indexed had the increscent

trend as prolonging the test time. The insulation resistance had little changes before and after spraying the dust and grease contamination (as shown in Fig.4). But after the first cycle test, the resistance dropped about 50%, which illuminated the dust and grease contamination to affect the resistance of the stator winding insulating. The resistance had little changes during the three test cycles, which showed the humidity and heat affected little the resistance.

### 3.3 Dielectric loss

This is one of the most efficient tests in order to establish the quality of an insulation system. A good insulation system should have a  $\tan\delta$ -U curve as linear as possible, where U represents the values of applied voltage. Fig.5 indicated the  $\tan\delta$  represent the values for all coils at different applied voltages. During the test voltage scopes, the  $\tan\delta$  of the 24kV and 26kV stator coils increased with the applied voltage increasing. And their relative was about linearity. Fig. 5 showed that the HEC insulation systems present very little dielectric loss factor and very flat characteristics [1]. Fig.6 indicated the values of  $\Delta\tan\delta$ , calculated for all of coils.  $\Delta\tan\delta$  is given by:

$$\square \tan \delta = \tan 1.0 U_N - \tan 0.2 U_N \quad (4)$$

Where:  $\tan\delta 0.2U_N$ ,  $\tan\delta 1.0U_N$  represented the average values of  $\tan\delta$  at a applied voltage of  $0.2 U_N$  and  $1.0 U_N$  respectively. After the first cycle test, the  $\Delta\tan\delta$  of the 24kV and 26kV stator coils had little obvious change [2].

The China electric power standard DL/T 492-92 ‘‘Epoxy Powder Mica Insulation Aging Identification Criterion of Generator Stator Winding’’ prescribes that the value of  $\tan\delta 1.0U_N$  should be lower than 0.07 and the value of  $\Delta\tan\delta$  should be lower than 0.06. Table VI indicated the test results  $\tan\delta 1.0U_N$  and  $\Delta\tan\delta$  conformed to DL/T 492-92 standard. All of the  $\Delta\tan\delta$  were almost less than 0.01. Fig. 6 indicated a good insulation system corresponds to values  $\Delta\tan\delta$  lower than 0.06, limited by the electric power norm DL/T 492.

Table VI The  $\tan\delta$  and  $\Delta\tan\delta$  of the 24kV and 26kV Stator Coils.

$U_N$	Tests and dates	$0.2 U_N$	$0.4 U_N$	$0.6 U_N$	$0.8 U_N$	$1.0 U_N$	$\Delta\tan\delta$
24kV	Before spraying, 09-08-11	0.0068	0.0089	0.0115	0.0136	0.0154	0.0086
	After spraying , 09-08-18	0.0071	0.0088	0.0113	0.0132	0.0148	0.0077
	After 1st test cycle, 09-10-08	0.0065	0.0089	0.0116	0.0141	0.0159	0.0094
	After 2nd test cycle, 09-11-13	0.0071	0.0096	0.0123	0.0147	0.0164	0.0093
	After 3rd test cycle, 09-11-18	0.0071	0.0095	0.0127	0.0146	0.0165	0.0094
26kV	Before spraying, 09-08-11	0.0070	0.0094	0.0119	0.0141	0.0162	0.0092
	After spraying, 09-08-18	0.0072	0.0092	0.0117	0.0136	0.0156	0.0084
	After 1st test cycle, 09-10-08	0.0065	0.0089	0.0122	0.0145	0.0165	0.0100
	After 2nd test cycle, 09-11-13	0.0073	0.0099	0.0130	0.0154	0.0174	0.0101
	After 3rd test cycle, 09-11-18	0.0073	0.0095	0.0131	0.0152	0.0172	0.0099

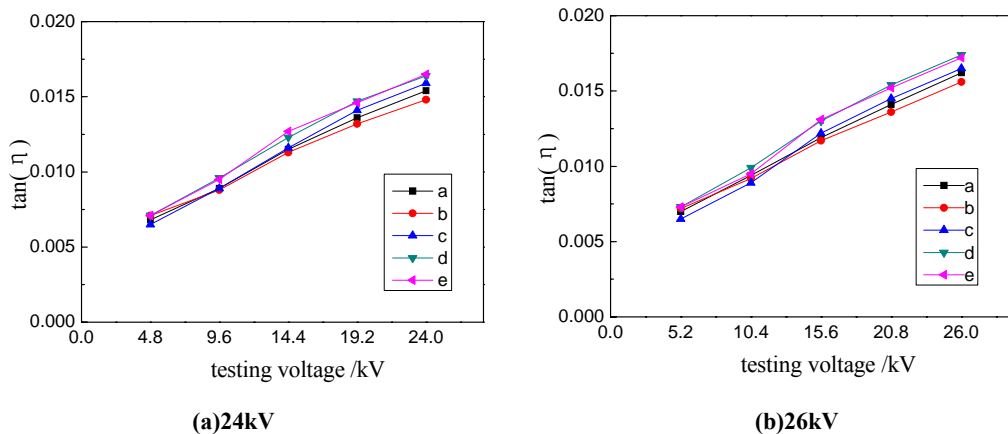
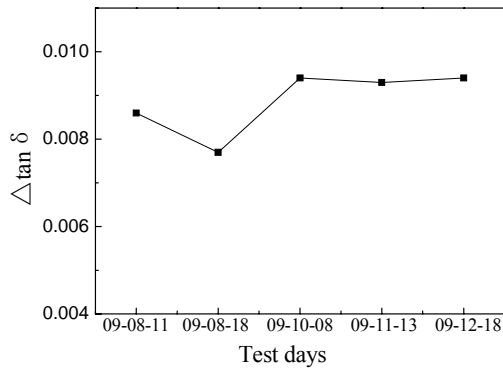
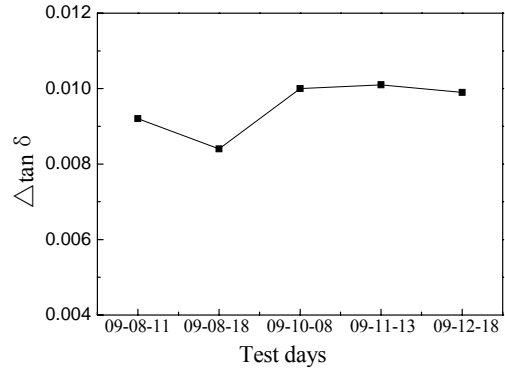


Fig. 5  $\tan\delta$  of the 24kV Stator Coils at Different Voltages. a: Before Spraying, 09-08-11; b : After Spraying, 09-08-18; c: After 1st Test Cycle, 09-10-08; d: After 2nd Test Cycle, 09-11-13; e: After 3rd Test Cycle,09-11-18.



(a) 24kV



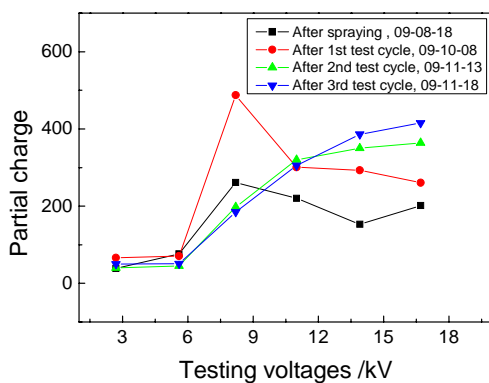
(b) 26kV

Fig. 6  $\Delta \tan \delta$  of the (a) 24kV, (b) 26kV Stator Coils at Different Test Times.

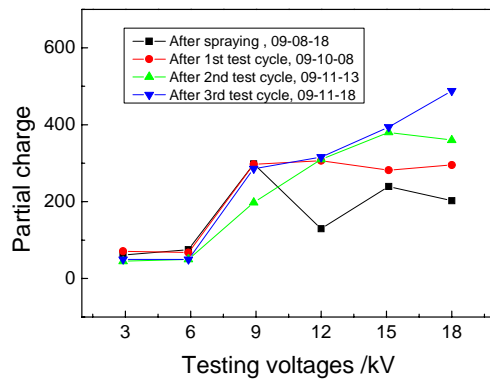
### 3.4 Partial discharge

The main insulation system is a critical component of a hydro-generator. Its degradation may cause the power units to fail while in service. The traditional test methods more accurately reflect the insulation condition, whereas a high-potential traditional test may cause insulation failure during the test period. For this reason, trending is recommended for the partial discharge testing. Partial discharges are recognized as the main cause of insulation deterioration process. Choosing a suitable partial discharge data evaluation method may provide a realistic statement about the hydro-generator insulation system [3]. The stator winding partial discharge had some increase above  $0.8U_{\phi}$  ( $U_{\phi} = U_N / \sqrt{3}$ .  $U_N=24\text{kV}$ ,  $0.8U_{\phi}=11\text{kV}$ ;  $U_N=26\text{kV}$ ,  $0.8U_{\phi}=12\text{kV}$ ), but the increment was not noticeable. The maximum partial discharge was less than  $10000\text{pC}$  at  $1.0U_{\phi}$  ( $U_N=24\text{kV}$ ,  $1.0U_{\phi}=13.9\text{kV}$ ;  $U_N=26\text{kV}$ ,  $1.0U_{\phi}=15\text{kV}$ ).

Fig. 7 indicated that a small increase in the partial discharge as adding test cycles when the test voltage was greater than  $0.8U_{\phi}$ . The results had an indication of loose coils and/or poor semi conductive coating, resulting in surface discharges between stator bar and grounded core iron. There may also not be delamination PD due to the small increase of PD [4].



(a)



(b)

Fig. 7 The Partial Discharge of the (a)24kV and (b)26kV Stator Coils.

The results of all insulation partial discharge tests were similar to the  $\tan \delta$  vs. voltage characteristic shown in Fig. 7, and this PD is similar to the favorable insulation performance characteristics verified experimentally with the large model coil [5].

### 3.5 High voltage test

After three cycles of environment simulation test, HEC 24kV voltage class stator windings were carried on the high voltage tests of  $1.3U_{\phi}$ ,  $1.05U_N$ ,  $1.5U_N$  and  $2U_N$  for 1 minute respectively. HEC

26kV stator windings also did such tests. No breakdown occurred during the tests (as shown in Table VII). Thus, the favorable insulation characteristics of the stator winding were verified [4].

**Table VII The Withstand Voltage Tests after the Third Cycle Test.**

Test conditions	$U_N=24\text{kV}$ $U_\phi=13.87\text{kV}$	Results	$U_N=26\text{kV}$ $U_\phi=15.02\text{kV}$	Results
$1.3U_\phi, 1\text{min}$	18.01kV	Pass	19.53kV	Pass
$1.05U_N, 1\text{min}$	25.20kV	Pass	27.3kV	Pass
$1.5 U_N, 1\text{min}$	36.00kV	Pass	39.0kV	Pass
$2.0U_N, 1\text{min}$	48.00kV	Pass	52.0kV	Pass

Note: test time: 2009/12/18~19 ; temperature: 13°C;humidity: 65%.

#### 4 CONCLUSIONS

HEC has carried out the environment simulation tests on the stator windings of 24kV and 26kV hydro-generators. The test results were analyzed and made some conclusions as follows:

- (1) The dielectric property of the stator coils had no notable changes before and after spraying the artificial dust and grease contamination in the environment simulation test.
- (2) During the three cycles tests, the 100°C equivalent insulation resistance decreased, while the absorptance and polarization index increased.
- (3) After the tests, dielectric loss  $\tan\delta$  increased little. The 24kV and 26kV stator windings  $\tan\delta$  increased by 7.1% and 6.2% than that measured before the tests. The 24kV and 26kV stator windings  $\Delta\tan\delta (= \tan\delta_{1.0U_N} - \tan\delta_{0.2U_N})$  increased by 13.9% and 7.6% than that measured before the tests.
- (4) After the tests, the stator windings partial discharges increased little. The 24kV coils maximum partial discharge measured at  $1.0U_\phi$  increased by 152.5% than that measured before the tests. The 26kV coils maximum partial discharge measured at  $1.0U_\phi$  increased by 177.1% than that measured before the tests.
- (5) After the tests, HEC carried out 24kV and 26kV withstand voltage tests. The 24kV and 26kV stator windings passed respectively the withstand voltage tests of  $1.3U_\phi$ ,  $1.05U_N$ ,  $1.5U_N$  and  $2U_N$ .
- (6) The test results showed that the dust and grease contamination, temperature and humidity could have effect on the properties of the stator winding insulation. But it needs to research further that the environment factors affect on the insulation aging of 24kV and 26kV hydro-generator stator windings.

**ACKNOWLEDGEMENTS:** We are grateful to Xi'an JiaoTong University and Dong Fang electric machinery company limited for their cooperation in the tests. And also thank our workmates for their carrying out the tests.

#### BIBLIOGRAPHY

- [1] Degeratu S, Ursache M, Bizdoaca N G, Rizescu S V. Performance Evaluation Of A Class F Electrical Insulation System For Three Phase Induction Motors. University politehnica of Bucharest Scientific bulletin Series C, 2010, 72(4) :219-230
- [2] Helgeson A, Gägvert U. Dielectric response during curing of a resin-rich insulation system for rotating machines//IEEE Conference on Electrical Insulation and Dielectric Phenomena, October 1999, 1:289-292
- [3] Naderi M S, Blackburn T R, Phung B T, Naderi M S, Nasiri A. Application of wavelet analysis to the determination of partial discharge location in multiple  $\alpha$  transformer windings. Electric Power Systems Research, 2008(78):202–208
- [4] Yeboah G. On-Line Partial Discharge Measurements on Turbine Generator Experience with KCPL Montrose Unit 2// Iris Rotating Machine Conference, New Orleans, June 2004:1-9
- [5] Niikura H, Inoue S, Yamazaki M. Global Vacuum Pressure Impregnation Insulation Applied to Hydrogen-cooled Generators. FUJI ELECTRIC REVIEW, 2009,55 (3): 93-99



Beijing, China

SC A1  
COLLOQUIUM ON NEW DEVELOPMENT OF ROTATING  
ELECTRICAL MACHINES

11~13 September, 2011

---

**Recent Technologies for Hydro Generators and Generator-Motors**

**Toru Kubo, Hideyuki Hachiya**  
**TOSHIBA CORPORATION**  
**Japan**

**Wu Jinshui**  
**TOSHIBA HYDRO POWER**  
**(HANGZHOU) CO., LTD.**  
**China**

**SUMMARY**

In the last ten years, more than 20,000MW new hydro electric power plants have been ordered per year in average around the world, and new construction has been remarkably progressed especially in China. Among them, many large power plants with the unit capacity of 200 MVA to 800 MVA are included. In the large capacity hydro generators, direct water cooling has been applied to stator and rotor winding in some cases. However at the view points in simple configuration and easy maintenance, air cooled type is preferable as far as applicable, and air cooled type is refocused in recent years. And in the low speed, large diameter generators, site welding structure may be adopted for the large sized components considering the transportation limit to the project site.

In China, not only large capacity power plants with vertical units, but also hydro power plants with horizontal bulb turbine generator have been constructed for low head project site. Recently large capacity bulb turbine generators with unit capacity of 30 to 45 MW have been commissioned. An application of new technologies for bearings and generator cooling will be expanded in bulb turbine generators.

In the pumped storage power plant, since the commissioning of the first adjustable speed pumped storage system in Japan in 1990, the adjustable speed system has been applied to several pumped storage power plants, especially in Japan and Europe. In the generator-motors for adjustable speed pumped storage, the rotor coil end support structures against the centrifugal force are one of the important technologies, and improvement is continued.

**KEYWORDS**

Synchronous generator, Bulb turbine generator, Generator-motor, Pumped storage, Adjustable speed

## 1 INTRODUCTION

Restraint of the climate change and environmental degradation has become a big issue on a global scale, and each country is focusing on reducing emissions of greenhouse gases. Under such circumstances, hydroelectric power has been re-evaluated as an environmental friendly electric power generation system, and the construction of hydro power plants are promoted in many countries, especially in China.

Also, the attention has been focused on pumped storage power plants. Pumped storage can supply electric power during times when demand for power is highest, and can store the energy during lower demand for power to balance power supply and demand in the power grid, and has been applied for many years. However, recently power grid stability is becoming one of major issues for utilities due to the increase of an intermittent renewable power, particularly wind power, and adjustable speed pumped storage as well as traditional pumped storage is becoming the focus of attention. The adjustable speed pumped storage can control the pump input by changing the rotating speed of the unit, and contribute to the stability of the power grid in more effectively.

Toshiba has been supplying hydro generators and generator-motors throughout the world for more than 100 years, and contributing to the expansion of hydroelectric power. This paper introduces recent technologies and technical trend of hydro generators and generator-motors including adjustable speed pumped storage system.

## 2 RECENT TECHNOLOGIES FOR HYDRO GENERATOR AND GENERATOR MOTOR

### 2.1 Large capacity synchronous generators

In the last ten years, more than 20,000MW new hydro electric power plants have been ordered per year in average around the world, and new construction has been remarkably progressed especially in China. Among them, many large power plants with the unit capacity of 200 MVA to 800 MVA are included. One of example is Guanyingyan hydro power plan in China, which consists of 5 units of 666.67 MVA hydro generators. The generator for this project is under designing stage and the commissioning of plant is scheduled in 2015. The sectional structure and the ratings of Guanyingyan generator are as shown on Fig.1 and Table I.

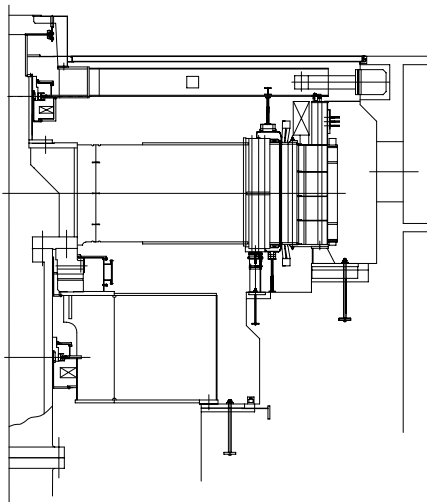


Fig. 1 Synchronous generator for Guanyingyan

Table I Ratings of Generator for Guanyingyan

Type	Semi-umbrella
Cooling method	Totally enclosed air cooling with water heat exchanger
Rated capacity	666.67MVA
Rotating speed	90.9r/min
Terminal voltage	20kV
Rated power factor	0.9

#### 2.1.1 Complete Air Cooling and 20kV Stator Winding

The Guanyingyan generator is of vertical shaft, semi-umbrella type synchronous generator, having large outer diameter stator core of approximately 17.2m, and total weight of generator of

approximately 2700 tons. The rated terminal voltage is 20kV and VPR (Vacuum pressurized resin rich mica tape) insulation system will be applied to stator bar. The cooling method of stator and rotor windings is air cooling. For large capacity generator, direct water cooling has been applied to stator and rotor winding in some cases. However at the view points in simple configuration and easy maintenance, air cooled type is preferable as far as applicable, and air cooled type is refocused in recent years. The complete air cooling technology for large capacity hydro generator have been realised in 805 MVA hydro generators for Guri II power plant in Venezuela in 1980s.

2.1.2 Site Welding Mechanical Construction

In the large diameter generators, the transportation limit to the project site need to be considered in designing and manufacturing the components. In Guanyingyan generator, site welding type structure will be applied to the large sized components such as stator frame, rotor spoke and bearing bracket considering the transportation limit and site installation. Fig.2 shows the rotor spoke consisting of individual center boss, outer elements, and sub ribs for keys which are assembled at site by welding.

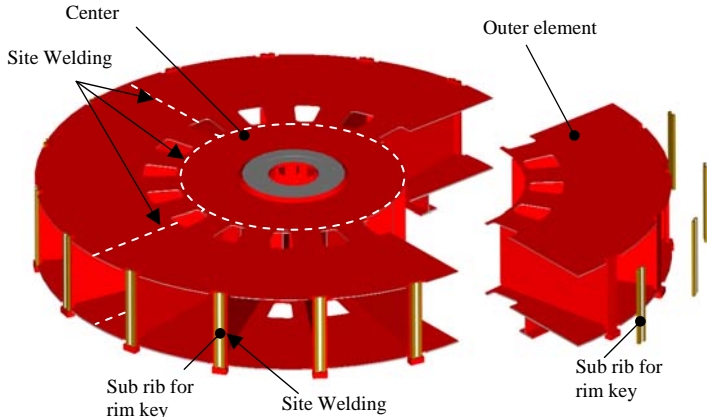


Fig. 2 Typical construction of site welding type rotor spoke

2.2 Bulb turbine generators

In China, not only large capacity power plants with vertical units, but also hydro power plants with horizontal bulb turbine generator have been constructed for low head project site, and recently large capacity bulb turbine generators with unit capacity of 30 to 45 MW have been commissioned. Fig.3 and Fig.4 shows the sectional structure and the generator rotor of the bulb turbine generator for Qingshuitang hydro power plant in China consisting of 4 units of 32MW unit with and rated speed of 62.5r/min. The ratings of this generator are shown on Table II . First unit of Qingshuitang has commissioned in September 2008.

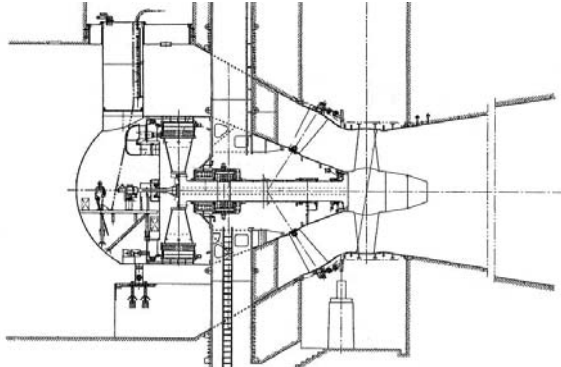


Fig. 3 Bulb turbine generator for Qingshuitang

Table II Ratings of generator for Qingshuitang

Type	Horizontal bulb turbine generator
Cooling method	Totally enclosed air cooling with water heat exchanger
Rated capacity	33.68MVA
Rotating speed	62.5r/min
Terminal voltage	10.5kV
Rated power factor	0.95



**Fig. 4 Generator Rotor for Qingshuitang**

### 2.2.1 Application of Non-metallic Guide Bearing for Horizontal Machine

The rotating parts of turbine and generator for Qingshuitang are supported by 2 guide bearings, and the maximum guide bearing load of 220 ton is very heavy load for horizontal hydro electric machine. The guide bearing of segmental type with non-metallic PTFE (Poly tetra fluoro ethylene) lined bearing pads are applied instead of conventional white metal journal bearing. The PTFE bearings have superior characteristics to white metal bearing in friction and abrasion under high bearing pressure. Further, high pressure oil system which is operated at starting and stopping of the machine can be eliminated. The PTFE bearing performance has been verified by the model test at the factory.

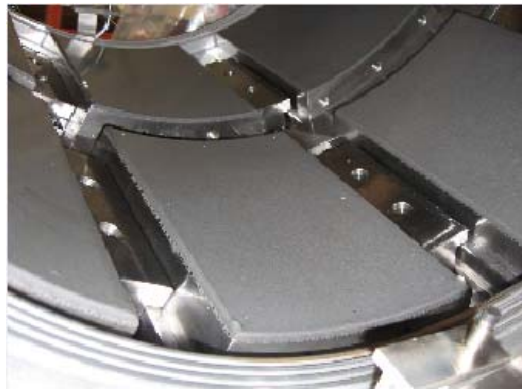


**Fig. 5 Segment type guide bearing for bulb turbine generator**

### 2.2.2 New Cooling Method of Bulb Turbine Generator

In general, it is difficult for bulb turbine generator due to low rotating speed and restriction of the bulb diameter to obtain sufficient cooling air volume and pressure by only radial ventilation of the rotor fan action. The stator and rotor of the generator for Qingshuitang is cooled by motor driven external fan and water cooled heat exchanger. However, improved cooling method such as direct cooling of the stator core through bulb shroud facing running water flow, and indirect cooling by cooling fin provided at inner surface of bulb shroud inner surface of bulb have been developed, and expansion of the application of such cooling methods are expected.

**2.3 Generator-motor for pumped storage**

Recent years, many pumped storage hydropower plants have been planned and constructed in China, and the most of the plants have the total capacity of more than 1000 MW consisting of large capacity and high speed units such as unit capacity of 200 to 300 MW and rotating speed of 375 to 500 r/min. As one of the example, the sectional structure and the ratings for the generator-motor for Qingyuan pumped storage in China are shown on Fig.6 and Table III.

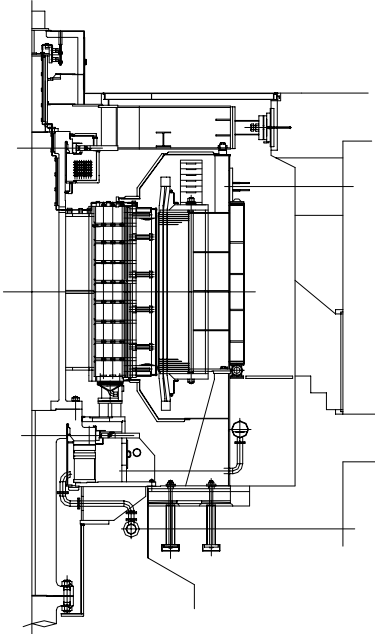


**Fig. 6 Generator motor for Qingyuan**

**Table III Ratings of Generator motor for Qingyuan pumped storage**

Type	Semi-umbrella
Cooling method	Totally enclosed air cooling with water heat exchanger
Rated capacity	356MVA/331MW (Generator / Motor)
Rotating speed	428.6r/min
Terminal voltage	15.75kV
Rated power factor	0.95 / 0.975 (Generator / Motor)

**2.3.1 Generator-Motor Construction and Ventilation Cooling Method**

The generator-motor for Qingyuan is of totally enclosed cooling system with water cooled surface air coolers. The rotor is of ring rim type which is constructed with high strength thick rolled plate stacking, and many radial air ducts are provided between ring rim plates to circulate the air through the air ducts of rotor and stator. The air flow of radial flow system is shown on Fig.7.

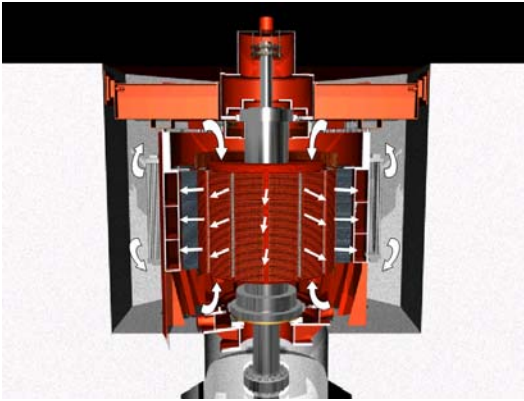


**Fig. 7 Radial flow cooling system for rotor and stator**

**2.3.2 Bearing for Generator-Motors**

The Qingyuan generator-motor is of semi-umbrella type with the combined thrust and lower guide bearing below the rotor and the upper guide bearing above the rotor. Each guide bearing and thrust bearing is center support type for reversible rotational machine, and the thrust bearing pads are supported by many coil springs. The thrust bearing pads for Qingyuan generator-motor are

conventional white metal lined type. However, recently, application of non-metallic thrust bearing which has superior friction and abrasion characteristics has been expanded to the generator-motors, and PTFE thrust bearings have been applied to 300 MW class generator-motors. The structure of the Non-metallic (PTFE) thrust bearing is shown on Fig.8, and the comparison of friction and wear for conventional white metal and the developed Non-metallic (PTFE with additives) is shown on Fig.9.

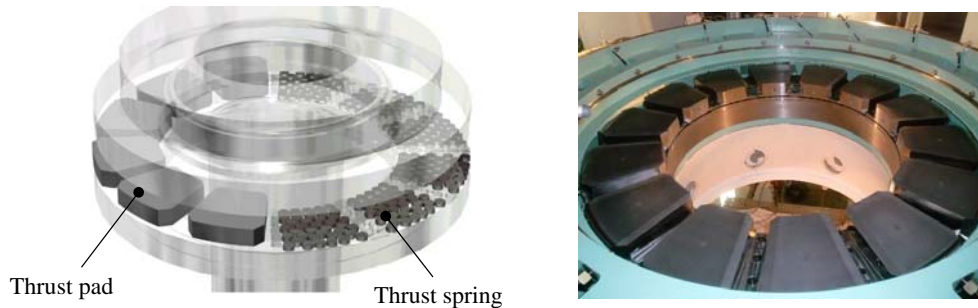


Fig. 8 Non-metallic (PTFE) thrust bearing for 300MW class generator-motor

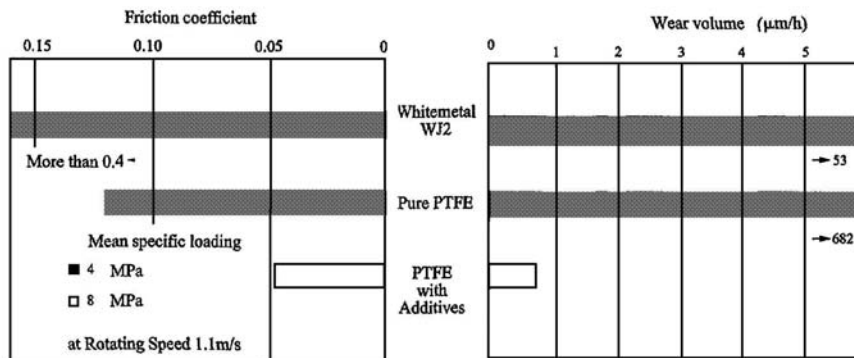


Fig. 9 Characteristics of Non-metallic (PTFE) thrust bearing

### 2.3.3 Bearing seal for prevention of oil vapour leakage

The labyrinth type seal has been traditionally widely adopted for the seal for bearing cover. However, since the rotor air intake will be close to bearing cover for high speed generator-motors with radial air flow, oil vapour was sometimes leaked from the gap between bearing cover and shaft. To prevent such problem, new type of seal named brush seal was developed, and has been applied for hydro generators as well as generator-motors. In the brush seal, plastic brushes having excellent friction abrasion characteristics keep contact with the shaft, and prevent the oil vapour leakage. The structure of the brush seal is shown on Fig.10, and the comparison of the seal performance for conventional labyrinth seal and the developed brush seal is shown on Fig.11.

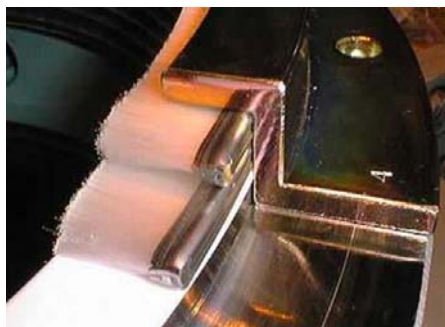


Fig. 10 Brush seal equipment for bearing cover

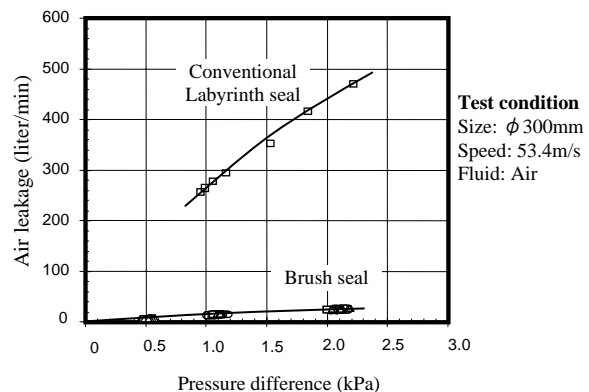


Fig. 11 Seal performance of brush seal equipment

## 2.4 Adjustable speed pumped storage

An adjustable speed pumped storage system can control pump input power by varying the rotating speed of the pump-turbine during pumping operation and contributes to the power system AFC (Automatic Frequency Control) operation. By this advantage, since the commissioning of the first adjustable speed pumped storage system at Yagisawa in Japan in 1990, the adjustable speed system has been applied to several pumped storage power plants, especially in Japan and Europe. The adjustable speed pumped storage system supplied by Toshiba is shown on Table IV.

**Table IV Generator-motors for adjustable speed pumped storage supplied by Toshiba**

Power station	Owner	Generator-motor capacity MVA/MW	Speed range r/min	Converter type	Operation
Yagisawa Unit 2	Tokyo Electric Power Co.	85/85	130 - 156	Cycloconverter	1990
Shiobara Unit 3	Tokyo Electric Power Co.	360/330	345 - 405	Cycloconverter	1995
Okukiyotsu No.2 Unit 2	Electric Power Development Co.	345/340	407 - 450	GTO Inv/Cnv	1996
Yanbaru sea water	Electric Power Development Co.	31.5/31.8	423 - 477	GTO Inv/Cnv	1999
Kyogoku Unit 1	Hokkaido Electric Power Co.	230/230	475 - 525	IEGT Inv/Cnv	2014
Kazunogawa Unit 3	Tokyo Electric Power Co.	475/460	480 - 520	IEGT Inv/Cnv	After 2020
Kazunogawa Unit 4	Tokyo Electric Power Co.	475/460	480 - 520	IEGT Inv/Cnv	After 2020

### 2.4.1 Configuration of Adjustable Speed Pumped Storage System

The system configuration of a converter-fed adjustable speed pumped storage system is shown on Fig.12. The system consists of pump-turbine, generator-motor, frequency converter and control system, and the generator-motor and frequency converter in particular are different from those of synchronous machine based conventional pumped storage system. The generator-motor has cylindrical rotor with three phase field windings, and rotating speed can be adjusted by controlling the AC current frequency of the frequency converter connected to the three phase field windings of the generator-motor.

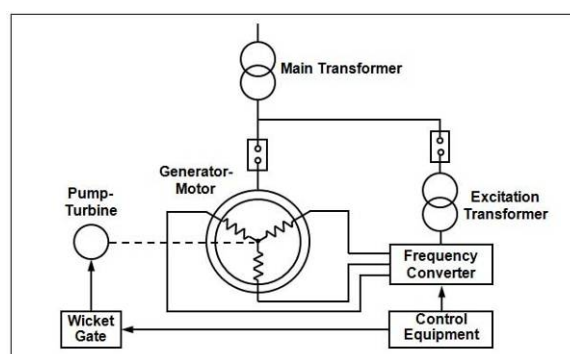


**Fig. 12 System configuration for adjustable speed pumped storage**

### 2.4.2 Generator-Motor

The rotor of the adjustable speed generator-motor is of cylindrical type with three phase distributed field windings and is different from that of the conventional synchronous generator-motor. The technical issues for high-speed large-capacity adjustable-speed generator-motors are the structures of rotor core lamination and rotor coils which need to endure large centrifugal force. The high tensile strength steel is applied for rotor core laminations. Since three phase coils like stator coils are inserted

in the rotor core slots for the adjustable speed generator-motor, the rotor coil end support structures against the centrifugal force are important. In the induction motors equipped with three phase distributed windings for the rotor, binding of non-magnetic steel wire to outer side of the rotor coil ends has been commonly used to support the coil ends against centrifugal force. However for the large-sized, large capacity generator-motors, U-bolt supporting structure has been developed and applied. The U-bolt supporting system has good advantages such as easy assembly and maintenance at site, good cooling of coil ends, free thermal expansion of the coils and no assembly facility requirement at site. The U-bolt supporting structure and generator motor rotor for adjustable speed pumped storage are shown on Fig.13 and Fig.14.

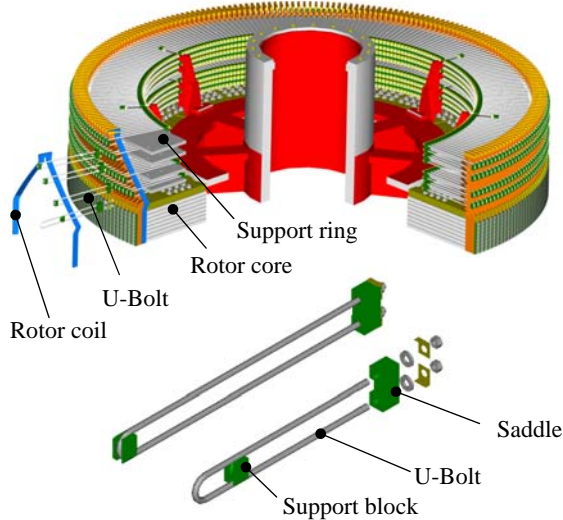


**Fig. 13 U-Bolt supporting system**



**Fig. 14 The Generator-Motor Rotor for Adjustable Speed pumped Storage**

**3 CONCLUSION**

The construction of hydroelectric power plants has been continued and the technologies for hydro generators including large capacity hydro generators and bulb turbine generators and generator-motors for pumped storage have been developed and improved.

Technical trends for hydro generators will be an expansion of complete air cooling application for large capacity hydro generators and generator-motors, an improvement of cooling method utilizing heat transfer through the bulb shroud facing the running water flow for bulb turbine generators, and development and improvement of maintenance free technology such as non-metallic bearings and high performance bearing seal.

With the increase of an intermittent renewable power such as wind power and solar power, power grid stability is becoming one of major issues, and equipment and/or system to stabilize the power grid such as adjustable speed pumped storage system will be introduced and developed.

**BIBLIOGRAPHY**

[1] Aguro K, Kato M, Kishita F, Machino T, Mukai K, Nagura O, Sekiguchi S, Shiozaki T. Rich operation experiences and new technologies on adjustable speed pumped storage systems in Japan. CIGRE-2008

[2] Namba S, Mikami M, Long T T, Arai H. The High Reliability Technology of Thrust Bearing for Hydrogenerator//Proceeding I of the 1<sup>st</sup> International Conference on Hydropower Technology & Key Equipment 2006, Beijing China



Beijing, China

SC A1  
**COLLOQUIUM ON NEW DEVELOPMENT OF ROTATING  
ELECTRICAL MACHINES**

11~13 September, 2011

---

**Development of Air-cooled Hydrogenerators for 700MW Level Capacity**

**Sun Yutian**, *Member, CIGRE*  
**Harbin Research Institute of  
Large Electrical Machinery  
China**

**Gao Qingfei**  
**Harbin Electrical Machinery  
Company Limited  
China**

**SUMMARY**

As a series of 700MW class totally air-cooled hydroelectric generators have been put into operation in China, the development of hydroelectric generators arrive at a new stage. To summarize the experience, taking the generator of Three Gorges Right Bank Power Station as an example, the design and operation features about 700MW class totally air-cooled hydroelectric generators are presented and discussed.

**KEYWORDS**

Hydroelectric generator, Air-cooling, Thrust bearing

# 1 INTRODUCTION

At present in China, there are some 100 hydroelectric generator units in operation with the ratings in the range of 550MW through 750MW, and the machines with the ratings above 700MW is about 70 units. From the year 2005 to 2020, the total capacity of new increased hydropower equipment will be more than 10 000MW every year, and it will be 5 times of the speed compared with the past(see in Fig.1).

For the design of large-capacity hydroelectric generators, cooling scheme is important. There are three cooling methods for hydroelectric generators at present, that is, totally air cooling, water inner cooling, and evaporation inner cooling.

For totally air-cooling scheme, only air is adopted as the cooling media inside the machine, and machine's cooling is realized by the flowing of air. The auxiliary equipment is only air coolers in this case. For water inner cooling scheme, the stator winding bar contains some hollow conducting strands with water flowing inside, and machine's cooling is realized partly by the flowing of water. In this case the auxiliary equipment contains not only air coolers, but also a set of complicated water-processing and circulation system to reduce the electricity-conductivity of water and drive water flowing. For evaporation-cooling scheme, the hollow conducting strands are also needed to form a set of evaporation circulation system of some special medium which similar to water inner cooling scheme<sup>[1]</sup>. In this case the auxiliary equipment contains only coolers. As the media is not electricity-conductive, and it can circulate automatically by cooling process, no pump and other devices are needed.

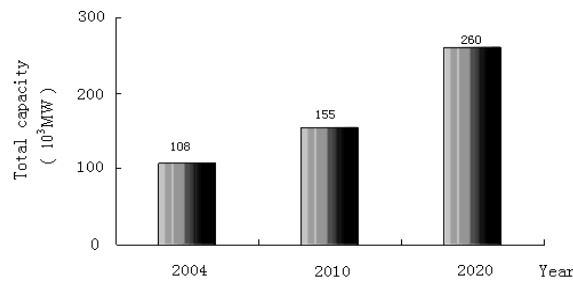


**Fig.1 The recent development and planning of hydroelectric generators units in China**

The comparison of three cooling schemes is shown in Table I. It shows that the dimension of the totally air cooled machine is a little larger, but it becomes not important when take into account system complicated extent. So the totally air cooling scheme will be preferred if feasible. Since 756MW totally air cooled hydroelectric generators operated in Three Gorges Right bank Power Station, all the orders for 700MW class hydroelectric generators in China have almost the same request of air cooling scheme.

**Table I Comparison of three cooling schemes**

	Size	System	Maintenance	Reliability
Totally air cooling	large	simple	small	high
Water cooling	small	Very complicated	Very large	low
Evaporation cooling	small	complicated	large	middle

In the sight of the customer, totally air cooling scheme is preferred to large hydroelectric generator products. For totally air cooled machines the temperature rise and its distribution in stator windings, thermal mechanical stress, expansion and deformation of stator core are emphasized to be solved. Those are perfectly solved in a series of 700MW class air cooled hydroelectric generators manufactured by Harbin Electric Machinery Company Limited (HEC). In this paper, taking the 700MW generator in Three Gorges Right Bank Power Station as an example, the design and operation features about 700MW class totally air-cooled hydroelectric generators are presented.

**2 ELECTROMAGNETIC DESIGN FEATURE**

For totally air cooled machines the temperature rise and its distribution in stator windings, thermal mechanical stress, expansion and deformation of stator core are emphasized to be solved. So in the design of the machine, thermal load should be controlled by optimization of parameters in order to decrease temperature rise and expansion of stator cores. Some countermeasures should be taken in the design.

The main parameters of Three Gorges Right Bank Power Station are listed in Table II.

**Table II Main data of three gorges right bank power station**

Capability (Max.)	700(756) MW
Rated voltage	20 kV
Rated power factor	0.9
rotating speed	75 r/min
Height of stator core	3.2 m
Max. Thrust load	5560 t

By electromagnetic calculation, incomplete transposition is adopted to replace conventional 360 degree transposition in stator windings in order to decrease additional loss and temperature difference among strands due to end magnetic field. Thus the lifetime of stator coils is improved.

The stator core material is made of an excellent, cold-rolled thin silicon steel sheet (50H250) with good quality, high magnetic permeability, low loss, and good mechanical characteristics. The loss per kilogram is not more than 1.05W/kg at magnetic flux density 1T, so the core temperature can be decreased. The stator core is pressed tight by using draw-in bolts and spring washer with epoxy glued at both core ends. The arrangement of draw-in bolts ensures that the stator core pressure is larger than 1.7MPa, thus the stator core becomes an integral body and core deformation is avoided.

Excitation brush bracket is an integral two-way conducting structure, it ensures that excitation cables are connected in one side so arrangement is easy, and the current can flow in from the middle of conducting ring so the current in each brush is uniform. Thus the sparking problem of brush in retaining ring under the condition of large excitation current is solved.

Stator frame has oblique plates. It makes the radial expansion force of stator core absorbed by deforming of frame oblique plates. Thus warp phenomena of stator core due to the pressure of frame at thermal state is avoided.

Staggered rotating windscreen technique is adopted at rotor part. That not only forms a screen for the wind, but also ensures the insulation distance of interpolar coil connection.

**3 VENTILATION DESIGN AND ANALYSIS**

With the increasing of machine’s capacity, cooling becomes more and more difficult. For Three Gorges 700MW hydroelectric generators, there is no precedent to use totally air cooling scheme in the world. For 700MW class hydroelectric generators, conventional cooling scheme is water inner cooling.

For the hydroelectric generators of Three Gorges Right Bank Power Station, as tangential velocity of rotor outer surface is high, the resulted cool airflow is sufficient for cooling. So the scheme of sealed double-path self-circulation radial ventilation system without fan is available, where the air goes back at the ends. For this scheme, the cool air flows into the inlet at rotor bracket by means of fan function that created by rotating of rotor bracket, rotor rim and poles, and goes across rotor rim ducts, interpolar space, air gap, stator radial ducts, finally get into the cooler from back of the machine with generator loss. After heat transfer with cooling water, the air goes in two paths of upper and bottom into rotor bracket again, that finishes an air circulation. Fig. 2 shows the ventilation system diagram.

In the study, a ventilation model test is made for 700MW class hydroelectric generator. The scale of ventilation model to Three Gorges Right Bank generator is chosen as 1:6. The body of ventilation model is designed on the basis of similarity criteria and some exceptions are specially considered. The material characteristic of model surface at air passage is made as closer to the situation in the real machine as possible. At cooling ducts, the iron material and structure are designed the same as the prototype to reach better test accuracy, even the sheet folding method.

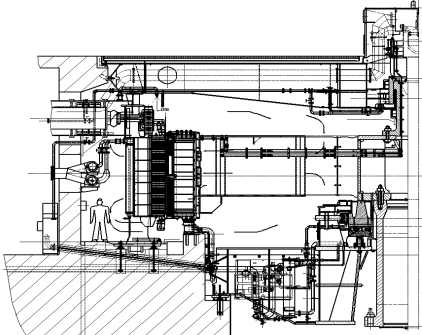


**Fig.2 Assembly and ventilation diagram for Three Gorges Right Bank generator**



**Fig.3 Ventilation model**

Test shows that the relation between air volume of the model and speed is linear (See Fig. 4), which means test condition is in the area of fluid similarity hence the test is valid. Table III shows comparisons of total air volumes and ventilation loss deduced from model test versus calculation.

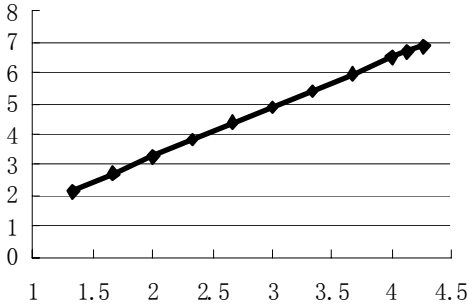


**Fig.4 Relation of air volume versus speed**

**Table III Comparison of air volume and ventilation loss**

Item	Air volume (m³/s)	Loss (kW)
Test	351	2300
Calculation	326.4	2460

Fig. 5 shows test results of air velocity in cooling ducts at different speed, which reflects air velocity in different ducts of the generator design are uniform. That ensures temperature rise of stator winding uniform.

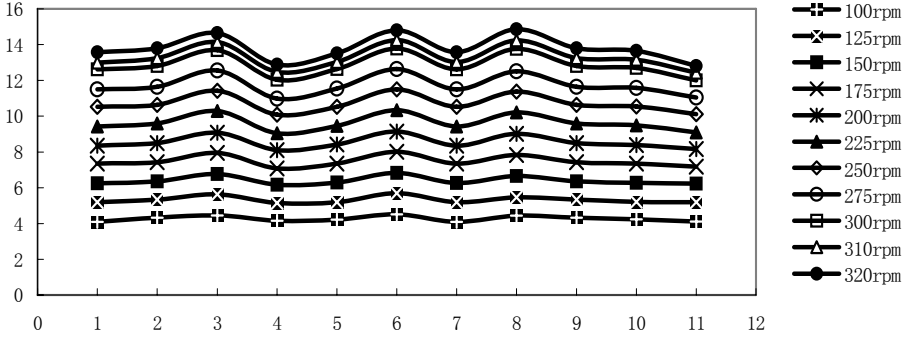


**Fig.5 Velocity distribution of cooling ducts in ventilation model**

Totally air-cooling scheme for Three Gorges Right Bank generators is obtained on the basis of comparison study of simulation test and calculation analysis. Systematic theory and test study show that, Total air cooling scheme is feasible for 700MW class hydroelectric generator. Fig. 6 is the stator bar temperature distribution of 700MW class hydroelectric generator from numerical calculation of three-dimension temperature field.

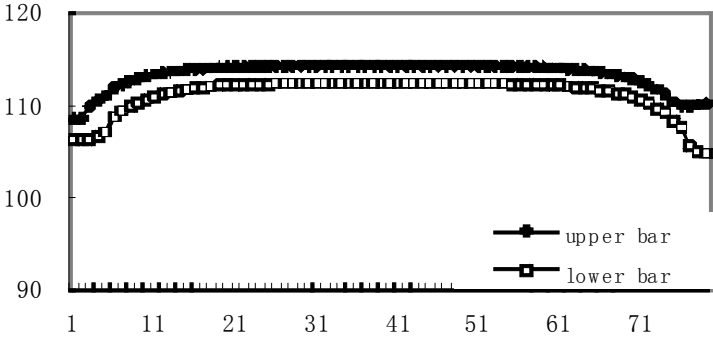


Fig.6 Calculation results of a stator bar temperature distribution at maximum load

**4 INSULATION STRUCTURE**

It is very important to develop high-performance insulation material and design reasonable structure. For air-cooled generator, in addition to electric and mechanical performance, thermal characteristic is also important to the insulation, it influences the heat transfer and reliability of the machines.

In the aspect of main insulation, the developed high electric field strength, epoxy frosting mica tape has excellent characteristics of electricity, strength, and heat, hence found successful application. For Three Gorges generator, the designed electric field strength reaches 2.5kV/mm.

By adopting slot-part anti-corona structure of stator bars with once-formed thin-type solidly fiberglass tape and manufacturing process of resin-rich epoxy fiberglass mica paper insulation, electric aging life index is greatly improved.

Stator winding is fixed by using silicon rubber in slot area and soft hoop at end part.

**5 THE DESIGN OF THRUST BEARING**

The thrust load of Three Gorges Right Bank hydroelectric generators is very large, up to 5560t, so it is difficult to be made. In the design, upper and lower guide bearings are made into complex bearing, and put into lower guide thrust oil tank. Thrust pad is double layer pad with a cluster of pins, and supported by adjustable spindle support with a supporting disk. Oil system includes self-pumped pad and external circulation structure.

**5.1 Characteristic analysis of thrust bearing**

The structure of thrust bearing is shown as Fig. 7, the bearing contains a running pad (thin pad) and a supporting pad (thick pad), in between is a cluster of pins with different diameters. At bottom of the supporting pad is a supporting disk, which is supported by a height-adjustable spindle support.

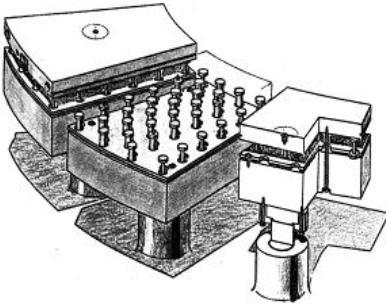


Fig.7 Babbitt pad thrust bearing

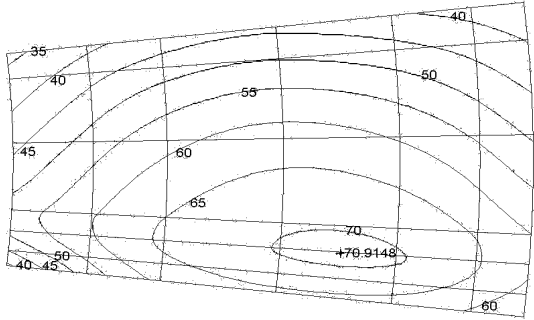
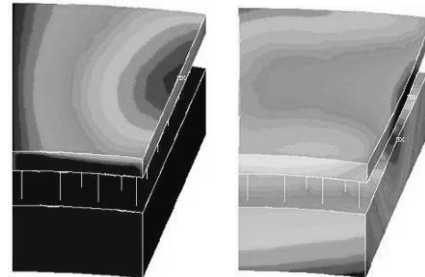
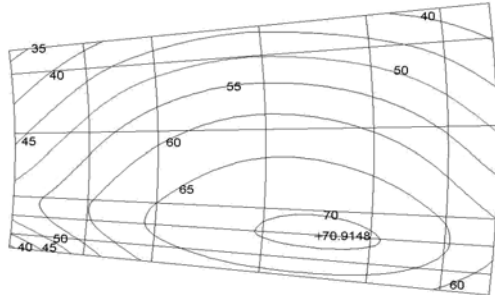


Fig.8 Temperature of thrust pad at 5mm below surface

As the pins detaches running pad and supporting pad, circulating oil can flow freely between the two pads, the temperature difference of running pad has little effect on supporting pad, thus the latter has uniform temperature distribution at directions of axial, radial, and peripheral tangential. The thermal deformation of supporting pad is very small. It has only elastic deformation on pins. As the thickness of running pad is small, by adjusting the diameters of pins, thermal-elastic deformation of the pad surface due to combined effect of oil film pressure and temperature can be controlled into small extend.



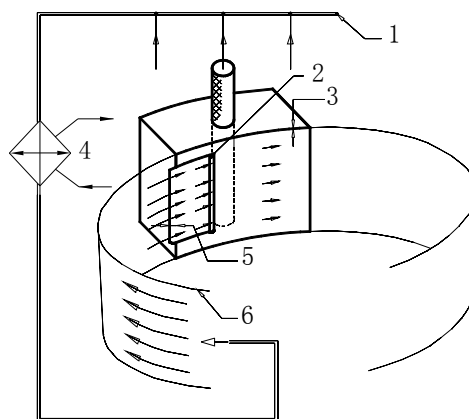
**Fig.9** Temperature of tray pad at 5mm below surface

**Fig.10** Calculated temperature and deformation

Test temperature distribution of Three Gorges thrust bearing is shown as Fig. 8 and 9, where surface temperature of the running pad is in the range of 35 to 37°C, and that of supporting pad is in the range of 32 to 34°C. Fig. 10 shows numerical calculation results of three dimensional temperature field and stress deformation for the bearing. As temperature distribution of supporting pad is nearly uniform, the thermal deformation becomes small. Deformation of running pad surface is a little concave along radial direction and runner surface is a little convex. So the effect of runner deformation on bearing characteristics is decreased. That is the results of pins optimization, it balances runner deformation greatly.

### 5.2 Oil circulation system

Fig. 11 shows the diagram of guide-pad pump external circulation system. The loss created by thrust bearing and lower guide bearing is evacuated out of oil tank by circulating oil, which is driven by guide-pad pump. The pad of guide bearing is self-pumped pad. When the machine rotates, the oil is taken by the outer surface of thrust runner into oil lumen (inner hole) of the guide-pad pump, and then flow into oil ring pipe. The oil ring pipe drives oil out of oil tank, which goes back to cool oil influx ring pipe under the bearing after cooled by external coolers. Then it flows up to every pad. Since no sealing elements and other frictional elements existed, there is no additional loss created.



**1** oil influx pipe, **2** thermal oil flow, **3** oil film, **4** heat transfer, **5** oil lumen (inner hole), **6** cool oil flow

**Fig.11** Diagram for self-pumped pad and guide-pad pump external circulation system

The thrust bearing of Three Gorges Right Bank hydroelectric generators adopts new technique like post-cluster double-layer pad, guide pad self-pumped oil circulation, etc, it shows excellent performance in the test of a 3000t thrust bearing test stand and practical operation of the machines.

## 6 Force on machine transients

### 6.1 Sudden short circuit current

By means of software SIMSEN, various short circuit accidents are simulated for Three Gorges Right Bank hydroelectric generators. Fig. 12 shows calculated stator current waveforms of the machine at different sudden short circuits under the conditions of load operation.

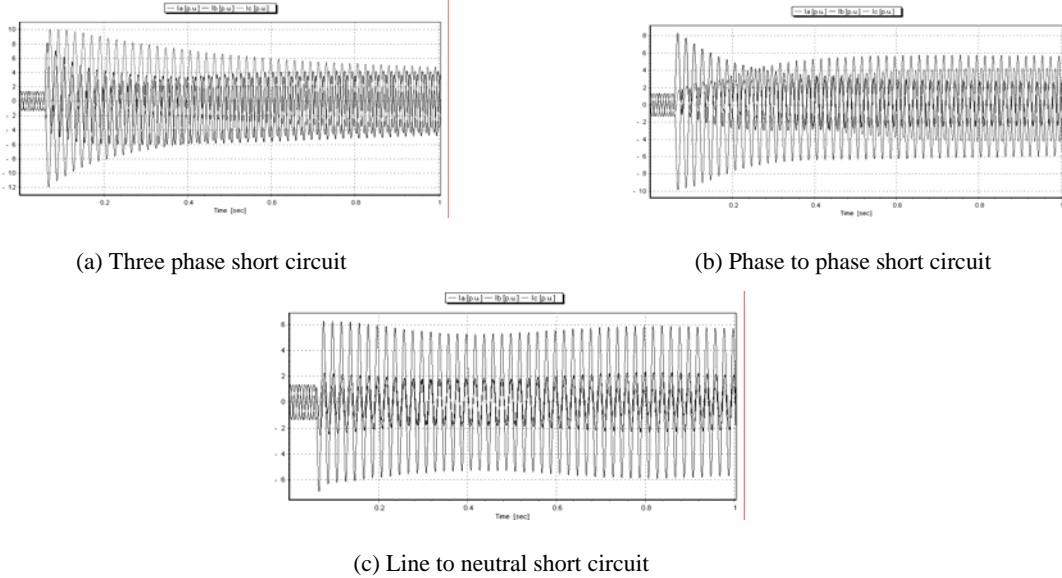


Fig.12 Calculation results of short circuit currents for Three Gorges Right Bank hydroelectric generators

### 6.2 Force of end connection copper ring

Based on short circuit current calculation, the force of end winding connection copper ring is calculated by analytical method. The most serious short circuit accident is three phase short circuit, where the largest current is 289 093A. The maximum force on copper ring connection is 192.4N/m under the condition.

### 6.3 Force of stator bar in slot

The force of stator bar in slot at three phase short circuit is calculated, the forces in unit-length are 101.51kgf/cm for upper bar and 135.34kgf/cm for lower bar.

### 6.4 Force of stator bar in end region

For winding overhang, calculation shows that maximum force takes place at out-of-phase synchronization of  $120^\circ$ . Fig. 13 shows initial waveform of stator currents and Fig. 14 three dimensional force.

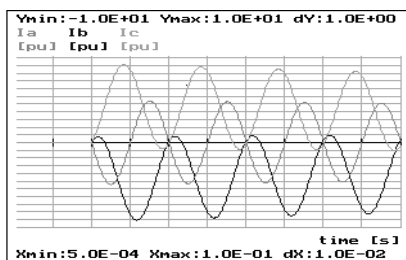


Fig.13 Initial stator currents

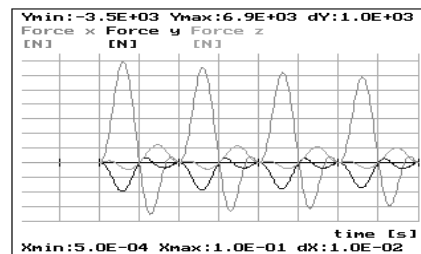


Fig.14 Force of winding overhang

## 7 OPERATION AND TEST ANALYSIS

Operation of Three Gorges Right Bank hydroelectric generators has shown excellent performance. Table IV shows the results of operation temperature.

**Table IV Temperature of the machines by test**

Power	Stator winding temperature	Stator core temperature	Rotor winding temperature	Remarks
500 MW	30 K	27 K	30 K	From Test
600 MW	36 K	29 K	34 K	From Test
700MW	39K	27K		From operation monitoring

The waveform distortion factor of the machine's line voltage is 0.26%, telephone harmonic factor is 0.20%.

By no-load and short-circuit test, the direct axis reactance  $X_d$  at rated condition is 1.129 (non saturated value) and 0.939(saturated value), and SCR is 1.065. Test transient parameters of the machine from three-phase sudden short-circuit test are,  $X_d'$  is 0.28, and  $X_d''$  is 0.235, direct axis transient short-circuit time constant  $T_d'$  is 1.45s, direct axis sub-transient short-circuit time constant  $T_d''$  is 0.08s, Armature winding short-circuit time constant  $T_a$  is 0.32s.

Generator efficiency is 98.58% at 500MW output and 98.68% at 600MW output. The operation results are satisfactory.

## 8 CONCLUSION AND PROSPECT

At present, a series of 700MW class totally air-cooled hydroelectric generators have been put into operation in China, like Three Gorges Right Bank Power station, Longtan Power Station, etc. Good operation effect and experience are obtained. By summarizing the design and operation, following conclusions are obtained.

- By optimization of electromagnetic design, adopting total air cooling scheme in 700MW class hydroelectric generators is realizable.
- By adopting the scheme of sealed double-path self-circulation radial ventilation system, 700MW class total air-cooled hydroelectric generators are able to realize airflow distribution uniform.
- In the aspect of main insulation, the developed high-voltage epoxy frosting mica tape has excellent characteristics of electricity, mechanical strength, and heat resistance, hence found successful application.
- Large-size heavy-load thrust bearing adopts new structure of post-cluster double-layer pad and guide pad self-pumped oil external circulation. It shows excellent performance both in test stand and machine's operation. It ensures normal operation of the machines.
- Force analysis of relative elements in transients provides reference for anti-impact design of the generator. It ensures the machine operating safe and reliable.

The operation success of 700MW class totally air-cooled hydroelectric generators brings experience and direction for larger hydropower products. For the development of larger capacity hydroelectric generators, possibility of total air-cooling scheme should be preferred to be taken into account.

## BIBLIOGRAPHY

- [1] Gu G, Xiong N. The Development of Evaporation-cooling Technology For Large Generator in China//Proceedings of the Third Chinese International Conference Electrical Machines (CICEM'99), Xi'an, China, August, 1996: International Academic Publisher
- [2] Schafer D, et al. Investigations into a 6000t Thrust Bearing with Teflon Layer or Babbitt Layer for the Three Gorges Units//Proceedings of the Fifth International conference :Electric Machines and System, Shenyang, China. August, 2001, I

**Optimization and Improvement on Vibration & Noise Performance of Unit 15~18  
for the Right Bank Power Station of TGP**

**He Jianhua, Chen Changlin, Duo Lin, Zhang Tianpeng**  
**DFEM**  
**China**

**SUMMARY**

A comprehensive and systematic testing and theoretical analysis were carried out on the abnormal vibration and noise level of generating Unit 15~18 at Right Bank Power Plant and 6 generators supplied by VGS Consortium for the Left Bank Power Plant. It was found that the electromagnetic design was the inherent cause for 100Hz electromagnetic vibration and noise, while the roundness deviations of both stator and rotor (uneven air gap) are the major reason to cause vibration of generators with 1~3 multiple rotating frequency. It was also found that the mechanical structure and installation accuracy of the units also produce rather impact on unit vibration and run-out. By changing the generator stator connections, the 100Hz electromagnetic vibration and noise were completely eliminated, while by controlling the installation quality and improving generator mechanical structure, the 1~3 multiple rotating frequency vibration amplitude and mixed-frequency amplitude were significantly reduced. Consequently, the above-mentioned abnormal vibration and noise of generators were basically resolved.

**KEYWORDS**

Generator, Electromagnetic vibration and noise, Improvement of stator connections, Structural optimization

## 1 INTRODUCTION

Dongfang Electric Machinery Co., Ltd (DFEM) independently undertook the design & manufacture contract of four units (unit15~18) for the right bank power station of Three Gorges. The electromagnetic scheme and main structure of VGS generators on the left bank power station were still used in generators on the right bank power station, and only the thrust bearing, collector ring and local structure that would influence manufacture and installation quality were optimized. While the first unit 18 was put into operation in October 2007, the vibration and noise of generator was a little large. In comparison test with VGS generator on the left bank power station, it was found that they had common character of large vibration and noise.

Therefore, DFEM carried out comprehensive and systematic tests and theoretical analysis, and finally found that the electromagnetic scheme of VGS generators had design defect, the intrinsic factor which caused 100Hz electromagnetic vibration and noise. The installation precision could significantly influence overall vibration & run-out. So, corresponding measures were taken for improving as actual installation progress. By improving the installation accuracy and part structure of unit17, vibration amplitude and noise had been sharply reduced. But, 100Hz electromagnetic vibration was not thoroughly eliminated. So, DFEM stuck to take measures to improve generator stator connections on unit16 and unit15, and finally eliminated the electromagnetic vibration, improving the vibration, run-out and noise to reach a good level. The unit18 improvement was completed in December 2008, solving the electromagnetic vibration and noise problem. With optimization and improvement of the four generators designed and manufactured by DFEM, the electromagnetic vibration and noise problems had been eliminated substantially.

## 2 VIBRATION ANALYSIS IMPROVEMENT SCHEME

### 2.1 Vibration analysis

In order to solve the larger vibration, with coordination of relative companies, DFEM performed a series of tests, mainly including: vibration comparison tests for unit18 and 3 & 7 units on left Bank power station, roundness measurement for stator and rotor of unit18, test for 100Hz electromagnetic vibration, and noise test, etc. Upon analysis on test result combined with electromagnetic vibration mechanism, we could make conclusions as below:

(1) Through vibration, noise test and spectrum analysis, vibration of unit18 was classified as two kinds:

a. One is low-frequency rotation frequency vibration, mainly 1~3 multiple rotation frequency (1.25Hz) vibration, in which double frequency (2.5 Hz) amplitude can reach as high as 54 $\mu$ m under 100%U<sub>e</sub> no-load speed condition. It has feature that it's very small under no-load speed condition and will increase as the excitation current (i.e. generator voltage) is increasing, while the amplitude will keep almost the same under different load condition.

b. The other one is high-frequency polar frequency vibration, mainly 100Hz vibration. It has feature that the amplitude is very small under 100%U<sub>e</sub> no-load condition and will increase as the load is increasing. While under 700MW load of unit, horizontal vibration amplitude of core reaches 47.7 $\mu$ m.

(2) Comparison test indicates the common characters of generators on left and right bank power station:

a. 100Hz vibration on core is a little large, with amplitude normally between 40 $\mu$ m and 50 $\mu$ m.

b. Electromagnetic noise is a little large, normally around 80dB (A).

c. Obvious vibration feeling: intensive resonance on components of cover plate and end shield, obvious "foot numbness" feeling and electromagnetic noise hum.

(3) Individual character of generators on left and right bank power station:

a. Low-frequency (1~3 multiple rotation frequency) vibration of 18 and 3 units is a little large but that of unit 7 is normal, which means low-frequency vibration has no necessary connection with design scheme but with installation precision;

b. Although amplitude of low-frequency vibration is large but its energy is small, so the direct perception is not so obvious.

100Hz high-frequency vibration is a little large, which is the common character existing in electromagnetic scheme for VGS generators. Meanwhile, low-frequency vibration of generators on left and right bank is sensitive to installation.

**Table I Comparison of vibration test data for unit18 and unit 3 on Left Bank power station  
(in which rotation frequency fr=1.25Hz) μm**

		Unit 18 (before improvement)					Unit 3 for the Left Bank Power Station					
		Totally Frequency	1fr	2fr	3fr	100Hz	Totally Frequency	1fr	2fr	3fr	4fr	100Hz
700MW	Frame level	122.0	25.0	60.0	46.0	5.0	117.0	14.0	74.0	31.0		2.0
	Core level	165.0	26.0	48.0	40.0	47.7	142.0	13.0	62.0	29.0	7.0	42.0
No-load	Frame level	134.0	26.0	68.0	47.0		134.4	15.0	82.0	35		1.1
	Core level	118.0	23.0	54.0	40.0	2.0	118.1		64.7			2.2

## 2.2 Cause analysis on low-frequency (1~3 multiple rotation frequency) vibration and measures for improvement

While rotor is not round enough and causes air-gap inequality, a series of geometric dimension harmonic (magnetic conductivities harmonic in magnetic field) were found during Fourier transform of air-gap data. Under excitation magnetic force, a series of low-order harmonic magnetic field will be produced among air-gap and force-wave will be produced due to the interaction of the harmonic field and dominant wave field, so that low-frequency electromagnetic vibration is produced, and this is the main cause to produce low-frequency electromagnetic vibration in hydraulic turbine generator.

Upon analysis on roundness test for stator and rotor of 18th generator, large out-of-roundness is found; especially cam and ellipse shape on rotor is obvious. After Fourier analysis, it is found that the geometric dimension harmonic amplitude of No.1, 2 and 3 antipodal is the largest, that is harmonic magnetic field of No.1, 2 and 3 antipodal is the strongest and 1~3 multiple rotation vibration will be produced if it is interactive with main wave magnetic field (40 antipodal).

It will be seen from the calculation principle of vibration amplitude that the relation between vibration amplitude  $A_m$  and electromagnetic wave node antipodal  $M$  is as following:  $A_m \propto 1/(M^2-1)^2$ . As 1~3 multiple rotation frequency vibration exciting force-wave node antipodal  $M=1\sim3$  which is a little small, so it's sensitive. Meanwhile, with regard to large water-cooling units like that of Three Gorges, the electromagnetic load is high and radial magnetic tensile force is directly proportional to square of magnetic flux density. Once the rotor is not round, unbalanced magnetic tensile force becomes big. It will be known by calculation that projection or recess of 1mm of each stage will produce 1.8t unbalanced magnetic tensile force. It will be seen from the rotor roundness wave-shape that roundness of unit 18 is a little bad, and unbalanced force calculation result for unit 18 will reach about 30t which is the main cause of big low-frequency vibration occurrence for unit 18. Because of excellent control on roundness of rotor and stator of unit15, low-frequency vibration amplitude is very small. Comparison figures for roundness of rotor and stator of 18 and 15 units is as Figure 1 and Figure 2.

Moreover, low-frequency vibration amplitude under load condition is generally the same, and the reason is that air-gap magnetic field remains almost unchanged (variety within 5%) under no-load rated voltage and load condition, i.e. exciting force-wave amplitude producing low-frequency vibration remains almost unchanged.

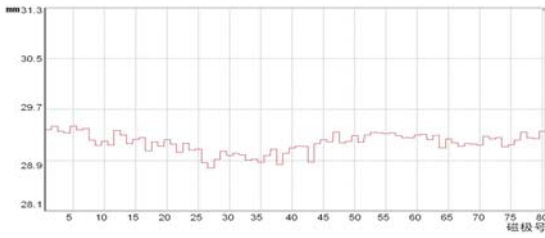


Fig. 1 Roundness of Generator Rotor of Unit 15

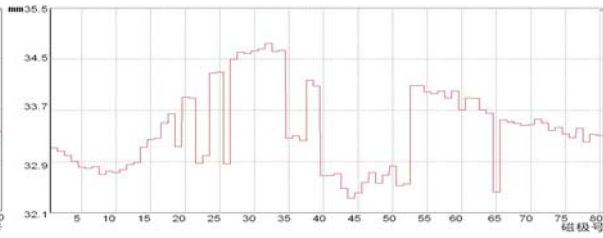


Fig. 2 Roundness of Generator Rotor of Unit 18

Low-frequency vibration can be improved by controlling installation requirement and improving local structure. Therefore, controlling measures including core lamination, rotor yoke lamination, stator & rotor roundness, tightness of magnetic yoke, shaft system accuracy, increasing upper bracket support etc. are intensified during generator installation for unit17, 16 and 15; and the actual effect indicates that control of low-frequency vibration has met good standards. Low-frequency vibration on unit18 generators is significantly reduced. Regarding vibration test result please see Table V.

### 2.3 Cause analysis of high-frequency (100hz) vibration and its improving measures

#### 2.3.1 Cause Analysis of Vibration and Judgment

Obvious “foot numbness” feeling and electromagnetic noise hum on cover-plate of unit18 is caused by high-frequency electromagnetic vibration. It will be seen from electromagnetic vibration principle that high-frequency vibration of hydro-generator is normally caused by exciting force produced due to interaction between fractional harmonic magnetic field and air-gap main-wave magnetic field. And reasons to produce fractional harmonic magnetic field are divided into two kinds:

(1) Because stator winding is matched with fractional slot (generally speaking, considering hydraulic generator has many poles and winding symmetry and different cooling mode and match of electromagnetic load, it’s difficult to find proper integral slot winding), for example, in Three Gorges VGS generators, slot number per phase per pole is , fractional harmonic is occurred in air-gap magnetic field and interaction between fractional harmonic and fundamental wave will cause vibration. Regarding this kind of harmonic especially the reversal harmonic, of which the number of pole-pairs is next to pole-pairs number of fundamental wave, because of its interaction with fundamental wave the force-wave node number produced in core is small, so it can cause big vibration.

(2) As the parallel branch is concentrated winding layout (that is concentrate together the five parallel branch that only occupy the circle), when air-gap is not uniform, electric potential induced by each branch is different so that circulation is formed among branches and the circulation will produce a series of fractional harmonic in air-gap magnetic field, which interact with fundamental wave to form force-wave.

As air-gap magnetic field under no-load and load condition only changes a little, so parallel branch circulation only changes a little, too. And vibration caused under no-load and load condition should be basically unchanged, i.e. vibration caused by circulation can be judged according to that under no-load condition. It will be seen from vibration test result for unit 18 on right bank power station of Three Gorges that 100Hz vibration under no-load 100%Ue is very small, only 1~2μm, therefore, the reason to cause vibration is not circulation.

Therefore, the most possible reason to cause 100Hz vibration on unit 18 on right bank power station of Three Gorges is fractional harmonic vibration caused winding itself. This kind of vibration will increase as the load increases (i.e. harmonic magnetic field-strengthening), and its amplitude is connected with stator slot number Z (510 slots for unit18 generator on the right bank power station of Three Gorges), connection mode of stator winding and elasticity modulus E1 after core lamination, etc.

#### 2.3.2 Calculation Method for Electromagnetic Vibration

Suppose the stator core and frame is a circle like that in Figure 3, the calculation formula for vibration of stator core is deduced as following:

Vibration amplitude :

$$A_m \propto \frac{F_m}{E_1(M^2 - 1)^2} \times \frac{1}{1 - \left(\frac{f}{f_0}\right)^2} \quad (1)$$

Natural frequency of corresponding vibration mode:

$$f_0 = \frac{M \times (M^2 - 1)}{\sqrt{M^2 + 1}} \sqrt{\frac{gE_1J_1}{2\pi G_1R_j^3}} \quad (2)$$

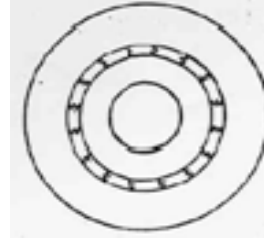


Fig.3

### 2.3.3 Analysis on Original Electromagnetic Design Scheme

The electromagnetic scheme same as left bank VGS units is applied for unit18 generators on the right bank power station of Three Gorges: 510 stator slots, 5 parallel branches, 40 rotor pole-pairs number, slot number per phase and per pole , motor number per unit t=10. Each phase of stator winding in original scheme is adopted with “10+7” type big & small phase zone layout, i.e. each positive phase has 10 series of slot number of which the electrical angle is the same and each negative phase has 7 series of slot number of which the electrical angle is the same. The reason to choose this layout scheme is that short distance for electric jumper lead is easy for connection.

The calculation indicates that under present winding connection, on load condition, there are 10, 20, 50, 70 and 80 antipodal and other magnetic harmonic in air-gap field, i.e. fractional harmonic. And the 10 and 70 antipodal harmonic is normal rotation harmonic, interacting with which the main wave (40 antipodal) produces force wave exciting node M which is very big and according to Formula (1), electromagnetic vibration will not be produced, so that it will not be taken into consideration. 20, 50, 70 and 80 antipodal harmonic is reverse and node number M of force-wave produced in stator core is few, and the corresponding natural frequency of stator core near 100Hz is the main cause for vibration.

Elastic modulus of core E1 is mainly related to unit dimension, lamination mode of core and tightness of core. Generally speaking, if it is whole-circle lamination with good tightness of core, the elastic modulus E1 will be high; oppositely it will be low. Test indicates that core elastic modulus E1 of middle-small type units with normal circle lamination is between 1.2~1.5×10<sup>5</sup>N/mm<sup>2</sup>. For big-dimension units like that in Three Gorges with whole-circle lamination, range of the elastic modulus E1 needs further study. In calculation and analysis on E1 with different value, when E1 = 1.2 × 10<sup>5</sup>N/mm<sup>2</sup>, the calculation is fitting with the actual measured value. Table II describes the calculation result for stator core vibration before and after connection change.

It can be seen from the calculation result that electromagnetic vibration caused by 50 antipodal harmonic is a little large. Because amplitude of 20 antipodal harmonic is large and is sensitive to elastic modulus, in order to further certify the reliability of theoretical calculation, a supplementary test on electromagnetic vibration respectively caused by 20 and 50 antipodal harmonic for unit17 and unit18 is performed. Vibration sensor is arranged according to force-wave node antipodal and space-distribution-pitch and the vibration amplitude of main harmonic can be obtained by signal operation. Please see Table III.

The result of supplementary test indicates that after removing the vibration produced by 50 antipodal field harmonic, the 100Hz electromagnetic vibration of generator is very small, which indicates that the 50 antipodal harmonic is the main cause for 100Hz electromagnetic vibration. And actual measured value is in accordance with the theoretical calculation.

### 2.4 Improving Scheme and Measures

It will be seen from the analysis on original scheme that there're two methods to reduce core vibration amplitude: one is to weaken amplitude of magnetic field harmonic and the other is to change elastic modulus of core. Regarding generators on right bank power station of Three Gorges, core installation has been completed and it's difficult to change its elastic modulus, and it is only possible to weaken 50

antipodal harmonic by change of winding connection. Therefore, changing stator winding mode for unit16 and unit15 as installation progress and changing stator winding for unit18 and unit17 can realize reducing core vibration amplitude.

**Table II Calculation of Stator core Vibration Before and After Connection Change**

	Harmonic Antipodal $p$	Percentage for Harmonic in Main Wave Amplitude/%	Node Number of Force Wave $M$	Natural Frequency of Stator Core /Hz	Amplitude of Stator Core / $\mu\text{m}$
Before Connection Change	20	6.4	20	442.8	0.594
	50	5.28	10	109.5	45.67
	80	1.418	40	1776.1	0.008
	Total				46.3
After Connection Change	20	6.075	20	442.8	0.56
	50	0.688	10	109.5	5.95
	80	3.29	40	1776.2	0.02
	Total				6.53

**Table III Test Result for 100Hz Electromagnetic Vibration Amplitude Produced by Main Fractional Harmonic of Unit18 and Unit17**

Operation condition		point 1	point 2	point 3	point 4	removing 50 antipodal harmonic(1、3 operation)	removing 50 antipodal harmonic(2、4 operation)	Removing 20 antipodal harmonic (1、3 operation)	Removing 20 antipodal harmonic (2、4 operation)
Unit 18	700MW amplitude	47.9	41.9	21.6	47.7	10.4	4.5	35.8	41.8
unit17	500MW amplitude	36.1	43.1	42.7	51	4.7	4.9	33.2	45.0
	700MW amplitude	37.9	49.0	47.1	57.3	4.6	5.8	42.0	51.0

Through the comparison calculation analysis on several schemes, it's known that it's better to change the "10+7" big-small phase zone layout of connection in original scheme into new type big-small phase zone layout (see Table II). In this way the 50 antipodal field harmonic caused by electromagnetic vibration is significantly weakened and amplitude is reduced from 5.28% to 0.688%. Meanwhile, amplitude of 20 antipodal field harmonic is also reduced a little from 6.4% to 6.075% and calculation value for stator core vibration is also reduced from 46.3 $\mu\text{m}$  to 6.53 $\mu\text{m}$ . As the new connection mode will not bring side-effect, i.e. free of other field harmonic, this scheme is practicable and reliable.

In this changed scheme, because utilization rate for winding has reduced by 1.85%, it may cause some small change in electromagnetic parameters and temperature rise. But the calculation results indicate the change is about 1%~2%, which can only influence the main performance parameters of generator little (see table IV) .

Structure of generator will be improved as follows according to above principle and scheme:

(1) Stator bar:

For implementation of improvement scheme for 16 and 15 units with the winding not installed, with full use of primitive bar, it only needs to change the location of extraction bar in slot to improve the scheme while installing winding. For 18 and17 units, it can be improved by new design and replacement of part lead bar.

**Table IV change of parameters after connection improvement**

Item	Before	After		Item	Before	After	
Winding Coefficient Kw	0.936	0.9187	(↓1.85%)	Rated Exciting Voltage Ufn /V	389	395	(↑1.54%)
Air-gap Flux Density Bδ/Gs	9134.8	9307	(↑1.9%)	Stator Core Temperature Rise /K	30.7	31.64	(↑3.1%)
Stator toot Flux Density (Bz1/3)/ Gs	15196	15483	(↑1.9%)	Exciting Winding Temperature Rise /K	37.7	38.69	(↑2.6%)
Stator Yoke Flux Density Bj/Gs	12631	12870	(↑1.9%)	Direct-axis Synchronous Reactance Xd	0.871	0.839	
Pole Body Flux Density Bm/Gs	15744	16050	(↑1.9%)	Direct-axis Transient Reactance $X'_d$	0.305	0.293	
Exciting Winding Current Density J2/ (A/mm2)	1.85	1.875	(↑1.35%)	Direct-axis Super-transient Reactance $X''_d$	0.24	0.232	
Rated Exciting Current Ifn /A	3563	3611	(↑1.35%)	Short-circuit Ratio	1.262	1.322	

(2) Copper ring, jumper line and water conduit.

Redesign and replace the copper ring, jumper line and water conduit. The primitive jumper line is with 6 slot pitch, while 20 slot pitch after connection change.

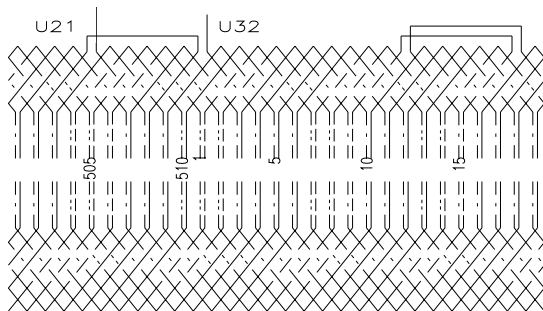


**Fig. 4 Primitive Connection Drawing (Local)**

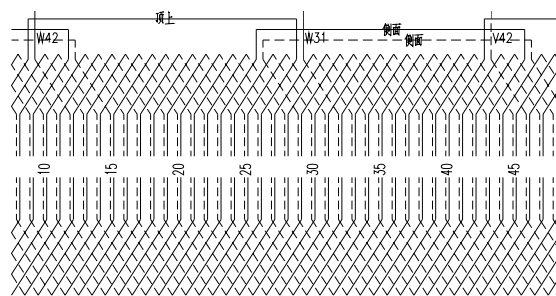


**Fig. 5 Connection Drawing (local) After Modification**

(3) Upper cover

Primitive three-section cover is formed with 48 pieces is changed into integrated cover formed with 16 pieces and its primitive thickness of 100mm is increased into 200mm, which is equivalent to that of units from other manufacturers. In this way, it can significantly weaken the vibration and noise on cover.

**3 IMPLEMENTATION EFFECT of IMPROVEMENT SCHEME for GENERATORS on RIGHT BANK POWER STATION**

Electromagnetic vibration of generators on right bank power station of Three Gorges is substantially removed and vibration, run-out and noise of units are reduced by measures of connection change, structural improvement and installation quality improvement, etc.

**3.1 General effect**

Vibration, run-out and noise of units on right bank power station of Three Gorges after improvement have met the excellent standard and can compare favourably with units from other manufacturers on right bank power station. Comparison for vibration on middle frame is shown in Table V.

- (1) 100Hz high-frequency electromagnetic vibration for generator is basically removed;
- (2) Noise of generator is significantly reduced by about 4~6dB(A);
- (3) Low-frequency vibration (1~3 multiple rotation frequency) for generator is significantly reduced by 50%~80%.
- (4) Run-out is obviously better than that of left bank units: the run-out at three guiding bearing is normally below 150um and the maximum run-out of left bank units can be 400 μm more.
- (5) Operation of units is stable and quiet. Feeling of “foot numbness” and “hum” is removed.

**Table V Comparison for radial vibration in middle of frame with rated load: m**

Unit No.	Amplitude for Total Frequency	Amplitude for 1 fr	Amplitude for 2 fr	Amplitude for 3fr	100Hz Amplitude
Unit 15	17.9	5.4	10.7	4.7	0.8
Unit 16	37.8	3.7	28.7	11.2	0.9
Unit 17 Before Improvement	50.4	7.5	14.2	13.3	6.0
Unit 17 After Improvement	36.8	6.3	18.8	15.3	1.31
Unit 18 After Improvement	65.2	7.2	21.5	38.8	1.8
Unit 18 Before Improvement	122.0	25.0	60.0	46.0	5.7
Unit 3	117.0	14.0	74.0	31.0	4.2
Unit 10	66.7	16.4	12.1	13.7	1.2

### 3.2 Improvement effect of high-frequency (100Hz) vibration

- (1) 100Hz vibration for stator core of 45~50um in primitive scheme is reduced to less than 10um, and 88% reduction is in accordance with theoretical calculation. 100Hz vibration on stator frame and neighboring components is obviously weakened, and table 6 shows the comparison on 100Hz vibration test for stator core of each unit.
- (2) Feeling of high-frequency vibration on cover and end shield has been removed.

**Table VI Comparison on test results after improvement of 100Hz vibration on stator core of generator**

Unit No.	Load (MW)	Point 1	Point 2	Point 3	Point 4	Point 5	Average
Unit 16	500	4.0	5.9	6.0	3.0	4.5	4.7
Unit 17 Before Improvement	500	36.1	43.1	42.7	51.0	36.2	41.8
Unit 18 Before Improvement	500	35.0	31.0	20.0	36.5	70.8	38.7
Unit 15	700	—	—	—	—	—	5.6
Unit 16	640	4.9	7.2	7.0	3.1	4.7	5.4
Unit 17 Before Improvement	700	37.9	49.0	47.1	57.3	43.5	47.0
Unit 17 After Improvement	700	—	—	—	—	—	4.4
Unit 1 Before Improvement	700	47.9	41.9	21.6	47.7	78.9	47.6
Unit 18 After Improvement)	703	6.2	5.7	4.1	6.1	7.8	6.0

### 3.3 Improvement effect on generator noise

(1) Noise on cover: According to Chinese national standard GB10069.2-88, 16 points measured on the circle 1m above the top cover uniformly and get the average value. With the results in Table VII, generator noise is significantly weakened. Compared with unit 18 before improvement and units on left bank power station, it has reduced by 4~6dB(A).

(2) Noise in wind tunnel: 16 points measured on 1m above the ground inside the upper wind tunnel uniformly and get the average value. The results show that primitive noise of 97.3 dB(A) in upper wind funnel before improvement is reduced after improvement to 96.2 dB(A), reduced by 1.1dB(A), in which the 100Hz noise component has reduced by 78.8%, better than units on left bank power station.

**Table VII Comparison on results of noise test on generator on left and right bank power station**

		Right Bank power Station/ DFEM Unit						Left Bank /VGS Unit		Left Bank /Alstom Unit
		Unit 15	Unit 16	Unit 17 Before Improvement	Unit 17 After Improvement	Unit 18 After Improvement	Unit 18 Before Improvement	Unit 3	Unit 7	Unit 10
Operation Condition	Active Power (MW)	697.7	640	700.2	700	750.0	700.5	679.0	679.0	700.0
	Reactive Power (MVar)	330.2	105.9	78.9	339	147.0	151.3	164.0	164.0	94.0
Average Value		74.1	76.4	77.7	76.1	76	79.2	78.9	81.8	80.3
After Background Noise Correction		72.3	73.5	75.3	73.1	73.2	78.3	78.1	/	79.5
Reduction Compared with the Primitive Before Improvement		-6.0	-4.8	-3.0	-5.2	-5.1	-	-	-	-

## 4 CONCLUSION

After implementing improvement scheme for generators on the right bank power station of Three Gorges, vibration and noise problem in unit 18 is successfully solved. What's more, solution scheme is also provided for the electromagnetic design defect found in VGS generators on left bank power station. Meanwhile, it proposes the systemic solution scheme and measures to make the vibration, run-out and noise of large hydraulic generators of or above 700MW reach a good level.

## Methods for Fixation of the Rotor Winding Overhang of Large Asynchronous Hydrogenerators

F.Neumayer, F.Ramsauer, M.Himmelreich, G. Kastner  
Andritz Hydro  
Austria

### SUMMARY

Variable speed units for pumped storage power plants are becoming state-of-the-art technology for optimized efficiency in turbine mode and a wide range of power control in pump mode. Benefits of this technology for grid operation and grid stability are already published, as well as optimization strategies for the hydraulic part.

The rotor winding is designed similar to a conventional 3-phase stator winding. This means, it consists of a two-layer bar-type winding. The bars are designed as transposed Roebel bars to minimize copper losses and insulated according to the specified test voltage with the stand-still voltage in the rotor winding as reference.

Compared to a standard high voltage winding in the stator, a major challenge is the design of the winding overhang. Required clearances and lengths of potential grading layers must be maintained, centrifugal forces at run-away speed must be withstood and sufficient and adequate ventilation must be provided.

In the past, ANDRITZ HYDRO provided a supporting system consisting of shrink-on outer retaining rings made of non-magnetic steel, inner support rings and a very special design of spacers inbetween the winding bars. This complex system enabled necessary support, proper cooling and protection of the high voltage insulation against mechanical damage. It also minimized relative movement between the laminated rotor body and the rotor winding. One of the most critical tasks was the forging and machining process of the rings given the precise requirements for material specification, dimensioning and accuracy. In a prior publication Scherer [1] presented some aspects and challenges for the design of the motor-generators including a description of retaining ring design.

In order to avoid the difficult and expensive manufacturing process of the shrink-on solution, ANDRITZ HYDRO developed a system using a large number of U-bolts supporting the bars. To provide the same functionality as that of the shrink-on ring mentioned above, a number of investigations were carried out.

These analyses include detailed mechanical simulations of load cycling and failures in combination with thermal stress and detailed ventilation calculations for different rotational speeds using *CFD* codes.

### KEYWORDS

Asynchronous, Variable Speed, Generator, Motorgenerator, Overhang, Rotor, Winding, Retaining, U-bolt, Shrink-On

## 1 MECHANICAL LAYOUT

Although variable speed pumped storage units undergo fewer start-stop cycles than synchronous units [2], their design must still allot for rigorous centrifugal load and temperature load cycling. Resultant alternating shear and tensile stresses within the high voltage insulation need to be minimized to avoid excessive fatigue.

Differential radial growth over the axial length due to centrifugal load may lead to shear and bending stress.

In order to minimize bending stresses of the Roebel bars in the overhang region, a pre-stressed system is needed. The required pre-tension may be achieved through two primary design solutions as described below. “Shrink-on retaining ring design” involves thermal shrinking of a steel ring and “U-bolt design” involves bolting bars towards inner retaining rings.

The former solution was successfully applied at the GOLDISTHAL pumped storage scheme in Germany and has proven a solid and reliable design over several years.

### 1.1 Shrink-on Retaining ring design

Except for the significantly larger dimensions of the shrink-on retaining ring, this solution is similar to the one used in turbo-generators. The main difference lies in the application of an inner ring. The properties of this ring are chosen in such a way that the expansion of the inner ring due to centrifugal load is similar to that of the rotor rim.

The parts involved in the mechanical system are depicted in Fig. 1.

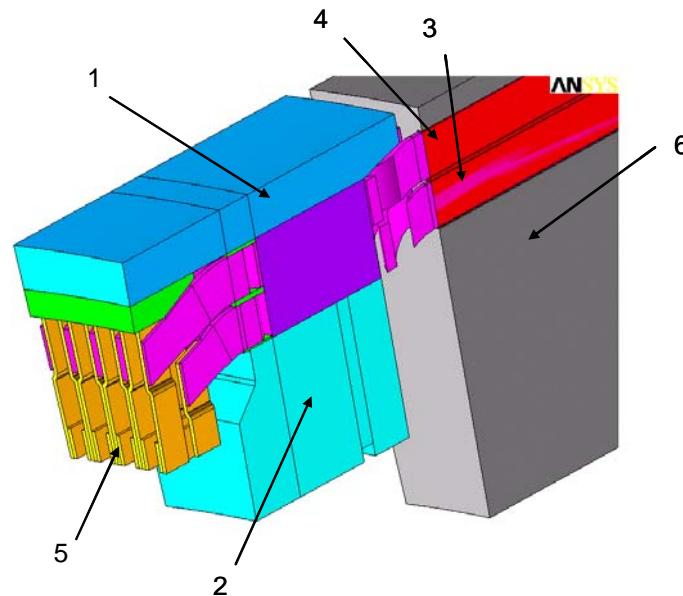


**Fig. 1 Parts of the Shrink-On Retaining Ring Winding Overhang Support System – Axonometric View.**

In the region of the laminated rotor body (6) the winding upper (4) and lower (3) bars are fixed in slots whereas in the winding overhang portion these bars are positioned between an outer (1) and an inner (2) ring.

Specially formed copper connectors (5) are brazed between the bars of the upper and the lower winding layers. Between the bars special rectangular profiles made of aluminium carry the radial compressive forces applied through the shrink fit. The bars are somewhat smaller in radial dimension than the aluminium profiles such that the bars will not be stressed due to the compressive shrink forces. Since this kind of assembly requires high dimensional accuracy, the bars have to be calibrated not only in the slot region of the rotor but also in the end winding region.

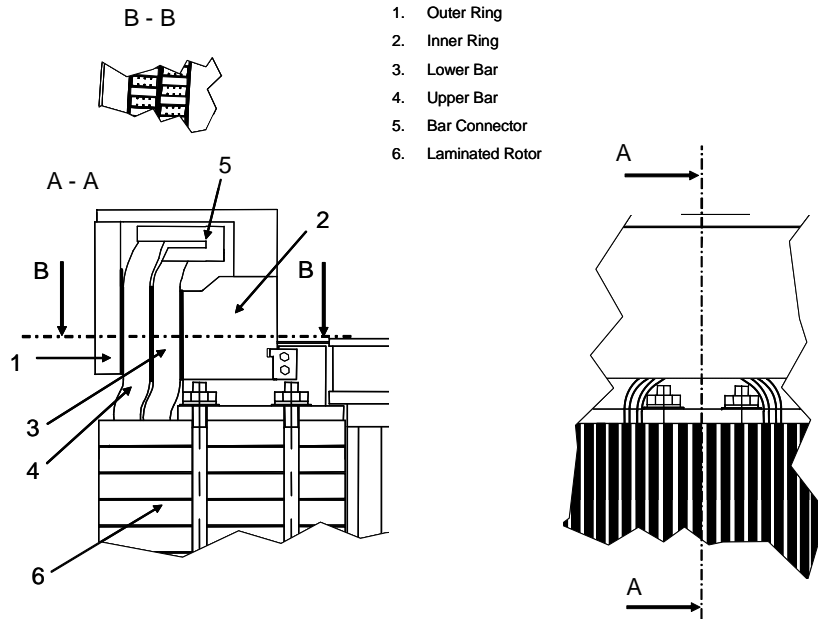


Fig. 2 Parts of the Shrink-On Retaining Ring Winding Overhang Support System – Sectional Views.

### 1.2 U-bolt design

An illustration of the design solution using U-bolts is shown in Fig. 3. Roebel bars (1) leaving the laminated rotor body (2) are supported by U-bolts (3) in the end winding region. These bolts are attached to retaining rings (4). Axial spacer plates (5) are mounted between two rings each and welded to both rings. Upper and lower bars are electrically connected via brazed-on copper plates. Special composite insulation caps (8) ensure radial support. These caps are held in position by hooking up to a groove formed by a two-part ring structure (6). The filling material of the caps is reinforced with randomly oriented glass fibres.

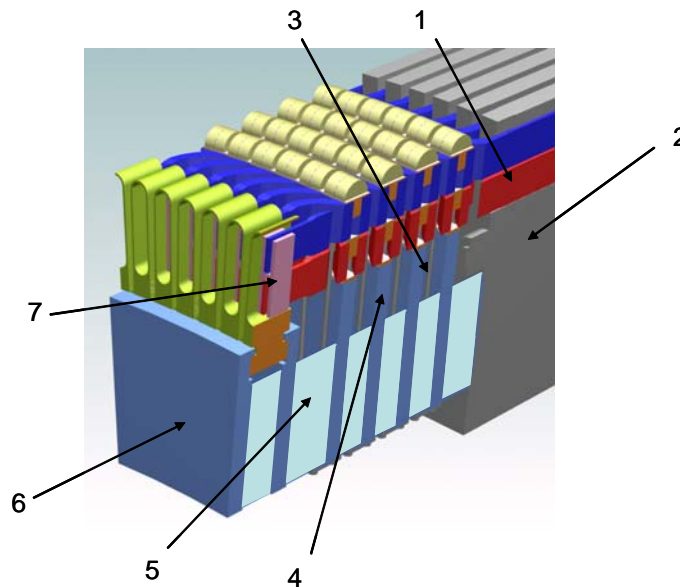


Fig. 3 Parts of the Winding Overhang Support System with U-Bolts.

The U-bolts, as shown in Fig. 4, are carefully pre-tensioned in such a way that compressive contact will be maintained up to runaway speed. For this purpose, nuts (9) at the inner ends of the U-bolts (5) have to be attached using a special hydraulic tensioning device. To avoid loosening of the nuts, securing plates (7) are used that secure two nuts each. The two nuts belong to the legs of two different U-bolts so that the two legs of individual U-bolts are electrically insulated from each other. This is

required to avoid looping currents in the U-bolts that might cause excessive heating and a loss of pre-tension.

The pre-tensioning of the long bolts at standstill causes a relatively constant tension of the bolts during start-stop cycles.

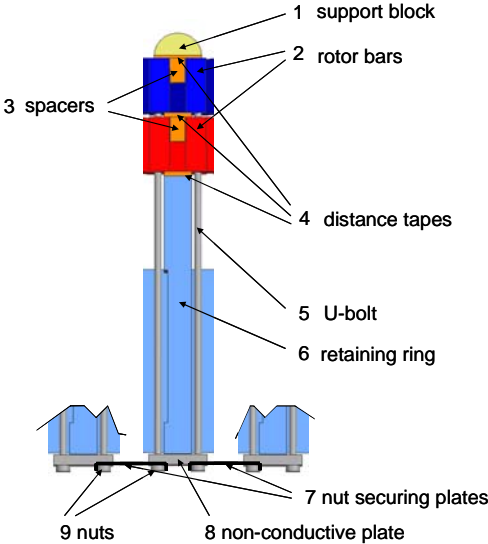


Fig. 4 U-Bolt Assembly.

The mechanical behaviour of the winding overhang under centrifugal load was carefully investigated using Finite Elements. Individual, optimised pre-tension was applied on each of the bolt rows. Fig. 5 shows the result of such an *FEM* calculation. Edges are plotted for the zero speed case and at runaway speed. Coloured contours contain data of radial displacement at runaway speed. The result indicates that the growth of the overhang is almost constant, approximately 2.5 mm, over the axial length. Maximum bending deflections of individual bars are limited to 0.5 mm. At nominal speed the radial bending is even lower.

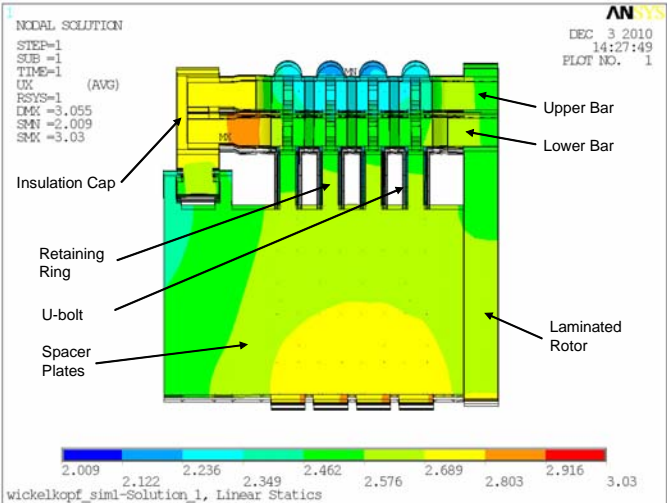
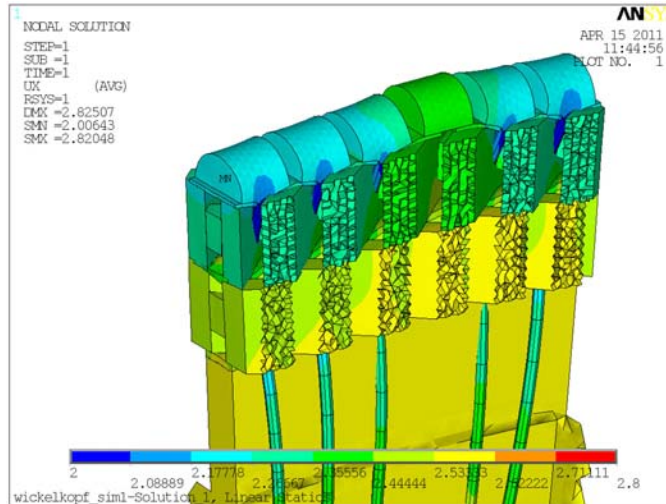


Fig. 5 Calculation Result of FEM Calculation Showing Radial Growth due to Centrifugal Load.

**1.3 Broken bolt test case**

Even though the bolts are designed to withstand an enormous number of cyclic loads, the case was investigated in which one leg of a single U-bolt fails. Fig. 6 shows the radial deformation of a portion of the winding overhang model with one missing U-bolt due to centrifugal forces at runaway speed. This picture illustrates that the deformation of the rotor bars at the location with the missing U-bolt are only 0.1 mm larger than at other positions.



**Fig. 6 Deformations of the Winding Overhang with a Broken Bolt due to Centrifugal Forces and Runaway Speed.**

Fig. 7 shows the distribution of tensile forces of the bolts at runaway speed. The bar plot to the left is the control case with all bolts intact. Forces are constant about the circumference. The bar plot to the right is the test case with a missing U-bolt toward the slip ring side. The distribution of bolt loads is no longer constant over the circumference. Neighbouring bolts have to carry additional loads. Also, at the neighbouring axial positions, U-bolts have to carry higher tension.

A detailed evaluation of the tensioning forces of the U-bolts surrounding the missing U-bolt shows that the maximum loaded U-bolt is loaded only 3% higher than the maximum loaded bolts in the control case.

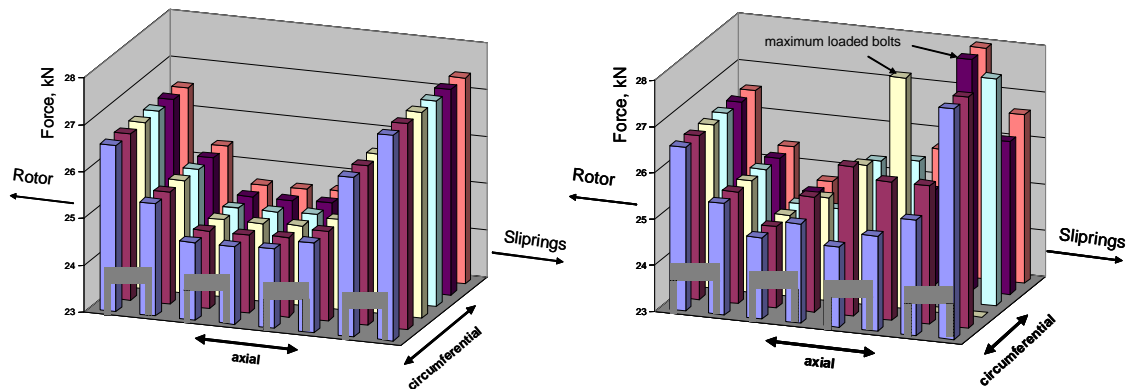


**Fig. 7 Calculation Result of FEM Showing Tensile Forces in the Bolts at Runaway Speed. Left: All U-bolts Tensioned. Right: One U-Bolt Missing.**

Another analysis demonstrated that if one leg of a U-bolt breaks, the second leg is capable of carrying the centrifugal load of the whole U-bolt, thus holding it safely in place.

## 2 VENTILATION LAYOUT

### 2.1 Shrink-on retaining ring design

As indicated in Fig. 8 Left, air is pumped by a radial fan to the winding overhang where the airflow is split. One part is pressed into the hollow aluminium profiles which are situated in-between the bars. Ribs inside the profiles which can be seen in section B-B of Fig. 2 significantly increase the heat transfer surface. The air flows through the profiles axially, passes the bar connections and leaves the rotor.

The other part of the airflow is aimed to cool the stator winding overhang and pressing plates before entering the stator housing cavity through adjustable bypass holes.

## 2.2 U-bolt design

Spacer plates between the retaining rings are positioned in axial-radial planes. The example has 48 spacers along the circumference. These plates create a radial pressure rise, similar to a radial fan. In this way, cold air is pumped first through the spacing between the rings and second through the array of lower and upper bars. Afterwards, the air flows through the overhang of the stator winding. This case is also shown in Fig. 8 Middle. The sizing of the flow areas between the rings controls the amount of volume flow and therefore temperatures and losses. These effective flow area can be controlled by use of simple covers at the hub of the retaining rings.

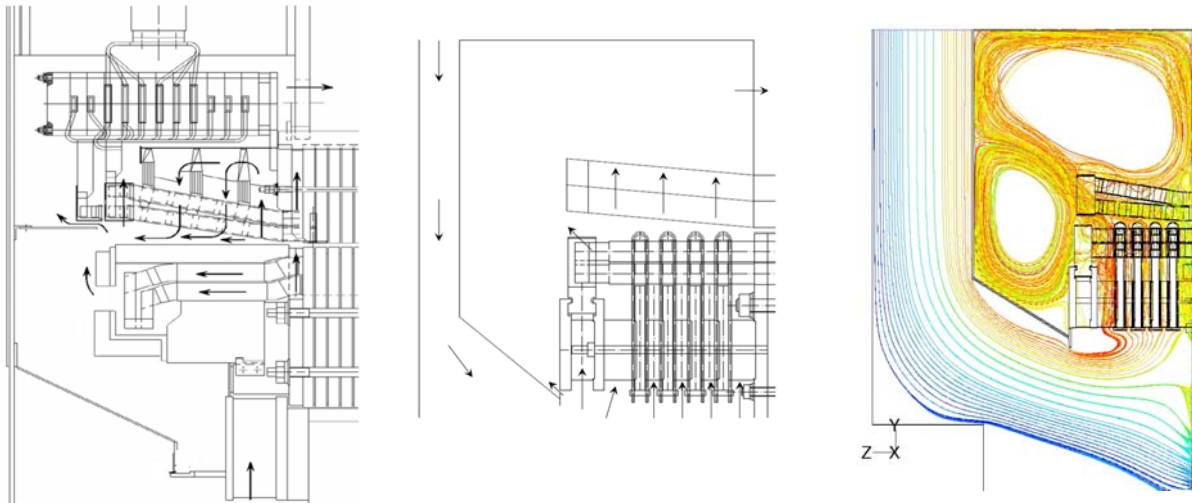


**Fig. 8 Left: Ventilation Air Circuit of the Shrink-On. Middle: Ventilation Air Circuit of the U-Bolt Solution. Retaining Ring Design Solution. Right: Ventilation Flow Path Lines of the U-Bolt Solution.**

Extensive CFD analysis for both solutions was performed. Fig. 8 Right shows a synopsis of the resulting ventilation path lines for the U-bolt option. Air flow begins at the CFD model inlet and is coloured by Particle ID.

## 3 INSULATION LAYOUT

Rotor windings of large double-fed asynchronous generators are designed at voltages of several kV. Special attention must be paid to voltage peaks caused by frequency converters.

### 3.1 Shrink-on retaining ring design

The outer corona protection that is typically only applied in the slot region of the rotor is required in the end winding region as well. Potential grading coating ensures a continuous raise of potential from the end of the aluminium profiles to the end of the bar insulation. The red area in Fig. 9 indicates the position of the grading coating. To ensure a compact fit of the bars in the winding overhang, necessary for sufficient heat transfer, the bars have to be geometrically calibrated in this region.

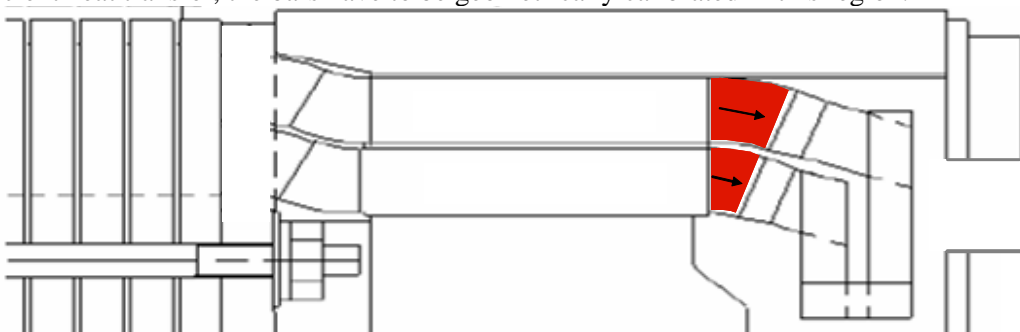


**Fig. 9 Potential Grading Coating.**

**3.2 U-bolt design**

Similarly for the U-bolt design, due to the presence of metal bolts, an outer corona protection has to be applied in the end winding region. In contrast to the shrink-on retaining ring solution, the bars do not have to be geometrically calibrated in the winding overhang portion. Potential grading coating is applied from the position of the last U-bolt to the end of the bar insulation near the brazing of the bar connectors. (See Fig. 10.)

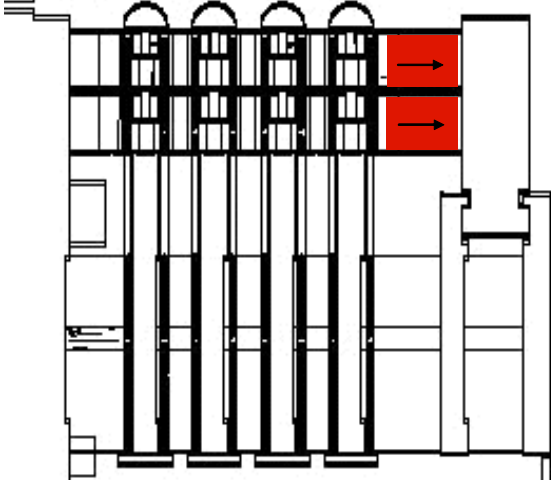


**Fig. 10 Potential Grading Coating.**

**4 CONCLUSIONS**

Pros and cons of the two support systems for rotor end windings of asynchronous hydrogenerators are listed in Table I.

**Table I Design Comparison.**

	Shrink-On Retaining Ring Design		U-Bolt Design
-	complicated fabrication of ring, few suppliers	+	simple parts, easy to manufacture
-	difficult shrinking process	+	easy assembly
+	quicker assembly	-	time-consuming assembly
-	limited diameter	+	unlimited diameter
+	few parts	-	high number of parts
+	no radial compression forces on bars	-	radial compression forces on bars
-	smaller airflow cross-sections	+	higher airflow due to larger flow cross-sections
-	indirect cooling of bars via aluminium profiles	+	good cooling of bars due to direct convection

Alternative solutions have been developed for large diameter machines where shrink-on retaining rings are difficult to build. However, for small diameter generators, the shrink-on retaining ring design remains an attractive, proven option.

For each project the two designs must be carefully weighed against each other in terms of design safety, procurement and manufacturing costs in order to select the optimum solution.

**BIBLIOGRAPHY**

- [1] Amler P. New Opportunities for Pump Storage//HYDROVISION RUSSIA 2011 Conference, Moscow, Russia
- [2] Scherer K. Variable Speed Units for Pumped Storage Power Plants// HYDRO 2004 Conference, Porto, Portugal
- [3] Stein G, Sertorio M, Kirchengast R. The biggest Retaining Ring ever made out of high Nitrogen Steel for 300 MW Asynchronmotors/ Generators in a Pumpstorage Power-Plant//15<sup>th</sup> International Forgemaster Meeting, Kobe, Japan ,2003



Beijing, China

SC A1  
COLLOQUIUM ON NEW DEVELOPMENT OF ROTATING  
ELECTRICAL MACHINES

11~13 September, 2011

---

**Inter-turn Short Circuit of Field Winding in Synchronous Machines**

**Sun Yuguang, Hao Liangliang ,**

**Sun Yutian**

**Wang Xiangheng**

**Dept. of Electrical Engineering,  
Tsinghua University,**

**Harbin Research Institute of  
Large Electrical Machinery**

**Beijing, China**

**Harbin, China**

**SUMMARY**

When inter-turn short circuit fault occurs in the field winding of a synchronous machine, the field current will increase and the reactive power output will decrease, aggravating the rotor vibration. Such faults will become to more severe accidents if they are not handled properly in a timely manner, which will effect the safe and stable operation of the machine and the electric power system. Existing research follows the experimental detection and qualitative analysis approaches, which are subject to practical limitations due to the fact that the fault current is not able to be calculated accurately. This paper sets up an extended multi-loop mathematical model for calculating all the currents of stator and rotor during the whole fault for the multi-branch synchronous machine with inter-turn short circuit of field winding, which considers the spatial harmonics of air-gap magnetic field, the unbalanced currents inside the phase windings, and changes of topological structure in excitation circuits due to the rotor faults. In addition, the field winding inter-turn faults experiments have been carried out on a 12kW model machine with three pairs of non-salient poles. The experiment data of both transient and steady-state processes coincide well with the simulation results obtained from the above mathematical model, which verifies the correctness of the mathematical model and accuracy of the simulation program. Based on the simulation and experiment results on the model machine, it is found that the characteristics of inter-turn faults in field windings are different from other faults such as stator internal short-circuits and external short-circuits in the terminal of synchronous machine. In fact this rule could be applied to most synchronous machines and inspire new ways to fault detection.

**KEYWORDS**

Synchronous machine, Inter-turn short circuit of field windings, Extended multi-loop mathematical model, Fault characteristics.

## 1 INTRODUCTION

Field winding short circuits occur frequently in synchronous generators, mostly due to abrasion of turn insulation caused by defective manufacture combined with mechanical, electromagnetic, or thermal forces in operation<sup>[1][2]</sup>. The slight faults of inter-turn short circuits in field windings usually produce unnoticeable change to the operation of the generator in a short term. If left unattended, the faults may develop progressively, causing field current increase, reactive power output decrease, and rotor vibration aggravation<sup>[3][4]</sup>. Local overheating in the short-circuit turns may lead to rotor one-point or even two-point earth fault, which then damages the rotor forging and even magnetizes the rotor shaft. In more severe conditions the shaft neck and bearing would be burned out, which threatens the safe and stable operation of the machine and the electric power system seriously.

If the inter-turn short circuit faults of field windings could be detected at their early stages and be monitored to determine when to maintain the machine, it is possible to avoid serious more faults such as earth faults. In order to effectively monitor and detect rotor inter-turn faults, the fault characteristics should be found out including the accurate distribution and variation rules of all the electrical state quantities of the machine during the faults.

Many researchers have pursued diagnostic approaches based on field current monitoring<sup>[5,6-8]</sup>. [6,7] analyzed the harmonic characteristics of field current in synchronous machines with inter-turn short circuit of field windings. However, compared with DC component of field current, the variety of AC components arising from inter-turn field windings faults are too small to serve as signature to distinguish the field winding faults from other types of faults, such as stator internal short-circuits<sup>[9,10]</sup> and external short-circuits outside of synchronous machine<sup>[11]</sup>, etc. In fact, the inter-turn short circuits of field windings lead to the asymmetry between the parallel branches in the same phase, which induces the circulating currents inside phase windings of the stator. Kryukhin first suggested that the inter-turn faults of field windings could be detected by measuring the even harmonic circulating currents between the two parallel branches in turbo-generators<sup>[12]</sup>, which has been applied on a number of turbo-generators in UK<sup>[13]</sup>. [14] also analyzed the harmonic characteristics and production mechanism of stator circulating currents in the typical two-pole turbo-generators with rotor faults. However, in most of the multi-pole generators with rotor faults, the circulating currents flowing inside phase windings not always contain even harmonics, some fractional harmonic currents usually occur with relatively high amperage<sup>[6,15,16]</sup>, which requires further study. In addition, measuring vibration of the machine offers another means of faults detection<sup>[4][17]</sup>, although up to now the cause of vibration may be difficult to distinguish from a wide variety of fault types including the electrical faults and mechanical ones. Furthermore, the characteristics of shaft voltage under inter-turn faults of field windings are also described in [18][19].

In summary, existent research on inter-turn short circuits of field windings has mostly resorted to experiments, on-site detection and qualitative analysis, and results from practical applications are still limited. If accurate distribution and variation rules of all the electrical state quantities of the machine during the faults could be worked out, the detecting approaches will be able to improved and effective monitoring schemes against the rotor inter-turn faults designed.

This paper proposes a digital simulation method for the multi-branch generator with field winding inter-turn short circuit faults. Currents flowing in all the parallel stator branches and rotor windings can be calculated accurately during the whole faulty process. Moreover the experiments on a model machine support the mathematical model and the according simulation program. Based on the simulation and experiment results on the model machine, it is found that the characteristics of inter-turn faults in field windings are different from other faults such as stator internal short-circuits<sup>[20-22]</sup> and external short-circuits in the terminal of synchronous machine<sup>[20]</sup>. In fact this rule could be applied to most synchronous machines and inspire new ways to fault detection.

## 2 MODELING OF SYNCHRONOUS GENERATOR WITH INTER-TURN SHORT CIRCUITS OF FIELD WINDING

In general, the inter-turn short circuits lead to the structure differences between field windings on every poles of the generator, the electric parameters will no longer be symmetrical. This asymmetrical

structure and parameters induce the distortion of air-gap magnetic field and circulating currents inside the phase windings, which makes it inappropriate to employ either the  $d,q,0$  coordinates system based on the ideal electric machine model or the phase coordinates method.

Considering the electric machine as the circuit consisting of many loops having relative motion, the Multi-Loop Method<sup>[20]</sup> analyzes the electro-magnetic relations of AC machine according to the actual loops of stator and rotor windings. For inductance parameters in the Multi-Loop mathematical model, the inductance of individual coils are derived firstly, then all the loop inductances could be worked out by superposition according to the actual connection. Then the currents and voltages distribution of all the stator branches and rotor windings could be solved numerically by Multi-Loop Method, which reckons in all the space-harmonics of air-gap magnetic field in AC machines. By now Multi-Loop Method have succeeded in the analysis of armature internal faults<sup>[20-22]</sup>, and that could also be used to study into the rotor windings thoroughly. So Multi-Loop Method is suitable to the calculation of inter-turn short circuits of field windings in synchronous machine as well.

This paper extends the multi-loop mathematical model of synchronous machine which is detailed in [20] to calculate all the electrical state variables under inter-turn short circuit of field windings including the currents of stator and rotor windings. In a general way, this paper only considers the machines with single-parallel field winding, and takes example for the single short-circuit loop.

## 2.1 Voltage equations of stator loops

The inter-turn short circuit in field winding induces unbalanced currents circulating between the branches in the same phase. Taking example for the stator winding with two parallel branches per phase shown in Fig.1, the currents of two branches in phase A are no longer equal due to the field winding fault, and other phases likewise, i.e.,  $i_1 \neq i_2$ ,  $i_3 \neq i_4$ ,  $i_5 \neq i_6$ . Considering the armature windings without neutral line, since the currents of three phases sum to 0, there are only 5 independent variables in stator currents. The 5 loop currents are selected as the independent variables in this paper shown in Fig.1, in which the dashed arrows and numbers in brackets represent the positive direction and sequence number of stator loops, while the straight arrows and numbers nearby represent the positive direction and sequence number of stator branches. Suppose that the three-phase machine has  $n$  parallel branches per phase, then the loop number  $N_s$  of stator winding in the Multi-Loop mathematical model is:

$$N_s = 3n - 1$$

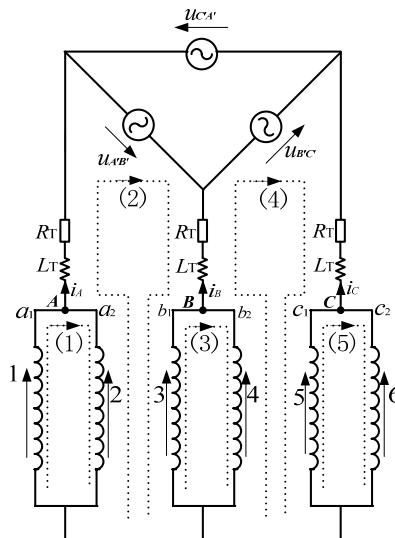


Fig. 1 Stator Loops

Taking the loop currents as the variables, the voltage equations for stator loops is then given in the following matrix form:

$$[U_\infty] = p[\Psi'_s] + [R'_s] \cdot [I'_s] + [M_{s,T}] p[I'_s] + [R_{s,T}] [I'_s] \quad (1)$$

where  $[U_\infty]$  is the known  $N_S$ -rank vector representing the line voltages of the power network;  $[\Psi'_S]$  and  $[I'_S]$  are the unknown  $N_S$ -rank vectors representing the flux-linkages and currents of the stator loops; as for the three  $N_S$ -rank constant square matrixes,  $[R'_S]$  is the loop resistance matrix,  $[M_{S,T}]$  and  $[R_{S,T}]$  represent the action of inductance and resistance of the supply side transformer.

## 2.2 Voltage equations of field winding with inter-turn short circuit

On fault condition the field winding has two independent loops. The normal field loop and the fault additional loop shown in Fig. 2 are selected in this paper, in which the current  $i_f$  and  $i_{fkL}$  flow respectively. The voltage equations of field winding are given by:

$$\begin{bmatrix} E_{ZF} \\ 0 \end{bmatrix} = p \begin{bmatrix} \psi_f \\ \psi_{fkL} \end{bmatrix} + \begin{bmatrix} r_f + R_{ZF} & r_{fk} \\ r_{fk} & r_{fk} + R_{fkL} \end{bmatrix} \cdot \begin{bmatrix} i_f \\ i_{fkL} \end{bmatrix} \quad (2)$$

where  $\psi_f$  and  $\psi_{fkL}$  are the flux-linkages of the normal loop and the fault additional loop in field winding respectively;  $r_f$  and  $r_{fk}$  are the resistances of the normal loop and the short-circuit turns in field winding;  $E_{ZF}$  and  $R_{ZF}$  are the EMF and the internal resistance of the field power supply;  $R_{fkL}$  is the short-circuit transition resistance which could be ignored in case of metallicity short circuit.

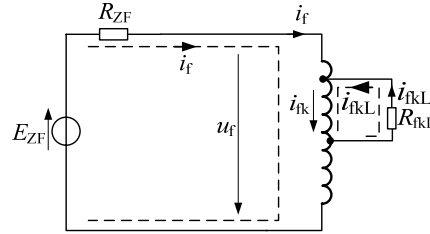


Fig. 2 Loops of Field Windings with Inter-Turn Short Circuit

## 2.3 Voltage equations of damper circuit loops

Considering the space-harmonics of air-gap magnetic field which contains the even harmonics and fractional harmonics (in multi-pole machine) besides the fundamental and other odd harmonics components, the practical mesh circuit of damper loops are selected in this paper as shown in fig.3. The voltage equations of these damper loops are

$$\begin{bmatrix} 0 \\ 0 \\ \vdots \\ 0 \\ 0 \end{bmatrix} = \begin{bmatrix} u_{d,1} \\ u_{d,2} \\ \vdots \\ u_{d,N_d-1} \\ u_{d,N_d} \end{bmatrix} = p \begin{bmatrix} \Psi_{d,1} \\ \Psi_{d,2} \\ \vdots \\ \Psi_{d,N_d-1} \\ \Psi_{d,N_d} \end{bmatrix} + [R_d] \cdot \begin{bmatrix} i_{d,1} \\ i_{d,2} \\ \vdots \\ i_{d,N_d-1} \\ i_{d,N_d} \end{bmatrix} \quad (3)$$

where  $[R_d]$  is the damper loop resistance matrix as follows:

$$[R_d] = \begin{bmatrix} r_{d,1} & -r_{c,2} & & -r_{c,1} \\ -r_{c,2} & r_{d,2} & \ddots & \\ & \ddots & \ddots & \\ & & r_{d,N_d-1} & -r_{c,N_d} \\ -r_{c,1} & & -r_{c,N_d} & r_{d,N_d} \end{bmatrix}$$

where  $r_{c,i}$  is the resistance of the  $i$ -th damper bar,  $r_{e,i}$  is the resistance of the  $i$ -th damper end ring,  $r_{d,i}$  is the resistance of the  $i$ -th damper loop expressed by

$$r_{d,i} = r_{c,i} + r_{c,i+1} + 2r_{e,i}$$

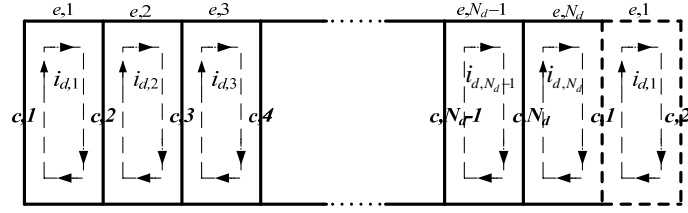


Fig. 3 Damper Loops in Rotor

## 2.4 State equations with variables composed of all stator and rotor loops currents

The voltage equations of all the loops in stator and rotor numbered (1) to (3) can be assembled into matrix form as follows:

$$[U] = p[\Psi'] + [M_T]p[I'] + ([R'] + [R_T])[I'] \quad (4)$$

where  $[\Psi']$  and  $[I']$  are column vectors representing the flux-linkages and currents of all the loops in stator and rotor,  $[U]$  is a known column vector composed of the voltages of the power network and field power supply,  $[R']$  is the loop resistance matrix,  $[M_T]$  and  $[R_T]$  are square matrixes with constant parameters that are related to the inductance and resistance of the supply side transformer as well as internal resistance of the field power supply.

In this paper the referential direction for currents and flux linkages is set that a positive current excites a positive flux linkage in all the loops. Therefore the flux linkages of all the loops in the Multi-Loop mathematical model could be expressed in the following matrix form:

$$[\Psi'] = [M'] \cdot [I'] \quad (5)$$

where the square matrix  $[M']$  represents the loop inductance matrix which is time-varying due to the relative movement between stator and rotor.

Substitute Eq. (5) into (4), then the state equations are obtained considering the currents of all the loops in stator and rotor as state variables

$$[U] = ([M'] + [M_T])p[I'] + (p[M'] + [R'] + [R_T])[I'] \quad (6)$$

This is a differential equation set with time-varying coefficients and can be solved by numerical method such as Longe-Kutta iteration algorithm. So all the currents and voltages of stator and rotor windings can be obtained, including both steady-state and transient ones under inter-turn short circuit of field winding.

## 2.5 Multi loop inductances for field winding inter-turn short circuit

It is necessary to calculate the time-varying loop inductance matrix  $[M']$  accurately for solving the mathematical model expressed in Eq.(6), especially for the inductances relating to the field winding with inter-turn faults. By means of the air-gap permeance analysis, [20] has calculated all the inductances in case of normal windings and internal faults in stator windings. In calculation of the inductances relating to the stator windings with internal faults, the inductances of a single armature is firstly worked out, then the loop inductances are obtained by superposition according to the actual connection of the stator loops.

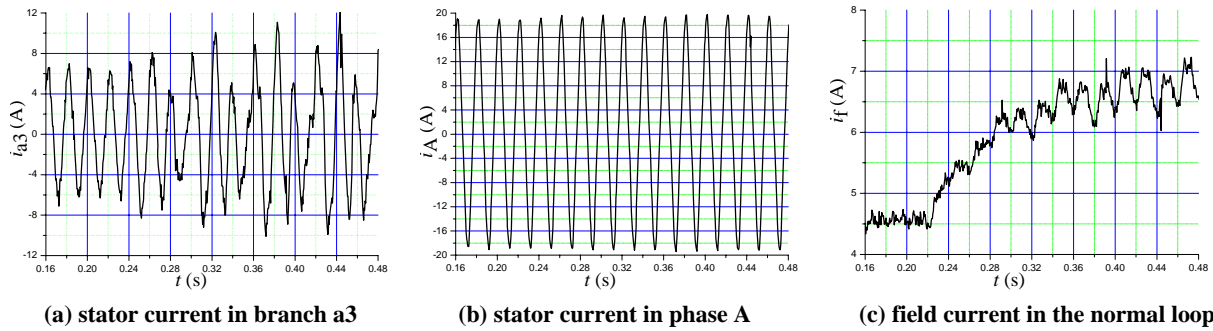
In the extended Multi-loop mathematical model proposed in this paper, the characteristics (such as periodicity) and calculation method of inductances relating to the imperfect field winding are different from those under normal condition as well as the stator internal faults, since the rotor inter-turn short circuit faults lead to the differences of field winding structure on every pole and break the symmetry in the electrical parameters. Focusing on the single-turn coil of the concentrated field winding on each salient pole of the hydro-generator, or the concentric coil with different pitches of the distributed field winding on each non-salient pole of the turbo-generator, the inductances relating to single field coil are worked out firstly. Then the inductances relating to the field loops are calculated by superposition

according to the actual connection of the normal loop and the fault additional loop in field winding. For the size of the paper, the derivation of the inductances calculation is not detailed in this paper.

As we know, the mutual inductances between stator and rotor windings are time-varying. The calculation results show that the variation periodicity of the mutual inductances between stator loops (or branches) and the fault additional loop in field winding is  $2P\pi$  in electrical radian, which is different from that relating to the normal loop of the field winding.

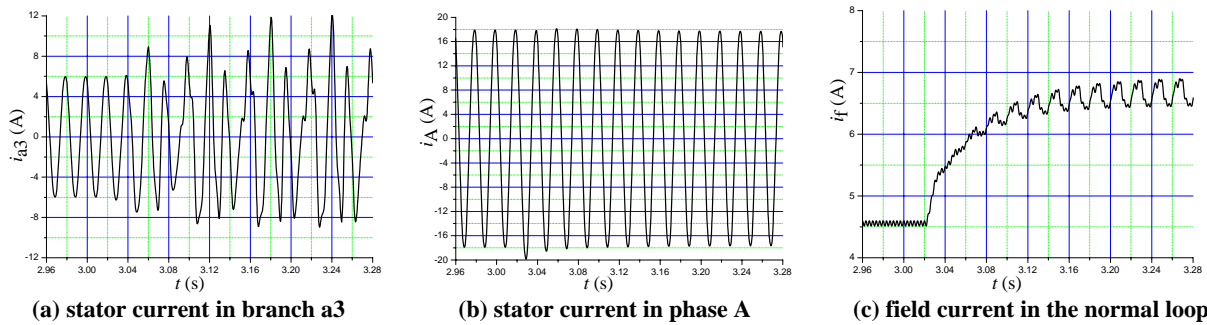
### 3 EXPERIMENT AND SIMULATION

A specialized three-pair non-salient pole synchronous machine labeled A1553, which has 5 extra taps within the field winding besides the two terminal taps to join to the individual posts on the control panel outside the machine through the brushes, has been tested with inter-turn short circuit in the field winding. Fig.4 shows the transient waveforms of stator current and field current during the field winding 43.5% inter-turn short circuit fault, in which the machine operated normally on load condition connected to network during  $t=0s\sim 0.225s$ , and the fault occurred on  $t=0.225s$ .



(a) stator current in branch a3 (b) stator current in phase A (c) field current in the normal loop  
**Fig. 4 Experimental Currents Waveforms of A1553 Model Machine with Field Winding 43.5% Inter-Turn Short Circuit on Load Condition Connected to Network**

Following the extended multi-loop mathematical model, digital simulation is conducted on A1553 model machine to obtain all the currents in stator and rotor windings throughout the fault. Fig.5 shows the simulation currents waveforms corresponding to the experiment in Fig.4, in which the fault is supposed to occur when  $t=3.022s$ .



(a) stator current in branch a3 (b) stator current in phase A (c) field current in the normal loop  
**Fig. 5 Simulation Currents Waveforms of A1553 Model Machine with Field Winding 43.5% Inter-Turn Short Circuit on Load Condition Connected to Network**

It is found that each experimental waveform in fig.4 corresponds well to the simulation result in fig.5 throughout the fault. The experiments on the model machine support the extended multi-loop mathematical detailed in section II, as well as the according simulation program, which is an effective means for research on fault monitoring and detection.

### 4 STEADY-STATE CURRENTS CHARACTERISTICS OF THE INTER-TURN FAULTS IN FIELD WINDING OF A1553 MODEL MACHINE

Fig.4 and fig.5 show that both the circulation currents in the same phase and the field currents increase gradually to reach the steady-state after the inter-turn short circuit in the field winding. So the steady-state currents have more significant meaning than the transient ones in fault monitoring and detection for inter-turn short circuit of field winding.

It is evident from Fig.4 and fig.5 that the periodicity of the steady-state fault currents in stator branches is 60ms instead of 20ms, i.e.,  $P$  times fundamental periodicity, in which  $P=3$  is pole-pair number of the model machine. Through FFT analysis on the steady-state waveforms of fault currents during  $P$  times fundamental periodicity, all the AC components with different frequencies could be calculated for both calculation and experiments. Then the steady-state fault characteristics of inter-turn short-circuits in field winding of A1553 model machines are concluded as follows:

(1) Circulation currents appear among branches of the same phase, which consist of only fractional harmonic components.

(2) After the faults, the phase currents mostly consist of fundamental frequency components with little change in their effective values.

(3) The major component of the field current is DC component, which increases obviously after the fault. The AC components of the field current only contain the fundamental and integer harmonic components, such as 2<sup>nd</sup> and 3<sup>rd</sup> harmonics, with minor effective values.

As we have known, under the occurrence of external faults at the stator terminals of the multi-branch machine, such as 2-phase short circuit<sup>[20]</sup> and single-phase short circuit, the branch currents are still balanced in the same phase, and only even harmonics exist in the field currents besides the DC component. As for the stator internal asymmetric faults<sup>[20-22]</sup> and rotor static eccentricity fault<sup>[23]</sup>, the unbalanced branch currents have only the fundamental and other odd harmonics, and the field current has only the even harmonics besides the DC component. As mentioned above, these fault characteristics of steady-state currents have many differences from those under field winding inter-turn short circuit, which may provide some clues for the fault monitoring and detection.

## 5 CONCLUSIONS

This paper sets up an extended multi-loop mathematical model for inter-turn short circuit of field winding in synchronous machines, by which all the currents in stator and rotor windings during the whole fault could be obtained. Supported by the experiments on a model machine, the mathematical model and the simulation program could act as an effective means for research on fault monitoring and detection.

The digital simulation and experimental results both indicate that, in the steady-state of the A1553 model machine after the rotor inter-turn fault, the circulation current inside each phases of stator consists of fractional harmonics, while the rotor current consists of the fundamental component and other integer harmonics, which is different from other faults such as stator internal short-circuits<sup>[20-22]</sup>, rotor eccentricity<sup>[23]</sup> and external short-circuits outside of synchronous machine<sup>[20]</sup>. These fault characteristics may provide some clues for the fault monitoring and detection of rotor inter-turn short-circuits.

## BIBLIOGRAPHY

- [1] Peter J T, James P. Condition monitoring of electrical machines. Hertfordshire:Research Studies Press,1987
- [2] Li W.Fault check and prevention of turbo generator.Beijing:China Electric Power Press,2002:80-81
- [3] Ramirez-Nino J, Pascacio A. Detecting Interturn Short Circuits in Rotor Windings.IEEE Computer Applications in Power, 2001, 14(4): 39-42
- [4] Huang H, Zhang K, Zhang Y. Detection of turbine generator field winding serious inter-turn short circuit based on the rotor vibration feature[C]//Universities Power Engineering Conference (UPEC), 2009 :Proceedings of the 44th International: 1-5
- [5] Streifel R J,Marks R J II,EI-Sharkawi M A.Detection of shorted-turns in the field winding of turbine-generator rotors using novelty detectors—development and field test. IEEE Transactions on Energy Conversion,1996,11(2):312-317

- [6] Penman J, Jiang H. The detection of stator and rotor winding short circuits in synchronous generators by analyzing excitation current harmonics[C]//Opportunities and Advances in International Electric Power Generation,18-20 March 1996,(419):137-142
- [7] Neti P, Nandi S. Analysis and modeling of a synchronous machine with structural asymmetries//Proceedings of 2006 IEEE Conference on Electrical and Computer Engineering, Ottawa, May 2006:1236-1239
- [8] Kim Y, Kim J, Yoon B, Lee S, Jung T. Detection of Shorted-Turns in the Rotor Winding of Cylindrical Synchronous Generators Using Discrete Wavelet Transform[C]//Proceeding of APEC'06:IEEE Applied Power Electronics Conference and Exposition, Dallas, TX, United states, 2006:1582-1586
- [9] Wang X, Chen S, Wang W, et al. A study of armature winding internal faults for turbogenerators [J].IEEE Trans. on Industry Applications,2002,38(3): 625-631
- [10] Wang X H, Sun Y G, Ouyang B, et al. Transient behavior of salient-pole synchronous machines with internal stator winding faults [J].IEE Proceedings-Electric Power Application,2002,149(2):143-151
- [11] Gao J, Zhang L, Wang X. AC Machine Systems: Tsinghua University Press and Springer, 2009
- [12] Kryukhin S S. A new principle for synchronous machine protection from rotor winding inter-turn and double earth faults. Elektrichestvo, 1972,2(5):47-59
- [13] Muhlhaus J, Ward D M, Lodege I. The detection of shorted turns in generator rotor windings by measurement of circulating stator currents[C]//Proceeding of 2nd Int. Conference on Electrical Machines-Design and Applications, London, 1985,254:100-103
- [14] Wan S, Wang A, Li Y, Wang Y. Reluctance Network Model of Turbo-Generator and its Application in Rotor Winding Inter-Turn Short Circuit Fault[C]// 2005 IEEE International Conference on Electric Machines and Drives, TX, 2005: 386-390
- [15] Foggia A, Torlay J E, Corenwinder C, Audoli A, Hbrigault J. Circulating Current Analysis in the Parallel-Connected Windings of Synchronous Generators under Abnormal Operating Conditions[C]//Proceeding of IEMDC'99:IEEE International Electric Machines and Drives Conference, Seattle, WA, USA, 1999: 634-636
- [16] Sottile J, Trutt F C, Leedy A W. Condition monitoring of brushless three-phase synchronous generators with stator winding or rotor circuit deterioration. IEEE Trans. on Industry Applications,2006,42(5):1209-1215
- [17] Trutt F C, Sottile J, Kohler J L. Detection of AC machine winding deterioration using electrically excited vibrations. IEEE Trans. on Industry Applications,2001,37(1):10-14
- [18] Torlay J É, Corenwinder C. Analysis of shaft voltages in large synchronous generators[C]//International Conference on Electric Machines and Drives, London, 1999
- [19] Alan M. Mirko C. Experimental research on rotor fault diagnosis using external coil voltage analysis and shaft voltage signal analysis[C]//Symposium on Diagnostics for Electric Machines, Power Electronics and Drives, Vienna, Austria, 2005
- [20] Gao J, Zhang L, Wang X. AC Machine Systems: Tsinghua University Press and Springer, 2009
- [21] Wang X, Chen S, Wang W, et al. A study of armature winding internal faults for turbogenerators [J].IEEE Trans. on Industry Applications,2002,38(3):625-631
- [22] Wang X H, Sun Y G, Ouyang B, et al. Transient behavior of salient-pole synchronous machines with internal stator winding faults [J].IEE Proceedings-Electric Power Application,2002,149(2):143-151
- [23] Zhu J H, Qiu A R. Inductance calculation of large salient-pole synchronous generator with air-gap Eccentricity[C]//Proceedings of the 12th Biennial IEEE Conference on Electromagnetic Field Computations (IEEE CEFC 2006), Miami, Florida USA, April 30 – May 3, 2006

**Simulation Test and Research on Evaporative Cooling of Hydraulic Generator  
for TGP Underground Power Plant**

**Liao Yigang, Hou Xiaoquan, Zhou Guanghou**  
**DFEM**  
**China**

**SUMMARY**

This paper describes the development and appliance of the evaporative cooling simulation platform of Three-Gorges Underground Plant Generator, based on which, a series of full simulation experiments were taken out, to acquire the characteristics of the temperature rise versus generator load, liquid pressure, liquid level and secondary cooling water flow rate, etc. Then a reasonable setting of the evaporative media level, flow rate and pressure is proposed, which will determine the cooling system scheme design, as well as the specifications of the employed condenser, pipe adapter connector, and cutting ferrules, to guarantee the reliability of the evaporative cooling system of Three-Gorges Underground Plant Generators.

**KEYWORDS**

Three-Gorges project , Hydraulic generators, Evaporative cooling, Simulation test

## **1 INTRODUCTION**

Evaporative cooling for hydraulic generator is a kind of self-circulation cooling system in which the state bars were cooled by latent heat of vaporization of low-boiling point liquid boiling at normal temperature after being heated with high-insulation performance. During operation of generator, heated, hydraulic medium in hollow copper strings of bar will change into vapor and then the evaporative cooling medium will be liquefied in condenser through steam-collecting tube at top bar; then it will return to bottom liquid-collecting tube and sealing pressure-difference self-circulation of a circle is formed for hydraulic medium which will enter the hollow copper wire of bar again to take away the heat inside generator for cooling.

Compared with water-cooling, evaporative-cooling has its unique advantage for high-load and large-capacity hydraulic generator, which is mainly presented as two aspects as following: evaporative cooling can form a self-circulation cooling system, never needs additional equipment for water treatment and can reduce the area for workshop layout. The other prominent advantage is that as pressure of evaporative cooling loop is very small, the possibility for leakage is relatively small; and even when leakage happens, as long as the leakage does not influence the normal operation of cooling system, it will not damage the safe operation of generator as well as the environment, because new-type cooling medium for evaporative cooling is non-poisonous, environment-protective, non-corrosive, high-insulated and fireproof. In this condition, it can be continuously operated or operated with lower loads and maintained after shutdown. It can maximum avoid the safety risk on unit operation and the economic loss due to shutdown.

## **2 DEVELOPMENT HISTORY of EVAPORATIVE COOLING**

In 1970s, Institute of Electrical Engineering, Academia Sinica and Dongfang Electric Machinery Company Limited(DFEM) jointly developed evaporative cooling technology for hydraulic generator, which was a new type cooling technology belong to our own proprietary intellectual property rights. Evaporative technology was first applied for 10Mw hydraulic generator in Yunnan Dazhai Hydraulic Power Plant in 1983; the second batches of hydraulic generators with evaporative cooling mode were put into operation in Shanxi Ankang Power Plant, with rated output of 52.5MW in 1992. And 7 years later, a 400MW evaporative cooling hydraulic generator in Liji Xia Power Plant was connected to the grid. Since the first evaporative cooling hydraulic generator of 10MW in Yunnan Dazhai Power Plant was put into operation, it has run for nearly 30 years. With long-term operation test, the unit is reliably operated with each performance parameters, meeting the expected requirement, and passes identification of relative national institution. It is awarded as the second National Prize for Progress in Science and Technology as well as the first Prize of Institute of Electrical Engineering, Academia Sinica for Progress in Science and Technology. It indicates that the generator evaporative cooling technology has come to mature and could be industrial-popularized.

## **3 CONTENT AND METHOD OF STUDY**

The theoretic study on evaporative cooling law in domestic is started early with much attention. The research was performed mainly by Institute of Electrical Engineering, Academia Sinica, of which the theoretic depth and breadth of research achievement leads the world. However, evaporative cooling refers to evaporative phase transition and two-phase flow of Hydrodynamics & Heat Transmission, which is a subject without finished theoretic system and solution. Therefore, so far it's very difficult to grasp the running discipline of evaporative cooling system under different condition only as per theory and further to guide the design on generator evaporative cooling system. So, for design on evaporative cooling system for large generator, except necessary theoretic analysis, study on evaporative cooling test is needed to ensure the research achievements with scientificness, rigor and engineering application value.

In order to scientifically guide the design of evaporative cooling system for hydraulic generator in Three Gorges Underground Power Plant and simulate real generator operation station, DFEM establishes a real unit simulator stand for Three Gorges Underground Power Plant in generator research room. The stand is designed and produced as per dimension and material of main components in real generator, can simulate the actual operation work condition under equivalent load of 700MW~

1000MW hydraulic generator. Some important information such as relation between parameters of generator capacity, pressure of cooling system, static liquid level & second water flow and generator coil temperature obtained from lots of test researches, provides important basis for design of evaporative cooling system for hydraulic generator in Three Gorges Underground Power Plant.

#### **4 OVERALL DESIGN of TEST STAND**

In order to simulate the real operation station of hydraulic generators of Three Gorges Underground Power Plant under evaporative cooling condition as far as possible, evaporative cooling stand is provided with stator bar, stator core, water fittings, fastening components, first & second cooling medium and other main components and material which are same as that of real generator. Simulation test stand is formed by below parts: test bed, simulation system for generator stator and environment, evaporative cooling circulation system (including steam connection tube, liquid collection tube, condenser, exhaust system, liquid feed/drainage system, connector and hose), test bar, large-current power supply system, ventilation system, parameter measurement system and cooling water circulation system, etc. Fig. 1 shows the evaporative cooling test stand after completion.



**Fig. 1 Appearance of Evaporative Cooling Test Stand**

##### **4.1 Test bar**

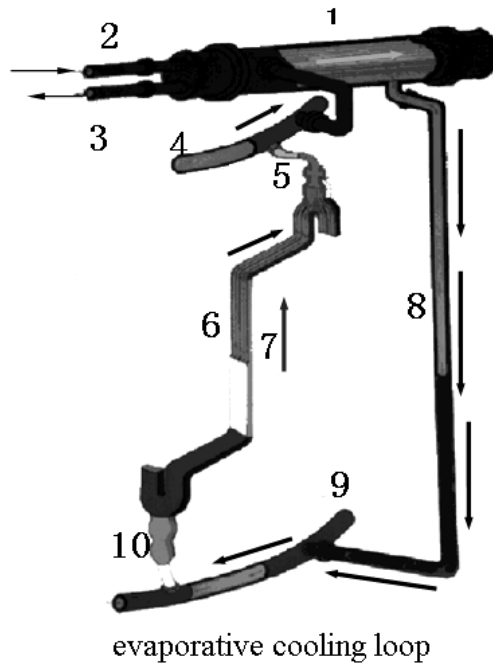
The test stand is equipped with 18 bars, in which 4 pieces are on one same hollow copper strings and one same solid copper strings of which the length direction is equipped with 126 thermocouples to test the distribution discipline of operation temperature.

##### **4.2 Simulation system for generator stator and environment**

The stator is composed of model foundation, stator base, stator core, heating system and ventilation system, etc. Back core is equipped with heating plate to simulate the temperature of core of real generator under operation station, and core section & ventilation U-steel is totally the same as that of real generator; meanwhile, on the top and bottom of stator core are equipped with 4 axial-flow fans to simulate the air flow station of real unit under operation.

##### **4.3 Evaporative Cooling Circulation System**

Cooling medium in bars with heat loss of bars will evaporate into steam which will form two-phase flow while mixing with un-evaporated medium. Because of the density difference and gravity impact, the gaseous cooling medium in bars after evaporation will flow up into steam connection tube and come to condenser together. In condenser, gaseous medium after heat release to condenser will re-liquefy into liquid state, and respectively flow into each bar along liquid collection tube at bottom of return flexible tube to complete a cooling circulation. See Fig. 2.



1. Condenser 2. Water inlet 3. Water outlet 4. Upper cannular tube 5. Upper connection tube  
 6. Stator coil 7. Evaporation section 8. Return flexible tube 9. Lower cannular tube  
 10. Lower connection tube

**Fig.2 Schematic Diagram for Evaporative Cooling Circulation System**

#### 4.3.1 Condenser

Condenser, an important component in whole evaporative cooling system, undertakes the important second heat exchange of cooling medium. The test stand is provided with condenser of which the cooling element is double-layer tube. Comparison performance test made for condensers manufactured by Dongwu, Dengfeng, GEA and other manufacturers. (See Fig.3)



**Fig.3 Condenser**

#### 4.3.2 Exhaust System

Condenser system of real generator is equipped with average-pressure loop, which makes the operation station of cooling parallel-connection branch of corresponding bar and collector ring keep in accordance and heat taken away by condenser is more uniform, and ensures temperature of generator stator winding along axial and circumferential direction distribute more uniform. Test stand is provided with exhaust system, and when pressure of evaporative cooling system rises and exceeds the specification, the high pressure needs to be released through exhaust tube and during exhaust process, the cooling medium will be retrieved by retrieving equipment which is equipped with pressure switch, pressure transmitter, solenoid valve, manual exhaust valve and other detecting elements in evaporative cooling system.

### 4.3.3 Liquid Feed/Drainage System

Because cooling medium in actual operation and test will be increased or reduced, it is provided with liquid feed/drainage device. During drainage, open the liquid drainage valve of liquid collection tube of stator bar and suck the cooling medium into liquid feed/drainage device with pump. During liquid feed, suck the cooling medium into stator bar evaporative cooling system with pump. And one liquid storage tank is used for both liquid feed and drainage. (See Fig.4)



Fig. 4 Evaporative Cooling Liquid Feed/Drainage System

### 4.3.4 Sealing Joints

There are many sealing joints in evaporative cooling system and their reliability directly influences the whole system reliability. Test stand is provided with sealing joints of real generator and simulation test for this installation and sealing is performed.

### 4.3.5 Teflon Hose

Teflon hose is selected to connect joints at two sides of stator bar and collector ring with steam collection tube and liquid collection tube. The plastic hose used in simulation test is totally the same with that of real generator.

### 4.4 The Measuring System

The measuring system is used to test the bar temperature, core temperature, flow rate & temperature of second cooling water and parameters like pressure of steam collection tube, liquid collection tube and condenser, etc. This system is composed of sensor, DX200 data acquisition & recording instrument and computer, performs the data transmission with Ethernet network and tests 154 parameters. Test software prepared on LABVIEW platform has function of acquisition, display, data comparison, imaging and data storage, etc. Please see Fig. 5 for main interface of the software.

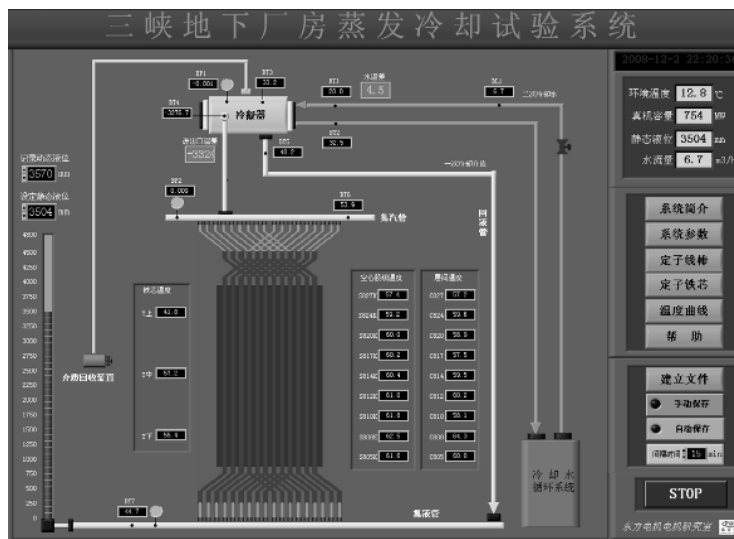


Fig. 5 Measuring System

#### 4.5 Cooling water circulation system

Cooling Water Circulation System is composed of water tank (including upper and lower water pipeline), valve, pump, flow-meter, water pipeline and condenser, etc. Under normal operation, the system can realize the remote control under the condition that water flow is within 0~32m<sup>3</sup>/h (1/60 of real unit) and water supply pressure within 0.25~0.4MPa. Feed water temperature  $\leq 40^{\circ}\text{C}$ .

### 5 TEST ITEMS and RESULT

The test is performed at the same water temperature as in summer time and the core temperature is controlled under operation of real generator. The simulation of real generator operation is realized with DC application, which produces same loss, on coil model as per coil loss of real generator. According to different capacity, pressure, hydraulic level and second cooling water flow, a series of real generator simulation tests are performed as well as some tests under complex work condition, including more than 30 work conditions such as low-load operation, changing core temperature, changing cooling air flow, limit small flow, limit low hydraulic level, and limit condenser pressure, etc. Some key tests are listed below:

#### 5.1 Simulation tests under different pressure in condenser

As the pressure in condenser directly influences the generator coil temperature, the discipline of condenser pressure influencing cooling system can be well known through comparison test under different pressure. The result indicates that different condenser pressure causes different system temperature and the higher the condenser pressure is, the higher the temperature of system bar is.

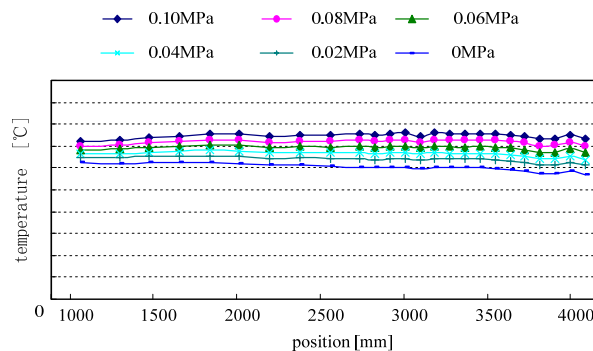


Fig. 6 Comparison for Hollow Strands Temperature

#### 5.2 Test on influence of cooling medium static hydraulic level on operation temperature

Static hydraulic level directly influences the operation temperature of generator coil. In order to determine a reasonable static hydraulic level value, several comparison tests under different static hydraulic level are performed on simulation stand.

It will be seen from data analysis curve displayed in Fig. 7 that the system can perform a good evaporative cooling circulation while hydraulic level is from 70% to 90%. Temperature differs not obviously. Operation pressure on condenser is near zero pressure.

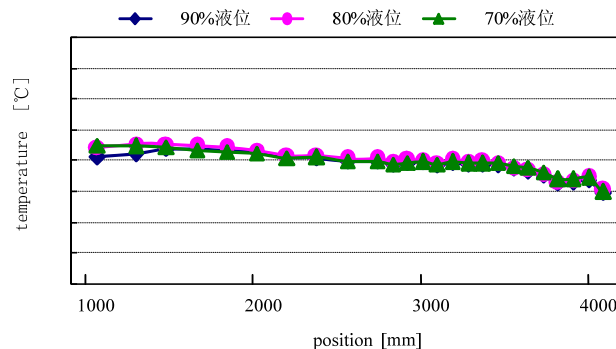


Fig. 7 Influence on Temperature from Static Level

### 5.3 Simulation test under different generator capacity

Different generator operation capacity produces different heat. In order to know cooling station of stator coil under different operation capacity of generator, study on simulation under different capacity conditions is performed. Test result indicates that under different operation capacity, generator cooling system can perform a good evaporative cooling circulation, with axial temperature difference of coil less than 10K. Fig.8 shows the coil temperature distribution under rated load condition and maximum load condition.

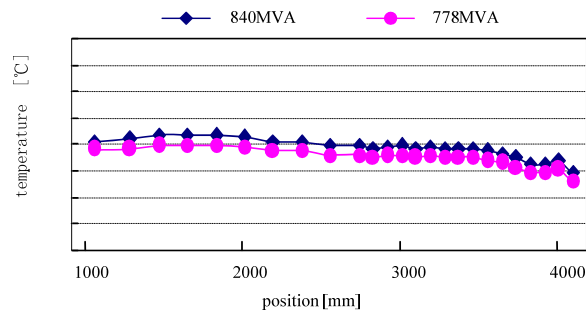


Fig. 8 Hollow Strands Temperature Under Different Simulation Real Generator Capacity

### 5.4 Studies on water break test

Water break is a possible fault that occurs during generator operation. In order to know generator coil temperature-change discipline under water break condition, simulation study on water break under different condition is performed to provide basis for protection parameters set for generator.

From the test result, under maximum load of 840MVA, if water break condition lasts for more than 397s, the pressure of evaporative cooling system reaches 0.1MPa, maximum temperature of strands is 78°C and generator coil is still in a safe station. Temperature change discipline is shown in Fig. 9.

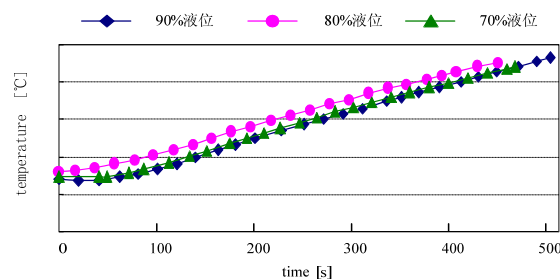


Fig. 9 Stator Coil Temperature Under Water Break

## 6 CONCLUSION

Through the simulation test study in laboratory for about two years, load-temperature relation, hydraulic level-temperature relation, system pressure-temperature relation, second water flow-temperature relation and other important parameters of evaporative cooling hydraulic generators in Three Gorges Underground Power Plant are obtained; and important discipline, performance curve and other basic research conclusion on rational design on these generators are summed. According to test results, reasonable set value (range) under different work conditions for hydraulic level, second water flow, system pressure and other main parameters in evaporative cooling system are proposed and set plan for alarm value & limit of temperature, pressure and hydraulic level under fault condition are made. It scientifically guides the design on evaporative cooling system of Three Gorges Underwater Power Plant and reasonable type-selection for condenser, pipeline connector and other components, ensures the reliability and rationality of evaporative cooling system here and creates good condition for development of larger-capacity evaporative cooling hydraulic generators, for example, 1000MW generator.



Liao Yigang(1963—): male; senior engineer; graduated from Hunan university in 1983 and majored in electric machine, Senior engineer, vice-director of researching & testing center of DFEM, engaged in research of ventilation and cooling . (email :DF-LYG@163.com)



Hou Xiaoquan(1962—): male; senior engineer; graduated from Qinghua university in 1984 and majored in electric machine,Senior engineer,gained engineering master's degree of Qinghua university in 2000, director of products developing department of DFEM now. (email : [houxq7859@163.com](mailto:houxq7859@163.com))



Zhou Guanghou (1970—), male, senior engineer; master degree from the Chongqing University, and engage in large electrical.machine electromagnetic analysis and testing study in DEC, China. ([zghdfem@163.com](mailto:zghdfem@163.com))

## **Thermal Analysis of Large Hydro-Generator Based on a Multi-physics Approach**

**Chaaban M. , Leduc J. , Hudon C., Merkouf A., Torriano F., Morissette J.F.**  
**Institut de Recherche d'Hydro-Québec (IREQ)**  
**1800 Boul. Lionel-Boulet, Varennes, Québec, J3X 1S1**  
**Canada**

### **SUMMARY**

The thermal analysis of the main components of hydro-generators, namely the stator, the rotor and the cooling system, is a complex issue that deals with several physical phenomena. The first to be addressed is the electromagnetic field which produces a significant portion of the losses. Secondly, the science of fluid mechanics is needed to evaluate the heat transfer between the cooling air and the solid parts of the generator as well as the windage losses and their distribution. Last but not least, is the phenomenon of heat transfer by conduction taking place through the various isotropic and anisotropic components of the generator. Ideally, a fully coupled multi-physics model should be used which would imply solving Maxwell's and Navier-Stokes equations coupled with the energy equation. As this is still computationally too demanding, the project presented herein has started with a more simple approach of simulating each aspect separately and exchanging results of one field with the other as a weak coupling. With this approach, the thermal analysis can readily include results from electromagnetic and computational fluid dynamics (CFD) simulations to evaluate the temperature field, and consequently the hot spot temperature and its location. This is done by solving the Fourier partial differential equation using Finite element/Finite volume methods. In parallel with simulations, on-site measurements of the various losses on existing generators at different loads and the measurement of several critical temperatures provide the data to calibrate and validate the models. This paper explains the step by step process and presents some computational and experimental results on an existing 122.6 MVA hydro-generator at Hydro-Québec.

### **KEYWORDS**

Stator temperature, Rotor temperature, Generator cooling system, Finite element

## 1 INTRODUCTION

Utilities around the world are thriving nowadays to increase the productivity of their existing generators by increasing their output without jeopardizing their life span. Beside mechanical and electrical considerations, the possibility of overheating these equipments represents a major obstacle that has to be examined thoroughly before any up-rating action is undertaken. The thermal analysis of a generator has to cover its three major components: the rotor, the stator and the cooling system since each of these components impacts the performance of the others. At any load, the temperature field in the stator and in the rotor must be calculated by balancing the electromagnetic, Joule and windage losses with the extracted heat by the cooling system via air-water heat exchangers. Thus, the losses and their spatial distribution have to be evaluated accurately, considering the various heat transfer coefficients between the fluid and the solid parts.

## 2 NUMERICAL SIMULATION

The procedure to analyze the thermal behavior of a generator consists of 4 main consecutive steps; namely the calculation of electromagnetic losses, the evaluation of air flow rate, its distribution and the windage losses, the heat dissipation in the solid part and finally the cooling performance of air/water heat exchangers.

**2.1 Electromagnetic losses**  
The magnitude and spatial distribution of the electromagnetic losses are obtained using in house and commercial software based on 3D finite element/finite volume methods. These losses are present in the damper bars, at the surface of the poles, in the teeth and the yoke of the stator core and to a lesser extent in other components such as pressure fingers, end plates, and vent-ducts spacers. The integration of loss densities in X, Y and Z (loss matrix) in the various components yields a global loss that can be compared to on-site measured values during a standard loss segregation test. Unfortunately, the measurement does not give the spatial distribution of these losses, but rather the losses per type (magnetic, Joule, stray and windage). The only possible validation of this distribution is to compare the subsequently calculated temperature field with several temperature sensors, installed in strategic locations inside the generator.

### 2.2 Cooling air flow parameters

The air flow induced by the rotor spiders and by the fans on top and bottom of the poles is extremely difficult to evaluate due to the complexity and the high number of passages that the cooling air may take to close the loop between the rotor, stator and the cooling system. Currently, a team at IREQ (Hydro-Quebec Research Institute) is actively developing a 3D CFD model for the entire generator based on the periodicity of a sector of rotor/stator assembly. The goal is to evaluate the followings:

- Air flow rate and its distribution
- Windage losses and its distribution
- Various heat transfer coefficient between cooling air and solid parts

Until such CFD simulation can be run effectively, the thermal simulation relies on local air flow measurements, especially at the back of the stator where a series of converging conduits provide axial distribution of the flow as well as the total air flow leaving the stator. As for the global windage losses, the current procedure is to use the value measured during the on-site calorimetric test. The various heat transfer coefficient required to carry out the heat dissipation analysis in the solid parts are obtained analytically from the literature. The flow is turbulent in all ducts and air passages in both stator and rotor due to the high velocities involved. The fully developed heat transfer coefficient in ducts ( $H_c$ ) is given by Colburn [1].

$$H_c = \left( \frac{k_{air}}{D_{duct}} \right) \left[ 0.023 \left( \frac{V D_{duct}}{\nu} \right)^{0.8} Pr^{\frac{1}{3}} \right] \quad (1)$$

Where  $k_{air}$  is the air thermal conductivity,  $D_{duct}$  is the hydraulic diameter of the duct,  $V$  is the air velocity,  $\nu$  is the air kinematic viscosity and  $Pr$  is the Prandtl number

At the entrance of ducts, the heat transfer coefficient has a higher value than further downstream. The ratio between the local ( $H_{cx}$ ) and the fully developed value, at a given distance from the entrance ( $x$ ), is given by the following equation [2]:

$$\frac{H_{cx}}{H_c} = 1 + 1.2513 \text{ EXP} \left( - \left( \frac{x}{D_{duct}} \right) \right) \quad (2)$$

In the air gap and around the poles, the heat transfer coefficient is given as a function of the tip velocity ( $V_{tip}$ ) by the following equations derived experimentally by Liebe [3].

$$H_c = 17.8(V_{tip})^{0.39} \quad (3)$$

Recent study by CFD [4], shown in equation (4) gives comparable results:

$$H_c = 15.6(V_{tip})^{0.45} \quad (4)$$

### 2.3 Heat dissipation in the solid part: Hot spot calculation

The heat conduction in the stator and in the rotor is analyzed by solving numerically the Fourier partial differential equation:

$$\left( K_x \frac{\partial^2 T}{\partial X^2} + K_y \frac{\partial^2 T}{\partial Y^2} + K_z \frac{\partial^2 T}{\partial Z^2} \right) + Q = \rho C \frac{\partial T}{\partial \tau} \quad (5)$$

Where  $K_x$ ,  $K_y$ ,  $K_z$ , are the thermal conductivity coefficients in x, y and z directions,  $T$  is the temperature,  $X$ ,  $Y$ ,  $Z$  are the spatial coordinates,  $Q$  is the heat source,  $\rho$  is the density,  $C$  the thermal capacity and  $\tau$  is the time.

The Finite Volume Method (FVM) is used to solve equation (5) in the stator and the Finite Element Method (FEM) in the rotor. In order to reduce the size of the problem to a manageable level, we have restricted the analysis to one slot in the stator and to one rotor pole. This implies that symmetry exists along the circumference which is the case most of the time. In the axial direction however, symmetry could not be used due to the different lengths and shape of upper and lower end-windings and to the possible axial non-uniformity of cooling air leaving the rotor and entering the stator. Figure 1 shows the mesh of these two components for a 122.6 MVA generator.

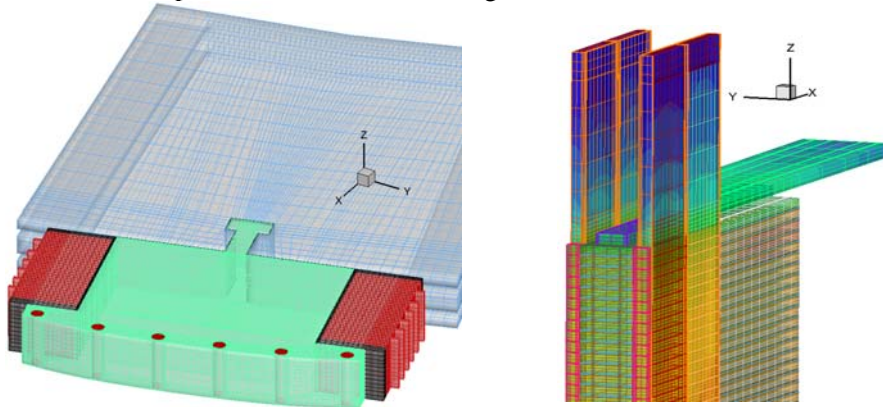


**Fig. 1 Meshes of a slice of the rotor (left) and the top end of the stator (right) of a 122.6 MVA hydro-generator**

#### 2.3.1 Analysis of the rotor

The heat losses in the damper bars are introduced as a volumetric heat source ( $W/m^3$ ). They are evaluated by integrating the  $RI^2$  loss resulting from the induced current harmonics in these bars and their AC resistance at the prevailing frequencies. The magnetic losses, calculated by Maxwell software for each domain discretized by the electromagnetic mesh, are interpolated to be transposed onto the thermal mesh by superposing both meshes as shown in Figure 2. Convection boundary conditions are set in the air gap and in the cooling ducts of the rim where equations (1-4) are used. The air temperature at the entrance of these ducts is set equal to the air temperature leaving the heat exchangers, plus the rise due to the heat transferred from the end-windings and a portion of the windage losses caused by the rotation of the end-plates and rotor spider arms. The air temperature

calculated at the air gap is based on the air flow rate, and the added losses from the rotor Joule and electromagnetic losses and of the entire windage losses. In the current version of the model, the windage losses beyond the rotor and the air gap are assumed to be negligible. Once the losses and the boundary conditions are set, we proceed with the calculation of temperature field in the rotor using equation (5). It should be noted that this is an iterative process. The calculated cooling air temperature in the air gap will be used as input boundary conditions for the stator. The air temperature leaving the stator is imposed at the entrance of the heat exchangers. The loop is closed by setting the air temperature leaving the exchangers as boundary condition at the entrance of the rotor and so on until convergence is reached. The calculated hot spot is difficult to validate by measurement because most locations inside the rotor are inaccessible. However, the calculated temperature field is partially validated with measurements at several locations where sensors are installed on few coil turns and on the surface of pole body and damper bars.

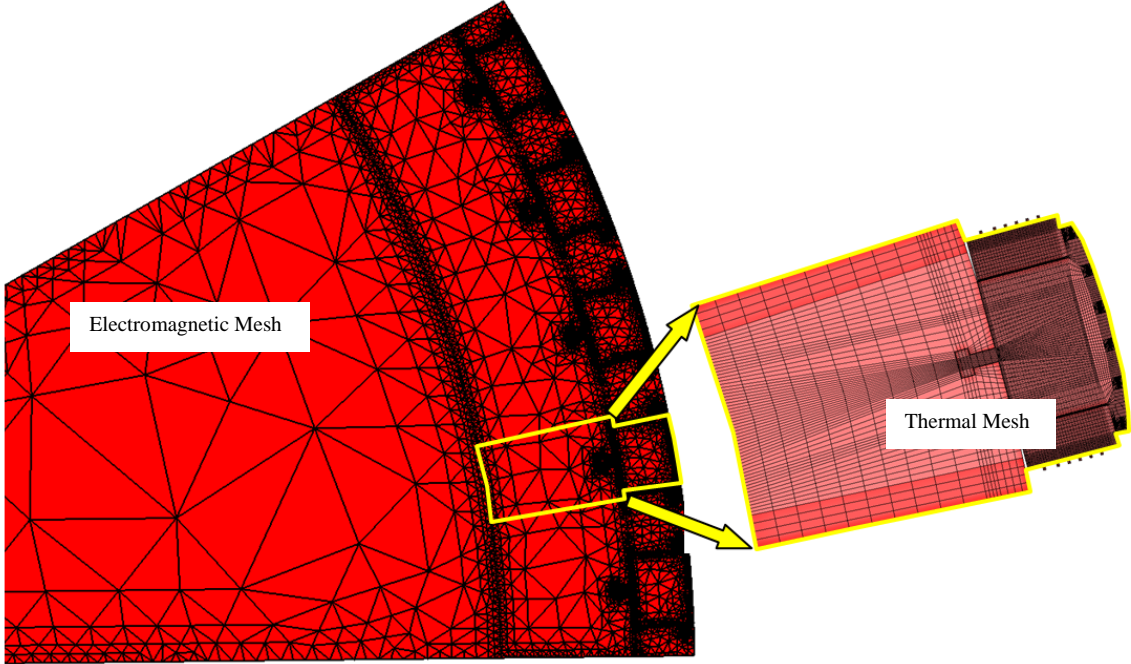


**Fig. 2 Interpolation of electromagnetic losses in the rotor by thermal mesh superposition**

2.3.2 Analysis of the stator

The heat losses in the yoke and teeth of the stator core are obtained in a similar fashion by superposing the electromagnetic mesh and the thermal mesh as shown in Figure 3. The electromagnetic loss matrix, calculated by Maxwell at every node, provides part of the heat source. In addition, the stray losses from circulation and Eddy current in the copper bars, end windings, vent duct spacers, end-plates and pressure fingers, is another heat source included in the thermal model. These losses are calculated using a combination of Maxwell and in-house analytical programs. Depending on the axial profile of air velocity leaving the stator that is obtained by measurement, uniform or non-uniform air velocity distribution is imposed as boundary condition at the entrance of the stator cooling ducts. Convection boundaries are also set at the back of the core and at both extremities of the stator. The heat transfer coefficient estimated at these locations, is based on an average air velocity of 3 m/s. Sensitivity analysis has shown that variation of the air velocity at these location have little impact on the calculation of hot spot inside the stator. The calculated temperature field yields the magnitude and location of the hot spot as well as the temperature at any location such as the one of the resistive thermal detectors (RTDs) normally installed between the top and bottom bars. A comparison with the readings of these sensors and with all other sensors is used to validate or calibrate the numerical model.

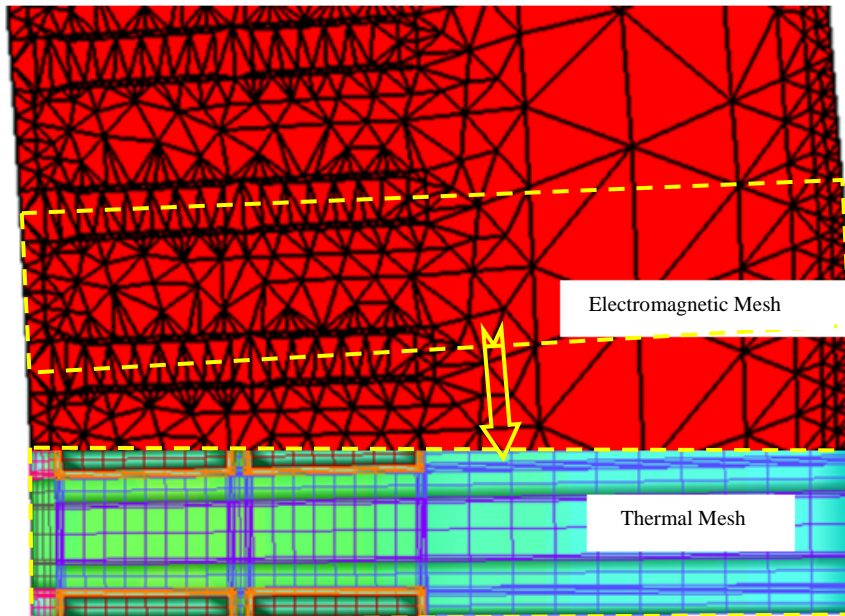


**Fig. 3 Superposition of the electromagnetic mesh of the stator onto the thermal mesh for interpolation of the magnetic loss matrix.**

## 2.4 Cooling system

The cooling system plays a major role in the overall performance of hydro-generators. The dam water temperature used in the system has a direct impact on the permissible load. It is well known that the maximum load of any generator drops substantially in summer compared with the winter condition when the cooling water, taken from the dam, is cooler. At Hydro-Québec, the majority of our generators are rated based on water temperature at 5°C during winter and 15°C during summer. Such variation in cooling water temperature leads to a difference in rating of 15% or more. Another major parameter that impacts the cooling system is the fouling of the water/air heat exchangers. In fact, it is well known that deposits, of various sources, in the water pipes of the radiator results in a gradual drop in exchanger performance because it creates an additional thermal resistance between the water inside the tubes and the air outside. This leads inevitably to higher air temperature leaving the radiators and consequently, to higher copper temperature in the stator bars and in the rotor coil. The fallout is a reduction in the generation capacity in order not to exceed the maximum temperature admissible by insulation system. A dedicated computer program to analyze the performance of water/air heat exchangers has been developed to evaluate the performance and fouling of the exchangers used on our generators. The inputs to the program are the physical dimensions (number of tubes, configuration of tubes, fins shape, dimensions, etc...) and the air and water inlet temperatures. The output is the exiting air and water temperature. This model and the fouling factor can be verified by comparing the outlet air and water temperature to the measured one at various loads.

## 3 STEP BY STEP CALCULATION PROCEDURES

The thermal analysis of the whole generator requires several parameters that are unknown in advance. The most important are the cooling air distribution in, and around the rotor and stator and copper temperature. The air temperature leaving the cooling system has an important impact on windage loss evaluation and on rotor temperature field calculation whereas the air temperature leaving the rotor influences heating of the stator components. On the other hand, the copper temperature dictates the Joule losses in the field coil and in the stator bars (or coils). For this reason, the analysis of the complete generator is an iterative process. In summary, the thermal analysis of an existing generator, identified for a potential uprate, consists of the following steps:

- Building the numerical finite element/finite volume models
- On site testing for losses, air flow rate and cooling system performance
- Calculating the electromagnetic losses and their spatial distribution
- Proceeding with thermal analysis at various load levels and comparison with measurements

- Potential adjustment of the model
- Extrapolating the losses for higher load
- Calculating the maximum power if uprating is possible

A future version of the model will also include iteration with CFD simulation to calculate convection coefficient in different air passages.

#### 4 REAL CASE STUDY

The procedure outlined in this paper was put to test for several generators at Hydro-Quebec with a potential for power increase [5, 6]. The current case study is a 122.6 MVA generator, operating at 0.9 power factor and at a nominal voltage of 13.8 kV. Figure 4 shows a comparison between the heat extracted by water, the heat released by air and the total losses at several power levels in this generator. These data are based on measured air flow and water flow rates and air and water temperatures upstream and downstream of the radiators. The losses are the sum of the windage, rotor and stator Joule losses, which are measured values and the magnetic, eddy and circulation losses which are calculated numerically as outlined previously.

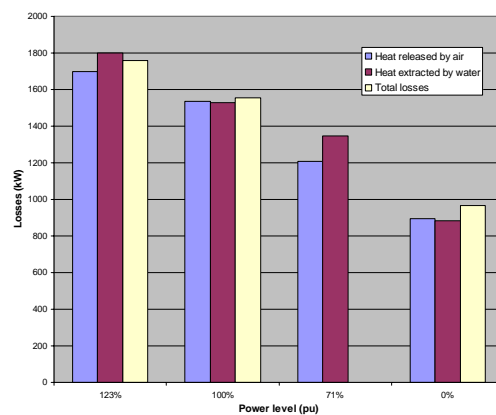


**Fig. 4 Comparison between the heat extracted by water, the heat released by air and the total losses in the generator**

It can be seen that the heat balance between air and water is not quite satisfactory, especially for the 71% heat run test. Ideally, the heat extracted by water and the one released by air across the radiators should be equal but because of uncertainty related to air flow rate measurements some difference was observed between the two. Also, the heat extracted by the radiators should be equal to the total losses in the generator, which was almost the case for the 123% and 100% conditions as shown in Figure 4. Simulation of electromagnetic losses distribution for the 71% test was not yet available at the time this paper was written and the model of the no load condition should be improved. Table I shows the comparison between measured and calculated critical temperatures in the stator and in the rotor of the generator. Figure 5 shows the isotherms in the rotor and stator.

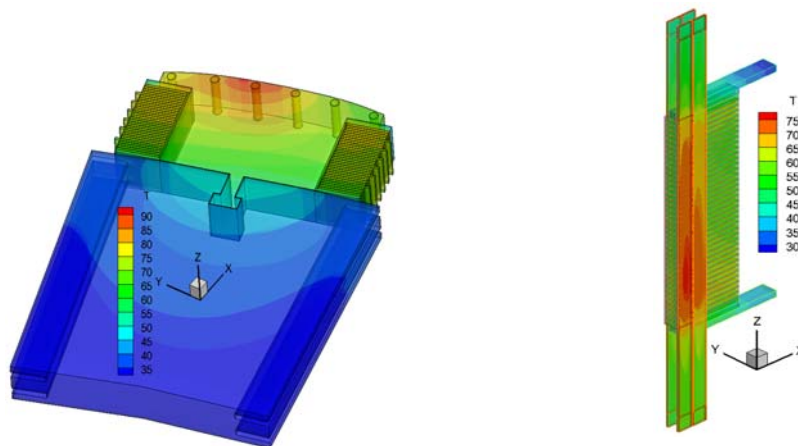


**Fig.5 Isotherms in the rotor and the stator at 123% power level**

**Table I Comparison between calculated and measured temperature (L.E.= leading edge, T.E= trailing edge)**

Power level	123%		100%		71%		0 %	
	Calc.	Measur.	Calc.	Measur	Calc	Measur.	Calc.	Measur.
T-air entering radiators	50.5	48.9	44.9	44.4		37.8	31.6	31.0
T-air exiting radiators	18.9	18.65	17.4	17.4		16.15	13.2	14.2
T-water exiting radiators	15.61	15.76	14.351	14.168		13.307	11.288	10.817
T-RTD location	70.6	67.1	60.8	58.0		45.7	34.6	32.8
Hotspot in stator	76.3	--	65.1	--			40.4	----
T-pole body surf. #1	79.4	72.2	70.1	66.5		56.0	40.9	41.7
T-pole body surf. #2	89.2	79.7	81.0	74.0		62.9	47.2	48.2
T-pole body surf. #3	86.2	75.7	76.6	70.2		60.0	50.1	49.1
T-pole body surf. #4	75.1	67.9	66.5	62.1		52.7	46.9	44.8
T-pole body surf. #5	68.4	64.7	60.4	58.7		49.9	40.8	40.9
T-damper bar #1	80.0	--	68.9	--		--	39.0	--
T-damper bar #2	83.6	88.6	74.8	80.8		67.4	43.9	48.8
T-damper bar #3	87.4	85.9	78.6	79.3		67.0	48.6	52.5
T-damper bar #4	80.0	80.0	71.1	73.8		62.3	48.4	51.4
T-damper bar #5	71.8	75.3	63.5	68.8		57.4	43.7	47.5
T-damper bar #6	69.9	--	61.2	--		--	38.9	--
T-coil, L.E., turn #3	76.3	77.5	65.3	65.8		51.2	37.8	34.8
T-coil, T.E., turn #3	79.2	85.9	67.9	72.6		56.5	37.8	36.6
T-coil, L.E., turn #15	73.7	75.3	63.1	63.3		50.0	36.5	31.8
Hotspot in rotor	91.6	----	82.9			----	50.5	----

## 5 DISCUSSION

The comparison between the measured and calculated temperatures in the stator for the air, water and RTD is fair, but poor in the rotor as shown in table I. The discrepancies can be attributed to the followings:

- In general, the measured temperatures are underestimated because the heat-run tests, at the four loads, were ended before reaching complete steady state conditions. By looking at the profile of recorded temperature rise, we estimate that the final steady state temperatures should be corrected by adding about 1-2°C with respect to the values reported in Table 1.
- As a first approximation, the convection heat transfer coefficient, calculated by equation (3), was considered constant all around the pole faces and winding. This simplification is not accurate as revealed by the measured coil temperatures in Table 1. For example, the measured coil surface temperature at 123% is equal to 77.5°C on the leading edge of turn #3, while the temperature on the same turn on the trailing edge is much higher reaching 85.9°C. This asymmetry in temperature suggests that the heat transfer coefficient at the trailing edge is lower than on the leading edge. This will be corrected in our model as soon as CFD calculations will be completed.
- Another source of discrepancy between the model and the measured values comes from the measured pole face temperature facing the air gap, which is believed to be a few degrees off from the actual surface temperature. In fact, it is very difficult to measure accurately the surface temperature of moving hot bodies at very high speed in a cooler medium. In the present case, the tip velocity is equal to 66.5 m/s (239 km/h). At this speed, a sensor, glued to the hot wall and protected by an external layer of silicon, is surely influenced by the relatively colder air nearby. Measurements and simulation in our laboratory indicate that the error in similar situations could reach 10°C or more, depending on the attachment configuration and protection of the sensors.

- Another important parameter that impacts the calculation of pole surface temperature is the thermal conductivity of pole's body in radial and circumferential directions. The exact thermal conductivity of the material used here is not known and theoretical evaluation of this conductivity is difficult due to the stacking of steel plates with thermal contact resistance between them. In our analysis, the conductivity was taken equal to 20 W/m°C whereas a solid bloc of the same steel has conductivity of 50 W/m°C. The heat convection coefficient along the surface is the other main factor that will have an impact on the maximum temperature in the rotor and has yet to be introduced.

Most of the hypothesis on parameters such as thermal conductivity, convection coefficient and potential discrepancy between measured and simulated values are still being fine tuned and the next version of our model is expected to give more accurate results. This is a mandatory condition to adequately calculate a new power output for a generator without jeopardizing its expected life.

## 6 CONCLUSIONS

The software developed at IREQ to analyze the performance of existing generators is a useful tool to evaluate the potential of power increase contemplated by Hydro-Quebec. This software combines the power of modern computational tools with on-site measurements. In the current version, multi-physic phenomena, namely, the fluid dynamics, the electromagnetic and the heat transfer are treated separately. The results are exchanged between fields in an iterative sequence that is repeated until convergence is reached. In a foreseeable feature, this process will be integrated with stronger coupling between all these phenomena.

The results outlined in the paper shows that the generator studied has a potential for power increase since the hot spot in both the rotor and the stator were well below the maximum limit of the insulation class. The next step will be concentrated on evaluating this maximum permissible load and make sure that other aspects, structural, vibrational, acoustical, are also acceptable at the new power level.

## BIBLIOGRAPHY

- [1] Özisik. Heat transfer, a basic approach: McGraw-Hill, 1985
- [2] Rohsenow, Harnett, Ganic. Handbook of heat transfer fundamentals: McGraw-Hill, 1985
- [3] Liebe W. Kühlung von Grossmaschinen. ETZ-A, 1966,87(13):434-442
- [4] Shanel M, Pickering S J, Lampard D// Application of computational fluid dynamics to the cooling of salient pole electrical machines, ICEM, 2000: 338-342
- [5] Chaaban M, Hudon C, Leduc J, Nguyen D N. The Use of Numerical Thermal Simulation and Distributed Temperature Sensing (DTS) for the Diagnostic of Large Hydro-Generator// Hydro Vision 2006 conference, Porto Carras, Greece, October 2006
- [6] Chaaban M, Leduc J, Hudon C, Nguyen D N. Thermal behavior of large hydro-generators[C]// The 12<sup>th</sup> International Symposium on Transport Phenomena and Dynamics of Rotating machinery, Honolulu, 2008

**Selection of Cooling Mode for Giant Hydro-generator**

**Li Dingzhong**  
**China Hydropower Engineering Consulting Group Co.**  
**China**

**SUMMARY**

This thesis reviews the selection of cooling mode for hydro generator in Ertan hydropower station. A new understanding of air cooling mode of hydro generator in recent years is developed. It is called “if air cooling mode is feasible, then it’s not necessary to adopt water cooling mode for stator winding of hydro generator”. The article also introduces the reasoning of air cooling mode and adoptive corresponding measures being selected for hydro generator in Longtan Hydropower Station, Xiaowan Hydropower Station and Laxiwa Hydropower Station, proposes the idea of “preferring to select evaporative cooling mode rather than water cooling mode for stator winding of hydro generator”

**KEYWORDS**

Hydro generator, Cooling mode, Air cooling, Water cooling, Evaporative cooling

The cooling system of giant generator is in relation to the parameter selection, structure design, weight and cost of hydro generators. It is one of the key techniques of hydro generator's insulation life as well as efficiency, reliable and stable operation of the generator. It is also the key point of breaking through the limits of generator capacity.

## **1 REVIEW OF CHOOSING AIR COOLED SYSTEM OF ERTAN HYDROPOWER TATION**

In the beginning of 1990s, the author was in charge of preparation work of hydro generator bidding documents of Ertan hydropower station in the Chengdu Survey, Design and Research Institute. The analysis of choosing the air cooled system for the hydro generators of Ertan hydropower station is given in the following ways.

### **1.1 Advantages and disadvantages between stator air cooled system and internal water cooling system**

The giant hydro generators with 500-800MVA stand-alone capacity have the internal water cooling system or air cooled system.

The advantages for air cooled system are good electric parameters and high efficiency at rated point; simple structure and arrangement; easy to install, run and maintain; low operation cost and high reliability; and beneficial to the payback of generating plants. The main problems are the relative bad uniform distribution of temperature in axial direction of stator coils. The mechanical stress and "buckling" which are made by heat expansion of stator iron core, compared with internal water cooling system, are more serious. It should be seen that, from 1970s, the main manufacturers in the world have researched and developed the disk type structure of rotors, float stator frame, oblique elastic supporting arms, eight-angular form upper bracket, radial direction ventilation system, F-class coil insulation and fixed systems, etc.; they have made relative big progresses in solving the key technique difficulties, such as, the cooling system of air cooled unit, heat-withstanding quality, deformation control and stacking of the stator core at Site; and big improvement of air cooling limits of generators have been made.

The temperature of stator bar is relatively low and well-distributed, which is good at improving heat stress and reducing "buckling" of iron core and prolonging the insulation life; under the regulated condition of  $GD^2$ , internal water cooling system can somewhat reduce the height, volume and weight of iron core; though some manufacturers have acquired the stator inter water cooling technique and have running experiences, the reliability of stator coil water connectors and water treatment devices is low. So the fatal disadvantage is danger of generator insulation damage and high risk of unsafe operation when water leaking; install, test, running management and overhaul are more difficult with heavy workload; and long starting time is not good to adjusting of frequency and power load of the station; the difficulty of underground equipment arrangement is increasing. At the same time, the cost of manufacturing, installation and maintenance of water treatment devices and its control system is relatively high.

### **1.2 Analysis from the aspects of generator's utilization coefficient and capacity per pole**

The utilization coefficient of generator is no more than 8.00 in the past (Grand Coulee is 7.31, Baishan Hydraulic Power Plant and Longyangxia Hydropower Station in China are respectively 7.76 and 7.80), while Gori II and Churchill Falls Hydropower Station have reached respectively 8.80 and 10.17, which have been great improvement comparing with the past. The capacity per pole of generator in Churchill Falls Hydropower Station made by GE company and put into operation in 1971 has reached 16.67MVA; in Grand Coulee II Hydropower Station, the generator, made jointly by SIMENS, TOSHIBA, HITACHI, and MITSUBISHI operating since 1983, has the unit capacity of 805MVA and capacity per pole of 15.1MVA. The generator in Ertan hydropower station has capacity per pole of 14.75MVA, which has no difficulty for major manufacturers in the world. The generator in Ertan hydropower station adopt pure air cooled system with utilization coefficient of about 10, which have reached the world advanced level and can be reached by its technology. The utilization coefficient of air cooled system is 95%-99%, while water cooled system is only 90%-95%.

### **1.3 Analysis from the cost of generator manufacturing**

According to the foreign technical exchange data, Canada GE Company previously estimated that the cost of generator stator with water cooling system in Ertan hydropower station is 15% higher than that with air cooled system; Alsthom estimated the cost is 9% higher; TOSHIBA considered that the generator using stator water cooling system which has complicated coils would have high price. Moreover, Ertan hydropower station is underground with large LV diversion channel section, so its required  $GD^2$  is no less than  $95000t.m^2$ . Under this condition, the weight of generator will not be reduced by using inter water cooling system, which have lost the main advantage of light weight of unit and relatively low price. In contrast, the general price of generator with inter water cooling system is higher than that with air cooled system.

### **1.4 Analysis from efficiency**

The efficiency of inter water cooling system and air cooled system is generally the same. The generator with inter water cooling system need small air flow, so have the relevant advantages of smaller wind-age loss and no-load losses, but higher efficiency when running under the rated capacity. According to the data provided by Alsthom, the highest efficiency of generator with air cooled system in Ertan hydropower station is 98.65%, while its counter part is 98.58%.

### **1.5 Analysis from stability of electric network**

Just at that moment, the 500kV network frame in Sichuan province is relatively thin, with the hope of small  $X_d'$ . The  $X_d'$  of generator with inter water cooling system in Ertan Hydropower Station is 0.36 or above, which can not satisfy the requirement of electric system—no more than 0.33.

In summary, according to the manufacture level in China and abroad at that time and the concrete conditions of Ertan hydropower station, we believe that the all air cooled generator has more advantages and thus recommend adopting this cooling system.

## **2 THE NEW UNDERSTANDING OF HYDRO GENERATOR USING THE ALL AIR COOLED SYSTEM**

### **2.1 No limits to capacity per pole of cooling system**

As a reference to the manufacturers in China and abroad, especially the technical data of the Harbin Electric Machinery Co. Ltd., alone with the improvement and development of ventilation and cooling technology, insulation technology, and anti-buckling technology of iron thermal expansion and cold shrinkage, the all air cooled generators have been widely used, and its capacity, slot current, and electric load value have significantly increased. The common hydro generator using the all air-cooled system, especially the generator of pumped storage power station can break through the limits of capacity per pole, with the value of 25-40MVA. It is generally thought that the cooling system has no longer been limited to capacity per pole, but to the rotate speed of machine set, rated voltage, stator winding branch number and proper distribution of stator slot current as well as the analysis and calculation of density of heat flow. In order to guarantee the safe and stable operation of all air cooled hydro generators, the slot current, electric load and heat load value must be controlled in a certain level, that is the slot current of all air cooled generator with high capacity is better to be 5500-7300A; heat load is better to be within the range of  $2000-2700A^2/(cm. mm^2)$ .

### **2.2 Attention to proper values of the loss density per unit volume and density of heat flow of key generator parts**

During the design of the electromagnetic, compare several alternatives, and then choose the optimized design of the generator. The main sizes (inside diameter of iron core and its height etc.) and the electric load should meet the requirements of efficiency, main reactance parameters, temperature rise,  $GD^2$ , stiffness and strength, and general layout for the generator. And calculate the matching between the loss by main heat parts and the sizes of relative structures, in order to have the proper volume loss density and heat flow density, so that the all air cooled ventilation system can be safe, reliable and economical.

After analyzing and calculating a lot of data from the big capacity generators with typical air cooled system, such as the Baishan, Yantan, Tianshengqiao (I, II), Geheyan, Xiaolangdi, Shuikou, Ertan, Wuqiangxi, Shuibuya hydropower stations, and the Guangzhou (I, II), Tianhuanpin pumped storage power stations, the Harbin Electric Machinery Co. Ltd. makes the range of volume loss density of stator windings with air cooled system between 0.15 to 0.45 W/cm<sup>3</sup>. The range of loss density of stator iron core volume is 0.025-0.04W/cm<sup>3</sup>; to the generators with capacity of 500MW and above, the range is better to be 0.024-0.034W/cm<sup>3</sup>. To high capacity of all air cooled generators, the proper value range of heat flow density made by stator iron core loss is 1.15-1.35W/cm<sup>2</sup>. The value of heat flow density made by stator winding loss is 0.5-0.77W/cm<sup>2</sup>, and higher capacity of all air cooled generator can choose the upper values.

In recent years, the value range of stator winding volume loss density and loss density of stator iron core volume for the generators of Longtan, Xiaowan, Laxiwa, and Three Gorges Right Bank Hydropower Stations, are all below the value range of all air cooled generators, such as, Geheyan, Ertan, Tianshengqiao I, and Shuibuya Hydropower Stations which were designed, manufactured and run after the 1990s, and even have the certain margin. Besides the stator iron loss volume density is reduced along with the increase of generator capacity (reducing the temperature rise in order to reduce the heat distortion and heat stress against the buckling of iron core), the other values of volume loss density and heat flow density would increase alone with the advancement of generator designing technology and increasing of the generator capacity.

### **2.3 Ventilation and cooling technology concerns not only about (Lt/ τ )**

In addition, considering that the ratio between the length of iron core and polar distance (Lt/ τ ) is the main characteristic data to judge the ventilation and cooling of air cooled generators, overlarge value of (Lt/ τ ) will directly affect the cooling and safe operation. The (Lt/ τ ) value of Xiaowan generator is 3.87, Longtan 3.92, Laxiwa 3.90, Three Gorges Right Bank 4.34, which are in the empirical scope of designing, building, and operation of all air cooled high capacity generators (such as 4.70 of Foz do Areia, 4.58 of Serra Da mesa, 5.01 of Xingo, 5.67 of Gori II, 4.17 of Liji Xia, 4.12 of Gezhouba and 3.27 of Ertan etc.). In fact, alone with the development of ventilation and cooling technology, for the median or low speed of high capacity hydro generators and high speed large capacity generator-motors using the two-way radial airtight self-circle air cooling system, their ventilation and cooling system do not only pay attention to the limits of (Lt/ τ ) value, but more to safe operation, total air ventilaton volume control, proper distribution of air volume and air flow speed as well as the expected cooling effect. All these can be guaranteed by the optimized design of ventilation system, more and more exact calculation, and ventilation model test.

On the basis of above comprehensive scientific analysis and demonstration, it is practicable to adopt the all air cooled alternative for 700MW hydro generator in Longtan, Xiaowan and Laxiwa Hydropower Station.

Proper design and selecting of equipment type play a primary role in engineering. In recent years, it is unnecessary to apply internal water cooled systems used in Three Gorge (Left Bank) hydro generators to all large capacity hydro generators in China.

### **3 DETERMINE THE ALL AIR COOLED GENERATOR ALTERNATIVE OF LONGTAN, XIAOWAN, AND LAXIWA HYDROPOWER STATIONS AND RELATIVE MEASUREMENTS**

In the recent years, with the commission from the owner, the author, on behalf of Hydropower and Water Resources Planning and Design General Institute, has been in charge of bidding document examination of hydroelectric generating units in Longtan and Xiaowan. Considering the willing of the owner, based on the technology data of Design Institutes, and especially analysis reports of the Harbin Electric Machinery Co., Ltd. and Dongfang Electric Machinery Co., Ltd. etc., agreed to change the cooling system from inter water cooling to all air cooled for generators.

### **3.1 Decision of hydro generator cooling system in Longtan Hydropower Station**

The author has given written consultant opinions of the choice of hydro generator cooling system in the technical consulting meeting for Longtan Hydropower Station in October, 2000 with a brief summary as the followings:

3.1.1 Inter water cooling system has the advantages to control the temperature difference of windings insulation in thermal and cold cycles and heat distortion when the generator is in the peak and off-peak regulation operation mode (especially when the length of the stator iron core is relatively longer. The length of the stator iron core of Longtan generator has reached 3.6m). But this water cooling alternative has too many water cooling connectors and one set of water treatment device, so its reliability is relatively lower comparing with the all air cooled alternative. One set of water treatment device per unit covers  $5 \times 7 \text{m}^2$ , which is more difficult to the layout of mechanical and electrical equipment of underground power house.

3.1.2 So far as we know, all air cooled system is technically mature alternative; the per-pole capacity of Longtan generator is in the normal design range of all air cooled system; proper design of all air cooled system can guarantee the even distribution ventilation of stator and rotor. Through the introduction of air cooled technology for Ertan project, Dongfang Electric Machinery Co., Ltd. has acquired the patent of ventilation technology from GE Company. The maximum capacity of the unit in Gori Hydropower Station is 805MVA, the length of stator iron core is 3.8m, and the capacity per pole is 15.1 MVA. In the past twenty or thirty years, the ventilation cooling technology has been largely developed. Two domestic main manufacturers have the experience of Ertan generating units (per-pole capacity has reached 14.6MVA). Compared with Ertan, per-pole capacity of Longtan Hydropower Station is 14.4 MVA (according to 700MW), which should be confident of success in technology.

3.1.3 With reference to the Longtan Hydropower Station beings underground, the layout of inter water cooling system has some difficulty; what's more, the regulation guarantee calculations of Longtan Hydropower Station has requirements to  $\text{GD}^2$ , so it is better to use air cooling system than inter water cooling system (additional on the basis of cooperation design with foreign manufacturers). It is better to have less compared alternatives in bidding documents. With the experience of successful examples, such as Tianhuangping Pumped-storage Power Station (per-pole capacity has reached 30MVA) etc., it is suggested that the technical specifications of the bidding documents should specify the manufacturers to provide calculation report of ventilation design and to make the ventilation model test for the generator. Then the ventilation design alternative would be carried out after the approval of owner.

Later, the review committee of the hydro generator bidding documents of Longtan Hydro Power Station, charged by the author, agreed that it is preferred to adopt the all air cooled alternative, and explicitly "suggest to cancel water cooled alternative." and point out that "the most important part in the technical specifications should be in accordance to the provisions and requirements of air cooling system, which need to have especial research and supplementary specifications."

### **3.2 Decision of hydro generator cooling system in Xiaowan Hydropower Station**

The Review Committee of the hydro generator bidding documents for Xiaowan Hydropower Station, charged by the author, has given this opinion: "agree to adopt preferentially the alternative of all air cooling system, and the stator inter water cooling alternative is workable as well. Bidders may recommend their alternative according to their practice, but shall provide all air cooling system as an option. The final choice should be given from the project owner.

### **3.3 Decision of hydro generator cooling system in Laxiwa Hydropower Station**

In the feasibility study report of Laxiwa Hydropower Station, the hydro generators use the inter water cooling system. The examination meeting, held by Hydropower and Water Resources Planning and Design General Institute, explicitly pointed out that "agree to use stator inter water cooling system and rotor air cooling system, further research should take the consideration to the rationality of all air cooling system in next stage." Later, according to the opinions of the meeting and aspiration of the project owner, "the 700MVA hydropower units research findings report and expert consulting meeting" was held. It explicitly suggested that all air cooling system should be adopted preferentially,

and no excluding to other cooling systems. Bidders may recommend their alternative according to their practice, but shall provide all air cooling system as an option. The final choice should be given from the project owner.

### **3.4 Corresponding measures should be adopted for hydro generator all air cooling mode**

Longtan, Xiaowan, and Laxiwa hydro generators have been the key developing giant all air cooled hydro generators in recent years in China. Due to large heat quantity made during the operation of generator, in order to effectively control the temperatures of stator and rotor windings, and iron core, so that the generator can operate safely and stably, we should pay attention to the design of ventilation and cooling system. Because Harbin Electric Machinery Co., Ltd. and Dongfang Electric Machinery Co., Ltd. have brought in new technology and it is the first time for them to design and manufacture the large scale air cooling generators of 700MW. the author has given special attention to the following measures in the situations of the design and review of generating units, bidding document consulting, contract negotiations and design liaison meetings etc.. Under the condition of no significant cost increase, it is better to have more design margins, so that the possible risk of the air cooling alternative will be reduced to the minimum. Its purpose is to make sure the smooth implementation of the air cooling alternative and a better foundation of successful operation in future. After the successful operation of air cooling generators, it is better to summarize the experience to review whether these margins and measures are conservative, necessary or rational.

3.4.1 Encourage the joint design of domestic manufacturers and qualified overseas manufacturers for the air cooling system, at the same time, trust that the major manufacturers in China with new technology transferred have sufficient experiences in designing, manufacturing and operating with substantial technical capability in computer software, model testing and talented pool through technology transfer and co-production. In several design liaison meetings, require the owners, design institutes, and manufacturers to research and analyze jointly the rationality of structure and design for ventilation and cooling system of generator.

3.4.2 Highlight for ventilation model test of generator: It is suggested to specify definitely making ventilation and cooling model test for generator before the bidding or after the award of contract, and provide ventilation and cooling calculation and analysis report of model test for generator with the bidding documents.

3.4.3 Strictly control the material of stator iron core and heat resources: suggest that the bidding document specify definitely specific loss per kilogram of silicon steel used for stator laminations not exceeding 1.05 W/kg when  $B=1T$ .

3.4.4 Agree the temperature rise limits of stator winding and rotor winding as 75K and 85K respectively, so that it can reduce heat stress and have some margins when the generator starts frequently and change greatly in output power.

3.4.5 Hope to have large design margin for generator air cooler: suggest “ capacity of air cooler shall at least have 15% of design margin. When 15% capacity of the air cooler (and at least one cooler) does not run, the generator shall be capable of long duration and continuous operation at rating conditions.

3.4.6 Attach importance to the selection of air cooler type: nowadays, there are many air cooler manufacturers in China and abroad with their technology developed very quickly, in improvement on heat conduction and wind resistance performance etc.. Good design of ventilation should be guaranteed by the air cooler with top-ranking quality and high efficiency of heat exchange. So the products of good quality in China and abroad will be preferentially used, in order to realize the designed ventilation effect.

3.4.7 Pay attention to the altitude effect of ventilation system design and have necessary modification.

It should be pointed out that, the main measures above, have gained the substantial support and active carrying-out of generator manufacturers, especially the Harbin Electric Machinery Co. Ltd. who has been awarded for the design and manufacture of giant hydro generator of above hydropower stations. With hard work in recent years, Harbin Electric Machinery Co. Ltd. has reached the world advanced

level in design, calculation and model test of ventilation and cooling system for giant air-cooled hydro-generator.

### **3.5 Cooling system of hydro generator in Three Gorges Left Bank Hydropower Station**

The left bank hydropower station of the Three Gorges Project use 14 units of 700MW generators with inter water cooling system, which is helpful to introducing effective technology of inter water cooling from abroad. According to opinions above, it is not necessary to adopt inter water cooling system in Three Gorges hydro generators with capacity per pole of 10MVA only, especially after the all air cooled system had been successfully used in Ertan hydro generators with capacity per pole of 14.57MVA. To our relief, the right bank power station of the Three Gorges Project has already used 4 all air cooled generators and these generators have been operating very well, which is advantageous to get experiences for the comparison of the two cooling modes.

### **4 EVAPORATIVE COOLING IS BETTER THAN INTERNAL WATER COOLING**

Evaporative cooling technology is new cooling method with proprietary intellectual property developed by our own country used in hydro generators since 1980s.

Evaporative cooling technology has the considerable cooling effect being equivalent to inter water cooling technology. With even low and well-distributed stator winding temperature rise, it is better to reduce heat stress and increase insulation life of the generator. These advantages are better to safe and stable operation. Compared with inter water cooling system, evaporative cooling system has the advantages as follows:

- Hollow wire would not have the problem of oxide blockage;
- No special requirements to adopt stainless hollow wire material;
- Abolish the expensive pure water treatment system (the price of ABB system and SIEMENS system is respectively 1,080,000 U.S. dollar and 2,200,000 U.S. dollar, so the total cost of generator will increase 2.5%-5.0% and the layout dimensions will increase too.);
- Evaporative medium is innocuous, safe and has good chemical stability;
- Environmentally friendly cooling medium have the advantages of insulation, anti-fire and arc extinguishing, which will fundamentally put an end to the problem of insulation fault by water leaking, so it has overcome the fatal shortcoming of inter water cooling system;
- The sealed problem of pipelines in the relative circle system is easy to solve, and no dirt will leave in the container and pipeline;
- Very low pressure (below the level of 0.03MPa, 1/12 of rated pressure of inter water cooling system) and no pump self-circled system, compared with high pressure forced-circled pure-water system (0.6MPa);
- Easy to operation, convenient to maintain and high reliability;
- Relatively short construction period.

Institute of Electrical Engineering Chinese Academy of Science, and Dongfang Electric Machinery Co., Ltd. have jointly developed, researched, and manufactured the evaporative cooled hydro generators of 10MW rated capacity, 1000r/min rated speed in Yunnan Dazhai Hydro Power Station in 1983; 50MW rated capacity, 214.3r/min rated speed in Shanxi Ankang Hydro Power Station in 1992; 400MW rated capacity, 125r/min rated speed in Qinghai Lijiaxia Hydro Power Station in 1999. The successful industrial trial operations of above generators indicate that the evaporative cooling technology is a reliable solution with industrial application value.

In recent years, under the substantial support and active calling from the China Three Gorges Project Corporation, Institute of Electrical Engineering Chinese Academy of Science and Dongfang Electric Machinery Co. Ltd. and Harbin Electric Machinery Co. Ltd. cooperate with each other in the use of evaporative cooling technology for 700MW unit size hydro-generator; carry out part of real machine model test and numerical simulation calculation; solve a series of technical difficulties of industrial

application on giant hydro generator by evaporative cooling technology. On that basis, Dongfang Electric Machinery Co. Ltd. and Institute of Electrical Engineering jointly present a design program for 840MVA hydro-generator to be used in Three Gorges Underground Power Station with evaporative cooling system. This program has already been passed by expert review. China Three Gorges Project Corporation decides to adopt this program. Nowadays, it is being carried out.

Certainly, if the technical performance and advantages of evaporative cooling system can be effectively put into play, and its quality and economical efficiency compared with other cooling system need industrial operation for testing.

## **5 CONCLUSIONS**

Selection of important electro-mechanical equipment should be taken serious consideration, because it influences the trend of equipment bidding, manufacturing, installation and operation in the next 5-10 years.

The author hopes that through the operations and all-round test of all air cooling generating units in Longtan, Three Gorges, Laxiwa, Xiaowan hydropower stations etc. , and mutual approval between calculation program and model test, we can make further summary of experience, so that air cooling technology of hydro generator will become more mature; At the same time, we need to speed up the industrialization that 840MVA or above hydro generator with evaporative cooling technology; Especially focus on the key technologies, such as hydraulic design of turbines, manufacturing of large steel casting and forgeable pieces, ventilation-cooling, thrust bearings and 24kV and above voltage stator winding insulation, to reach the world most advanced design and manufacturing of hydro generators; and accumulate experience of cooling system on 1000MW unit size hydro generator, which will be beneficial to implementation of Western Development Strategy and West-to-East Electrical Power Transmission Projects in China.

### **Brief introduction of the author**

Li Dingzhong, born in May 1945, is a Professor of Engineering in China Hydropower Engineering Consulting Group Co. He has worked on hydropower engineering design as well as technical management in Electro-Mechanical speciality for years.

**Research on Transposition Methods of the Stator Bars for  
Huge Hydro-generator**

**Sun Yang, Liang Yanping**  
**Harbin University of Science  
and Technology**  
**Harbin, China**

**Sun Yutian**  
**Harbin Research Institute of Large  
Electrical Machinery**  
**Harbin, China**

**SUMMARY**

There are a lot of circulating current existed between strands of the stator bars. The circulating current losses could be limited in a certain range by the traditional transposition methods , while the losses can not be reduced more. In this paper, the arrangement of the strands of the transposition methods is improved which named odd strands arrangement. On the basis of the detailed description of the odd strands arrangement, taking a huge hydro-generator as an example, the circulating current losses of traditional strands arrangement and odd strands arrangement under the four stator bar transposition methods are calculated accurately using leakage potential method, the distributions of circulating current and the circulating current losses of all the strands in a bar are also obtained. The results show that odd strands arrangement is beneficial to decrease the circulating current losses in the stands of the stator bars of hydro-generator obviously. The conclusion provides a theoretical reference for the project design.

**KEYWORDS**

Huge hydro-generator ; Stator bar transposition ; Odd strands arrangement

## 1 INTRODUCTION

The stator bars of huge hydro-generator are composed of many strands, which are connected together at the end region. Because the position of the strands are varied in the magnetic field, the electric potential difference between different strands will lead to circulating current. The average temperature of the stator bars is increased caused by the circulating current losses, therefore the service life and reliable operation of the generator will be harmed seriously. In recent years, with the unit capacity of hydro-generator increasing, the issues caused by the circulating current losses in the strands become more and more prominent. Stator bar transposition methods are usually used in order to reduce circulating current losses in China. There are four common transposition methods for hydro-generator, which are  $360^\circ$  bar transposition,  $0^\circ/360^\circ/0^\circ$  bar transposition with void, deficient  $360^\circ$  void bar transposition, and  $0^\circ/360^\circ/0^\circ$  extended bar transposition. The four transposition methods have different characteristics, and the circulating current losses could be limited in a certain range, while the losses can not be reduced more.

An improved stator bar transposition method which named odd strands arrangement is proposed in this paper. Arrangement of strands in the stator bar transposition is improved, and the circulating current losses can be reduced more. The principle and arrangement of odd strands arrangement are introduced in detail and on this basis taking a huge hydro-generator as an example, the circulating current losses of traditional strands arrangement and odd strands arrangement under  $360^\circ$  bar transposition,  $0^\circ/360^\circ/0^\circ$  bar transposition with void, deficient  $360^\circ$  void bar transposition, and  $0^\circ/360^\circ/0^\circ$  extended bar transposition are calculated accurately using leakage potential method, the distributions of circulating current and the circulating current losses of all the strands in a bar are also obtained. The results is compared and analyzed in detail.

## 2 ARRANGING METHOD

The number of the stator strands are even in the common bar, and there are one blank at the top of the bar and another at the bottom of the bar in order to make the strands transposition conveniently such as Fig.1A. The method of odd strands arrangement is adding a strand to fill in the lower blank of the bar which leakage magnetic is smaller, thereupon the number of the stator strands is odd.



Fig. 1 Strands arrangement of stator

A transposition pitch of odd strand transposition is shown as Fig.2. The principle of odd strands arrangement is transposed by the blank. The number strands of the odd strands arrangement is one more than the traditional strands. The advantage of this method is that it can make the slot filling factor increase and the circulating current losses also can be reduced obviously.

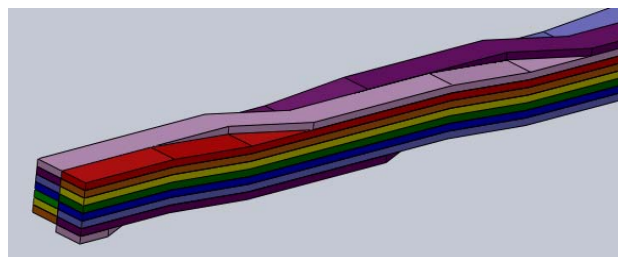
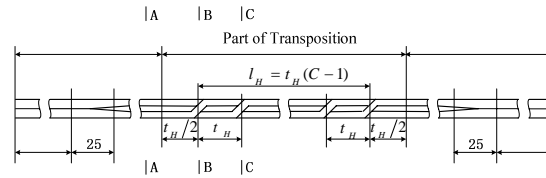
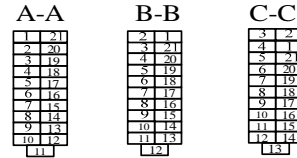


Fig. 2 Odd strands arrangement model

The transposed pitch and transposition method of odd strands arrangement and traditional strands arrangement are the same, odd strands arrangement method is shown as Fig.3.



**A The odd strand arrangement transposition**



**B Strands arrangement in the transposition cross-section**

**Fig.3 The odd strands arrangement method**

As the Fig.3 show, cross-section A, cross-section B and cross-section C are the three cross-sections in front. Cross-section A is the strands arrangement of the first cross-section, strand 1 is transposed when it pass through cross-section B, strand 2 is transposed when it pass through cross-section C, and so on.

### 3 THE RESULTS OF CIRCULATING CURRENT LOSSES IN THE STRANDS

The number of the strands of single bar of the huge hydro-generator is 80 when traditional strands arrangement is used, and the number of the strands is 81 when odd strands arrangement is used.

#### 3.1 360° bar transposition

Because induced potential of the strands in the stator slot part is counteracted, only consider the induced potential in the end of the hydro-generator. The circulating current losses of odd strands arrangement and traditional strands arrangement is shown as Fig. 4.

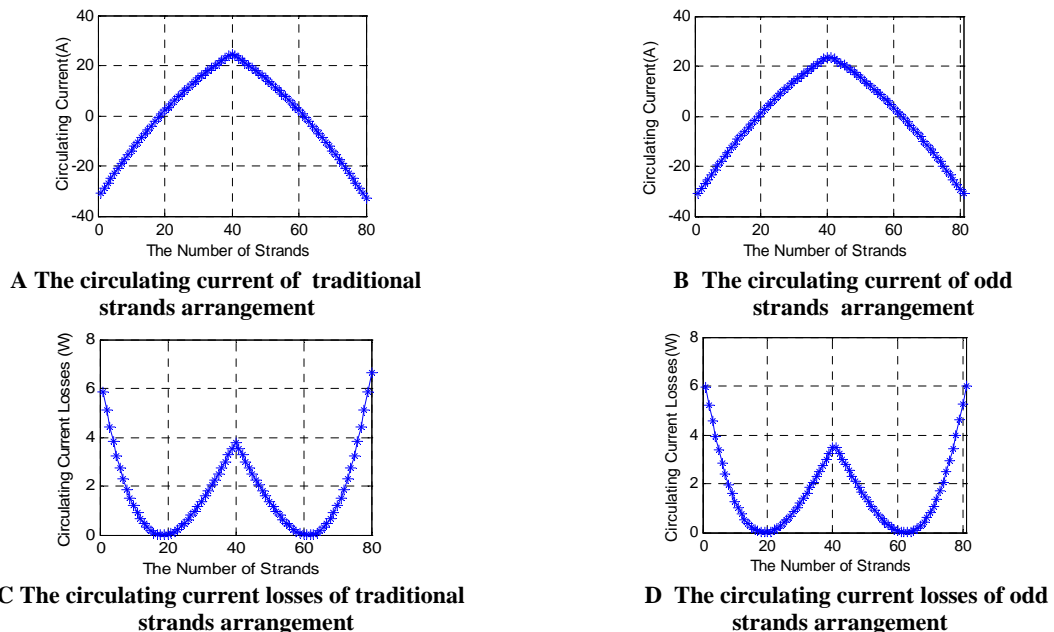


**Fig.4 The circulating current and losses under 360° bar transposition**

As the A and C of Fig.4 show, the circulating current in the strands is distributed as half cycle sinusoidal, the circulating current losses in the strands is distributed as ‘W’, when 360° bar transposition. The maximum circulating current in the strands is 32.74A, the maximum circulating current losses of the single bar is 6.61W, the total losses of a single bar with 80 strands is 137.84W. Therefore, the total circulating current losses of the hydro-generator will be 185.26kW.

As the B and D of Fig.4 show, the maximum circulating current in the strands is 31.10A, when odd strands arrangement. The maximum circulating current losses of the single bar is 5.98W, the total

losses of a single bar with 81 strands is 133.51W. Therefore, the total circulating current losses of the hydro-generator will be 179.44kW.

Comparison of the graphs in Fig.4 is easy to know, the odd strands arrangement compare with traditional strands arrangement the change trend of the circulating current and the circulating current losses are similar. But the circulating current losses and its maximum value will be reduced.

**3.2 0°/360°/0°bar transposition with void**

A void is added in the right position of the strands in the stator slot part, when 0°/360°/0°bar transposition with void. So that the circulating current produced by the magnetic leakage of the stator slot part and the circulating current produced by the magnetic leakage of end of the hydro-generator will be counteracted from each other, to reduce the circulating current losses. Taking the best void length, the circulating current losses of odd strands arrangement and traditional strands arrangement is shown as Fig. 5.

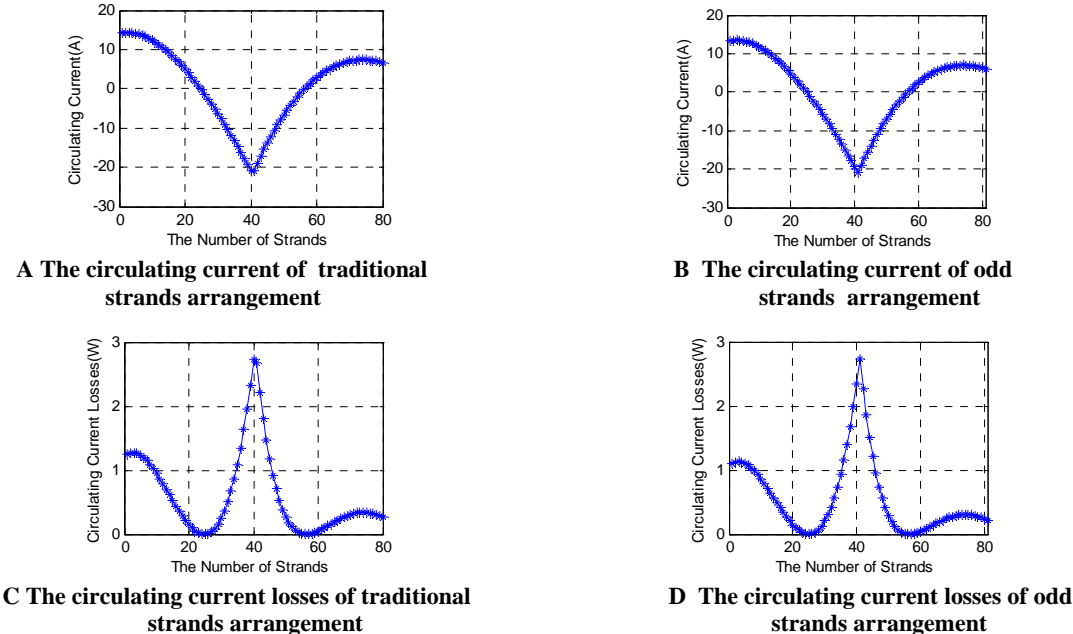


**Fig.5 The circulating current and losses under 0°/360°/0°bar transposition with void**

As the A and C of Fig. 5 show, the circulating current in the strands is distributed as ‘V’, when 0°/360°/0°bar transposition with void. The maximum circulating current in the strands is 20.98A. Compared with the 360° bar transposition, the circulating current losses are decreased a lot at this time. The circulating current losses of most strands less than 1W. The maximum circulating current losses of the single bar is 2.73W, the total losses of a single bar with 80 strands is 48.74W. Therefore, the total circulating current losses of the hydro-generator will be 65.51kW.

As the B and D of Fig.5 show, the maximum circulating current in the strands is 20.00A, when odd strands arrangement. The maximum value of the circulating current losses of the single bar is 2.73W, the total losses of a single bar with 81 strands is 45.11W. Therefore, the total circulating current losses of all the bars of the stator of the hydro-generator will be 60.62kW.

**3.3 Deficient 360° void bar transposition**

The transposition angle is less than 360° in the stator slot part when deficient 360° void bar transposition. So that the circulating current produced by the magnetic leakage of the stator slot part and the circulating current produced by the magnetic leakage of end of the hydro-generator will be counteracted from each other. The circulating current losses of odd strands arrangement and traditional strands arrangement is shown as Fig. 6.

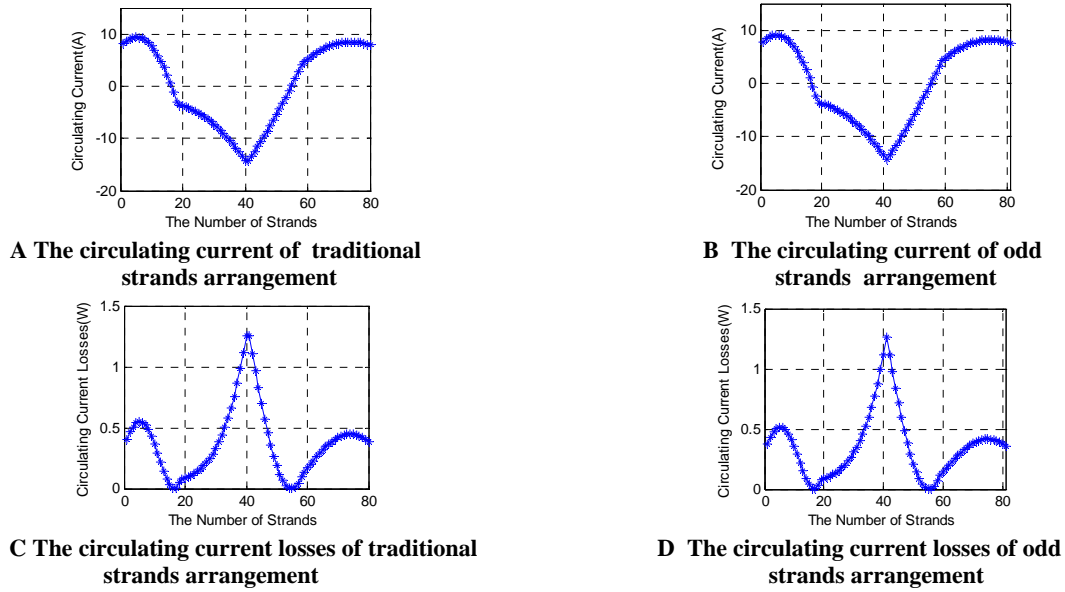


**Fig.6 The circulating current and losses under Deficient 360° void bar transposition**

As the A and C of Fig.6 show, the circulating current in the strands is distributed as ‘V’, when deficient 360° void bar transposition. The maximum circulating current in the strands is 15.71A. The maximum circulating current losses of the single bar is 1.52W, the total losses of a single bar with 80 strands is 35.70W. Therefore, the total circulating current losses of the hydro-generator is 48.00kW.

As the B and D of Fig.6 show, the maximum circulating current in the strands is 14.27A, when odd strands arrangement. The maximum circulating current losses of the single bar is 1.26W, the total losses of a single bar with 81 strands is 28.89W. Therefore, the total circulating current losses of the hydro-generator will be 38.82kW.

### 3.4 0°/360°/0° extended bar transposition

The strands in the end of the hydro-generator are also transposed, when 0°/360°/0° extended bar transposition. The same as extend 360° bar transposition. The circulating current losses of odd strands arrangement and traditional strands arrangement is shown as Fig. 7.

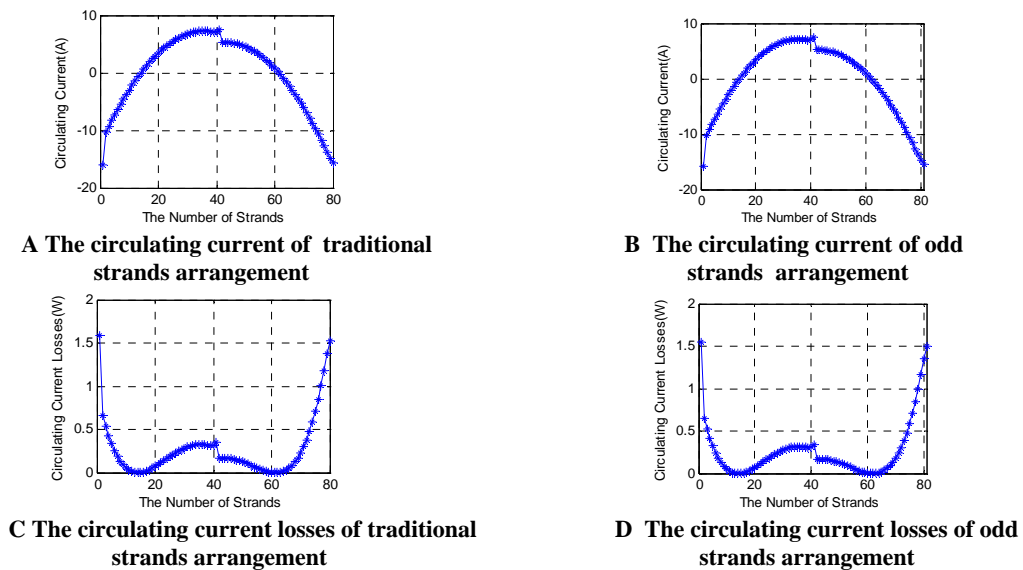


**Fig.7 The circulating current and losses under 0°/360°/0° extended bar transposition**

As the A and C of Fig.7 show, the circulating current in the strands is distributed as half cycle sinusoidal, when 0°/360°/0° extended bar transposition. The maximum circulating current in the strands is 13.46A. The maximum circulating current losses of the single bar is 1.52W, the total losses

of a single bar with 80 strands is 21.03W. Therefore, the total circulating current losses of the hydro-generator will be 28.26kW.

As the B and D of Fig.6 show, the maximum circulating current in the strands is 13.11A, when odd strands arrangement. The maximum circulating current losses of the single bar is 1.49W, the total losses of a single bar with 81 strands is 20.79W. Therefore, the total circulating current losses of the hydro-generator will be 27.94kW.

### 3.5 Results comparison

The circulating current losses of a single bar is shown as table1 when odd strands arrangement and traditional strands arrangement under the four cases.

**TableI Results comparison of a single bar**

	360° bar transposition	0°/360°/0°bar transposition with void	deficient 360° void bar transposition	0°/360°/0° extended bar transposition
the circulating current losses of traditional strands arrangement (W)	137.84	47.74	35.70	21.03
the circulating current losses of odd strands arrangement (W)	133.51	45.11	28.89	20.79
Reduce percentage	3.4%	7.4%	4.2%	2.4%

It can be known from table1 that comparison of the circulating current losses under different transposition method horizontal, the total circulating current losses of all the bars of the stator is the lest, when 0°/360°/0° extended bar transposition. It accounts for 15.26% of the circulating current losses of a bar under 360° bar transposition.

It can be known that comparison of the circulating current losses under different transposition method vertical, the circulating current losses of a bar is much smaller.

### 4 CONCLUSION

The circulating current and the circulating current losses of the bars of huge hydro-generator under various transposition method are calculated and analyzed in detail in this paper, when odd strands arrangement and traditional strands arrangement are used. The conclusion is as followed:

- (1) All the transposition method could be realized by odd strands arrangement and the the distributions of circulating current and the circulating current losses of all the strands in a bar are similar ;
- (2) The odd strands arrangement can increase the slot filling factor and reduce the circulating current losses obviously ;
- (3) The circulating current losses can decline 3.4% under 360° bar transposition, decline 7.4% under 0°/360°/0°bar transposition with voids, decline 4.2% under deficient 360° void bar transposition, decline 2.4 under 0°/360°/0° extended bar transposition using odd strand transposition method. The conclusions can provide theory basis for engineering design.

### BIBLIOGRAPHY

- [1] Jiang T , Song W . Analysis of the 0°/360°/0° Stator Bar Transposition with Voids for Large A.C. Machines[J]. TRANSACTIONS OF CHINA ELECTROTECHNICAL SOCIETY, 1989(4):23-30
- [2] Guo Y, Wang X. Analysis of Cirulating Currents among the Stator Bar Strands of Large Turbine-Generators[J].J. Huazhong Univ. of Sci. & Tech.,2000,28(4):83-86

- [3] Wang G. Research on Key Technologies of Installed in Three Gorges Right Bank Station Fully Air Cooled Hydro-generators[J]. Proceeding of the Csee,2009,29(15):74-79
- [4] Jiang T, Wang H, Song W. The Theoretical Analysis of Strand Circulating Current in the Stator Barrel Type Coil of AC Machines[J]. TRANSACTIONS OF CHINA ELECTROTECHNICAL SOCIETY,1991(3):11-16
- [5] Haldemann J. Transpositions in Stator Bars of Large Turbogenerators[J]. IEEE TRANSACTIONS ON ENERGY CONVERSION,2004,19(3):553-560
- [6] Guo Y, Wang X. Simplified Calculation Model of Circulating Currents among the Stator Bar Strands of Electrical Machines[J]. J. Huazhong Univ. of Sci. & Tech.,2000,28(5):86-88
- [7] Guo N, Han L, Shi X. Analysis and Comparison of Four Transposition Methods in the Stator Bar of Hydrogenerator [J]. Journal of Chongqing Unibersity, 2007,30(2):42-45
- [8] Jiang K, Han L. Calculation and analysis on stator bar transposition of Hydro-generator of tian ba qi[J].Dong fang Electrical Machine, 1995(2):23-30
- [9] Han L, Shi X, Guo N. New Methods for the Stator Bar Transpositions of Hydrogenerators[J]. Large Electric Machine and Hydraulic Turbine,2009(3):1-5

### **Experience with Turbine Generator Life Cycle Management Process**

**G.C. Stone**  
**Iris Power LP**  
**Canada**

**J. Kapler**  
**Iris Power LP**  
**Canada**

**J. Stein**  
**EPRI**  
**United States**

#### **SUMMARY**

Nuclear power plants are applying the Life Cycle Management (LCM) processes to manage aging degradation and obsolescence of important plant systems. The Electric Power Research Institute (EPRI) has developed an LCM process and some supporting software to help plant engineers to develop such LCM plans for systems important to plant reliability, availability and profitability. The Institute of Nuclear Power Operations (INPO) has integrated LCM in its equipment reliability industry guidance. The general objective of the LCM process is to provide system engineers with generic information, data and guidance to generate long-term equipment reliability plans and focus on areas where there may be opportunities for cost-effective improvements in the remaining plant life. The LCM process was applied to the main generator since it is subject to significant degradation and requires costly maintenance. This paper describes a typical LCM process for the main generator and exciter. The process includes assessment of the industry operating experience with generators, plant specific performance review, and the aging and obsolescence assessment. The process has been applied to 17 generators at 13 plants in the USA and Spain, to date.

#### **KEYWORDS**

Turbine generator, Reliability, Maintenance planning.

## **1 INTRODUCTION**

The majority of nuclear units throughout the world are 25 to 35 years old. Presently, plant asset managers are assessing the condition of their major equipment and systems and evaluating the required investments necessary to extend the operating licenses to 60-year reliable plant life.

The expected operating design life of generators and exciters was originally defined at 30 years. All active generator components are subject to wear and degradation. The rate of this degradation is affected by initial design, fabrication and installation, preventive and corrective maintenance practices, operating conditions such as temperature, vibration, and grid disturbances. Expected life is defined as the time from start of service to the point when reliable service cannot be maintained with normal periodic maintenance.

The end of a generator life is not necessarily defined as the end of life for the whole machine, but rather of its main components: stator winding, stator core, rotor and excitation system. The renewal of these components is usually the strategy to extend the generator's operating life to the end of a generating plant as a whole.

The recognition of gradual or accelerated aging of individual generator components is required to plan for timely preventive and corrective maintenance, including replacement, to ensure that the generator performs reliably within the defined parameters. The following is a description of a process designed to help plant engineers to develop such plans and present them for implementation. The life cycle management process (LCM) for the main generator and excitation systems was developed by EPRI and published in 2001 [1]. It has so far been used by 13 nuclear power plants in the US and Spain to examine their maintenance and component replacement strategies for the current periods and for the anticipated future license extensions.

In this process the past plant forced outages due to failures of generator and excitation components are compared to the average industry failure rates from 104 generators and exciters over a 10-year period. The future failure rates for a specific main generator are evaluated from the current condition of the components, (derived from the past on-line monitoring data, off-line tests and from detailed visual inspection of the equipment) and from corrective/replacement activities planned in the future. A set of alternative maintenance strategies can be developed and life cycle costs calculated. Alternatives with the lowest net present value (NPV) or best benefit-to-cost ratio (B/I) can be identified and presented for implementation. EPRI-developed software programs such as LcmPLATO or LcmVALUE [2] can be used to facilitate the calculations.

## **2 INDUSTRY OPERATING EXPERIENCE**

A review of industry experience with generator performance included failure data on 65 of 104 generators and exciters at 45 nuclear power plants in a 12-year period from 1990 to 2001. A total of 115 forced plant outages were recorded, causing 1120 forced outage days. Although much of generator preventive (PM) and corrective (CM) maintenance is completed during reactor re-fueling outages, the number of forced outages and of forced extensions of PM and CM outages is still considerable. The data indicates the following dominant component contributions to unit downtimes: stator winding, rotor winding, rotor forging and excitation system with voltage regulator.

The resulting failure rate from these data was calculated at 0.092 per generator-year and the average forced outage time to 9.74 days (234 hours) per event. The forced outage rate (FOR) was calculated at 0.31 %. The average Lost Power Generation at a power price of \$50 per MWH amounts to about \$12 million dollars per event for a 1000 MW plant. The annual risk is the failure rate of 0.092 times the event cost, or about a million dollars for a 1000 MW plant.

The review of performance statistics from other databases such as NERC/GADS, Canadian Electrical Association and French EdF [3] reports on nuclear units indicate some discrepancies with the Equipment Performance Information Exchange (EPIX) (managed by INPO) data because of the differences in the reporting systems. However, the review confirms that the generator reliability is comparable when similar maintenance programs and performance monitoring criteria are used.

It is suggested that the Nuclear Power Reliability Data System (NPRDS)/EPIX (managed by INPO with NPRDS discontinued and replaced by EPIX) data be used as a benchmark in plant specific failure rate evaluations. It is also proposed that the number of generator components in the analyses be limited to a manageable number and to those that have the largest contributions to the unit downtime and are the costliest to repair or replace. The generator components and associated failure rates, derived from NPRDS/EPIX data, are presented in Table I .

**Table I Generator Major Component Average Failure Rates**

<b>Generator Component</b>	<b>Failure Rate (per year)</b>
Stator Winding and Core	0.016
Rotor Winding and Forging	0.010
Exciter and Voltage Regulator	0.035
Other	0.0136

**3 PERFORMANCE AND CONDITION ASSESSMENT OF A GENERATOR AND EXCITATION SYSTEM**

This is perhaps the most important and most critical component in the evaluation of the fitness of the main generator system for future service. The current condition will reflect the extent of the aging, wear, and degradation of the main generator and exciter components. Recognition of the early stages of deterioration and timely repair play an important role in the generator longevity. The steps in this review include the following:

**3.1 Compiling the operating and performance history**

The operating and performance history will identify past corrective actions, including replacements and upgrades already completed or planned in the near future. This may identify evidence of generic problems on individual components and the likelihood of their occurrence in the future.

Review of the number of unit outages and their durations attributed to the generator and exciter will indicate the cost of loss of unit production and also provide the basis for the assessment of the generator component failure rates. The calculated failure rates are used in the economic evaluation of current maintenance costs and for comparison of the alternative LCM maintenance plans.

The records of past inspections and tests may provide information about already observed degradation and the presence of active failure mechanisms. The trending of the progression of the component degradation by on-line monitoring or periodic testing will indicate the urgency for future corrective actions.

**3.2 Compiling maintenance history**

The maintenance history provides a record of PM and CM activities, such as correction of normal aging degradation, design changes, enhancements and replacements. The costs of these activities are extracted for economic analyses. The work orders or work plans of these activities can be extracted from plant records. They include descriptions of problems, root cause analyses, parts required for corrections, man-hours required to complete them and all associated material costs. The manpower and cost data often have to be extracted from other associated records. These activities are normally separate from the routine work done when the unit is on-line and actions completed off-line during re-fueling or other planned outages.

This information is used to identify the need for additional preventive maintenance or predictive maintenance work, potential improvement to the current maintenance programs and the need for replacement of degraded components. Some upgrades and redesign may also be required in anticipation of the potential unit up-rates associated with the upgrades of the reactor, steam generator and turbine systems.

The definitions of the PM and CM may differ from plant to plant. In LCM economic evaluations it is important to use consistent definitions. The EPRI LCM process uses the definitions from “Nuclear Power Plant Common Aging Terminology” [4]. A simplified general rule is: PM is done on an un-failed component, CM on a failed component.

### **3.3 Inventory of current maintenance activities**

Each plant normally develops a set of maintenance procedures for all their systems, including the generator. These procedures are founded on applicable national codes and standards (IEC, IEEE, government), insurance carriers, and plant reliability targets. A review of these activities provides the basis of the inputs for the base case in LCM planning alternatives. It also provides a benchmark for comparison to industry practices and is the source to identify the need for additional activities, enhancements and possible reduction opportunities.

### **3.4 Generator monitoring systems**

Generator and exciter condition and status are supervised with monitoring and protection systems. With severe and sudden fault events, such as stator and rotor winding ground faults, phase to phase shorts, core faults and the like, the generator protection systems take the unit off-line in a forced outage. Long unit outages and expensive repairs are frequent in such conditions.

The **on-line monitors**, continuous or periodic, provide real-time status of some generator components [5]. They detect long-term trends for dominant aging mechanisms. Temperature monitoring of insulation, endwinding vibration, partial discharge testing, rotor shorted-turn detection, core condition monitors are all examples of on-line monitors. The normal expected values from the monitors are often defined by the generator OEM. Deviations from these values indicate the severity of a problem and may be presented in multi-stage alarms. Sudden unit trips are normally not triggered by these devices. They provide information necessary to plan for PM and CM actions.

The main purpose of **off-line testing** is to diagnose, locate and assess the severity of component deterioration. These tests may confirm the aging or failure mode already indicated by on-line monitors. A group of these tests is normally included in any major generator inspection plan.

A review of the results from monitoring will aid in detecting the developing failure mechanism and will point to the need for immediate or planned PM. It will also indicate the effectiveness of the current monitoring and provide evidence for the necessity of implementing additional monitors.

### **3.5 Condition and performance assessment**

Information on the current condition of generator components is required to assess their suitability for service and the evaluation of future failure probabilities. A detailed inspection and a number of tests are required for this task [6]. Rotor withdrawal is normally required to gain access to internal components. A review of recent inspection and test reports, including records of any correction of defects, modifications or parts replacements will provide further information about the condition of generator parts. This condition assessment will identify the extent of the aging of some components like insulation or accelerated deterioration from vibration, abrasion, overheating, fatigue cracking, coolant leaks and other. The need for future PM and remedial actions need to be assessed.

The records of unit forced outages, or forced extensions to planned outages, attributed to the generator, exciter and voltage regulator should be extracted and reviewed. This review will provide information for calculation of the plant-specific failure rates of major components. These failure rates can be compared to the average industry data, shown in Table 1. If significant discrepancy is found, there may be a need for PM enhancement. The range of options for such enhancements will be evaluated in the LCM alternatives and economic assessments will show the ranking for possible implementation.

## **4 GENERIC AGING AND OBSOLESCENCE ASSESSMENT**

### **4.1 Review of aging mechanisms**

All active generator components are subject to wear and degradation from operating stresses such as temperature, mechanical loading, dielectric stress and environmental conditions. Normal aging of generator components occurs when a generator operates within rated power, at rated voltage and frequency, within rated temperatures and within normal system operating conditions over time. The limits of these parameters are defined in national standards; manufacturers may apply additional internal design standards in order to meet the user Performance Specifications for plant life expectancy.

Generator life expectancy implies that some preventive or condition based maintenance will take place at defined intervals or as indicated by condition monitoring systems. In addition, the generator will be protected against system operating events, which would result in non-repairable accelerated deterioration. Recognition of the early signs of deterioration and timely repair play a very important role in generator component life expectancy.

Operational experience indicates that generators, as a whole machine, seldom “die” suddenly and without any early indication of gradual deterioration. There are records of sudden loss of whole generators from catastrophic events such as internal fires, rotor forging bursts and retaining ring explosions. These are rare and do not represent the normal aging. Rather the gradual aging of individual generator parts, particularly the insulation systems in the stator winding, stator core and rotor winding, lead to repetitive breakdowns, high repair costs and unacceptable production losses.

A comprehensive outline of winding insulation failure and aging mechanisms in generator stators and rotors can be found in EPRI Volume 16, Handbook to Assess Rotating Machine Insulation Condition [6].

#### **4.2 Expected life of major components**

There is general expectation that a generator, under normal operating conditions, will perform at average generator reliability and without major upgrades, for about 30 years. Many power generating plants, including nuclear plants, have extended the expected operating life to 40 years. This was obtained by extending the licensing permits and in consultation with their respective equipment OEM.

Actual in-service experience of large generators indicates that the actual life of generator components may be significantly different from the expected design life of 30 years. All active generator components are subject to wear and degradation. The rate of component degradation is affected by initial design and fabrication, operating conditions, and maintenance practices.

The life expectancy periods can be used for long range planning of component replacements and upgrading. Although they reflect the field experience, they may not be applicable to all generators. As an example, the life of a sound rotor forging is expected to last more than 60 years. However, a life of less than 5 years was experienced on a few forgings having design flaws, which were not recognized during the design and manufacturing stages.

The plant specific life expectancy of any generator component should be evaluated from the condition assessment results and evaluation of generic problems known to exist for each component.

#### **4.3 Technical obsolescence**

A number of generator and exciter systems are sensitive to technical obsolescence. The stator cores, and stator and rotor windings are generally not considered to be obsolete even after long service. The design function, basic materials and dimensions parameters have not changed substantially in the last half-century, although significant progress has been achieved in design optimization and material properties. Replacements of these components, even if they are many decades old, are readily available from the OEMs and after market sources.

Electronic control, monitoring and protection components and circuit cards in exciters are examples of components sensitive to technical obsolescence. These components are used in most nuclear units and were designed and assembled in the sixties and early and mid-seventies. In LCM, planning the replacement of components should be considered when the availability of spare parts becomes limited and the failure rates on the system are rising to unacceptable levels. The availability of parts from alternative sources and some reverse engineering of obsolete components can be considered, if they are cost effective.

### **5 DEVELOPMENT OF ALTERNATIVE LCM PLANS**

The LCM planning alternatives at each plant are determined largely on the basis of current reliability performance of its generators and exciters. Therefore, the LCM planning alternatives proposed for evaluation at each plant will be very much plant-specific.

Following the assessment of the condition of the generator and exciter components and after the review of past reliability performance, potential alternative LCM plans can be identified. If the significant aging of some components has been identified, these components may require upgrading or replacement before there is high risk of their sudden failure in service. A review of past performance may indicate higher failure rates than the industry average. The objective of alternative LCM plans is to explore whether there are potentially better ways of managing the equipment aging in the remaining plant life period [7].

The following guide includes the identification of possible plant operating life strategies and the development of alternative LCM plans that are compatible with or integral to the strategies identified.

Alternative plant strategies may be developed for different expected life periods of the plant. In one strategy, the 40-year life of the currently licensed period may be examined, in the other an operating license extension to 60 years may be considered. In each strategy the current maintenance practice forms a base case against which 3 or 4 alternatives are examined to identify an economically optimized option. A typical approach to an LCM plan may include:

**Plant Strategy 1: Operate the plant to its currently licensed period of 40 years.**

- **LCM Plan Alternative A:** A base case to determine the cost of the activities performed under the current maintenance plan, assuming that the current activities will continue to the end of the licensed plant life. This case assumes the continuation of the existing maintenance programs without any major capital investments unless they are necessary for continuation of plant operation.

- **LCM Plan Alternative B:** A plan where the current maintenance plan is optimized and an enhanced PM program is implemented to reduce equipment failures, lost power production and regulatory risk. The plan may include the purchase of additional generator component condition monitors to detect aging mechanisms in the early stages, enabling timely repairs and limiting the risk of sudden failures. Replacement of major parts may also be required in order to secure a 40 year operating life at target performance levels, e.g. planned replacement of obsolete exciters.

- **LCM Plan Alternative C:** An alternative in which the current maintenance plan is optimized and degraded generator components are upgraded, e.g. stator and rotor rewinds. The target of such a plan is to reduce the current level of the generator failure rate and lower unit production losses.

- **LCM Plan Alternative D:** An alternative in which further upgrades are considered with the purchase of new stator, new rotor and new exciter.

**Plant Strategy 2: Operate the plant for 60 years under a License Renewal Program**

Similar alternatives can be developed for their cost evaluation. In each alternative all costs and benefits should be considered. Typical components of these costs related to the generator are:

- Plant maintenance costs with unit at power.
- Plant outage planning and plant outage maintenance costs during outage. The outages here are refueling outages and costs include manpower and materials.
- Contract cost of external contractors.

The critical component is the cost of lost production assigned to generator and exciter. These costs are derived from the failure rate probabilities of individual generator components and their repair cost to return the unit to service.

**6 ESTIMATING FUTURE FAILURE RATES**

The plant specific past failure rates for each component of the generator and exciter system can be calculated from the forced outage failure data caused by and assigned to individual components [8]. These values can be compared to the industry average for the same components. Significantly higher values may point to generic problems, lack of monitoring for detection of aging modes and lack of appropriate PM and CM actions.

The future failure rates used in Base Alternatives will be close to these values, unless the already completed PM/CM actions justify a reduction, e.g. stator or rotor rewinds already done, additional monitoring implemented, etc. In cases where no failures were recorded on a component, the industry average values can be used, because it is not likely that the component will sustain the zero failure rate over the life of the plant. The selection of the failure rates should also consider the current, or the most recent, assessment of the actual physical condition of the evaluated components.

The future failure rates of other examined alternatives should be evaluated on the basis of merits of the proposed maintenance actions. For example, implementation of enhanced on-line monitoring will help to detect developing problems such as excessive winding temperatures and vibrations, water leaks, rising trend in partial discharge activity, rotor shorted turns, and others. Reductions in failure rates may be justified on the basis of improved PM and CM actions from such information. Major upgrades such as rewinds of stators and rotors, or purchase of new components and major spares, significantly reduces the estimated future failure rates. The enhanced designs and application of advanced technologies may justify adoption of failure rates lower than the industry average.

Evaluation of future failure rates normally requires advanced familiarity with component failure mechanisms, their recognition and the effect on life expectancy. In addition, the average repair costs and repair times need to be considered. These capabilities may sometimes not be available to personnel at the plant level and the services of external consultants or OEMs may be needed.

The failure rates for generator stators and rotors may look something like Table II. In alternative 1B the application of enhanced on-line monitoring is evaluated, in alternative 1C the stator and rotor will be re-wound, in alternative 1D the purchase of new stator and new rotor is considered.

**Table II Generator Stator and Rotor Failure Rates Inputs**

Plant	Stator Failure Rates (FR)					
	Industry FR	Plant FR	Alternatives			
			1A	1B	1C	1D
ABC	0.016	0.05	0.05	0.03	0.016	0.01
	Rotor Failure Rates (FR)					
	0.01	0.03	0.03	0.02	0.01	0.01

The failure rates shown in 1B, 1C and 1D are artificial and reflect a possible assessment of enhancements considered in the respective alternatives.

The calculations of yearly and cumulative costs to the end of plant operating life can be modeled in software applications such as EPRI LcmVALUE and LcmPLATO, or similar commercial applications.

**7 ECONOMIC COMPARISON OF LCM ALTERNATIVES**

The above inputs in calculation of net present values (NPV) and benefit-to-cost ratios (B/I) on a 1200 MW nuclear unit may produce results as demonstrated in Table III.

The B/I ratio in this table represents the benefit-to-investment ratios of Alternatives B, C, and D relative to base case Alternative A. In the 40 year life, Alternative C appears to result in the lowest NPV cost and the best B/I ratio and would be recommended. In 60 year life Alternative D appears the best, despite the higher cost of a new stator and a new rotor.

**Table III LCM Alternatives**

<b>LCM Plan Alternatives</b>	<b>NPV Cost Total 40 Years</b>	<b>B/I</b>	<b>NPV Cost Total 60 Years</b>	<b>B/I</b>
Alternative A	\$24,000,000	N/A	\$32,000,000	N/A
Alternative B	\$21,500,000	1.12	\$29,000,000	1.1
Alternative C	\$15,200,000	1.58	\$26,000,000	1.23
Alternative D	\$26,800,000	0.89	\$22,300,000	1.43

The NPV cost reduction results from the reduction in the cost of lost generation (lower failure rates), despite higher PM cost from implementation of the component upgrades.

## **8 CONCLUSIONS**

- Evaluation of life cycle costs of all maintenance costs and probable lost production costs is an effective process to define the optimized maintenance cost strategy.
- Assessment of the current condition of the main generator components and evaluation of the future failure probabilities from the identified failure modes are critical for estimating the expected generator life.
- The presented LCM process, sponsored by EPRI, has so far been used successfully at 13 of nuclear plants for assessment of optimized maintenance alternatives of the main generator and excitation systems.

## **BIBLIOGRAPHY**

- [1] EPRI Technical Report 1003058:Life Cycle Management Planning Sourcebooks-Overview Report, December 2001
- [2] EPRI Software 1003435:LcmVALUE, Version 1.0a, LCM Planning Tool, June 2002
- [3] European Industry Reliability Data Bank, EIReDA,1998:Crete University Press
- [4] Nuclear Power Plant Common Aging Terminology, EPRI, TR-100844
- [5] Guide for On-Line Testing and Monitoring of Turbine Generators, EPRI Report 1006861, March 2002
- [6] Culbert I M, et al. Handbook to Assess the Insulation Condition of Large Rotating Machines, Power Plant Electrical Reference Series ,16, EPRI
- [7] Miller R, Creed W. Technical Workshop and Vendor Exposition Life Cycle Management, EPRI, NOC ,Winter 2007
- [8] Anders G.Probability Concepts in Electric Power Systems:John Wiley & Sons Canada Ltd., 1990
- [9] EPRI.Plant Support Engineering: Main Generator End-of-Life and Planning Considerations, Report 2007. 1014783, Palo Alto, CA

## **Temperature of Turbo-generator Stator Strands**

**Y.Satake, K.Hattori, K.Takahashi**  
**Hitachi, Ltd.**  
**Japan**

### **SUMMARY**

In this paper, the results and consideration of temperature measurement of turbo-generator stator strands are described. Embedding resistor temperature detectors (RTDs) between stator coils are usually the only way to detect the temperature of the stator coils, but it doesn't show the temperature of the stator strands. Although the critical temperature that may damage the insulation system is the temperatures of the conductors, they cannot be measured easily.

As had been reported since year 2004, we have developed calculation tools that can predict temperature distribution in stator strands. Also temperatures of stator strands were measured directly in actual generators. We obtained many useful data and have been accumulating databases on developed turbo-generators. Now it is the time to reveal the measured values of stator strands in actual generators.

As the calculation predicted that the temperature at the series loop connection shows the hottest depending on the generator design, sensors for stator strand temperatures were installed both at the end and in the slot. To verify these phenomena, several stator test models were also manufactured. The measured values were positively correlated with calculated values.

In conclusion, the actual temperature of the stator strands that had not usually been measured is reported in this paper. The accurate temperature calculation tools and measurement techniques were developed and continue to progress.

### **KEYWORDS**

Turbine generator, Stator coil, Stator strands, Temperature distribution, RTD

## 1 INTRODUCTION

Today, generator design demands large capacity and low environmental burden with less material used for construction. In addition, many customers require generators that combine high energy efficiency with user-friendly operation and the long term reliability of the unit. To achieve these requirements, a generator's amount of heat increases, so the temperature becomes severe. Consequently, to reduce temperature rise, 540 degree transposition and ICVS (inner cooler ventilation system)<sup>[1]</sup> are often used to minimize generator losses and improve cooling performance, lowering and averaging the maximum temperature. Also, the generator can ensure high efficiency at the same time by reducing losses. We have developed air-cooled generators up to 300MVA class and added it to its product line up. These generators optimize the cooling by ICVS and configuring a stator coil to achieve a better cooling by using augmented air flow. These measurements improved the precision of various design tools. Since then, the design tools have been constantly evolving. Now, we have come to be able to predict a detailed temperature distribution of the stator coil strands by using this tool<sup>[2]</sup>.

## 2 TEMPERATURE MEASUREMENT FOR GENERATOR

Generally, temperatures of stator coils are measured with RTDs embedded between top and bottom coils, as shown in Fig.1. Historically, the temperature of RTDs has been believed to be the mean temperature of the top and bottom coils. In fact, temperature measurement on an actual generator revealed it often becomes lower than those of the top and bottom coils. The RTD cannot detect the temperature of stator coil strand itself. It is important to reliably measure temperature of stator strands or to accurately predict the temperature of stator coil strands. Provided that we know the relationship between the temperature of stator coil strands and that of RTDs, measuring only RTD temperatures gives some information on the temperature of the stator coil strands.

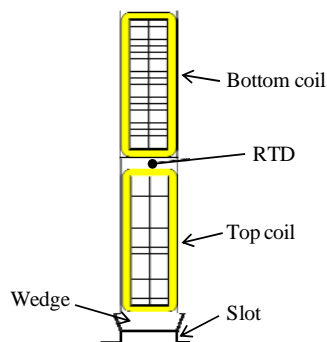


**Fig.1 Coils and RTD in a Stator Slot.**

In other words, if we know how to estimate strand temperature from the value measured with RTDs, we can prove the reliability of the generator. However, the direct temperature of the stator coil strand is not measured easily because it is in a high voltage range of about 10-30kV. The high magnetic field there also prevents the measurements. To measure temperature of stator coil strands, optical temperature sensors that are not usually used were installed in the stator coil strands. And temperature distribution of the strands was measured. The calculation result of the temperature was evaluated and compared with the measured value. Fig. 2 shows installed optical temperature sensors. Although the result of the measurement has not been explicitly revealed, this paper discloses the measured temperature distribution of stator coil that is not usually observable.

On the other hand, the rotor coil temperature is estimated by comparing the rotor coil resistance, measured prior to the rotation test, with the resistance obtained from the field current and field voltage measured in the rotation test. However, this is the average temperature, so a maximum temperature cannot be taken. There should be a special scheme to measure rotor coil temperature because of high rotational speed and high centrifugal force, but this is not within the main scope of this paper.

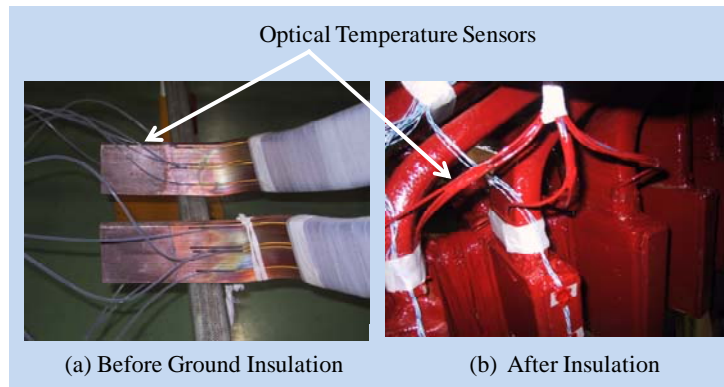


**Fig. 2 Installed Optical Temperature Sensors.**

### 3 COMPONENTS THAT AFFECT TEMPERATURES AND HOW TO DESIGN GENERATORS

#### 3.1 Generator heat source

Temperature is determined by the quantity of heat and cooling. This subsection discusses the origin of the temperature rise or heat source, or in other words, loss of each part. The losses that affect generator temperature are as follows.

- (1) Mechanical and ventilation loss
- (2) Iron loss
- (3) Armature  $I^2R$  loss
- (4) Field  $I^2R$  loss
- (5) Stray load loss

All these losses affect the temperature of stator coil. Some of these losses are easily estimated while the others are very complicated. Consequently, the summation of the losses is very complicated. These losses are calculated in detail by using three-dimensional analysis<sup>[3]</sup>. This calculation considers armature  $I^2R$  loss, eddy current loss and circulating current loss. Also, this calculation considers strands in transposed coil. As the loss distribution is very complicated, so is temperature distribution.

#### 3.2 Ventilation

Generators are equipped with cooling paths. Examples of the paths are the air gap between the stator and the rotor, air ducts between core laminations, and ventilation grooves or radial ventilation holes on rotor conductors, etc. For generator design, all of these ventilation paths are estimated as a flow resistance and combined to build up ventilation network analysis<sup>[4]</sup>. This calculation estimated total air volume in the generator and air flow distribution in each part of the generator. The part that is predicted to become a complex flow is calculated in detail by using three-dimensional flow analysis. The results are fed back to the network analysis. Fig. 3 shows an example of three-dimensional flow analysis.

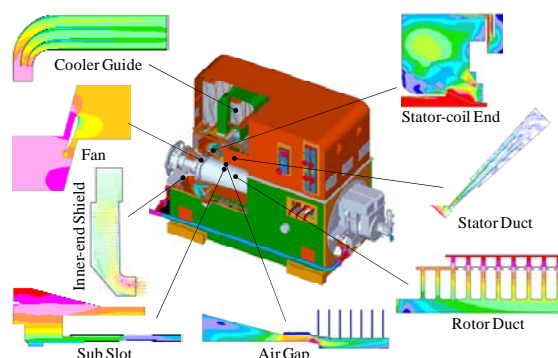


**Fig. 3 Example of Flow Analysis.**

### 3.3 Temperature calculation of stator coil

The network analysis calculates the temperature of stator coil [2]. Fig. 4 shows an example of a thermal network for a generator. This calculation begins with the series-connected components and expands to the center point in an axial direction. This network model takes into consideration the stator coil, core, air gap, stator ducts, and all the other components, including the stator wedges and ripple springs. We take into account the actual configuration of the strand transposition in slot area as shown in Fig. 5. With all the losses in the generator taken into consideration, the temperature distribution can be calculated.

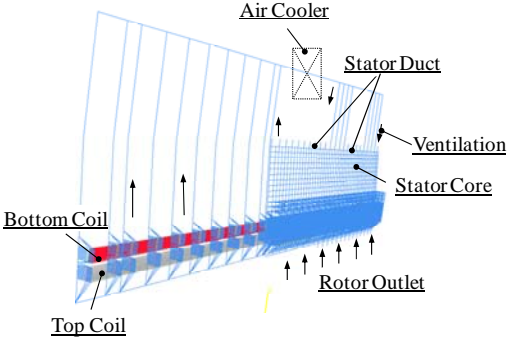


Fig. 4 Thermal Network for Generator.



Fig. 5 Stator Strand Transposition.

Although the rotor temperature may not seem important for stator temperature, it does affect stator temperature because the rotor sometimes produces 10-20 percent of total loss and the outlet gas of the rotor sometimes exceeds 100 degrees Celsius. Thus, as with the stator coil, this calculation takes into consideration the all parts and all losses including the rotor.

### 4 VERIFICATION TEST

For a 250MVA class air-cooled generator, the temperature of stator coil was calculated and verified with measurement. The specifications of this generator are listed in Table I . More than 1000 temperature and ventilation sensors were installed in this generator including the sensor for directly measuring the stator and rotor coil strands. In accordance with the findings regarding the calculation, temperature sensors were placed in a concentrated manner, particularly in places where the stator coil temperature was high. The locations of these sensors are shown in Fig. 6.

Table I Specifications of 250MVA Class Generator

Item	Specifications
Output power	250 MVA
Voltage	20 / 18 kV
Short-circuit ratio	0.5
Power factor	0.85 / 0.90
Number of poles	2
Rotation speed	3,600 / 3,000 min <sup>-1</sup>
Insulation class	class F
Temperature rise class	class B
Efficiency (measured)	98.80 %
Cooling method	Totally enclosed

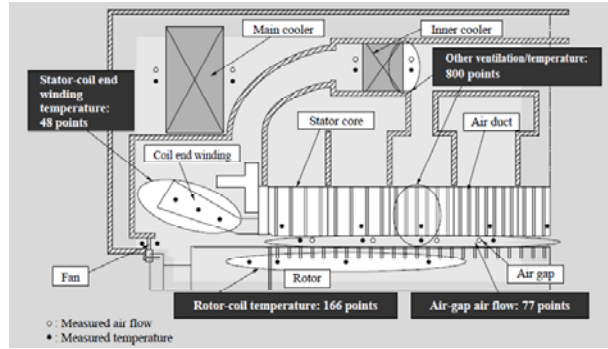


**Fig. 6 Main Measurement Points of Generator.**

On the stator coil strands, optical temperature sensors were installed in slots and the coil-end region. The optical temperature sensor is suitable for measuring this part because it has superior electric strength and is magnetic field performance-resistant. The locations of the installed optical temperature sensors are shown in Fig. 7. The optical temperature sensors were installed in the upper, middle, and lower parts of the stator coil strands in order to measure the temperature distribution and the maximum temperature in the stator coil strands.

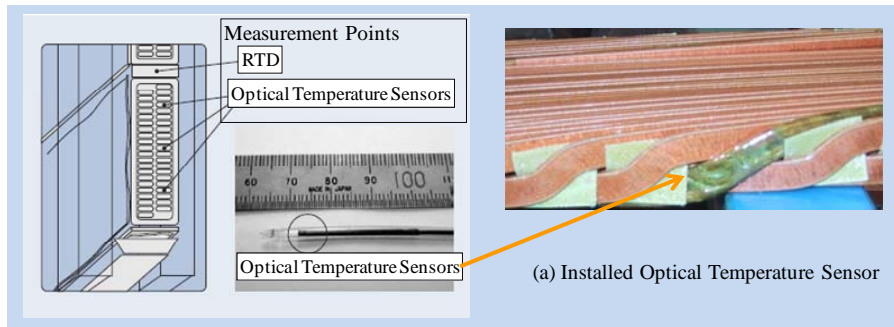


**Fig. 7 Temperature Measurement Points and External View of Optical Temperature Sensor.**

Fig. 8 shows the contour of calculated stator coil loss. This calculation includes armature  $I^2R$  loss, eddy current loss, and circulating current loss. Some strands have high density while some have low density, because the calculation is taking into account the actual configuration of the transposition. Fig. 9 shows the contour of calculated stator coil strands temperature. The contrast of the temperature distribution is not as strong as that of loss distribution.

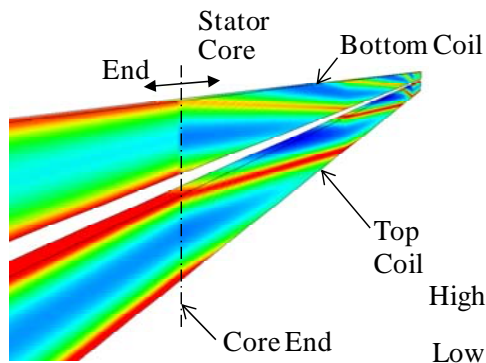


**Fig. 8 Loss Distribution in Stator Coils.**

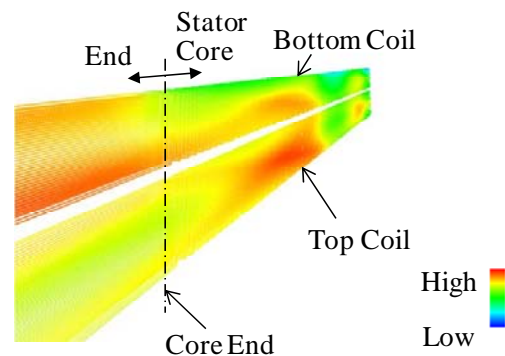


**Fig. 9 Temperature Distribution in Stator Coils.**

The axial temperature distribution in the stator top coil strands during copper loss operation is shown Fig. 10. The horizontal axis of the figure represents the axial position in the generator. The value of 0.0 pu indicates the edge of the stator core and 0.5 pu represents the center of the generator. The calculated and the measured temperature distribution agreed well. In addition, we also measured temperature of the stator coil end with different insulation methods. One model has the insulation with current design, while the other has that with traditional design. The calculation showed that the

temperature of the stator coil end was greatly influenced by the insulation method, which was demonstrated by the measurement.

Fig. 11 compares calculated and measured top coil strands temperature at around 0.2 pu in Fig. 10. The 0.0 pu value in the horizontal axis denotes the innermost position of the strands in the slot. The calculated temperature distribution agreed well with the measured one. Within this cross-section, the highest temperature is at the center of the top coil. From the result, we can see that the highest temperature of stator coil does not necessarily occur at uppermost position of the top coil. In addition, as shown by Fig. 11, the RTD temperature is less than the bottom coil strand's temperature. This result contradicts the widely held belief that RTD temperature is the mean average of top and bottom coil temperatures.

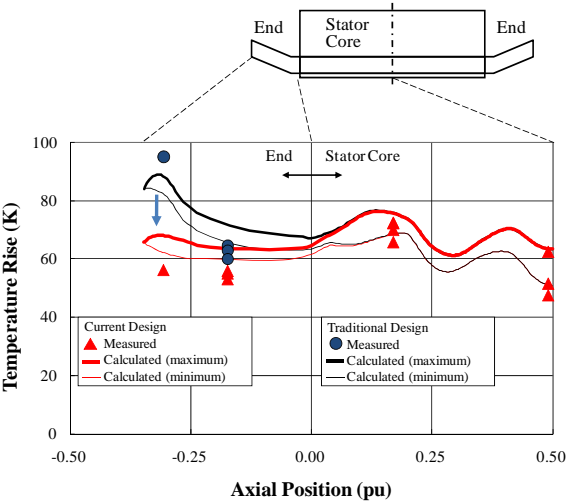


**Fig. 10 Measured and Calculated Stator Top Coil Temperature Distribution of 250MVA Air-Cooled Generator.**

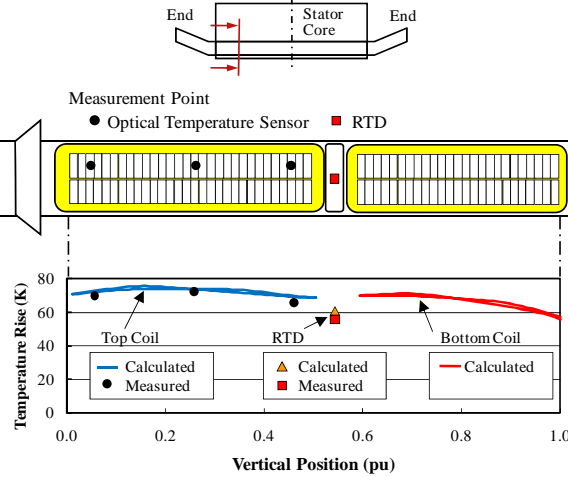


**Fig. 11 Measured and Calculated Strand Temperature Distribution.**

For another generator, a customer gave us a chance to measure strand temperature at the site. In this generator, 12 optical temperature sensors were installed in the series-connection. And the temperatures are measured at site with full load. Fig. 12 compares measured and calculated temperatures of stator coils. As the figure shows, RTD and series-connection temperature agreed well. Note that this generator is designed as F class temperature rise. Both the calculated values are the designed value, and no corrections after the measurement were added.

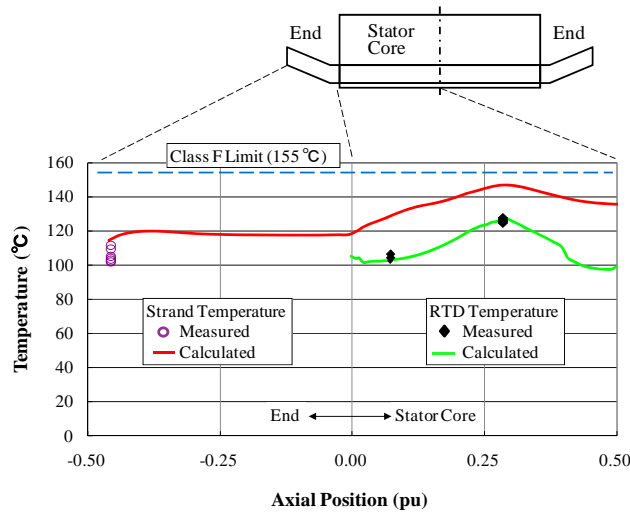


**Fig. 12 Measured and Calculated Stator Coil Temperature Distribution in Operation.**

As we mentioned before, the temperature of stator coil strand are usually measured with only RTDs. As Fig. 11 and Fig. 12 shows, the calculated temperature of stator coil strand and RTD agree with the measured values. And so, we can predict the temperature of stator coil strand by the tools from the temperature of RTD. Fig. 13 shows a comparison of measured and calculated RTD temperatures of generators developed within last 10 years. A generator has various measurement points in the axial direction and all the measured temperatures are in the figure. The data include both air-cooled and hydrogen-cooled generators. The ratios of measured and calculated temperature rise are within the range of 0.76 to 1.08. Even if measured and calculated temperatures are exactly the same, when the temperature distribution shifts in the axial direction, the ratio gets out of 1.0. It gets higher or lower than 1.0. But the shift in the axial direction should be allowed for design. Considering the shift, we use Fig. 14 for designing a generator. Fig. 14 shows the comparison of the calculated and measured hottest temperatures. If further accuracy is required, loss and temperature distribution are calculated iteratively. Because the electrical conductivity of copper varies with temperature, loss at each location also varies with the temperature at the location. For circulating current, the mean temperature of each strand is important because it determines the resistance of the circuit. We have experience of the iterative calculation, but it will be reported in another chance. For our daily use, non-iterative calculation is enough, if the average conductivity is selected correctly.

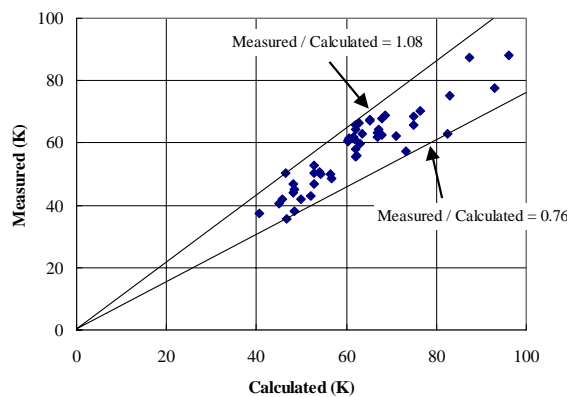


**Fig. 13 Measured and Calculated Temperature Rise of RTD.**

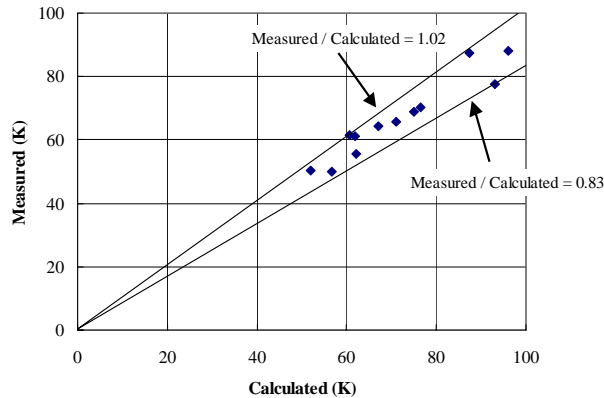


**Fig. 14 Measured and Calculated Hottest Temperature Rise of RTD.**

After each measurement, the design tool is slightly modified for further accuracy. Design tools are better developed on the basis of the measurement result and we have been accumulating the data.

## 5 CONCLUSIONS

This paper disclosed the actual temperature of the stator coil strands that have not usually been measured with a generator.

The following conclusions were obtained.

- We measured the temperature of the coil strands. The measured RTD temperature was different from average of top and bottom coil temperature. And the temperature distribution was different from what was conventionally believed.
- The accurate temperature calculation tools were developed. The calculation tools continues to progress.
- These technologies are applied to all generators including hydrogen-cooled and water-cooled generators.
- An example of temperature design database is shown.

## BIBLIOGRAPHY

- [1] Okabe H, Hattori K, Miyashita I, Sawada S, Sawada I, Watanabe T. Performance Evaluation of a Turbine Generator through a thorough Measurement on the Actual 250MVA-Class Machine, IEE Japan, RM-02-129 (2002-10) (in Japanese)
- [2] Hattori K, Ide K, Takahashi K, Kobashi K, Okabe H, Watanabe T. Performance Assessment Study of a 250MVA Air-cooled Turbo Generator, IEMDC, 2003
- [3] Takahashi K, Ide K, Onoda M, Hattori K, Sato M, Takahashi M. Strand Current Distributions of Turbine Generator Full-Scale Model Coil[C]// Int. Conf. on Electrical Machines, Proceedings paper 139, 2002
- [4] Watanabe T, Takahashi K, Ide K, Hattori K. Turbine Generators Progress with Highly precise Analysis Design. IEE Japan, RM-04-143 (2004-10) (in Japanese)
- [5] Mori H, Shiobara R, Hattori K. Heat transfer Characteristic of Rectangular channel Rotating on a Parallel Axis, JSME B, 2000-10:66 (650) (in Japanese)



*Beijing, China*

SC A1  
**COLLOQUIUM ON NEW DEVELOPMENT OF ROTATING  
ELECTRICAL MACHINES**

*11~13 September, 2011*

---

**The Developing Road of HEC Turbine Generator**

**Shen Liangwei**  
**Harbin Research Institute of Large**  
**Electrical Machinery**  
**China**

**Jiao Xiaoxia**  
**Harbin Electric Machinery**  
**Company Limited**  
**China**

**SUMMARY**

The electric power supply was lack in China from 1980s to 1990s, however for 21 century energy conservation and emission reduction become more and more important. Harbin Electric Machinery Company Limited (HEC) play important role for this two steps. Under steering of reform and open policy, HEC find developing road to get succeed using technology introduction, assimilation and independent innovation. In this paper some information will be shared and 600MW class Turbine generator of HEC is presented as an example.

**KEYWORDS**

600MW class turbine generator

## 1 INTRODUCTION

China steps on reform and open road from 1978, it provides a foundation for the development of electric power industry. The electric power supply was lack in China from 1980s to 1990s. The manufacture technology of 300MW and 600MW turbine generator units was introduced from US Westinghouse (WH) organized by the former Ministry Machine Building Industry and former Ministry of hydropower in 1980. Moreover, domestic manufactories were rebuilt in large scale, so the capacity of produce and manufacture is enlarged. Since 2005, the through put of power equipments annually was already exceeding 100 million kW. The electric power supply is abundant.

In 21 century, energy conservation and emission reduction and development of low carbon economic become more and more important. From 2006-2010, On the one hand the products with high energy consumed such as the thermo power 100MW and below total 60000MW was eliminated, on the other hand nuclear power, wind power, water power and thermal power with high parameter are developed. HEC pay important role at this two steps. In this paper 600MW class turbine generator of HEC is presented as an example, because it already had gone whole process included the technology introduction, assimilation and independent innovation of key technology.

Until 2010 end, domestic 600MW class Turbine generators have produced about 400 sets, among it 350 sets already put in to operation. In addition, 600MW class Turbine generators export contracts have exceeded 65 millions kW. HEC occupied about 33% in the whole market.

## 2 REGARD TO DEVELOPING ROAD TO SUCCEED OF HEC

HEC was established in 1951. It was China largest manufacturer in Turbo-generator, Hydro-generator, Hydro-turbine . In 1954-1960 it main depended on Russia .From 1961-1980 it was self-dependence. From today point of view these two ways are not success.

Since 1980s , HEC has found developing road to get succeed using technology introduction, assimilation and independent innovation. Now HEC has developed own key technology and style. The HEC technology introduction until to 2010 end sees table I .

**Table I HEC technology introduction and developing (from 1981 to 2010 end)**

year	name	product	technology introduction company	technology introduction mode	number of operated units	number of units delivered	Total number of contracts
1981~2010	Short circuit generator	6500MVA		self-developed	1	2	4
		3200MVA		self-developed	3	6	9
1981-2010	Thermal power	Air cooling 60~150MW	TOSHIBA	self-developed	115	142	149
		200MW		manufacture cooperation	3	6	9
		300~350MW	WH	self-developed	0	0	0
		Hydrogen-water cooling 300~350MW		whole sets introduction	135	180	220
		600~670MW	TOSHIBA	manufacture cooperation	115	129	190
		1000MW		manufacture cooperation	5	5	12
Combine cycle 9F 390H 468MVA	GE	manufacture cooperation	23	23	23		
Hydrogen cooling 300~350MW 60 Hz		self-developed	1	1	3		
2007~2010	Nuclear power	650MW		self-developed	2	2	4
		AP1000 1250MW	MELCO	manufacture cooperation	0	0	12

1997-2008 2004-2010	Hydro power	Three Gorge 700MW units	ALSTOM	whole sets introduction	12	14	16 (8sets subcontract)
		Pumped storage 300MW	ALSTOM	whole sets introduction	0	0	2
2010	Wind power	0.15~0.5MW	GE	joint venture	0	0	
2003-2010	excitation	300-660MW	ABB	parts assembly	100	105	110
2007-2010		300-660MW	GE	EX2100H, OEM	2		9

Manufacture cooperation mode is adopted by HEC according to the domestic market needs. It just like a car which is market needs, technology introduction and factories rebuilt are wheel, assimilation and independent innovation are engine, and that HEC is the driver.

From Table I, we can see that technology introduction is proceeding continuously following the products development. In additional, HEC should be a main role during the technology introduction.

### 3 THE EXAMPLE: 600MW CLASS TURBINE GENERATOR

#### 3.1 Technology introduction and assimilation

PINGWEI plant#1 600MW project was pointed as the reference unit of technology introduction and assimilation. Generator is only a subsystem in this big project. This subsystem is involved in technology introduction, technical reconstruction, manufacture of unit, test of the unit, the stator transportation, installation and testing etc. Every item in this subsystem contains a great deal of works. In the process of technology introduction and assimilation, HEC organized the manufacture strictly in terms of WH drawings, craft and standard, and distinguished the advantage and disadvantage of the introduced technology and how to deal with it.

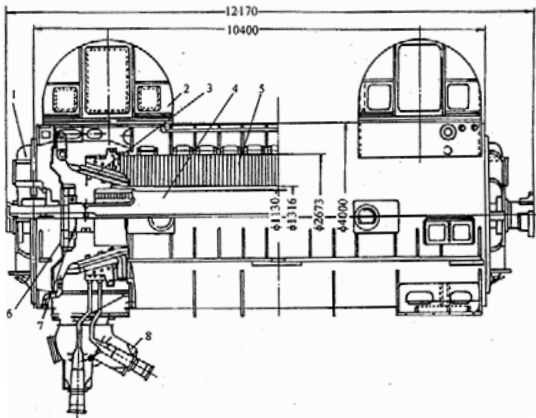
#### 3.2 Optimization design

Through the operation of 600MW reference units, it demonstrated WH technology is mature, reliable and advanced. Because 600MW reference units design is based on WH 60Hz units which is not suitable for Chinese market. It was optimized by WH and HEC under WH instrumental leadership. The optimization design not only improved the performance of generator, but also made an advantageous condition for localization. The comparison of 600MW reference units and optimization units is showed in table II.

**Table II the comparison of 600MW reference units and optimization units**

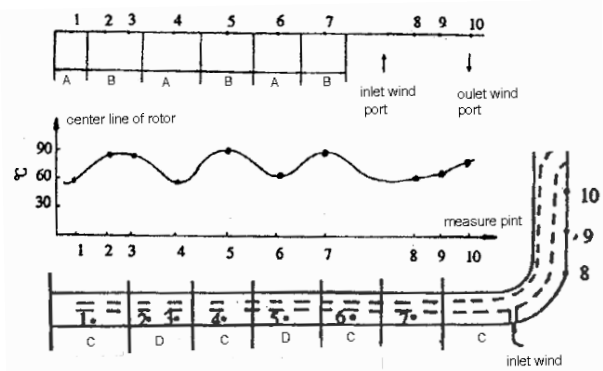
number	item	reference units (PINGWEI #1)	optimization units (HARBIN NO.3#1)	remark
1	capacity(MVA)	666.67	722.22	customer's requirement
2	power factor	0.9	0.9	customer's requirement
3	MCR (MW)	630	680	
4	rated voltage( KV)	20	20	consult with customer
5	hydrogen pressure (MPa)	0.52	0.4	
6	Efficiency ( %)	98.67	98.94	
7	excitation voltage $U_{fN}$ (V)	429	460	

8	excitation current $I_N$ (A)	4202	4503	
9	excitation system ceiling voltage ratio	1.67	2	according to the domestic power grid requirement
10	outer diameter of stator frame(mm)	4115	4000	according to limit of domestic railway transportation
11	ventilation type of rotor	multi-staged blower and axial ventilation	Air gap-pickup with diagonal flow ventilation	adopted HEC technology
12	excitation type	brushless excitation	brushless excitation or static excitation	according to the customer's requirement
13	Localization rate (%)	47 (average value of two units)	>90	according to the government police



1- Bearing, shaft seal and end cover 2- Cooler 3- Stator winding 4-Rotor winding  
5- Stator core 6- Wind guide ring and internal end cover 7- Fan 8- Bushing assembly

Fig.1 the general arrangement of 600MW optimization turbine generator



A- inlet wind zone B- outlet wind zone C- cold wind zone D- hot wind zone

Fig.2 measure elements location and rotor winding temperature distribution (exciter end)

In optimization design, except for the ventilation type of rotor winding is changed to air gap-pickup, the other design is not changed. Since eliminate high-pressure blower, the structure is simplified, ventilation loss is reduced and the temperature distribution of rotor winding is homogeneous. The maximal temperature rise of rotor winding of reference units is 74K at 0.517MPa hydrogen pressure and 600MW, for the optimization units it is only 66.6K at 0.4MPa hydrogen pressure and 680MW. The cooling effect is improved obviously. It is also verified by the following test, see Fig.1 and table III.

Through the optimization design, almost hundred aspects were improved and the cost was decreased about 50%. The main succeed is the localization of stator bar. HEC settled it by developing resin-rich model mould pressing and F class insulation technology (see the reference). During the localization, the technology performance and standard of WH must achieve or exceed, and the quality and standard can not reduce. The test results of the first optimization units are shown in table III. It is noticed that the temperature rise test of air gap-pickup rotor is made using the reverse connection of rotor coil and with rated rotor current in the test bed. The distribution of temperature of rotor winding is shown in Fig.2 and Table IV.

The main performances of generator achieved international advanced level. When the 600MW optimization unit just has operated three years, the equivalent availability coefficient is above 90%

already. The unit coal loss: 320g/kw.h for sub-critical condition, 305g/kw.h for super-critical condition, 290g/kw.h for ultra super-critical condition.

**TableIII Test collection of 600MW generator in the test bed**

Item name		measure data			standard	
rated excitation current $I_{fn}$ (A)		4140 (4202 design value)				
short circuit ratio S.C.R		0.541			>0.5	
D axis synchronous reactance (%) $X_d$		216.13 (215.5 design value)				
D axis transient reactance (%) $X'_d$		30.01 (22.28 design value)				
D axis sub transient reactance (%) $X''_d$		21.38 (22 design value)			>10%	
Efficiency (%)		98.94				
temperature rise (K)	stator winding k	21.3			<40K	
	stator core k	38			<80K	
	rotor winding (average) k	43			<70K	
rotor critical speed (rpm)		n1	n2			
		768(731 design value) 2220 (2136 design value)				
The ellipse frequency of stator end winding (cold condition) (Hz)		turbine side	exciter side		f>110 or <94 Hz	
		58	62			
The vibration amplitude of stator end winding P-P ( $\mu$ m)		$I_k=1.0I_N$	21.25 (radial)		<100 $\mu$ m	
		$U_o=1.05U_N$	18.7 (radial)		<100 $\mu$ m	
The vibration amplitude of frame P-P ( $\mu$ m)		amplitude	2 $\mu$ m			
		frequency	111Hz			
The vibration amplitude of stator core P-P ( $\mu$ m)		amplitude	18.5 $\mu$ m			
		frequency	218Hz			
The temperature rise of stator end core (K)			end core	Pressing finger	magnetic shield	
		$I_k=1.0 I_N$	18.6	11.2	9.0	
		$U_o=1.05U_N$	19.2	9.0	7.7	
The shaft vibration amplitude P-P ( $\mu$ m)		exciter side		turbine side		
		13 (perpendicular)		12 (perpendicular)		
						<76 $\mu$ m

**TableIV the temperature distribution of rotor coil #8 (top turn, gas inlet temperature 24°C)**

Capacity(MW)	$I_f$ (A)	1	2	3	4	5	6	7	8	9	10
700	4744	57.7	91.3		59.1	92.4	58.5	89.8	73.8	79.1	84.6
680	4682	57.4	89.7		58.0	91.1	57.7	88.5	73.3	78.4	82.9
650	4503	52.8	84.6		54.2	85.7	52.1	79.6	69.6	75.9	79.6
600	4052	43.6	72.7		45.6	74.2	44.5	67.2	60.4	67.2	71.2
	3602	37.7	63.2		38.8	65.0	38.3	59.1	51.2	58.4	63.4

In Order to meet market demand, HEC 600 MW class generator now had developed following design:

- There are two power factor 0.9 or 0.85 could be selected.
- There are two SCR 0.5 or 0.45 could be selected for 660MW.
- There are two excitation system could be selected brushless excitation or static excitation.
- The fleet includes 600MW、650MW、660MW、670MW...
- It fit to different kind of turbine type: sub-critical、sup-critical、ultra super-critical、air cooling...

### 3.3 The main faults of hec 600mw generator

HEC 600MW generator reliability index which come from China electric power reliability manage center is shown in Table V. From TableV, we can see 600MW class generator of HEC is steady and reliable.

The main faults were listed in Table VI.

**Table V HEC 600MW generator reliability index**

year	The number of units	Equivalent non-planned stop (h/u.y)		Effect on unit equivalent availability coefficient (%)	
		total	caused by equipment effect	total	caused by equipment effect
2005	9	4.55	4.55	0.05	0.05
2006	14	21.46	20.31	0.24	0.23
2007	36	0.17	0.17	0	0
2008	57	12.76	10.01	0.15	0.11
2009	69	1.62	0.21	0.02	0.00

**TableVI the main faults of HEC 600MW generator**

number	name	the total number	settle measure	faults evaluation
1	Gas block for phase ring	four generators	Have settled the measure is clear.	Drawing is not clear.
2	Adjustable banding ring of stator winding is loose.	one generator occur short circuit, three generators occur coil abrasion	recheck fifty generators manufactured during the 2007~2009 , retighten ten generators.	The control of craft is not strict.
3	The filler strip of rotor leading wire is broken.	two generators rotor occur earth ground	Recheck about ninety generators	The filler strip of leading wire occur fatigue fracture
4	Sub-synchronous oscillation (SSO)	two generators	one rotor discard useless, one rotor changed shaft coupling	TSR is not used in the protection.

The phenomena of gas block for phase ring is shown in Fig.3. The reason is the outside connection pipe (about 10m long) at the spot in Fig.4 should be  $D_N40$ , in fact it used  $D_N20$ . So the water flow is reduced to 60%.

The adjustable banding ring tighten system is shown in Fig.5. The individual banding ring is loosed because the control of the craft is not strict.

The filler strip of rotor leading wire broken is shown in Fig.6. The broken filler strip stretch and touch with the over bridge line at the bottom of rotor winding, causing rotor winding earth ground.



**Fig.3 gas block of the phase ring**

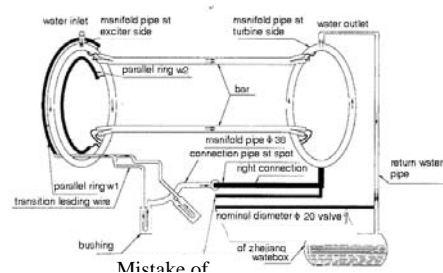


**Fig.4 stator waterway sketch of 600MWgenerator**

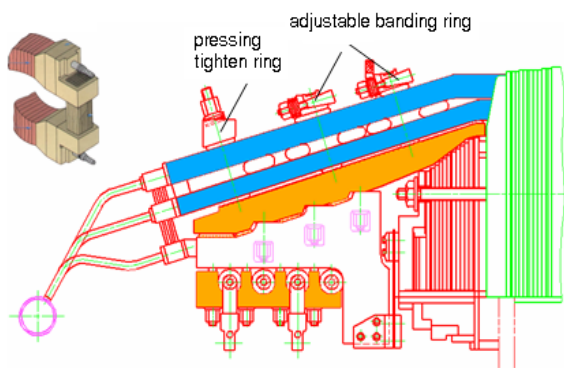


**Fig.5 the adjustable banding ring tighten system of stator winding**

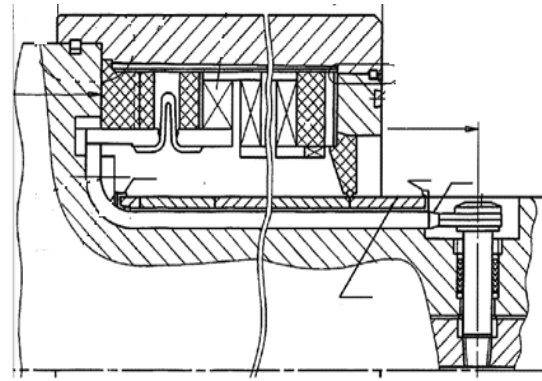


**Fig.6 the filler strip of rotor leading Wire broken schematic**

The Sub-synchronous Oscillation (SSO) occurred in thyristor controlled series capacity (TCSC) test from March to May in 2008 at some power plant. At that time, the electric frequency 21.33 and second order mechanical frequency 28.67 are complemented. The mode effective value tested by the TSR is 0.3rad/s at the machine head and 0.5rad/s at the machine end. It lasted 778 hours while TSR is not used in the protection. SSO induced the shaft coupling and shaft extension crack, shown in Fig.7. After the accident, four measures were developed to prevent SSO in the electric net, the effect is good. In additional, HEC sets the trip value for the TSR protection. Therefore, the possibility of the fault destroy is eliminated.

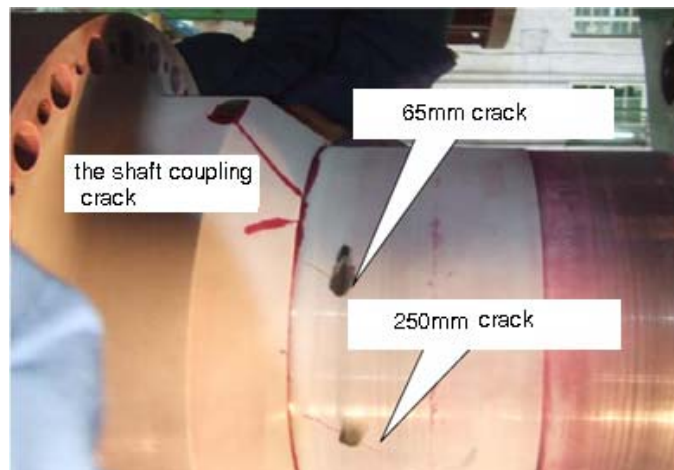


**Fig.7 the shaft coupling and shaft extension crack caused by SSO**

From the results in the Table6, you can believe the main problem is not technology itself. It is important to enhance the scientific management following the output of production increased rapidly.

#### **4 ABOUT INDEPENDENT INNOVATION**

The new product development is very important in order to meet the domestic market need. Technology introduction insures high initial and high product quality and avoid the initial and long time explore. It is the best way to meet market demand quickly. After technology introduction, technology should be optimized and localization, otherwise it will be behind as the technology development is rapidly. Therefore, HEC should have the independent innovation ability. Harbin Research Institute of Large Electric Machinery (HILEM) is an important department of HEC. HILEM has 309 employees engaged with the insulation, cooling method, structure intensity, metal material, auto-control for electric machine and design and test of the hydraulic turbine model etc. HEC has developed resin-rich model mould pressing and F class insulation technology. The results exceed the

performance of original so it had already been used in the introduced products and got a great appreciation because of outstanding achievement.

Though it is convenient for HEC that technology only just introduced from one company. But China market is big it can't meet the various kinds need so as to HEC had introduced technology from GE and WH according with different product. The key of independent innovation is holding the improvement of electronic, information and material to increase the machine's life and efficiency and adopting the advantages of technology introduction and considering the domestic condition to fit. At present, there are three cooling methods for turbine generator in HEC.

1) air-cooling : Air cooled inside rotor coils and outside of stator bars, the installment and operation is easier than other cooling modes;

2) hydrogen-cooling : Hydrogen-cooled inside rotor coils and outside of stator bars. There is not inner water cooling system;

3) hydrogen-water cooling : Water cooled inside the stator bars, hydrogen-cooled inside rotor coils, hydrogen-cooled stator core. This mode is applied to large generators. Because the manufacture is complex and efficiency is lower for the high pressure blower, so we prefer to use self ventilation system liked sub slot ventilation and air gap pick-up system...etc.

For excitation, there are two types could be selected by customer brushless excitation or static excitation.

For stator bar, there are two types could be selected by customer rich resin or VPI.

The independent innovation of HEC for turbine generator is shown in TableVII.

**TableVII independent innovation of HEC turbine generator**

capacity range	cooling type	Technology introduction	HEC produce's characteristics
60-150MW 200-350MW	air cooling	self-developed TOSHIBA 200MW	60~150MW full impregnation for stator, sub-slot ventilation for rotor
			200~350MW, thin main insulation for stator bar, sub-slot ventilation for rotor.
300~500MW	hydrogen-cooling	GE390H	For combine cycle, 50Hz and 60Hz fleet, sub-slot ventilation for rotor winding.
600~700MW	water-hydrogen-cooling	WH 600MW	Fit to various turbine type (sub-critical, super-critical, ultra super-critical, air cooling, reheating, nuclear), 50Hz and 60Hz, brushless or static excitation, preparation on-line monitoring, air gap pick-up ventilation for rotor winding.
2 pole 1000~1200MW	water-hydrogen-cooling	TOSHIBA 1000MW	Developed new frame for the railway transportation, 30KV stator insulation system, air gap pick-up ventilation for rotor.
Nuclear power 4 poles 1400-1700MW	water-hydrogen-cooling	MELCO 1250MW	Expect substitute self ventilation for axial ventilation.

From 1998 to 2008, the turbine generator output capacity of HEC has increased from 1,800 MW to 28,000 MW per year. If the goal in table7 has finished in five years, HEC will becomes more strong and competitive and will more contribute to domestic and international electric power industry.

## 5 CONCLUSION

Under steering of reform and open policy, HEC find developing road to get succeed using technology introduction, assimilation and independent innovation.

Through adopt the advantage of introduced technology and combine with independent innovation, HEC turbine generator have achieved international level and has bright future.

## **BIBLIOGRAPHY**

- [1] LU C , MAN Y . The Development Of HEC Insulation System



Beijing, China

SC A1  
COLLOQUIUM ON NEW DEVELOPMENT OF ROTATING  
ELECTRICAL MACHINES

11~13 September, 2011

---

**Calculation of Electric Field and Structure Design of Semi-conduction Layer  
for Stator Bar of 1000MW Turbo-generator**

**Sun Liang, Hu Haitao  
Gao Junguo, Zhang Xiaohong  
Key Laboratory of Engineering  
Dielectric and Its Application Ministry  
of Education, Harbin University of Science  
and Technology, Harbin, China**

**Yuan Xiaohong  
Hu Chunxiu  
Insulation Research Department,  
Harbin Research Institute of  
Large Electrical Machine,  
Harbin, China**

**SUMMARY**

The 1000MW class super critical turbo-generators are becoming the key developing points due to their excellent economical performances, but some unfavorable factors to effect on the operation stability of generator insulation are caused by larger unit capacity. With the increasing of the unit installed capacity, the rated voltage of generators is markedly heightening, as a result it is more strictly demanded to eliminate the partial discharge and corona for generators insulation.

The section of the stator bar is rectangle; therefore, there will be the concentration area of electrical stress at the corner of the conductor. In the practical stator bar, the corner of the conductor is the circle of the electromagnetic wire, whose radius of curvature is very small. To reduce the concentration distribution of electrical stress, curvature radius of conductor should be increased by introducing the equipotential layer structure. The determination of distance between the contact points is significant. If the distance is too long, the effect of the contact point will be weakening; on the contrary the difficulty in manufacture will be increased.

In the present paper finite element method (FEM) and equivalent circuit method are used to calculate the distribution of electrical stress at the corner of conductor and perfect distance between the contact points. Body capacitance and surface capacitance of the stator winding ending are calculated via CMATRIX command in ANSYS, and it is very important that concentrative parameters should be used in the circuit analysis. The equivalent circuit analysis is performed by Tina Pro. This method has the practical significance in engineering applications. The data acquired by actual measurement is validated through the numerical simulation. The results indicated that (1) with increasing in curvature radius of conductor, the distribution of electrical stress is obviously improved, when the curvature radius of the conductor is about 2mm, the maximum electrical stress at corner of conductor reduces from 13.2kV/mm to 8.65kV/mm, and the nonuniform coefficient of electrical stress comes down from 3.03 to 1.99, both of which reduces 34.47%. (2) when the distance between contact points is less than 300mm, the electric potential of the equipotential is familiar with the conductor's, therefore, the perfect distance between contact points should be less than 300mm.

**KEYWORDS**

Calculation of electric field, Turbo-generator, Stator bar, Finite element method

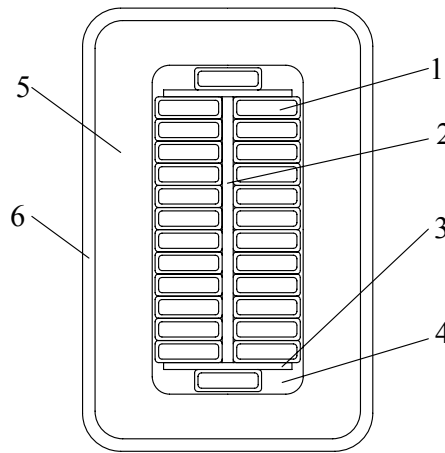
## 1 INTRODUCTION

The stator winding insulation plays a very important role in HV electric machine, which deeply affects the service life and the reliability of the electric machine. Insulation structures are more important effect factors comparison with insulation materials in improving the insulation level of generator<sup>[1]</sup>, because the phenomenon of electric field concentrates happens at the corner of stator bar more easily according to other parts. So to improve the distribution of electrical field at the corner of conductor in stator bar and to prolong the life of insulation in the stator bar are given more attention in the insulation design of high capacity HV electric machine<sup>[2][3]</sup>.

## 2 CALCULATION OF ELECTRIC STRESS AT THE CORNER OF STATOR BAR

### 2.1 The structure of the stator bar

The section of the stator bar is shown in Fig.1. Except of the stator winding insulation and the semi-conduct anti-corona layer, the inner structure is called Roebel bar. Outside the transposition insulation, there is an electrostatic shielding layer to reduce and uniform the inner electric field. It can improve the effect of electrical corrosion resulted by the partial discharge of the void in the transposition insulation under high electrical stress during the long term service<sup>[4]</sup>. The layer is called equipotential layer.



1.electromagnetic wire 2.insulation between turns 3.transposition insulation  
4.transposition filled insulation 5. grounding insulation 6. semi-conductor equipotential layer

Fig.1 The section of the stator bar

Generally the electrical stress at the corner of stator bar is several times higher than the average electrical stress of the bar, which is due to small curvature radius at the corner of conductor. In the broadside of the stator bar, the electric stress can be considered as approximately uniform distribution. It's electrical stress can be calculate by the formula (1):

$$E_a = \frac{U}{d} . \quad (1)$$

The electrical stress at the corner of conductor can be calculated by the experience formula(2):

$$E_{\max} = \frac{U}{d} \sqrt[3]{1.8(1 + \frac{d}{r})} . \quad (2)$$

The ratio of the maximum electrical stress to the average electrical stress is termed concentration coefficient  $f_m$ , it is expressed as follows:

$$f_m = \frac{E_{\max}}{E_a} = \sqrt[3]{1.8(1 + \frac{d}{r})} . \quad (3)$$

Where  $r$  is the curvature radius of the conductor,  $d$  is the thickness of the grounding insulation.

According to the formula (3), when  $d$  decreases or  $r$  increases,  $f_m$  will reduce. In the practical stator bar, the corner of the conductor is the circle of the electromagnetic wire, whose radius of curvature is about 0.5mm~0.8mm. To increase the curvature radius, the semi-conductor equipotential layer structure is introduced<sup>[5]</sup>. Then a bigger corner of the conductor is formed, whose curvature radius go up to 2mm.

**2.3 Calculation of electric field**

Because the symmetrical structure is characteristic of the section of stator bar, the distribution of electrical field on it is also symmetrical. A quarter section of the stator bar was chosen to carry out the finite-element analysis. Assume that the connections between the copper conductor and inner semi-conduct equipotential layer, outer semi-conductor anti-corona layer and the stator slot are perfect, and then the equipotential layer and anti-corona layer have the same electric potential as the conductor and the stator slot, respectively. Moreover, all of the things inside the semi-conductor equipotential layer are considered as one copper conductor, grounding insulation, semi-conductor equipotential layer models are built in sequence. As shown in Fig.2, parts distinguished by the colors are conductor, grounding insulation, and anti-corona layer from the inner to the external.

As an example, the calculate result of the 2mm radius is shown in Fig.3. The distribution of maximum electrical stress appears at the corner of the copper conductor, the value is  $8.65 \times 10^3$  kV/mm. Compared to other areas, the electrical stress at the corner of conductor is much higher and more concentrated.

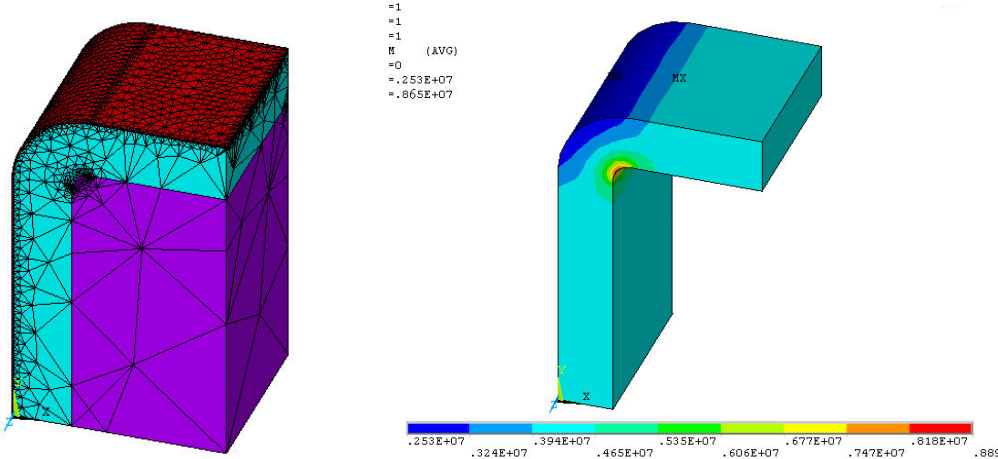


**Fig.2 The grid division diagram of stator bar**

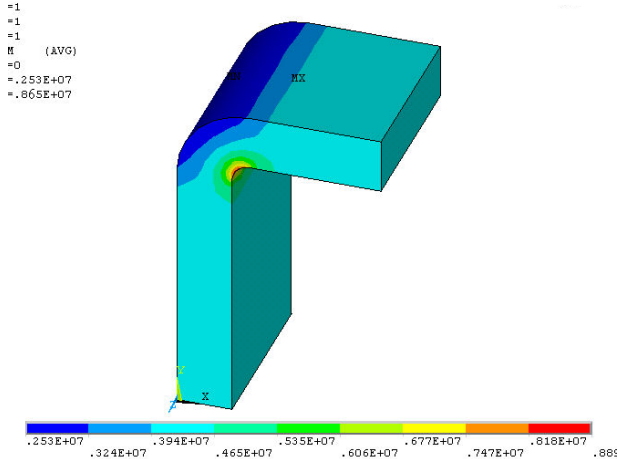


**Fig.3 The nephogram of field strength**

Because of the nonuniform distribution, electrical stress at the corner of stator bar reduces rapidly with grounding insulation thickness increasing, as shown in Fig.4. The average electrical stress calculated is 4.35kV/mm, based on the curve in Fig.4.

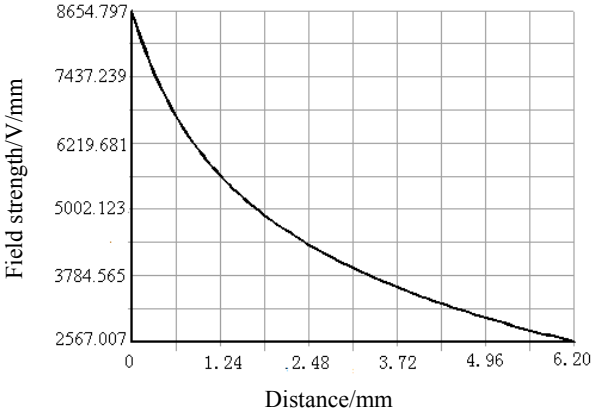


**Fig.4 The change of electric stress at the corner of stator bar with insulation thickness**

## 2.4 Results and discussions

By means of ANSYS software, the maximum electrical stress at the corner in different curvature radius is acquired, as listed in table I .

table I Calculated results of different curvature

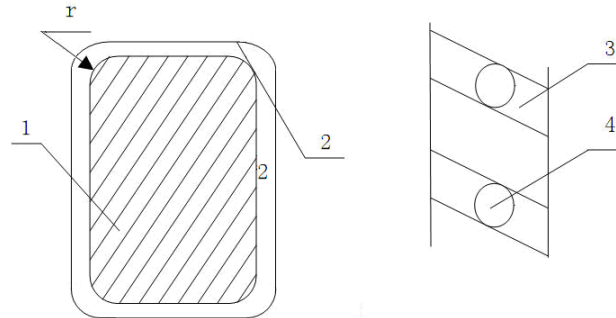
R/mm	0.5	1.0	1.5	2.0	2.5	3.0	3.5
$E_m$ /kV/mm	13.20	10.80	9.48	8.65	8.07	7.64	7.29
$E_a$ /kV/mm	4.35	4.35	4.35	4.35	4.35	4.35	4.35
$f_m/E_m / E_a$	3.03	2.48	2.18	1.99	1.86	1.78	1.68

It can be seen in the table that when the curvature radius increases from 0.5mm to 2mm,  $E_m$  and  $f_m$  reduces obviously, the maximum electrical stress and nonuniform coefficient decrease from 13.2kV/mm to 8.65kV/mm, and from 3.03 to 1.99, respectively, both reduces 34.47%. However, when the curvature radius increases from 2mm to 3.5mm, these two parameters fall much slowly. Moreover, in consideration of the stator slot to be filled with wire, the more perfect curvature radius of the conductor with semi-conductor equipotential layer should is 2~2.5mm.

## 3 CALDULATION OF CONTACT POINTS

### 3.1 Structure of the contact points

Semi-conductor Equipotential layer could evidently improve the distribution of electrical stress in stator bar, however the distance between contact points of copper conductor is also a very significant effect factor. If the distance is too far, the effect of semi-conductor equipotential layer would be weakened, and the maximum electrical stress in the stator bar will be higher, so the service life of the stator bar insulation will be reduced. Conversely, if the distance is too near, more complex processing technique will be needed, and more time will be wasted in the manufacturing. The diagram of the contact point structure is shown in Fig.5.



1.conductor 2.semiconductor 3.transposition conductor 4.contact points

Fig.5 the structure of the contact points

### 3.2 Calculation of the capacitance

Calculation of electrical stress distribution between the contact points of copper conductor belongs to dynamic electric field problem, the method of solving electrostatic field cannot be directly used. However, if the problem is transformed to a circuit problem, it will become easier. Then the lumped parameters, which can be solved in the circuit analysis, are used during the calculation of electrical stress distribution. By means of ANSYS CMATRIX command, the lumped parameters of body and surface capacitance could be calculate based on the geometric dimensions and the parameters of materials known. Applying the capacitance and the resistance of the semiconductor equipotential layer into the circuit analysis, and the distribution of electric potential between contact points of the copper conductor can be easily calculated.

The three electrodes system in the stator bar is given for the model built in ANSYS, as shown in Fig. 6. In Fig.7 the half-round area is airflow field, the rectangle area is grounding insulation, and the round area is assuming electrode. Airflow field is built because the surface capacitance is directly relevant to the air, and the radius of the airflow should be eight times longer than the distance between the electrodes.

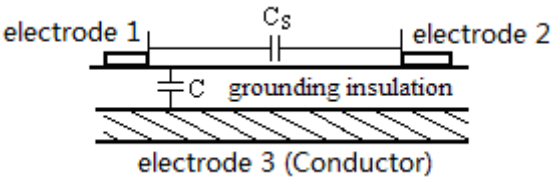


Fig.6 The diagram of three electrodes system given

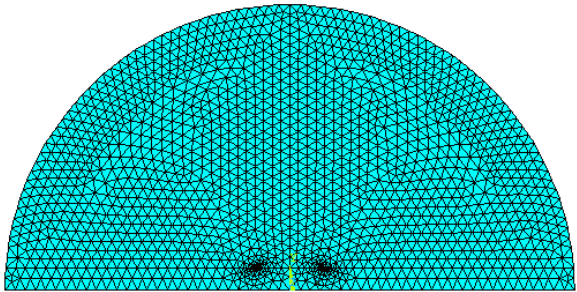


Fig.7 model used for calculation capacitance

**3.3 Analysis of the equivalent circuit**

According to the structure of the stator bar, equivalent circuit with distributed parameter is used to numerical analysis, it is shown in Fig.8. Because the influence of the surface capacitance could be ignored, only the body capacitance is considered. The length of every unit in Fig.8 is fixed 20mm. Body capacitance of grounding insulation (in the first row)  $C1=5.868 \times 10^{-15}F$ , Body capacitance of electromagnetic wire (in the second row)  $C2=6.213 \times 10^{-14}F$ , Resistance of semiconductor per unit  $R=5 \times 10^5 \Omega$ .

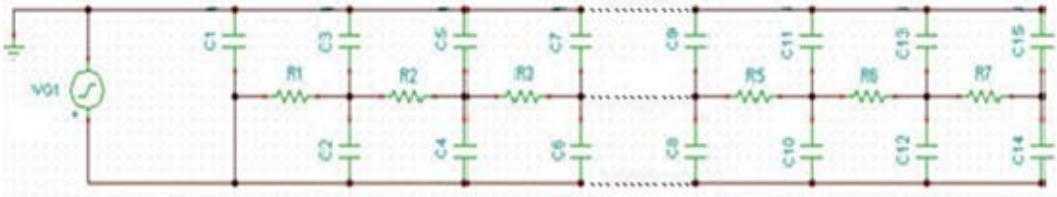


Fig.8 The equivalent circuit of stator bar with the equipotential surface

**3.4 Results and discussions**

The changes of electric potential and the electrical stress with distances between the contact points of copper conductor are respectively shown in Fig. 9.

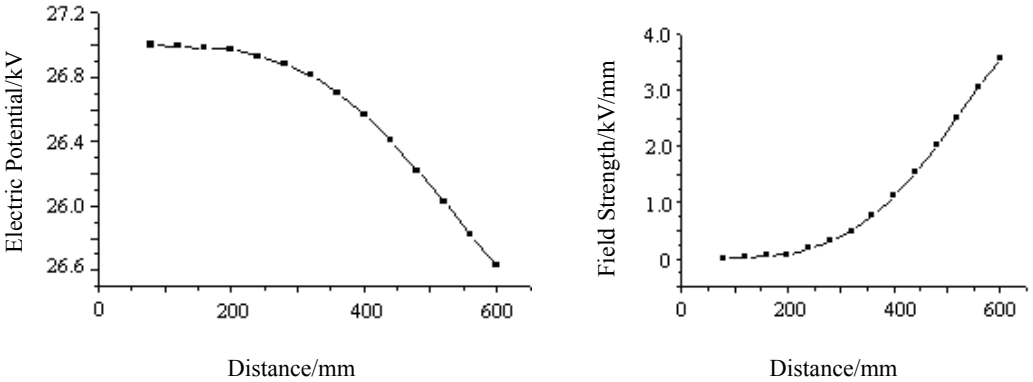


Fig.9 electric potential and strength with different distances between contact points

It can be seen in Fig.9, that when the distance between contact points of copper conductor is more than 300mm, the electric potential of the equipotential layer is reduced obviously, while the electrical stress is raised strongly. When the distance between contact points of copper conductor is less than 300mm, the electric potential of the equipotential is familiar with the conductor's, which means the electric potential gradient approximate zero. Therefore, the perfect distance between contact points of copper conductor should be less than 300mm.

## CONCLUSIONS

(1)When the curvature radius of the conductor is increased to 2mm, the distribution of electrical stress is obviously improved. The maximum electrical stress and nonuniform coefficient reduces from 13.2kV/mm to 8.65kV/mm, and from 3.03 to 1.99, respectively, both reduce 34.47%. The perfect curvature radius of the conductor with semiconductor equipotential layer should be 2~2.5mm.

(2) When the distance between contact points of copper conductor is less than 300mm, the electric potential of the semiconductor equipotential layer is familiar with the conductor's, and the distribution of electric potential tends to more uniform. So the perfect distance between contact points of copper conductor with the semiconductor equipotential layer is considered as being less than 300mm.

## ACKNOWLEDGEMENT

Research was supported by National Nature Science Foundation of P. R. China (51077029), National Basic Research Program of China (973 Program) (2010CB736208), and Science &Technology Research Program of Heilongjiang Province (GC10A203).

## BIBLIOGRAPHY

- [1] Nagano S, Kitajima .T, Yoshida K. Development of World's Largest Hydrogen-cooled Turbine Generator[C]//Power Engineering Society Summer Meeting, 2002: 657-663
- [2] Nakayama A, Haga H, Muraoka M. Development of Generrator Stator Coil with 22kV Global VPI Insulation[C]//2004 Annual Report Conference on Electrical Insulation and Dielectric Phenomena, Kawasaki Japan, 2004: 224-227
- [3] Boulter E A, Stone G C. Historical Development of Rotor and Stator Winding Insulation Materials and Systems[J]. Electrical Insulation Magazine, 2004, 20(3): 25-39
- [4] MA W , LI Y, KONG L. Research on the Characteristic of the Winding Cable in High Voltage Motor[J]. High Voltage Engineering, 2006, 32(3): 24-26
- [5] Akinobu N, Inoue S, Haga K. Numerical Analysis on Electric Field and Taping for Stator Coil With Global Insulation[C]//2001 International Symposium, Himeji, 2001: 641-644

## **Nonlinearity of Torsional Damping and its Effect on SSR Characteristics of Turbine Generators**

**Xie Xiaorong, Zhang Xiaojin**  
State Key Laboratory of Power System,  
Department of Electrical Engineering,  
Tsinghua University, Beijing China

**Dong Xiaoliang, Li Guoqing**  
School of Electrical Engineering,  
Northeast Dianli University,  
Jilin China

### **SUMMARY**

For a series compensated system, when the mechanical damping of a torsional mode is overcome by the electrical damping caused by series capacitor, the stability of torsional interactions will suffer. So the mechanical torsional damping is a key parameter in the risk evaluation of subsynchronous resonance (SSR). However, for a long time, the determination of mechanical torsional damping is a controversial issue. In theory, it varies with a lot of factors, for instance, the material and structure of the shaft, the pressure and temperature of the steam, and the electrical load. Since it is too complicated, the general treatment is to simplify it into a fixed value and a linearly changing value with a specific operating parameter. However, the shortcoming is obvious. The damping is the only function of steady-state loading of the generator. It doesn't reflect the intense of the subsynchronous oscillation or transient dynamics. Actually, these fixed damping under a certain operating condition can hardly explain some practical phenomena, for instance, the persistent SSR. In this paper, a nonlinear shaft model is developed first, in which the modal torsional damping is presented as a nonlinear function of the modal speed and the power output. Then, for a 600 MW generator in a real series-compensated power system, the recorded data of a phase-to-phase short-circuit fault occurring at the terminal are used to identify the torsional mechanical damping. The relationship between the modal damping and the amplitude of the torsional vibration is analyzed and the nonlinear mathematical model obtained. This model is incorporated into the electromagnetic simulation software PSCAD/EMTDC. With nonlinear simulation, the effect of nonlinearity of torsional mechanical damping on SSR is studied in several importance respects, such as the critical compensation degree, the small-signal damping, the transient torque and the fatigue life loss during large disturbances. The nonlinear and linear mechanical damping is compared through simulation study in a real multimachine series-compensated system. The results present insight into the SSR phenomena in practical systems. The novelty of the paper lies in three aspects, i.e., the mechanical damping measured in a real system following a short-circuit fault, a nonlinear damping model and its effect on SSR characteristics of series-compensated power systems.

### **KEYWORDS**

Subsynchronous resonance; Series compensation; Nonlinear model; Mechanical damping; Modal speed.

## 1 INTRODUCTION

Fixed series capacitors have been extensively used in long-distance lines to increase transmission capability. However, they may bring about subsynchronous resonance (SSR), which would lead to turbine-generator shaft damages if not handled properly [1]. Therefore, it is necessary to perform a thorough SSR-risk evaluation of the series-compensated system before it is put into practical operation.

It is well-known that when the mechanical damping of a torsional mode is overcome by the electrical damping caused by series compensation (an event prone to happen when the electrical resonant frequency of the compensated network is close to the complement of the torsional frequency of the shaft), the stability of torsional interactions will suffer. So the mechanical torsional damping is key parameters in SSR-risk evaluation. However, for a long time, the determination of mechanical torsional damping is one of the most controversial issues. In theory, it varied with a lot of working conditions, for instance, the material and structure of the shaft, the pressure and temperature of the steam, and the electrical load. Since it is too complicated, the general treatment is to simplify it into a fixed value or a linearly changing value with a specific operating parameter. For instance, in [2], the mechanical damping is simply ignored, i.e., the damping is zero. Consequently, the result of SSR evaluation is conservative. In some other works [3], the mechanical damping is set as a fixed values. For instance, in the IEEE second benchmark model, the damping has been chosen proportional to inertia so that each mode has the same torsional damping in rad/sec. Still other reports used mechanical damping measured at several loading conditions [4]. For different load, the mechanical damping is obtained by linear interpretation. The latter approach is relatively accurate and widely used. However, the shortcoming is obvious. The damping is the only function of steady-state loading of the generator. It doesn't reflect the intense of the subsynchronous oscillation or transient dynamics. Actually, these fixed damping under a certain operating condition can hardly explain some practical events. For instance, it has been noticed in the operation of North-Western American Power System (NWAPS) that the Subsynchronous Resonance (SSR) oscillations at one of the mechanical shaft modes may be limited instead of increasing exponentially [5, 6].

Another important issue is the variation of the torsional damping in different disturbances. As some literature reported [7], the damping is a time-varying value. It changes with the amplitude of the torsional oscillation. In other words, it is different between large disturbances (e.g., short-circuit fault) and small disturbances (e.g., load variation). However, no actual data could be found in literatures.

In this paper, the torsional mechanical damping was identified using the recorded data of a phase-to-phase short-circuit fault that occurred at the terminal of a 600 MW generator. Its relationship with oscillatory amplitude was analyzed. Then a nonlinear model is derived, which presents the modal torsional damping as a nonlinear function of modal speed. Based on the model, the effect of nonlinearity in torsional mechanical damping on SSR is studied on several aspects. The results present insight of the SSR. The novelty of the paper lies in three aspects, i.e., a really measured mechanical damping following system fault, a nonlinear damping model and its effect on SSR characteristics.

The rest of this paper is organized as follows: In section 2, the dynamic model of the turbine-generator shaft system is described. Section 3 presents the measured torsional damping. Electromagnetic simulations are applied in section 4 to evaluate the effect of nonlinearity of damping on SSR characteristics. Section 5 draws some conclusions.

## 2 DYNAMIC MODEL OF THE TURBINE-GENERATOR SHAFT SYSTEM

For SSR evaluation, a turbine-generator (T-G) shaft system is generally represented as a spring and lumped-mass model [2,3,8]. For instance, the widely deployed 600MW turbine generator in China can be represented as a 4-mass spring model, as described in Fig. 1

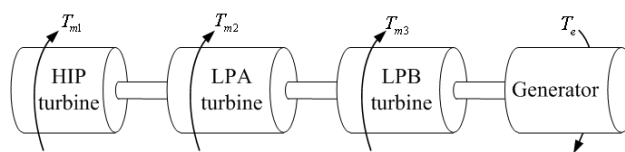


Fig. 1 The lumped T-G shaft system

The turbine-generator consists of four rotors, i.e., a high-and-intermediate-pressure turbine (HIP), two low-pressure turbines (LPA and LPB), and the generator rotor, thus resulting in three torsional modes. The self-parallel excitation system is used. So there is no separate mass to represent the exciter.

Representing the turbine sections as inertias connected by shafts of appropriate stiffness, the dynamic equations for the turbine-generator mass system may be written as (1)

$$2H\ddot{\theta} + D\dot{\theta} + K\theta = T_m - T_e \quad (1)$$

Where:

$\theta$  is the angular displacements column matrix;

$H$  is a diagonal matrix representing the inertias of masses;

$D$  is the damping coefficients symmetric matrix;

$K$  is a tri-diagonal matrix of torsional stiffness with the following properties

$$K_{ij} = K_{ji} \text{ and } \sum_{j=1}^N K_{ij} = 0.$$

$T_m$  and  $T_e$  are vectors of mechanical and electrical torques respectively.

Model (1) can be transformed into the canonical form as (2)

$$2H_c \ddot{\theta}_c + D_c \dot{\theta}_c + K_c \theta_c = T_c' \quad (2)$$

In (2), the coefficient matrices  $H_c$ ,  $K_c$  are both diagonal matrix. As shown in [9], the system described by (2) has  $n-1$  natural frequencies and mode shapes. These modes are not completely uncoupled because the damping matrix  $D_c$  is generally not diagonal. However, it is convenient to define an equivalent modal damping so that the various modes can be uncoupled. Thus each natural mode is governed by an equation of the form

$$\ddot{\theta}_i + D_i \dot{\theta}_i + \omega_{ni}^2 \theta_i = T_i \quad (3)$$

Where  $D$  is the decoupled modal mechanical damping,  $\omega_n$  is the natural angular frequency; the subscript  $i$  denotes the  $i$ th torsional mode.

From (3), it can be observed that the modal damping has vital effect on the stability of the torsional oscillation. In the small-signal sense, the SSR stability is determined by the following formula.

$$D_i + D_{ei} > 0 \quad (4)$$

In (4)  $D_e$  is the electrical damping caused by the electrical interaction of the generator and the series compensated networks, which is defined as

$$D_{ei} = \text{Re} \left\{ \left. \frac{\Delta T_{ei}}{\Delta \omega} \right|_{\omega=\omega_i} \right\} \quad (5)$$

For a series compensated network, when the natural frequency of the electrical network is near the complement of the torsional frequency,  $D_e$  tend to be negative. And if it cannot be overcome by the mechanical damping, instable torsional oscillation, or SSR, occurs. Mechanical torsional damping has great effect on SSR characteristics. However, it is very hard to be accurately measured. Actually it is handled too simple in practice. To explain the nonlinear behavior, dynamic system (3) can be extended to the nonlinear ODE given by

$$\ddot{\theta}_i + D_i(\theta_i, \dot{\theta}_i) \dot{\theta}_i + \omega_{ni}^2 \theta_i = T_i \quad (6)$$

Eqn. (6) indicates that the net damping is in general form a nonlinear function of deviations in position and speed. Eqn. (3) is a special case of Eqn. (6), in which the damping is a fixed value.

### 3 NONLINEARITY OF MECHANICAL TORSIONAL DAMPING

#### 3.1 Mechanical damping measurement

As reported in literatures [4, 10, 11], there are several ways of measuring mechanic torsional damping. These ways involved shaft excitation, recording of the vibration and identification of modal damping with the obtained data. These methods are generally categorized into two groups. The first group is to measure with the generator synchronized to the grid. In this method, the obtained damping is actually the system value, which means it is composed of the mechanical and electrical damping. Thus the latter should be separated to get the purely mechanical damping. The second group of method is to measure the damping with the generator disconnected from the grid. This is achieved by load-reject test. By this method, the mechanical damping can be obtained. However, both methods can only be performed with a very small disturbance to ensure the safety of the generator shaft. Therefore, the damping is in the small-signal sense. There is no report on the measurement of mechanical damping following large-disturbance, for instance, short-circuit fault.

#### 3.2 Mechanical damping measurement following an inter-phase short-circuit fault

In May 19, 2009, during the synchronizing operation of Unit 1 of Shangdu Power plant, a phase B to C short-circuit fault was caused because the mechanical failure of the breaker. The fault was cleared by protective relay. The speed deviation of the HIP turbine was recorded during the event, as shown in Fig. 2. Spectrum analysis was carried out on the recorded data and the result is illustrated with Fig. 3. Obviously, there are three subsynchronous torsional modes, with frequencies being 15.33Hz, 26.12Hz and 30.54Hz respectively. By filtering the HIP speed deviation with band-pass filters, modal torsional speeds can be obtained and shown in Fig. 4.

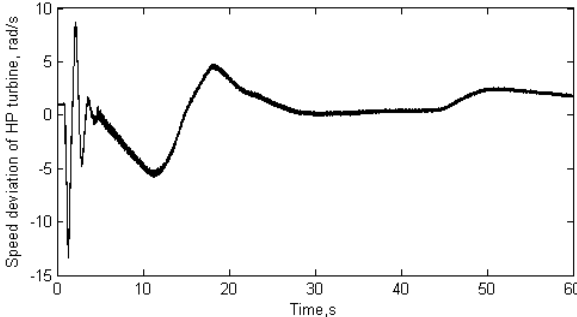


Fig. 2 The Speed deviation of HP turbine following the fault

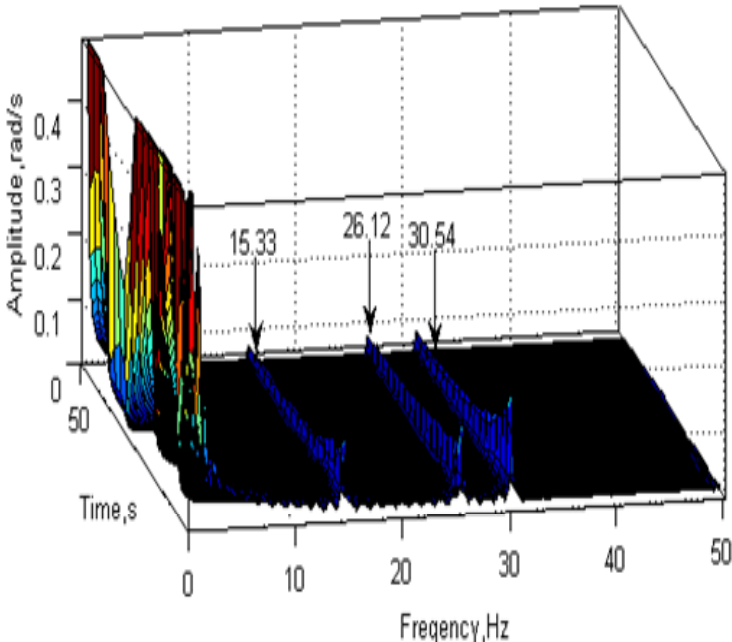
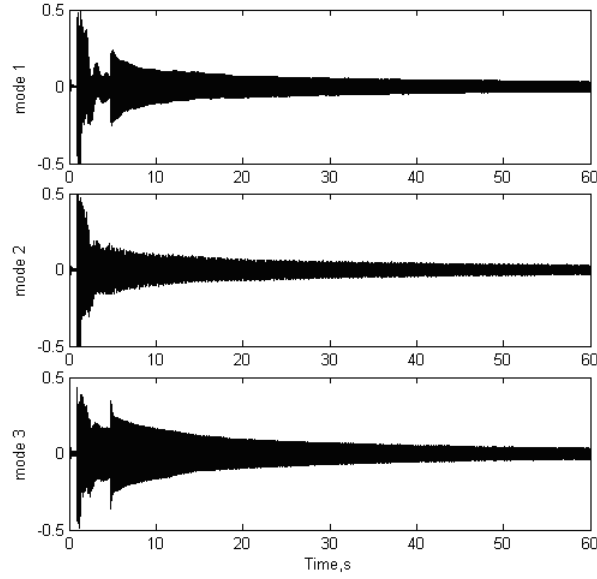


Fig. 3 Spectrum analysis of the speed deviation of HP turbine following the fault



**Fig. 4 The dynamics of the modal speed of HP turbine following the fault**

For each mode, the modal damping is calculated with the following formula [4]

$$D_m = \ln(A_1 / A_2) / (t_2 - t_1) \quad (7)$$

Where

$D_m$  is the obtained modal mechanical damping with unit s<sup>-1</sup>;

$A_1, A_2$  are the amplitudes of modal speed at the time  $t_1, t_2$ .

Thus the mechanical torsional damping can be calculated. It is illustrated in Fig. 5, from which it is observed the mechanical damping varied with time. In other words, it is not a fixed value.

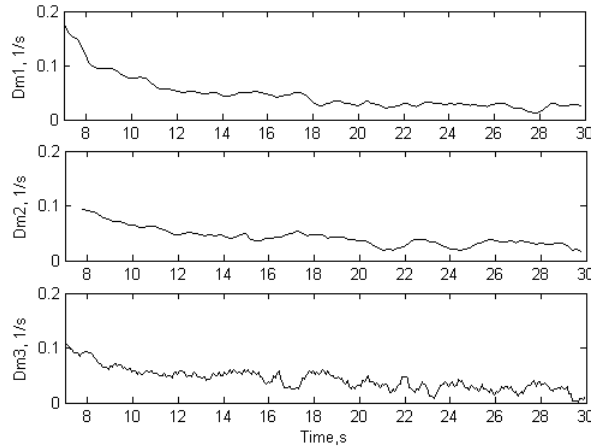


**Fig. 5 The mechanical damping dynamics**

### 3.3 Modeling of the mechanical torsional Damping

If the mechanical damping is plotted with reference to the modal speeds, as in Fig.4, it is shown that the former can be represented as the function of the latter. Consequently, a fitting function can be obtained for each mode, as described in (8).

$$D_{m,i} = a_i \exp(b_i \cdot \Delta\omega_{m,i}) + c_i \quad (8)$$

Where  $D_m$  is the mechanical damping,  $\Delta\omega_{m,i}$  is the modal speed; a, b, c are coefficients, the subscript  $i$  denoted the  $i$ th torsional mode.

The mechanical torsional damping is proportional to the load [4], thus if different loading level is considered, the damping model (8) can be rewritten as (9).

$$D_{m,i} = a_i \exp(b_i \cdot \Delta\omega_{m,i}) + kP + c_i \quad (9)$$

Where P is the output power and k is the coefficient.

By using the formula (9) and the measured damping values as shown in Fig.6, the fitting coefficients can be obtained, as displayed in Table I . Fig.6 illustrates the comprison of the measured damping and thosed calculated with the formula (9) and the coefficients listed. Obviously, they fit very well. It must be pointed out that these coefficients are calculated when the modal speed is in the range of 0 to 0.2 rad/s. When even larger transient events occur, which may cause more severe torsional vibration, the modal speed possibly exceed 0.2 rad/s. It is still an issue to be further verified that these coefficients be appropriate for torsional vibration caused by even severe system fault.

**Table I The parameters of the mechanical damping**

Coefficient Mode	<i>a</i>	<i>b</i>	<i>c</i>	<i>k</i>
1	0.010	25.2	0.005	0.135
2	0.007	31.0	0.006	0.135
3	0.005	20.0	0.012	0.180

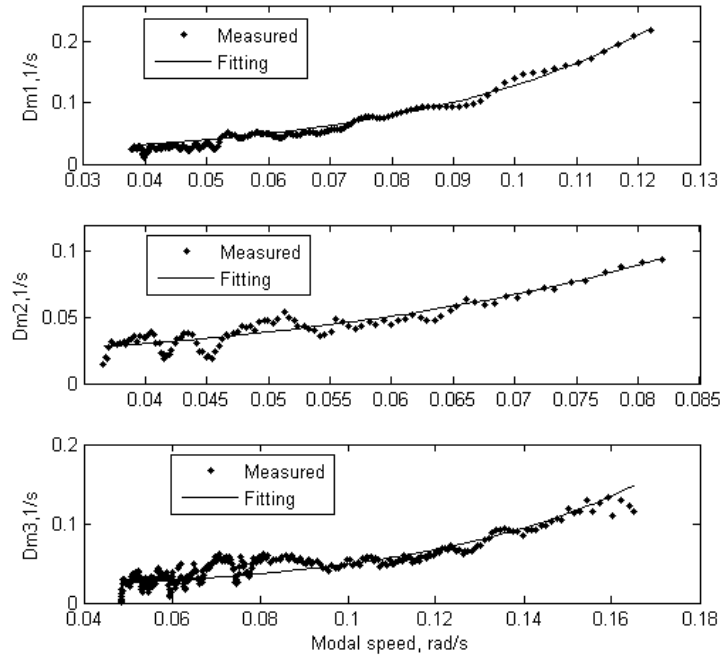


**Fig. 6 Comprison of the measured and fitting mechanical damping dynamics**

#### 4 EFFECT OF NONLINEAR TORSIONAL DAMPING ON SSR CHARACTERISTICS

Three aspects are investigated about the effect of nonlinear torsional damping on SSR characteristics.

##### 4.1. The critical compensation degree

The critical compensation degree (CCD) means the degree of series compensation that makes the system is on the edge of torsional stability.

For the test system, the CCD is calculated respectively with the fixed mechanical damping and the nonlinear damping represented in formula (9) for the 4-machine and one-line operating condition at its most vulnerable generator output (when all machines are lightly loaded). The used fixed mechanical

damping is calculated just by set  $\Delta\omega_{m,i} = 0$ ,  $P = P_0$  in (9). In the time-domain simulation, the disturbance triggered is manually switching off one of the Shangdu-Chengde lines to transmit to the one-line condition. The compensation degree is increased step by step until the system become critically unstable and thus the CCD is obtained.

The results of the analysis indicate that: CCDs for the fixed and nonlinear torsional damping are the same, i.e., 0.303, 0.312, 0.700 for the three torsional modes. In other words, the nonlinearity of mechanical damping doesn't affect the CCD.

#### 4.2. Large-disturbance stable case

In the test system, a three-phase short-circuit is triggered and the faulted line is cleared 0.1 second later. Due to the severe SSR impact, the protection device called torsional stress relay (TSR) is initialized to trip one of the four online generators. Then the system is stabilized. Both the fixed and nonlinearly varying mechanical damping are applied. The torque between masses are recorded and displayed in Fig. 7. The fatigue loss-of-life is calculated, as shown in Table II. It is observed that with the nonlinear mechanical damping, the torsional oscillation attenuates with a higher speed and causes low fatigue loss-of-life.

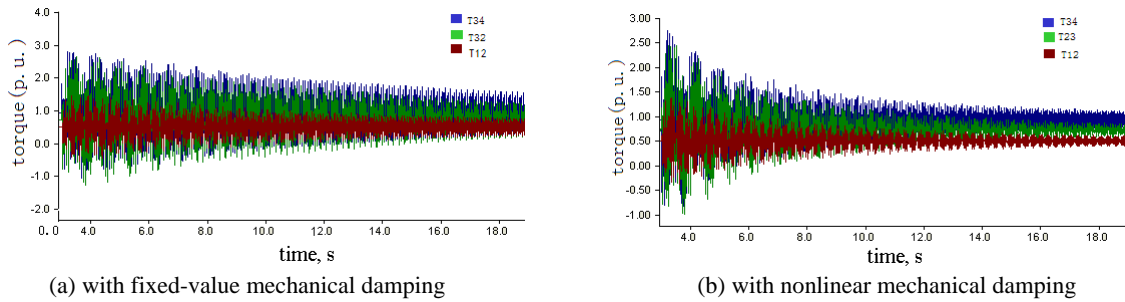


Fig. 7 Torque between masses after three-phase fault

Table II The fatigue loss-of-life caused by the three-phase fault (unit: %)

damping \ Position	HIP-ALP		ALP-BLP		BLP-GEN	
	HIP side	LPA side	LPA side	LPB side	LPB side	GEN side
Fixed damping	0.3746	0.0249	1.1394	1.7871	0.5065	0.5015
Nonlinear damping	0.1038	0.0051	0.2310	0.3839	0.0898	0.0847

#### 4.3 Large-disturbance instable case

The same fault as in 4.3 is applied to the system, however without the trip action of TSR. The system becomes SSR instable. Both the fixed and nonlinearly varying mechanical damping are used in the simulation. Fig.8 displays the speed deviation of HP turbine following the fault. It can be seen that with the fixed damping, the speed deviation increases exponentially. However, when the nonlinear damping is applied, the modal speed grows at the beginning and then become persistent oscillation with constant amplitude. This phenomena is similar with that once was observed in the reference [12].

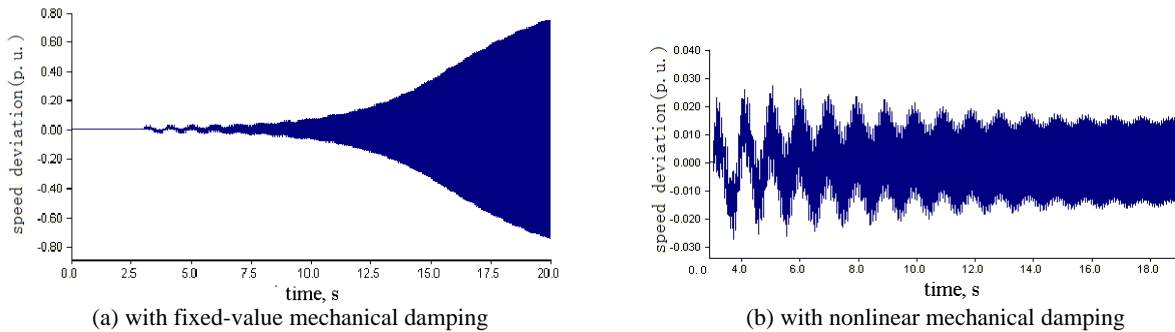


Fig. 8 The Speed deviation of HP turbine following the fault

## 5 CONCLUSIONS

A nonlinear turbine-generator shaft model is derived first, in which the modal torsional damping is presented as a nonlinear function of the modal speed and the power output. Then, for a practical 600 MW generator in a series-compensated power system, the recorded data of a phase-to-phase short-circuit fault occurring at the terminal are used to identify the torsional mechanical damping, which demonstrates obvious nonlinearity. The relationship between the modal damping and the amplitude of the torsional oscillation is analyzed and the nonlinear mathematical model obtained. This model is incorporated into the electromagnetic simulation software PSCAD/EMTDC. The effect of nonlinearity of torsional mechanical damping on SSR is studied in several importance respects, i.e., the critical compensation degree (CCD), the small-signal damping, the transient torque and the fatigue life loss during large disturbances. The nonlinear and linear mechanical damping is compared through simulation study in the Shuangdu series-compensated system. The results indicate that the nonlinear torsional damping doesn't affect the CCD, however leads to different dynamics of torsional oscillation when large disturbances occur in the system. For stable cases, nonlinear damping accelerates the speed of convergence and reduces the fatigue loss-of-life. While for unstable cases, nonlinear damping results in persistent instead of exponentially diverging torsional oscillation. And this is confirmed by practical phenomena.

## ACKNOWLEDGEMENTS

This work was supported in part by National Natural Science Foundation of China (51077080).

## BIBLIOGRAPHY

- [1] IEEE Subsynchronous Resonance Working Group of the System Dynamic Performance Subcommittee, Power System Engineering Committee. Countermeasures to subsynchronous resonance problems. IEEE Trans. PAS-99, 1980 :1810–1818
- [2] IEEE Committee report: First Benchmark Model for Computer Simulation of Subsynchronous Resonance. IEEE Trans. on Power Apparatus and Systems, 1977, PAS-96:1565-1572
- [3] IEEE Committee report : Second Benchmark Model for Computer Simulation of Subsynchronous Resonance. IEEE Trans. on Power Appa. Sys., 1985, PAS-104 :1057-1066
- [4] Agrawal B L, Farmer R G. Effective damping for SSR analysis of parallel turbine-generators[J]. IEEE Trans. Power Systems, 1988, 3( 4): 1441-1448
- [5] Iranvani M R, Semlyen A. Hopf bifurcation in torsional dynamics. IEEE Trans. on Power Systems, 1992, 7(1): 28-36
- [6] Zhu W, Mohler R R, Spee R, et al. Hopf bifurcation in a SMIB power system with SSR. IEEE Trans. on Power Systems, 1996, 11(3): 1579-1584
- [7] Dong L. The simple analysis of mechanical damping in shaft torsional vibration of turbogenerator, 1995, 19(8): 29-33
- [8] Baker D H, Boukarim G E, D'Aquila R. Subsynchronous resonance studies and mitigation methods for series capacitor applications[C]//PES 2005 Conference and Exposition in Africa, Proceedings of the Inaugural IEEE Durban, 2005: 386-392
- [9] Fouad A A, Khu K T. Damping of torsional oscillation in power systems with series-compensated lines, IEEE Trans. ,1978,PAS-97 :744–753
- [10] Bigret R. Measuring the Torsional Model Frequencies of a 900MW Turbinegenerator. IEEE Trans. on Energy Conversion, 1986
- [11] Brown M D , Moran C G . Torsional System Parameter Identification of Turbine-Generator Sets. IEEE Transactions on Energy Conversion, 1997, 4(11):304-309
- [12] Zhu W , Mohler R R. Hopf Bifurcation Analysis for an Electric Power System Experiencing Subsynchronous Resonance[C]//Proceedings of the 33rd Conference on Decision and Control Lake Buena Vista. FL, 1994: 613-614

**Sensitive Analysis on Electrical Parameters of Generators to Sub-synchronous Resonance**

**Song Peng<sup>1</sup>, Xie Xiaorong<sup>2</sup>, Zeng Fang<sup>3</sup>**

**Liang Yanjun<sup>3</sup>, Gao Xun<sup>4</sup>, Bai Kai<sup>1</sup>, Liu Ping<sup>1</sup>**

**1. North China Electric Power Research Institute Co., Ltd, China**

**2. Tsinghua University, China**

**3. Datang International Power Generation Co., Ltd, China**

**4. North China Grid Co., Ltd, China**

**SUMMARY**

In order to improve the capacity and the stability of the transmission lines, with the large application of the series compensation techniques to the electric grid in China, the sub-synchronous resonance (SSR) which may be harmful to the generator and the electric grid, was brought forth. More accurate parameters of the generators are needed to analyze and resolve the SSR problems. In this paper, the parameters of the generator which are obtained using the load rejection method based on the time-domain simulation technology, was applied to the SSR analyses on the long-distance transmission system with the series compensation techniques. Through the eigenvalue simulation analysis, the sensitivity of the different generator parameters on the SSR problems including the torsional oscillation and the asynchronous self-excitation were studied. Moreover, the demand of the SSR problem to the parameters identification of the generator was assessed accurately, which can be beneficial to precisely identifying the generator parameters.

**KEYWORDS**

Series compensation technique, Sub-synchronous resonance, Torsional oscillation, Asynchronous self-excitation, Generator, Parameter identification.

# 1 INTRODUCTION

With more and more application of the series compensation technique to the electric grid in China, especially its application to the transmission lines from the large coal power plant to the main grid in order to improve the capacity and the stability of the transmission lines, the sub-synchronous resonance (SSR) which may be harmful to the generator and the electric grid, was brought forth[1-5].

The SSR problem is a special stability problem caused by coupling between the mechanical or electrical systems of the generator and the transmission lines with the series compensation equipment. The SSR problem mainly involves the dynamic process of the generator and the electrical grid in the range of subsynchronous frequency, which is different from the dynamic process of the power frequency (50Hz). The five-order, 3-order and even lower order equivalent model of the generator is applied in studying the general electro-mechanical transient process and its stability[6]. However, in order to analyze the SSR problem precisely, the more detailed Park equation model of the generator should be adopted, which needs more accurate generator parameters.

In this paper, the parameters of the generator which are obtained using the load rejection method based on the time-domain simulation technology, was applied to the SSR analyses on the long-distance transmission system with the series compensation techniques. Through simulation analysis, the sensitivity of the different generator parameters on the SSR problems including the torsional oscillation and the asynchronous self-excitation were analyzed. Moreover, the demand of the SSR problem to the parameters identification of the generator was investigated. This means that precise identification of the generator parameters is greatly important to make the measurements which can effectively inhibit the SSR problems.

# 2 SENSITIVE ANALYSIS OF GENERATOR PARAMETERS TO SSR PROBLEM

In order to improve the transmission capacity of the transmission lines of the power plant, the series compensation devices were fixed on the each transmission line. However, the operation of the series compensation devices resulted in the torsional oscillation between the series compensation devices and the shaft of the generator. Based on each SSR modal frequency, Blocking filters (BF) are mounted at the neutral point of the high voltage side of the main transformers to inhibit the torsional oscillation. When the BF were put in operation, the asynchronous self-excitation of the generator was brought forth.

Based on the NO.1~8 generator of a power plant and its transmission lines with the series compensation devices, the effects of the electrical parameters of the generator on the two kinds of SSR problems including the torsional oscillation and the asynchronous self-excitation are studied. The schematic diagram of the generators and their transmission lines with the series compensation devices can be seen in Fig.1.

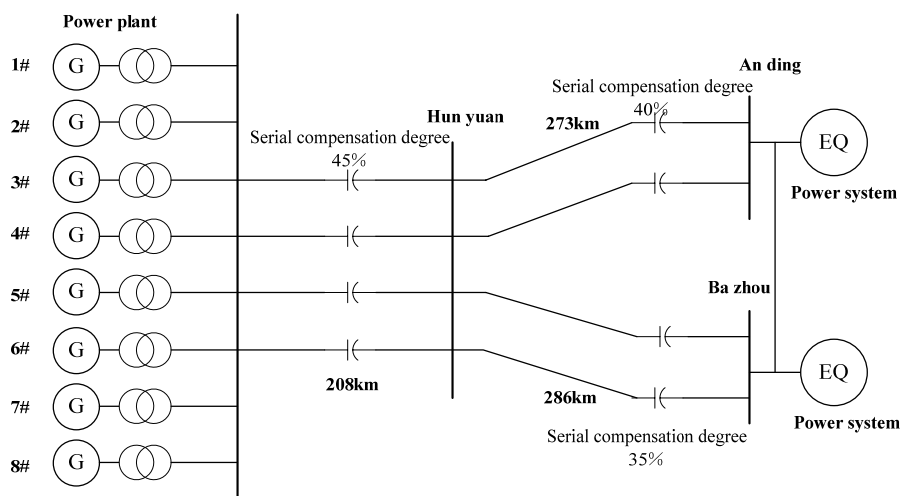


Fig. 1 Schematic diagram of series compensation transmission lines of a power plant

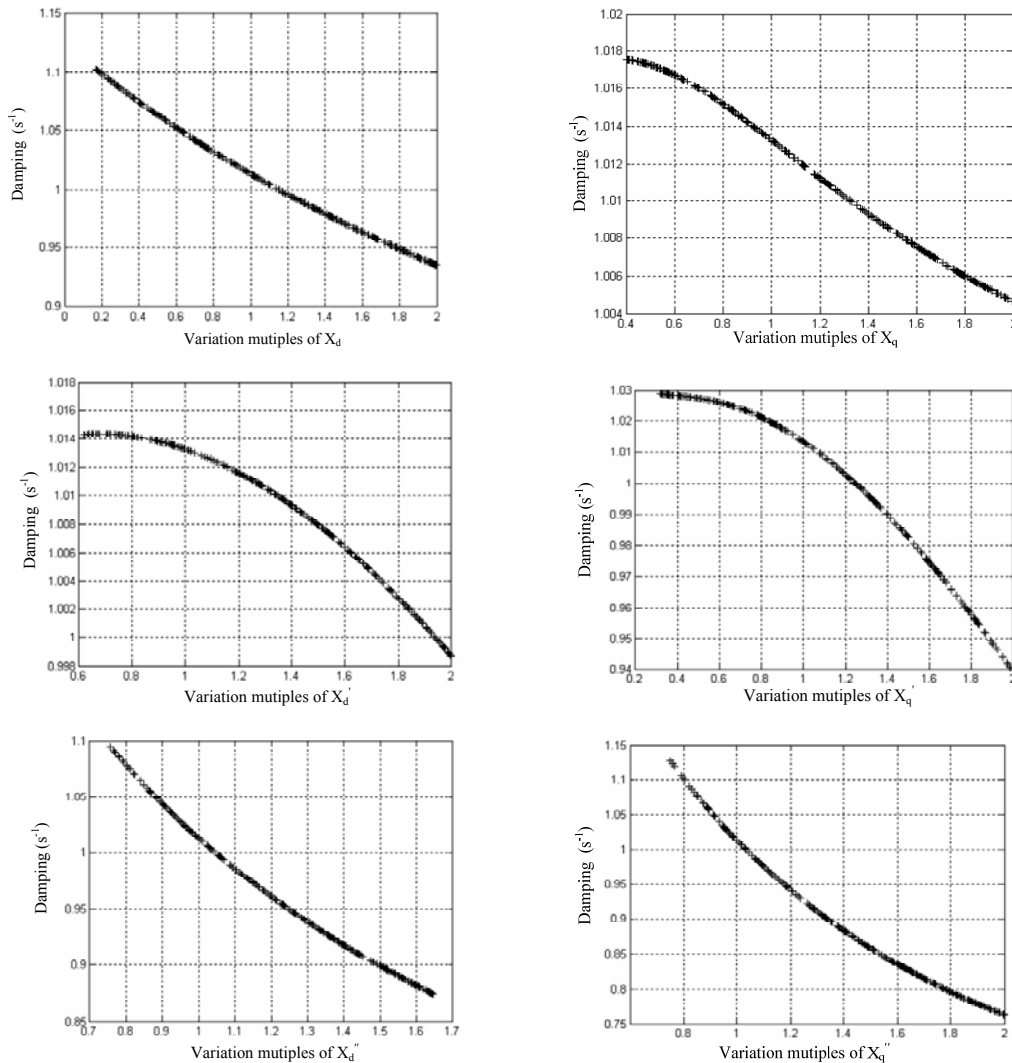
## 2.1 Sensitive analysis of parameters to torsional oscillation

On the operation condition of NO.1~8 generator that each generator takes the half active power and all the transmission lines with the series compensation devices are put into operation, the torsional oscillation modal frequency 1, 2 and 3 of NO.2 generator are taken for example, effects of the electrical parameters of the generator including  $X_d$ ,  $X_q$ ,  $X_d'$ ,  $X_q'$ ,  $T_{d0}$ ,  $T_{q0}$ ,  $T_{d0}''$  and  $T_{q0}''$  on each modal frequency are analyzed. The analytical results are shown in Table I.

**Table I Variation of the torsional oscillation modal frequency 1, 2 and 3 with different generator parameters.**

	Larger SSR risk with larger parameters	Smaller SSR risk with larger parameters	Almost no effects (<5%) of the variation of parameters on SSR risk
Modal frequency 1	$X_d''$ , $X_q''$	$T_{d0}''$ , $T_{q0}''$	$X_d$ , $X_q$ , $X_d'$ , $X_q'$ , $T_{d0}$ , $T_{q0}$
Modal frequency 2	-	$X_d$ , $X_q$ , $X_d'$ , $X_q'$ , $X_d''$ , $X_q''$ , $T_{d0}''$ , $T_{q0}''$	$T_{d0}'$ , $T_{q0}'$
Modal frequency 3	-	-	All parameters of the generator

Taken the modal frequency 2 (24.94Hz) for example, through eigenvalue simulation program, the damping variation tendency of modal frequency 2 with the variation of each generator parameter are obtained, which can be seen in Fig.2.



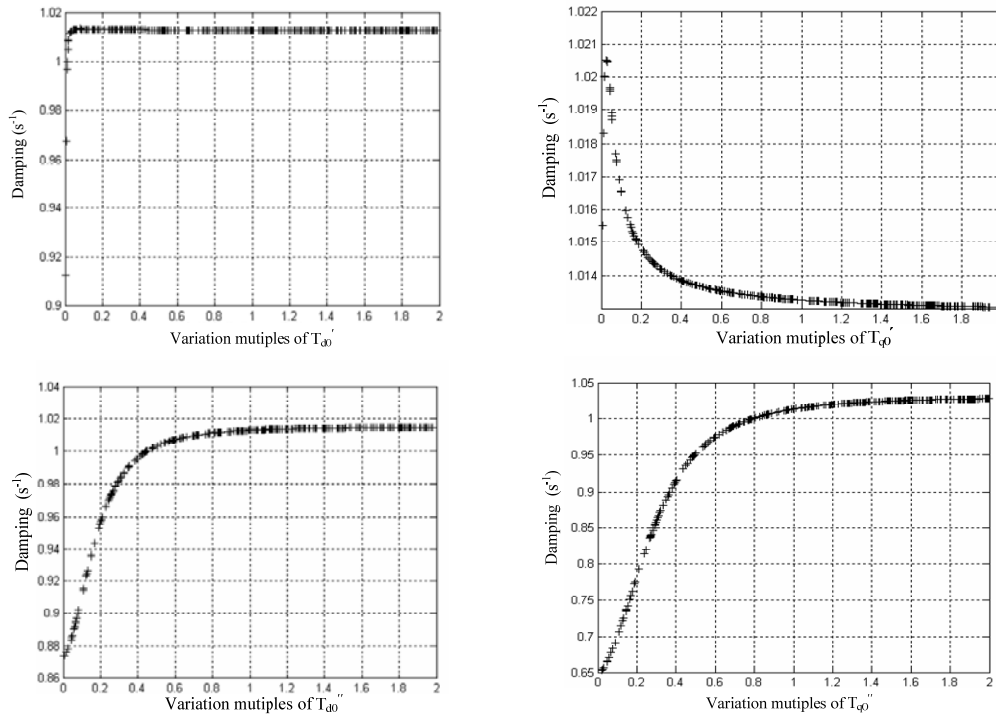


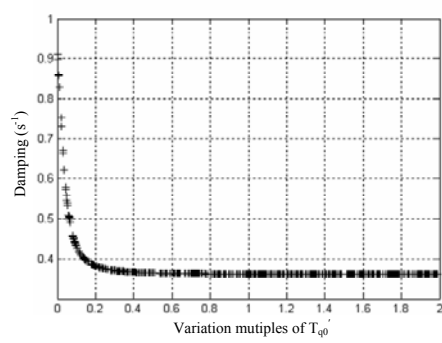
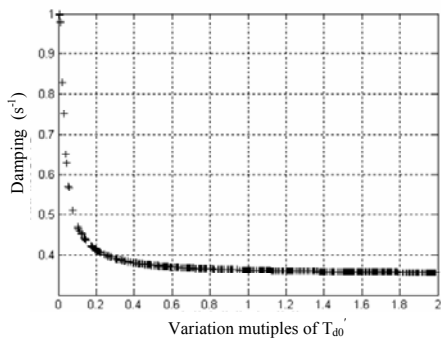
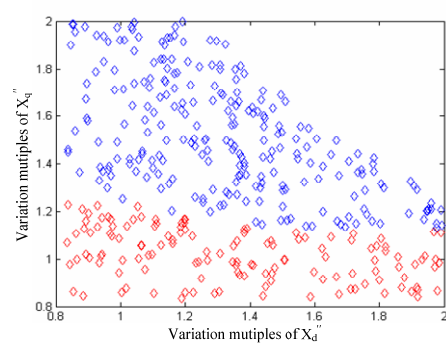
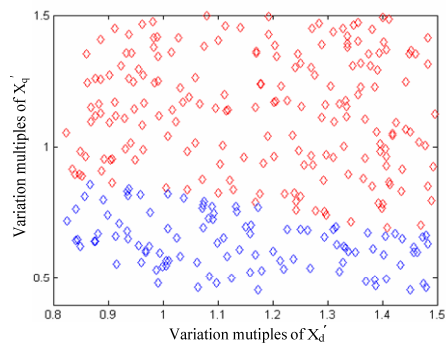
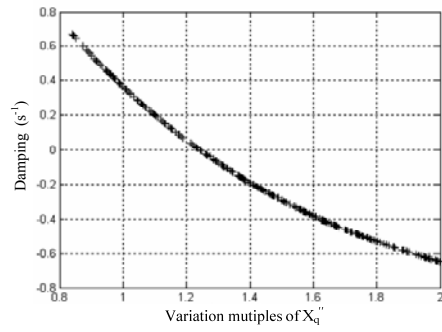
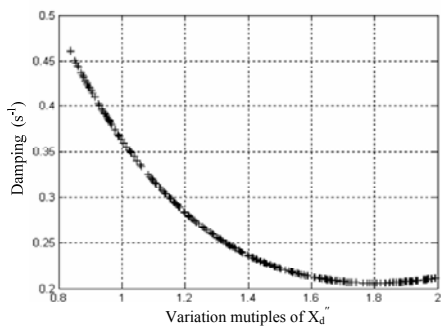
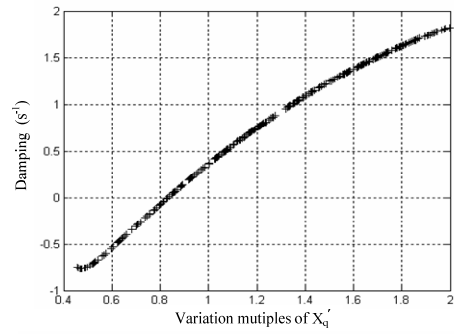
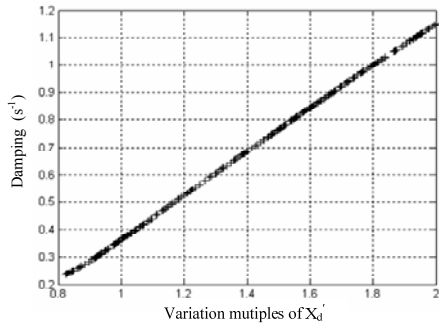
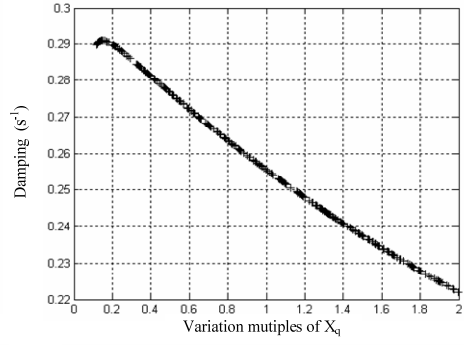
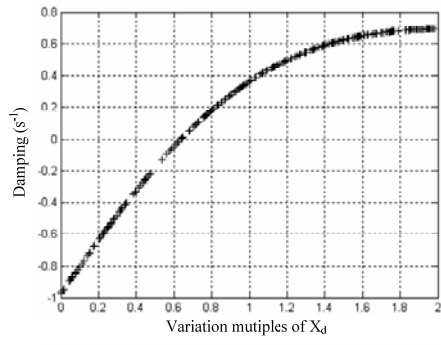
**Fig. 2 Damping variation tendency affected by different generator parameters.**

Through calculation and analysis, It can be found that the reactance and the time constant of the generator basically represents the reactance and the resistance connected serially in the equivalent circuit of the system with the modal frequency 2. From Table I and Fig.2, the analytical results can be obtained as below.

- (1) Larger transient time constant means the smaller resistance connected serially in the equivalent circuit of the system, which can result in larger risk in torsional oscillation. However, because the generator resistance takes a small percentage of the whole equivalent resistance in the circuit, the variation of the transient time constant ( $T_{d0}'$  and  $T_{d0}''$ ) has no apparent effect on damping of the modal frequency.
- (2) Larger reactance means the larger reactance value connected serially in the equivalent circuit of the system. This will reduce the equivalent series compensation degree of the system. With different modal frequency of the torsional oscillation, the relationship between the series compensation degree of the transmission line and the SSR risk is accordingly different.
- (3) Because the sub-transient parameters of the generator are represented in the sub-synchronous resonance range, the sub-transient parameters have more obvious effect on the torsional oscillation.
- (4) Generally, the effect of generator parameters on the torsional oscillation depends on the relationship between the mechanical modal frequency  $f_m$  and the electrical modal supplement frequency  $\bar{f}_e$ . Regularly, the closer to  $f_m$  the  $\bar{f}_e$  is, the larger effect on the SSR problem the parameters have.

## 2.2 Sensitive analysis of parameters to asynchronous self-excitation

Taken the asynchronous self-excitation modal frequency 2 (24.27Hz) for example, the operation mode of the power plant is that, NO.1~6 generator is normally operating connected to the electrical grid with half rated active power, and all the series compensation devices are not put into operation. The sensitive analyses of the generator parameters on the asynchronous self-excitation are conducted, which can be seen in Fig.3.



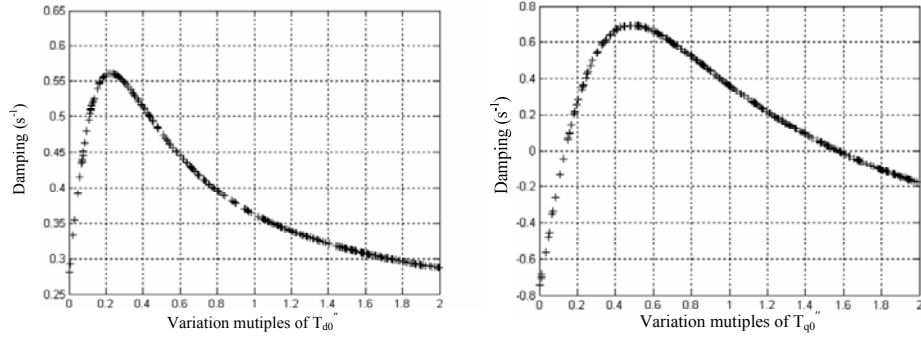


**Fig. 3 Damping variation tendency of asynchronous self-excitation affected by different generator parameters.**

Through above eigenvalue calculation analysis, for the modal frequency of the asynchronous self-excitation, the conclusions can be obtained as below.

(1) Larger time constant means smaller resistance serially connected to the equivalent circuit of the system and smaller negative resistance reflected in the rotor side, and thus reduce the risk of the asynchronous self-excitation. This is opposite to its effects on the torsional oscillation. Because the resistance reflected in the rotor side depends on the time constants of the generator, the time constants especially the sub-transient time constants have larger effects on the asynchronous self-excitation.

(2) Larger reactance of the generator means larger reactance serially connected to the equivalent circuit of the system. It can increase the original reactance value which forms resonance with the BF capacitance value, and thus reduce the risk of the asynchronous self-excitation. On the other side, with the same time constants, larger reactance can lead to the larger negative resistance reflected in the rotor side, and accordingly enhance the risk of the asynchronous self-excitation. From Fig.3 we can see that, the transient reactances ( $X_d'$  and  $X_q'$ ) will enhance the risk in direct proportion, and the sub-transient reactances ( $X_d''$  and  $X_q''$ ) will enhance the risk in inverse proportion.

(3) The generator parameters have more apparent effects on the asynchronous self-excitation than that on the torsional oscillation.

### 3 NECESSITY ANALYSIS OF THE PARAMETER IDENTIFICATION OF GENERATOR

With the equivalent reactance of the generator and the electrical grid, the BF reactance leads to the series resonance. The negative resistance of the equivalent circuit can result in divergence of the self-excitation. Therefore, when the BF is adopted to inhibit the torsional oscillation, the asynchronous self-excitation probably caused by the BF operation must be considered. In this paper, the simulation was conducted respectively based on the design parameters and the identified parameters of the generator, which is shown in Fig.4.

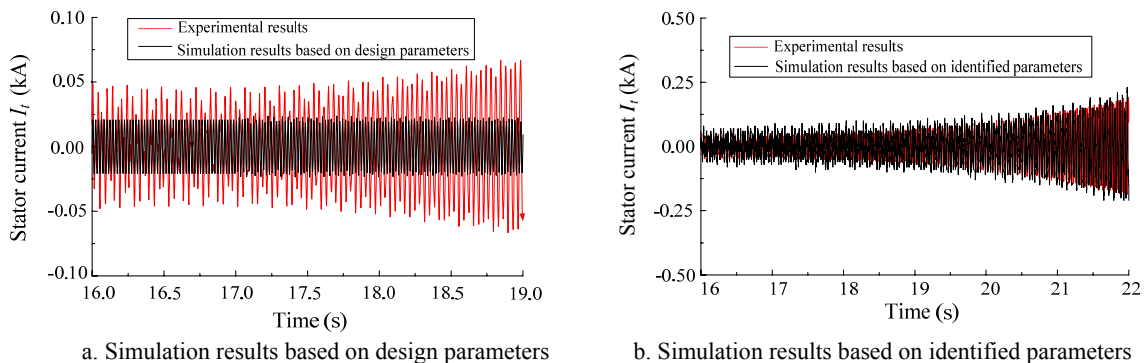


**Fig. 4 Comparison of the experimental results with the simulation results.**

Simulation results indicate that, the simulation curve based on the design parameters (Fig.4(a)) shows no diverge asynchronous self-excitation; the simulation curve based on the identified parameters (Fig.4(b)) manifests the diverge asynchronous self-excitation, which coincides greatly with the experimental curve. This is because that the design parameters of the generator, especially the key

parameters including the transient and sub-transient reactance and resistance to the asynchronous self-excitation, have no enough precision for the asynchronous self-excitation.

From above analysis, it is indicated that if the BF is adopted to inhibit the SSR problem of the transmission system with the series compensation devices, the higher precision of the generator parameters must be satisfied to accurately design the BF parameters. Therefore, the generator parameters should be accurately identified. The reasons are as below.

(1) The torsional oscillation is sensitive to the sub-transient reactance of the generator except other parameters. The asynchronous self-excitation has great sensitivity to lots of parameters of the generator.

(2) The effects of some parameters of the generator on the torsional oscillation and the asynchronous self-excitation are opposite to each other. Therefore, precisely identifying these parameters plays an important role in accurately assessing the SSR risk and the design of the BF parameters.

(3) The effective BF parameters are greatly sensitive to the generator parameters. The more parameters of the generator are provided, the BF can be designed to inhibit the torsional oscillation and avoid the asynchronous self-excitation more effectively. In the BF design, the inaccurate parameters of the generator may result in weakening the blocking effect on the SSR, reducing the capability of inhibiting the torsional oscillation and enlarging the losses.

### 3 CONCLUSION

In this paper, the analysis on the effects of the generator parameters on the torsional oscillation and the asynchronous self-excitation are conducted, which can provide the guidance to the actual measurement of the generator parameters, also establish the strong technical support to effectively inhibit the asynchronous self-excitation, and accurately assess the risk of the SSR problem. From the above analysis in the paper, the conclusions were obtained as below.

(1) The parameters which have the most apparent effects on the torsional oscillation are the D-axis and the Q-axis sub-transient reactances ( $X_d''$  and  $X_q''$ ).

(2) The parameters which have relatively large effect on the asynchronous self-excitation include  $X_d'$ ,  $X_q'$ ,  $X_d''$ ,  $X_q''$ ,  $T_{d0}''$  and  $T_{q0}''$ . The analyzing results indicate that, larger  $X_d'$  and  $X_q'$  can enhance the asynchronous self-excitation risk, however, larger  $X_d''$  and  $X_q''$  can reduce the asynchronous self-excitation risk. The results also show that larger time constant and smaller rotor resistance will reduce the asynchronous self-excitation risk.

(3) Both the transient and the sub-transient parameters have great effects on inhibiting the SSR problem. The transient and the sub-transient parameters of the generator are closely related to the design of the damping structure, which brings forward a demand of the planning of the coordination between the generators and the electric grid. Therefore, it is necessary that, the parameters of the generators, especially as the important power suppliers in the power system, should be accurately identified.

### BIBLIOGRAPHY

- [1] IEEE Sub-synchronous Resonance Working Group. Countermeasures to Sub-synchronous Resonance[J]. IEEE Trans. On PAS, 1980, 99(5): 1810-1818
- [2] Xu Z, Luo H, Zhu R. Review on Methods of Analysis For Sub-synchronous Resonance Analysis and Solutions[J]. IEEE Trans. on PAS, 1977, 96(4): 1226-1232
- [3] Xu Z, Zhang F. SSR Analysis of Series Compensation Transmission Scheme For Tuoketuo Power Plant[J]. Electric Power, 2006, 39(11): 21-26
- [4] Jiao X, Shen L. Discussion on The Reaction of Turbo generator to Sub-synchronous Resonance[J]. Large Electric Machine and Hydraulic Turbine, 2010 (2): 1-6
- [5] Liu X. Analysis of Suppression Strategy of Sub-synchronous Resonance In Power Generators[J]. Journal of Electric Power, 2010, 25(5): 394-396
- [6] Ni Y, Chen S, Zhang B. Theory and Analysis of Dynamic power system[M]. Beijing: Tsinghua University Press, 2002

**Resistance Analysis on the Gap-pickup Diagonal Flow Passage in Turbine  
Generator Rotors**

**Hu Lei, Yuan Jianhua  
Liang Xubiao, Xian Zhelong  
Shanghai Electric Power Generation Group  
China**

**Hu Xiaohong, Yuan Yichao  
University of Shanghai for Science  
and Technology, China**

**SUMMARY**

The gap-pickup diagonal flow ventilation system has been widely employed because of its short cooling channels, simple fan configuration, high reliability and efficiency. The diagonal flow passage is an important section in where heat exchanges between rotor winding and cooling gas, and it directly influences the cooling condition of the gap-pickup diagonal flow system. The resistance characteristic of the diagonal flow passage is analyzed, and the formula for the total resistance of diagonal flow passage has been obtained in this paper. The results should be helpful for the calculation of the gap-pickup ventilation system.

**KEYWORDS**

Turbine generator ,Rotor ,Gap-pickup , Diagonal flow passage

## 1 INTRODUCTION

The directly hydrogen-cooling rotor winding method has been employed widely as a high performance rotor cooling system<sup>[1]</sup>. Several different arrangements for directly hydrogen-cooling rotor windings have been used in domestic and abroad to improve the efficiency of turbine generators. The two primary methods currently used are radial flow cooling system and gap-pickup diagonal flow cooling system<sup>[2-4]</sup>. Because of the shorter channel, lower temperature rise, more uniform for temperature distribution, simpler fan configuration, and higher reliability etc, gap-pickup diagonal flow ventilation system has been widely applied in large-scale turbine generator rotors and provided with reliable and efficient performance.

The diagonal flow passage is an important section in where the heats transfer between rotor winding and coolant in the gap-pickup diagonal flow system. The fundamental flow of coolant in the diagonal cooling ducts is affected not only by the friction, local resistance of inlet and outlet, but also by the thermal resistance and rotating centrifugal force. These factors make the flow pattern of coolant more complex in the diagonal cooling ducts. The resistance characteristic of the diagonal flow passage under thermal resistance and rotating centrifugal force is analyzed, and the formula for the total resistance of diagonal flow passage has been obtained in this paper.

## 2 INFLUENCE OF THERMAL RESISTANCE

In order to facilitate the influence of temperature rise of rotor winding on the flow pattern of coolant, we first neglect the friction resistance, local resistance and the additional resistance which is caused by rotating centrifugal force, and simplify the flow pattern as non viscous, one dimension, internal flow(shown in Fig 1). Some assumption are as follow: the coolant is ideal gas, the heat distribution is uniform in the cooling ducts, inlet velocity and temperature distribution is also uniform, stagnation static pressure at the inlet is constant, the outlet back pressure is independent of outlet velocity. The governing equation is as follows:

Mass conservation equation:

$$V_1\rho_1 = V_2\rho_2 \quad (1)$$

Momentum conservation equation:

$$P_1 - P_2 = m(V_2 - V_1) \quad (2)$$

Energy conservation equation:

$$q = c_p(T_2 - T_1) + \frac{(V_2^2 - V_1^2)}{2} = c_p(T_{02} - T_{01}) \quad (3)$$

$$c_p T_{01} = c_p T_1 + \frac{V_1^2}{2} \quad (4)$$

Stagnation pressure at point 1 and 2 are:

$$p_{01} = p_1 \left( 1 + \frac{k-1}{2} M_1^2 \right)^{\frac{k}{k-1}} \approx p_1 \left( 1 - \frac{k}{2} M_1^2 \right) \quad (5)$$

$$p_{02} = p_2 \left( 1 + \frac{k-1}{2} M_2^2 \right)^{\frac{k}{k-1}} \approx p_2 \left( 1 - \frac{k}{2} M_2^2 \right) \quad (6)$$

In the above equations, M represents ach number, m means flow mass of coolant, q denotes density of heat flow, K is entropic exponent,  $T_{01}$ 、 $T_{02}$ 、 $P_{01}$ 、 $P_{02}$  represent stagnation temperature and pressure at point 1 and 2.

In the gap-pickup diagonal flow ventilation system, when  $P_1$ 、 $V_1$ 、 $T_1$  keep constant which means the inlet mass flow is fixed, however, the coolant density and outlet pressure will decrease , the velocity

will increase as the coolant absorb the heat which is generated in the rotor windings. This effect named thermal resistance  $\Delta P_h$  is caused by temperature rise<sup>[4]</sup>.

$$\Delta P_h = P_1 - P_2 = \xi_h \cdot \frac{1}{2} \rho_2 V_2^2 \quad (7)$$

In equation 7,  $\xi_h$  represents thermal resistance coefficient, and when the coolant is affected only by thermal resistance, then  $\Delta P_h = P_1 - P_2$ .

From equation 1 to 6, one can get the formula for thermal resistance coefficient, shown in equation 8:

$$\xi_h = 2 \left[ 1 + \frac{q}{c_p T_0} - \frac{(1 + k M_1^2) \left( 1 + \frac{k-1}{2} M_2^2 \right)}{(1 + k M_2^2) \left( 1 + \frac{k-1}{2} M_1^2 \right)} \right] \bigg/ \left( 1 + \frac{q}{c_p T_0} \right) \quad (8)$$

When the value of He ( $He = q/c_p T_0$  represents the ratio of heat absorption per unit mass to initial stagnation enthalpy) is minor, which means  $M_1^2 \approx M_2^2$ , equation 8 is equivalent to the follow equation:

$$\xi_h = \frac{2 \frac{q}{c_p T_{01}}}{1 + \frac{q}{c_p T_{01}}} = \frac{2He}{1 + He} \quad (9)$$

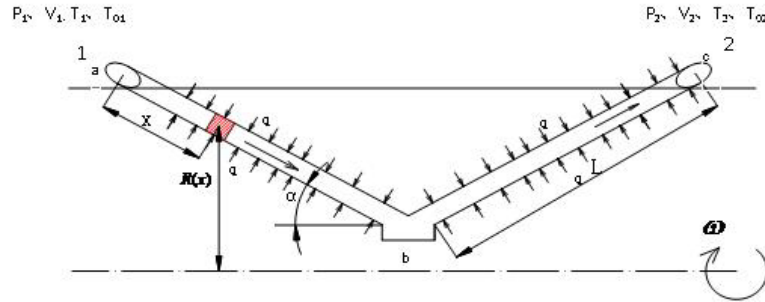


Fig.1 Schematic of gap-pickup diagonal flow passage

### 3 INFLUENCE OF TOTATING CENTRIFUGAL FORCE

In the gap-pickup diagonal flow ventilation system, thermal resistance, rotating centrifugal force and friction affect the coolant in the cooling ducts at the same time, and the total resistance equation is as follows:

$$\Delta P_d = \Delta P_r + \Delta P_c + \Delta P_h \quad (10)$$

In the above equation,  $\Delta P_r$ ,  $\Delta P_c$  and  $\Delta P_h$  respectively represent the pressure drop caused by friction, rotating centrifugal force and thermal resistance.

In order to calculate  $\Delta P_c$ , from the infinitesimal analysis view point for fluid flow shown in Fig 2, we analyze the influence of centrifugal force on the coolant. In Fig 2,  $R(x)$  denotes the distance between infinitesimal body and rotating axial, and then  $R(x) = (L-x) \sin \alpha$ ,  $L$  represents the length of line section  $ab$ ,  $\alpha$  expresses the included angle between rotor axial and diagonal duct.

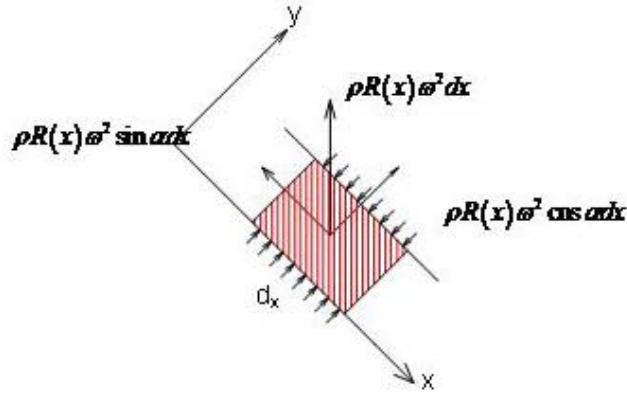


**Fig.2 Decomposition of centrifugal force of the diagonal flow passage**

In order to calculate the component of centrifugal force,  $F_{ab}$ , which is parallel to diagonal duct, one should make the integration of infinitesimal body, shown in Fig 2, along the diagonal duct ab section.

$$\begin{aligned}
 F_{ab} &= \int_0^L \rho R(x) \omega^2 \sin \alpha dx = \int_0^L \rho(L-x) \omega^2 \sin \alpha^2 dx \\
 &= \rho \omega^2 \sin \alpha^2 \left( L - \frac{1}{2} L^2 \right)
 \end{aligned} \tag{11}$$

Based on equation 11, one can calculate the pressure  $\Delta P_{ab}$  which is caused by centrifugal force named  $F_{ab}$  :

$$\Delta P_{ab} = \frac{F_{ab}}{A} = \rho \omega^2 \sin \alpha^2 \left( L - \frac{1}{2} L^2 \right) \tag{12}$$

Using the same method, one can get the pressure  $\Delta P_{bc}$ :

$$\Delta P_{bc} = \frac{F_{bc}}{A} = \rho \omega^2 \sin \alpha^2 \left( L - \frac{1}{2} L^2 \right) \tag{13}$$

In Fig 1, the direction of centrifugal force is opposite to coolant flow along the diagonal duct ab section, and keeps the same direction along bc section. Because of  $L_{ab}=L_{bc}=L$ , then  $\Delta P_{ab}=-\Delta P_{bc}$ , so the formula for  $\Delta P_c$  is:

$$\Delta P_c = \Delta P_{ab} + \Delta P_{bc} = 0 \tag{14}$$

And the simplification for equation 10 is:

$$\Delta P_d = \Delta P_r + \Delta P_h \tag{15}$$

#### **4 INFLUENCE OF FRICTION IN ROTATING DIAGONAL DUCT**

In the gap-pickup diagonal flow ventilation system, the secondary flow which is caused by centrifugal force and Coriolis force will influence the flow pattern of the coolant, and change the friction loss coefficient. The formulas for Coriolis force and centrifugal force are as follow <sup>[5]</sup>:

$$f_k = 2\vec{\omega} \times \vec{V} = 2\omega V \sin \beta \tag{16}$$

$$f_L = \rho R \omega^2 \tag{17}$$

In the above equations,  $\vec{\omega}$  denotes angular velocity vector,  $\vec{V}$  expresses velocity vector,  $\omega$  means angular velocity,  $\beta$  is the included angle between the central line of the rotating body and rotating axial.

The rotation motion of the diagonal duct is shown in Fig1 which can be decomposed into radial rotating and parallel rotating. For example, as for diagonal duct section ab, it can be decomposed into radial rotating around axial L1 and parallel rotating around axial L2, shown in Fig3(a); about section bc, it can be decomposed into radial rotating around axial L1' and parallel rotating around axial L2', shown in Fig3(b):

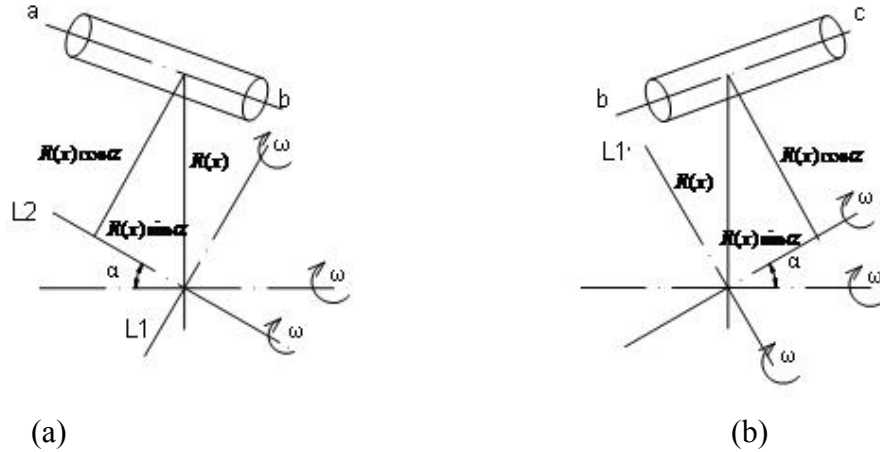


Fig.3 Decomposition of rotational movement of the diagonal flow passage

When the diagonal duct is radial rotating, velocity field and temperature field is not uniform in the same cross-section, therefore, the value of Coriolis force and centrifugal force at any point in the same cross-section is different from each other. At the centre of the cross-section, based on equation 16 and 17, because of its high velocity, low temperature and high density, the value of Coriolis force and centrifugal force achieve the highest value, and vice versa in the wall vicinity. When the diagonal duct is parallel rotating, there is no Coriolis force, however, it exist temperature difference for the coolant, and the centre part temperature is lower than the wall vicinity in the same cross-section. The secondary flow is caused by density difference which is the result of the temperature difference. The secondary flow which is caused by Coriolis or centrifugal force can alter the friction loss coefficient and surface heat transfer coefficient of the coolant in the diagonal duct.

Friction loss named  $\Delta P_r$  in the rotating diagonal duct includes two parts, one is frictional head loss and another is local head loss.

$$\Delta P_r = \left( \lambda_{rab} \frac{L}{d_1} + \lambda_{rbc} \frac{L}{d_1} + \xi_r \right) \frac{1}{2} \rho V_2^2 \quad (18)$$

In the equation 18,  $\lambda_{rab}$  is the frictional loss factor for diagonal duct section ab,  $\lambda_{rbc}$  denotes section bc,  $\xi_r$  represents the local loss factor,  $d_1$  is equivalent diameter for the diagonal duct.

(1) frictional loss factor for radial rotating

While  $Re \leq Re_{cr}$ , frictional loss factor for radial rotating duct is as follows<sup>[6]</sup>:

$$\lambda_{kr} = \frac{64}{Re^{0.8}} \frac{u}{V} \sqrt{\frac{d_1}{R_{av}}} \quad (19)$$

In equation 19,  $R_{av}$  is the average rotating radius for diagonal duct,  $u$  denotes the velocity at the average rotating radius,  $V$  represents average velocity for the coolant,  $Re$  means Reynolds number,  $Re_{cr}$  is the critical Reynolds number and its definition formula is:

$$Re_{cr} = 2300 \left[ 1 + \left( \frac{u}{V_c} \sqrt{\frac{d_1}{R_{av}}} \right)^2 \right] \quad (19a)$$

Where  $V_c$  is the velocity for  $Re=2300$  in above equation.

While  $Re > Re_{cr}$ , frictional loss factor for radial rotating duct is:

$$\lambda_{kr} = c\lambda \quad (20)$$

In equation 20,  $\lambda$  is the frictional loss factor under statics, and its definition is  $\lambda = 0.3164/Re^{0.25}$ ,  $c$  denotes the compensation factor for frictional loss factor, and its value is 0.75 for centripetal rotating, 1.25 for centrifugal rotating.

(2) frictional loss factor for parallel rotating

$$\lambda_{pr} = \lambda' \left[ 1 - 0.037 \left( \frac{u}{V} \right)^{2.772} \right] \quad (21)$$

In equation 21,  $\lambda'$  means the frictional loss factor which does not consider the rotating effect. In fact, there are radial rotating and parallel rotating in the diagonal duct, based on equation 21, and then we get the formula [6]:

$$\lambda_r = \lambda_{kr} \left[ 1 - 0.037 \left( \frac{u}{V} \right)^{2.772} \right] \quad (22)$$

(3) local loss factor for diagonal rotating duct

While  $Re \leq Re_{cr}$ , local loss factor for rotating duct is as follows [6]:

$$\xi_r = \xi \left[ 1 + 0.52 Re^{0.25} D_r^{0.86} \right] \quad (23)$$

In above equation 23,  $\xi$  is the local loss factor under statics which definition formula is  $\xi = \xi_d + \xi_{in} + \xi_{out}$ .  $\xi_d$ ,  $\xi_{in}$ ,  $\xi_{out}$  respectively denotes the local loss factor, inlet local loss factor, outlet local loss factor under statics;  $D_r$  is the rotating diameter for local loss calculation.

When  $Re > Re_{cr}$ , the value of local loss factor is independent of rotating.

$$\xi_r = \xi = \xi_d + \xi_{in} + \xi_{out} \quad (24)$$

In the end, the formula for total resistance of diagonal duct is as follows:

When  $Re \leq Re_{cr}$ :

$$\begin{aligned} \Delta P_d &= \left( \lambda_{rab} \frac{L}{d_1} + \lambda_{rbc} \frac{L}{d_1} + \zeta_r + \zeta_h \right) \frac{1}{2} \rho V_2^2 \\ &= \left[ \frac{64}{Re^{0.8}} \frac{u}{V} \sqrt{\frac{d_1}{R_{av}}} \left[ 1 - 0.037 \left( \frac{u}{V} \right)^{2.772} \right] \frac{2L}{d_1} + \left[ \xi_d + \xi_{in} + \xi_{out} \right] \left[ 1 + 0.52 Re^{0.25} D_r^{0.86} \right] + \frac{2He}{1+He} \right] \frac{1}{2} \rho V_2^2 \end{aligned} \quad (25)$$

When  $Re > Re_{cr}$ :

$$\Delta P_d = \left( \lambda_{\text{rab}} \frac{L}{d_1} + \lambda_{\text{rbc}} \frac{L}{d_1} + \zeta_r + \zeta_h \right) \frac{1}{2} \rho V_2^2$$

$$= \left[ \begin{array}{l} (0.75 + 1.25) \frac{0.3164}{Re^{0.25}} \left[ 1 - 0.037 \left( \frac{u}{V} \right)^{2.772} \right] \frac{L}{d_1} + \\ \left[ \zeta_d + \zeta_{\text{in}} + \zeta_{\text{out}} \right] + \frac{2He}{1 + He} \end{array} \right] \frac{1}{2} \rho V_2^2 \quad (26)$$

## 5 CONCLUSIONS

The total resistance, which is caused by thermal resistance, centrifugal force, and viscous, is associated with the amount of heat transfer, velocity at the average rotating radius, average velocity of the coolant etc. The formulas of 25 and 26 should be helpful for the calculation of the gap-pickup ventilation system.

## BIBLIOGRAPHY



**Hu Lei** (1980~), on-job doctorate. He received a BE degree in Architecture Environment & Equipment Engineering from Central South University in 2002 and a ME degree in Fluid Mechanics from University of Shanghai for Science and Technology in 2006. He is now the director of Ventilation Cooling Technology Institute, Shanghai Electric Power Generation Group R&D Center.

- [1] ХыропеЦКИЙ Г М. Gas cooled for rotor of two pole turbine generator [J]. *Abroad Large Scale Electric Motor*, 1991 (5) :18~22
- [2] Wang G, Ding S. Sum-up of design and research for 1000MW turbine generator [J]. *Shanghai Large Scale Electric Motor*, 2001(3):2~5
- [3] Wei S. Review for the development of cooling technology of abroad turbine generator [J]. *Abroad Large Scale Electric Motor*, 1979(1):1~7
- [4] Guo Z. *Thermal fluid mechanics*. Beijing : Tsinghua University Press, 1992
- [5] Tong B, Yin X. *Theory of vortex motion*. University of Science and Technology of China Press, 1994
- [6] Wei Y, Meng D, Wen J. *Heat exchange in electric motor*. Beijing China Machine Press, 1998

## **Negative Sequence Eddy Current Field Analysis and Temperature Calculations of 1100MW Turbo-generator with 3D Finite Element Methods**

**Zhong Houhong, Xian Zhelong, Zhao Wei  
Liang Xubiao, Liu Minghui  
Shanghai Electric Power Generation Equipment Co., Ltd.  
/ Shanghai Generator Works, China**

### **SUMMARY**

Generally speaking, there's negative current in the stator windings of turbo-generators when operating with unbalance currents. Then a negative direction rotating magnetic field with twice power frequency will be caused in the machine. It's important to limit the negative sequent current level and its duration. Therefore, detailed calculations or analysis of negative sequence eddy current field and temperature field is required, especially during the period of new type turbo-generator development.

In this paper, a parametric 3D negative sequence eddy current field analysis model of 1100MW 4-pole turbo-generator is established. The 1100MW 4-pole turbo-generator is a new type turbo-generator using in nuclear power plants. The 3D negative sequence currents arising from unbalance system operations in large turbo-generators are studied by using the finite element method. And the physical theory base of negative sequence eddy current field analysis is Maxwell equations. The mathematical models of large capability 4-pole turbo-generators are proposed to predict the negative sequence eddy current and temperature fields. In order to emulate the distributed exciting sources of the negative sequence current fields with enough precisions, the geometrical complication of the stator are accurately modeled in the proposed solid models, making it be readily to take into account of practical distributions of the negative sequence exciting currents. The sequence eddy current fields analysis of large turbo-generators includes both steady state and transient state analysis.

To obtain temperature calculation results, some solving techniques of coupled fields are introduced. The temperature field analysis of large turbo-generators also includes both steady state and transient state analysis. And finally, the eddy current, loss and temperature distributions of the 1100 MW generator operating with negative current are obtained, for both analysis states. The computational results are shown in 3D colored figures, thus it's easy to get an overview of the eddy current, loss and temperature distributions.

The results of steady state and transient state negative sequence analysis are in accordance with the standard IEC 60034-3. This study provides a basis for the design and operation of large capability turbo-generator.

### **KEYWORDS**

1100MW, 4 poles, Turbine generator, Eddy current field, Finite element, Negative sequence

## 1 INTRODUCTION

In the first decade of 21 century, because of global warming, more and more countries consider nuclear power as a low-carbon energy source. Therefore, QFSN type 1100MW 4poles turbo-generator was developed and already machined since 2010, in Shanghai, China. It's a new type turbo-generator using in nuclear power plants.

As is well known, negative sequence current exists during the unbalanced operations of the turbo-generator. Subsequently, a 100Hz A.C. harmonic current will occur in rotor surface, including rotor teeth surface, rotor slot wedge etc. This kind of harmonic current brings additional loss to the rotor part of the machine. Once the negative sequence current level or the acting time of negative sequence current exceed the allowed value, over-heat will occur on the rotor surface. If this results in long time shut-down, the power plant has to undergo losses. Thus, it's important to bring up a study of negative sequence analysis.

Since 1950s, hundreds of theses about negative analysis has been published. With the rapid development of calculation science and computer technology, theses of negative sequence eddy current field analysis also appears recently. The major analysis method of negative sequence eddy current field is Finite Element Analysis (FEA).

In this paper, a Three Dimensional (3D) negative sequence analysis model of 1100MW 4poles turbo-generator was created using 3D drawing software (such as PRO/E). After automatic meshing of FEA software (such as ANSYS), a FEA model was obtained. Based on this FEA model, steady state and transient state negative sequence eddy current field and thermal results were acquired.

## 2 SOLID 3D and NUMERICAL MODEL

### 2.1 Electrical-magnetic analysis model

In order to calculate the negative electric-magnetic field and temperature of 1100MW 4-poles turbo-generator, solid 3D models of stator slots(with slot wedge), stator tooth, rotor slots(with slot wedge),rotor tooth were created, using 3D drawing software(such as PRO/E). With the purpose of keeping the magnetic path complete, solid 3D models of stator yoke with a size of 20mm under stator slots, rotor yoke with a size of 20mm under rotor slots were also created. As is well known, that the penetrate depth of 100Hz negative current field in the material of iron or copper is less than 1mm. The 20mm models are deep enough.

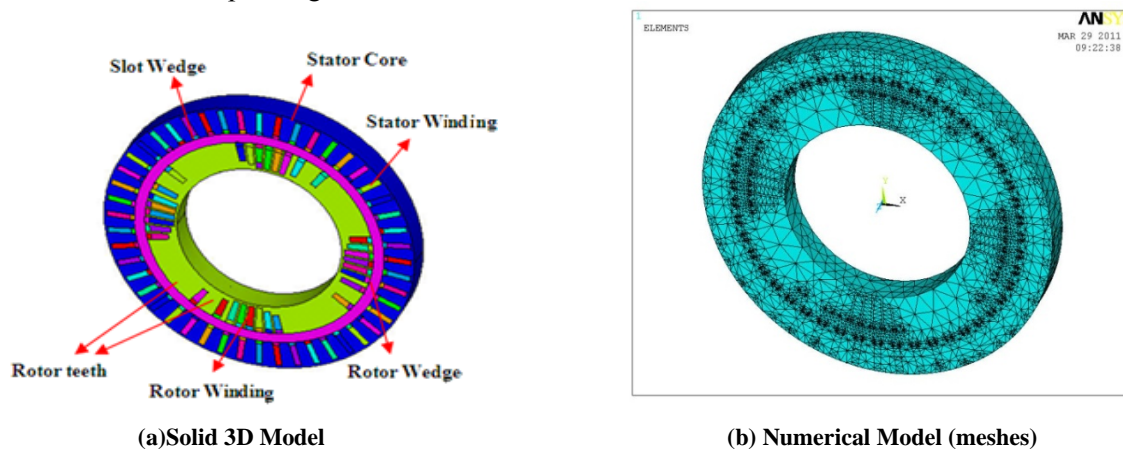
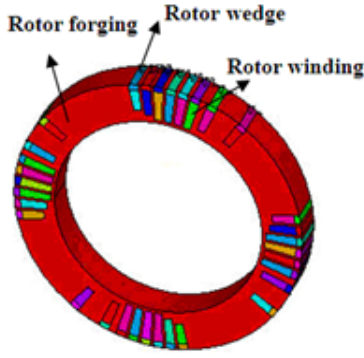


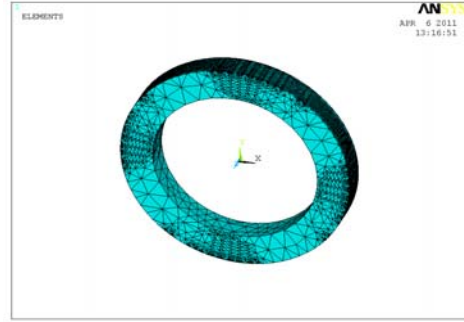
Fig.1 Models of 1100MW 4poles Turbo-generator Eddy Current Analysis

### 2.2 Thermal analysis model

The focus of thermal analysis is the temperature of the rotor. It's not necessary to rebuild a new model for thermal analysis. In ANSYS, the model for eddy current field was transformed to thermal analysis model.



(a) Solid 3D Model



(b) Numerical Model (meshes)

Fig.2 Models of 1100MW 4poles Turbo-generator Thermal Analysis

### 3 BASIC THEORY

#### 3.1 FEA method for electrical-magnetic analysis

The theory base of Electrical-magnetic Analysis is 3D Finite Element Methods. As is well known, Maxwell Equations are used to describe the instinct property of electrical-magnetic field.

$$\begin{cases} \nabla \cdot D = \rho \\ \nabla \cdot B = 0 \\ \nabla \times E = -\frac{\partial B}{\partial t} \\ \nabla \times H = J + \frac{\partial D}{\partial t} \end{cases} \quad (\text{Maxwell Equations})$$

Where:

- D — Electrical displacement vector, unit: C/m<sup>2</sup>;
- E — Electrical field strength, unit: V/m;
- B — Magnetic flux density, unit: T;
- H — Magnetic field strength, unit: A/m;
- ρ — Magnetic flux density, unit: C/mm<sup>3</sup>;
- J — Current density, unit: A/mm<sup>2</sup>.

All flux-lines at the boundary of the negative calculation model are paralleled with the edges of the model boundary. Therefore the boundary condition is natural boundary condition. With these boundary conditions, the differential equations of the whole calculation region are as follow:

$$\begin{cases} \nabla \times (v \nabla \times \dot{A}) - \nabla \times (v \nabla \cdot \dot{A}) + j\omega \sigma \dot{A} + \sigma \nabla \dot{V} - \dot{J}_s = 0 \\ \nabla \cdot (-j\omega \sigma \dot{A}) - \sigma \nabla \dot{V} = 0 \end{cases}$$

Where:

- A — Magnetic vector,  $\nabla \times \dot{A} = \dot{B}$ ;
- v — Permeability, unit: T/(A/m);
- ω — Angular velocity, unit: rad/s;
- σ — Electrical conductivity, unit: Ω/m;
- V — Volume, unit: mm<sup>3</sup>;
- J<sub>s</sub> — Current density, unit: A/mm<sup>2</sup>.

The current eddy field is described by the differential equations above.

Using the symbol " $\vec{n}$ " or " $\vec{N}$ " to symbolize vertical direction vector of one surface, the internal boundary conditions of the analysis model are as follow:

$$\begin{cases} \vec{n}_{12} \cdot (\nabla \times \dot{\vec{A}}_1) = \vec{n}_{12} \cdot (\nabla \times \dot{\vec{A}}_2) \\ \frac{\nabla \times \dot{\vec{A}}_1}{v_1} \times \vec{n}_{12} = \frac{\nabla \times \dot{\vec{A}}_2}{v_2} \times \vec{n}_{12} \end{cases}$$

The Galerkin's weighting margin equations of the calculated model are as follows:

$$\begin{cases} \int_{\Omega} \left\{ v \nabla \times \vec{N}_1 \cdot (\nabla \times \dot{\vec{A}}) + v \nabla \cdot \vec{N}_1 (\nabla \cdot \dot{\vec{A}}) + \right. \\ \left. j \omega \sigma \cdot \vec{N}_1 \cdot \dot{\vec{A}} + \sigma \vec{N}_1 \cdot \nabla \dot{V} - \vec{N}_1 \cdot \dot{\vec{J}}_s \right\} dV = 0 \\ \int_{\Omega} \left\{ \nabla \vec{N}_1 \cdot (j \omega \dot{\vec{A}} + \sigma \nabla \dot{V}) \right\} dV = 0 \end{cases}$$

Finally, the Galerkin's weighting margin equations above were convert to matrix form.

$$\begin{bmatrix} \int_{\Omega} \left[ v \nabla \times \vec{N}_1 \cdot \nabla \times () + v \nabla \cdot \vec{N}_1 \nabla \cdot () + j \omega \sigma \cdot \vec{N}_1 \cdot () \right] dV & \int_{\Omega} j \omega \sigma \vec{N}_1 \cdot \nabla () dV \\ \int_{\Omega} j \omega \sigma \nabla \vec{N}_1 \cdot () dV & \int_{\Omega} j \omega \sigma \vec{N}_1 \cdot \nabla () dV \end{bmatrix} \cdot \begin{bmatrix} \dot{\vec{A}} \\ \frac{1}{j \omega} \dot{V} \end{bmatrix} = \begin{bmatrix} \int_{\Omega} \left\{ \vec{N}_1 \cdot \dot{\vec{J}}_s \right\} dV \\ 0 \end{bmatrix}$$

And the matrix equation above describes the 3D eddy current field of the negative sequence.

### 3.2 Basic equations for thermal analysis

The theory base of Thermal Analysis is also 3D Finite Element Methods. According to principles of heat transferring, the temperature distribution is conformed to the following equation:

$$\begin{cases} \frac{\partial}{\partial x} \left( \lambda_x \frac{\partial T}{\partial x} \right) + \frac{\partial}{\partial y} \left( \lambda_y \frac{\partial T}{\partial y} \right) + \frac{\partial}{\partial z} \left( \lambda_z \frac{\partial T}{\partial z} \right) = \rho C \frac{\partial T}{\partial t} - q \\ T|_{\Omega_1} = T_0 \\ \frac{\partial T}{\partial n} |_{\Omega_2} = 0 \\ -k \frac{\partial T}{\partial n} |_{\Omega_3} = \alpha (T - T_f) \end{cases}$$

Where:

- T —— Temperature of the calculated model, unit: °C;
- $\lambda_x$  —— The thermal conductivity of x direction (horizontal), unit: W/m/K;
- $\lambda_y$  —— The heat conductivity of y direction (vertical), unit: W/m/K;
- $\lambda_z$  —— The heat conductivity of y direction (axial), unit: W/m/K;
- $\rho$  —— The density of the calculated model, unit: kg/m<sup>3</sup>;
- C —— The specific heat of the calculated model, unit: J/kg/K;
- $\Omega_1$  —— The heat isolation boundary condition I  
(equal temperature surface boundary condition);
- $\Omega_2$  —— The heat isolation boundary condition II  
(parallel heat flux boundary condition);
- $\Omega_3$  —— The boundary condition of heat convection.

## 4 ADDING EXCITATION SOURCE FOR ELECTRICAL MAGNETIC ANALYSIS

There're two coils in each stator slot, and 48 stator slots in the whole model. It's no need to give excitation current for the top coil and the bottom coil. By synthetizing, the excitation source can be set only once.

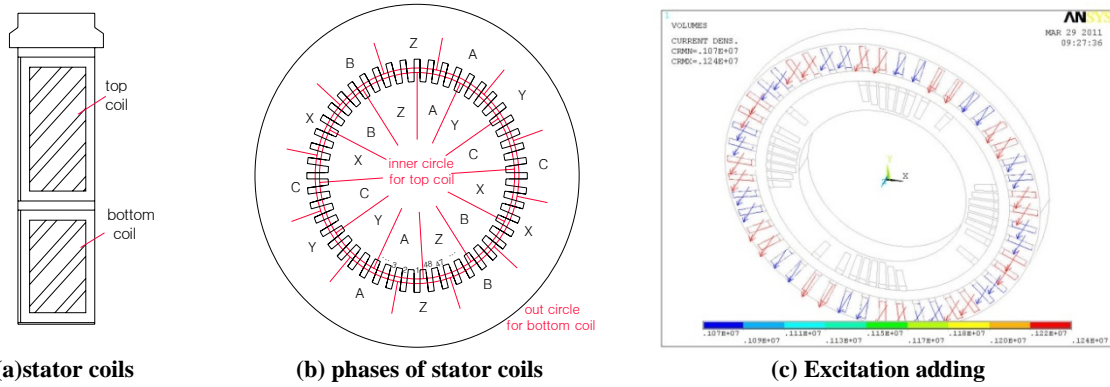


**Fig.3 Stator Slots and its Excitation Source**

The negative currents are calculated as follow:

$$J_2 = \frac{I_2^* \cdot \sqrt{3} \cdot I_N}{A_c}$$

Where:

- $J_2$  — Negative current density, unit: A/mm<sup>2</sup>;
- $I_2^*$  — Negative current, per unit, for example 5%,6% ,etc;
- $I_N$  — Rated stator current of the turbo-generator , unit: A;
- $A_c$  — Copper section area, unit: mm<sup>2</sup>.

The negative sequence currents of each stator slot and its phase angle are as follows:

**Table I Data of negative sequence currents of each stator slot**

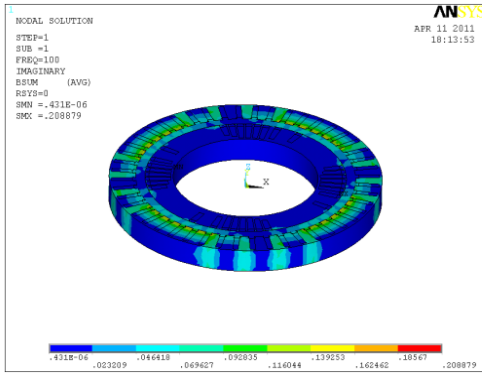
Item	Data of Negative sequence current	
	Stator Slot No.	Negative sequence current
1	1~2;25~26	$J_2 \angle 0^\circ + J_2 \angle 0^\circ = 2J_2 \angle 0^\circ$
2	3~4;27~28	$J_2 \angle 0^\circ + J_2 \angle 240^\circ = \sqrt{3}J_2 \angle 330^\circ$
3	5~6;29~30	$J_2 \angle 300^\circ + J_2 \angle 300^\circ = 2J_2 \angle 300^\circ$
4	7~8;31~32	$J_2 \angle 300^\circ + J_2 \angle 240^\circ = \sqrt{3}J_2 \angle 270^\circ$
5	9~10;33~34	$J_2 \angle 240^\circ + J_2 \angle 240^\circ = 2J_2 \angle 240^\circ$
6	11~12;35~36	$J_2 \angle 240^\circ + J_2 \angle 180^\circ = \sqrt{3}J_2 \angle 210^\circ$
7	13~14;37~38	$J_2 \angle 180^\circ + J_2 \angle 180^\circ = 2J_2 \angle 180^\circ$
8	15~16;39~40	$J_2 \angle 180^\circ + J_2 \angle 120^\circ = \sqrt{3}J_2 \angle 150^\circ$
9	17~18;41~42	$J_2 \angle 120^\circ + J_2 \angle 120^\circ = 2J_2 \angle 120^\circ$
10	19~20;43~44	$J_2 \angle 120^\circ + J_2 \angle 60^\circ = \sqrt{3}J_2 \angle 90^\circ$
11	21~22;45~46	$J_2 \angle 60^\circ + J_2 \angle 60^\circ = 2J_2 \angle 60^\circ$
12	23~24;47~48	$J_2 \angle 60^\circ + J_2 \angle 0^\circ = \sqrt{3}J_2 \angle 30^\circ$

## 5 RESULTS

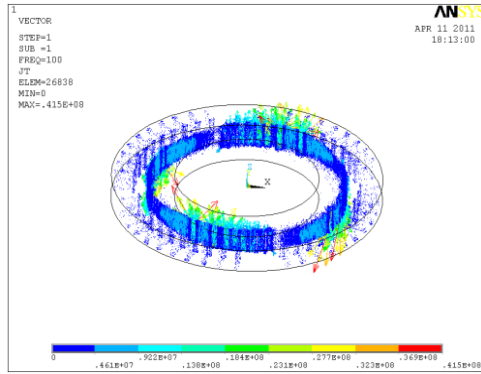
### 5.1 FEA calculation results for electrical-magnetic analysis

#### 5.1.1 Results prepared for the follow-up steady thermal analysis

Using FEA method mentioned in part 3, the negative sequence current field of 6% the rated stator current can be solved out. The solving steps of this FEA matrix equation are automatic.



(a) Magnetic Flux Density Distribution



(b) Eddy Current Distribution

**Fig.4 Current Field Analysis Results(Negative Currents of 6% the Rated Stator Current)**

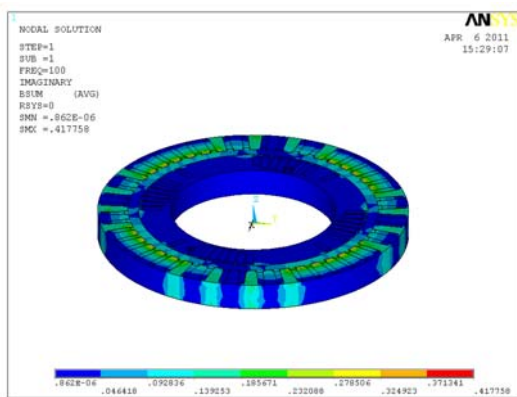
Furthermore, the eddy current losses were obtained. Both the negative currents of 6% the rated stator current and 5% the rated stator current are taken into account. The losses results are as follow:

**Table II Results of Eddy Current Losses**

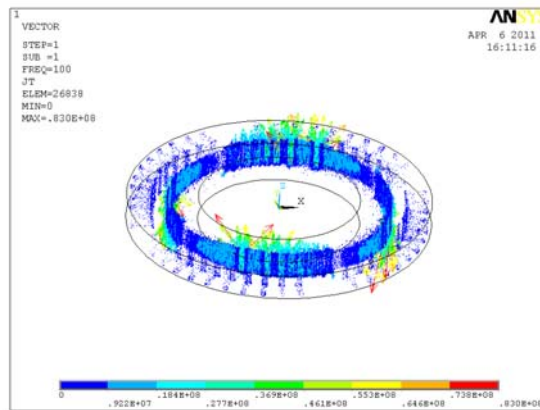
Item	Data of eddy current losses (W)		
	Parts	Negative currents of 5% the rated stator current	Negative currents of 6% the rated stator current
1	Rotor wedge	2390	3442
2	Rotor forging	23593	33974
3	Rotor(in all)	26010	37454
4	Model(in all)	26165	37678

### 5.1.2 Results prepared for the follow-up transient thermal analysis

When the negative sequence current is 12% the rated stator current and its acting time lasts 416 second, transient  $I_2^2t$  can reaches 6 seconds. The negative sequence current field of 12% the rated stator current can be solved out by using ANSYS.



(a) Magnetic Flux Density Distribution



(b) Eddy Current Distribution

**Fig.5 Current Field Analysis Results (Negative Currents of 12% the Rated Stator Current)**

## 5.2 Thermal analysis results

### 5.2.1 Results of steady thermal analysis

After electrical-magnetic calculation results imported directly into thermal analysis, thermal analysis can be done. Under the negative currents of 6% the rated stator current, the temperature distribution of steady state is as follow :

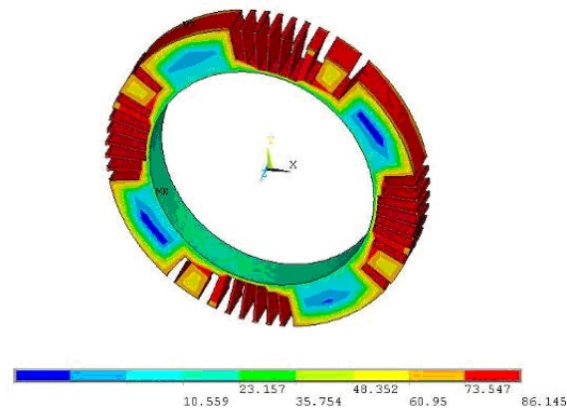


**Fig.6 Temperature Distribution of steady state  $I_2=6\%$ (Negative Currents of 6% the Rated Stator Current)**

Viewing from Fig.6, the steady temperature is lower than the admit value. The admit value is  $130^{\circ}\text{C}$ , according to the standard IEC 60034-3.

### 5.2.2 Results of transient thermal analysis

Temperature distribution of transient state was also solved out. Under the negative currents of 12% the rated stator current, the transient temperature distribution at 416 second is as follow:

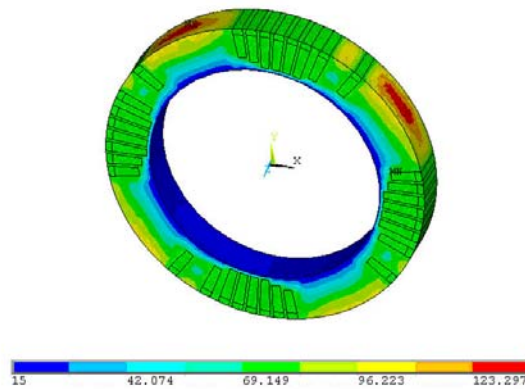


**Fig.7 Temperature Distribution of transient state  $I_2^2 t = 6\text{s}$  (Negative Currents of 12% the rated Stator Current & 416s)**

Viewing from Fig.7, the transient temperature is also lower than the admit value.

## 6 CONCLUSION

In this paper, a 3D model for QFSN type 1100MW 4-pole turbo-generator negative sequence analysis was established. Eddy current distribution and losses of different parts were obtained. Then, these results were imported into latter thermal analysis. By multi-field coupling analysis, the temperature distribution of both transient state and steady state were solved out. The method using in this paper can be easily transplanted to other turbo-generator. This study provides a way to consider the negative sequence ability of large capability turbo-generator.

## BIBLIOGRAPHY

- [1] Dong J. Negative Sequence Analysis for 1000MW-class Turbo-generator (Master's thesis of Zhejiang University, 2006)
- [2] Wang G, Li X. Design, Manufacturing and Operating of Large Capability Turbo-generator. Shanghai : Shanghai Science and Technology Publication House , 2000
- [3] Zhou D, Gong B. Operating Technology and Practice of Turbo-generator. Beijing: Chinese Electrical Power Press, 2004

## **Study and Application of Mitigation and Protection Technology To SSR/SSO**

**Zheng Wei, Chang Fujie, Ji Han, Liu Quan, Jiao Shaohua, Zhang Tao**  
**Beijing Sifang Automation Co.,Ltd.,**  
**China**

### **SUMMARY**

Series compensation transmission technology and high-voltage direct current transmission technology are two major economic power transmission modes to improve transmission capacity and enhance the transient stability of the power system. After 2000, these technologies are applied widely in China, but they cause the sub-synchronous resonance (SSR) and sub-synchronous oscillation (SSO), which become a focus of power grid construction. This paper studies the mitigation and protection measures on SSR / SSO, combines with the SiFang Company's products and engineering practice, introduces the application of technology in China.

The causes and impacts of SSR can be described in three different aspects: Induction Generator Effect (IGE), electrical and mechanical torsional interaction (TI) and transient torque amplification (TA). The core study of SSO is the damage to the shaft by torsional stress. It will directly affect the stability of the power system and the economic interests of large numbers of users.

This paper describes study results and practice on the SSR / SSO mitigation and protection, introduces digital supplementary excitation damping control (SEDC) and torsional stress relay(TSR) which are based on multi-mode control technology. The technology identifies the torsional vibration modals of the shaft online, judges the trend of SSR and SSO. SEDC can improve the damping of the power system by providing control signal which has opposite phase to excitation system. TSR is a special protection equipment to protect the system security. The combination application of these two technologies have been carried out in China as the solution measures of SSR/SSO, they have the characteristics with solving problems through controlling and protection completely, less investment and high efficiency. The scheme has been proved in practice, it effectively mitigate the SSR/SSO to prevent the turbine shaft torsional oscillation from damage. It not only solves the transmission problem from plant of energy base, also shows that the SSR of point to network transmission system problem have found a better solution. It helps the large power plants establish the scheme of point to network ,to address the domestic concern technical issues, establish a viable technological route.

### **KEYWORDS**

Sub-synchronous resonance, Torsional vibration, SEDC, TSR.

## 1 INTRODUCTION

At present, Chinese power industry experiences her rapid progress period, as the construction of extra-high voltage/ultra high voltage power grid, the large capacity Series compensation transmission technology and high-voltage direct current transmission technology are widely adopted in China, while the sub-synchronous oscillation (SSO) are the problem demanding prompt solution.

Since 2000, as the construction of the power grid has brought more and more problems caused by SSR/SSO, the relative research and solution has aroused wide concern in China; We take the early scholar's theoretical research documents [1] as the account case and theoretical principle of SSO. The documents [15] provided detailed research on the SSO occurred in power plants adopted series compensation transmission. The documents [10][11][12] provided practical analysis methods of SSO, such as frequency sweep method, torque parameter method and characteristic root method, these documents also adopt simulation tools to implement time domain analysis test. These theories have considerable directive significances for the SSO mitigation research, but they were limited in theoretical research, so how to resolve the concrete issues through engineering practice became the most urgent problem.

This paper expounds how to mitigate SSO/SSR by the combination technique of digital supplementary excitation damping control and torsional stress relay based on multimode control technology, introduces the engineering and applications of this technology in China.

## 2 THE KEY TECHNOLOGY OF DIGITAL SUPPLEMENTARY EXCITATION DAMPING CONTROL AND TORSIONAL STRESS RELAY

The mitigation and protective method of SSO involves multiple academic categories, including detection technique, digital signal processing, and relay protection, we will introduce the key technology of digital supplementary excitation damping control and torsional stress relay in the following paragraphs, which have been applied in engineering.

### 2.1 Self adapting online identification of unit and grid SSO

It is well-known that the generator unit will receive electrical excitations and mechanical excitation during operation, the excitation signal will generate responses of different characteristics, how to obtain the relative SSR response signal is the key to implement the further analysis, control and protection.

#### 2.1.1 Mains side SSO detection and demodulation method

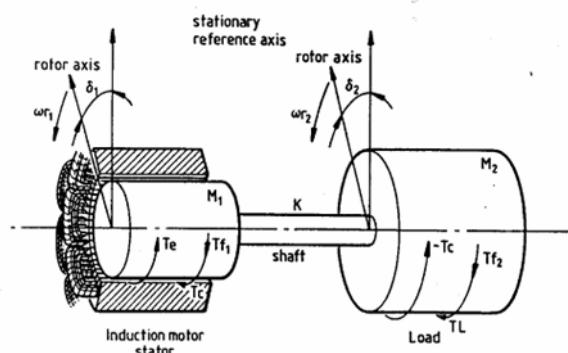


Fig. 1 rotor movement chart

First we should focus on the mathematic model of torsional vibration, as Fig.1 shows, the rotor is equivalent to two mass blocks, when the single frequency simple harmonic torsional vibration occurs on the rotor; we suppose the angular displacement should be:

$$\nu(t) = A \sin(\omega_r t + \theta) \quad (1)$$

In this formula,  $\omega_r$  is the vibration angular frequency, A is the vibration amplitude of the section, and  $\theta$  is the initial phase of the section.

If the rotor works in stable rotate speed, when it was impacted by the periodicity exciting torque, the torsional vibration of the rotor contains simple harmonic components of different frequency and amplitude, and we can suppose that:

$$\phi(t) = \omega_r t + \sum_k A_k \sin(\omega_k t + \theta_k) \quad (2)$$

The rotation speed of the shaft equals to the superimposing of the average rotation speed and torsional vibration rotation speed.

$$\omega = \omega_r + \sum_k A_k \omega_k \cos(\omega_k t + \theta_k) \quad (3)$$

Then the variable quantity of the rotation speed on the steam turbine side should be:

$$\Delta\omega = \sum_k A_k \omega_k \cos(\omega_k t + \theta_k) \quad (4)$$

The major input signal of the SSO mitigation and protection is rotation speed difference signal  $\Delta\omega$ . By analyzing  $\Delta\omega$ , the shaft superimposed response of frequency signal on different mode could be expressed.

The rotation speed sensor mounted on the shaft will real-time measure the shaft rotation speed. The obtained  $\Delta\omega$  should get double sampling to avoid incorrect process and improve the reliability of the signal acquisition to meet the needs of analysis and calculation.

### 2.1.2 Self adapting mode filter technology of generator SSO

The rotation speed signal contains not only the sub-synchronous frequency component signal, but also the signal of power frequency, low frequency and high frequency. Only the sub-synchronous frequency component signal is needed for supplement damping control. For power frequency and high frequency signal, we adopt low pass filter to isolate them, for low frequency signal and DC signal, we adopt high pass filter to isolate them. The combination of low pass filter and high pass filter has composed a band pass filter with a comparatively large bandwidth.

The object of model band pass filter is to decouple SSO in multiple modes and control them. So the following problems should be considered:

#### 1) Decouple level

The filter should filter the different torsional vibration mode separately to implement the decoupling control.

#### 2) The robustness of the filter

If there's minor deviation occurred in centre frequency and parameter, the amplitude frequency and phase frequency of relative mode signal should not be affected greatly. So the slight variation of filter parameter will not affect the SEDC control ability greatly. This is to make allowance for deviation brought by digitalization; the transfer function is as follows:

$$Y(t) = L^{-1} \left\{ \frac{G \cdot \left(\frac{s}{\omega_c}\right) \cdot X(s)}{1 + 2 \cdot \zeta \cdot \left(\frac{s}{\omega_c}\right) + \left(\frac{s}{\omega_c}\right)^2} \right\} \quad (5)$$

The centre frequency of the mode filter can be adjust flexibly, the damping parameter could also be adjusted, the design of bandwidth could adapt the shaft mode frequency change, which could make it have excellent filtration ability in the range of 1.5Hz centre frequency and reach the best result of comb filtration. The amplitude frequency and phase frequency characteristics of the filter are shown in Fig.2

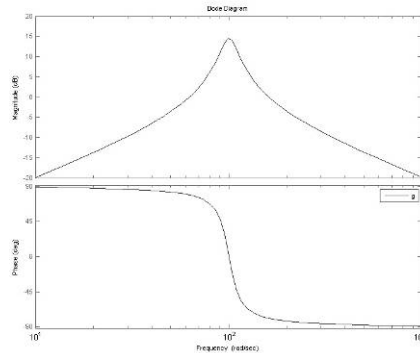


**Fig.2 The amplitude frequency and phase frequency characteristics of the filter**

## 2.2 The coordinated solution of SSO mitigation implemented by supplementary excitation damping control (SEDC) and torsional stress relay (TSR)

The system solution of supplementary excitation damping control (SEDC) and torsional stress relay (TSR) should consider the cooperative relationship between the adjustment control and protection action. Fig.3 is typical system diagram of point-to-grid large capacity and long distance, the configuration method are shown in the figure. The coordinated solution is the first defend line of SSO, SEDC's main function is to continuous inspect and analyze the rotation speed of the shaft system, when SSO occurred in units, SEDC will inhibit it by control and regulation method that complemented on the excitation system. TSR is the last defend line of mitigating SSO, its main function are as follows: it will judge the divergence of torsion vibration according to the characteristics of the steam turbine's rotation speed, it will also provides the judgments of the fatigue loss according to the generator's electric value, if the judgment value reaches the set value, or the sub-synchronous torsional vibration with characteristic frequency is excited, and the progressive divergence will threaten the security of units operation, it will make protective trip, alarm and adopt a series of protection.

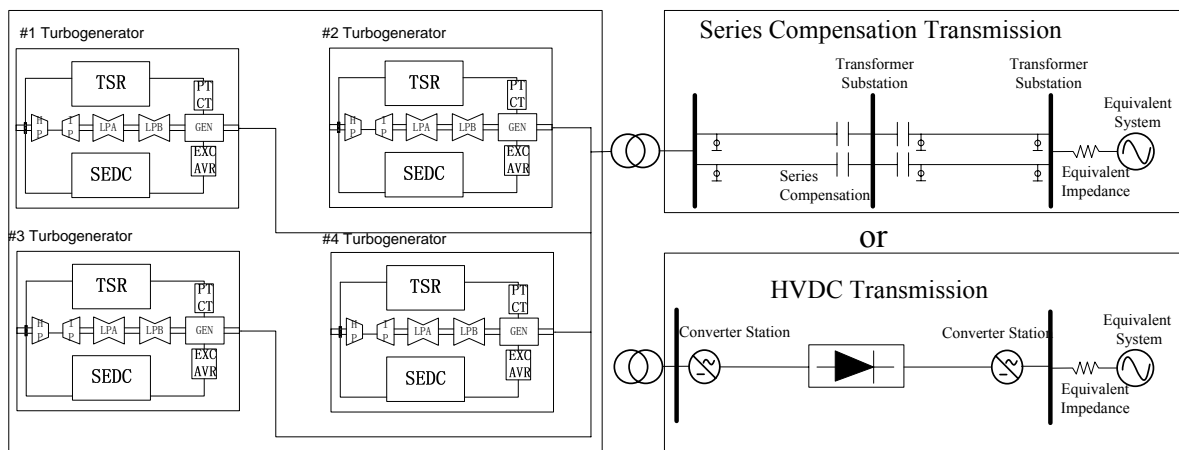


**Fig 3 typical system diagram of point-to-grid large capacity and long distance**

According to the detailed situations of SSO that might occurred, the following points of SEDC+TSR coordinated solution should be concerned:

1) When there are miniature perturbations, the transient torsion moment of initial shaft dangerous section is minor, and the initial torsional vibration mode is not diverged rapidly, SEDC should be the main regulation function, SEDC will provide positive damp to inhibit SSO to slow down the process of divergence or make the torsional vibration of constant amplitude convergent as soon as possible.

The TSR will be the protection device of the shaft system, and it will trip the unit when the shaft system is damaged.

2) For bigger perturbations, the amplification effect of SSO transient torsion moment will exist, the initial transient torsion moment of shaft dangerous section will be very big, and the mode will be diverged rapidly. Because of the limitation of unit excitation, SEDC will mitigate the SSO when perturbation starts, and TSR will monitor the fatigue damage of the dangerous section, if the fatigue damage set value is reached, TSR will trip. For the same type units in a power plant, a single perturbation will cause sub-synchronous torsional vibration of multiple units, and after 1 unit has been tripped by TSR, the torsional vibration of other units will be weakened by SEDC, SEDC and TSR will interact and cooperate.

There are some other methods to mitigate SSO: on the power grid side, for series compensation transmission, the controllable series compensation could be mounted, for high-voltage direct current transmission, the SSDC could be mounted. On the mains side, there are some other available methods, such as block filters, SVC, but the investment will be high. SEDC+TSR could be the default solution of SSO, based on this solution, other additional mitigation method can be considered according to the particularity of the specified engineering.

### 3. THE PRINCIPLE OF SEDC AND TSR

#### 3.1 The principle of SEDC

Supplementary excitation damping control is to separate the independent torsional vibration mode from generator unit rotation speed signal, make closed loop gain and adjust the phase shift according to each torsional vibration mode. SEDC will modulate magnetic torque moment to inhibit the torsional vibration according to the output signal of each mode control. The output signal will form as Fig. 4 shows, and it will act on the generator excitation controller to inhibit the shaft torsional vibration[17].

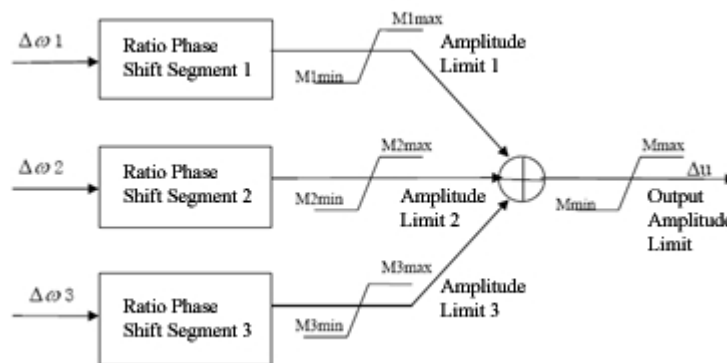


Fig.4 the principle diagram of master control module control

The whole system adopts PID control; the structure of control system is shown in Fig.5

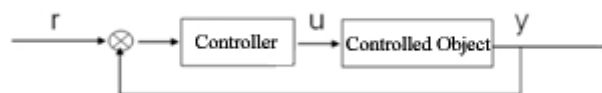


Fig. 5 basic structure of control system

The parameter adjustment of the controller should consider the following principle:

- (1) The control parameter should consider the control effect of different perturbation, and evaluate the typical system operation mode, the control parameter should guarantee the rapid convergence when minor perturbation occurs, and keep the convergence stability of the system when large perturbation occurs.
- (2) The control parameter should be adjustable, so the parameter could be adjust according to different control object characteristics.

### 3.2 The principle of TSR

#### (1) Mode divergence judgment

Based on conjugated observation window and torsional mode stable robust identification technology, the mode time sequence will be obtained by real-time measuring the generator shaft rotation speed difference, and the torsional vibration mode divergence will be distinguished by the statistics of mode diversification trend in a period of time. The mode data (as Fig.6 shows) could be real-time generated according to the self adapting online identification technology, the mode stability will be identified according to the data generated amplitude change curve (as Fig.7 shows).

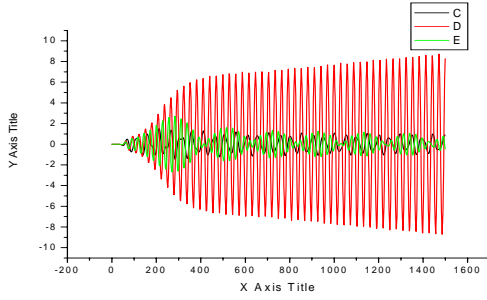


Fig.6 Mode analysis diagram

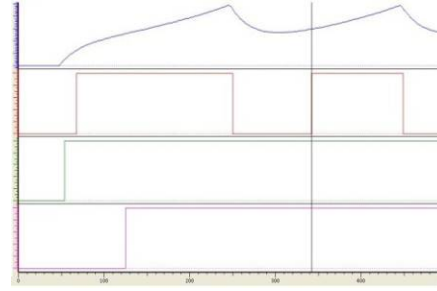


Fig.7 Identification process diagram

#### (2) Fatigue inverse time lag judgment

The generator shaft mass model is required for researching the shaft torsional vibration. The mass model is shown in Fig.8. The calculation of fatigue adopts the online fatigue inspection method based on real-time rain flow method, to real-time measure the generator shaft system mechanical fatigue. According to the mode frequency [13] of steam turbine generator units, vibration mode curve and equivalent rigidity, the torque moment  $T_{ij}$  ( $i=1, 2, 3; j=1, 2, 3$ ) generated by each mode unit strength single stress (the stress cycles in each calculated section) will be calculated. After the torque moment – time course curve of this perturbation is obtained, the rain flow method is adopted to locate the stress cycle, and the equivalent stress amplitude of each cycle will be obtained; according to the peak values which forms the circle and the appropriate average stress convert parameter, the equivalent stress amplitude will be obtained. After calculated all the stress cycle of linear accumulation by the S-N torsion curve, the generated fatigue loss will be obtained.



Fig.8 continuous mass model of the shaft system

The computation formulas are as follows:

$$\text{Vibration equation: } \mathbf{M}\{\ddot{x}\} + \mathbf{C}\{\dot{x}\} + \mathbf{K}\{x\} = \{\mathbf{Q}(t)\} \quad (6)$$

$$\text{Composed Vibration matrix } \mathbf{A} = \begin{bmatrix} 0 & \mathbf{M} \\ \mathbf{M} & \mathbf{C} \end{bmatrix}, \quad \mathbf{B} = \begin{bmatrix} -\mathbf{M} & 0 \\ 0 & \mathbf{K} \end{bmatrix}, \quad \mathbf{E}(t) = \begin{bmatrix} 0 \\ \mathbf{Q}(t) \end{bmatrix}, \quad y = \begin{bmatrix} \dot{x} \\ x \end{bmatrix} \quad (7)$$

The differential equation of system vibration could be expressed by 8 first order simultaneous equation:

$$\mathbf{A}\{\dot{y}\} + \mathbf{B}\{y\} = \{\mathbf{E}(t)\} \quad (8)$$

$$\text{After the linear transform of modal coordinate } \{y\} = \mathbf{U}\{z\} \quad (9)$$

$$\text{We will get } \mathbf{P}\{\dot{z}\} + \mathbf{Q}\{z\} = \{\mathbf{F}(t)\} \quad (10)$$

This equation is in complete decoupling form.

After calculate the torsional vibration response of the modal, we can get the torsional vibration displacement and velocity of each mass block at all times in modal coordinate, then we can transform them to the actual coordinate  $y$ , the linear transform are as follows:  $\{z\} = \mathbf{U}^{-1}\{y\}$ , then the actual torsional vibration displacement and velocity of each mass block, so we can calculate the fatigue loss by the obtainable torque moment.

#### 4 ENGINEERING APPLICATION

At present, Sifang Company's SEDC+TSR SSO mitigation solution has been applied on 6 600MW steam turbine generator units in China, TSR has been individually applied in 34 large steam turbine generator units various of various types.

##### 4.1 The application of TSR

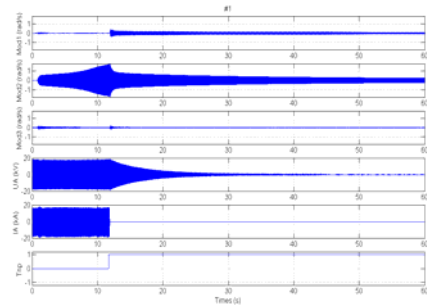


Fig.9 TSR oscilloscope diagram of unit 1

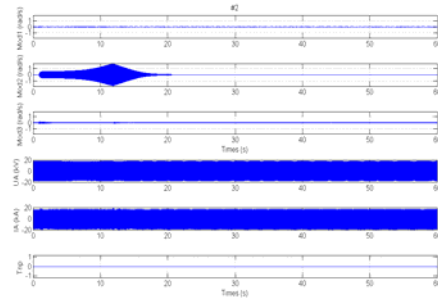


Fig.10 TSR oscilloscope diagram of unit 2

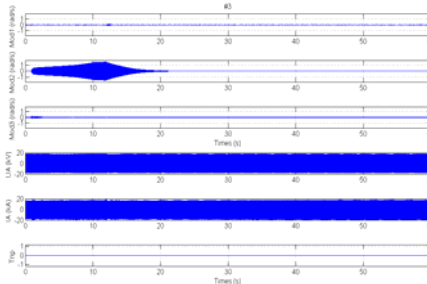


Fig.11 TSR oscilloscope diagram of unit 3

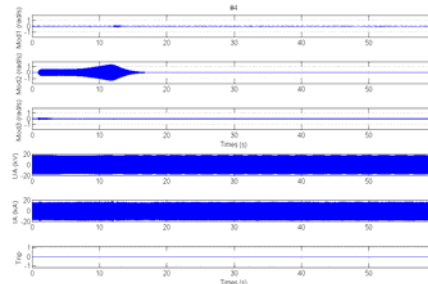
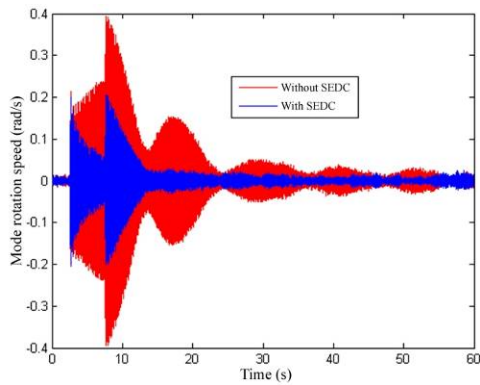


Fig.12 TSR oscilloscope diagram of unit 4

Fig.9 - Fig.12 are the oscilloscope diagram of TSR, that TSR was applied the in unit 1 – 4 of a power plant which occurs SSO, the horizontal axis expresses time, the vertical axis expresses amplitude. The curves from top to bottom are: mode 1, mode 2, mode 3,  $U_a$  (stator voltage),  $I_a$  (stator current), protective act signal. We can see that the mode 2 of SSO caused by this accident is diverged, and the transient torque moment is comparatively large, it is an accident of large perturbation. Fig.9 also shows that after 11 seconds that mode 2 occurred, the TSR divergence protection judgment of unit 1 acted, and then the unit 1 stepped out. Fig.10 is the oscilloscope diagram of unit 2, mode 2 began to diverge when the accident occurred, but it was weakened by the SEDC after unit 1 tripped, different with the curve which is weakened slowly by the mechanical damp after unit stepped out, because of action judgment was not satisfied during the whole perturbation process, the TSR of unit 2 did not tripped. Fig.11 and Fig.12 are the oscilloscope diagram of unit 3 and unit 4, same as unit 2, the curve was weakened by SEDC soon after unit 1 tripped, and the TSRs of them were not tripped.

##### 4.2 Application of SEDC

SEDC and TSR has been both applied in the 4 synchronized units (units of the 1st stage and the 2nd stage) of this power plant. In Oct.10, 2008, the experiment of SEDC inhibition was completed, in this experiment, 3 units was operating, and the oscilloscope data of the SEDC are as follows:



**Fig.13 SEDC inhibition oscilloscope diagram**

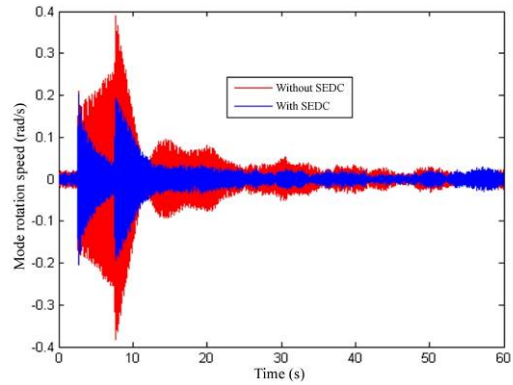


**Fig.14 SEDC inhibition oscilloscope diagram**

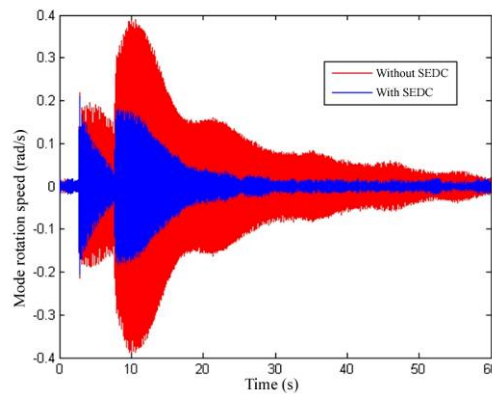


**Fig.15 SEDC inhibition oscilloscope diagram**

Fig.13~Fig.15 shows the mode 2 diagram of unit 1, unit 2 and unit 4 SEDC oscilloscopes, the horizontal axis expresses time, the vertical axis expresses amplitude. Because of the series compensation transmission mode this power plant adopted, when the primary circuit trips, SSO will diverge, the experiment will show the contrast of SSO trend in with and without SEDC situation. The initial part expresses that the circuit was broken, and then circuit was reclose after 5 seconds. The red curve shows the oscilloscope without SEDC, the blue one shows the oscilloscope with SEDC. We can see that SEDC inhibit the SSO divergence obviously from the contrast of oscilloscope diagrams.

## 5. CONCLUSION

This paper introduces the SEDC+TSR system solution, it also introduces the system application of large thermal power plant adopted this technology in China. We consider that as the developing the construction of China power grid, SSO will attach enough attention and more method will be applied to mitigate SSO. SEDC+TSR is the most basic and effective method which should be applied in most of the thermal power plant and nuclear power plant. At the same time, to prevent SSO, the establishment of global torsional vibration monitors systems is very necessary; the torsional vibration monitors systems should be widely applied. The advantage of SEDC+TSR scheme is that it can resolve the problem completely by control and protection thought, its investment is lower, its benefit is higher. The practice shows that this scheme could mitigate SSR/SSO effectively, and prevent steam turbine generator shaft damage from torsional vibration.

## BIBLIOGRAPHY

- [1] IEEE Sub-synchronous Resonance Working Group. First benchmark model for computer simulation of Sub-synchronous resonance. IEEE T-PAS,1977,96(5)
- [2] IEEE Sub-synchronous Resonance Working Group. Countermeasures to sub-synchronous resonance problems. IEEE Trans on Power Apparatus and Systems,1980,99(5):1810-1818
- [3] IEEE Sub-synchronous Resonance Working Group. Terms,Definitions and Smbols for Sub-synchronous Oscillations [J] . IEEE Trans,1985,104 (6) :1326 - 1334

- [4] LI Q, ZHAO D, YU Y. A new pole-placement method for excitation control design to damp SSR of a nonidentical two machine system. IEEE Trans on Power System s,1989,4(3):1176-1181
- [5] Sub-synchronous Resonance Working Group of the System Dynamic Performance Subcommittee. Reader's guide to sub-synchronous resonance. IEEE committee report. IEEE Trans on Power Systems,1992,7(1):150-157
- [6] IEEE Sub-synchronous Resonance Task Force.Second benchmark model for computer simulation of sub-synchronous resonance.IEEE Trans on Power Apparatus and Systems,1995,104(5):1057-1066
- [7] Hong J H, Park J K.A time-domain approach to transmission network equivalents via Prony analysis for electromagnetic transients analysis[J].IEEE Trans on Power Systems,1995,10(4)
- [8] Houry M P, Bourles H.Rotation speed measurement for turbine generator: torsion filtering by using kalman filter[J].IEEE Trans on PD,1996,11(1):110-115
- [9] Chen C, Yang Y. DISCUSSION OF SEVERAL ANALYTICAL APPROACHES AND TOOLS ABOUT SUBSYNCHRONOUS RESONANCE (SSR). Power System Technology,1998,22(8)
- [10] Xu Z, Luo H, Zhu R. REVIEW ON METHODS OF ANALYSIS FOR SUBSYNCHRONOUS OSCILLATIONS OF POWER SYSTEMS. Power System Technology,1999,23(6):36-39
- [11] Yang Y,Chen C.SSR in Yimin—Daqing 500 kV transmission system[J].Power System Technology,2000,24(5):11-12
- [12] EPRI. Steam turbine-generator torsional vibration interaction with the electrical network: tutorial.California: EPRI of US,2006:1~200
- [13] GUO X. SSR analysis and prevent measures comparison on series compensation transmission line system. Inner Mongolia Electric Power,2006,24(3):1-4
- [14] YANG Y,HU R,HONG C, Ren C. The Subsynchronous Oscillation Problem and the Damping Control Strategy at the Monopolar Operation Stage of Xingan HVDC Transmission Project. SOUTHERN POWER SYSTEM TECHNOLOGY,2007,1(2):25-30
- [15] XIE X,LIU S,ZHANG S,GUO X,LI Y. Basic Principles and Key Issues of Depressing Multi-mode SSR by Supplementary Excitation Damping Control. AUTOMATION OF ELECTRIC POWER SYSTEMS,2007,21
- [16] LIU S,XIE X, WANG Z. SSR Problem in Compensated Transmission System of Thermal Power Bases in China. POWER SYSTEM TECHNOLOGY,2008, 32(1): 5-8
- [17] Zhang D, Xie X, Liu S, Zhang S. An Intelligently Optimized SEDC for Multimodal SSR Mitigation. Electric Power Systems Research,2009, 79(7): 1018-1024; 2008, 32(1): 5-8
- [18] Wu T, Su W, Wang Bi, Wang Z, Yao Q, Gao X. Simulation and test on supplementary excitation damping control. ELECTRIC POWER,2009,42(11)
- [19] Liang X, Zheng W, Chang F, Liu Q.CSC-812P Series Steam Turbine Generator Shaft System Torsional Stress Relay Specification. V2.0, 2010
- [20] Chang F, Zheng W, Liu Q. CSC-811P Steam Turbine Generator Supplementary Excitation Damping Controller Specification. V1.0, 2008



SC A1  
COLLOQUIUM ON NEW DEVELOPMENT OF ROTATING  
ELECTRICAL MACHINES

*Beijing, China*

*11~13 September, 2011*

---

**Test Analysis of 600MW Generator Stator Bar Temperature Measure**

**Xing Xuhui, Wang Yunshan, Zhuge Wenbing, Li Zhi**  
**Beijing BEIZHONG Steam Turbine Generator Co., Ltd**  
**China**

**SUMMARY**

The material of hollow conductors in the 600MW stator bar has been studied in many years, but it is rarely to do the stainless steel conductor test and the available data is also not clear. It is significative to do the stator bars temperature measure test. The test can tell us the temperature distribution of the copper conductors on the influence of the large current when we respectively use stainless steel conductors and copper conductors. The test can help us to get the temperature change in the 600MW steam generator stator bars when the generator is running. The test can help us to know the grads and the effect on heat exchange using stainless steel conductors or copper conductors. The paper introduces the main parts of test, such as the design and manufacture of the large current generator, the design and manufacture of the cooling water system, the choice and distribution of temperature measure, the data collection system design, etc. The paper also discusses the experimental method and the difficulty with the existing test equipment under the limited condition, and shows the test methods formulation and implementation. Finally, it is obtained that the different temperature distribution gradient and temperature curve with copper hollow conductors and stainless steel hollow conductors by the test and calculation.

**KEYWORDS**

Stator bar, Large current generator, Compensation capacitor, Hollow conductor.

# 1 TEST METHODS ANALYSIS

## 1.1 The preparation of the bars tested

The bar is composed of the copper solid conductors and the hollow conductors made of copper or stainless steel material, the total length is 7.874 /7. 873m.

Copper resistance rate(when it is 20°C): 0.01724 Ω mm<sup>2</sup>/ m

The thickness of the insulating layer: 0.125mm

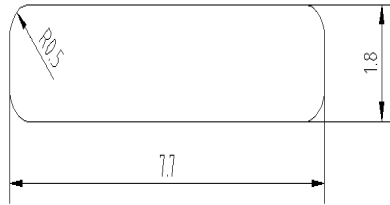


Fig.1 The section of the copper solid conductors

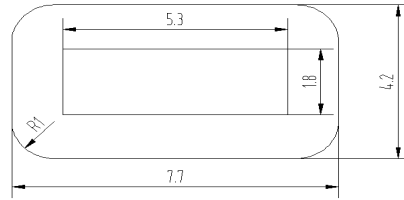


Fig.2 The section of the copper hollow conductors

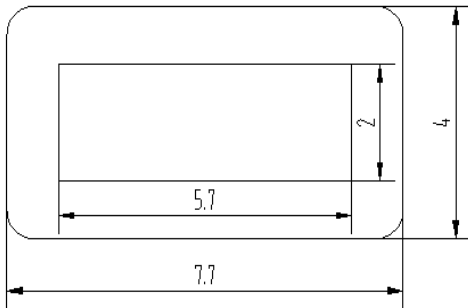


Fig.3 The section of the stainless steel hollow conductors

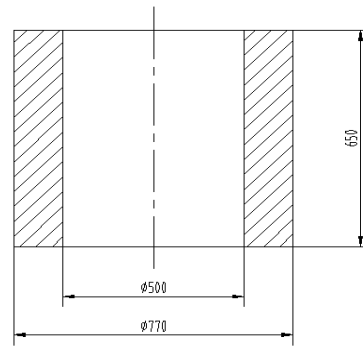


Fig.4 The section of the silicon steel strip roll

## 1.2 Reference calculation

a) The stainless steel hollow conductor

The total numbers of the solid conductors in each bar: N=72

the conductor length: 7.873m

The area of the solid conductor section:

$$S = 1.8 \times 7.7 - 4 \times 0.5 \times 0.5 \times (1 - \pi/4) = 13.645 \text{ (mm}^2\text{)}$$

The proportion of the hollow and the solid: 1 and 6

Rows number: 4

The groups number of each row: 3

The total electric area:

$$S_n = S \cdot N = 13.645 \times 72 = 982.44 \text{ (mm}^2\text{)}$$

The resistance of the bar (when it is 20°C):

$$R_{20} = \rho L / S_n = 0.01724 \times 7.873 / 982.44 = 0.138 \text{ (m} \Omega \text{)}$$

The temperature of the bar during test: more than 40°C

The resistance of the bar during test:

$$R_{40} = R_{20} (235 + 40) / (235 + 20) = 0.138 \times 275 / 255 = 0.149 \text{ (m} \Omega \text{)}$$

The current through the stator bar: I=9339A

The flux of the water cooling: 0.231L/s

The copper loss of the bar:

$$P = I^2 R_{40} = 9339 \times 9339 \times 0.149 \times 10^{-3} = 12994.7 \text{ (W)}$$

The raise of the water temperature:

$$\Delta t = P / C_v = 12994.7 / 4.18 / 0.231 / 1000 = 13.4 \text{ (K)}$$

Copper thermal coefficient: 385W/(m.K )  
 Copper specific heat at constant pressure: 0.39 kJ/(kgK)  
 Stainless steel thermal coefficient: 16.3 W/(m.K )  
 Stainless steel specific heat: 0.5 kJ/(kgK)  
 The insulating layer thermal coefficient: 0.22 W/(m.K )  
 Water thermal coefficient: 0.6 W/(m.K )  
 Water specific heat at constant pressure: 4.18 kJ/(kgK)  
 Water density: 1g/cm<sup>3</sup>

Length after conversion: 7.863m  
 Thickness of the stainless steel hollow conductor wall: 1mm

Loss of the unit copper conductor:  
 $P_0 = P/N/L = 12995/72/7.873/1000 = 0.0229W$

Unit length loss of three copper conductors:  
 $P_3 = 3 P_0 = 0.0229 \times 3 = 0.0687W$

The temperature rise on the 1mm thickness wall of the hollow conductor:  
 $\Delta t_0 = P_3 \delta / (\lambda S) = 0.0687 \times 1/1000/16.3/5.7 \times 1000000 = 0.74K$

The temperature rise on the first single insulating layer from the hollow conductor:  
 $\Delta t_1 = P_3 \delta / (\lambda S) = 0.0687 \times 0.125/1000/0.22/7.7 \times 1000000 = 5.08K$

Unit length loss of two copper conductors:  
 $P_2 = 2 P_0 = 0.0229 \times 2 = 0.0458W$

The temperature rise on the first double insulating layers from the hollow conductor:  
 $\Delta t_2 = P_2 \delta / (\lambda S) = 0.0458 \times 0.25/1000/0.22/7.7 \times 1000000 = 6.77K$

The temperature rise on the second double insulating layers from the hollow conductor:  
 $\Delta t_3 = P_0 \delta / (\lambda S) = 0.0229 \times 0.25/1000/0.22/7.7 \times 1000000 = 3.38K$

The temperature rise on the first solid conductor from the hollow conductor:  
 $\Delta t_4 = P_0 \delta / (\lambda S) = 0.0229 \times 2.5 \times 1.8/1000/385/7.7 \times 1000000 = 0.035K$

The temperature rise on the second solid conductor from the hollow conductor:  
 $\Delta t_5 = P_0 \delta / (\lambda S) = 0.0229 \times 1.5 \times 1.8/1000/385/7.7 \times 1000000 = 0.021K$

The temperature rise on the third solid conductor from the hollow conductor:  
 $\Delta t_6 = P_0 \delta / (\lambda S) = 0.0229 \times 0.5 \times 1.8/1000/385/7.7 \times 1000000 = 0.007K$

b) Copper hollow conductor

The total numbers of the solid conductors in each bar: N=48

The conductor length: 7.874m

The section area of the hollow conductor:

$$S_2 = 4.2 \times 7.7 - 1.8 \times 5.3 - 4 \times 1 \times 1 \times (1 - \pi/4) = 21.94 \text{ mm}^2$$

The section area of the solid conductor:

$$S_1 = 1.8 \times 7.7 - 4 \times 0.5 \times 0.5 \times (1 - \pi/4) = 13.645 \text{ mm}^2$$

The proportion of the hollow and the solid: 1 and 2

Rows number: 4

The groups number of each row: 6

The total electric area:

$$S_n = 24 (2 \times S_1 + S_2) = (13.645 \times 2 + 21.94) \times 24 = 1181.52 \text{ mm}^2$$

The resistance of the bar (when it is 20°C):

$$R_{20} = \rho L / S_n = 0.01724 \times 7.874 / 1181.52 = 0.115 \text{ m} \Omega$$

The temperature of the bar during test: more than 40°C

The resistance of the bar during test:

$$R_{40} = R_{20} (235 + 40) / (235 + 20) = 0.115 \times 275 / 255 = 0.124 \text{ m} \Omega$$

The current through the stator bar: I=9339A

The flux of the water cooling: 0.231L/s

The copper loss of the bar:

$$P=I^2 R_{40}=9339 \times 9339 \times 0.124=10806.5W$$

The raise of the water temperature:

$$\Delta t=P/Cv=10806.5/4.18/0.231/1000=11.2K$$

The insulating layer thermal coefficient: 0.22 W/(m.K)

Length after conversion: 7.863m

Thickness of the copper hollow conductor wall: 1.1mm

Loss of the unit solid copper conductor:

$$\begin{aligned} P_0 &= PS_1/(2S_1+S_2)/L/24 \\ &= 10806.5 \times 13.645/(2 \times 13.645+21.94)/24/7.873/1000 \\ &= 0.0158W \end{aligned}$$

Loss of the unit solid copper conductor and hollow conductor:

$$P_3=P/L/24/2=10806.5/7.873/1000/24/2=0.029W$$

The temperature rise on the 1.1mm thickness wall of the stainless steel hollow conductor:

$$\Delta t_0= P_3\delta/(\lambda S)= 0.029 \times 1.1/1000/385/5.7 \times 1000000=0.014K$$

The temperature rise on the single insulating layer from the hollow conductor:

$$\Delta t_1= P_0\delta/(\lambda S)=0.0158 \times 0.125/1000/0.22/7.7 \times 1000000=1.17K$$

The temperature rise on the first solid conductor from the hollow conductor:

$$\Delta t_4= P_0\delta/(\lambda S)=0.0158 \times 2.5 \times 1.8/1000/385/7.7 \times 1000000=0.024K$$

### 1.3 The preparation of the large current generator

We should utilize a large transformer in order to get current generator. The transformer secondary side will be connected directly with the stator bar. For the stator bar is a very low impedance load, when the transformer primary side is connected with the voltage source, the secondary side will be in short and get a large current with low voltage. The difficulty of design is how to utilize limited equipment to achieve the requirement of the test with low cost.

Firstly, we use an O type transformer to get a high efficiency. This kind of transformer has many advantages such as low impedance, high efficiency and low loss. The silicon steel strip roll with low loss is a good core to the test transformer.

The rate capacity provided by this iron core:

$$P= K_0(K_1S)^2$$

For the large capacity transformer,  $K_0$  is 1.  $K_1$  is compaction coefficient and can be 0.7.

$$\text{so: } S=(770-500)/2 \times 675 \times 10^{-2}=910 \text{ (cm}^2\text{)}$$

$$P= K_0(K_1S)^2=1 \times (0.7 \times 910)^2 \approx 400 \text{ (kVA)}$$

For the test current is less than 10000A and the test voltage is about 10V,

The capacity needed by test:  $Q=IU \approx 100kVA$

So the silicon steel strip roll meets the capacity needs and can be the transformer's core with abundant redundance.

We enwind the copper cables to get the transformer winding. Considering the conveniently enwinding and the electric section area, the cable with  $95mm^2$  section area is better. The current through the transformer primary winding is about 500A, so the two copper cables should be enwind in parallel. The current through the transformer secondary winding is about 10000A, so the copper cables should be enwind in parallel too. Considering that they are different in length, tightness, and position, the currents through each cable of the secondary are inequality. The number of the cables in parallel is 20 because the current redundancy should be 50% and electric current density is less than  $5A/mm^2$ . We can get a three-phase varied transformer to be the voltage source of the transformer primary side. Its basic parameters are as follows:

Output capacity: 250kVA	Phases number: 3
Frequency: 50Hz	Input voltage: 380V
Output voltage: 0—650V	The maximum output current: 222A

For the varied transformer is voltage source of the O type transformer primary side, the max input voltage of the O type transformer should be less than 650V, and the max input current should be less than 222A.

In order to get the large current from the secondary side of the transformer, we should choose a right ratio of the turns. Too many turns can lead the inductance rise, while too few turns will lead that the secondary output current cannot meet the requirement of test. On the other hand, the input power of the transformer primary side lies on the output of the varied transformer. When the output voltage and current of the varied transformer reach the rate point, the transformer input power will be maximum, and the varied transformer will be utilized fully.

We do the test of the several ratios and find that the ratio of 20/1 can get the largest current.

**Table I The result of transformer current measure without compensation**

O type transformer			
Primary turns	18	20	22
Secondary turns	1	1	1
Input current	200A	200A	180A
Secondary current	3000A	3400A	2800A

According to the test data, we can see that the current generator impedance is very big, the secondary output power largely lost in the inductance, and the active power is small. The transformer, the bar, and the connection copper cable are the big inductive load. In order to improve the output current, we should increase capacitive load which needs to connect compensatory capacitance to the circuit. Consequently it can be achieved that the purpose on providing the large current. There are several existing capacitors. The parameters are as follows:

- capacitor: 600 μ F ( 2 sets ) , 1200 μ F (2sets) , 500 μ F ( 1set)
- capacitor voltage: 380V
- connection: Δ

If we connect all the capacitor in parallel and make a phase of each capacitor in short, the capacitance will be the twice of the single phase capacitance. For example each branch of the 1200 μ F capacitor has 400 μ F because of Δ connection. After we make a branch of each capacitor in short, the others will be use in parallel.

The total capacitors:

$$C=2 \times ( 600+600+1200+1200+500 ) /3=2733 ( \mu F )$$

The current of the compensation

$$Z= ( \omega C )^{-1}$$

$$\omega =2 \pi f$$

$$I=U_1 \times Z^{-1}= U_1 2 \pi f C=380 \times 314 \times 2733 \times 10^{-6}=326 A$$

**Table II The result of transformer current measure with compensation**

O type transformer			
Primary turns	16	18	20
Secondary turns	1	1	1
Varied transformer input current	200A	200A	160A
Compensation current	230A	300A	300A
Secondary current	7500A	10000A	7500A

The calculation shows that the transformer primary current can be increased when connecting the compensation capacitors. For the rated voltage of capacitors is 380V, the output voltage of varied transformer should be less than 380V. In order to realize the purpose on the output current reaching 9339A, we should consider both the varied transformer input power and compensation capacitor input current so as to make the input power of the transformer achieve maximum. In addition, it is important to reduce the loop impedance. The inductance led by the copper cables has great influence on the

current output. We put the cable tightly around the bar, reducing surround area formed by the bar and connecting cables. So the load impedance will be decreased, which forms the foundation for output of large current. We change the ratios and check the test data to get the max current. The ratio of 18/1 is better than the others.

**1.4 Current measurement**

- a) A current transformer (the rate current is 15kA/5A) can be used to measure the secondary current. Two shunts (rate values are 600A and 5V) are used to measure the primary current.
- b) Because the copper cables current uneven, the temperatures of these copper cables are different. We use the clamp ampere to measure the higher temperature in them, preventing some cables overheating.

**1.5 Cooling water system**

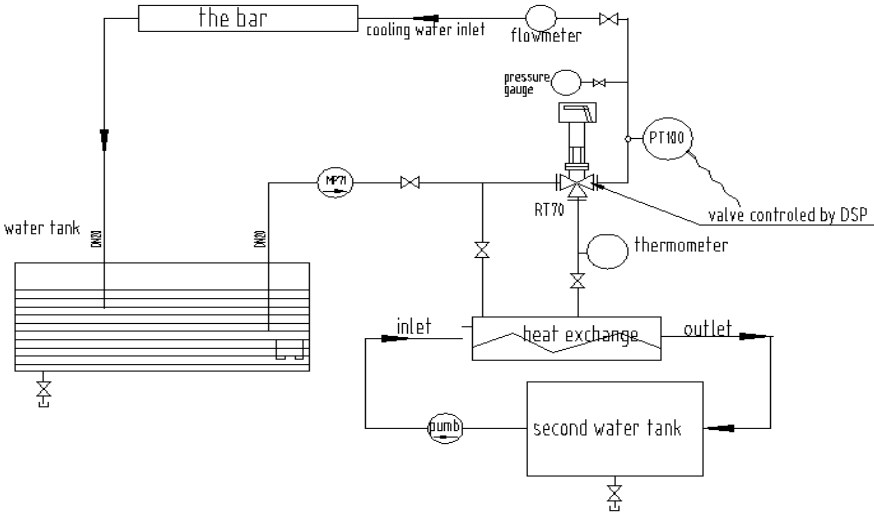


**Fig.5 Cooling water principle diagram**

The cooling water of the bar in the system is provided by the cooling water tank. After cooled by water cooler, the cooling water is mixed with itself in the temperature control valves and forms constant temperature water. The water runs through the bar and returns to the water tank. The flux of the cooling water is 0.231L/s. DSP controller which is mainly PI adjustment adjusts the amount of valve opening and travel position to control the water mixture ratio according to the feedback from thermal resistance at the entry of water. Cooling water system is a high delay feedback loop, so integral time constant should not be too small. To get stability of the system, proportional coefficients should not be too big. After several tests, it will get the better result that proportional coefficients is 12~15 and integral time constant is 20~25.

**1.6 The temperature measuring points layout**

The T-type copper-constantan thermocouples can be used to measure temperature. The thermocouples are stucked on the surface of conductors covered with epoxy resin and asbestos felt, preventing heat dissipation.

Temperature position:

- At the water inlet of the bar: 1point in the water
- At the water outlet of the bar: 1point in the water
- At the 1740mm apart from water inlet: a group of measurement points (one point at each conductor)
- At the 6110mm apart from water inlet: a group of measurement points (one point at each conductor)
- At the water outlet of the bar: a group of measurement points (one point at each conductor)

**Table III The temperature arrangement of the bar with the hollow conductors**

Position	The points at the 1740mm apart from water inlet		The points at the 6110mm apart from water inlet		The points at the water outlet of the bar	
	stainless steel	copper	stainless steel	copper	stainless steel	copper
Measurement points mark(up to down)	21	18	42	36	63	54
	20	17	41	35	62	53
	.....	.....	.....	.....	.....	.....
	2	2	23	20	44	38
	1	1	22	19	43	37

**1.7 Test data collection system**

At first, all the millivolt data measured by the thermocouple are sent into the temperature test device in that the millivolt data can be changed to the temperature data. Then the temperature data will be sent to computer through the RS232 interface. By the labview software program, these data can be gathered, disposed, and recorded. Finally, we can get the data result of time-temperature table and curve.

**2 TEST RESULTS**

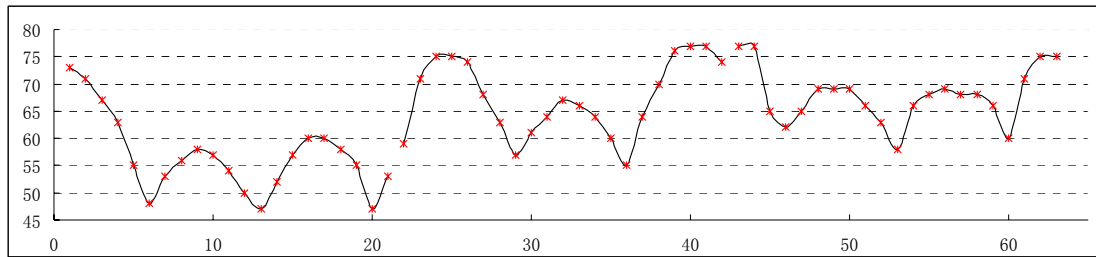


**Fig.6 The time-temperature curve when using the stainless steel hollow conductors**

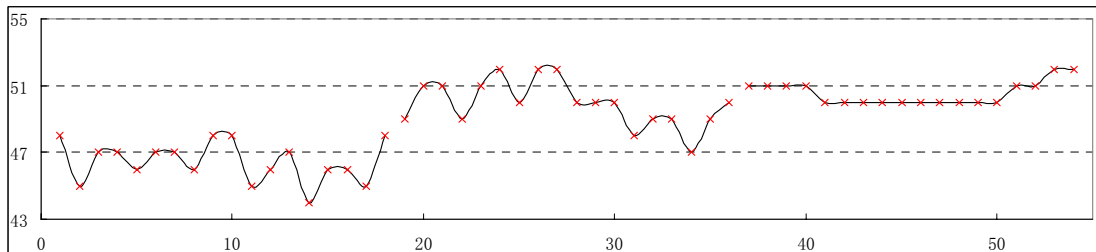


**Fig.7 The time-temperature curve when using the copper hollow conductors**

**3 THE CONCLUSION**

Experimental bar calculations show that on the same section in the bar with stainless steel hollow conductor, 11K can be reached between solid conductor which has the highest temperature and the hollow conductor. It means that the thermal gradients are very big and the temperature distribution uneven. Yet the thermal gradient on the same section in the bar with the copper hollow conductor is 1.2K, and there are small differences in the solid conductors temperature. The result of calculation is the same with the test. The test show that there are 12~22K temperature differences between the lowest temperature solid conductor and the highest on the same section of the bar with stainless steel hollow conductor while there are 1~3K temperature differences on the same section of the bar with the copper hollow conductor. In the bar with the stainless steel, generally the third solid conductor from the hollow conductor has the highest temperature. Because the bar conductor converse, the temperature may rise 5K on the fourth and the fifth solid conductor. This condition in the whole conductor of bar appears very little, and the temperature gradient are not high between neighboring conductors from the third to the fifth, so we can only considered it in general condition.

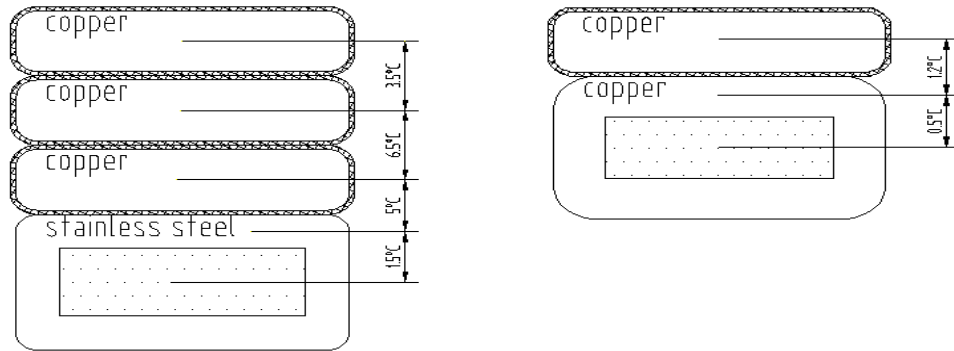


**Fig.8 temperature gradient chart of the section of bars**

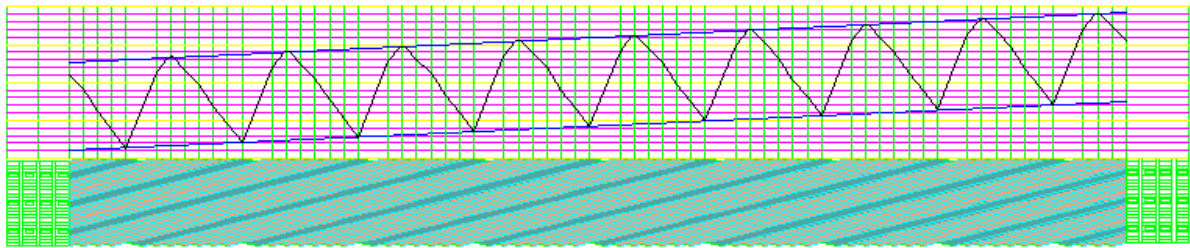


**Fig.9 temperature distribution tendency of the bar with stainless steel hollow conductors**

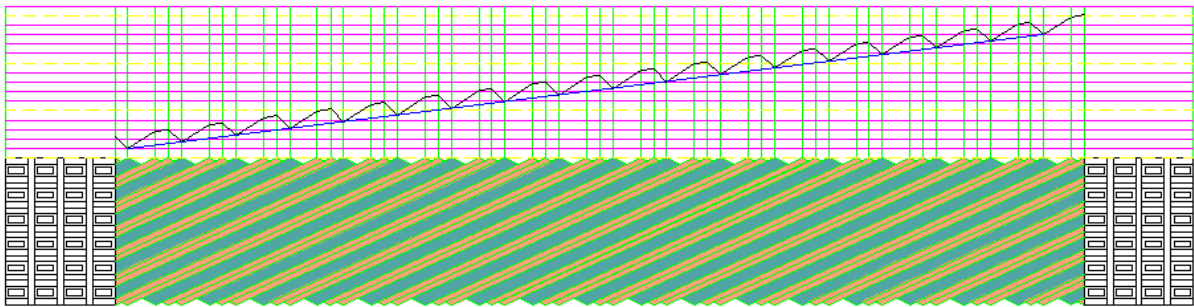


**Fig.10 temperature distribution tendency of the bar with copper hollow conductors**

The best way to decrease the temperature gradient of the bar is decreasing the current density of section. When we design the bar with the stainless steel hollow conductor, we should get a right current density to control the temperature difference in the conductors at reasonable range. We should avoid the insulation problem led by the uneven expansion of the conductors in the bar due to high temperature gradient and improve the safety of generator operation.

#### **4 PERORATION**

The temperature measurement test is finished successfully and economically based on the existing conditions, forming the test foundation for the application of stainless steel hollow conducts. It is helpful to electrical tests. At last, express our sincere gratitude to the experts who participate and guide this experiment.

#### **BIBLIOGRAPHY**

- [1] Ding S.heat and cooling of the large generator.Beijing:Science Press, Chapter. 7, 1992
- [2] Yang L, Li H.Labview advanced programming.Beijing: Tsinghua university press

**Study on Internal Cooling Water Quality and Coils Corrosion  
of Large Generators**

**Cui Yibo, Ruan Ling**

**High Voltage Department of Hubei Electric Power Testing & Research Institute  
China**

**SUMMARY**

In recent years, along with the improvement of manufacture and operation levels of large generating unit, the operation and management levels of large generators internal cooling water are more and more important. As the main editors of the power industry standard DL/T 801<< Requirements for internal cooling water quality and It's system in large generators>> (revised vision), the authors have researched the problems of large generators internal cooling water occurred in these years.

With the increasing of unit capacity and the development of stator coils design and manufacture, the requirement of the large generators internal cooling water quality is higher and higher. This paper takes the quality of large generators internal cooling water for object and researches the blockage fault in stator coils caused by copper corrosion. The authors analyses the reasons of the coils copper corrosion in PH value, oxygen content, conductivity, etc. And it comes to the conclusion that PH value is the main factor on copper corrosion in stator coils. Some suggestions were put forward about the quality of internal cooling water to improve the standard DL/T 801. For example, decrease the copper content, distinguish the PH value between different oxygen contents, delete the index of hardness, modify the value of conductivity on basis of the relationship between conductivity and pH value, etc. (the advises above were adopted in the revised vision of DL/T 801). Meanwhile the question that how to choice the oxygen-poor system or oxygen-rich system was discussed in the paper, which shows that the oxygen-rich system isn't always rich in oxygen. And the oxygen-rich system can't work as well as it should be in theory.

The paper tries to conclude the views and basis on the process of standard revision. It can help the professionals to understand and execute the new standard. Also it can provide the basis for the operation control of new generator unit internal cooling water and the technical transformation of old generator units.

**KEYWORDS**

Generator, Internal cooling water, Water quality, Corrosion

## 1 INTRODUCTION

At present, a majority of large generators apply the internal water cooling technology, which can help to preferably solve the heat dissipation inside the stator & rotor windings of large generator, to effectively control the temperature rise of the generator and provide necessary guarantee to the long-term safe & stable operation of the generating equipment. Meanwhile, since cooling water of the generator acts as the cooling medium in high-voltage electric field, quality assurance of generator cooling water is of great importance to the safe and economical operation of the generator.

To meet the requirements for production and operation, Electric Power Industry Standard, *Requirement of Water Quality and Internal Cooling Water System for Large Generator* (DL/T 801—2002) was issued by the original State Economic & Trade Commission in 2002. In view of the inadequacy of operation and management levels in China, internal cooling water quality index was eased correspondingly [1]. With the increasing commissioning of 600MW and 1000MW large generators in recent years, the operation, maintenance and management levels of the internal cooling water system equipment in the thermal power plant shall be further improved, to further improve the quality standard of internal cooling water, so as to create possibility for the unit to be operated under the optimum condition.

## 2 CONTROL OF INTERNAL COOLING WATER QUALITY

Internal cooling water quality of large generator unit is mainly controlled from two aspects such as insulation and corrosion prevention. In respect of insulation, hollow copper conductor is charged during the generator operation and a relatively high insulation level must be maintained, which requires that the cooling water must have a certain degree of resistivity (conductivity). Requirement on conductivity in control standard for generator cooling water quality is put forward from the aspect of insulation. From the point of view of corrosion prevention, it is the foremost problem exists during the practical operation of the internal cooling water system at present. Hollow copper conductor of the generator is mainly made of pure copper or copper-silver alloy with low silver content. Due to various factors, hollow copper conductor may encounter with corrosion, sometimes even quite serious event. On one hand, the corrosion may lead to the increase of copper ion in the internal cooling water, to increase the leakage current of the generator. On the other hand, corrosion products will deposit in the hollow copper conductor, to possibly block the inside of the hollow copper conductor, so as to lead to the temperature rise, insulation damage and even burnout of the copper conductor.

At present, the following viewpoints are mainly expressed on the corrosion mechanism and influence factor of hollow copper conductor of large generator:

- (1) Water conductivity is the main reason for copper conductor corrosion. The corrosion degree shall be lower if the water purity is higher. Similar opinions were expressed during the communication of the author with some professionals from the power plant. It is based on the principle that the copper ion produced by corrosion shall lead to the conductivity increase, that is to say the corrosion degree will be extremely low if the conductivity can be well controlled.
- (2) Main reasons for copper conductor corrosion are oxygen dissolved in the water and carbon dioxide in the air. Therefore, cooling water tank of the generator shall be subject to nitrogen-sealed treatment.
- (3) PH value of the cooling water is the main factor for controlling the corrosion of copper conductor. PH value is concerned with oxygen content and conductivity etc. Copper conductor corrosion of the generator is mainly caused by low PH value.

## 3 INTERNAL COOLING WATER INDEX SPECIFIED IN CURRENT STANDARDS

To meet the requirements on ground insulation of the generator and corrosion protection of the copper bar, a series of standards for internal cooling water quality has been put forward by the state and the ministry of power industry at different times. Refer to Table I for details.

**Table I Standard for Internal Cooling Water Quality at Different Times [2]**

Standards	SD163-85	DL/T561-95	GB/T12145-1999	DL/T801-2002
PH (25°C)	>7.6	>7.0	>6.8	7.0~9.0
Conductivity ( $\mu$ s/cm, 25°C)	$\leq 5$	$\leq 10$	$\leq 5$	$\leq 2$
Copper content ( $\mu$ g/L)	$\leq 200$	$\leq 200$	$\leq 40$	$\leq 40$
Dissolved oxygen ( $\mu$ g/L)	—	—	—	$\leq 30$
Hardness ( $\mu$ mol/L)	—	—	—	$\leq 2.0$
Ammonia content ( $\mu$ g/L)	—	—	—	<300
Notes: ① Requirement of Water Quality and Internal Cooling Water System for Large Generator (DL/T801-2002) is applicable to large generator unit. ② “—” means that there is no such stipulation on this item.				

#### 4 INFLUENCE OF MAJOR INDEXES ON COPPER CONDUCTOR CORROSION

Copper content refers to the mass of copper dissolved in each liter of water. Although the content of copper ion may have some effect on the corrosion rate, the influence is relatively low when comparing with other factors. Since copper ion is produced by corrosion, it is hereby only taken as the direct index for measuring the corrosion degree.

##### 4.1 PH Value

From the point of view of chemical thermodynamics, the copper is corroded by oxidation. Whether the corrosion reaction can be continued depends on the property of corrosion products. If deposition velocity of the corrosion products on the copper surface is very quick and the deposits are quite dense, protection role is realized and the so-called protective film is formed. On the contrary, if protective film can not be formed by corrosion deposits, the corrosion shall be continued unceasingly. From the investigation and research executed by the author and bibliography [3], [4] and [5], the professionals believe that the formation and corrosion prevention performance of the copper oxidation film is closely related to PH value of the solution; and the influence of PH value on copper dissolution is higher than other factors. As shown in Fig.1, it is known that PH value is approximately 7-10 when the copper dissolubility in pure water is the lowest, on the basis of relationship between copper – water PH value and the copper dissolubility. The reason is that oxidation state exists on the surface of most metal, including the copper sealed in the stator bar. In neutral and meta-acid water, excessive hydrogen ion concentration will lead to the instability of the oxidation film; but the film will be quite stable in alkaline water. According to theoretical analysis and tests, comparing with neutral and meta-acid environment, a certain degree of high PH value will be better for mitigating the corrosion on the hallow copper conductor [3]. In bibliography [4], Japan, Britain, Switzerland and the original Soviet Union stipulate the highest upper limit for PH value, i.e. 9-10; and other countries specify the upper limit as 7-8. On the basis of the analysis and combining with the previous operation status in China, the upper limit is determined as 9.

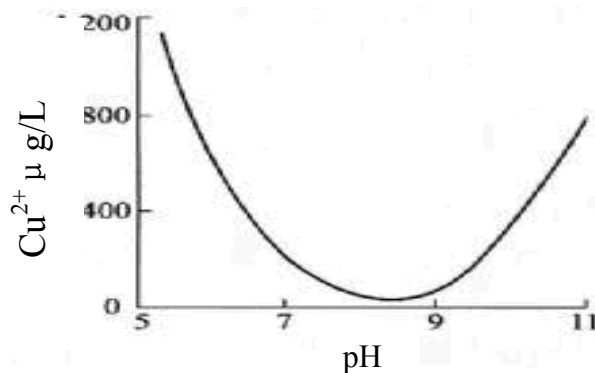


**Fig. 1 Relation between Copper Dissolubility (Corrosion) and PH Value**

## 4.2 Oxygen Content

As shown in Fig. 2, it is known from the relation curve for copper corrosion in pure water and oxygen content in water that the copper dissolubility is quite low when the oxygen content is very low (less than  $50 \mu\text{g/L}$ ) or quite high (greater than  $1000 \mu\text{g/L}$ ). The reason is that, when oxygen content is great enough in the water, a layer of dense oxidation film will be formed on the surface of the stator bar after the copper being oxidized, to protect the stator bar, so as to greatly prevent the further oxidation. However, according the curve, it is also known that: theoretically, the copper corrosion is close to 0 when the dissolved oxygen approaches to 0; however, copper corrosion still exists when the oxygen content approaches to infinite and approximately equal to the value with  $30 \mu\text{g/L}$  oxygen content (up to  $6\sim 13 \text{mg/L}$  when the dissolved oxygen is saturated in the water; content of dissolved oxygen in water is normally  $1.4\sim 3.2\text{mg/L}$  when contacts with the air).

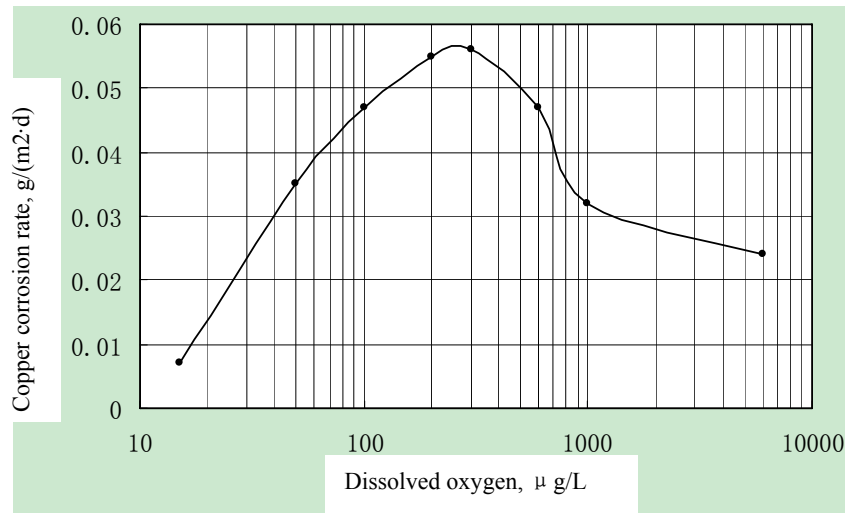


Fig. 2 Relation between Copper Dissolubility and Oxygen Content in Pure Water

Meanwhile, according to Fig. 3 – relation curve between copper corrosion rate and PH value & content of dissolved oxygen in water, it is known that different PH value will cause dissimilar effects on the copper corrosion even if the oxygen contents are identical. As per the forgoing paragraphs, when PH value is equal to 7, the corrosion rate will be greatly affected by the oxygen content, which must be controlled beyond the range of  $40 \mu\text{g/L}$ — $1000 \mu\text{g/L}$  to meet the standard requirement; when PH value is greater than 8, influence of oxygen content on corrosion rate shall be obviously decreased; when PH value is greater than 8.3, content of dissolved oxygen will cause little influence, and the corrosion degree will be less than the mild corrosion in pure water even if the oxygen content is within the active corrosion range of  $40 \mu\text{g/L}$ — $1000 \mu\text{g/L}$ . Thus, it can be known that, comparing with the oxygen content, PH value of the internal cooling water will bring about the more significant influence on corrosion of copper core bar. If PH value can be well controlled, influence of oxygen content on the corrosion can be greatly reduced.

A part of water quality indexes for cooling water of generator provide with no any control standard for oxygen content in our country, but it is required to be less than  $20\text{—}50 \mu\text{g/L}$  in Russia and lower than  $20\text{—}100 \mu\text{g/L}$  in Japan [6]. Combining with the foresaid content, the author believes that the oxygen content shall be controlled below  $20 \mu\text{g/L}$  theoretically. However, in view of practical situation during the existing operation and manufacture procedure, it is very difficult to change into the totally enclosed internal cooling water system within a short period, which makes the carbon dioxide and oxygen dissolved in the water exert an influence on PH value. Therefore, it is recommended that the oxygen content shall not be controlled when PH value is within the range of 8-9. If the operation is instable and PH value is below 8, the oxygen content shall be controlled below  $30 \mu\text{g/L}$ .

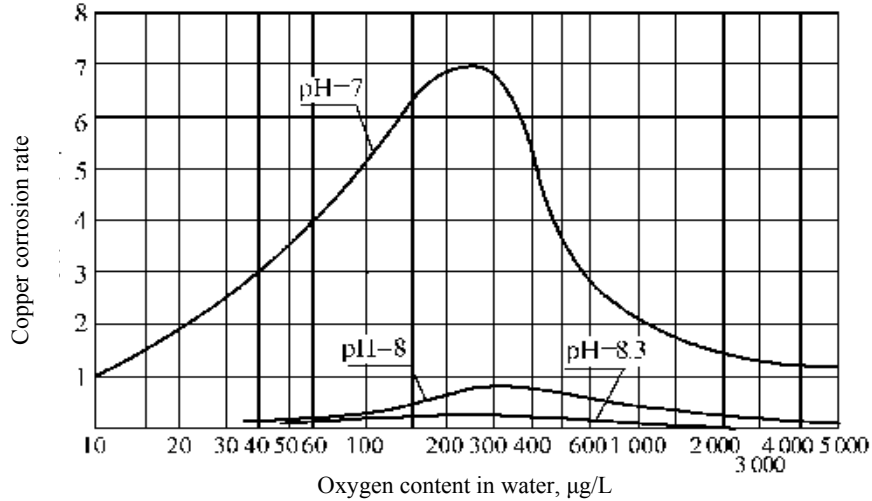


Fig. 3 Relation between Copper Corrosion Rate and PH Value & Content of Dissolved Oxygen in Water

### 4.3 Conductivity

Conductivity will have a certain effect on the copper conductor corrosion. As shown in Fig. 4, from the relation curve between the dissolubility of copper in the water and the conductivity, both excessively high and low conductivity may cause adverse effect on the copper corrosion; when the conductivity is too low or too high, the corrosion rate will be greatly increased. Thus, it is observed that Opinion (1) in Section 2 is wrong because that pure water is a type of solvent which can dissolve many substances and metal is somewhat dissoluble in the water. Comparing with their compounds, metals (besides platinum and gold) have a higher free energy and can form into oxidation and other compounds through reactions, so as to trend to a higher stability. Even if putting aside the oxidation factor, metal can be directly dissolved in the water in a state of ion or free particle [7].

Meanwhile, metal dissolved in the water may increase the conductivity. If the conductivity of internal cooling water will be maintained within the range of relative low by means of unceasingly changing water to remove the dissolved metal, the dissolution velocity of copper will be increased. In brief, the copper deposits can be prevented in a certain degree, but the copper corrosion can not be fundamentally solved and a large amount of water will be wasted. Therefore, corrosion of copper conductor can not be mitigated by excessively decreasing the control value of cooling water conductivity of the generator. Control of cooling water conductivity of the generator is not mainly decided by the corrosion, but the insulation requirement. Combining with the requirements of corrosion and insulation, conductivity limit shall be determined as 0.4-2.

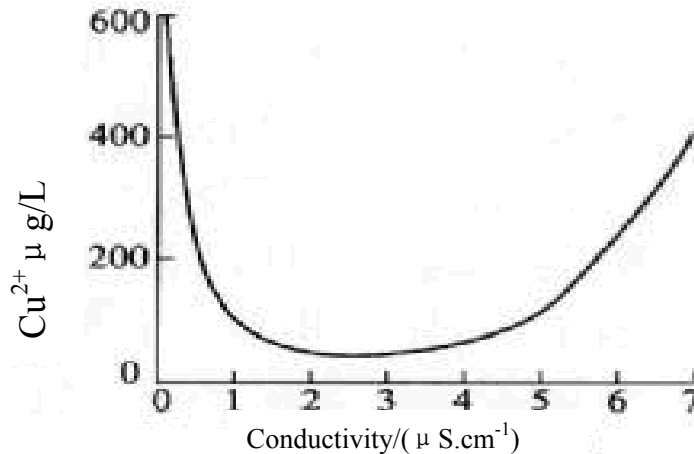


Fig. 4 Influence of Water Conductivity on Copper Corrosion Rate

#### **4.4 Hardness**

Viewed from the investigation and research executed by the author, a majority of professionals believe that the formulation of hardness index has no great valuable meaning under the existing technology and management level. The hardness will surely not exceed the standard when conductivity and PH value etc. meet relevant requirements. Some power plants which have been normally operated for several years were never provided with hardness test. Therefore, it is somewhat reasonable to abrogate the hardness index.

#### **5 SELECTION BETWEEN OXYGEN-POOR SYSTEM AND OXYGEN-RICH SYSTEM**

At present, internal cooling water system of water-hydrogen-hydrogen unit operated in China are mostly of two types; one is the open type, i.e. there is air pipe in the water tank to directly connect to the open air, which is known as oxygen-rich system; the other is the closed type, that is the entire internal cooling water system is the totally enclosed structure, nitrogen, hydrogen or other rare gas will be filled in the water tank from its upper part for sealing off, to reach the purpose of air isolation, and it is called as oxygen-poor system.

From the foresaid relation between the oxygen content in water and the copper corrosion, the copper corrosion rate is quite slow no matter the oxygen content is very high or too low, that is, when relevant conditions are satisfied, the copper corrosion can be well controlled both for the oxygen-rich system and the oxygen-poor system. It is theoretically believed that the system with the oxygen content no less than  $1000 \mu\text{g/L}$  is defined as oxygen-rich system, while the system with the oxygen content no greater than  $40 \mu\text{g/L}$  is named as oxygen-poor system. From the point of view of structure and cost, only one pipeline is required to be connected out of the water tank to the open air, but the oxygen-poor system is more complicated since sealing gas shall be filled into the tank and the cost will be higher. A majority of earlier water-hydrogen-hydrogen units adopt the oxygen-rich system in China.

However, from the operation experience of various power plants in China for the past several years, control of copper corrosion rate in the oxygen-rich system is actually far away from the theoretical level [8]. The author believes that there are mainly two reasons. Firstly, when dissolved oxygen is saturated in normal water, the oxygen content can be up to  $6\text{-}13\text{mg/L}$  theoretically; and oxygen content in water is  $1.4\text{-}3.2\text{mg/L}$  when normally contact with the air. However, it is obviously that the foresaid expression “normally contact with the air” is not direct at the internal cooling water system of the generator. There is a certain difference between the internal cooling water system of the generator and other systems which directly contact with the air. Internal cooling water system of the generator is only provided with one pipeline to connect with the air, with quite limited air inflow; and there is no enough time for internal cooling water to sufficiently calm down in the water tank to contact with the air, since the internal cooling water is under unceasingly circular flow. And that makes the oxygen content in the internal cooling water system can not meet the theoretical requirement during the practical production, that is “oxygen enrichment fails to live up to its name”, so that the oxygen content of the entire internal cooling water system is decreased to the range of severe corrosion. Secondly, carbon dioxide gas exists in the air and will dissolved in the water since the internal cooling water is quite pure and the buffer is narrow, so that the original low PH value will be further decreased and the copper corrosion rate will be increased accordingly.

Besides, even if the requirement of oxygen content can be satisfied, a certain degree of corrosion may also exist in the oxygen-rich system. However, in respect to the oxygen-poor system, since nitrogen etc. can be used to check the equipment failure such as hydrogen leakage during the normal operation of the generator, totally enclosed internal cooling water system can be gradually adopted in future design and production, to prevent “the oxygen enrichment fails to live up to its name”.

#### **6 CONCLUSION**

From the foresaid analysis, it is known that in respect of control indexes for internal cooling water of the generator, the copper content only directly reflects the corrosion degree of copper conductor, but PH value, oxygen content and conductivity will have different degree of influence on the corrosion of copper conductor. However, among those influence factors, PH value leads to quite great influence on

the copper corrosion in water. In a sense, PH value of the internal cooling water will directly determine the corrosion degree of copper bar caused by internal cooling water. Therefore, copper corrosion can be favorably prevented once PH value is well controlled. However, the current standard limit value for the internal cooling water takes the operation & management level at the time of formulation into account and does not use the limit value to guarantee the optimum operation of the unit, so the problem shall be considered and resolved at the time of standard revision.

## **BIBLIOGRAPHY**

- [1] Description for drawing up requirement of water quality and internal cooling water system for large generator, October 2001
- [2] Huang Z. Study on new treating technology for internal cooling water in generator. Colloquium on Water Conservation Technology in Thermal Power Plant, October 2006
- [3] Bai Y., Dai J.i, Song Z. Method and measures of optimizing generator cooling-water to prevent copper corrosion. *Electric Power Equipment*, 2006, 4
- [4] Excerpt of characteristic curve for relation between conductivity, PH value & oxygen and copper corrosion
- [5] Comprehensive investigation report on winding corrosion of water-cooled turbine generator. CIGRE Committee for Rotating Electrical Machine (SC11) 1984 ~ 1994 Publications (Electra) Translation – J. GHEARD 11.01 Working Group
- [6] Wen R, Ding H, Du Fg, Wang L. Analysis on copper conductor corrode caused by cooling water in generator. *North China Electric Power*, March 2003
- [7] Liu J, Han X, Kang S. Technical analysis on corrosion and output of cooling water system inside generator. *Inner Mongolia Electric Power*, 2003, 21(6)1.3, 1.4,
- [8] Li Z, Ye H, Wan Y. Corrosion control of stator bar of internal cooling water generator in three gorges left bank power station. *Mechanical & Electrical Technique of Hydropower Station*, 2008( 4, 2, 3.1, 3.2)

**Technical Characteristics of 1100MW Nuclear Power Generator  
Designed by Shanghai Generator Works**

**Wang Tingshan, Hu Jianbo, Wei Yanfei**  
**Shanghai Electric Power Generation Equipment CO., Ltd. Shanghai Generator Works**  
**Shanghai, China**

**SUMMARY**

Shanghai Generator Works (SGW), belonging to Shanghai Electric Power Generation Equipment Co.,Ltd, is a large R&D and manufacturing enterprise, ranking in a leading position in China, engaged in the manufacture of large turbine generator and related equipments.

In recent years, with the national energy structure adjustment and the need to accelerate clean energy development, China's nuclear power has made significant progress, and the nuclear power industry has entered a new stage of rapid development. To meet the domestic and foreign demands for 1000MW class nuclear power generator and to promote independent of the national nuclear power industry, Shanghai Generator Works has developed 1100MW class 4-pole nuclear power generator with independent intellectual property rights, based on the combination of the own generator technology and the imported technology. The first 1100MW nuclear power generator has begun manufacturing in Shanghai Generator Works, and will be delivered in 2011.

In this paper, the main technical specifications, performance and structure technical characteristics of 1100MW nuclear power generator designed by Shanghai Generator Works are presented. The development of this generator enhances the capability of independent innovation, and enhances the strength of China's equipment manufacturing industry.

**KEYWORDS**

Turbogenerator, Nuclear power, 4-pole, Ventilation, Generator stator, Generator rotor, Brushless exciter

## 1 INTRODUCTION

Shanghai Generator Works (SGW), belonging to Shanghai Electric Power Generation Equipment Co.,Ltd, is a large R&D and manufacturing enterprise, ranking in a leading position in China, engaged in the manufacture of large turbine generator and related equipments.

In recent years, with the national energy structure adjustment and the need to accelerate clean energy development, China's nuclear power has made significant progress, and the nuclear power industry has entered a new stage of rapid development.

To meet the domestic and foreign demands for 1000MW class nuclear power generator and to promote independent of the national nuclear power industry, Shanghai Generator Works has developed 1100MW class 4-pole nuclear power generator with independent intellectual property rights, based on the combination of the own generator technology and the imported technology. The first 1100MW nuclear power generator has begun manufacturing in Shanghai Generator Works, and will be delivered in 2011.

## 2 GENERATOR MAIN TECHNICAL PERFORMANCE ATTRIBUTES

This 1100MW class nuclear power generator is 4-pole, 3-phase, non-salient pole turbine generator, using enclosed ventilation and water-hydrogen-hydrogen cooling method. The main technical performance attributes are shown in table I.

**Table I 1100MW-class nuclear power generator technical performance**

Generato Type	QFSN-1100-4 / 24
Rated Power	1100 MW
Power Factor	0.9
Rated Voltage	24k V
Rated Current	29402 A
Rotating Speed	1500 r/min
Frequency	50 Hz
Cooling Methods	Stator winding: Water Rotor winding: Hydrogen Stator core: Hydrogen
Rated Hydrogen Pressure	0.52MPa (g)
SCR	0.6
Level of Insulation	Level F (with Level B temperature )
Efficiency	98.9%
Excitation	Brushless
Rated Excitor Current	8200 A
Rated Excitor Voltage	480 V

## 3 GENERATOR MAIN STRUCTURES TECHNICAL CHARACTERISTICS

### 3.1 Ventilation and cooling

1100MW class generator is a hydrogen-cooled generator, equipped with an all water-cooled stator winding. The rotor winding is axially hydrogen-cooled, and the stator core is primarily axially hydrogen-cooled, with radial ducts at each end for supplemental cooling. Hydrogen is circulated with one multi-stage, axial flow blower mounted on the shaft at the turbine end of the generator. The closed circuit hydrogen is cooled with four hydrogen coolers installed vertically on the stator frame in the turbine side of generator. As illustrated in Fig.1, ventilation is divided into three branches totally to cool the rotor windings and the stator core.

Circulation 1:

Cold hydrogen flows from the coolers at the turbine end (TE), through the ducts at the back of stator frame, arriving at the exciter end (EE). Then a portion of the gas flows into the stator core along the axial vents, and after absorbing the heat generated by stator core, flows to the coolers due to the pressure of the multi-stage blower.

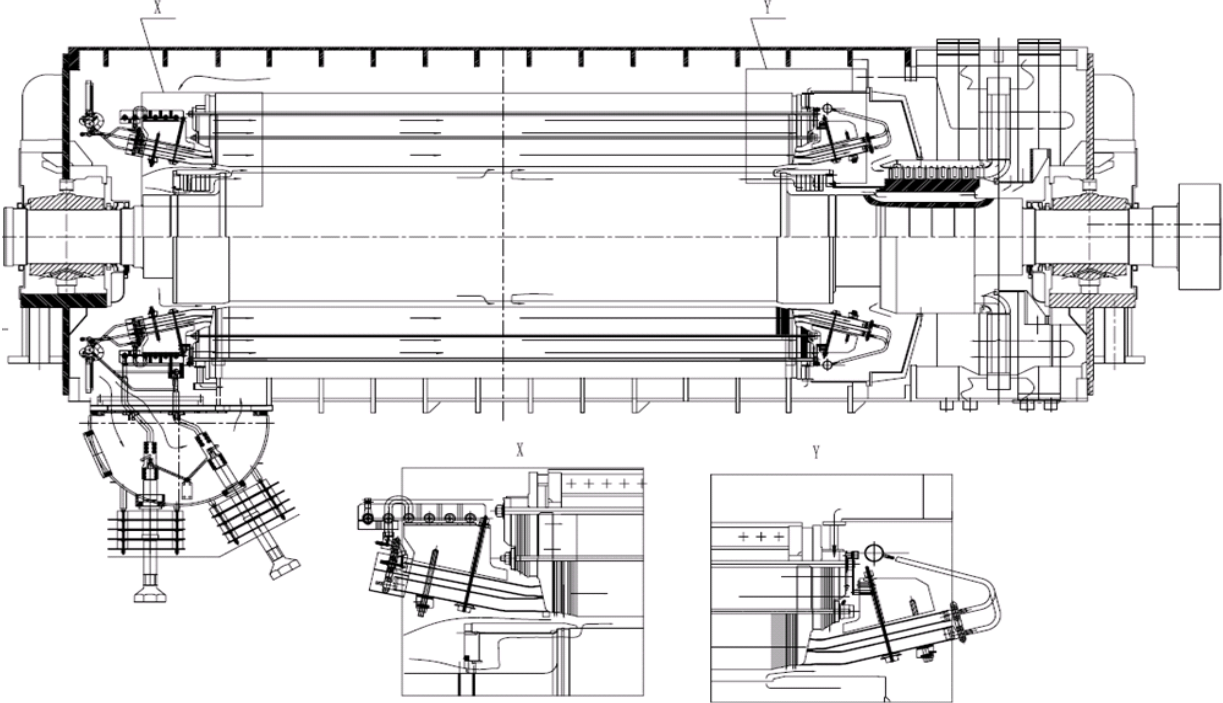


Fig. 1 Closed ventilation circuits for generator.

Circulation 2:

This cold hydrogen is the other portion gas of Circulation 1 at the EE, directed by means of baffles and ventilating passages through the rotor winding, and after cooling the half rotor winding in the exciter side, flows into the gap, finally to the coolers due to the pressure of the multi-stage blower.

Circulation 3:

Cold hydrogen directly enters the rotor end winding region from beneath of the blower hub, flowing through the ventilation passages provided in the rotor winding itself, and is discharged into the gap at the center of the rotor after cooling the half rotor winding in the turbine side, finally flows to the coolers as Circulation 2.

3.2 Stator frame

1100MW class generator stator frame design consists of an inner and outer frame construction, which could meet both water transportation and railway transportation, and shorten the manufacturing cycle effectively. The core and frame could be assembled either in the manufactory or at the site according to the transportation need of customs.

Inner Frame:

The inner frame is a single piece construction and consists of several clamping rings and two beams, for supporting the core, as shown in Fig.2.



**Fig. 2 The inner stator frame structure.**

#### Outer Frame:

The outer frame consists of 2 separate sections, one for outer frame turbine end and the other for the remaining section, welded into an integrated frame after being connected with bolts. A stress relieving treatment is performed after welding, and all the gas-tight welds are detected for flaw. It has radial and axial steel ribs having adequate strength and rigidity.

There are flange faces on the top and bottom of outer frame at TE of generator for mounting the hydrogen coolers, and one on the bottom at EE for installing the terminal box. Some temperature lead holes, manhole, interfaces for gas charge and discharge, interfaces for monitoring instruments, etc are designed on the outer frame also.

Several sets of vertical big spring plates on the side face are connected between the inner and the outer frame along the axial direction, with some small spring plates on the bottom, maintaining the stability of the entire core, as illustrated in Fig.3.

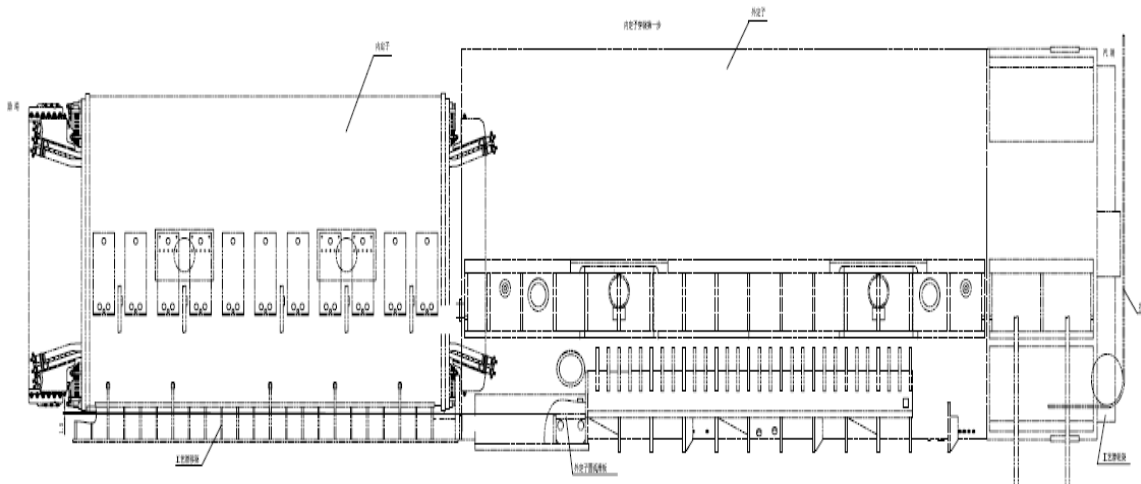


**Fig. 3 The inner and outer stator frame structure.**

### 3.3 Stator core

The stator core is made of 5mm thin non-oriented cold-rolled silicon steel punching with high permeability and low losses, and stacked in the inner frame on axial key bars which are welded to the clamping rings inside diameter. Stator laminations are coated with water soluble synthetic varnish. By using the axial core key bars and insulated through-bolts, the stator core is tightened into a entire block between steel clamping plates with non-magnetic pressing fingers, after compressed and heated for several times. The stator core can be retightened after running for a certain time by means of the hydraulic screw nuts mounted on the through-bolts at the exciter end, as shown in Fig.4.

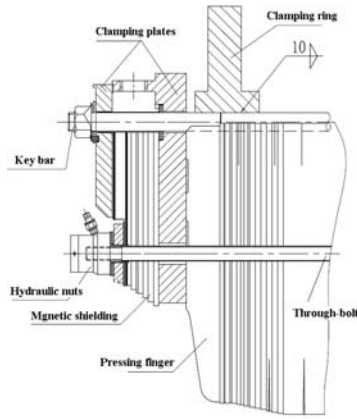


**Fig. 4 The structure of stator core end.**

In order to reduce the losses of end magnetic flux leakage, the edge core is designed ladder shape along the radial direction. Magnetic shielding is used also at the stator core end to effectively shield the leakage flux and increase the capability of the generator. Full compensation for the entire core can prevent from the creep loose after a long time running.

### 3.4 Stator coil and fixation for stator windings

The stator windings consist of two layers in one slot. To minimize losses, the stator bars are composed of separately insulated strands, four columns of mixed hollow and solid copper strands with two to one solid to hollow strand ration. In the straight slot portion, the strands are transposed by 540 degree to reduce the stray losses. The cross section for top bar is larger than the one of bottom bar, which could balance the temperature rise of bars in a slot. The stator coil involute end use non-equidistant structure, decreasing the distance between two bars of the same phase and enlarge the distance of two bars belonging to different phases, as illustrated in Fig.5. The winding insulation is obtained by vacuum press impregnation (VPI), which has excellent electrical, mechanical and thermal properties, and the insulation level is F class.

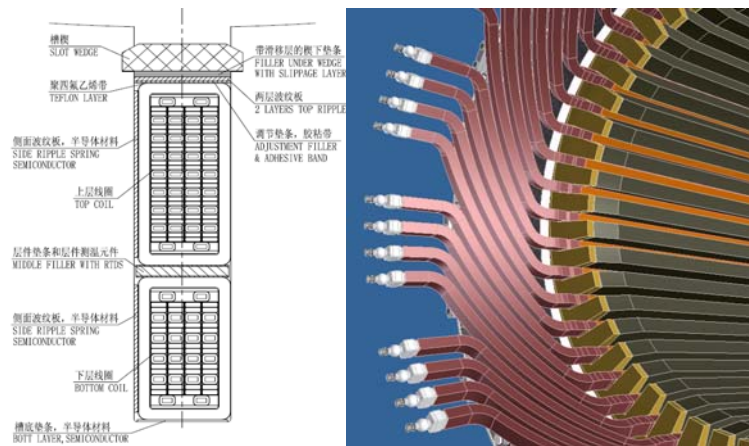


**Fig. 5 The stator coil construction.**

Ball connecting structure for stator winding is used as Fig.6, the welds between hollow stands and water box, between water box and ball connector, using intermediate frequency brazing process.

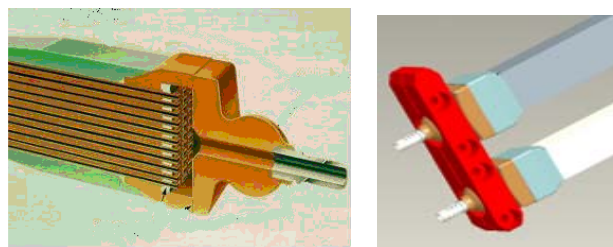


**Fig. 6 The ball connecting structure for stator winding.**

Stator slot fixed structure: stator bars in the slot are fastening by the high strength wedges, and the closing wedges at both sides are locked to the core by adhesive, preventing the wedges from moving axially due to the operation vibration. Two layers ripple springs under the wedge and a sumicoducted ripple spring in slot side ensure the bars fixed tightly.

Stator end windings fixed structure: The stator end winding fixation is a rigi-flex structure, as shown

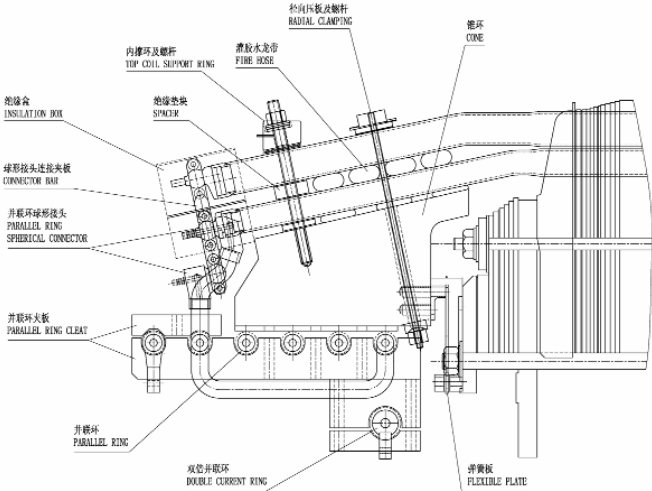


Fig. 7 The stator end winding fixed structure.

in Fig.7, the end winding fixed structure consists of cone, radial clamping, spacer, resin impregnated fire hose, and support ring, binding the top and bottom end windings to the cone as a whole structure. The cone is fixed to the core end by flexible plates circumferential distributed uniformly. This structure makes the end windings in the radial, tangential directions with good integrity and rigidity, while in the axial direction with free expansion ability, effectively alleviating the mechanical stress effect due to the temperature changes during the operation.

The stator terminals connect to parallel ring with flexible copper bars, and to the bushings with copper fittings. The terminal box is welded with the anti-magnetic stainless steel plates, bearing the same level of pressure and tightness tests for the stator frame. Also, it is needed to ensure the design for strength and modal frequency of terminal box, bushings and current transformers meet the security requirements.

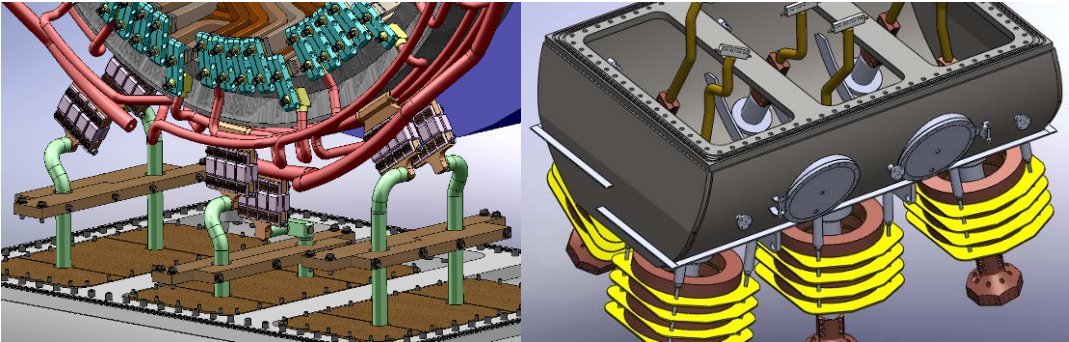
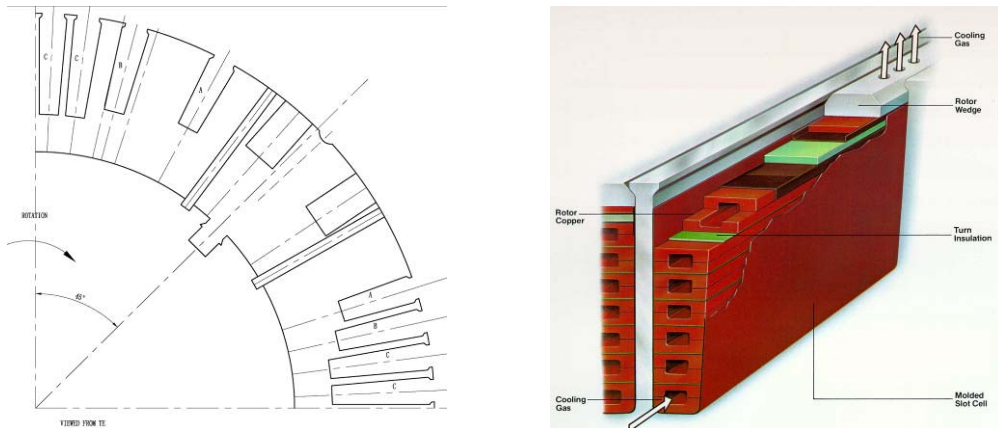


Fig. 8 The terminals and terminal box structure.

**3.5 Rotor**

1100MW class generator rotor is 4-pole, with multi-stage blower and axial-radial ventilation. The rotor with different slot sections and partial slot structure, effectively improves the magnetic field waveform, reducing the additional loss of stator windings.

The slots of rotor are ladder shape. Each turn of the coil consists of two concave silver coppers, constrained by the alloy copper wedge with high strength and good conductivity. The wedges and the retaining ring together constitute the rotor damping systems.



**Fig. 9 The rotor slots and winding structure.**

The inner surfaces of both rotor slot insulation and retaining ring cylinder insulation, contacting with the rotor windings, are affixed with slipping layers to prevent the winding deformation and insulation damage caused by thermal expansion and contraction.

Rotor retaining ring is manufactured of 18Mn18Cr forging with anti-magnetic high-strength alloy steel, which has good resistibility to stress corrosion. Long retaining ring structure is used for 1100MW generator, and this structure increases with the interaction surface of the rotor, consequently reduces the stress and improves fatigue life.

### 3.6 Brushless exciter

The brushless exciter is mainly consisting of AC main exciter, pilot exciter and rectifier wheels, installed in one shaft. The exciter is enclosed in housing in which air circulation and cooling system is formed, to ensure the exciter runs with low temperature rise and low noise pollution, as shown in fig.10.

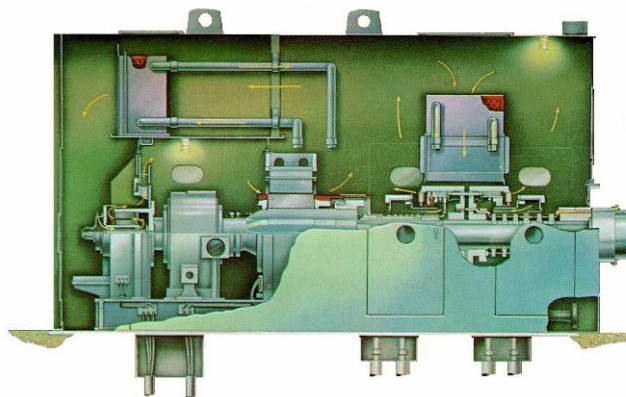


**Fig. 10 The brushless exciter structure.**

Brushless exciter has large capacity and low operating temperature. By using large capacity permanent magnet exciter and improving the diode over-current and reverse voltage capability, the brushless exciter response and forced excitation could be improved.

## 4 CONCLUSION

In this paper, the main technical specifications, performance and structure technical characteristics of 1100MW nuclear power generator designed by Shanghai Generator Works are presented. The development of this generator enhances the capability of independent innovation, and enhances the strength of China's equipment manufacturing industry.

## **Refurbishment Model of Turbine Generator in Nuclear Power Plant**

**A. Semba, M. Sugiyama, T. Sano, K. Hosokawa, M. Toyota**  
**Hitachi, Ltd.**  
**Japan**

### **SUMMARY**

One of the techniques most widely used throughout the world to extend the lifetime of turbine generators is "rewinding," which involves updating the insulation system. This paper suggests a different approach for extending the lifetime that has many advantages in plant operation. In this approach, the entire generator is replaced in a very short period of time. The new generator brings state-of-the-art technologies to the plant and extends its lifetime dramatically. Another advantage is that the generator is able to increase its rated output and/or efficiency per plant requirements in many cases. The main disadvantage to the replacement, though, is the cost. However, if a replacement is completed much faster than an insulation update, the operation period that is saved covers the cost, especially in base load plants. This means that generators in large thermal and nuclear power plants are the preferable targets for this scheme.

We were involved in a project to replace four generators at a power plant in the Republic of Korea from 2005 to 2009. One of the generators was updated in its capability by approximately 10%. The duration from the shut-down of the former generator to 100% output of the new generator was less than 50 days. In particular, the fourth replaced generator was rated at 1,222 MVA, 22 kV, and 60 Hz, for a weight of approximately 500 tons and required only 43 days for the refurbishment in 2009. We estimated that an insulation update for this class of turbine generator would have taken 50 to 60 days including disassembly and reassembly of the rotor. Therefore, this plant was able to save approximately two weeks by replacing the whole generator by our estimation. The operational profit from this period basically covered the extra cost of replacing the generator.

Although this business model can offer significant benefits to the parties concerned, it is essential that the work be carried out under a very strict schedule with full collaboration among the related parties. Additionally, the proper experience and thorough preparation are required in order to do these kinds of refurbishment. In the case mentioned above, we were not the original manufacturer, so it was necessary to measure the dimensions of the equipment and to understand the restrictions of the structure in order to plan the replacement. In addition to the generator and auxiliary system design, the strength of the foundation and the crane load had to be measured and evaluated. The installation plan was discussed and agreed on based on this "reverse engineering" process.

In summary, this refurbishment model is often effective and is cost-effective for large thermal and nuclear power plants. Our objective is to share this information with various parties throughout the world who are interested in achieving a stable electrical power supply over the long term.

### **KEYWORDS**

Turbine generator, Re-winding, Replace generator, Reverse engineering

## 1 BACKGROUND

To meet the huge increase in electric power consumption, many new power plants are being established all over the world, and their plant outputs tend to be increased over time. This approach normally requires a large budget that must be carefully managed, and it also takes a long period of time not only for the construction, but for assessment and approval by governments. An easier and shorter way to boost electric power is to increase the existing plant output. In particular, even a small improvement in the heat balance and/or plant auxiliary system efficiency in large thermal and nuclear power plants would produce additional plant output by 10 to 100 MW, which is similar to the output of a small power plant.

An increase in the power output is based on a new generator rating. The new rating normally depends on the mechanical output of the new turbine. One common technique to meet the new generator rating is to improve its cooling method. Installing new insulation with a higher heat-transfer coefficient is sometimes effective for this. Another idea is to increase the amount of cooling medium such as water or hydrogen. Furthermore, a decrease in electrical system losses in the plant would also be taken into account.

On the contrary, insulation system updates or rewinding, are standard to extend the generator lifetime after many years of operation. Rewinding is carried out after analyzing data from diagnostic results of the insulation and information based on former practical cases. In these cases, the uprating mentioned above is practical. However, rewinding involves some physical constraints. For instance, it is difficult to change the stator and rotor slot size and length, so the improvement of the cooling capability is somewhat limited. If a much higher improvement in mechanical output is planned on the turbine side, the selected generator sometimes cannot meet the requirements.

Thus, replacing, i.e., refurbishing, the whole generator is another way to improve the output. In this approach, the generator can be designed more freely against physical constraints, while limitations in the foundation or equipment still exist. In such cases, the manufacturer can offer a more attractive plan, and the plant user can select from various uprating solutions.

This paper focuses on the refurbishment model for turbine generator.

## 2 ACTUAL PROJECTS

We started working on a generator replacement project in the Republic of Korea in the mid-2000s. The project involved a total of four generators at a nuclear power plant. Table I lists the original generator details. At that time, it was standard to take 50 to 60 days for rewinding in armature coils. Therefore, a replacement project required the same number of days or less than the rewinding work.

**Table I Original Generator Information.**

	Unit 1	Unit 2	Unit 3	Unit 4
Generator rating [kVA]	700,000	764,700	1,222,222	1,222,222
Generator voltage [kV]	22	22	22	22
Armature current [A]	18,370	20,068	32,075	32,075
Insulation class	B	B	B	B
Stator weight [ton]	230	242	340	340
Rotor weight [ton]	124	130	180	180
In-service date	1978/4	1983/7	1985/9	1986/4

In nuclear power plants, a high utilization rate and high reliability are strongly required. Thus, we planned to shorten the overhaul period as much as possible. Moreover, it was promised that many improvements such as rotor vibration and ease of maintainability as well as refreshment of armature

and field insulation, which had an advantage by applying the whole generator replacement with reasonable cost instead of just re-winding cost.

## **2.1 Approach on the project**

At the bid, we collected as much information on the plant as possible because the original generators had been manufactured by another company. This was a disadvantage for us, as we did not have any manufacturing drawings or designs. To compensate for this, we dispatched several engineers to the site to create some rough drawings as if we were the original manufacturer. However, access was limited, so some parts of the designs were estimated based on practical knowledge. This initial “reverse engineering” was very important.

After being selected in the bidding process and receiving the order, we investigated the customer’s requests for the new generator. We wanted to offer the best solution we could in order to implement this “refurbishment” model. As a result, we dispatched 5 to 10 engineers to the site more than five times per unit. Each time, the customer’s thorough cooperation and understanding were helpful for the reverse engineering.

In addition, the construction required planning the disassembly of the existing equipment and installation of the new equipment. The main issue in the early stage was how to install the equipment. The generator stator was the heaviest component, so we had to arrange to have a lifting device in some units. The installation of the auxiliary system was also difficult. Because the auxiliary equipment had to be set in a basement or underground floor, we managed the installation plan using a very limited opening space and a lifting device. Some parts had to be disassembled in order to put them into such a narrow space after being assembled for a test at the shop.

Moreover, many regulations regarding construction are in place in each country. In particular, a national licence for construction is needed in most cases. One of the solutions is to establish a partnership with a company that has such a license, which we did in this project.

At the design proceeded to some degree, we wanted to confirm the actual data and interface at the site again. One of the priorities of the project was to finish the replacement in a very short period. This meant that small defects or mismatches between our design and the actual equipment at the site would result in wasted time. Thus, we felt that the visit for the final confirmation was very important.

## **2.2 Engineering**

In addition to designing the new generator and auxiliary system, the following procedures were executed.

- (1) Analysis of overall flow balance for lube oil system
- (2) Analysis of all interfacing system (auxiliary system, IPB, excitation system)
- (3) Pedestal concrete crack investigation
- (4) Pedestal vibration analysis (resonance check)
- (5) Structural integrity examination for the existing anchor bolts
- (6) Structural integrity examination of temporary lifting device
- (7) Transportation route load examination
- (8) Torsional analysis and measuring of turbine-generator rotor train
- (9) Turbine-generator thrust force calculation
- (10) Generator thermal expansion analysis
- (11) Turning gear capacity and load analysis
- (12) Rotor dynamics analysis

Plant utilities such as lubrication oil, cooling water, and auxiliary power were carefully estimated. If new requirements for these utilities affected the existing conditions, we had to change the balance that affected the pump and motor capacity as well as set points such as those for pressure and flow.

Examining and reducing the rotor vibration was one of the major tasks. In this project, we did not have sufficient original turbine and generator rotor data. Therefore, conducting a thorough analysis and comparing it with the actual data were key steps. We checked feedback from the analysis with the measured data many times to ensure accurate results.

The main physical interfaces between the original equipment and the new one occurred at the IPB, T-G coupling, DC bus bar, and rotor end with the main oil pump. Most of these interfaces could not be investigated or measured when the rotor was pulled out. Therefore, it was very important not to miss such limited timing in the customer’s plant operation schedule.

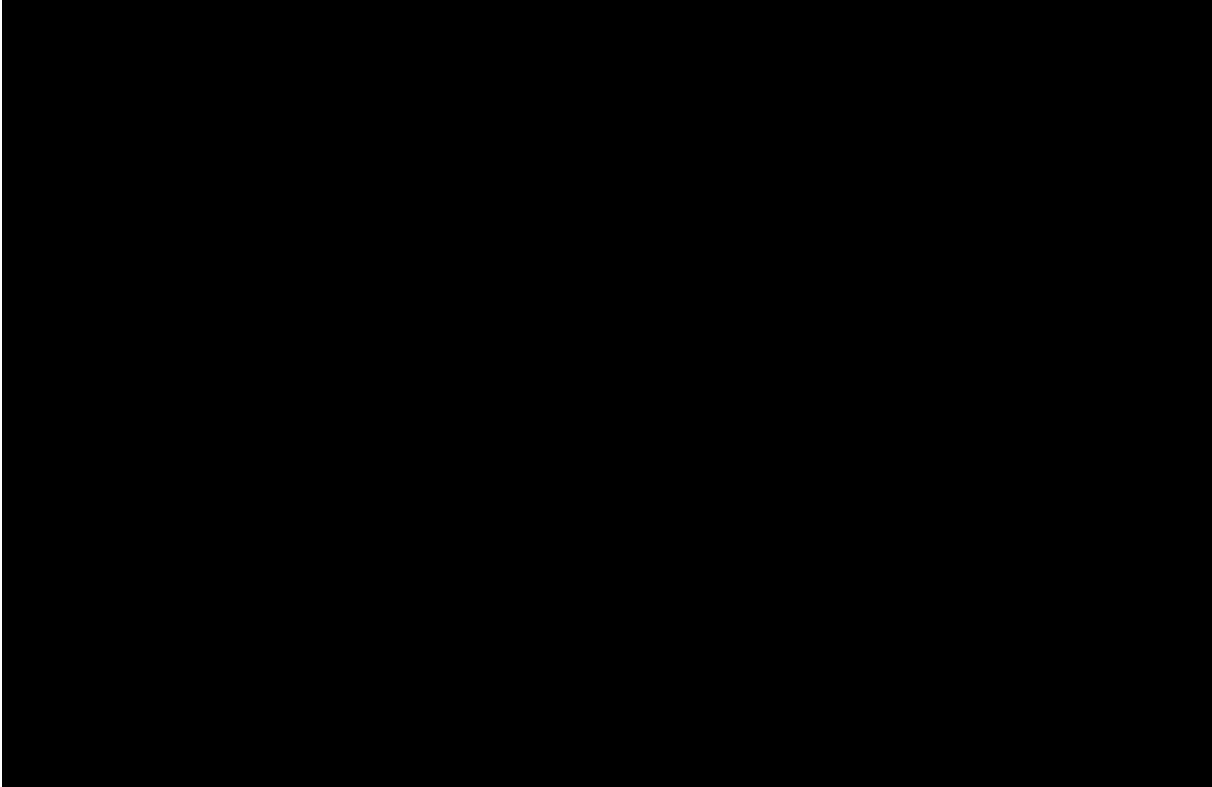
**2.3 Disassembly and installation**

Adequate preparation before the planned overhaul was carried out. First of all, adequate reinforcement of the transportation route where heavy equipment would pass was conducted. Trailers over 300 tons could possibly damage underground conduits. An actual load test of a temporary lifting device was also performed. In one of the units, a heavy generator had to pass over the turbine. Therefore, it was necessary to verify the actual load capacity of the crane before the replacement. If the crane did not have sufficient lifting capacity, we had to factor in extra days for countermeasures such as reinforcing the wire and/or exchanging the motor.

This prior engineering and preparation took about one month. At the same time, the complete set of new generator was shipped from the factory and arrived at the site in time for the project. Frequent meetings were necessary at this stage because many key personnel had little time to get together after the overhaul began. Obtaining everyone’s mutual understanding and confirmation for the work ahead was helpful for the smooth running of the project.

Table II lists the actual planned working schedule from the shut-down to 100% reload. Fig. 1 shows some photographs of actual working scenes.

**Table II Planned Schedule from Shut-down to 100% Re-load.**



After the rotor turning had ended, the dismantling of the existing generator was started. Concurrently, the removal of the auxiliary system and its piping were also carried out on each floor. It took only 16 days after the shut-down to set the new stator on the base. To keep this schedule, we had a crew of more than 100 people working two shifts (day and night).

The foundation and flushing work took a certain period of time, so minimizing these tasks was the key to meeting the schedule. Moreover, this schedule did not include field balancing work. If that had been required, the rotor would have had to be stopped and started again, which would have taken a couple of days for turning and purging. Previous calculation of rotor dynamics and shop balancing was another key issue.



(1) Just before positioning on the base (at turbine floor)

(2) Working on the base



(3) Completion

**Fig.1 Replaced Generator**

## 2.4 Experience

Table III indicates the new generator specifications and the actual replacement working days. Replacement of the first unit took 53 days from shut-down to 100% reload. However, the next two units required fewer days, and the last unit took only 43 days, which is comparable to the time required for rewinding. Two main external conditions were necessary to achieve such a fast replacement,

One condition was having the unrestricted use of the overhead crane to do this work. In a planned overhaul period, many inspections, such as of the turbine rotor, are normally performed using the overhead crane. If the crane has to be shared to carry out various tasks, the replacement work might be interrupted, which wastes a lot of time. Therefore, the manager had to consider this in advance and coordinate a proper time schedule with the relevant personnel.

The other condition was establishing clear communication between related parties (customers, partner, and so on). Having frequent and regular meetings together was very important even though there was little time for each person to speak. With such a tight schedule, people tend to concentrate on their own jobs. Sharing the status of the entire project in the overhaul was very important to accomplish the common goal. At these meetings, it was especially important to make prompt decisions regarding actions on unexpected troubles. Of course, it goes without saying that very skilled and experienced persons should be engaged in making quick decisions. A good relationship based on mutual trust is a strong driving force for such trouble-shooting.

**Table III Replaced Generator Information.**

	Unit 1	Unit 2	Unit 3	Unit 4
Generator rating [kVA]	749,000	840,000	1,222,222	1,222,222
Rating increase [%]	107	110	100	100
Generator voltage [kV]	22	22	22	22
Armature current [A]	19,656	22,044	32,075	32,075
Insulation class	F	F	F	F
Planned replacement days *1	46	53	53	53
Actual replacement days *2	53	45	43	49
In-service date	2005/5	2008/7	2009/12	2009/2

\*1: From unit shut-down to 100% power output

\*2: Including other work not attributable to generator

## 3 BENEFITS OF REPLACEMENT

It is true that replacing a whole generator is more expensive than rewinding. However, the following advantages should be evaluated.

### 3.1 Latest technology

Electrical equipment around the generator can be replaced easily. Digital redundant AVR and IPB having much capability are one of the targets. A change in the excitation method is also taken into consideration. From a brushless exciter with or without a permanent magnet generator (PMG) to a static exciter and vice versa are typical changes. A new diode and/or thyristor might bring lower losses and more compactness in size.

Additionally, new diagnostic equipment is now being installed in generators, for example, a flux probe, partial discharge monitor, generator condition monitor, and armature winding vibration sensor. Although most of these components can be installed in operating generators, it is important to evaluate the trends of such diagnostic data from the initial status. New generators can provide the initial data, which helps the operator understand the generator condition.

### **3.2 Operational cost**

Improvements in iron core materials have been achieved recently, and loss is typically lower than before. If this material was adopted, plant output efficiency would increase, and the core insulation would be refreshed. Sufficient cooling in the generator can extend the insulation lifetime. These improvements can decrease the future operating cost.

To ensure long-term operation over the years, many generator components must be maintained. However, it is possible that original suppliers or components such as carbon brushes, diodes, and bushings will be unavailable or lost. As time passes, this risk might increase. Therefore, a continuous supply framework has to be taken into consideration.

### **3.3 Flexibility of operation**

New generators can easily meet a large uprating demand if the turbine can increase its mechanical output through various means. Operation at a large leading power factor and with frequent starts and stops can also be incorporated into the generator design if the operating conditions require them.

Noise and vibration problems are potentially improved when the whole generator is replaced. For instance, it is difficult to dramatically change the natural frequency and resonance, which are determined mainly by the physical dimensions of the rotor and stator. A new rotor design and a support system for the winding assemblies would improve them.

## **4 SUMMERY**

A business model involving replacement of a whole generator is suggested. Many advantages are gained with this model compared with the rewinding model for extending the plant lifetime. The disadvantage to establishing this model is the cost. However, various engineering procedures can shorten the replacement period as described above, which would cover the cost in some cases. In particular, large thermal and nuclear power plants have large potential to gain from this model because they produce large amounts of electric power over a long term. Therefore, the trade-off in cost and benefits should be carefully analyzed when both the generator lifetime and power plant output needs to be improved. We hope to share such information with a lot of parties throughout the world who desire a stable and continuous electrical power supply over the long term.

Finally, we thank the many related companies and persons who were involved in the successful project reported here.

**Study on Electromagnetic Design of Special Brushless Exciter Used for Synchronous Motors**

**Sun Yutian, Zhang Chunli**  
**Harbin Research Institute of Large Electrical Machinery**  
**China**

**SUMMARY**

The purpose of the special brushless exciter studied in this paper is to provide the field current through the rotating rectifier for the synchronous motor at speed from zero to rated. The rotor of the brushless exciter and the rectifier are mounted on the same shaft with the motor. The structure of the exciter is similar with the wounded rotor induction machine, where the rotor windings are connected to the field winding of the motor by the rectifier, and the stator windings are connected to the voltage regulator, so the current of the rotor windings can be controlled through the adjustment of the regulators. The principle of the brushless excitation system is presented in this paper. Moreover, the equivalent circuit, power flow and the relative parameters of the brushless exciter are studied in this paper. A comparison between computation and test is made in a brushless exciter. Results show a good coincidence.

**KEYWORDS**

Brushless exciter, Equivalent circuit, Power flow, Synchronous motor

## 1 INTRODUCTION

With the development of electronic technology, the brushless exciting system was developed rapidly. For the brushless exciting system, the reliability of driving system increased and the maintenance reduced. It eliminates the faults caused by the electric brush, such as the poor contact between the carbon brush and the slip ring, the carbon brush abrasion, particularly the electric arc and spark etc. Therefore, nowadays it is applied widely in explosion proof fields, such as the mining, the petroleum and the chemical industry etc.

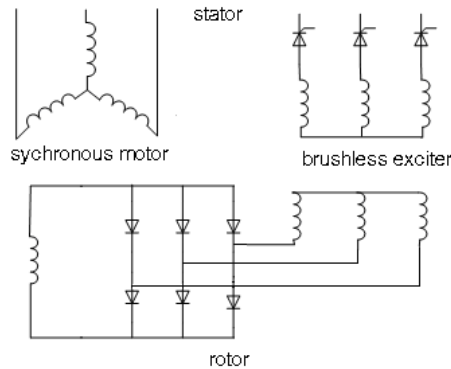


**Fig. 1 Schematic of the Brushless Excitation System.**

A synchronous motor needs field current. Fig.1 shows the schematic of the brushless exciting system and the synchronous motor. The structure of the brushless exciter is similar with the wound rotor induction motor, that the stator windings and the rotor windings of the exciter are all connected as the three-phase windings, but the stator windings are connected to the voltage regulators consisting of the thyristors, and the rotor windings are connected with the field winding of motor as the rotor of the brushless exciter and the rotating rectifier are mounted on the same shaft with the motor. The current in the rotor windings of the exciter can be controlled by the delay angle of the thyristors in stator side, so the field current of the synchronous motor can be controlled.

When the currents flow through the stator windings of the exciter, the rotating electromagnetic field will be caused, and the field will induce the currents in the rotor windings of the exciter. But if the number of the poles in the exciter is the same with the number of the poles in the synchronous motor, the currents in the rotor windings of the exciter will no longer be induced, because there is no relative motion between the rotating electromagnetic field and rotor winding. Therefore, in such case, the currents in the stator windings should be obliged to be the negative phase sequence. If the number of the poles in the exciter differs from which in the synchronous motor, the stator windings can be connected in any phase sequence (positive or negative), in such way the exciter can always provide the exciting current for the synchronous motor. But if the difference between them is close, it is better to make the stator windings connected in negative phase sequence, so the field current can meet the requirement. The test machine in this paper is in accordance with the latter case.

The equivalent circuit, the power flow and the relative parameters are studied in this paper, and the details are presented in the following sections.

## 2 EQUIVALENT CIRCUIT

The equivalent circuit method is one of the important methods in the analysis of electrical machine. Because the structures of brushless exciter are similar with wound rotor induction machine, there must have some relation between the equivalent circuit of exciter and the equivalent circuit of induction machine. In order to design the brushless exciter, the equivalent circuit must be established.

The voltage equation for the stator windings is expressed as

$$\dot{U}_1 = \dot{I}_1(R_1 + jX_{1\sigma}) - \dot{E}_1 \quad (1)$$

Where  $\dot{U}_1$  is the stator terminal voltage;

$\dot{I}_1$  is the stator current;  
 $R_1, X_{1\sigma}$  are the stator resistance and leakage reactance respectively;  
 $\dot{E}_1$  is the phase emf in the stator windings. It can be expressed as

$$\dot{E}_1 = -\dot{I}_m Z_m \quad (2)$$

Where  $\dot{I}_m$  is the exciting current;  
 $Z_m$  is the exciting impedance.

The positive direction is shown in the equivalent circuit of one phase in the stator windings as Fig.2 (a).

Similarly the voltage equation for one phase in the actual rotor winding can be written as:

$$\dot{U}_2 = -\dot{I}_2 (R_2 + jX_{2\sigma}) - \dot{E}_{2s} \quad (3)$$

Where  $\dot{E}_{2s}$  is the phase emf in rotor windings;  
 $\dot{I}_2$  is the rotor current;  
 $\dot{U}_2$  is the rotor voltage;

$R_2, X_{2\sigma}$  are the rotor resistance and leakage reactance respectively.

The equivalent circuit in one phase of the rotor windings and the positive directions are shown as Fig.2 (b) at the slip frequency.

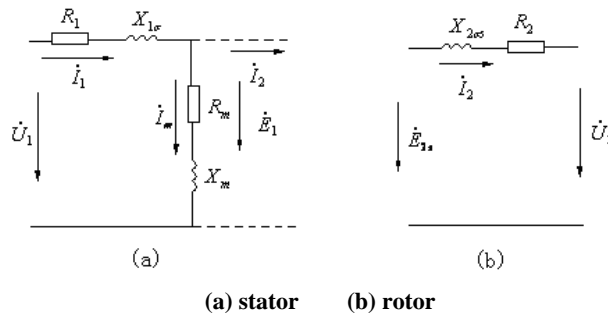


**Fig. 2 The Equivalent Circuit in One Phase.**

As the frequency and the number of the effective turns per phase between the stator and the rotor are different, they can not be linked together directly. In order to get an integral equivalent circuit, the voltages, the currents and the impedances in actual rotor should be referred to the stator. The converting method is the same with converting the secondary quantities to the primary ones in static transformer theories. Firstly, the frequency of the rotor's parameters in the equivalent circuit should be converted. Then Eq.(3) can be changed into

$$\frac{\dot{U}_2}{s} = -\dot{I}_2 \left( \frac{R_2}{s} + jX_{2\sigma} \right) - \dot{E}_2 \quad (4)$$

Where  $\dot{E}_2 = \frac{\dot{E}_{2s}}{s}$ ,  $X_{2\sigma} = \frac{X_{2\sigma}}{s}$ .

Secondly, the rotor winding should be referred to the stator side, i.e. the number of the phases and the number of the effective turns per phase in the rotor winding should be substituted for the equivalent winding with the same number of the phases and the effective turns as the stator winding. Consequently, the rotor voltage equation Eq.(4) is changed as

$$\frac{\dot{U}'_2}{s} = -\dot{I}'_2 \left( \frac{R'_2}{s} + jX'_{2\sigma} \right) - \dot{E}'_2 \quad (5)$$

Where  $I'_2 = \frac{I_2}{k_i}$ ,  $U'_2 = k_e U_2$ ,  $E'_2 = k_e E_2$ ,  $R'_2 = k_e k_i R_2$ ,  $X'_2 = k_e k_i X_2$ ,  $k_i = \frac{m_1 N_1 k_{w1}}{m_2 N_2 k_{w2}}$ ,

$$k_e = \frac{N_1 k_{w1}}{N_2 k_{w2}} \circ$$

With  $N_1$  and  $N_2$  are the numbers of turns of the stator winding and rotor winding respectively;  $m_1$  and  $m_2$  are the numbers of the phases of the stator winding and rotor winding respectively;  $k_{w1}$  and  $k_{w2}$  are the winding factors of the stator and rotor respectively.

The T-shape equivalent circuit can be achieved through the voltage equations of the brushless exciter (1), (2) and (5), as shown in Fig.3.

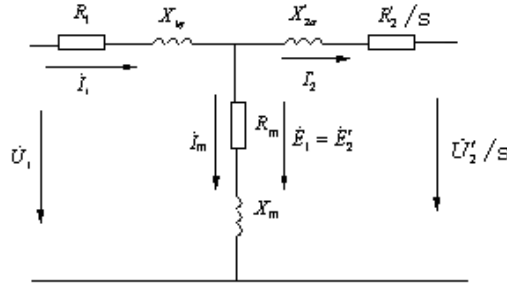


Fig. 3 The Referred Equivalent Circuit of the Brushless Exciter.

Based on the Fig.3, after some algebraic manipulation, the rotor voltage  $\dot{U}'_2$  and current  $\dot{I}'_2$  can be written in terms of the stator voltage  $\dot{U}_1$  and current  $\dot{I}_1$ :

$$\dot{I}'_2 = \frac{(Z_1 + Z_m)\dot{I}_1 - \dot{U}_1}{Z_m} \quad (6)$$

$$\frac{\dot{U}'_2}{s} = [Z_m - \frac{(Z'_2 + Z_m)(Z_1 + Z_m)}{Z_m}]\dot{I}_1 + \frac{Z'_2 + Z_m}{Z_m}\dot{U}_1 \quad (7)$$

Where stator impedance  $Z_1 = R_1 + jX_{1\sigma}$ , referred rotor impedance  $Z'_2 = R'_2/s + jX'_{2\sigma}$ , exciting impedance  $Z_m = R_m + jX_m$ , where the  $s$  is the slip ratio. Eq.(6) and (7) show the relationship among the rotor current, the rotor voltage, the stator winding quantities and the machine parameters. For the test machine, the phase current which is in negative sequence to the stator winding will create a reverse rotating field, whose speed is  $-n_s$ . So the slip ratio  $s$  is  $(-n_s - n)/-n_s$ , where the  $n$  is the rotor speed. In the test machine this paper,  $s=3$ , its basic data are shown in table I.

### 3 POWER FLOW

The brushless exciter has two AC terminals, one is at the stator side, and the other is at the rotor side. They both take part in the process of the energy transfer in operation. Therefore, the operating characteristics of the brushless exciter are complicated. The relationship between these powers is analyzed in detail as below.

Observing the equivalent circuit in Fig.3, it's easy to found that  $P_1$ , the supplied power in the stator winding, is consumed partly on the stator resistance, i.e. the stator copper loss  $P_{cu1}$ , partly on the stator core, i.e. stator core loss  $P_{Fe1}$ , and the rest is mostly as the electromagnetic power  $P_{m1}$ . So the following equation can be obtained.

$$P_1 - P_{cu1} - P_{Fe1} = P_{m1} \quad (8)$$

Where

$$P_1 = m_1 U_1 I_1 \cos \varphi_1 ;$$

$$P_{cu1} = m_1 I_1^2 R_1 ;$$

$$P_{Fe1} = m_1 I_m'^2 R_m \circ$$

For the rotor, the output power  $P_2$  of the rotor winding is derived from the rotor electromagnetic power  $P_{m2}$ . The difference between them is consumed at the rotor copper  $P_{cu2}$  and rotor iron loss  $P_{fe2}$ . The equation as below:

$$P_2 = P_{m2} - P_{cu2} - P_{fe2} \quad (9)$$

Where

$$P_2 = m_1 U_2' I_2' \cos \phi_2 ;$$

$$P_{cu2} = m_1 I_2'^2 R_2' \circ$$

The relationship between  $P_{m2}$  and  $P_{m1}$  can be derived from their definition in the equivalent circuit.

$$P_{m2} = s P_{m1} \quad (10)$$

Eq.(10) shows that, if the brushless exciter can provide current to the field winding of the synchronous motor, the slip ratio  $s$  should greater than zero. When  $s > 1$ , according to the energy conservation theory, the rotor electromagnetic power  $P_{m2}$  is supplied by both the stator electromagnetic power  $P_{m1}$  and the rotor mechanical power  $P_{meg}$ . When  $0 < s < 1$ , the stator electromagnetic power  $P_{m1}$  partly will be the  $P_{m2}$ , and partly costs on the  $P_{meg}$ . Therefore, in case of the large field current of the synchronous motor,  $s$  should be greater than 1. In such case, the expression can be written as

$$P_{m1} + P_{meg} = P_{m2} \quad (11)$$

For the test machine,  $s=3$ , the  $P_{m2}$  is obtained mostly from the mechanical power  $P_{meg}$ , few from the  $P_{m1}$ .

The actual mechanical power  $P_{meg}$  of the rotor can be expressed as

$$P_{meg} = P_M - P_{mec} - P_{ad} \quad (12)$$

Where  $P_M$  is the input mechanical power from the synchronous motor,

$P_{mec}$  is the mechanical loss (including the bearing loss and the ventilation loss),

$P_{ad}$  is the additional loss.

On the basis of the above analysis and eq.(8), (9), (11),(12), the diagram of power flow can be described as Fig.4.

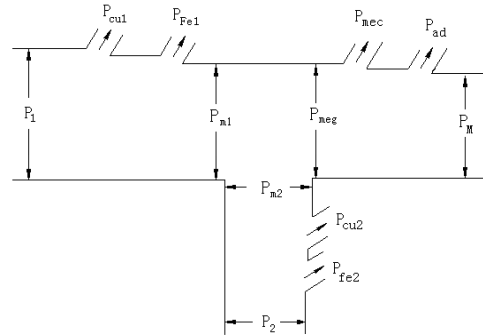


**Fig. 4 The Power Flow Diagram of the Brushless Exciter for Synchronous Motor.**

Moreover, the brushless excitation system is not only included the brushless exciter, but also involved in the rotating rectifier. It is necessary to analyze the relationship of the parameters before and after commutating.

#### 4 PARAMETER CALCULATION

The field current of synchronous motor is provided by the rotor output current of the brushless exciter through the rectifier. Because the field winding is a large nonlinear inductance load for the brushless exciter and the rotor winding of exciter itself is inductance, the rotor current could not jump immediately from one phase to another phase. It needs some time, and the commutating angle  $\gamma$  is used to represent it. The output current waveforms of the exciter's rotor winding are shown in Fig.5. To simplify the calculation, the current in one phase is approximated in Fig.6. Moreover, the direct current  $I_d$  in the field winding of the synchronous motor could keep constant, as the field winding of the synchronous motor being a large inductance load to the exciter.

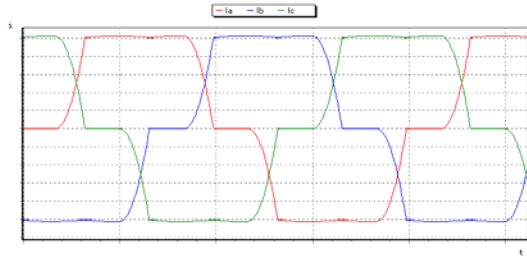


Fig. 5 The Current Waveforms for the Exciter's Rotor Winding.

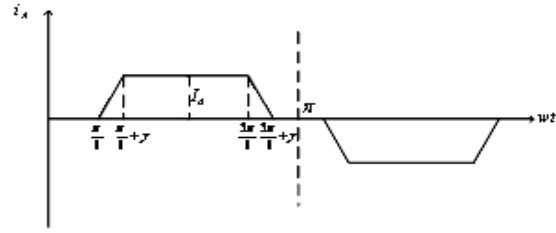


Fig. 6 The Current Waveform of the A Phase

The brushless exciting system is applied widely in fields of explosion proof, as the mining, petroleum and chemical industry etc. So the diodes are used in the rectifier. In this paper, the rectifier system is a three-phase six-pulse bridge, the other types of the rectifier are not discussed at here.

From the Fig.6, the function expression of A phase current can be represented as

$$i_A = \begin{cases} 0 & 0 \leq \omega t < \frac{\pi}{6} \\ \frac{I_d}{\gamma} (\omega t - \frac{\pi}{6}) & \frac{\pi}{6} \leq \omega t < \frac{\pi}{6} + \gamma \\ I_d & \frac{\pi}{6} + \gamma \leq \omega t < \frac{5\pi}{6} \\ \frac{I_d}{\gamma} (\frac{5\pi}{6} + \gamma - \omega t) & \frac{5\pi}{6} \leq \omega t < \frac{5\pi}{6} + \gamma \\ 0 & \frac{5\pi}{6} + \gamma \leq \omega t < \pi \end{cases} \quad (13)$$

The description of RMS amplitude for rotor current of exciter is

$$I = \sqrt{\frac{1}{\pi} \left\{ \int_{\frac{\pi}{6}}^{\frac{\pi}{6} + \gamma} i_{A1}^2 d\omega t + \int_{\frac{\pi}{6} + \gamma}^{\frac{5\pi}{6}} i_{A2}^2 d\omega t + \int_{\frac{5\pi}{6}}^{\frac{5\pi}{6} + \gamma} i_{A3}^2 d\omega t \right\}} \quad (14)$$

according to eq.(13),

$$i_{A1} = \frac{I_d}{\gamma} (\omega t - \frac{\pi}{6}); i_{A2} = I_d; i_{A3} = \frac{I_d}{\gamma} (\frac{5\pi}{6} + \gamma - \omega t)$$

Substitution of  $i_{A1}$ ,  $i_{A2}$ ,  $i_{A3}$  into Eq.(14), the relationship between the rotor current of the exciter and the field current of the motor can be obtained. It is as

$$I = \frac{I_d}{\sqrt{3\pi}} \cdot \sqrt{2\pi - \gamma} \quad (15)$$

where commutating angle is

$$\gamma = a \cos^{-1} \left( 1 - \frac{2I_d X_B}{\sqrt{6}U_2} \right) \quad (16)$$

Where the  $X_B$  is the total leakage reactance referred to the rotor. The  $U_2$  is the induced voltage of the rotor winding in the brushless exciter. The value of  $U_2$  is determined by the value of the voltage

and the current in the field winding in the synchronous motor. This relationship in Eq.(15) is important during the process of the electromagnetic design and calculation.

Moreover, the Eq. (13) is decomposed after the Fourier series theory.

$$i_A(t) = \sum_{n=1}^{\infty} \frac{8I_d}{\pi m^2} \sin n \frac{\gamma}{2} \sin n \left( \frac{\pi}{2} + \frac{\gamma}{2} \right) \sin n \frac{\pi}{3} \sin n \omega t \quad (17)$$

Observing the eq.(17), there are not triple harmonic currents in the rotor current of the exciter. This may be useful in the future study.

## 5 THE ELECTROMAGNETIC CALCULATION ON THE TEST MACHINE

Based on the operating principle, the equivalent circuit, the power loss and parameters for the brushless exciter and the excitation system as above mentioned, the software for the electromagnetic calculation on the brushless exciter for the synchronous motor is developed.

The test machine is calculated through the developed software. The basic data of the test synchronous motor and the exciter in the brushless excitation system are show in Table I. The results are shown in Table II.

**Table I The Basic Data of Experimental Motor and Exciter**

	value
synchronous motor	
rated power (kW)	42000
rated voltage (v)	10500
the number of pole	2
field current (A)	675
field voltage (V)	190
brushless exciter	
the number of pole	4
the number of stator slot	48
stator slot type	pear
stator winding	two-layer
the number of rotor slot	60
number of parallel circuit	2
rotor winding type	wave

**Table II The Results of Exciter's Magnetic Calculation**

parameter	value
stator current density (A/mm <sup>2</sup> )	4.43
flux density in stator tooth (T)	0.67
flux density in stator yoke (T)	0.55
flux density in the air gap(T)	0.35
rotor current density (A/mm <sup>2</sup> )	5.51
flux density in rotor tooth (T)	0.85
flux density in rotor yoke (T)	0.59
stator input power $P_1$ (kW)	56.29
mechanical power caused by motor $P_M$ (kW)	110.99
rotor output power $P_2$ (kW)	158.14
rotor line current (A)	545.61
rotor line voltage(V)	167.35
stator line voltage (V)	244.56
stator line current (A)	145.41
stator apparent power (kVA)	61.60

When the field current of the motor is 675A in testing, the stator voltage and current of the exciter are 265V and 150A respectively. Observing the Table II, the calculated results and tested results are approximate well. The absolute errors of them are 7.71% and 3.06% respectively.

## **6 CONCLUSION**

The equivalent circuit and the power flow of the brushless exciter used for synchronous motor are presented in this paper. The relationship between the rotor current of the exciter and the field current of the motor is given. Thus, the software for the electromagnetic calculation on the exciter is developed based on the study. The analysis is proved valid according to the test results.

## **BIBLIOGRAPHY**

- [1] Tang Y, et al. Electric Machinery,1993(In Chinese)
- [2] Dionysios C.Aliprantis ,et al. A brushless exciter model incorporating multiple rectifier modes and Preisach's hysteresis theory. IEEE Transactions on Energy Conversion,2006,2(1)
- [3] Yamamoto M. Active and reactive power control for doubly fed induction generator. IEEE Transactions on Power Electronics,1991,4(6)
- [4] Machmoum M.Steady-state analysis of a doubly-fed asynchronous machine supplied by a current-controlled cycloconverter in the rotor.PIEE-B. 1992,139(2):114-122

**Asymmetry of Windings Inductance in High-torque Low-speed Multi-unit  
Permanent Magnet Synchronous Motor**

**Zou Jibin**  
Harbin Institute of Technology  
China

**Zhao Bo**  
Harbin Institute of Technology  
China

**SUMMARY**

The high-torque low-speed PMSM directly driving the load without speed reducer can be widely used in electric propulsion fields. It is necessary to employed for the superpower drivers (i.e. higher level power device) which can support the large current. However, it would increase the cost of the PMSM drivers extremely. In order to solve the contradiction between the power output of the PMSM and the limitation of single driver output of power, the multi-unit winding topology with five units including five independent three-phase star-connected windings is proposed aiming to develop the PMSM with high-torque low-speed performance and high reliability. The unit motor can be operated independently or jointly.

During normal operation, the multi-unit PMSM is similar to the conventional three-phase PMSM. However, it is no longer regarded as a conventional three-phase PMSM when part of the units motor is in operation or the some of the units are in fault condition.

The mathematical model of the multi-unit PMSM is established. The mutual inductance and eletromagnetical torque under various of operation are derived by analysis method. Meanwhile, the expression of torque ripple are obtained under normal and faulty operation. On the other hand, the asymmetric mutual inductances is computed by using 2-D Finite Element Method (FEM). The harmonic components of torque ripple is computed with different currents of phase winding. The validity of analysis method can be verified by 2-D FEM.

**KEYWORDS**

Permanent magnet synchronous machine (PMSM), Multi-unit, Mutual inductance, Asymmetry, Torque ripple

# 1 INTRODUCTION

The high-torque low-speed PMSM directly driving the load without speed reducer can be widely used in electric propulsion fields. However, the superpower PMSM drivers need higher level power device which can support the large current, the cost of the PMSM drivers will be increased extremely. In order to solve the contradiction relation between the increasing PMSM output of power and limitation of single driver output of power, the multi-unit winding topology is proposed [1-2].

The parallel drive topology of multi-unit PMSM system is shown in Fig.1. In the parallel drive system, the five units can be constructed by CAN bus. One of them works as master unit, and the other four units work as slave units. The master unit harmonizes the five drive units operating parallel and gets the position signal, and broadcasts the speed and current to the slave units by CAN bus. The slave units can follow the current command rapidly through controlled by the current loop algorithm.

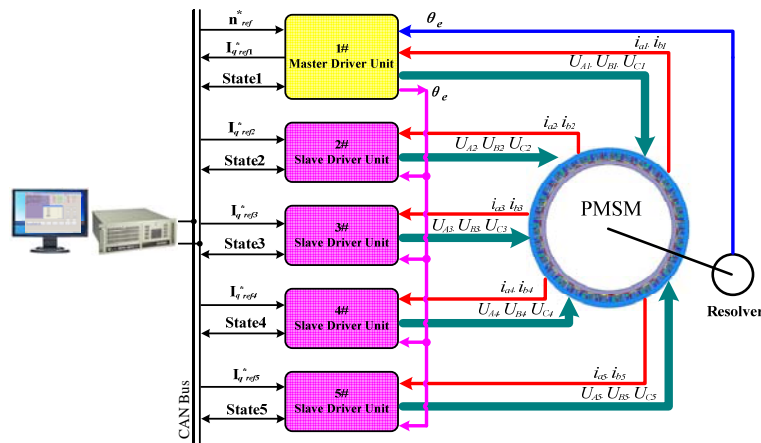


Fig. 1 Multi-unit PMSM System.

The Space Vector PWM (SVPWM) control algorithm is adopted in the five unit parallel operation drive system. The water-cooling method is adopted in the system. The high-torque low-speed PMSM system (i.e. multi-unit PMSM) consists of five units and each unit is composed of a driver and a set of independent three-phase star-connected windings. The power of 400kW is provided by each unit at the speed of 100rpm, and the PMSM can output of 2MW steadily if all units are adopted under normal operation. The fault tolerance and reliability can be improved by selection of the multi-unit construction. During the faulty operation, the faulty unit can be separated from the power supply, and the other units can be worked under normal condition.

# 2 WINDINGS CONNECTION AND MATHEMATICAL MODEL

The multi-unit PMSM windings connection is shown in Fig. 2.

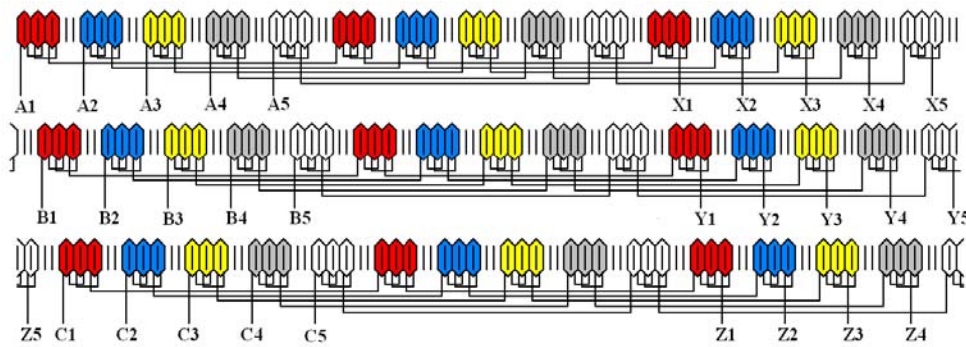


Fig. 2 Five units' Windings Connection.

Each unit has the three-phase star-connected windings, which can work independently and adjacent 120° electrical degree. Every unit windings occupy a fan-shaped region in the stator. For Example,

the unit 1 is composed of the winding A1, B1, and C1. In Fig. 2, the different background colour windings mean different units and each phase winding consists of three pole-phase groups.

## 2.2 Mathematical model

The basic voltage equation [3-4] can be expressed as following

$$\begin{bmatrix} U_{A1} \\ U_{B1} \\ U_{C1} \\ U_{A2} \\ U_{B2} \\ U_{C2} \\ U_{A3} \\ U_{B3} \\ U_{C3} \\ U_{A4} \\ U_{B4} \\ U_{C4} \\ U_{A5} \\ U_{B5} \\ U_{C5} \end{bmatrix} = R_a \begin{bmatrix} I_{A1} \\ I_{B1} \\ I_{C1} \\ I_{A2} \\ I_{B2} \\ I_{C2} \\ I_{A3} \\ I_{B3} \\ I_{C3} \\ I_{A4} \\ I_{B4} \\ I_{C4} \\ I_{A5} \\ I_{B5} \\ I_{C5} \end{bmatrix} + p \begin{bmatrix} L_{A1} & M_{A1B1} & M_{A1C1} & M_{A1A2} & M_{A1B2} & M_{A1C2} & M_{A1A3} & M_{A1B3} & M_{A1C3} & M_{A1A4} & M_{A1B4} & M_{A1C4} & M_{A1A5} & M_{A1B5} & M_{A1C5} \\ M_{A1B1} & L_{B1} & M_{B1C1} & M_{B1A2} & M_{B1B2} & M_{B1C2} & M_{B1A3} & M_{B1B3} & M_{B1C3} & M_{B1A4} & M_{B1B4} & M_{B1C4} & M_{B1A5} & M_{B1B5} & M_{B1C5} \\ M_{A1C1} & M_{B1C1} & L_{C1} & M_{C1A2} & M_{C1B2} & M_{C1C2} & M_{C1A3} & M_{C1B3} & M_{C1C3} & M_{C1A4} & M_{C1B4} & M_{C1C4} & M_{C1A5} & M_{C1B5} & M_{C1C5} \\ L_{A2} & M_{A2B2} & M_{A2C2} & L_{A2} & M_{A2B2} & M_{A2C2} & L_{A3} & M_{A3B3} & M_{A3C3} & L_{A4} & M_{A4B4} & M_{A4C4} & L_{A5} & M_{A5B5} & M_{A5C5} \\ M_{B2A2} & L_{B2} & M_{B2C2} & M_{B2A3} & M_{B2B3} & M_{B2C3} & M_{B2A4} & M_{B2B4} & M_{B2C4} & M_{B2A5} & M_{B2B5} & M_{B2C5} \\ M_{C2A2} & M_{C2B2} & L_{C2} & M_{C2A3} & M_{C2B3} & M_{C2C3} & M_{C2A4} & M_{C2B4} & M_{C2C4} & M_{C2A5} & M_{C2B5} & M_{C2C5} \\ M_{A3A3} & M_{A3B3} & M_{A3C3} & M_{A3A4} & M_{A3B4} & M_{A3C4} & M_{A3A5} & M_{A3B5} & M_{A3C5} \\ M_{A1B3} & M_{B1B3} & M_{C1B3} & M_{A2B3} & M_{B2B3} & M_{C2B3} & M_{A3B3} & L_{B3} & M_{B3C3} & M_{B3A4} & M_{B3B4} & M_{B3C4} & M_{B3A5} & M_{B3B5} & M_{B3C5} \\ M_{A1C3} & M_{B1C3} & M_{C1C3} & M_{A2C3} & M_{B2C3} & M_{C2C3} & M_{A3C3} & M_{B3C3} & L_{C3} & M_{C3A4} & M_{C3B4} & M_{C3C4} & M_{C3A5} & M_{C3B5} & M_{C3C5} \\ M_{A1A4} & M_{B1A4} & M_{C1A4} & M_{A2A4} & M_{B2A4} & M_{C2A4} & M_{A3A4} & M_{B3A4} & M_{C3A4} & L_{A4} & M_{A4B4} & M_{A4C4} & M_{A4A5} & M_{A4B5} & M_{A4C5} \\ M_{A1B4} & M_{B1B4} & M_{C1B4} & M_{A2B4} & M_{B2B4} & M_{C2B4} & M_{A3B4} & M_{B3B4} & M_{C3B4} & M_{A4B4} & L_{B4} & M_{B4C4} & M_{B4A5} & M_{B4B5} & M_{B4C5} \\ M_{A1C4} & M_{B1C4} & M_{C1C4} & M_{A2C4} & M_{B2C4} & M_{C2C4} & M_{A3C4} & M_{B3C4} & M_{C3C4} & M_{A4C4} & M_{B4C4} & L_{C4} & M_{C4A5} & M_{C4B5} & M_{C4C5} \\ M_{A1A5} & M_{B1A5} & M_{C1A5} & M_{A2A5} & M_{B2A5} & M_{C2A5} & M_{A3A5} & M_{B3A5} & M_{C3A5} & M_{A4A5} & M_{B4A5} & M_{C4A5} & L_{A5} & M_{A5B5} & M_{A5C5} \\ M_{A1B5} & M_{B1B5} & M_{C1B5} & M_{A2B5} & M_{B2B5} & M_{C2B5} & M_{A3B5} & M_{B3B5} & M_{C3B5} & M_{A4B5} & M_{B4B5} & M_{C4B5} & M_{A5B5} & L_{B5} & M_{B5C5} \\ M_{A1C5} & M_{B1C5} & M_{C1C5} & M_{A2C5} & M_{B2C5} & M_{C2C5} & M_{A3C5} & M_{B3C5} & M_{C3C5} & M_{A4C5} & M_{B4C5} & M_{C4C5} & M_{A5C5} & M_{B5C5} & L_{C5} \end{bmatrix} \begin{bmatrix} I_{A1} \\ I_{B1} \\ I_{C1} \\ I_{A2} \\ I_{B2} \\ I_{C2} \\ I_{A3} \\ I_{B3} \\ I_{C3} \\ I_{A4} \\ I_{B4} \\ I_{C4} \\ I_{A5} \\ I_{B5} \\ I_{C5} \end{bmatrix} \quad (1)$$

Where  $U_{Ai}$ ,  $U_{Bi}$ ,  $U_{Ci}$  is the three-phase windings voltage of unit driver  $i$  ( $i=1, 2, 3, 4, 5$ ),  $E_{Ai}$ ,  $E_{Bi}$ ,  $E_{Ci}$  is the three-phase windings EMF of unit motor  $i$ ,  $I_{Ai}$ ,  $I_{Bi}$ ,  $I_{Ci}$  is the three-phase windings current of unit  $i$ ,  $R_a$  is windings resistance matrix,  $p$  means differential operator.

The inductance matrix in the equation (1) could be transformed into different forms when different number and space position of unit operating. The inductance matrix is also expressed as equation (2)

$$L = \begin{bmatrix} L_1 & M_1 & M_2 & M_3 & M_4 \\ M_1^T & L_1 & M_1 & M_2 & M_3 \\ M_2^T & M_1^T & L_1 & M_1 & M_2 \\ M_3^T & M_2^T & M_1^T & L_1 & M_1 \\ M_4^T & M_3^T & M_2^T & M_1^T & L_1 \end{bmatrix} \quad (2)$$

The sub matrix is expressed by equation (3), and all different unit quantity or space position operation can be composed by different sub-matrix.

$$L_1 = \begin{bmatrix} L_A & M_{AB} & M_{AC} \\ M_{AB} & L_B & M_{BC} \\ M_{AC} & M_{BC} & L_C \end{bmatrix} \quad M_1 = \begin{bmatrix} M_{A1A2} & M_{A1B2} & M_{A1C2} \\ M_{B1A2} & M_{B1B2} & M_{B1C2} \\ M_{C1A2} & M_{C1B2} & M_{C1C2} \end{bmatrix} \quad M_2 = \begin{bmatrix} M_{A1A3} & M_{A1B3} & M_{A1C3} \\ M_{B1A3} & M_{B1B3} & M_{B1C3} \\ M_{C1A3} & M_{C1B3} & M_{C1C3} \end{bmatrix} \\ M_3 = \begin{bmatrix} M_{A1A4} & M_{A1B4} & M_{A1C4} \\ M_{B1A4} & M_{B1B4} & M_{B1C4} \\ M_{C1A4} & M_{C1B4} & M_{C1C4} \end{bmatrix} \quad M_4 = \begin{bmatrix} M_{A1A5} & M_{A1B5} & M_{A1C5} \\ M_{B1A5} & M_{B1B5} & M_{B1C5} \\ M_{C1A5} & M_{C1B5} & M_{C1C5} \end{bmatrix} \quad (3)$$

The inductance matrix in the voltage equation (1) is decomposed into each sub-matrix. For example, when unit 1# and 3# operating, the inductance matrix in the voltage equation will be composed by  $L_1$  and  $M_3$  sub-matrix.

## 3. ASYMMETRIC MUTUAL INDUCTANCE AND TORQUE RIPPLE

### 3.1 Asymmetric mutual inductance

#### 3.1.1 Mutual Inductance Analysis and Parker Transform

Multi-unit PMSM inductance is correspond with the ideal motor assumptions, and the self inductance and mutual inductance can be expressed as from equation (4) to (13). The inductance can be approximately composed by constant component and the 2<sup>nd</sup> harmonic component.

$$\begin{cases} L_A = L_{S0} - L_{S2} \cos 2\theta \\ L_B = L_{S0} - L_{S2} \cos 2(\theta - 120^\circ) \\ L_C = L_{S0} - L_{S2} \cos 2(\theta + 120^\circ) \end{cases} \quad (4) \quad \begin{cases} M_{A1B1} = -M_{S00} - M_{S20} \cos 2(\theta + 120^\circ) \\ M_{B1C1} = -M_{S00} - M_{S20} \cos 2(\theta) \\ M_{A1C1} = -M_{S01} - M_{S21} \cos 2(\theta - 120^\circ) \end{cases} \quad (5)$$

$$\begin{cases} M_{A1A2} = -M_{S02} + M_{S22} \cos 2(\theta) \\ M_{B1B2} = -M_{S02} + M_{S22} \cos 2(\theta - 120^\circ) \\ M_{C1C2} = -M_{S02} + M_{S22} \cos 2(\theta + 120^\circ) \end{cases} \quad (6)$$

$$\begin{cases} M_{A1A3} = -M_{S05} + M_{S25} \cos 2\theta \\ M_{B1B3} = -M_{S03} + M_{S23} \cos 2(\theta - 120^\circ) \\ M_{C1C3} = -M_{S03} + M_{S23} \cos 2(\theta + 120^\circ) \end{cases} \quad (7)$$

$$\begin{cases} M_{A1A4} = -M_{S05} + M_{S25} \cos 2\theta \\ M_{B1B4} = -M_{S05} + M_{S25} \cos 2(\theta - 120^\circ) \\ M_{C1C4} = -M_{S05} + M_{S25} \cos 2(\theta + 120^\circ) \end{cases} \quad (8)$$

$$\begin{cases} M_{A1A5} = -M_{S02} + M_{S22} \cos 2\theta \\ M_{B1B5} = -M_{S02} + M_{S22} \cos 2(\theta - 120^\circ) \\ M_{C1C5} = -M_{S02} + M_{S22} \cos 2(\theta + 120^\circ) \end{cases} \quad (9)$$

$$\begin{cases} M_{A1B2} = -M_{S03} - M_{S23} \cos 2(\theta + 120^\circ) \\ M_{B1A2} = -M_{S01} - M_{S21} \cos 2(\theta + 120^\circ) \\ M_{B1C2} = -M_{S03} - M_{S23} \cos 2(\theta) \\ M_{C1B2} = -M_{S01} - M_{S21} \cos 2(\theta) \\ M_{A1C2} = -M_{S04} - M_{S24} \cos 2(\theta - 120^\circ) \\ M_{C1A2} = -M_{S00} - M_{S20} \cos 2(\theta - 120^\circ) \end{cases} \quad (10)$$

$$\begin{cases} M_{A1B3} = -M_{S06} - M_{S26} \cos 2(\theta + 120^\circ) \\ M_{B1A3} = -M_{S04} - M_{S24} \cos 2(\theta + 120^\circ) \\ M_{B1C3} = -M_{S06} - M_{S26} \cos 2(\theta) \\ M_{C1B3} = -M_{S04} - M_{S24} \cos 2(\theta) \\ M_{A1C3} = -M_{S07} - M_{S27} \cos 2(\theta - 120^\circ) \\ M_{C1A3} = -M_{S03} - M_{S23} \cos 2(\theta - 120^\circ) \end{cases} \quad (11)$$

$$\begin{cases} M_{A1B4} = -M_{S04} - M_{S24} \cos 2(\theta + 120^\circ) \\ M_{B1A4} = -M_{S06} - M_{S26} \cos 2(\theta + 120^\circ) \\ M_{B1C4} = -M_{S04} - M_{S24} \cos 2(\theta) \\ M_{C1B4} = -M_{S06} - M_{S26} \cos 2(\theta) \\ M_{A1C4} = -M_{S03} - M_{S23} \cos 2(\theta - 120^\circ) \\ M_{C1A4} = -M_{S07} - M_{S27} \cos 2(\theta - 120^\circ) \end{cases} \quad (12)$$

$$\begin{cases} M_{A1B5} = -M_{S01} - M_{S21} \cos 2(\theta + 120^\circ) \\ M_{B1A5} = -M_{S03} - M_{S23} \cos 2(\theta + 120^\circ) \\ M_{B1C5} = -M_{S01} - M_{S21} \cos 2(\theta) \\ M_{C1B5} = -M_{S03} - M_{S23} \cos 2(\theta) \\ M_{A1C5} = -M_{S00} - M_{S20} \cos 2(\theta - 120^\circ) \\ M_{C1A5} = -M_{S04} - M_{S24} \cos 2(\theta - 120^\circ) \end{cases} \quad (13)$$

Where  $M_{AiAj}$ ,  $M_{BiBj}$  and  $M_{CiCj}$  is same phase mutual inductance between different unit ( $i, j=1, 2, 3, 4, 5$  and  $i \neq j$ ),  $M_{AmBn}$ ,  $M_{BmCn}$  and  $M_{AmCn}$  is different phase mutual inductance between different unit ( $m, n=1, 2, 3, 4, 5$  and  $m \neq n$ ),  $M_{S0x}$  is the constant component of mutual inductance and  $M_{S2x}$  is the second harmonic component ( $x=0, 1, 2, 3, 4, 5, 6, 7$ ).

Each  $M_{S0x}$  and  $M_{S2x}$  is not same value due to the different magnetic conductivity between phase windings, therefore the inequality (14) and (15) is founded.

$$M_{S00} > M_{S01} > M_{S02} > M_{S03} > M_{S04} > M_{S05} > M_{S06} = M_{S07} \quad (14)$$

$$M_{S20} > M_{S21} > M_{S22} > M_{S23} > M_{S24} > M_{S25} > M_{S26} = M_{S27} \quad (15)$$

From equation (5)~(15), it draws a conclusion that the mutual inductance between different windings is asymmetric. Further more, the Park Transform is used to analyse the multi-unit PMSM torque ripple. The last Park Transform results of equation (3) is shown as follow

$$M_{dq} = \frac{2}{3} \sin(2\theta - \frac{\pi}{3}) \cdot (M_{S00} - M_{S01}) + \frac{1}{3} \sin(4\theta + \frac{\pi}{3}) \cdot (M_{S20} - M_{S21}) \quad (16)$$

$$M_{d1q1} = \frac{\sqrt{3}}{6} (-M_{S00} + 2M_{S01} - 2M_{S03} + M_{S04}) + \frac{1}{3} \sin(2\theta - \frac{1}{3}\pi) \cdot (-M_{S00} + M_{S01} + M_{S03} - M_{S04}) + \left[ \frac{1}{6} \sin(2\theta) + \frac{1}{6} \sin(2\theta + \frac{\pi}{3}) \right] \cdot (M_{S20} + M_{S21} - M_{S23} - M_{S24}) + \frac{1}{6} \sin(4\theta + \frac{\pi}{3}) \cdot (-M_{S20} + M_{S21} + M_{S23} - M_{S24}) \quad (17)$$

$$M_{q1d1} = \frac{\sqrt{3}}{6} (M_{S00} - 2M_{S01} + 2M_{S03} - M_{S04}) + \frac{1}{3} \sin(2\theta - \frac{1}{3}\pi) \cdot (-M_{S00} + M_{S01} + M_{S03} - M_{S04}) + \left[ \frac{1}{6} \sin(2\theta) + \frac{1}{6} \sin(2\theta + \frac{\pi}{3}) \right] \cdot (-M_{S20} - M_{S21} + M_{S23} + M_{S24}) + \frac{1}{6} \sin(4\theta + \frac{\pi}{3}) \cdot (-M_{S20} + M_{S21} + M_{S23} - M_{S24}) \quad (18)$$

$$M_{d2q2} = \frac{\sqrt{3}}{6} (-M_{S03} + 2M_{S04} - 2M_{S06} + M_{S07}) + \frac{1}{3} \sin(2\theta - \frac{1}{3}\pi) \cdot (-M_{S03} + M_{S04} + M_{S06} - M_{S07}) +$$

$$\left[ \frac{1}{6} \sin(2\theta) + \frac{1}{6} \sin(2\theta + \frac{\pi}{3}) \right] \cdot (M_{S23} + M_{S24} - M_{S26} - M_{S27}) + \frac{1}{6} \sin(4\theta + \frac{\pi}{3}) \cdot (-M_{S23} + M_{S24} + M_{S26} - M_{S27}) \quad (19)$$

$$M_{q2d2} = \frac{\sqrt{3}}{6} (M_{S03} - 2M_{S04} + 2M_{S06} - M_{S07}) + \frac{1}{3} \sin(2\theta - \frac{1}{3}\pi) \cdot (-M_{S03} + M_{S04} + M_{S06} - M_{S07}) +$$

$$\left[ \frac{1}{6} \sin(2\theta) + \frac{1}{6} \sin(2\theta + \frac{\pi}{3}) \right] \cdot (-M_{S23} - M_{S24} + M_{S26} + M_{S27}) + \frac{1}{6} \sin(4\theta + \frac{\pi}{3}) \cdot (-M_{S23} + M_{S24} + M_{S26} - M_{S27}) \quad (20)$$

$$M_{d3q3} = \frac{\sqrt{3}}{6} (-M_{S07} + 2M_{S06} - 2M_{S04} + M_{S03}) + \frac{1}{3} \sin(2\theta - \frac{1}{3}\pi) \cdot (-M_{S07} + M_{S06} + M_{S04} - M_{S03}) +$$

$$\left[ \frac{1}{6} \sin(2\theta) + \frac{1}{6} \sin(2\theta + \frac{\pi}{3}) \right] \cdot (M_{S27} + M_{S26} - M_{S24} - M_{S23}) + \frac{1}{6} \sin(4\theta + \frac{\pi}{3}) \cdot (-M_{S27} + M_{S26} + M_{S24} - M_{S23}) \quad (21)$$

$$M_{q3d3} = \frac{\sqrt{3}}{6} (M_{S07} - 2M_{S06} + 2M_{S04} - M_{S03}) + \frac{1}{3} \sin(2\theta - \frac{1}{3}\pi) \cdot (-M_{S07} + M_{S06} + M_{S04} - M_{S03})$$

$$\left[ \frac{1}{6} \sin(2\theta) + \frac{1}{6} \sin(2\theta + \frac{\pi}{3}) \right] \cdot (-M_{S27} - M_{S26} + M_{S24} + M_{S23}) + \frac{1}{6} \sin(4\theta + \frac{\pi}{3}) \cdot (-M_{S27} + M_{S26} + M_{S24} - M_{S23}) \quad (22)$$

$$M_{d4q4} = \frac{\sqrt{3}}{6} (-M_{S04} + 2M_{S03} - 2M_{S01} + M_{S00}) + \frac{1}{3} \sin(2\theta - \frac{1}{3}\pi) \cdot (-M_{S04} + M_{S03} + M_{S01} - M_{S00}) +$$

$$\left[ \frac{1}{6} \sin(2\theta) + \frac{1}{6} \sin(2\theta + \frac{\pi}{3}) \right] \cdot (M_{S24} + M_{S23} - M_{S21} - M_{S20}) + \frac{1}{6} \sin(4\theta + \frac{\pi}{3}) \cdot (-M_{S24} + M_{S23} + M_{S21} - M_{S20}) \quad (23)$$

$$M_{q4d4} = \frac{\sqrt{3}}{6} (M_{S04} - 2M_{S03} + 2M_{S01} - M_{S00}) + \frac{1}{3} \sin(2\theta - \frac{1}{3}\pi) \cdot (-M_{S04} + M_{S03} + M_{S01} - M_{S00}) +$$

$$\left[ \frac{1}{6} \sin(2\theta) + \frac{1}{6} \sin(2\theta + \frac{\pi}{3}) \right] \cdot (-M_{S24} - M_{S23} + M_{S21} + M_{S20}) + \frac{1}{6} \sin(4\theta + \frac{\pi}{3}) \cdot (-M_{S24} + M_{S23} + M_{S21} - M_{S20}) \quad (24)$$

### 3.1.2 Mutual Inductance of the Numerical Calculation

It is essential to establish two-dimensional (2-D) finite element method (FEM) to accurately predict the asymmetric mutual inductance. Fig.3 shows the flux distribution of the multi-unit PMSM. Fig. 4 presents the coefficient mutual inductance of single unit. It can be seen that the fundamental and 2<sup>nd</sup> harmonic components of  $M_{A1C1}$  is smaller than those of  $M_{A1B1}$  and  $M_{B1C1}$ . In other words, the mutual inductance of three phases are asymmetric in waveform.

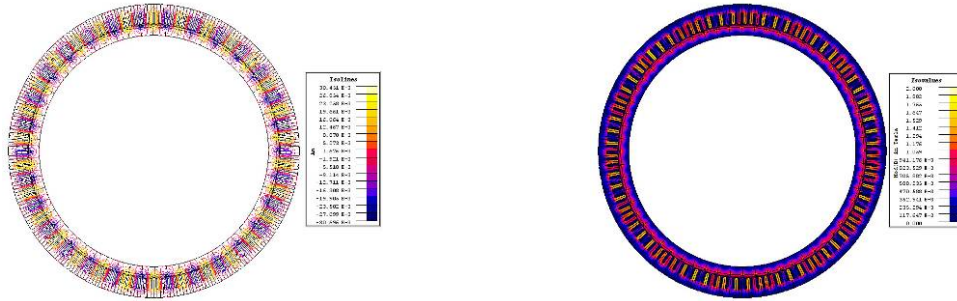


Fig. 3 (a) Flux Line distribution on no-load condition. (b) Flux Density distribution on no-load condition.

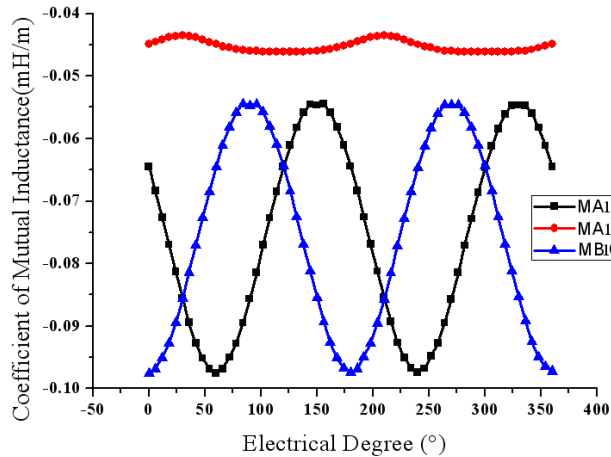


Fig. 4 Asymmetric Mutual Inductance in One Unit.

### 3.2 Torque ripple analysis

#### 3.2.1 Electromagnetic Torque Equation Mathematical Analysis

The maximum current/torque control strategy is adopted in the multi-unit PMSM system, (i.e. the D-axis current is equal to zero). It is assumed that three-phase currents are strictly symmetrical in all of units machine. When the unit 1# is adopted under normal operation and the other units are adopted under fault or downtime operation, the electromagnetic torque can be expressed by the following equation (25)

$$T_e = p_n \left[ \psi_f i_q + (L_d - L_q) i_d i_q + M_{dq} i_q^2 - M_{qd} i_d^2 \right] \quad (25)$$

Considering  $I_d=0$ , equation (25) can be also expressed by equation (26)

$$T_e = p_n (\psi_f i_q + M_{dq} i_q^2) \quad (26)$$

Similarly, when the unit 1# and 2# are adopted under normal operation, electromagnetic torque can be written as follows equation (27). The torque equations in other operations are also easily obtained.

$$T_e = p_n \left[ (\psi_{d1} i_{q1} - \psi_{q1} i_{d1}) + (\psi_{d2} i_{q2} - \psi_{q2} i_{d2}) \right] = p_n \left[ 2\psi_f I_q + (2M_{dq} + M_{d1q1} + M_{q1d1}) I_q^2 \right] \quad (27)$$

The different kinds of multi-unit PMSM operation are listed in the Table I, according to the variety of space distribution and number of the unit motor. The 2<sup>nd</sup> and 4<sup>th</sup> harmonic components of torque ripple is presented.

**Table I Torque Ripple When Different Unit Operation.**

Unit Numbers	Harmonic order torque	Harmonic torque amplitude
Unit 1#	2nd	$ T_{\Delta 2}  = \frac{2}{3} p_n I_q^2 (M_{s00} - M_{s01})$
	4th	$ T_{\Delta 4}  = \frac{1}{3} p_n I_q^2 (M_{s20} - M_{s21})$
Unit 1# and 2#	2nd	$ T_{\Delta 2}  = \frac{2}{3} p_n I_q^2 (M_{s00} - M_{s01} + M_{s03} - M_{s04}) \approx \frac{2}{3} p_n I_q^2 (M_{s00} - M_{s01})$
	4th	$ T_{\Delta 4}  = \frac{1}{3} p_n I_q^2 (M_{s20} - M_{s21} + M_{s23} - M_{s24}) \approx \frac{1}{3} p_n I_q^2 (M_{s20} - M_{s21})$
Unit 1# and 3#	2nd	$ T_{\Delta 2}  = \frac{2}{3} p_n I_q^2 (2M_{s00} - 2M_{s01} - M_{s03} + M_{s04}) \approx \frac{4}{3} p_n I_q^2 (M_{s00} - M_{s01})$
	4th	$ T_{\Delta 4}  = \frac{1}{3} p_n I_q^2 (2M_{s20} - 2M_{s21} - M_{s23} + M_{s24}) \approx \frac{2}{3} p_n I_q^2 (M_{s20} - M_{s21})$
Unit 1# 2# and 3#	2nd	$ T_{\Delta 2}  = \frac{2}{3} p_n I_q^2 (M_{s00} - M_{s01} + M_{s03} - M_{s04}) \approx \frac{2}{3} p_n I_q^2 (M_{s00} - M_{s01})$
	4th	$ T_{\Delta 4}  = \frac{1}{3} p_n I_q^2 (M_{s20} - M_{s21} + M_{s23} - M_{s24}) \approx \frac{1}{3} p_n I_q^2 (M_{s20} - M_{s21})$
Unit 1# 2# and 4#	2nd	$ T_{\Delta 2}  = \frac{2}{3} p_n I_q^2 (2M_{s00} - 2M_{s01} + M_{s04} - M_{s03}) \approx \frac{4}{3} p_n I_q^2 (M_{s00} - M_{s01})$
	4th	$ T_{\Delta 4}  = \frac{1}{3} p_n I_q^2 (2M_{s20} - 2M_{s21} - M_{s24} + M_{s23}) \approx \frac{2}{3} p_n I_q^2 (M_{s20} - M_{s21})$
Unit 1# 2# 3# and 4#	2nd	$ T_{\Delta 2}  = \frac{2}{3} p_n I_q^2 (M_{s00} - M_{s01})$
	4th	$ T_{\Delta 4}  = \frac{1}{3} p_n I_q^2 (M_{s20} - M_{s21})$
Unit 1# 2# 3# 4# and 5# (All Units)	2nd	$ T_{\Delta 2}  = \frac{2}{3} p_n I_q^2 (M_{s06} - M_{s07}) = 0$
	4th	$ T_{\Delta 4}  = \frac{1}{3} p_n I_q^2 (M_{s26} - M_{s27}) = 0$

### 3.2.2 Electromagnetic Torque Ripple FEM Analysis

The FEM is employed in order to verify the validity of analysis method. Fig. 5 shows the variation of electromagnetic torque ripple as function of phase currents, assuming that the only one unit of motor is adopted under normal operation. It can be seen that the 2<sup>nd</sup>, 4<sup>th</sup> and 6<sup>th</sup> harmonic components increase as the phase current increases. For the further analysis, the value of 2<sup>nd</sup> harmonic component is the same as that of 4<sup>th</sup> harmonic component, and they are main portion in the harmonic of torque ripple due to the existence of asymmetric inductance.

Fig.6 presents the variation of electromagnetic torque ripple as function of phase currents, assuming that the only two units of motor are adopted under normal operation. It can be seen that the 2<sup>nd</sup> and 4<sup>th</sup> harmonic components of unit 1# 3# are higher than those of unit 1# 2# given the same current. A similar trend is observed, the 6<sup>th</sup> and 12<sup>th</sup> harmonic components of unit 1# 3# are higher than those of unit 1# 2# given the same current.

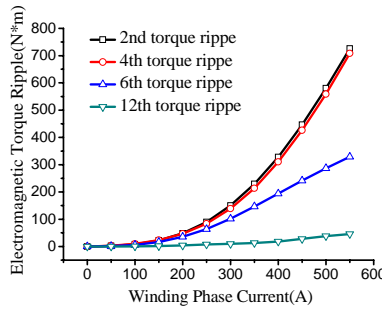


**Fig. 5 Torque Ripple When Only Unit 1# Running.**

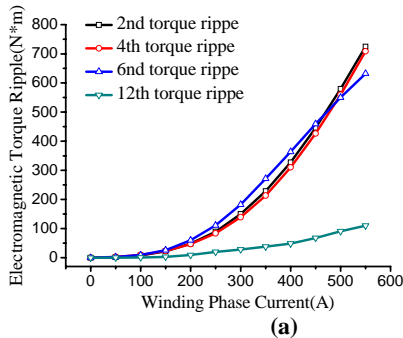
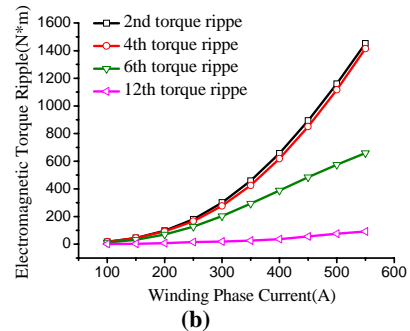


**Fig.6 (a) Torque Ripple When Unit 1# and 2# Running.**



**(b) Torque Ripple When Unit 1# and 3# Running.**

Fig.7 presents the variation of electromagnetic torque ripple as function of phase currents, assuming that the only three units of motor (i.e. unit 1# 2# and 3# or unit 1# 2# and 4#) are adopted under normal operation. It can be seen that the 2<sup>nd</sup>, 4<sup>th</sup> and 6<sup>th</sup> harmonic components increase as the phase current increases.

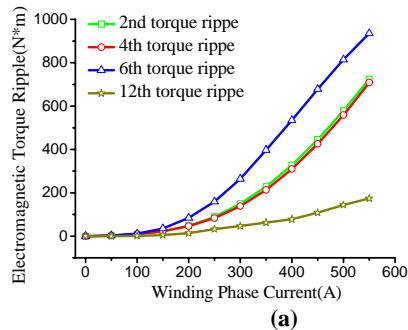
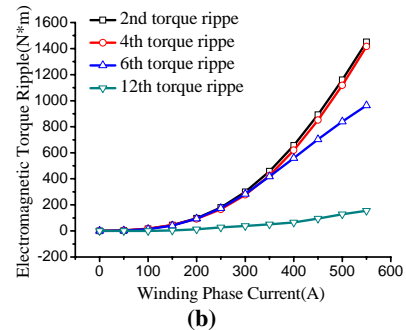


**Fig.7 (a) Torque Ripple When Unit 1# 2# and 3# Running.**



**(b) Torque Ripple When Unit 1# 2# and 4# Running.**

Fig.8 shows the variation of electromagnetic torque ripple as function of phase currents, assuming that the only four units of motor (i.e. unit 1# 2# 3# and 4#) are adopted under normal operation. It can be seen that the 2<sup>nd</sup>, 4<sup>th</sup> and 6<sup>th</sup> harmonic components increase as the phase current increases. It should be noted that the 6<sup>th</sup> harmonic component is main portion in the harmonic of torque ripple.

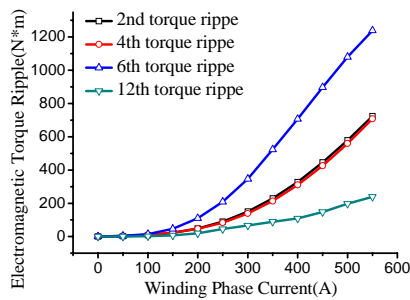


Fig. 8: Torque Ripple When Unit 1# 2# 3# and 4# Running.

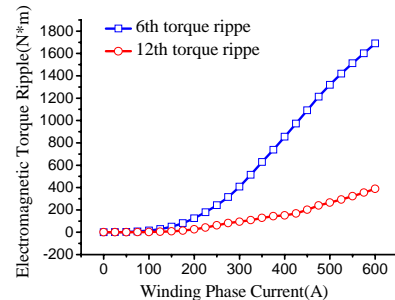


Fig. 9: Torque Ripple When All Units Running.

Fig.9 presents the variation of electromagnetic torque ripple as function of phase currents, assuming that the five units of motor are adopted under normal operation. It can be seen that only the 6<sup>th</sup> and 12<sup>th</sup> harmonic components exists.

#### 4 CONCLUSION

- (1) During normal operation, multi-unit PMSM is very similar to the conventional three-phase PMSM, and the torque ripple is relative minimum. However, the multi-unit PMSM is no longer regarded as a conventional three-phase PMSM, due to the existence of asymmetric mutual inductance.
- (2) The 2nd harmonic component of torque ripple is caused by the asymmetric constant of mutual inductance in unit motor. The 4th harmonic component of torque ripple is caused by the asymmetric amplitude 2nd harmonic of mutual inductance in unit motor.
- (3) The amplitude of 2<sup>nd</sup> harmonic torque ripple of one unit is equal to that of the several adjacent units. The same conclusion also applies to 4<sup>th</sup> harmonic torque ripple. The amplitude 2<sup>nd</sup> and 4<sup>th</sup> harmonic torque ripple of several units spacing one unit is twice that of adjacent units. In other words, it had better choose the adjacent units to reduce the toque ripple under the fault condition.

#### BIBLIOGRAPHY

- [1] Zhao P , Yang G , Liu J.Multi-unit motor parallel drive system for electric vehicle application[C]//IEEE Vehicle Power and Propulsion Conference, 2008
- [2] Zhang B, Liu Y, Feng G.Study on low voltage high power multi-branch permanent magnet synchronous motor[C]//Power and Energy Engineering Conference, 2010
- [3] Gao J, Wang X, Li F. Analysis of AC Machines and Their systems.Beijing:Tsinghua University Press, 2005:15-18
- [4] Sun J, Ma W, Wu X.Study on mathematical model of 3-&12-phase synchronous generators with AC and bridge rectified DC output.Proceedings of the Chinese Society for Electrical Engineering2003, 23(1):93-96

## **Overview of Permanent Magnet Wind Generators in China**

**Tang Renyuanm, An Zhongliang, Tong Wenming**  
**National Engineering Research Center for Rare Earth Permanent Magnet Machine**  
**China**

### **SUMMARY**

Wind energy conversion systems have become a focal point in the research of renewable energy sources. China has a vast land and long coastline and is rich in wind energy resources. China was the world's largest market in 2010. Nearly half of the global wind turbine installations in 2010 came from China. China is now the country with the largest installed wind power capacity in the world. Four Chinese manufacturers are part of the world's top ten largest wind turbine manufacturers.

Because of better overall system efficiency, reliability and grid compatibility, permanent magnet wind generator (PMWG) system is the most promising wind energy conversion concept. Although direct drive (DD) PMWG is widely used, the market interest of PMWG system with a multiple-stage gearbox or a single-stage gearbox is increasing. Presently, 5MW DD PMWG which is already for commercial use is produced by Xiangtan Electric. More powerful PMWGs are under developing.

Through the comparison of different topologies, radial flux (RF) structure is the most suitable concept for large wind generators. However, some special generator-configurations are promising, including dual air gap RF and hybrid excitation generator.

Some design technologies for PMWG are also discussed in this paper, including PMWG design integration with PWM converter, reliability improvements of stator insulation system and permanent magnets, efficiency improvement and weight reduction.

There is a possibility of irreversible demagnetization for permanent magnets in the case when magnets are hot and a three-phase short circuit takes place in the generator terminals. The working point of permanent magnet at this condition must be calculated. On the other hand, permanent magnets losses need to be calculated by considering all the factors, including stator magnetomotive force (MMF) harmonics, permeance harmonics and current time harmonics. For low speed high power PMWGs, the copper losses are dominated among all the losses. PMWG with fractional slot concentrated winding (FSCW) is beneficial due to short end winding, high efficiency. Weight reduction can be carried out by adopting a lightweight structure and an effective cooling system. Finite element method has to be applied to calculate the stiffness and strength of the compact structure and temperature distribution within the generator to verify effectiveness of the design.

### **KEYWORDS**

Wind power, Permanent magnet wind generator, Dual air gap, Hybrid excitation, Reliability improvements, Permanent magnet losses, Efficiency improvement, Weight reduction

# 1 INTRODUCTION

Wind power is the leading electricity generation technology in the fight against climate change, enhancing energy security, stabilising electricity prices, cleaning up our air and creating thousands of quality jobs in the manufacturing sector. During the past 15 years, wind energy conversion is the fastest-growing source of new electric generation in the world

China has a vast land and long coastline and is rich in wind energy resources. Studies show that the potential for exploiting wind energy in China is enormous, with a total exploitable capacity for both land-based and offshore wind energy of around 700-1 200GW.

China's wind market doubled every year between 2006 and 2009 in terms of total installed capacity, and it has been the largest annual market since 2009. In 2010, China was the country with the most installed wind energy capacity by adding 18.9GW over the course of the year, a 73.3% increase on 2009 in terms of cumulative capacity, reaching 44.7GW in total. Nearly half of the global wind turbine installations in 2010 came from China. Fig. 1 shows the annual and cumulative installed wind capacity in China between 2000 and 2010. The top 10 new installed capacity manufactures of China and their share in 2010 are shown in Fig. 2. Fig. 3 provides the top 10 cumulative capacity manufactures of China by the end of 2010 [1].

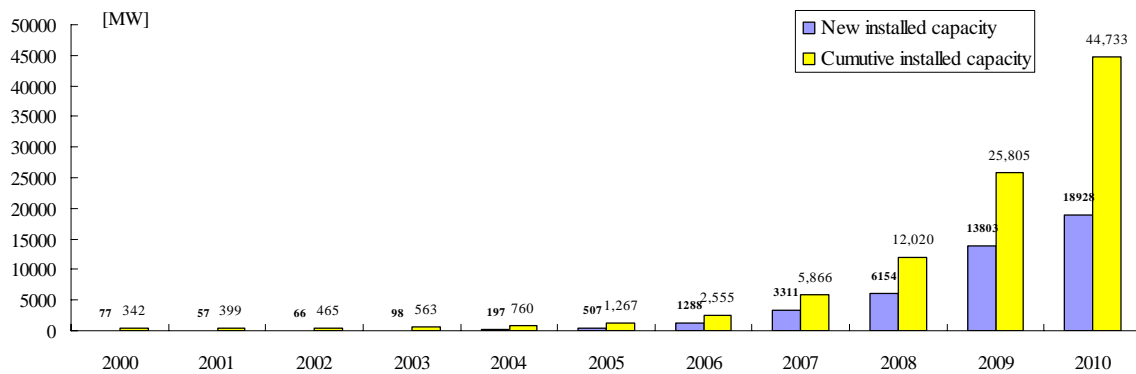


**Fig. 1 Annual and Cumulative Installed Capacity in China 2000-2010.**

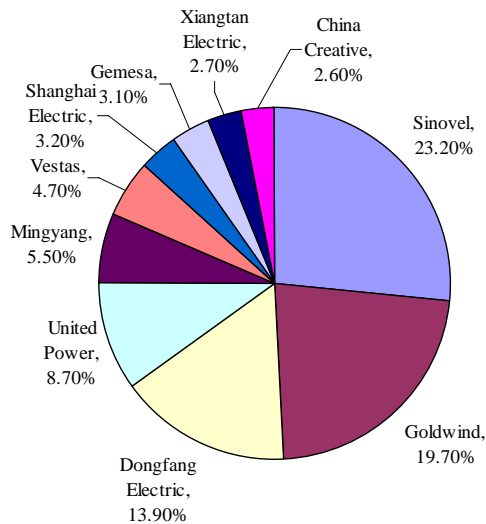


**Fig. 2 Top 10 New Installed Capacity Jan-Dec 2010.**

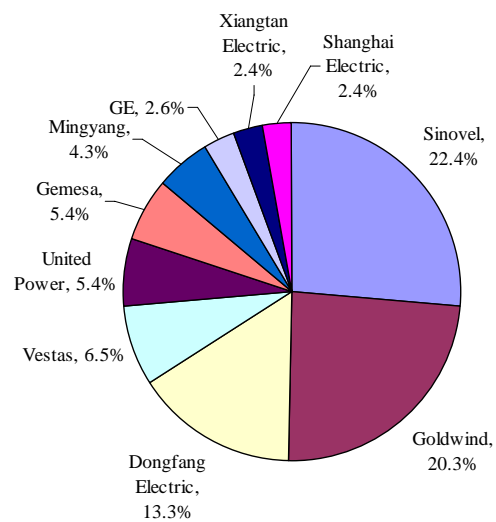


**Fig. 3 Top 10 Cumulative Capacity by Dec 2010.**

The Chinese wind turbine companies such as Sinovel, Goldwind, Xiangtan Electric and so on, start from technology import to independent research. The Chinese manufacturing industry is becoming increasingly mature, stretching over the whole supply chain. China has now become the world's largest producer of wind energy equipment, and components made in China are now starting to not only satisfy domestic demand, but also meet international needs. Among suppliers of wind turbines, China dominates the market, with four Chinese manufacturers, including Sinovel, Goldwind, United

Power and Dongfang Electric, are part of the world's top ten largest wind turbine manufactures in 2010. Driven by global development trends, Chinese firms have entered the competition to manufacture wind turbines of high power. Presently, 5MW DD PMWG which is already for commercial use is produced by Xiangtan Electric for offshore wind turbines. More powerful PMWGs are under developing.

Although the installed capacity is largest in the world, China still encounters the grid interconnection problem of wind farms. Microgrid is one of the methods to solve this problem.

## **2 ADVANTAGES OF PMWG**

The generators used in the variable speed wind turbine system can be classified into double fed induction generator, electrically excited synchronous generator and permanent magnet generator. With the development of high performance permanent magnet, high power density PMWGs are more and more attractive. More than half of the world's top 10 turbine manufacturers are investigating PMWG technology or are already offering PMWG to the market. The representative companies of PMWG system in China are Goldwind and Xiangtan Electric. Goldwind is the second largest wind turbine manufacture in China, and ranks fourth in the world. According to the data from Chinese Wind Energy Association (CWEA), PMWGs occupy more than 22.4% of new installed capacity in 2010, and more than 22.7% of cumulative capacity by the end of 2010 in China [1].

PMWG has a lot of advantages, can be listed as follows:

- Without excitation, simplified drive chain, so high overall efficiency can be achieved.
- High reliability, suitable for offshore application.
- High grid compatibility.

Because of the advantages stated above, PMWG system is the most promising wind energy conversion concept. Although DD PMWG is widely used, the market interest of PMWG system with a multiple-stage gearbox or a single-stage gearbox is increasing.

## **3 PMWG CLASSIFICATION**

PMWGs allow a great deal of flexibility in their geometry, so that various topologies may be used. According to the direction of flux penetration, PMWG can be classified into the following types: RF, axial flux (AF) and transversal flux (TF). In RF PMWG, the length of the stator and the air gap diameter can be chosen independently. The structural stability of RF PMWG is easy to make sufficient, and the assembly process is simple and mature. The main strength of AF and TF PMWGs can be summarized as higher torque density. Contrary to the strengths, the construction and assembly process are very complicated, so they have not been used for large wind turbines. Most of the megawatts wind generators are RF machines that seem to be the most interesting machine type for the large scale wind generators. However, some special generator-configurations are promising, including dual air gap RF and hybrid excitation generator.

### **3.1 Dual air gap rf configurations**

High torque density and high efficiency are two of the most desirable features for an electrical machine. One of the solutions to the problem is to adopt a novel machine class—dual air gap PMWG. The dual air gap PMWG includes two configurations, dual-rotor RF PMWG and dual-stator RF PMWG.

#### **3.1.1 Dual-rotor RF PMWG**

The dual-rotor RF PMWG can possess a variety of topologies based on different structure of windings, slots and magnet arrangements. Toroidal winding is a promising choice for this type of machine, because the winding end portion is greatly shortened. This results in an improved machine efficiency. The configuration of dual-rotor RF PMWG is shown in Fig. 4.

Dual-rotor RF PMWGs have some specific features caused by their unique mechanical configuration: rotor-stator-rotor structure and double air gaps. Since the output torque is proportional to the air gap surface area for the constant electrical and magnetic loadings, the most straight forward observation

coming from the doubled air gaps in a slightly enlarged volume is that the torque density will be substantially boosted [2]. Another aspect for the dual-rotor topologies is that the radial forces are balanced. In the topologies, these forces can be balanced by an equal and opposite attractive forces due to symmetry. In this case, the mechanical stress is greatly reduced. In addition, the ratio of the torque density of the dual-rotor RF PMWGs to conventional PM machines increases as the rated power increases.

### 3.1.2 Dual-stator RF PMWG

Similar to the dual-rotor structure, the dual-stator topologies also can improve the torque density and efficiency by doubling the air-gap and keeping the machine volume unchanged. Slotted or slotless structures and N-N type or N-S type magnets all can be used. The end winding in the dual-stator structure will be much longer than that in the dual-rotor structure since the conventional winding has to be used. This is a feature that causes the efficiency and torque density to be lower than dual-rotor RF PMWG. The configuration of dual-stator RF PMWG is shown in Fig. 5.

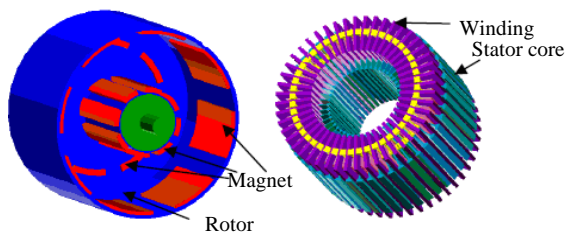


Fig. 4 Configuration of Dual-rotor RF PMWG.

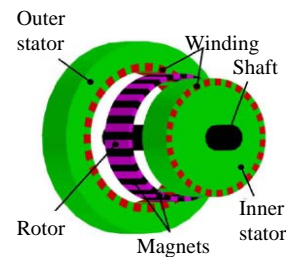


Fig. 5 Configuration of Dual-stator RF PMWG.

## 3.2 Hybrid Excitation Wind Generator (HEWG)

HEWG is a combination of conventional RF PMWG and electrical-excitation generator to achieve constant voltage in the case of variable speed. For PMWG, the changes of rotating speed, working temperature and load level may cause a huge fluctuation of generator terminal voltage. By supplying DC excitation of different magnitude and direction according to the variation of the voltage, the magnetic field can be adjusted, and constant voltage is achieved. The configuration of a HEWG is shown in Fig. 6. The type of generator system has a good capacity of realizing constant voltage in the case of minimum consumption because of simple control system, and can be applied to DC microgrid for distributed generation system. The full power inverter is unnecessary in DC microgrid.

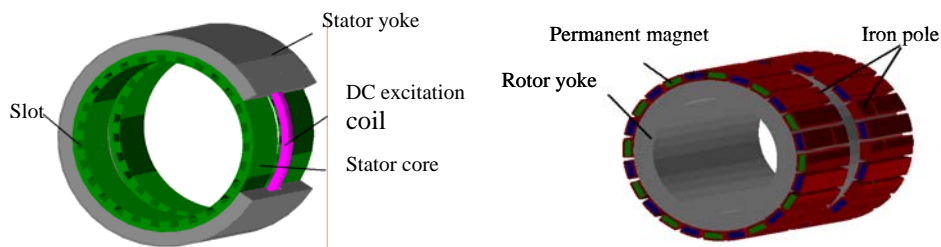


Fig. 6 Configuration of Hybrid Excitation Wind Generator.

## 4 PMWG DESIGN TECHNOLOGIES

### 4.1 Pmwig design integration with pwm converter

Most of large power PMWGs connect with back-to-back PWM converters. This type of converter can control the current phase angle to supply the generator with different reactive power. The output voltage of the generator changes along with the power factor. Three different ways to control the generator terminal voltage are shown in Fig. 7. As can be seen from the Fig. 7a, maximizing the terminal power factor ( $\cos\phi=1$ ) does not maximize the power, because the terminal voltage is much lower than the no-load EMF due to the existence of armature reactance. Instead, the terminal voltage can be kept at the same as the no-load EMF by supplying some reactive power, as shown in Fig. 7b. This control method will reduce the generator weight compared to Fig. 7a. If the generator is designed according to  $I_d=0$  control, the no-load EMF is lower than the rated voltage. The advantage of this

generator design is that the least active material is used, but the drawback is that the kVA rating of PWM converter is larger. To maximize the active power at rated current, the product of the voltage, current and power factor has to be maximized.

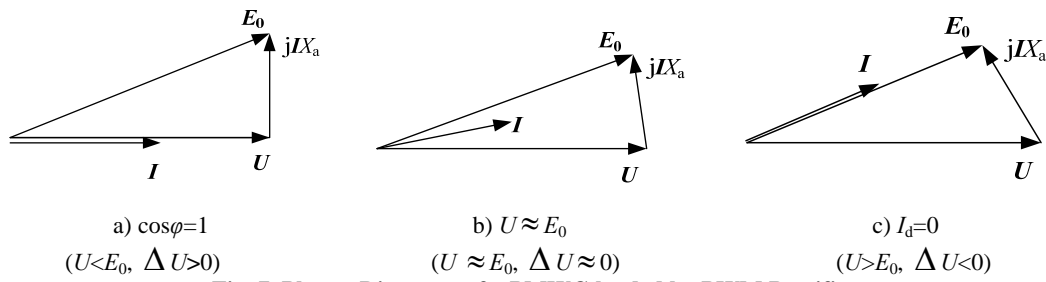


Fig. 7 Phasor Diagrams of a PMWG loaded by PWM Rectifier.

## 4.2 Reliability improvements

### 4.2.1 Insulation Reliability

Some effects of the PWM waveform need to be considered when using a generator in wind energy conversion application: The fast rate of voltage changes results in high voltage stresses that have a detrimental effect on the conductor insulation of the generator windings. These surge voltages can be 2 to 3 times higher than the nominal voltage of the generator which may cause partial discharge and dielectric breakdown. To avoid winding failure of PMWG connected by PWM converter, the insulation has to be designed to withstand these high voltage stresses.

### 4.2.2 Permanent Magnet Reliability

One of the main design issues is to make sure that permanent magnets never lose the polarization. The main improvements in the recent development of NdFeB magnets have been reached in corrosion resistivity and temperature tolerance. By using a proper application design, modern NdFeB magnets can be kept stable for decades.

#### ■ Prevent Local Demagnetization under Short Circuit Condition

At temperatures below the Curie temperature, the demagnetization is caused by an opposing magnetic field. Coercivity can be understood as the capability of a material to resist opposing fields. It determines the opposing field strength at which magnets become demagnetized. The coercivity of NdFeB magnets decreases with increasing temperature. It means that there is a possibility of losing the polarization in the case when magnets are hot and a three-phase short circuit takes place in the generator terminals. This is a rare occasion in a converter-operated machine, but must still be kept as a design criterion. The working point of permanent magnet at this condition must be higher than the knee point of the demagnetization curve. The current curve of a 2MW PMWG during three-phase short circuit at the highest working temperature is calculated by using finite element software, as shown in Fig. 8. Fig. 9 gives the working point of a permanent magnet at extremely condition.

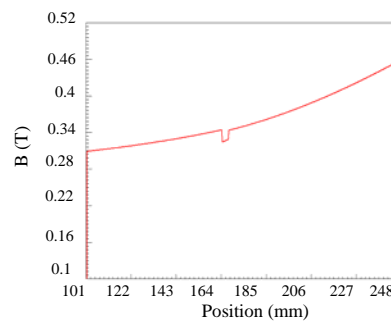
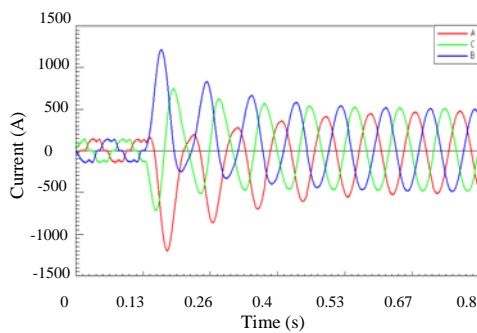


Fig. 8 Three-Phase Short Circuit Current Curve. Fig. 9 Magnet Working Point at extremely condition.

## ■ Permanent Magnets Losses Calculation

Eddy current losses in the permanent magnets will not only affect the generator efficiency, but may also result in excessive heating, which could lead to irreversible demagnetization of the magnets. Eddy current losses in the permanent magnets are caused by three different reasons. First, the stator winding distribution produces a large amount of MMF harmonics travelling across the permanent magnets, thereby causing eddy currents. Secondly, permeance harmonics cause flux density variations that induce eddy currents in the permanent magnets. Finally, stator current time harmonics caused by PWM converter produce extra losses in the rotor. Therefore, permanent magnets losses need to be calculated by considering all these three factors. The magnets loss of a 40-pole 45-slot PMWG is shown in Fig. 10.

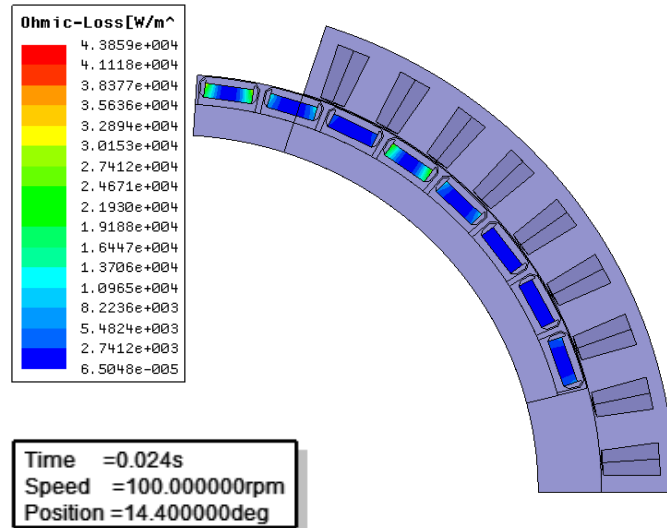


Fig. 10 Eddy Current Loss Density Distribution.

### 4.3 Efficiency improvements

For low speed large power PMWGs, the copper losses are dominated among all the losses. To achieve high efficiency, the copper losses should be reduced. Generally, large power PMWG has a small ratio of length to diameter, so the end winding occupies a large portion of conventional distributed winding. PMWG with fractional slot concentrated winding (FSCW) is beneficial due to short end winding, high efficiency, simple structure and high capacity of fault tolerance. Table I gives a comparison between FSCW and conventional distributed winding for a 10kW PMWG. As can be seen from the table, the end winding of FSCW is greatly reduced, and the efficiency is improved by 2.4%.

Table I End Winding Comparison between Fractional Slot Concentrated Winding and Conventional Winding.

Parameter	Fractional slot concentrated winding	Conventional winding
$q$	0.375	1
End winding weight (kg)	7.67	24.7
Total weight of winding (kg)	31.23	48.26
End wind weight/Total weight of winding	0.246	0.512
Efficiency (%)	91.05	88.62

### 4.4 Weight reduction of PMWG

#### 4.4.1 Light Weight Structure

According to [3], the structural mass of a large power DD generator can be in excess of 80% of the total mass. To reduce the weight of PMWG, a reliable and compact structure should be designed. Fig. 11 presents 4 kinds of main mechanical structures of DD PMWGs. Among these basic structures, single-bearing structure is attractive in compactness and light weight. Fig. 12 shows a 2MW single-bearing DD PMWG. The generator structure is part of the turbine load carrying parts in combination with the single-bearing construction [4]. The main bearing is a specially designed two row cylindrical

roller bearing of large diameter. The inner non-rotating ring is mounted to the generator stator. The outer rotating ring is mounted between the hub and generator rotor. The bearing takes axial and radial loads as well as bending moments. The bearing is provided with a fully automatic lubrications system monitored by the turbine controller. FEM calculations must be made to determine strength and stiffness of structure and bolted connections under extreme loads. The deformation distributions within stator frame and rotor conical support are shown in Fig. 13 and 14 respectively. The single-bearing structure is adopted for 5MW and 2.5MW DD PMWGs in China.

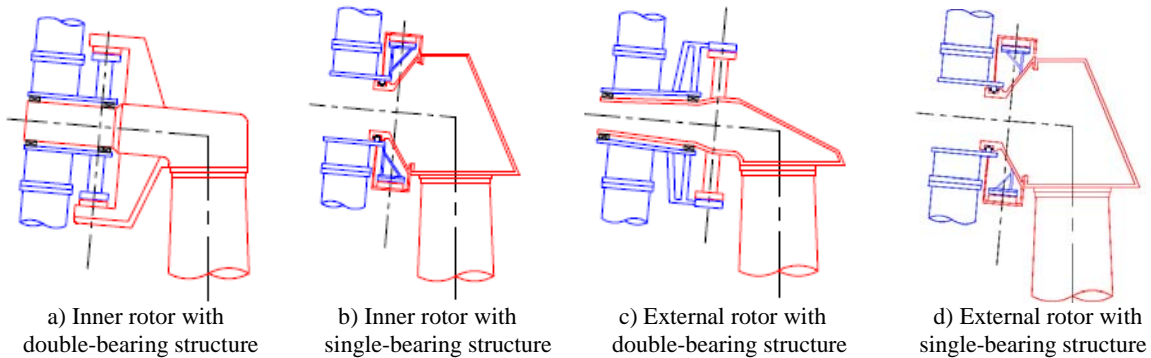


**Fig. 11 Main mechanical structures of DD PMWGs.**

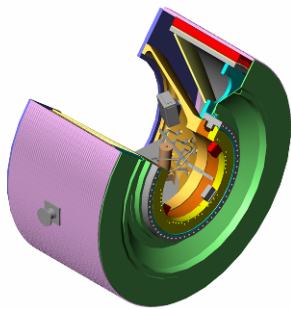


**Fig. 12 Model of a Single-Bearing DD PMWG.**

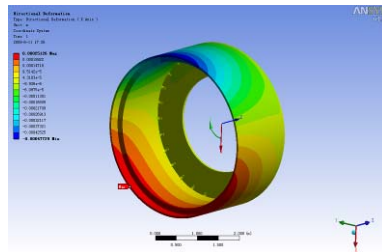


**Fig. 13 Deformation of Stator Frame.**

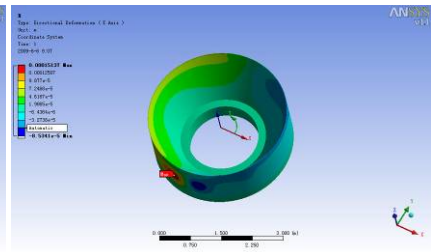


**Fig. 14 Deformation of Rotor Conical Support.**

#### 4.4.2 Cooling System

A reliable and effective cooling system can improve the thermal load of PMWG, so both the weight of active material and structural material can be reduced. In order to make full use of the natural air flow of wind farm and simplify the cooling system, a 2MW DD PMWG and a 1.5MW DD PMWG are cooled directly by natural wind blowing through the ventilated ribs that mounted on the surface of frame, as shown in Fig. 15 and 16. The 1.5MW PMWG is outer rotor structure, which is inherently the best alternative from a permanent magnet temperature point of view. As the magnets are attached to the inner surface of the outer rotor whose outer surface rotates in free air, the cooling of the magnets takes place most effectively.

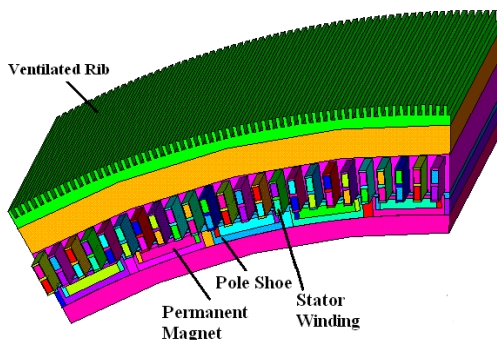


**Fig. 15 2MW PMWG with Ventilated Ribs.**

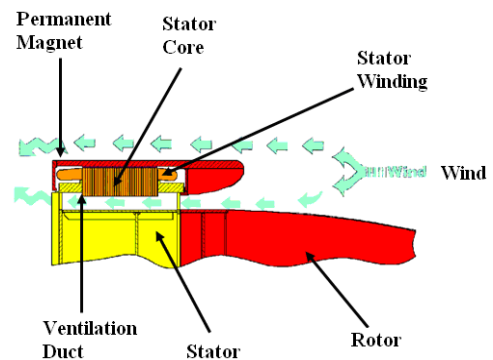


**Fig. 16 Schematic Diagram of 1.5MW PMWG Ventilation System.**

Forced air cooling is better than natural cooling from the generator weight reduction point of view. An axial forced air cooling system for 1.5MW semi-DD PMWG is design by the collaboration between Chinese National Engineering Research Center for Rare Earth Permanent Magnet Machine (NPMCC) and Harbin Electric Machinery Co., Ltd, as shown in Fig. 17. The velocity vector distribution is shown in Fig. 18. Through the temperature field calculation as seen in Fig. 19 and 20, the temperature distribution within the PMWG can be obtained to verify the effectiveness of the cooling system.

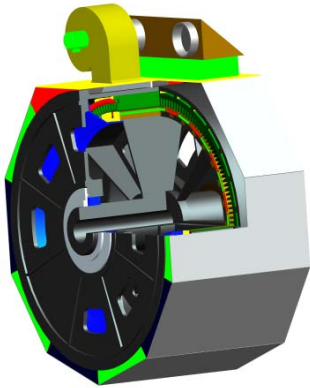


Fig. 17 Configuration of 1.5 MW Semi-DD PMWG.

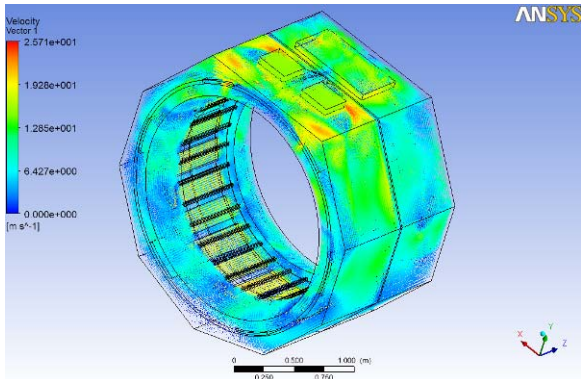


Fig. 18 3D Velocity Vector Distribution of the Cooling Air

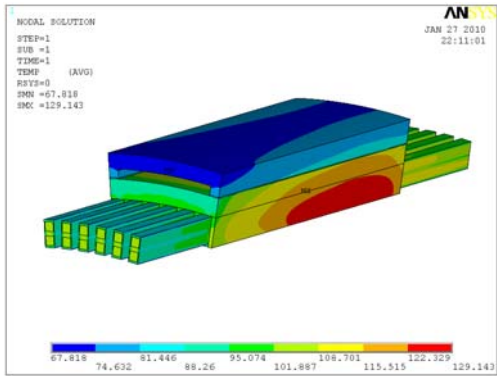


Fig. 19 Stator Temperature Distribution of 1.5 MW Semi-DD PMWG.

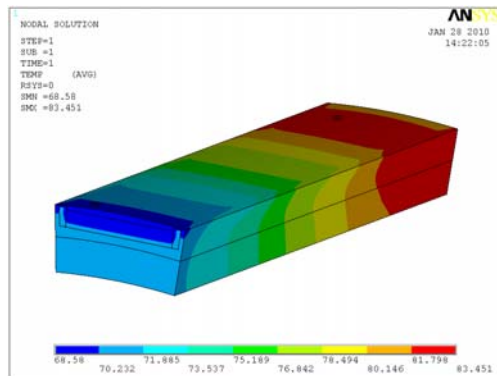


Fig. 20 Rotor Temperature Distribution of 1.5 MW Semi-DD PMWG.

**CONCLUSION**

China is now the country with the largest installed wind power capacity in the world. Four Chinese manufacturers are part of the world’s top ten largest wind turbine manufactures, but China still encounters the grid interconnection problem of wind farms.

Because of better overall system efficiency, reliability and grid compatibility, PMWG system is the most promising wind energy conversion concept. Although DD PMWG is widely used, the market interest of PMSG system with a multiple-stage gearbox or a single-stage gearbox is increasing. Presently, 5MW DD PMWG which is already for commercial use is produced by XEMC. More powerful PMWGs are under developing.

RF structure is the best choice for large wind turbines. Some special generator-configurations are promising, including dual air gap RF and hybrid excitation generator. The design technologies of RF PMWG, including PMWG design integration with PWM converter, reliability improvements of stator insulation system and permanent magnets, efficiency improvement and generator weight reduction, are discussed in this paper.

**BIBLIOGRAPHY**

[1] CWEA. Statistics of wind turbine installed capacity in China 2010

- [2] Qu R, Lipo T A. Dual-rotor, radial-flux, torodially wound, permanent-magnet machines. IEEE Transactions on Industry Applications ,November/December 2003,39(6)
- [3] Mueller M A, McDonald A S. A lightweight low-speed permanent magnet electrical generator for direct-drive wind turbines.Wind Energy ,2009
- [4] Bang D, Polinder H, Shrestha G, Ferreira J A.Review of generator systems for direct-drive wind turbines[C]// European Wind Energy Conference & Exhibition(EWEC 2008), Belgium, 1-4 April, 2008

## **2G HTS Wind Turbine Generators**

**Yu.F. Antonov**  
**Ya.B. Danilevich**  
**Institute of Silicate Chemistry**  
**Russian Academy of Sciences**  
**Russia**

**Li Weili**  
**Harbin University**  
**of Sciences and Technology**  
**China**

### **SUMMARY**

Justified by technical feasibility and economic viability of a fully superconducting wind farms megawatt power level. The technical details of hybrid and fully superconducting wind turbine generators capacity of 1.5 and 5.0 MW. Along with mini hydro generators wind turbine generators form a cluster low-potential, renewable and environmentally friendly sources of electrical energy. Hydro turbine work practically at constant pressure (flow) of water, determines the distance between the top and tail water. This distance can be quite large. As a result, speed turbines reaches one thousand of rpm. However, wind turbines are used in air flow with a substantially low rate. Wind turbines are strictly low-speed units. Therefore, they are equipped with direct (1:1) or half (1:10) transmissions. Stator has a fractional number of slots per pole and phase. Winding material for the stator and rotor is belt high-temperature superconductor of the second generation (2G HTS). Hybrid wind turbine has an inductor with permanent magnets. Alternatively, permanent magnets are replaced by massive 2G HTS samples. Their magnetization is carried out on the installation site (in situ) topological method at the operating temperature. The recommendations on manufacturing technology of superconducting windings of the rotor and stator. Considered modes cryostating.

### **KEYWORDS**

Wind turbine generator, High-temperature superconductor, Cryogenic cooling, Fully superconducting, Hybrid, Compound.

# 1 INTRODUCTION

## 1.1 Current status of wind energy

According to [1] the use of wind energy for electricity generation in the foreseeable future will be implemented with the help of powerful wind turbine generators with a horizontal or vertical shaft. In connection with the intensive development of wind energy rapidly growing wind power unit. The greatest share purchase wind turbine generators capacity increased, 1-12 MW. Among the most common is the wind turbine generators capacity of 1.5 MW. The number of wind turbine generators GE Energy capacity of 1.5 MW, in operation, is 7 700 units. In Harbin (Heilongjiang Province, China) industrial enterprise “Hafey” created by the parent model windmill power of 1.5 MW. For the release of wind farms in the Russian Federation created a joint venture between Russian Technologies, RusHydro and Siemens. The company will launch the production of energy wind-power plants with a unit capacity 1.5 MW plant in Volgograd “Khimprom”. By 2020, Russia will develop several wind farms with total installed capacity of 7 GW [2].

Megawatt-level wind turbines are essentially low rpm. To transfer large momentum from the wind turbine generator to apply a direct (1:1) or a half (1:10) transmission. Because of the low speed 10-15 rpm powerful wind turbine have impressive weight and dimensions. For example, a wind turbine has a capacity of 10 MW three-blade rotor diameter of 200 m. It is mounted on a supporting tower height of 250 meters. Installation of windmill weight of 350 tons at a height of 250 meters is a complex technological task, dictating the high capital costs.

A significant decrease in weight and size of wind turbine generator possible by the use of superconductors. Thus, by replacing the conventional (copper) on the superconducting windings, including the high-temperature superconductors, and reduce the amount of steel in the magnetic mass of wind turbine generator capacity of 10 MW could be reduced by three times, up to 120 m. The relatively lightweight HTS generators can greatly simplify and cheapen the construction of large capacity wind turbines. With the commissioning of production HTS magnet materials cost about 25 dollars per kA·m and below, opens up real prospects of a fully superconducting wind turbines.

Zenergy Power commissioned by UK Department of Trade and Industry produced a prototype of a superconducting synchronous generator with capacity of 8 MW direct drive of the wind turbine. The generator is made from 1G (first generation) HTS production Zenergy Power. In AMSC developed wind turbine based on 2G (second generation) high-temperature superconductors [3]. Megawatt wind turbine prototypes level made hybrid (stator windings - copper wire, field winding - superconducting).

## 1.2 Problem statement

Fully superconducting and hybrid wind turbine generators are high rating electrical machines. Therefore, at the design stage is crucial to obtain the calculated and experimental data of thermal and electromagnetic states of the rotor and stator windings.

## 2 DESIGN AND PARAMETERS OF WIND TURBINE GENERATORS OF VARIOUS TYPES OF POWER OF 1.5 AND 5 MW

Powerful wind turbines with a mini-hydro form a cluster of renewable and cleaner sources of electricity. However, if the turbines are working practically at constant pressure and flow rate, determines the distance between the top and tail water, the wind turbines used by the air flow with very small pressure and speed. Wind turbines are strictly low-speed units. Consequently, they applied stator windings to the fractional number of slots per pole and phase (Table I , Fig. 1).

**Table I The scheme of the stator windings to the fractional number of slots per pole and phase.**

1	-3	2	-1	3	-2	-2	1	-3	2	-1	3	3	-2	1	-3	2	-1
-1	3	-2	1	-3	2	2	-1	3	-2	1	-3	-3	2	-1	3	-2	1
etc. -----																	

$$1 \equiv A; -1 \equiv A^1; 2 \equiv B; -2 \equiv B^1; 3 \equiv C; -3 \equiv C^1$$

Traditional (option № 1) and hybrid (option № 3A,B) have the main field wind turbine generator rotors, fully superconducting (option № 2) – implicit-pole (Table II). Rotor core (option № 1, 3) are made from thick sheets of electrical steel strapped to each other pins. Laminated poles are made. Rotor

core (option № 2) - a non-magnetic. The stator core of traditional and hybrid types of wind turbine generators consist of a package drawn from the electrical sheet steel of thickness 0.35 mm.

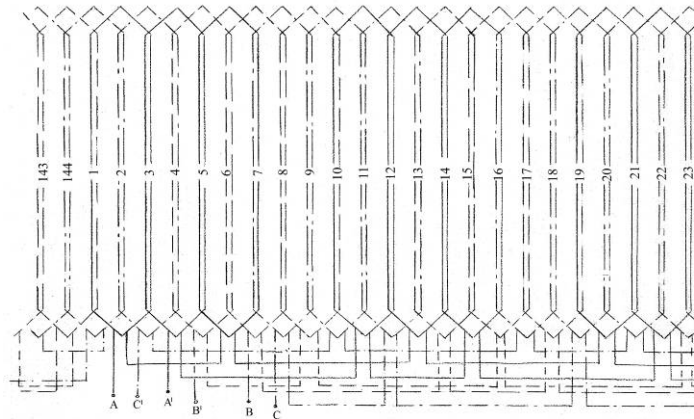


**Fig. 1** Scheme of the three-phase two-layer fractional winding loop with  $Z = 144, 2p = 20, q = 1 \frac{1}{5}, a = 1, y = 3, \tau = 0,155 \text{ m}, \beta = 0,833$ .

**Table II** Technical data of wind generators 1.5 and 5.0 MW.

Parameter	Option № 1	Option № 2	Option № 3A,B
Type	Traditional	HTS completely	HTS - a hybrid
Rated Power $P_H$ , MW	1,5	5,0	1,5
Rated voltage (linear) $U_H$ , kV	6,3	6,3	6,3
Rated speed $n_H$ , rpm	150	150	150
Frequency $f$ , Hz	50	50	50
$\cos \varphi$	0,8 (lagging)	0,8 (lagging)	0,8 (lagging)
Efficiency (including cryogenic maintenance) $\eta$	0,95 (No cryogenic maintenance)	0,995	0,98
Weight, t	6,9	6,9	2,1
Cooling	Air	cryocooler (via heat exchanger gas - neon)	cryocooler (via heat exchanger gas - neon)
Rated speed wind turbine $n_T$ , rpm	15	15	15
Gear ratio $n = n_H/n_T$	10 (half-transmission)	10(half-transmission)	10 (half-transmission)
Rotor diameter (three-blade) turbines $2R$ , m	61,6	116,4	61,6
Torque on the shaft $M_T$ , N·m	$0,7 \times 10^6$	$3,5 \times 10^6$	$0,7 \times 10^6$
Maximum linear speed blades of wind turbines $v_{max}$ , m/s	61,6	89,8	61,6
Height axis $h$ , m	55,8	55,8	83,2
Rated phase voltage (connection of stator windings - into a star) $U_{n,F_3}$ , V	3462	3462	3462
Nominal full power $S_n$ , MVA	1,894	5,647	1,894
Rated phase current $I_{F_3}$ , A	176	587	176
Number of pole pairs $p$	20	20	20
Inner diameter of stator $D_i$ , m	1,97	1,97	0,994
Outside diameter of stator $D_o$ , m	2,22	2,22	1,2
Pole pitch $\tau$ , m	0,155	0,155	0,078
The length of the stator $l_\delta$ , m	0,846	0,846	1,0
Magnetic induction in the gap $B_\delta$ , T	0,8	1,6	0,8
A linear load, A/m	$45 \times 10^3$	$149 \times 10^3$	$147 \times 10^3$

In traditional (option № 1) and hybrid (option № 3A.B) wind generators with stator winding of the conventional (copper) conductor is cooled by air through axial channels, the open-loop operation (Fig. 2).

In the fully superconducting (option № 2) and hybrid (option № 3B) wind generator of winding material in the rotor is belt 2G HTS for the stator - the cable transposed scheme Roebel. Traditional (option № 1) and hybrid (option № 3A) wind turbines are inducers, respectively, of the permanent

magnets and bulk superconductors. Permanent magnets and magnetization of bulk HTS can be installed in the slots (tangential position) or on the surface of the pole (radial position). Magnetization of bulk HTS is carried out on the installation site (*in-situ*), topological methods to work (cryogenic) temperature.

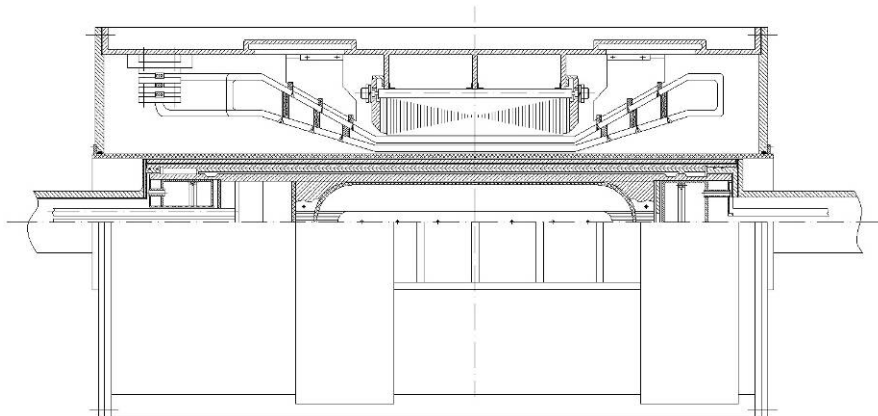
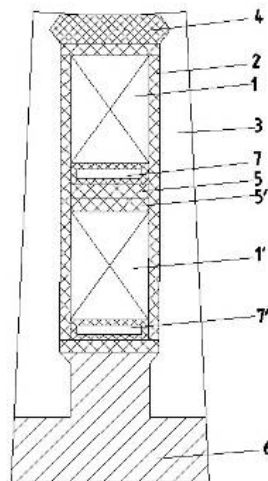


Fig. 2 Longitudinal section of a hybrid (option № 3B) wind turbine.

### 3 TYPES OF LTS/HTS STATOR AND ROTOR WINDINGS

#### 3.1 Stator windings

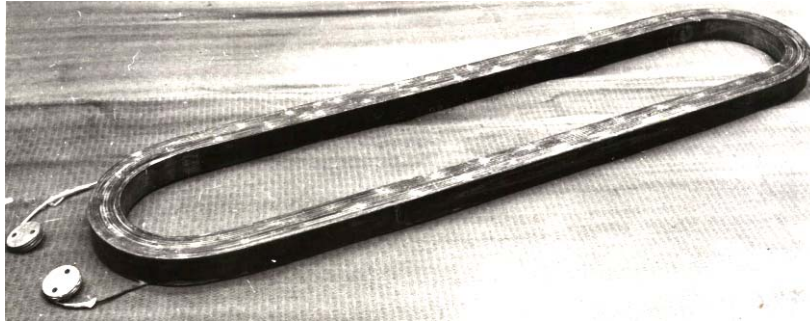
The stator windings are conventional (option № 1) and hybrid (option number 3A,B) wind turbine made from rod transposed to the system Roebel stranded copper wire [4]. They consist of coil groups, placed in the slots provided in the stator according to Table I circuit installation (Fig. 3).



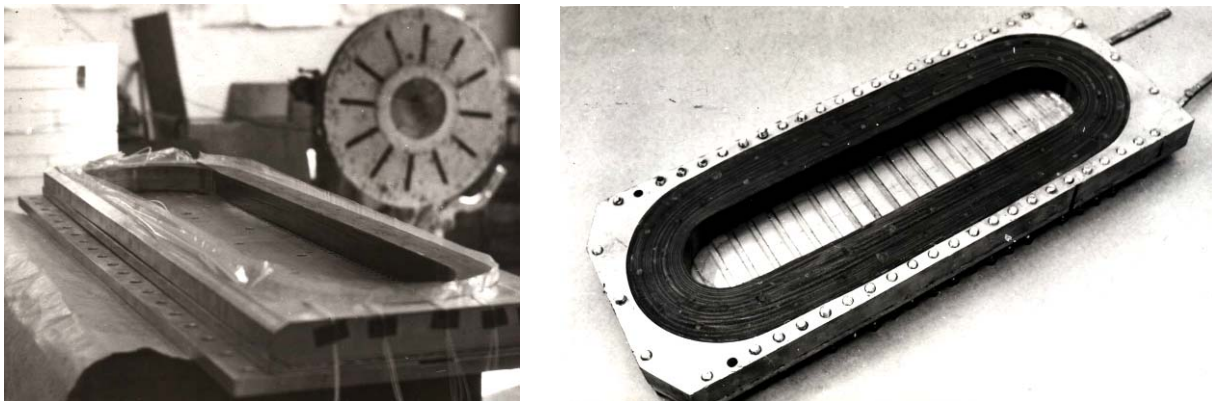
1, 1' - active side track module of the stator winding, 2 - slot insulation, 3 - edge of the groove, 4 - wedge, 5, 5' - interlayer insulation, 6 - ferromagnetic screen, 7 - channel cooling.

Fig. 3 Stator slot.

In the fully superconducting wind generator (option № 2) of the stator winding coil groups in the form of tracking modules (Fig. 4). The main advantage of a tracking module - is the relative simplicity of its winding, compounding and installation in the stator slots (Fig. 3) [6]. The Research Centre Forschungszentrum Karlsruhe (FZK) made from a 2G HTS tape transposed current-carrying element type Roebel length 1.1 m. Critical current of 2.63 kA at 77.4. More promising (as compared to Roebel) is transposed HTS wire developed at the University of Colorado in cooperation with NIST (USA). Current-carrying element Ø7.5 mm in a copper Former Ø5.5 mm, around which wound 24 2G HTS tapes 4 mm in width. Critical current of 2.8 kA at 77.4. Bending radius of 125 mm.



**Fig. 4 Model of a tracking module superconducting stator winding is fully superconducting wind turbine generator(option № 2).**



**Fig. 5 The technology section of track winding superconducting modules.**

To ensure the desired shape track superconducting module used industrial equipment, consisting of a collapsible frame with a lid, drum brakes and a spring dynamometer (Fig. 5). The frame and cover are made of duralumin Д16 brand. Along the perimeter of the frame are blind threaded holes. They are designed to connect the cover and frame bolts. Two through holes provide vacuum cavity tooling, with accommodation in its module, and fill it with liquid compound. Monolithic module occurs during hot curing compound in a vacuum furnace. In order to safely remove the module from the inner walls of tooling polished and coated with adhesive stamps anti-adhesion KJIT30M. Cabinet insulation is fluoroplastic film.

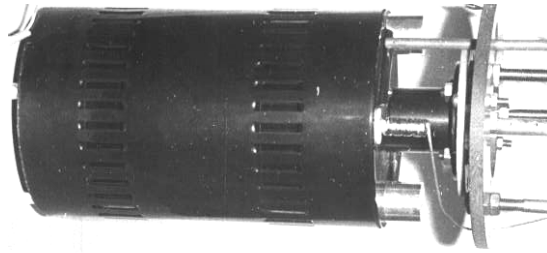
Track module is impregnated with epoxy resin brands ЭТ-10 [5], designed specifically for cryogenic electrical machines with a working temperature range 4.2-77.4 K. This compound satisfies the basic technological requirements, having high impregnating ability and adhesion, forming together with winding monolithic capsule that will not crack after polymerization in the process of cyclic cooling down, having high thermal conductivity and moisture (Table III). Compound marks ЭТ-10 is based on epoxy resin ЭД-5 and isometric tetrahydrophthalic anhydride with the introduction of a plasticizer based on liquid synthetic rubber compound to give increased flexibility.

### 3.2 Excitation system

In traditional (option № 1) and hybrid (option № 3) wind generators excitation system implemented on the basis of permanent NdFeB magnets with high coercive force  $H$ . Experiments with permanent magnetization of NdFeB magnets in the three environments showed a tendency to increase the coercive force  $H$  with decreasing temperature:  $1.3 \cdot 10^6$  A/m (300 K);  $3.2 \cdot 10^6$  A/m (77.4 K) and  $5.1 \cdot 10^6$  A/m (4.2 K). Magnetization in the "room" temperature (300 K) and liquid nitrogen (77.4 K) is satisfied by the pulse method. In liquid helium (4.2 K) used for this purpose superconducting solenoid type CC-89 with magnetic induction at the geometric center of  $B_0 = 8.7$  T and an aperture diameter  $D_B = 30$  mm (Fig. 6).

**Table III Basic physical and chemical properties of the compound ЭТ-10.**

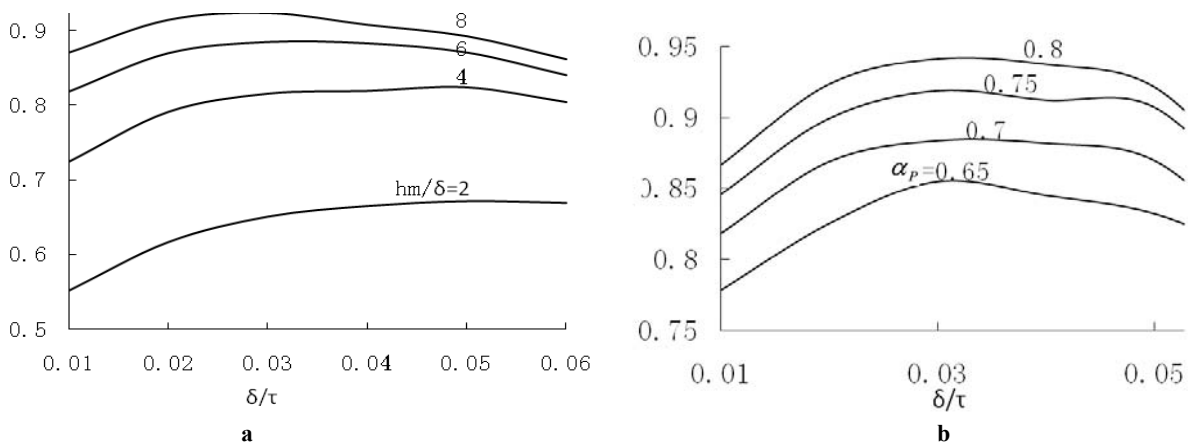
Breaking stress at break  $\sigma_p = 11.4$  MPa  
 Breaking stress in compression  $\sigma_c = 38.0-31.6$  MPa  
 Modulus of elasticity  $E = 2.5 \cdot 10^4 - 2.5 \cdot 10^3$  MPa  
 Thermal conductivity  $\lambda = 0.178 - 0,167$  W/(m°C)  
 Specific heat  $C = 1.662 - 2.418$  kJ/(kg°C)  
 Volume resistivity  $\rho = 6 \cdot 10^{12}$  Ohm·cm  
 Thermal diffusivity  $\alpha = 4.5 - 6.5 \cdot 10^{-5}$  °C<sup>-1</sup>  
 Dielectric strength  $E = 30$  kA/mm  
 Loss tangent  $\text{tg } \delta = 0.016$   
 Permittivity  $\varepsilon = 4$



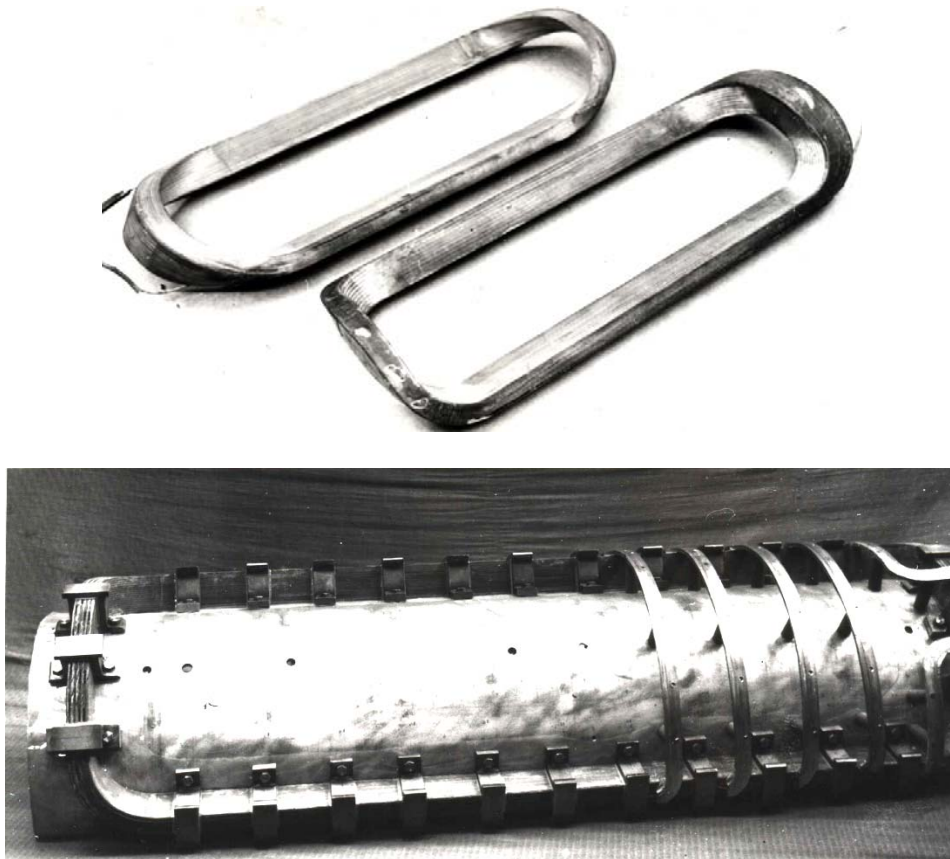
**Fig. 6 Solenoid CC-89: rated current of  $I_H = 172$  A; maximum magnetic induction in the geometric center of  $B_0 = 8.7$  T, and the constant  $C_0 = 50.6$  T/kA, the stored energy  $W = 20$  kJ; mass  $m = 14$  kg; field 10 mm; inductance  $L_H = 1.7714$  H; no uniformity over the length of  $\pm 10$  mm; wire NbTi Ø1, 0 mm, number of turns  $w = 10$  163, the number of layers  $n = 62$ , the fill factor of winding  $k = 0,775$ ; outer diameter  $D_n = 128$  mm internal diameter  $D_B = 30$  mm, height  $2b = 210$  mm, total length of magnet wire  $l = 2$  km.**

Fig. 7a for the traditional (option № 1) and hybrid (option № 3A) shows the wind turbine generators magnetic induction in air gap  $B_\delta$  the ratio of the air gap  $\delta$  and the pole arc  $\tau$  at different values of the pole arc. Fig. 7b shows similar curves for different values of the ratio of height poles of a magnet  $h_m$  to the air gap  $\delta$ , provided that the coefficient of the pole arc  $\alpha_p = 0.7$ . The optimal relations: the air gap to the length of the pole arc  $\delta / \tau = 0.025 \div 0.03$ , height permanent magnet by the air gap  $h_m / \delta = 4.5 \div 6.0$  [7].

In the hybrid version № 3A instead of permanent magnets used magnetization of bulk superconductors. Rotor design also provides for a combination of permanent magnets and bulk superconductors. On the effective work of the permanent magnets and/or magnetized HTS bulk affects the reaction anchor. It is therefore necessary to take protective measures against the longitudinal response anchors. It should not exceed a critical threshold of irreversible demagnetization of the magnets. Re-magnetization magnets expedient to carry out without dismantling the machine. To this end, developed several methods of magnetizing the place of installation (*in-situ*) magnets. In the fully superconducting (option № 2) and hybrid (option № 3B) wind generators field winding consists of a set of track (Fig. 4, 5) or saddle-shaped (Fig. 8) modules. Design tracking modules of the rotor and stator are similar, except for winding data.



**Fig. 7 Магнитная индукция: (a)  $B_\delta = f(\alpha_p, \delta / \tau)$ ;  $h_m / \delta = 6$ ; (b)  $B_\delta = f(h_m / \delta, \delta / \tau)$ ;  $\alpha_p = 0,7$ .**



**Fig. 8 Models of a saddle-shaped module superconducting rotor winding is fully superconducting (option № 2) and hybrid (option № 3B) wind turbine generator.**

The pole cores and pole shoes made according to the type of excitation windings (Table IV). In traditional (option № 1) and hybrid (option № 3A) wind generators for the production of cores of the poles and pole shoes of the rotor plate is used, for example, Ст. 3, of a thickness of 1-2 mm (Fig. 9). In the fully superconducting (option № 2) and hybrid (option № 3B) wind generators pole cores and pole pieces made of nonmagnetic material, such as stainless steel or fiberglass. Permanent magnets and/or magnetized bulk HTS set in place the pole shoes (radial position) or in the gap between the pole cores (tangential position). In the fully superconducting (option № 2) and hybrid (option number 3B) or saddle-shaped track wind generators are installed in the gap between non-magnetic pole cores. Their band is designed as a thin-walled tube of stainless steel or fiberglass.

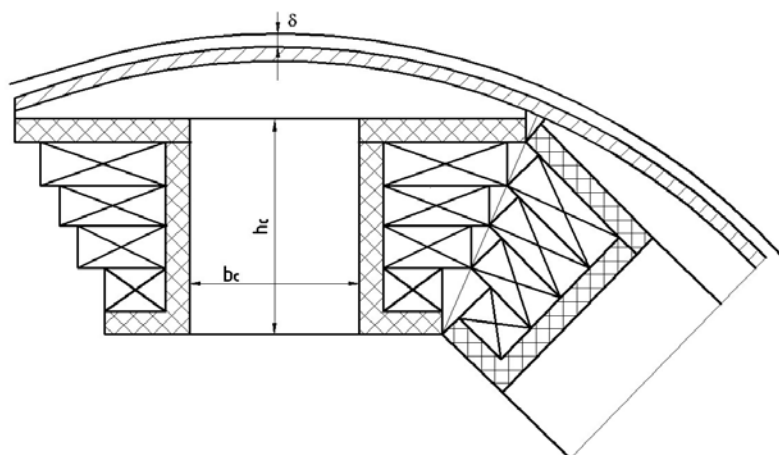


**Fig. 9 Rotor poles.**

**Table IV Specification of the poles.**

Parameter	Option № 1	Option № 2	Option № 3A,B
Type	Traditional	HTS completely	HTS - hybrid
Working gap $\delta$ , mm	3,9	3,9	3,9
Width of the pole piece $b_p$ , mm	70	70	37
Width of the pole core $b_c$ , mm	60	60	30
Height of pole piece $h_p$ , mm	16	16	12
Core length of the pole and pole piece $l_m$ , mm	830	830	1060
Height of the pole core $h_c$ , mm	124	124	115

#### 4 CRYOGENIC COOLING AND SEALING

Autonomous and trouble-free operation HTS wind turbine requires the development of reliable systems for cryogenic cooling, with highly efficient and cost-effective, low mass and size and long-life cryogenic refrigeration or cryocooler. Technical requirements depend on the losses in the cryogenic region and the scheme cryostating. For example, in a fully superconducting wind generator (option number 2) losses in the HTS stator winding is 300 W, the total background heat leak into a stationary and a rotating cryostats 40 W. The largest share of the loss falls on the ferromagnetic stator core,  $\sim 20$  kW. Therefore, in a fully superconducting wind generator (option № 2) the stator core to produce a nonmagnetic material (position 3 in Fig. 3). Ferromagnetic screen (position 6 in Fig. 3) should be imposed beyond a static cryostat. In this context, they are reduced to the following indicators: cooling capacity up to 500 W at 77.4, to the resource without maintenance  $\sim 30000$  hours. Promising are the pulsation tubes with high efficiency, working on the Stirling cycle.

In a cryogenic electric machine uses two types of seals - the labyrinth and magnetic fluid. To create a hydraulic resistance of outflow of the shaft has a number of separated annular gap arranged in series along the shaft cells, forming "a labyrinth". The basis of the labyrinth seal is the centrifugal force acting on gas particles. Centrifugal force is greater the higher the tip speed of rotating parts of the labyrinth site, and the greater efficiency of labyrinth seal. Thus, in low-speed wind turbine generator labyrinth seals are of little use.

Is more appropriate noncontact slit magnetic-fluid seal. The sealing unit includes a stainless steel shaft (or attachment to it) of a ferromagnetic steel, a permanent magnet and two magnetic core. Sealable gap between node from the ferromagnetic steel and the shaft (paddle) is filled with magnetic fluid. Magnetic fluid is retained in the gap of the magnetic field. Magnetic fluid is a colloidal mixture of ferromagnetic (or ferrite) nano particles with an organic solvent. Heavy enough to ferromagnetic nano particles provide an effective seal work because they do not perform Brownian motion. To avoid agglomeration of nano particles covered with surfactant.

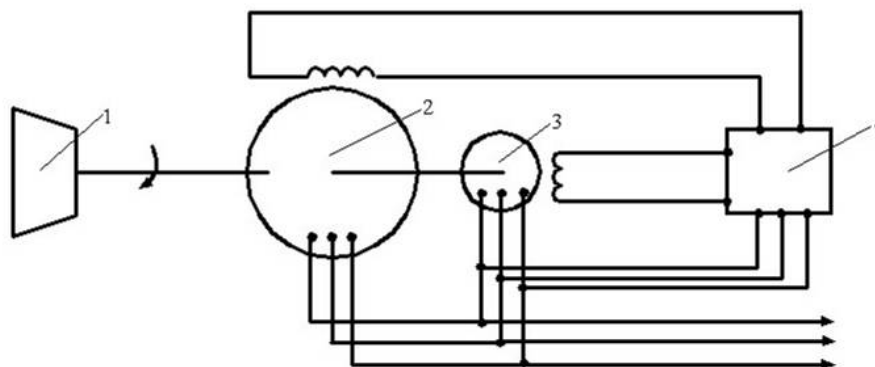
Experience of application of magnetic fluid seals in a superconducting synchronous generator KTF-20 power 20 MW shows that it provides a reliable separation of the helium vapor flows through several channels at the shaft rotates with a frequency of 3000 rpm [6]. Unlike other helium cryogenic agents less fluid and thus do not create additional problems with sealing.

#### 5 WORK IN POWER SYSTEM

Parallel operation with grid system makes windmill to the requirements for maximum development and the quality electricity in a wide range of wind speeds. Most wind turbine megawatt level have a direct or semi-direct transmission. As a result, the generated alternating current has a low frequency. To obtain the current of commercial frequency, he straightens up, and then converted to an inverter into alternating current line frequency. With short, strong gusts of wind or a sudden change in load in the network may be transient voltage spikes ("flicker effect"). They are extinguished with the help of electronic devices.

In wind turbines, which use a transmission with adjustable pitch, the reaction control system to changes in wind speed is ensured by changing the angle of the blades of wind turbines. However, this system of active stabilization speed windmill is a complex and expensive.

For this purpose, we can apply simple and effective way by installing the same shaft as the wind-power plants auxiliary synchronous motor relatively low power (Fig. 9) [8]. Auxiliary synchronous motor maintains constant speed windmill as an increase or decrease in wind speed.



1 - wind turbine, 2 - synchronous generator, 3 - auxiliary synchronous motor, 4 – control.  
Fig. 9 Scheme to maintain a constant speed windmill.

Installing on a common shaft auxiliary synchronous motor 3 increases the synchronizing power generator 2, ensuring its operation without loss of synchronism with the network even with significant changes in the moment. With increasing speed of the wind flow auxiliary synchronous motor 3 becomes regenerative, giving power to the load-carrying network. In nominal operation windmill auxiliary synchronous motor 3 operates as a synchronous compensator, does not consume active power.

## BIBLIOGRAPHY

- [1] Milford E. BTM Wind Market Report: International Wind Energy Development – World Market Update 2009; Forecast 2010-2014, 20 July 2010
- [2] [http://www.fedpress.ru/federal/moscow/Business\\_finance/id\\_216542.html](http://www.fedpress.ru/federal/moscow/Business_finance/id_216542.html) 01.02.2011.
- [3] <http://www.amsc.com/.../windEnergy/seatitan.html>.
- [4] Домбровский В В, Хуторецкий Г М. Основы проектирования электрических машин переменного тока. – Л. – Энергия, 1974: 504 с
- [5] Пономарев Л Т. Закономерности физико-химической технологии создания материалов и конструкций изоляции. – СПб. – ОЭЭП РАН, 2004: 112 с
- [6] Антонов Ю Ф, Данилевич Я Б. Сверхпроводниковые топологические электрические машины. М.: Физматлит, 2009: 368 с
- [7] Вэйли Ли, Пэн Чэн, И Сюе, Данилевич Я Б, Антонов Ю Ф. Расчет и анализ электромагнитного и температурного полей синхронного ветрогенератора мощностью 1,5 МВт с возбуждением от постоянных магнитов. Электричество, 2010(N 12): 29–34 с
- [8] Антонов Ю Ф, Данилеви Я Б ч, Кручинина Патент И Ю. 2 408 126 С1 (RU). Устройство преобразования электрической энергии, 01.07.2009

**Brushless Excitation System 2G HTS Wind Turbine Generator  
Based on Topological Generator (Flux PUPM)**

**Yu.F. Antonov  
Institute of Silicate Chemistry  
Russian Academy of Sciences  
Russia**

**SUMMARY**

With an increase in unit capacity of wind turbines have increasingly high utilization of active materials. As a consequence, the growth capacity of excitatory systems outpaced the power turbines. This is accompanied by an increase in excitation current. In wind generators of 10 MW it could be ~ 2 kA.

Achieved in superconducting topological generators (flux pump) high-current parameters, together with their main advantage - to form a closed superconducting circuit with the load, allowing for creation on their basis of effective systems for the excitation of superconducting high-power turbines. Topological generator (TPG) - is a fully superconducting electrical machine dc phase resistive superconducting switch. Its main purpose - power superconducting magnetic systems (SMS) in a short mode, in which SMS during the excitation and subsequent work is a closed-circuit superconductor.

Technical possibility of brushless excitation system based on rotating and static exciters topological proved by the example of a synchronous generator capacity of 18 kW with Nb-Ti (LTS) and Y123 (HTS) coil excitation, cooled with LHe or LN.

As shown by experimental studies, the use of superconducting topological generator enables us to exclude from excitation circuit of synchronous turbine power contact device or significantly limit the function of resistive current leads. Current leads are used only for emergency withdrawal of the electromagnetic energy of the excitation windings or for short-field forcing (if required by the terms of the power system).

**KEYWORDS**

HTS, Wind turbine, Topological generator, Flux pump, Excitation, Technology.

## 1 INTRODUCTION

In wind power have the greatest proportion of units with a unit capacity in the range 1.5 ÷ 12 MW. Such wind-power assemblies have significant size and mass. Threefold decrease in mass and size of wind generators with capacity 1.5-12 MW is possible in the application of superconductors in the windings and the reduction of steel in the magnetic circuit. The consequence is that the construction of the wind farm is much cheaper and easier installation of its high altitude. Superconducting wind turbine generators power 1.5-12 MW are meant primarily for use in the power system. Much less often they are used in micro grid. This implies the need to ensure the dynamic stability of superconducting wind turbine in the power system. Compliance with this requirement by changing the current in the field winding is difficult. In this mode the excitatory system should provide twice the voltage and current is forced for 10-20 sec. For this goal will require three to four times to increase the nominal capacity of excitatory systems of wind turbine. Such a regime is difficult to implement because there are speed limits of current variation inherent in a superconductor. On this basis, to ensure the dynamic stability of wind turbines in power system must apply the means of external influence, especially on the wind turbine. It is difficult to implement. Thus, in practice one can only provide continuous nominal mode of operation of wind turbine. He implemented a fairly simple way. In this respect, superconducting wind turbines to megawatt-level perspective is the use of brushless excitation system based on superconducting topological generators [1].

The objective of the report is evidence of the technical possibility of establishing a brushless excitation system based on the topological exciter embedded in a superconducting rotor wind turbine.

## 2 PARAMETERS AND CHARACTERISTICS OF SUPERCONDUCTING TOPOLOGICAL EXCITER

To calculate the parameters and the construction of the superconducting properties of topological exciter needs to know the electromagnetic energy  $W_H$ , superconducting winding of the wind turbine. In a symmetric steady wind generator power  $P_g$  is related to electromagnetic energy  $W_H$  ratio

$$W_H = \frac{(\alpha + 1)^2 + (Q_m + Q_L)^2}{2k^2 Q_m \omega} P_g .$$

Here  $\alpha = R_a/R$ ;  $Q_m = (3\omega L_a)2R$ ;  $Q_L = \omega L/R$ ;  $k = M/(L_a L_H)^{1/2}$  - coefficient of coupling between the windings of the stator and rotor;  $R_a$  - active resistance of the phase stator windings;  $R$  - active load resistance per phase;  $L_a$  - inductance stator windings per phase;  $L_H$  - inductance field winding;  $L$  - load inductance per phase;  $M$  - mutual inductance between the windings of the stator and rotor;  $\omega$  - angular frequency of rotation.

Let  $Q_m = 1$ ,  $R_a = 0$  and, consequently,  $\alpha = 0$ . Then the maximum power of wind turbine at a power factor  $\cos \varphi = \frac{1}{\sqrt{1 + Q_L^2}} = 1$  (where  $Q_L = 0$ ) depends linearly on the stored energy:  $W_H = \frac{1}{\omega_k^2} P_{g \max} \cdot$

In a superconducting turbine possible mode of constant flux linkage winding. This mode provides a topological pathogen. In this case, the electromagnetic energy of the  $W_N$  is defined as

$$W_H = P_{g \max} \frac{1}{\omega_k^2} \frac{\left[ 1 + (3/2)k^2 + \sqrt{(9/4)k^4 + 1 - k^2} \right]^2}{2 \left[ 1 + (1/2)k^2 + \sqrt{(9/4)k^4 + 1 - k^2} \right] \sqrt{1 - k^2} \sqrt{(3/2)k^2 + \left[ (9/4)k^4 + 1 - k^2 \right]^{1/2}}}$$

In the presence of a half-transmission gear ratio 10, the rotation frequency of wind turbine  $n_g = 150$  rpm, the coupling coefficient  $k = 0,5$  and maximum power  $P_{g \max} = 10$  MW, stored in a superconducting coil excitation energy for the case of the symmetric steady state is  $W_H = 41$  kJ. Power turbine will decrease by about two times compared to its maximum value. If the safety factor from the current in a superconducting field winding to be equal to 1.4 (relative to the nominal value), then increase the power of wind generator at constant flux linkage is impossible.

Thus, as input data for calculating the parameters and characteristics of the exciter can take the following values:  $L_H = 2 \cdot 10^{-3}$  H; nominal current of the wind turbine  $I_v = 2$  kA. In accordance with these values required power superconducting topological exciter  $P_v = 24$  W,

voltage  $U_v = 12 \cdot 10^{-3}$  V, the load current (it is the nominal current wind generator)  $I_v = 2$  kA; efficiency  $\eta_v = 0,8$ . These parameters satisfy the superconducting generator topological type of TPG-4 (Table I) [1].

## 2 MODEL OF SUPERCONDUCTING WIND GENERATOR WITH THE TOPOLOGICAL EXCITERS CAPACITY OF 18 kW: CONSTRUCTION AND SPECIFICATIONS

For experimental studies established the scale model wind generator hybrid type (stator - the traditional, the rotor - superconducting) capacity of 18 kW. Fig. 1 shows the main components (except the rotor), and in Fig. 2 - internal (cryogenic) part of the rotor vertical hybrid model of wind turbine rotor with a built-in superconducting topological exciter.

**Table I Specifications of superconducting topological exciter.**

Parameter	TPG-4	TPG-LTS (HTS)
Outer diameter of the armature core, mm	185	100
Bore anchor, mm	167	90
The length of anchor, mm	250	100
Sectional area of the pole shoe mm <sup>2</sup>	90×15	64×10
Number of poles	4 or 6	4
The diameter of inductor coils (on the wound), mm internal/external	20/140	12/84
Height inductor coils (on the wound), mm	15	10
The fill factor for winding	0.4	0.5
Number of inductor coils	2	2
Number of turns of armature winding	5	1
The number of parallel conductors armature winding	10	9
Material switch - tape thickness, μm	25	50/50
Emf, mV	30	3/1.7
Load current, A	2000 (4.2 K)	260/170 (4.2 K); 55 (77.3 K)
Permanent solenoid load (for the geometric center), T/A	$1.7 \cdot 10^{-3}$	$5,3 \cdot 10^{-2}$
Inductance of the load test (normal state), H	$13 \cdot 10^{-3}$	0,37
Stored in a test load of electromagnetic energy, kJ	26	4.15



**Fig. 1 The nodes of the superconducting wind generator model with a topological exciter**

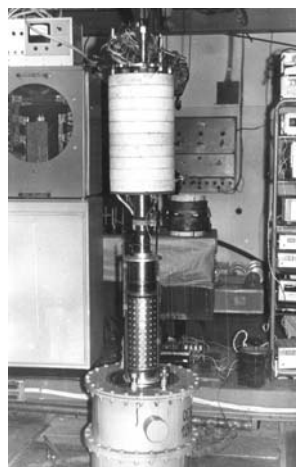


**Fig. 2 The interior of the rotor of the superconducting wind generator model before diving into the technological cryostat.**

### 2.1 Stator

The stator has a stand, core, winding and nitrogen vessel. Bed is a hollow cylinder of stainless steel. It is fastened to the frame. The frame is welded to the bedplate., At the bottom of the frame is installed electric power. Top frame with the lid, stainless steel, which has a built-in diameter. The cover also serves as the upper end shield. Go to the top cover of the bed on a thin-walled aluminum cylinder

suspended from a ferromagnetic stator core with a copper coil. The core is made of sheet electrical steel thickness of 0.35 mm. In contrast to the conventional technology, the package lists are isolated from each other epoxy curing cold. Core has axial ventilation ducts. At the core sheets are semi-closed slots for stacking stator conductors. The winding is partitioned. Her slot insulation made of Insulating. Provided by cooling coils with liquid nitrogen. The upper bearing shield has fittings for filling and draining its nitrogen vapor. In the central part of the shield is placed drive the exciter. Bottom to the frame through a rubber seal on the bolt is fastened a massive flange with a central hole for passage end rotor. Go to the flange inside docked two coaxial cylinders. Cylinders made of glass tape by its layer-winding on templates with simultaneous sizing epoxy curing cold. Annular gap between the cylinders is filled with liquid nitrogen. Liquid nitrogen is used to cool the stator windings. Between the outer dielectric cylinder and the bed is placed a layer of plastic foam, intended to reduce the freezing bed. The number of grooves 48, bore diameter 254 mm; Detent division 16.6 mm pole pitch 24 slots (400 mm); winding factor of 0.828, the magnetic flux  $4.26 \cdot 10^{-3}$  Wb; active length of 104 mm, the coefficient of pole overlap 0.64; winding pitch by grooves 16, the amplitude of magnetic induction in the working gap of 0.16 T, the number of turns of phase 280, the number of conductors in the slot 36, wire Nb+50% Ti Ø1.62/1.73 mm in the varnish insulation, outer diameter 366 mm, length place the front part of 145 mm, diameter 550 mm barrel.

## 2.2 Rotor

The rotor consists of a barrel and two massive ends. Barrel of a rotor with the upper end forms cryostat. Massive lower end is an intermediate docking between the rotor and the driving mechanism. Connection with the barrel bottom end rotor detachable. This allows the notch flanks of the rotor from the stator without disassembling the driving mechanism.

Upper end with the barrel of the rotor is bolted connection. It mounted angular contact ball bearing and knot collect return flow of helium gas. Nodes of liquid helium, and the collection of gaseous rotating seals have made on the basis of Fluor plastic polyurethane and rubber parts. Inside the upper end rotor installed electric insulation pipe. It is equipped with external longitudinal ventilation ducts, underemployed measuring wires in Teflon insulation. Test leads are derived on the slip rings through the radial hole in end rotor, located above the bearing. Under the slip rings is placed a protective shield that protects the bearing from contamination copper graphite dust. The outer casing of the cryostat is a thick-walled cylinder made of stainless steel. It connects to a thin-walled cylindrical inner shell development of thermal bridges on the one hand, and through a vacuum tube with another. The inner thin-walled cylinder is wound multi-layer insulation, metal films and glass veil. Multilayer insulation is surrounded by a polished brass shell (see Fig. 2). Copper sheath soldered to the two mechanical copper rings, which, in turn, soldered to the inner thin-walled cylinder. All vacuum-tight connections are welded. The diameter of the outer shell of the cryostat of 180 mm, diameter of the inner (cryogenic) cryostat shell 120 mm tank height for cryo agent 455 mm height to the neck of 605 mm, barrel length 805 mm rotor, the number of turns of field winding 568; wire Nb+50% Ti Ø1.5 mm in the varnish insulation. Total length 1800 mm generator.

Superconducting field winding at the bottom of the rotor. Her wound carried a piece of wire without the use of bonding compound. Torque is transmitted to the winding through the trapezoidal finger-sliding splinted connection. In the axial direction, it can be shifted only towards the top end rotor.

## 2.3 Superconducting topological exciter

As the superconducting exciter is used topological generator TPG-LTS (HTS) (Table I ). Its body is fastened with screws to a perforated flange. Flange separates the main helium volume and the neck of the cryostat. On the outer surface of a ferromagnetic cylindrical shell topological agent, longitudinal vents depth of 1 mm and 2 mm wide. Ventilation ducts made with a step on the circle at 150.

Resistive superconducting switch topological agent is placed in the gap between the ferromagnetic body and textolite cylinder having a wall thickness of 2 mm. Cabinet insulation resistance-superconducting switch is made of thick cardboard electrical 0,15 mm, insulation between coils - from the Mylar film of thickness 20 microns. Tubular propeller shaft drive mechanism has an outer diameter of 20 mm and wall thickness of 1 mm. At the bottom it ends perforated flange, which is welded hinge. At the top of the tubular shaft planted gear drive transmission unit topological pathogen. Coaxially with the tubular shaft is stock standard helium siphon overflow.

## 2.4 Electric drive

Electric drive, replacing the wind turbine consists of a DC motor ПИИ-85, V-belt transmission with pulleys and a sealed gear mechanism. The shaft runs inside the bellows, the ends of which are soldered to the bearing outer ring. Through the splined connection shaft is joined to the lower end rotor.

## 3 TOPOLOGICAL EXCITER FROM LOW AND HIGH TEMPERATURE SUPERCONDUCTORS

### 3.1 Construction of topological exciter

The principle of operation of superconducting topological exciter presented in [2]. Topological exciter is made in two ways: from the low-temperature (LTS) and high-temperature (HTS) superconductors. Their designs do not differ from each other. This is evidenced by the scheme of the longitudinal section (Fig. 3). Thus, low and high temperature versions are interchangeable.

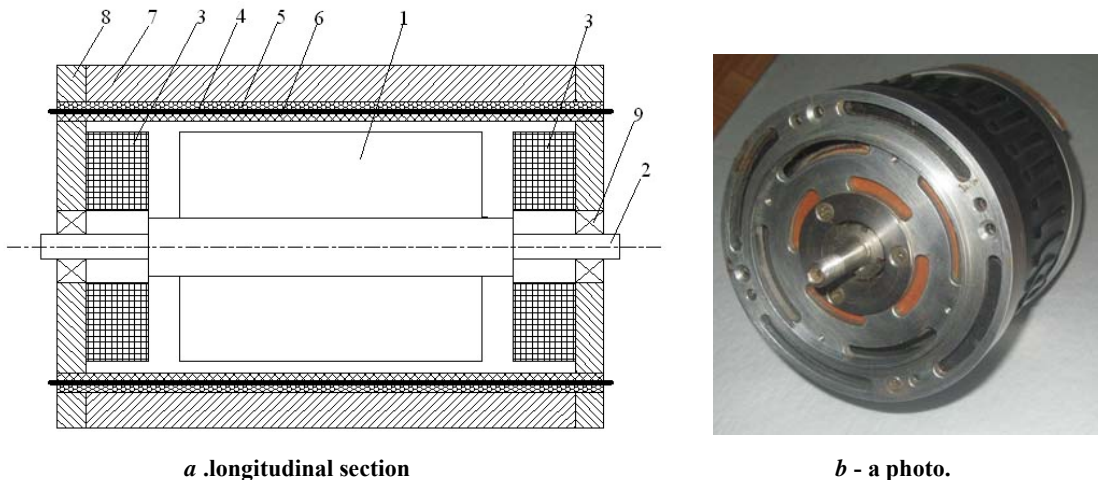


**Fig. 3 Superconducting topological exciter with the resistive superconducting switch from Nb +1,5% Zr and  $\text{YBa}_2\text{Cu}_3\text{O}_{7-x}$ . Rated load  $I_v \equiv I_N = 260 \text{ A}$  ( $T = 4.2 \text{ K}$ );  $170 \text{ A}$  ( $T = 4.2 \text{ K}$ ),  $55 \text{ A}$  ( $T = 77.3 \text{ K}$ ).**

Outer diameter of 100 mm, length 100 mm, number of parallel armature winding turns 12; material resistive superconducting switch - the film of Nb+1,5%Zr thickness of 50 nm and 80 mm wide, the number of winding of the coils 2, the inner and outer diameters and height (winding) 11, 84 and 10 mm respectively, the wire of Nb+50%Ti  $\varnothing$ , 33 mm; insulation varnish, and the number of poles 4, the length and width of the pole piece 60 and 10 mm ball bearings angular contact, single row with the separator of Teflon-4 (without lubrication), the topological exciter mass 8 kg. In the topological exciter TPG-HTS armature winding and the resistance-superconducting switch (RSS) 4 constitute a whole they are made of 2G HTS ribbon width  $d = 100 \text{ mm}$  and a thickness of  $\delta = 50 \text{ microns}$ . Deposited layer superconducting ceramic  $\text{YBa}_2\text{Cu}_3\text{O}_{7-x}$  has a thickness  $\delta_s = 1 \text{ }\mu\text{m}$ , and bilateral stabilizing copper coating  $\delta_{\text{Cu}} = 25 \text{ }\mu\text{m}$ .

Armature winding and RSS 4 are set on an insulating cylinder 6. Bandage 5 provides their electrical isolation from the housing 7. Split housing 7 serves as a ferromagnetic core armature. Inductor consists of a field winding 3 and the toothed ferromagnetic core 1. Field winding 3 is made of two identically wound coils 3 with a rectangular cross-section. Coil 3 attached to a ferromagnetic bearing shields 8 mirror each other. They create the opposite direction along the magnetic field, which is concentrated at the poles, the teeth 1. Pole-teeth have a homopolar magnetization. Notched a ferromagnetic core is rigidly mounted on a shaft 2. Shaft rotates in bearings 9. Connection between RSS and the superconducting load performed by the application of indium at the contact surface using an ultrasonic soldering iron. Specific contact resistance  $\rho = 5 \cdot 10^{-6} \text{ Ohm}\cdot\text{m}^2$ . Experimental studies of the compounds showed that the contact resistance is almost independent of temperature. Measurements were carried out in liquid nitrogen (77.3 K), liquid helium (4.2 K) and air (300 K).

### 3.2 Options and Features

Preliminary tests of topological exciter TPG-LTS held in technological cryostat. Achieved the following parameters: load current 260 A, voltage of 3 mV. Rotational speed and the excitation current varied in the range  $f = 1 \div 50$  Hz,  $I_i = 2 \div 5$  A. Similar testing topological exciter TBC-HTS performed in two cryogenic mediums - liquid helium and nitrogen. Fig. 4 and 5 show the experimental characteristics obtained in tests in liquid nitrogen.

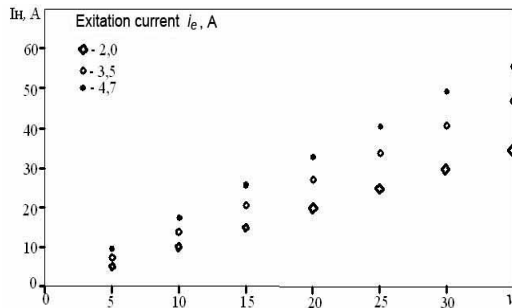


Fig. 4 Cyclic v dependence of the current load  $I_H$ .

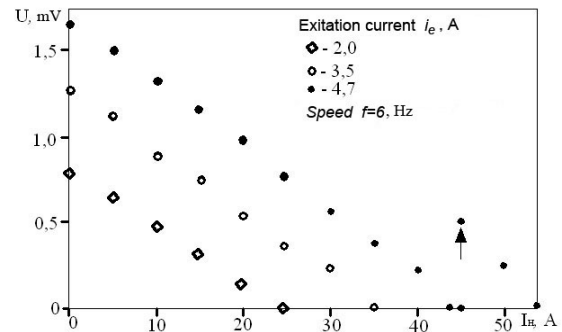


Fig. 5 External characteristics.

## 4 RESULTS OF EXPERIMENTAL RESEARCH MODEL SUPERCONDUCTING WIND TURBINES THE TOPOLOGICAL EXCITER

Phased testing sites superconducting rotor turbine hybrid performance were held in various cryogenic media - liquid helium and nitrogen. As can be seen in the photo Fig. 2, the topological exciter is installed above the superconducting winding of the wind turbine. This is due to the need to accommodate the mechanical drive from the top of a topological exciter. Such a constructive solution for virtually no effect on the topological characteristics of the exciter, because it has a higher critical current than a superconducting field winding wind turbine. Due to lack of current leads in wind turbine modal been regulated solely by the topological exciter.

As a result, helium (4.2 K) cryogenic static tests of the rotor in the technological cryostat, the following data. In the superconducting field winding wind turbine under static conditions the critical current of 450 A, which is estimated at 1.7 above the nominal excitation current car is idling. The distribution of the magnetic field produced by a superconducting coil excitation, obtained with the help of five converters Hall. Hall transducers mounted on the outer surface of the thin-walled cylinder made of stainless steel, which houses the coil. The distribution of the radial component of magnetic induction takes the form of a cosine wave.

Topological exciter TPG-LTS has been tested in the indirect and "pseudo load" modes. "Pseudo load" mode is provided as follows. Terminal ends of the superconducting armature winding TPG-LTS should be soldered to current leads. On them from the DC generator, located outside the cryostat, the transport current is fed into the winding. Transport current models current "load". The current in the armature winding TPG-LTS rose above the critical current of superconducting winding of the turbine at 30 A (7%). Experimentally established the dependence of the voltage at the terminals of TPG-LTS on the transport current "load". At a maximum current 480 A in a superconducting armature winding TPG-LTS voltage at its terminals does not exceed 0.9 mV, while at the nominal (for wind generator) current of 262 A, it reached 3 mV.

The task of the research also included the determination of current-carrying capacity of connections between niobium-zirconium current-carrying elements of the resistive superconducting switch and output ends. All connections are made by contact welding. They stand without going to a normal state of the superconducting armature winding DC current 480 A, with an average of 40 A for the connection.

During helium cryogenic testing of the rotor in the static current in superconducting excitation winding was wound up in 20 minutes. Within 1.5 h ensured persistent current mode. The initial voltage of the topological exciter 4 mV, of course - when the current in the field winding 260 A did

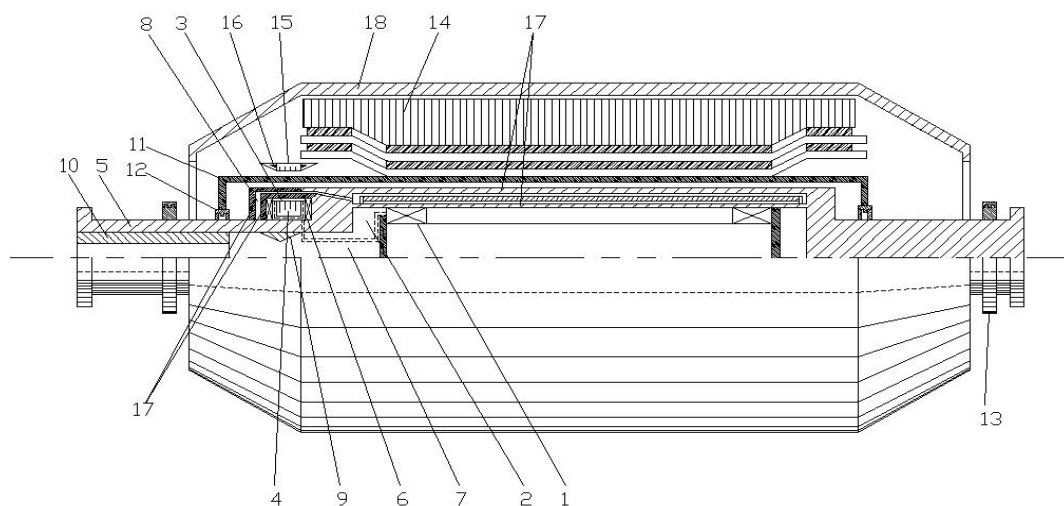
not rise above 2 mV. The total consumption of liquid helium in the cooling down and all the tests was 250 liters.

Assembling a model wind turbine and its drive was carried out directly on the experimental stand. During the assembly of the stator and the drive did not stop vacuuming the rotor. Before installation of the rotor bearings are produced to the preliminary cooling down by pouring liquid nitrogen into the rotor and its removal from the rotor, followed by ventilation of internal volume. Pouring liquid helium into the rotor was carried out in static and rotating the rotor. Steady level of liquid helium in a rotating rotor remained ~ 1 hour. Current in superconducting excitation winding wind turbine was introduced at various rotor speed  $5 \div 10$  Hz. Voltage topological pathogen was maintained at least 2 mV at a current excitation 3 A. During the 15 minutes in the superconducting excitation winding was introduced current 200 A, which accounted for 75% of the rated current load excitation. After the first test bench cycle completion design superconducting wind turbines has been reduced to the reconstruction drive topological agent and search for technical capabilities, simplifying cryo agent fill in the rotor during its rotation.

The second cycle bench test model of the superconducting wind generator consisted in the removal characteristics in the indirect and load conditions with access to the design parameters. In the area of the measurement range no-load characteristic is linear. Topological exciter works steadily and reliably, not only in conditions of constant filling of liquid helium into the rotor, but if the system of liquid helium is disconnected from the rotor and the rotor rotates at a frequency of 25 Hz for 20 min. Investigation of load-limit operation model of the superconducting wind turbine on a local area network (micro grid).

Since the field winding model of wind turbine capacity of 18 kW is made of niobium-titanium wire (LTS), the test topological exciter TPG-HTS in standard conditions were performed in liquid helium. Achieved the following parameters: load current 173 A, voltage 1.6 mV. This is more than 3 times the load current TPG-HTS in liquid nitrogen, but 67% of the nominal value of excitation current models of wind turbines.

Because of the structural complexity of the placement of the drive, with the restrictions on the speed of its rotation, not to install a topological exciter rotor outside the filler and the consequent difficulty in pouring the liquid cryo agent rotating rotor, there is a need to develop a static topological exciter [4, 5] (Fig. 6)



- 1.superconducting field winding 2.cryostat 3.resistive superconducting switch 4.ferromagnetic core 5.shaft  
6. superconducting coil bias 7. axial channels 8. radial channels 9. differential washer 10. tube filling cryo agent  
11. fixed dielectric screen 12.vacuum seal 13. bearing 14.stator core 15.stationary ferromagnetic screen,  
16.three-phase exciter winding 17.vacuum shell cryostat 18. electromagnetic screen.

Fig. 6 Schematic drawing of the superconducting wind turbine generator with a topological exciter.

## BIBLIOGRAPHY

- [1] Глебов И А ,Шахтарин В Н ,Антонов Ю Ф.Проблема ввода тока в сверхпроводниковые устройства.Ленинград: Наука, 1985: 208 с
- [2]Антонов Ю Ф,Данилевич Я Б.Сверхпроводниковые топологические электрические машины. Москва: Физматлит, 2009:368 с
- [3] Антонов Ю Ф. Топологический генератор с фазовым коммутатором из 2G ВТСП// Труды МАИ. Электронный научный журнал. Выпуск № 35. <http://www.mai.ru/science/trudy/> - 2009
- [4] Antonov Y F, Glebov I A, Shakhtarin V N. Contactless superconducting synchronous electrical machine :USA, Patent 4352033. 1982-09-28
- [5] Antonov J F, Glebov I A , Shakhtarin VN. Kontaktlose supraleitende Synchronmaschine:FRG, Patent 3027340. 1983- 10- 27



**The Development of 5MW Off-shore Direct-drive Wind Turbine Generator**

**Lei Xiangfu, Yang Guowei, Li Chunlin, Wang Buyao, Li Suping**

**State Key Laboratory of Off-shore Wind-power Technology and Testing- XEMC**

**Xiangtan, Hunan, China**

**SUMMARY**

XE115 5MW direct-drive permanent magnet synchronous generators for gearless wind turbine are of a new type that developed by XEMC in order to expand the off-shore wind power area. This paper describes the main design basis, design principles, main design features and advantages, as well as the application prospects. From the view point of the type test results, the 5MW grade direct-drive permanent magnet synchronous generators for gearless wind turbine has been developed successfully, with its excellent performance showing that XEMC has been at the advanced level of the world in the development of MW grade direct-drive permanent magnet synchronous generators for gearless wind turbine.

**KEYWORDS**

Generator for wind turbine, Direct-drive, Permanent magnetic, Medium voltage, Insulation Configuration, Slot-pole combination, Demagnetization

## 1 INTRODUCTION

With the deteriorating environment and the growing energy crisis around the world, the full development and utilization of renewable energy has become the consensus of the world countries. As one of the most common renewable clean energy sources, wind energy has been made widely attention, and wind power technologies have made a rapid development in the past two decades. Without the typical gearbox in wind-generating system and the disadvantages caused by gearbox, the permanent magnetic Synchronous generator is directly driven by the wind turbine at low speed, which makes the operation of the generator more liable. Having successfully developed various permanent magnetic generators for gearless wind turbines, such as the series XE72 (22.5RPM, 2MW), XE82 (19RPM, 2MW), XE93 (17RPM, 2MW) and XE93 (18RPM, 2.5MW), XEMC R&D teams<sup>[1]</sup> have accumulate rich experience in designing and manufacturing permanent magnetic Synchronous generators for direct-drive gearless wind turbine, in which the design and process provide a good reference for developing 5MW large and low-speed permanent magnetic Synchronous generator. In order to accommodate the requirement of the off-shore wind turbine to run steadily and maintained easily, this type of generator utilizes the advanced model of the prior generators and uses modern design and manufacturing process, bringing to a successfully development of the 5MW permanent magnetic synchronous generator for direct-drive gearless wind turbines. This paper focuses on the features of this type of generator.

## 2 MAIN TECHNICAL DATA

5MW direct-drive permanent magnetic synchronous generator main technical data as follows

Type: XE115 TFYD5000-1

Rated Power: 5273KW

Rated Voltage: 3000V

Rated Speed: 18 r/min

Rated Frequency: 12Hz

Efficiency: 95%

Phases: 3

Insulation: Class F (for temp. rise utilizes Class B)

Cooling Method: CACA, with outside nature air cooled ribs.

Altitude: 1000 m

Protection: IP54

Ambient Temp.: -10~40°C

Weight: 130000Kg

## 3 DESIGN OF PERMANENT MAGNET GENERATOR

### 3.1 Design Principles

#### 3.1.1 Using a Design of Flat Disc Shape

According to the following equation of the main parameters of generator,

$$D_1^2 l_{ef} = \frac{6.1}{K_{N1}} \cdot \frac{1}{\alpha_p AB_\sigma \eta} \cdot \frac{P_N}{n} \quad [2] [3]$$

where,  $D_1$  is the inner diameter of the generator stator.

$l_{ef}$  is the length of the generator's stator core.

$k_{N1}$  is the generator winding factor.

$\alpha_p$  is the pole embrace.

$A$  is the linear load.

$B_\sigma$  is the flux density of air gap.

$\eta$  is the efficiency.

$P_N$  is the rated power.

$n$  is the rated speed.

The developed 5MW permanent magnetic generator for direct-drive gearless wind turbines has an extremely low rated speed of 18 RPM and a huge size. In order to make use of its linear velocity at the circumference and to minimize its size to form a structure with larger diameter and shorter length, maximizing the stator inner diameter is necessary. The design of flat disc shape can improve the material utilization. However, limited by the size of the VPI container, the stator dimensions are restrictive. The stator outer diameter of this 5MW generator is close to the diameter of 6m of the VPI container.

### 3.1.2 Selecting 3000V Medium Voltage Design

The 5MW permanent magnetic generator for off-shore direct-drive gearless wind turbines is selected with a design of 3000V medium voltage. Comparing to the design of 690V low voltage, the design of 3000V has a higher output voltage hence less cables and lower losses on cables. At least 60KW loss on cables can be avoided in the 3000V medium voltage design than that of the 690V low voltage one. Furthermore, for the rated currents of 3000V and 690V designs, respectively 1100A and 4500A, only 9 (3\*3) cables are required in the 3000V design while 48 (16\*3) cables are required in the 690V design provided that 70mm<sup>2</sup> cables are used. The quantity of cables used has adverse effect on installing the cables. Moreover, there is a cable twist problem to be solved during the yaw operation of wind turbines. Also, the cooling cost of low voltage converter is higher than that of a converter that operates at higher voltage. Therefore, the wind turbines of MW ratings equipped with 3000V medium voltage generator follow the development trend<sup>[4]</sup>.

## 3.2 Electromagnetic Design

### 3.2.1 Insulation Configuration

The insulation configuration is important for improving the uniformity of electric field of the stator windings to minimize the uniformity coefficient of electric field and enhance the breakdown voltage, as well as to eliminate the field concentration and local discharge due to various factors in manufacturing process such as the air spaces, sharp corners and foreign substances existing in the primary insulation, which affect the service life of the generator<sup>[5] [6]</sup>. As the generator supply the grid via a converter, the PWM (Pulse Width Modulation) and switching operation of this converter will exert sharp peaks on the generator windings, which put higher requirements on its inter-turn and coil-ground insulation. The generator equipped with surge protector has to withstand 2-2.5 rated voltage and the one without surge protector has higher requirements on the insulation. The wind turbine generator with 3000V rating has to be tested according to 7.2kV rated voltage so that the thickness of to-ground insulation plus the corona-proof layers and the inter-turn insulation has to be specially enhanced. To accommodate the requirement between turns against the corona, a insulation

system using Class F less-adhesive mica material that is then treated by VPI process with solvent – free epoxy/anhydride resin is employed. Impregnation using solvent-free epoxy resin gives higher depth of impregnation and enhanced overall insulation level. With this insulation system, the generator has the features of thinner insulation, good electrical and mechanical performance, steady thermal characteristics, strong resistance to ambient conditions, simple design, energy-saving, green production environment and environment-friendly and safe operation.

### 3.2.2 Slot-Pole Combination

The cut-in wind speed depends on the start resisting moment of the wind turbine generator, less resisting moment of the generator brings to lower cut-in wind speed and better utilization of wind resource. To minimize the start resisting moment, fractional slot windings with suitable pole-slot combination are used. The slot number per pole per phase is  $q = \frac{b+c}{d}$ , in which larger  $d$  results in more cycles and lower amplitude of start resisting moment. Thus, to minimize the start resisting moment,  $d$  shall be maximized<sup>[7] [8]</sup>. Electromagnetic noise results from electromagnetic vibration, which arises from the electromagnetic force acting on the core due to the air gap field of the generator. The distortion of the radial electromagnetic force that results from air gap flux and acts on the core teeth is the main source of the electromagnetic noise<sup>[9]</sup>. Carefully select the pole-slot combination can also reduce the electromagnetic noise. Because the fractional slot windings of XE72, XE82 and XE93 types present good results, the 5MW permanent magnetic generator keeps the same design of slot number per pole per phase, i.e.  $1\frac{3}{5}$ <sup>[10]</sup>.

### 3.2.3 Anti-Demagnetization Design of Permanent Magnet

In design of the magnetic circuit of permanent magnetic generators, parameters of the permanent magnet directly affect the overall performance of the generator. Therefore, the performance, design and manufacturing features and application of permanent magnetic generators are highly depend on the performance of the permanent magnetic material. When demagnetization occurs in Nd-Fe-B permanent magnetic in a generator, the residual magnetism will be reduced and the potential generated lowered, which will change various parameters of the generator, resulting in such as lower output, higher current and increased temperature rise. To prevent the demagnetization from occurring, the conventional method is, in design phase, keeping a larger allowance in the length in the magnetizing direction of permanent magnet and using electromagnetic steel with high coercive force. The consequence is an increased manufacturing cost of the permanent magnetic generator. In design of this type of generator, the highest demagnetization point and the inflection point of the demagnetization curve under that temperature are checked to improve its reliability so as to keep the working point be above the inflection pint of the permanent magnet's demagnetization curve even under the worst conditions (incl. at high temperature and with high current), assuring that the non-reversible demagnetization of the permanent magnet is less than 1%. Furthermore, a mounting design for box-type permanent magnet of laminated silicon steel sheets, which has intellectual property rights<sup>[11]</sup>, is used. This reduced the eddy loss and the demagnetizing effect of the permanent magnet resulted from sudden short-circuit current.

The magnetic steel part of 5MW permanent magnetic generators for off-shore gearless wind turbines has a larger magnetizing area and put high requirement on the magnetizing uniformity of the magnetic steel part. These 5MW generators employ Nd-Fe-B permanent magnets with high

performance, which exert restrictive requirements on protecting the magnetic steel. In order to enhance the chemical stability of the permanent magnet, Nickel-Copper-plated and electrophoresis epoxy coatings are designed on the surface of magnetic steel.

**4 DESIGN OF VENTILATION AND COOLING**

Comparing to the types of XE72, XE82 and XE93, this 5MW generator has higher unit capacity and uses higher electromagnetic loading to enhance the material utilization. Thus, the generation has to be designed with its cooling system improved to enhance it’ s heat sinking capacity. According to the losses from the electromagnetic calculation, 60% of the heat generated is dissipated by the outside nature air cooled ribs and 40% of the heat generated dissipated by its CACA design. Because the material of Aluminum has higher heat sinking capacity (the heat conductivity of Aluminum is more than 4 times that of Ferric), the ribs of Aluminum that are used improve the heat dissipation conditions of the generator, better resolving the heat dissipation problem of the large permanent magnetic synchronous generator for wind turbines under nature air cooling conditions. The patent application about these Aluminum heat-sink ribs has been filed to the national patent office.

The construction, electromagnetic and heat sinking considerations in large generator design affect each other. In designing this 5MW permanent magnetic synchronous generator, the calculation about heat dissipation is done following the preliminary design of the generator and the electromagnetic design is adjusted according to the calculation results above. The generator reliability is ensured by using existing reliable design and materials as well as by utilizing matured design means and comparable methods, giving a successful development of this new type of generator.

**5 RESULTS OF TYPE TEST**

Two 5MW permanent magnetic synchronous generators are tested in back-to-back configuration. The driving machine drive the generator to its rated speed via the coupling and the power generated by the generator in full output operation is fed back to the grid via a converter<sup>[12]</sup>. Photo 1 shows the back-to-back full power test bench.



**Fig.1 5MW permanent magnetic synchronous generator back-to-back full power test bench**

**Table I Designed Data vs. Tested Results of 5MW Permanent Magnetic synchronous Generator**

Main Data	$P_N$	$U_N$	$I_N$	$\eta$	Stator Temp. Rise	Waveform Distortion	Noise (sound power level)
Designed	5273KW	3000V	1046A	96%	105K	5%	107dB (A) <sup>[13]</sup>
Tested	5273KW	(cold 20°C) 2999V (hot 100°C) 2849V	1092A	95.3%	93.3K	1.25%	101dB (A)

From Table I, we can see that the prototype of 5MW permanent magnetic synchronous generator for off-shore direct-drive gearless wind turbines achieved or even exceed the design target. The prototype of 5MW generator has been developed successfully and it went off the line on Oct. 25<sup>th</sup>, 2010.

## 6 APPLICATION

One of the two prototypes of 5MW permanent magnetic synchronous generator for off-shore gearless wind turbine will be installed in a domestic off-shore wind farm and the other in a Europe wind farm. Furthermore, various owners of overseas wind farms have shown great interests in these new generators. At present, a memo of cooperating in off-shore wind power at 5MW level has been signed between XEMC and the state of Delaware of USA.

## 7 CONCLUSION

Owing to the implementation of developing the 5MW permanent magnetic synchronous generator for off-shore gearless wind turbines, XEMC will be in the position to have a design and manufacturing capacity of annual output of more than a hundred 5MW large generators for off-shore direct-drive gearless wind turbine<sup>[14]</sup>. This is consistent with the aim for manufacturing enterprises that was initiated by the government to be robust in developing new equipment. These products of generator will form an industrial output of more than 1000 million yuan(RMB) and bring to considerable tax income and enterprise profit, which will greatly help the national energy resource structure transit and make energy renewable as well as protect the environment. Moreover, this type of independent developed product has intellectual property rights and is comparative to the overseas equivalent products in technical advantages. Additionally, as the dominant position of China as far as the raw materials and supporting industries such as those about Rare-earth permanent magnet, steel & iron industry and machinery industry, these generators are bound to have a dominant share in international market.

## BIBLIOGRAPHY

- [1] XEMC.State Key Laboratory of Off-shore Wind-power Technology and Testing- XEMC [J] .Electric Machines & Control Application, 2010
- [2] Tang R. Modern Permanent Magnet Machines-Theory and Design[M].Publication, 1997:328~329
- [3] Chen S. Electric Machinery Fundamentals [M]. Publication, 2000 :9~11

- [4] Xiao H, Huang S. The study and design of MW permanent-magnet synchronous generator in the wind power generation system [D] :3~5
- [5] Wan Y, Li Z. Methodology Study of On-line Partial Discharge Monitoring and Analysis for Large Generator [D] :1~5
- [6] Cai J, Zhang X. Research and preparation of VPI resin for dry mica tape for high-voltage motors. *Insulating Materials* [J] ,2004
- [7] Lin Y, Tang R. Research on Technology of Demagnetization Proof of Permanent Magnet Machine on High Temperature [D] :2~3
- [8] Wang W, Tang R. Calculation and Suppression of Electromagnetic Noise for Disc Type PMSM with Multi-Pole and Few-Slot [D]
- [9] Song Z, Tang R. Research on Recognition of Electromagnetic Noise and Vibration of Permanent Magnet Synchronous Machine [D]
- [10] Liu L, Tang R. Study on key technology of MW grade direct-drive permanent-magnet synchronous generators for wind turbines [D] :69~71
- [11] XEMC. Rotor structure of wind turbine permanent magnet synchronous generator. CN101212154A
- [12] Wind turbine low-speed permanent magnet synchronous generator-Testing methods. GB/T 25389. 2010-2
- [13] Measurement of airborne noise emitted by rotating electrical machines and the noise limits. GB 10069.3-2008/IEC 60034-9:2007
- [14] XEMC .XEMC 5MW PMSG for off-shore wind power will large scale yield next year [J] 2004 Electrical Manufacturing , 2010

## Development of Permanent Magnet Wind Generators with Fractional Slot Concentrated Winding

Tang Renyuan, Tong Wenming, An Zhongliang  
National Engineering Research Center for Rare Earth Permanent Magnet Machine  
China

### SUMMARY

Permanent magnet wind generators (PMWGs) are more superior in terms of energy yield, reliability, and maintenance problem than other generator concepts. Permanent magnet machines with fractional slot concentrated winding (FSCW) have been gaining interest over the last few years, due to the several advantages that this type of windings provides. However, presently most of the FSCW permanent magnet machines are used for low power industrial applications, and they are not yet frequently used in larger electrical machines.

In this paper, firstly the slot and pole number combinations for large power PMWGs with FSCW are discussed by considering all the parasitic effects. The curve that fundamental winding factors vary with  $q$  (slots per pole per phase) is obtained. The maximum winding factor for double-layer FSCW is 0.955, which appears at  $q$  equals  $1/m$ . The closer  $q$  is from  $1/m$ , the higher fundamental winding factor is achieved. Especially, the winding factor of slot harmonics is equal to fundamental winding factor. Thus, if the orders of slot harmonics are lower than 1, the amplitudes of these harmonics will be larger than that of fundamental wave. The factors that affect sub-harmonics and harmonic spectrums are analyzed in this paper. A very low cogging torque can be obtained if the slot and pole numbers are chosen so that the least common multiple between them is large. The closer the number of slots to the number of poles, the higher their least common multiple can be achieved. An even number of slots or a multi-unit machine combination should be used for large PMWGs from the unbalanced magnetic pull point of view. As stated above, the conventional combinations of slot and pole number are not suitable for large power PMWG because of the stator MMF harmonics and the possibility of unbalanced magnetic pull. Multi-unit machine combination is a good choice from the comprehensive point of view.

Secondly, the thermal management work is carried out for a 100kW prototype generator with FSCW. Then, a modular structure with closed-slot is presented in order to improve fault tolerance capacity. At last, a 100kW modular PMWG with FSCW is manufactured. Measurements on the prototype generator have demonstrated that FSCW generators are favourable.

### KEYWORDS

Permanent magnet wind generator, Fractional slot concentrated winding, Winding factor, MMF harmonics, Cogging torque, Unbalanced magnetic pull, Modular structure, Thermal management

## 1 INTRODUCTION

PMWGs are more superior in terms of energy yield, reliability, and maintenance problem than other generator concepts. Permanent magnet machines with FSCW have been gaining interest over the last few years. This is mainly due to the several advantages that this type of windings provides, including high efficiency, short end turns, high slot fill factor when modular structure is used, low cogging torque, and high fault tolerance capacity. However, presently most of the FSCW permanent magnet machines are used for low power industrial applications, and they are not yet frequently used in larger electrical machines [1]. This is due to an increased amount of parasitic effects like low fundamental winding factor, alternating magnetic fields in the rotor, unbalanced radial forces and acoustic noise and vibration. In this paper, firstly the slot and pole number combinations for large power PMWGs with FSCW are discussed by considering all the parasitic effects. Secondly, the temperature distribution over a 100kW PMWG with FSCW is calculated by taking into account the copper losses, iron losses and rotor losses. Then, a modular structure is presented in order to improve fault tolerance capacity. At last, a 100kW modular PMWG with FSCW is manufactured. Measurements on the prototype generator have demonstrated that FSCW generators are favourable.

## 2 SLOT AND POLE NUMBER COMBINATIONS

### 2.1 Winding factor

The winding factors of an electrical machine are proportional to the generated electromagnetic torques. So the fundamental winding factor of the PMWG must be high and its sub- and super-harmonic winding factors as low as possible. The pitch factor  $k_{pv}$  of different harmonic orders for three-phase double-layer FSCW is computed by

$$k_{pv} = \sin\left(v \frac{y}{y_\tau} \frac{\pi}{2}\right) = \sin\left(v \frac{\pi}{6q}\right), \quad (1)$$

where  $v$  is harmonic order, coil pitch  $y$  equals 1 for FSCW,  $y_\tau$  is pole pitch and  $q$  is the slots per pole per phase, which can be written as  $q = \frac{c}{d}$ .

For three-phase double-layer FSCW having a phase spread of  $60^\circ$ , the distribution factor of different harmonic orders can be calculated from the equation [2]

$$k_{dv} = \frac{\sin c \frac{\alpha_v}{2}}{c \sin \frac{\alpha_v}{2}}. \quad (2)$$

If  $d$  is even, then  $\alpha_v = Y_0 d \alpha_m v + \pi$ . If  $d$  is an odd number, the value of  $\alpha_v$  should be calculated in two cases. If  $G$  is even, then  $\alpha_v = Y_0 d \alpha_m v$ , otherwise,  $\alpha_v = Y_0 d \alpha_m v + \pi$ . In these formulas,  $\alpha_m = \frac{\pi}{3c}$ ,

$Y_0 = \frac{3cG + 1}{d}$  and  $G$  is the smallest integer to make  $Y_0$  become an integer.

For a three-phase double-layer FSCW generator, the winding factor of different harmonic orders can be solved from the equation

$$k_{dqv} = k_{pv} k_{dv} = \sin\left(v \frac{\pi}{6q}\right) \frac{\sin c \frac{\alpha_v}{2}}{c \sin \frac{\alpha_v}{2}}. \quad (3)$$

The fundamental winding factor  $k_{dp1}$  is calculated according to formula (3), as shown in Fig. 1. In order to improve the torque density of PMWG, the slot and pole number combinations with a high  $k_{dp1}$

should be adopted. As can be seen from Fig. 1, the maximum  $k_{dp1}$  for double-layer FSCW is 0.955, which appears at  $q$  equals  $1/3$ . Whether  $q$  is greater than or less than  $1/3$ ,  $k_{dp1}$  is reduced. The closer  $q$  is from  $1/3$ , the higher  $k_{dp1}$  is achieved. To make sure that  $k_{dp1}$  is greater than 0.93,  $q$  must be selected between 0.28 and 0.4.

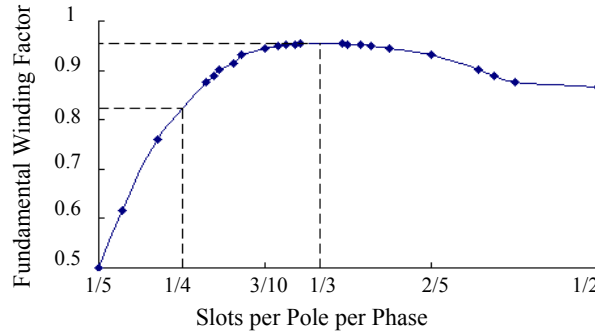


Fig. 1 Fundamental Winding Factor Varies with Slots Per Pole Per Phase.

## 2.2 Stator MMF harmonics

PMWGs with FSCW have a stator MMF distribution containing a rich set of space harmonics and a pulsating flux component caused by air gap reluctance variations. These phenomena result in lower and higher order space MMF harmonics with rotational speed asynchronous to the rotor, which induce eddy current losses in the magnets.

The rotation speed of  $v^{\text{th}}$  harmonic is  $1/v$  of the fundamental wave. The relationship between the amplitude of  $v^{\text{th}}$  harmonic and fundamental wave can be shown as

$$F_v = \frac{F_1}{vK_{dp1}} K_{dpv}, \quad (4)$$

where  $F_1$  and  $F_v$  are the amplitudes of fundamental wave and  $v^{\text{th}}$  harmonic respectively.

As can be seen from formula (4), the amplitude of  $v^{\text{th}}$  harmonic is inversely from the number of  $v$ . For sub-harmonics,  $v$  is less than 1, so the amplitudes of such harmonics will be much larger than the super-harmonics when the same winding factor is assumed. It is demonstrated that the sub-harmonics are the main causes of rotor losses. Especially, the winding factor of slot harmonics  $v=2mqk \pm 1$  ( $k=1, 2, 3 \dots$ ), is equal to fundamental winding factor. Thus, if the orders of slot harmonics are lower than 1, the amplitudes of these harmonics will be larger than  $F_1$ . This is quite dangerous for large PMWG. To make sure that the lowest order of slot harmonic ( $v_1=2mq-1$ ) is larger than 1,  $q$  must be larger than  $1/m$ . For some regular slot and pole number combinations, like  $Q=2p-1$  and  $Q=2p-2$ , the value of  $q$  is smaller than  $1/m$ , which means that a sub-harmonic with a larger amplitude than fundamental wave is existed in the space, and rotates with the speed of  $1/v$  of the fundamental wave. This kind of slot and pole number combinations should be avoided for large power PMWGs.

The choice of the combinations of slot and pole number should be influenced by the stator MMF harmonic spectrum and specially the quantity and amplitude of the sub-harmonic components with a view to minimizing the rotor losses. The stator MMF harmonics aroused from different slot and pole number combinations need to be calculated. If  $d$  is even, the stator MMF harmonics are [3]

$$v = \pm \frac{1}{d}(2mk + 2). \quad k = 0, \pm 1, \pm 2, \pm 3, \dots \quad (5)$$

If  $d$  is odd, the stator MMF harmonics are

$$v = \pm \frac{1}{d}(2mk + 1). \quad k = 0, \pm 1, \pm 2, \pm 3, \dots \quad (6)$$

According to formula (5) and (6), the number of sub-harmonics has a relationship with the value of  $d$ , which is shown in Fig. 2. As can be seen from the figure, the number of sub-harmonics increases greatly along with the increasing of  $d$ . Similar conclusion can be obtained: the number of harmonics

below seventh increases also along with the increasing of  $d$  as shown in Fig. 3. The combinations of slot and pole number should be chosen with a small value of  $d$ . For large power PMWGs, hundreds of poles may be used. If  $Q=2p \pm 1$  or  $Q=2p \pm 2$  is used, the value of  $d$  will be quite large. Take 45-slot 40-pole and 42-slot 40-pole for example, the values of  $d$  are 8 and 20 respectively. The number of sub-harmonics is 2 for 45-slot 40-pole and 6 for 42-slot 40-pole. There are 18 different orders of harmonics below seventh for 45-slot 40-pole, but this number becomes 47 for 42-slot 40-pole. The stator MMF harmonic spectrums for both cases are shown in Fig. 4 and 5 respectively.

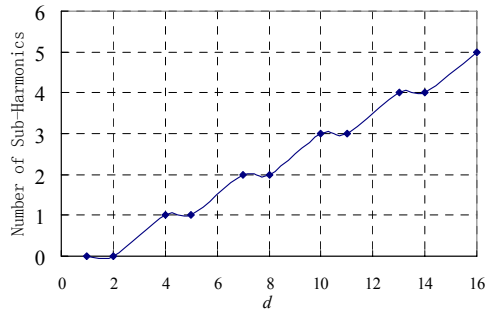


Fig. 2 Number of Sub-Harmonics Varies with  $d$

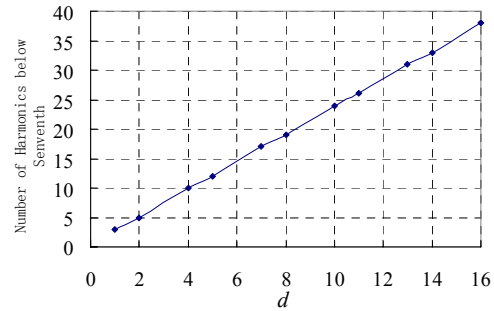


Fig. 3 Number of Harmonics below Seventh Varies with  $d$ .

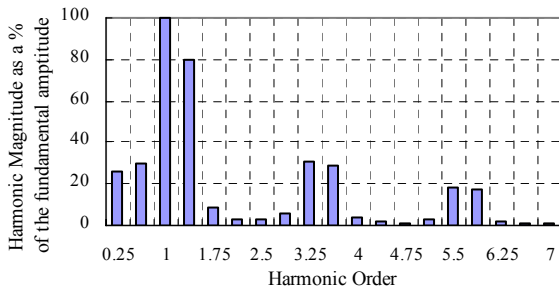


Fig. 4 Stator MMF Harmonics of 45-Slot 40-Pole

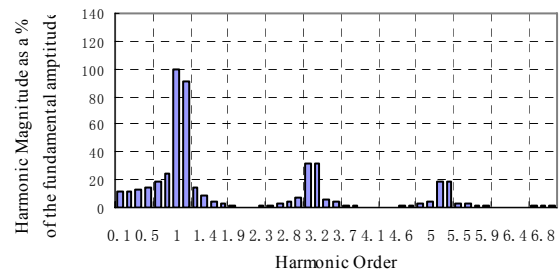


Fig. 5 Stator MMF Harmonics of 42-Slot 40-Pole.

### 2.3 Cogging torque and unbalanced magnetic pull

Cogging torque results from the interaction of the rotor permanent magnets with the stator teeth. The use of a fractional number of slots per pole reduces the amplitude of the cogging torque greatly. In general, the higher the least common multiple between the number of poles and the number of slots, the lower the cogging torque, while the smaller the greatest common divisor between the number of poles and the number of slots, the lower the cogging torque.

A very low cogging torque can be obtained if the slot and pole numbers are chosen so that the least common multiple between them is large. The closer the number of slots to the number of poles, the higher their least common multiple can be achieved. For example, the smallest common multiple is 360 for 45-slot 40-pole, while this number is 240 for 48-slot 40-pole. Hence, the lower cogging torque is achieved with machines having 45-slot 40-pole.

If the radial magnetic forces are not regularly distributed along the air gap, their sum results in an unbalanced magnetic pull that rotates with time and generates noise and vibration in the machine. This resulting force is due to the asymmetry in the windings. When the combinations of slot and pole number with  $Q=2p \pm 1$  are chosen, the unbalanced magnetic pull will exist. Therefore, an even number of slots or a multi-unit machine combination should be used for large PMWGs from the unbalanced magnetic pull point of view.

### 2.4 Fault tolerant capacity

For double-layer FSCW PMWGs, the phase windings are effectively isolated magnetically, and a high per-unit self-inductance can be achieved to limit the short-circuit current by utilizing the relatively high air gap inductance and leakage flux at the slot openings. Due to the negligible mutual-inductance between phases, the possibility of a phase-to-phase short-circuit fault is minimized. The self- and

mutual-inductance of a 45-slot 40-pole PMWG is calculated, as shown in Fig. 6 and 7 respectively. As can be seen from the two figures, the self-inductance is almost 12 times higher than mutual-inductance. Therefore, a good fault tolerant capacity can be achieved by using the combination of 45-slot 40-pole.

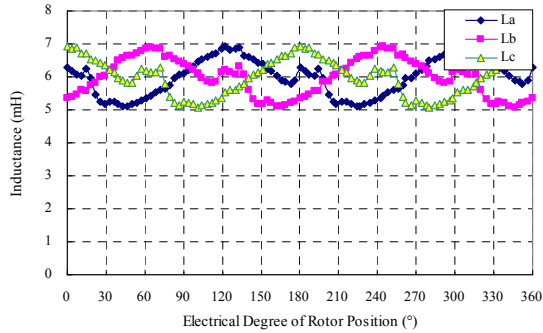


Fig. 6 Self-Inductance of a 45-Slot 40-Pole PMWG.

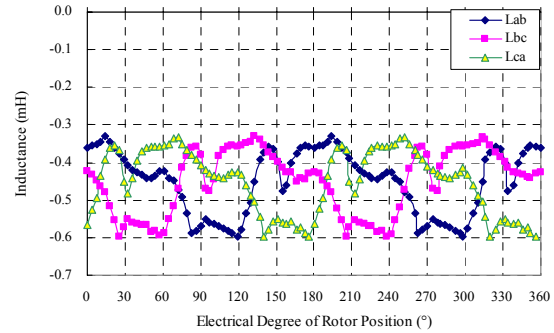


Fig. 7 Mutual-Inductance of a 45-Slot 40-Pole PMWG.

To achieve a unit synchronous inductance, the slot opening width and height should be optimised by magnetic field calculation.

As stated above, the combinations of slot and pole number like  $Q=2p \pm 1$  or  $Q=2p \pm 2$  are not suitable for large power PMWG because of the stator MMF harmonics and the possibility of unbalanced magnetic pull. Multi-unit machine combination is a good choice from the comprehensive point of view. The combinations of slot and pole number such as multi-9-slot-8-pole (45-slot 40-pole, 90-slot 80-pole and etc.), multi-12-slot-10-pole, are suitable for large power module PMWGs. 45-slot 40-pole is adopted for a 100kW prototype generator developed in this paper.

### 3 THERMAL MANAGEMENT

#### 3.1 Ventilation system description

Effective cooling is of paramount importance for PMWGs due to their high power density and complex working conditions. The generator should be totally enclosed because protection grade IP54 is used. Ambient air is not allowed to enter the generator in order to reduce the risk of water condensation on the windings and salt and dust in the generator.

In order to make full use of the natural air of wind farm and simplify the cooling system, the PMWG can be cooled directly by natural wind blowing through the surface of stator frame. For large power generators, the stator frame is manufactured with ventilated ribs on its surface to increase the heat dissipation capacity. In this paper, the development of a 100kW prototype generator is conducted. Natural air cooling system is applied to the prototype generator. In order to save the manufacturing cost and time, the ventilated ribs is not adopted in the prototype generator.

#### 3.2 Temperature field calculation

In Heat Transfer, steady heat conduction equation of anisotropic solid material with inner heat sources can be written as

$$\text{div}(\lambda \cdot \text{grad}T) + q_v = 0, \quad (7)$$

where  $q_v$  is heat generation in unit volume,  $T$  is the temperature and  $\lambda$  is thermal conductivity of solid.

There are three kinds of common boundary conditions in thermal field, this paper use two of them:

- Heat Flow Boundary Condition

$$\lambda \frac{\partial T}{\partial n} \Big|_{S_1} = 0. \quad (8)$$

- Convection Boundary Condition

$$-\lambda \frac{\partial T}{\partial n} \Big|_{S_2} = \alpha(T - T_0), \quad (9)$$

where  $T_0$  is the ambient temperature that surrounds surface  $S_1$ , and  $\alpha$  is heat transfer coefficient of surface  $S_2$ .

The insulation layers of each conductor are very thin, so the copper for both upper winding and lower winding are considered as one isothermal conductor respectively, and the insulations including material of the impregnation, residual air as another which equivalent thermal conductivity is 0.26W/m/K [4]. The model of stator winding is shown as Fig. 8.

Before finite element analysis, necessary boundary conditions have to be identified. One of the most important boundary conditions is heat transfer coefficient between ambient and frame. It can be calculated as follows [5]

$$\alpha = \alpha_0(1 + k\sqrt{U}), \quad (10)$$

where  $\alpha$  is heat transfer coefficient in calm air,  $k$  is coefficient of efficiency and  $U$  is air velocity.

Based on the analysis stated above, a 3-D finite element model with only one tooth pitch is solved by using Ansys software. The temperature distribution of the 100kW prototype generator is shown in Fig. 9. By thermal analysis, the thermal load of the prototype generator is modified to fit for the cooling system.

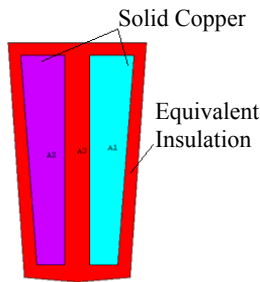


Fig. 8 Model of Stator Slot.

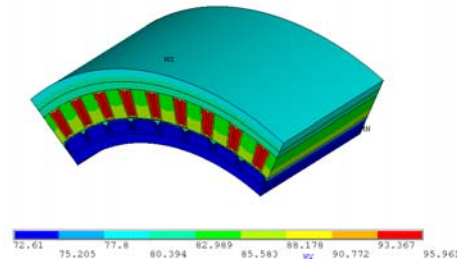


Fig. 9 Temperature Distribution of 100kW Prototype Generator.

#### 4 MODULAR STRUCTURE

To improve the fault tolerant capacity, a modular structure is presented in this paper for a 100kW prototype generator. The stator core and rotor pole are all composed of basic elements as shown in Fig. 10 and 11. After assembling these lamination elements, the modules of stator tooth and rotor pole are completed, as shown in Fig. 12.



Fig. 10 Stator Core Lamination Element.



Fig. 11 Rotor Pole Shoe Lamination Element.

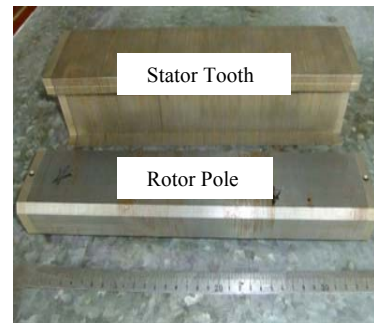


Fig. 12 Photo of Stator Tooth and Rotor Pole Module.

Fig. 13 shows the schematic of the stator teeth modules assembly process. Each stator tooth module is fixed to the inner surface of the solid stator back yoke by two bolts. Before the assembly process, the position for each stator tooth module is marked out accurately. The stator photo of the 100kW modular

PMWG after tooth modules assembling is shown in Fig. 14. Closed-slot structure is realised as can be seen from the figure. The photo of complete machine is shown in Fig. 15.

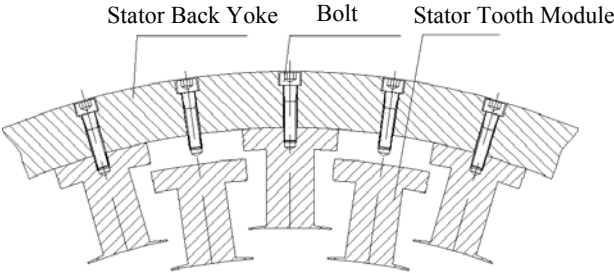


Fig. 13 Schematic of Stator Teeth Modules Assembly.



Fig. 14 Photo of Stator frame with Teeth Modules.



Fig. 15 Photo of the Prototype Generator.

**5 EXPERIMENTAL RESULTS**

The experimental platform is developed for PMWGs in this paper, as shown in Fig. 16. The platform contains complete facilities, such as cooling fan, gearbox, DC driving motor, back-to-back full power converter produced by ABB and other instruments used for data testing.

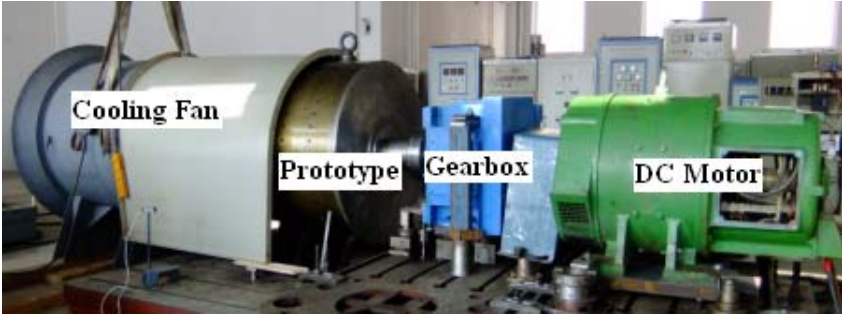


Fig. 16 Self-Inductance of a 45-Slot 40-Pole PMWG

The no load EMF waveform of the prototype generator is tested by using digital oscilloscope, as shown in Fig. 17. The harmonic spectrum is shown in Fig. 18. It can be seen that the EMF waveform is very sinusoidal, with a total harmonic distortion less than 1.8%.

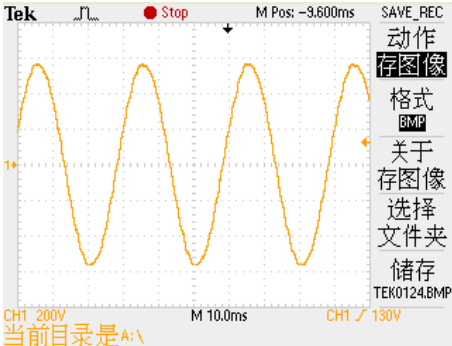


Fig. 17 Experimental Waveform of No Load EMF

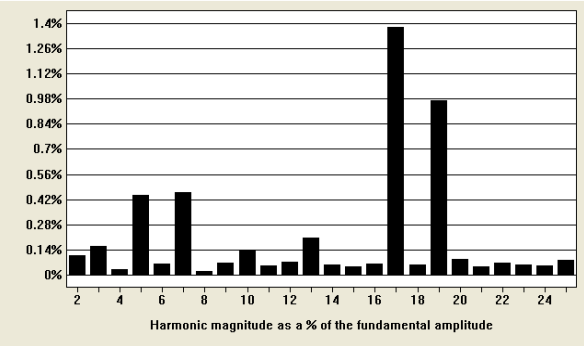
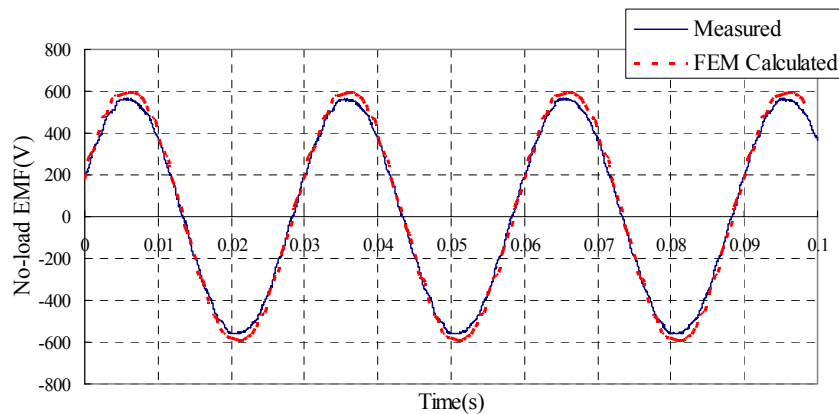


Fig. 18 Harmonic Spectrum of No Load EMF.

The waveforms of the FEM calculated and measured no load EMF of the prototype generator are shown in Fig. 19, which match very well. The difference in amplitudes is mainly a result of a larger equivalent air gap in the fabricated generator due to segmented stator and rotor structure.



**Fig. 19 Measured and Calculated No Load EMF**

The measured cogging torque is less than 0.5% of rated torque, which is due to the adoption of closed-slot and a good selection of slot and pole number combinations. The measured average temperature rise of stator winding is almost identical with the calculation result. Because of the employment of FSCW, the high efficiency is achieved for this prototype generator. The rated efficiency is more than 95.3% in the case of 95°C of operating temperature.

## CONCLUSIONS

Presently most of the FSCW permanent magnet machines are used for low power industrial applications, and they are not yet frequently used in larger electrical machines.

The maximum winding factor for double-layer FSCW is 0.955, which appears at  $q$  equals  $1/m$ . The closer  $q$  is from  $1/m$ , the higher fundamental winding factor is achieved. Then, the factors that affect sub-harmonics and harmonic spectrums are analyzed. The combinations with small  $d$  are more attractive. A very low cogging torque can be obtained if the slot and pole numbers are chosen so that the least common multiple between them is large. The closer the number of slots to the number of poles, the higher their least common multiple can be achieved. An even number of slots or a multi-unit machine combination should be used for large PMWGs from the unbalanced magnetic pull point of view. As stated above, the conventional combinations of slot and pole number are not suitable for large power PMWG because of the stator MMF harmonics and the possibility of unbalanced magnetic pull. Multi-unit machine combination is a good choice from the comprehensive point of view.

The thermal management work is carried out for a 100kW prototype generator with FSCW. Then, a modular structure with closed-slot is presented in order to improve fault tolerance capacity. At last, a 100kW modular PMWG with FSCW is manufactured. Measurements on the prototype generator have demonstrated that FSCW generators are favourable.

## BIBLIOGRAPHY

- [1] Freedy M, Chandur S. Winding factors and joule losses of permanent magnet machines with concentrated windings. IEMDC-2003
- [2] Bai Y. Design and calculation of hydro-generators: Beijing: China Machine Press, Inc., 1972
- [3] Pia S, Markku N, Juhu P, Juhani M. Performance analysis of fractional slot wound PM-motors for low speed applications[C]//39<sup>th</sup> IAS Annual Meeting-2004
- [4] Wei Y, Meng D, Wen Ji. Heat exchanges in electric machines. Beijing: China Machine Press, Inc., 1998
- [5] Chen S. Electrical machine design. Beijing: China Machine Press, Inc., 2000

**Modeling and Simulation of Direct-coupled Permanent Magnet Wind  
Generators System with Maximum Power Point Tracking Control Using  
Simplorer**

**Yan Cheng, Shumin Sun**  
Shandong Electric Power Research Institute  
  
Jinan, China

**Jinhua Du, Deliang Liang**  
State Key Laboratory of Electrical  
Insulation and Power Equipment, Xi'an  
Jiaotong University  
Shaanxi, China

**SUMMARY**

This paper presents a maximum power point tracking (MPPT) method which does not need information like wind turbine characteristic and wind speed. The MPPT method is effective especially when air density of the environment changes. A wind system based on a low-speed direct-coupled permanent generator is constructed in this paper.

Firstly, the theoretical principle of the MPPT method is analyzed, which includes two basic steps: wind turbine speed disturbance and output power measurement. Increase the speed disturbance when the output power increases, and decrease the speed disturbance when the output power decreases as well. This method will not be effected by the ageing problem and have better control result.

Secondly, the simulation of the wind turbine is proposed, which is based on a DC motor. Wind turbine is a power source whose amplitude changes continuously. Thus the simulation of wind turbine is to describe its characteristics and make equivalent output power. Using a DC motor to model the wind turbine is a practical and feasible method to obtain a better approximation.

Thirdly, accounting for the permanent magnet generator and main circuit as well as control scheme, the model of wind generation system was built in Simplorer, which is a useful FEM tool for the applications in motor control, electrical transmission, aerospace industry and power electronic device.

Finally, the control system based on TMS320LF2407 was constructed. Voltage and current sampling, IGBT driver, thyristor control, speed detect and snubber circuit are designed respectively. The current, output power and speed are measured at constant wind speed. The experiment of controlling wind turbine speed and output power at constant wind speed on a DSP platform verifies the feasibility of the MPPT method presented in the paper.

**KEYWORDS**

Maximum power point tracking method, Permanent magnet wind generator system, Simplorer.

## 1 INTRODUCTION

Shortage of power and pressure of environment are more and more serious in the world. Wind power is a kind of clean and reproducible energy. In recent years, the research about wind generation is a popular area. Permanent magnet generator has high efficiency and good performance at low speed. Direct-coupled wind system with low speed generator and low speed wind turbine was widely used because of its no gear operations. How to capture the maximum power of wind turbine is one of the most important questions because it decides the efficiency of wind generation system.

MPPT method is a popular control strategy of capturing the maximum wind power. To capture the maximum wind power, the wind turbine needs to keep the optimum status. Nowadays the MPPT methods can be divided into the following types:

1. By measuring wind speed, the optimum speed of the wind turbine can be calculated. To capture the maximum wind power, wind turbine speed need to keep at the optimum speed point. And then the MPPT can be realised by measuring the wind speed [1]. However, this method increases the system complexity and cost, and decreased the reliability.

2. By measuring wind turbine speed, the optimum current of generator at different wind turbine speed can be calculated to follow the maximum output power point of the wind turbine. This method only needs the relationship curves of maximum output power vs. speed of the wind turbine, however, these curves will be changed with the wind turbine ageing and the MPPT efficiency will be worse and worse [2, 3]. In additional, this method does not take the efficiency of generator and transmission, therefore, the control of wind generator output power will bring an error with the maximum power point of the wind turbine which is determined by the efficiency of the generator and transmission [4].

3. By disturbing the wind turbine speed and measuring the output power of the generator, the maximum output power point of the generator can be found. Increase the speed disturbance when the output power increases, and decrease the speed disturbance when the output power decreases as well. This method does not need the relation curves of maximum output power vs. speed of the wind turbine, therefore, the method efficiency will not be effected by the ageing problem and have better control result [5-8].

In this paper, based on the third maximum power point tracking above, the theoretical analysis, simulation method as well as results and experimental results will be presented in this paper.

## 2 THEORETICAL ANALYSES

### 2.1 Analysis of MPPT method

The captured power of a wind turbine  $P$  is related to surface area of wind turbine  $A$ , air density  $\rho$ , wind speed  $v$  and power coefficient  $c_p$  shown in (1).

$$P = \frac{1}{2} c_p \rho A v^3 \quad (1)$$

If wind speed  $v$  is constant, the approximate relationship of the captured power and angular speed of wind turbine is shown in Fig. 1. Based on the maximum power point tracking by disturbing the wind turbine speed and measuring the output power of the generator, the MPPT process can be obtained in Fig. 2.

The maximum power point tracking method includes two steps: speed disturbance and power measurement. Assuming the initial wind turbine speed is  $n_1$ , the captured power of wind turbine will be  $P_1$  at steady state. If the wind turbine speed increases to  $n_2 = n_1 + \Delta n$ , the captured power of wind turbine will be  $P_2$  at steady state. From Fig. 2, it can be seen  $P_2 > P_1$ , which shows the speed increment is beneficial for wind power capture. Therefore, add another  $\Delta n$  to achieve  $n_3 = n_2 + \Delta n$ , and the captured power of wind turbine will be  $P_3$  at steady state. Repeat the process until the captured power of wind turbine is  $P_m$ , which is the optimum captured power and the optimum wind turbine speed is  $n_m$ . If keep increase the wind turbine speed, the captured power will decrease in Fig. 2, which is harmful to the wind power capture. Therefore, the next time the wind turbine speed will

decrease  $\Delta n$  to track the maximum power capture. By using such control strategy, the captured power of wind turbine will fluctuate near the optimum power capture point and make sure the power captured by wind turbine will be always tracking the maximum power point.

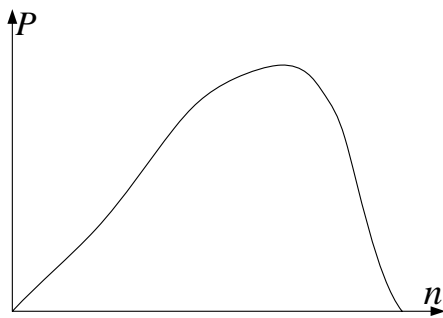


Fig. 1 Power vs. Speed.

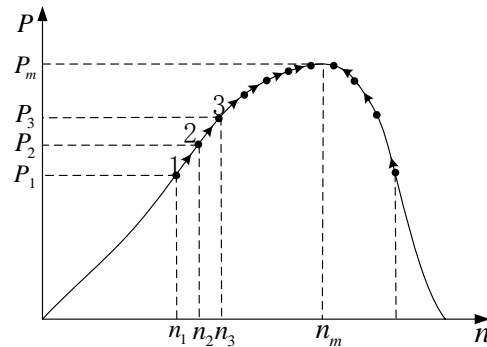


Fig. 2 MPPT Process.

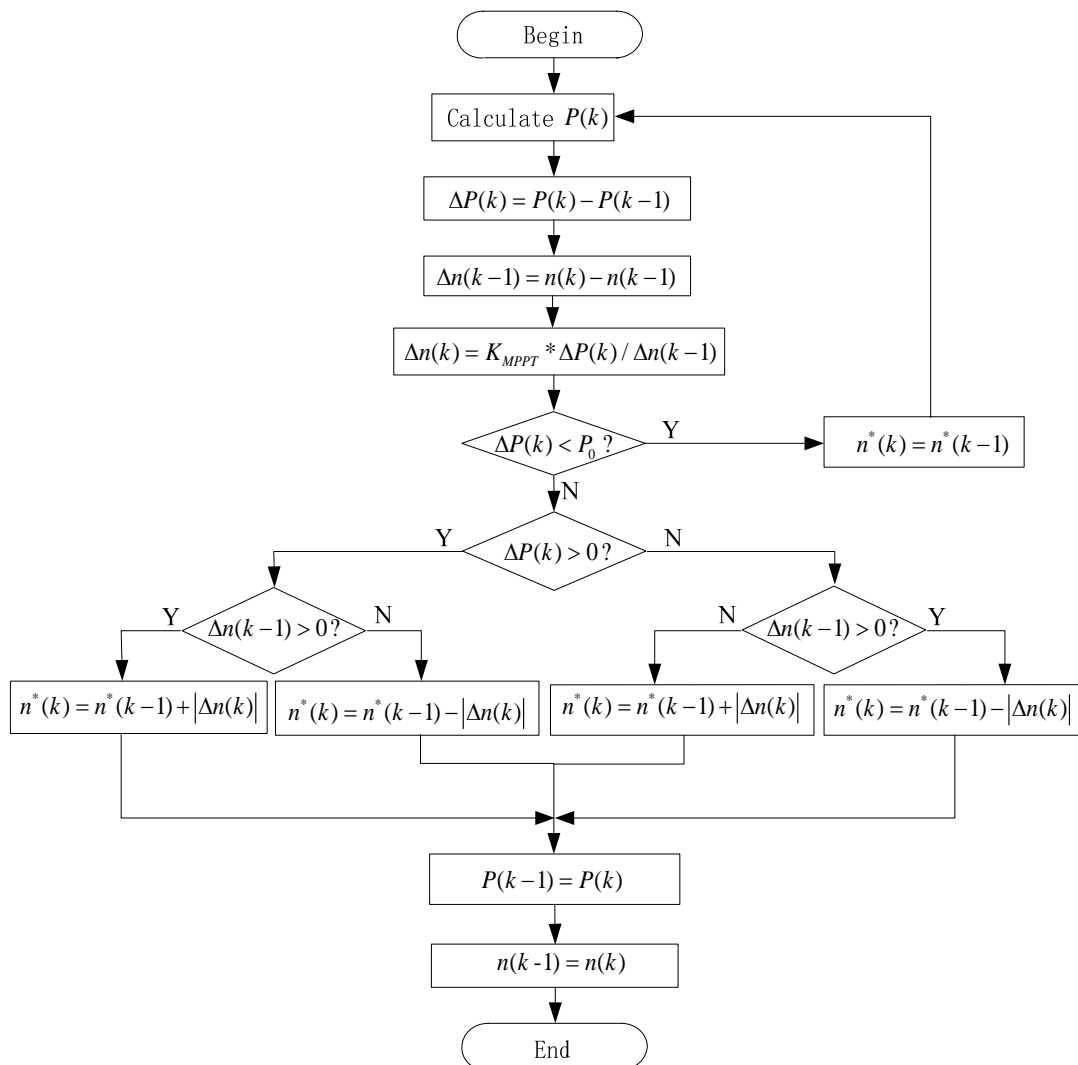


Fig. 3 MPPT Flow Chart.

According to the MPPT method mentioned above, the flow chart of MPPT can be obtained in Fig. 3 and  $P_0$  is the minimum power error. Wind turbine will finally operate near optimal point after several periods.

## 2.2 Principle of wind turbine simulation

The wind turbine can be simulated by a DC motor if output power of the DC motor is equal to the captured power of the wind turbine. Torque of the DC motor is proportional to armature current. Therefore, output power of the wind turbine can be controlled if the armature current is controlled.

Based on the above principle, the simulation model of the wind turbine can be obtained if the speed of the simulated wind turbine can be detected. The idea can be illustrated in Fig. 4. According to the assuming wind speed  $\omega_w$  and detected motor speed  $v$ , the output torque  $T_w^*$  can be calculated from the wind turbine mathematic model as Fig. 5. Power coefficient  $c_p$  is the function of tip speed ration  $\lambda$  and  $D_w$  is the wind turbine diameter.

And then the required current of DC motor can be obtained which is the control variable to generate commands as shown in Fig. 6. The thyristor converter is used in DC motor control system, whose turn-on and turn-off angle are controlled according to the error of given and actual current. In the end, the given power can be output from the DC motor controlling system.

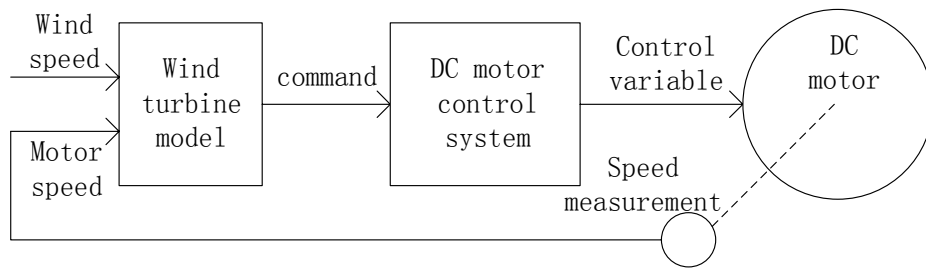


Fig. 4 Principle of Wind Turbine Simulation.

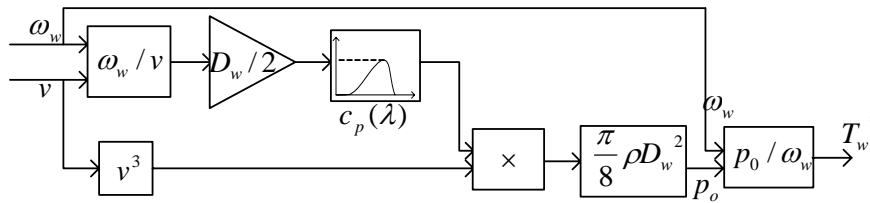


Fig. 5 Wind Turbine Model.

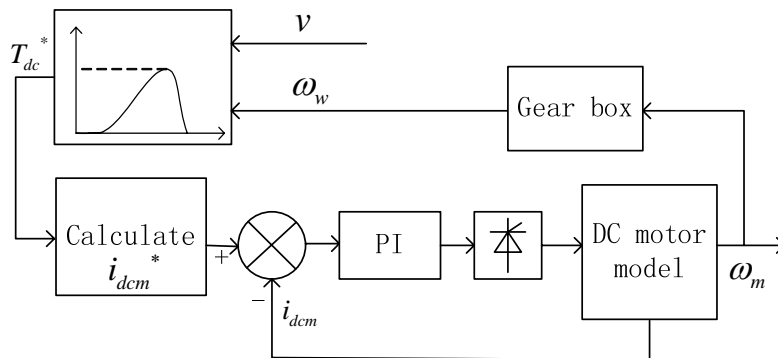


Fig. 6 Torque control of DC Motor.

## 3 SIMULATION METHOD AND RESULTS

In order to validate the control scheme, professional software simplorer was used to simulate the wind system shown in Fig. 7. A low speed permanent magnet generator was designed and the Cuk chopper and speed current double close loop control arithmetic was used to control the speed of generator. The

MPPT control arithmetic was employed to track the maximum output power. The simulation results including generator speed and output power of generator at 7.2m/s of wind speed are shown in Fig.8.

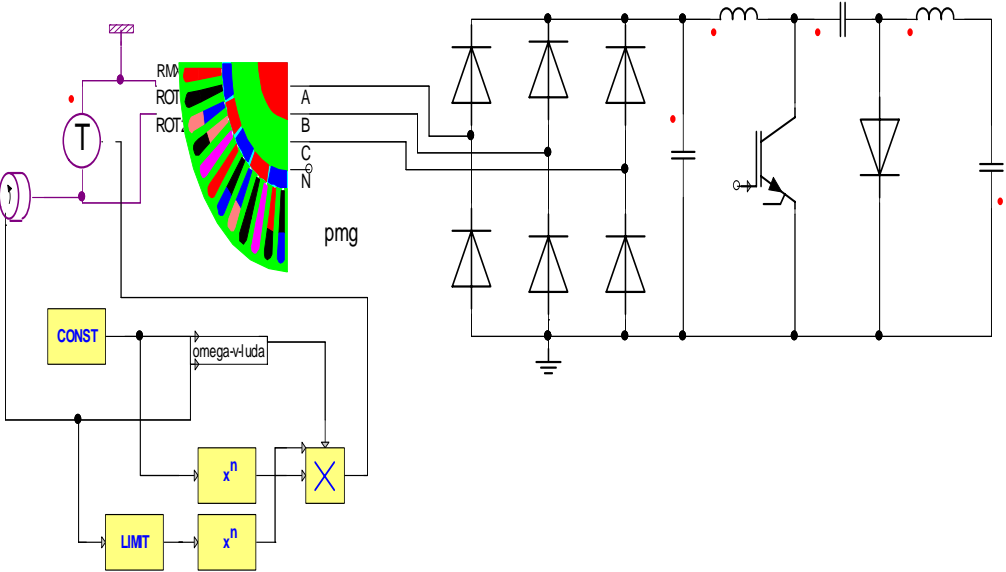
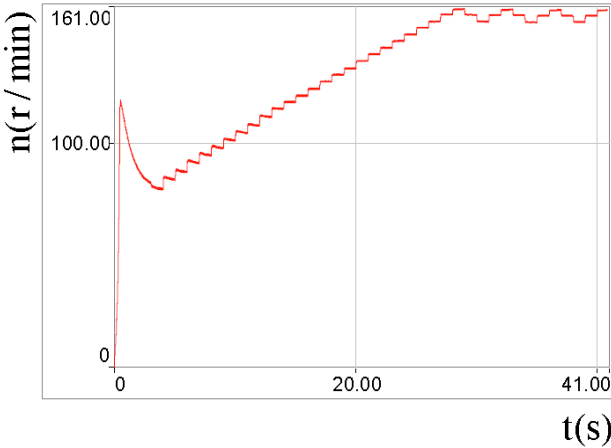
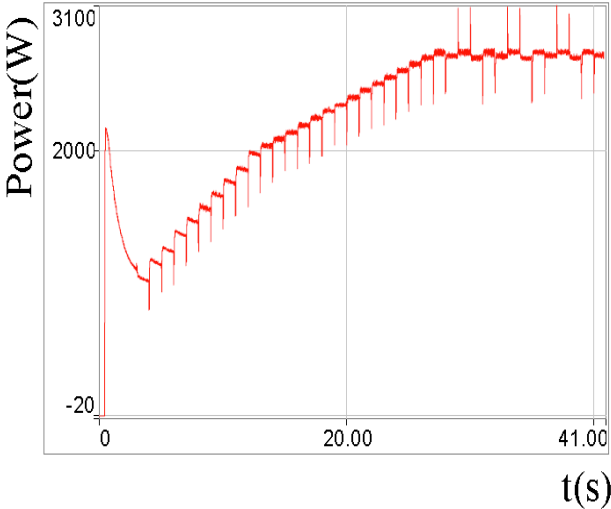


Fig. 7 Model of PM Wind Generation System Based on Ansoft/Simplorer



(a) Wind Turbine Speed



(b) Output Power

Fig. 8 Simulation results

## 4 EXPERIMENT RESULT

The experiment was performed in order to verify the simulation result and the feasibility of the proposed MPPT method. The wind system with the core controller TMS320LF2407 shown in Fig. 9 was built and the experiment was carried at 3m/s of wind speed. The experiment results are shown in Fig.10. The experiment results showed the wind turbine operates near the optimal speed and the wind system can capture the maximum power.



Fig. 9 Experiment Setup (a) DC Motor and PM Generator (b) Converter

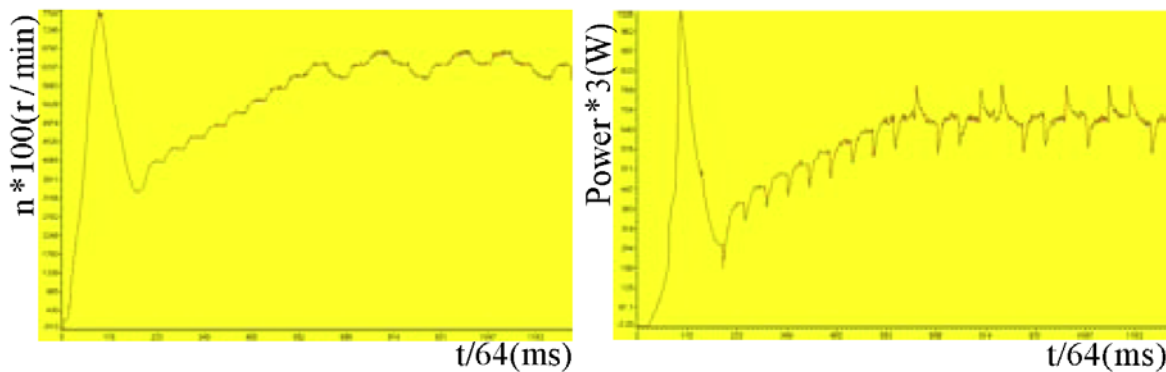


Fig. 10 Experiment Results (a) Wind Turbine Speed (b) Output Power

## 5 CONCLUSIONS

This paper presents a wind power generation system based on a PM generator, and the MPPT control. The principle of the wind turbine is formulated on a DC motor model and the control strategy based on wind turbine speed disturbance and output power measurement is introduced. Meanwhile the control principle and scheme of maximum power point tracking for PM generators used in wind power generation system were discussed. To verify the MPPT control strategy used in the PM wind generation system, the simulation models of the wind turbine and PM wind generation system were built based on the FEM by using Ansoft/Simplorer. By using the simulation model, the control principle and scheme of MPPT for PM generators used in wind energy conversion system were simulated and analysed. The tests and experimental results of the whole system had been done and verified the feasibility of the MPPT method.

## BIBLIOGRAPHY

- [1] Esmaili R, Xu L, Nichols D K. A New Control Method of Permanent Magnet Generator for Maximum Power Tracking in Wind Turbine Application[C]// Power Engineering Society General Meeting, 2005(3):2090-2095
- [2] Hashimoto S, Nitta M, Tani T, et al. A Stand-alone Wind Turbine Generator System for a Small-scale Radio Base Station[C]// Telecommunications Energy Conference, 2003:404-409

- [3] Koutroulis E, Kalaitzakis K. Design of a Maximum Power Tracking System for Wind-Energy-Conversion Applications. *Industrial Electronics*, 2006, 53 (2): 486-494
- [4] Pena R S, Cardenas R J, Asher G M, et al. Vector Controlled Induction Machines for Stand-Alone Wind Energy Applications[C]//*Industrial Application Conference*, 2000(3): 1409-1415
- [5] Datta R, Ranganathan V T. A Method of Tracking the Peak Power Points for a Variable Speed Wind Energy Conversion System. *Energy Conversion*, 2003, 18(1): 163-168
- [6] Jia Y, Yang Z, Cao B. A New Maximum Power Tracking Control Scheme for Wind Generation. *Power System Technology*, 2002(1): 144-148
- [7] Borowy B S, Salameh Z. Dynamic Response of a Stand-Alone Wind Energy Conversion System with Battery Energy Storage to a Wind Gust. *Energy Conversion*, 1997, 12(1): 73-78
- [8] Jang J, Lee D. Output Voltage Control of PWM Inverters for Stand-Alone Wind Power Generation Systems Using Feedback Linearization[C]//*Industrial Application Conference*, 2005(3): 1626-1631

**Research on Low-voltage Ride-through Technology of grid-connected Doubly-Fed Wind Power Generation System**

**Fujia Chen<sup>1</sup>, Hongyu Wang<sup>2</sup>, Jianeng Tang<sup>3</sup>**

**School of Electrical and Electronic Engineering, North China Electric Power University,  
China**

**SUMMARY**

According to the demand of the regulations of the grid, within a certain period of time after power failure, the wind power systems should be able to maintain uninterrupted power supply to the grid, which called for low voltage ride through capability (LVRT) of the wind power systems.

To achieve the LVRT ability, a relatively common practice is to install the rotor side crowbar protection circuit. When the grid voltage dips happen, Crowbar protection circuit will be activated in order to protect the converter. But in this way, DFIG will degenerate into a wire-wound induction motor with a variable resistor connected to the rotor side. At this time the motor needs to absorb reactive power from the already vulnerable power grid in order to establish the motor's magnetic field. This will undoubtedly result in a negative impact to the rapid recovery of the grid voltage.

On the bases of the research of the transient characteristics of DFIG in the case of the grid voltage dips, this paper introduced the concept of LVRT and its relevant standards in our country, and analyzed the various kinds of schemes which has already been proposed to achieve the LVRT ability. With the most common practice which installs the rotor side crowbar protection circuit, a proved protection and control strategy to enhance the LVRT capability of a wind turbine driven by DFIG was proposed. In this strategy, we will add a RPC circuit in the stator side to compensate the reactive power demand of the DFIG during the LVRT period with the expectation of reducing the reactive power load of the already blooey power grid as much as possible. The simulation results reviewed that the proposed strategy could help the power grid survive during the shot period of voltage dip and the grid could eventually return to the stable operation conditions.

**KEYWORDS**

Wind power, DFIG, LVRT, Crowbar, Reactive Power, RPC.

## 1 INTRODUCTION

Recent years, with the gradual depletion of fossil energy, as a clean, green and renewable energy, the Wind power generation develops at an amazing pace. The theory of Wind Power is also becoming more and more sophisticated. However, with the great development of Wind Power and its growing proportion in the grid, the grid-connecting technical requirements of the large-scale wind farms are also more and more rigorous. In terms of wind power generator, one of the most important technical requirements is the low voltage ride through (LVRT) capacity. LVRT means that when there is a dips of the grid-connecting voltage of the wind farm caused by power grid failure or disturbance, within a certain period of time after power failure, the wind power systems should be able to maintain uninterrupted power supply to the grid.

At present, double-fed generator is the mainstream type generator for the Wind Power generation. The generation technology of DFIG can improve the efficiency of wind energy capture and conversion, Improve and optimize wind turbine operating conditions, and could make the connection between the generator and the Power System achieve a better flexibility and make the grid-connecting operations much easier. Therefore, DFIG is an optimization with a good prospect of wind power solutions. But precisely because the DFIG wind power generation system uses a small capacity converter, it weakens the ability of the DFIG system to withstand the grid voltage dip. Therefore, during the grid voltage fault, a method that could keep the DFIG grid-connecting and can provide support for the grid to improve power system stability issue has currently become a hot research topic.

In order to avoid the over current and over voltage during the grid voltage dips, researchers and scholars have put forward a variety of approaches. Reference [1] proposed that we can achieve the goal by changing the control strategy, however its effects depend on the control capacity of the converter and motor parameters and the control effect is limited. Reference [2] proposed a way to achieve the LVRT ability by changing the excitation method of the rotor circuit. Reference [3] also proposed a Crowbar circuit, but it was not active that its Crowbar circuit's on and off is uncontrollable which lead to a limited LVRT capability. Reference [6] studied the dynamic response of the DFIG during the grid voltage dips, and proposed a strategy of reducing the flux and comparing the rotor current to control the Active Crowbar circuit, and then, gave out the simulation waveform.

In this paper, the simulation model of the wind power system has been build, and the proposal strategy was verified that it could reduced the reactive load of DFIG from the grid and was favourable to the rapid recovery of the grid voltage.

## 2 THE TECHNICAL STANDARDS OF LVRT IN CHINA.

In accordance with the technical requirements of the State Grid Corporation for wind farms connecting into power grid(released at December 22, 2009), wind farms across the low voltage requirements are as follows:

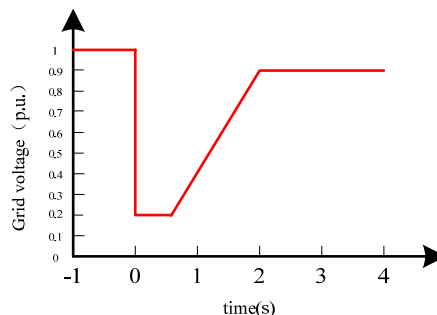


Fig. 1 Requirements of LVRT for Wind Farms

Fig.1 shows the requirements of low voltage ride through for wind farms. When the voltage of the grid-connecting point is above the contour line, the wind power systems must be able to maintain uninterrupted power supply to the grid, and when the voltage of the grid-connecting point is below the contour line, the wind turbines are allowed to remove from the grid.

The specific requirements of LVRT for wind farms are as follows:

- 1) The wind turbines in the wind farm should have the capability of low voltage ride through to maintain connecting to the grid for about 625ms during the voltage of grid –connecting point fell to 20% of the rated voltage.
- 2) Within 2s after the grid voltage dips, if the grid-connecting point voltage could be able to recover to the 90% of the rated voltage, the wind turbines in the wind farm should be able to keep connected to the grid.

The technical requirements from the State Grid are for the whole wind farm.

### 3 THE TRANSIENT CHARACTERISTICS OF THE DFIG AND THE CONTROL STRATEGY OF THE CROWBAR CIRCUIT

#### 3.1 The transient characteristics of the dfig

After the grid voltage dips occurs, owing to the characteristic of the flux that it could not mutate, a DC component of the flux will be induced during the transient process, and its magnitude is determined by the degree of voltage drop and the fault type. The more the voltage drops, the larger the magnitude of DC component is induced. However, the stator and rotor leakage inductance of large scale DFIG are generally small (about 0.1pu), this makes that it needs a large short-circuit current (about 5 to 10 times the rated current) to establish the DC flux component, this will inevitably produce great harm to the DFIG convertor with a small capacity and the winds of stator and rotor. [7] On the other hand, the grid voltage sag, makes a vast part of the input power from the rotor side cannot be effectively output, We can see from the energy conservation principle that this part of the energy could only consumed within the DFIG units itself. This will lead to a sharp rise in DC bus voltage, and thus pose a huge threat to the DC link capacitor and it may even be punctured. At the same time, large fluctuation of the stator and rotor currents will lead to violent oscillation of the electromagnetic torque. This will caused a great torque impact to the mechanical system of the Wind Power generation system.

#### 3.2 The control strategy of the crowbar circuit

We can know from the transient characteristics of the DFIG that when the grid voltage drop, especially a significant drop occurs, the fault would cause great harm to the DFIG system. To avoid this hazard, the traditional practice is to remove the DFIG system from the grid directly during the power failure, and connect to the grid after the grid returns to normal. However, this approach obviously does not meet the requirements of low voltage ride through performance. A more commonly used approach is to install the rotor side of the Crowbar protection circuit. When the grid voltage dips occurs, once the current in the stator and rotor windings of DFIG exceeds a set upper limit, put in the rotor side Crowbar circuit and blockade the rotor side converter output pulse. When both the stator and rotor current is lower than the set lower limit, cut out the rotor side Crowbar circuit and restore the rotor side converter's work. It depends on the fact that whether there is over-current to cut-in or cut out the Crowbar circuit, rather than on the failure signal detection of the grid. After the Crowbar was cut in, DFIG will run as an induction motor. In this running state, DFIG will absorb a certain amount of reactive power from the grid.

### 4 THE MODEL OF THE CROWBAR AND THE RPC CIRCUIT

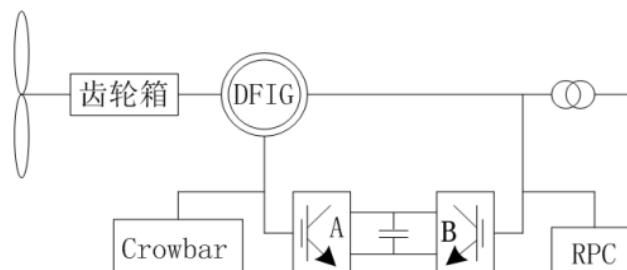
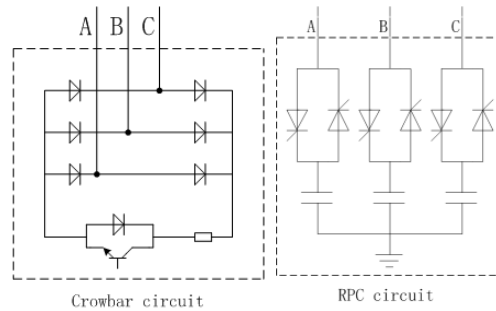


Fig.2 LVRT Control Model

As is shown in Fig.2, a crowbar protection circuit is fixed to the rotor side and a reactive compensation circuit is added to the grid side. When there is a voltage dip, the crowbar protection circuit and the reactive power compensation circuit will be both triggered instantly and work together.



**Fig. 3 Crowbar and RPC Model**

Crowbar protection circuit is to protect the converter from damage and to achieve LVRT performance, while the reactive power compensation circuit is to balance the reactive power demand of the DFIG after the crowbar circuit is triggered.

### 5 SIMULATION OF THE LVRT CONTROL STRATEGY

A simulation of a practical DFIG wind turbine has been carried out using Matlab/Simulink2008.

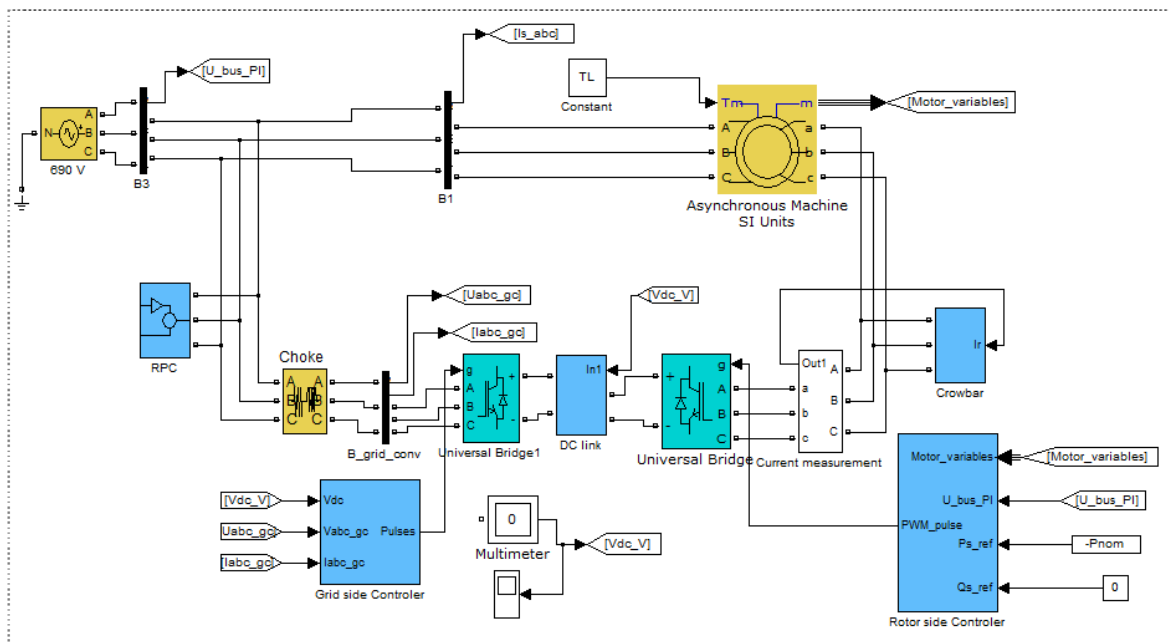


**Fig. 4 Simulation Model**

In this model, we choose a back to back converter, and use a stator flux oriented vector control strategy for the rotor side control system and a stator voltage vector control strategy for the stator side control system. The rotor side control system aims at providing the excitation current for the rotor side and controlling the output power of DFIG system. By tracking changes of the DC bus voltage, the stator side control system aims at controlling the stator side converter in order to maintain the stability of the DC bus voltage and control the power factor of the DFIG system's output.

In this model, a three-phase programmable voltage source block is used to simulate the infinite power grid. At the time of 1s, the grid voltage drops to 20% of the rated voltage and at the time of 1.625s, the grid voltage restored to 90% of the rated voltage. And the duration time of voltage dips is 0.625s.

Hysteresis compare strategy is used to control the Crowbar and RPC circuit. When the rotor side current is greater than 4000A or the DC bus voltage is greater than 1280V, and then put in the Crowbar protection circuit and RPC reactive power compensation circuit and latch the rotor side converter at the same time. When the rotor side of the current is less than 2000A and the DC bus

voltage is lower than 1200V, remove the Crowbar and RPC circuit, and let the converter return to work.

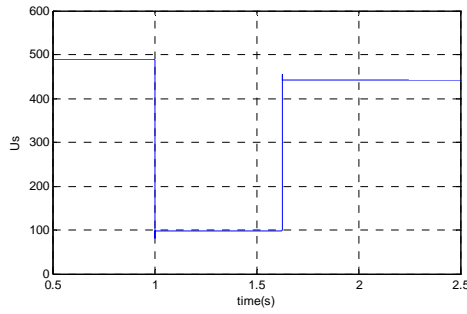


**Fig.5 Stator Voltage Amplitude**

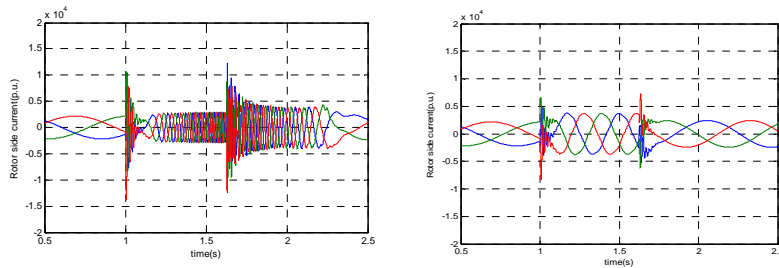


**Fig.6 Rotor Side Current**

As can be seen from Fig.6, the rotor side over current has been effectively suppressed and the converter be well protected from the damage of the over current.

## 6 CONCLUSION

This paper proposes a solution to the LVRT performance of a wind turbine driven by DFIG. In this solution, a crowbar protection circuit is fixed to the rotor side and a reactive power compensation circuit (RPC) is added to the grid side. Compare with the solution which uses the crowbar protection circuit merely, the combined solution could not only realize the performance of LVRT effectively, but also reduce the requirement of reactive power from the Power Grid and provide a favourable help to the system to return to normal conditions as soon as possible.

## 7 APPENDIX

**Table I DFIG Simulation Parameters**

Rated power	$P_{nom}$	1.5	MW
Rated voltage	$V_{nom}$	690	V
Rated frequency	$F_{nom}$	50	HZ
stator resistance	$R_s$	$3.26 \times 10^{-3}$	$\Omega$
rotor resistance	$R_r$	$2.7 \times 10^{-3}$	$\Omega$
stator leakage inductance	$L_{ls}$	$5.68 \times 10^{-5}$	H
rotor leakage inductance	$L_{lr}$	$3.35 \times 10^{-5}$	H
magnetizing inductance	$L_m$	$5.57 \times 10^{-3}$	H
the pole pairs	$n_p$	2	
moment of inertia	$J$	340	$kg \cdot m^2$

## BIBLIOGRAPHY

- [1] RODRIGUEZ M, ABAD G, SARASOLA I, et al. Crowbar control algorithms for doubly fed induction generator during voltage dips [C] // 2005 European Conference on Power Electronics and Applications. Dresden, Germany :IEEE,2005 :1-10
- [2] XIANG Di, YANG S, RAN L. Ride-through Control Strategy of a Doubly Fed Induction Generator for Symmetrical Grid Fault .Proceedings of the CSEE, Feb. 2006 ,26 (3)
- [3] Muyeen S M , Takahashi R , Murata T , et al . Low voltage ride through capability enhancement of wind turbine generator system during network disturbance [J].IET Renewable Power Generation , 2009 , 3 (1) : 65274
- [4] WEI L, CHI Y, ZHAO JI, WANG W. Control of Low Voltage Ride-Through in Doubly Fed Induction Generators[J].Power System and Clean Energy,2009,25(2)
- [5] He Y , Hu J , Zhao R.Modeling and control of wind turbine used DFIG under network fault conditions [A]//Proceedings of the Eighth International Conference on Electrical Machines and Systems [C].Nanjing , 2005
- [6] Zhou P, HE Y. Control strategy of an active crowbar for DFIG based wind turbine under grid voltage dips [C] // The International Conference on Electrical Machines and Systems. Seoul, South Korea: IEEE,2007 :1489-1494
- [7] He Y, Zhou P. Overview of the Low Voltage Ride-Through Technology for Variable Speed Constant Frequency Doubly Fed Wind Power Generation Systems. TRANSACTIONS OF CHINA ELECTRO- TECHNICAL SOCIETY ,Sep. 2009 ,24 (3)
- [8] Li D(IEEE Member), Zhang H. A combined protection and control strategy to enhance the LVRT capability of a wind turbine driven by DFIG //IEEE International Symposium on Power Electronics for Distributed Generation Systems
- [9] FELTES C, WREDE H, KOCH F W, ERLICH I.Enhanced fault ride through method for wind farms connected to the grid through VSC-based HVDC transmission .IEEE Trans. Power Syst., 2009, 24, (3), pp. 1537–1546
- [10] MUYSEEN S.M., TAKAHASHI R., MURATA T., ET AL.: Low voltage ride-through capability enhancement of wind turbine generator system during network disturbance', IET Renew. Power Genre., 2009, 3 (1) :65–74
- [11] ZHU Y,LI J,ZHAO B. Simulation of LVRT strategy for DFIG wind power system. Electric Power Automation Equipment .Jun.2010 ,30(6)
- [12] Liu Q,He Y,Bian S.Study on the no-load cutting-in control of the Variable Speed Constant Frequency (VSCF) wind-power generator[J].Proceedings of the CSEE, 2004, 24(3) :6-11

## **Study on Maximum Power Point Tracking Control for Switched Reluctance Generator Used in Wind Power Generation**

**Shumin Sun**  
Shandong Electric Power Research Institute  
China

**Wen Ding, Deliang Liang**  
Xi'an Jiaotong University  
China

### **SUMMARY**

As the problems of environment protection, energy sources shortage and conservation are being noticed gradually, people are paying more and more attention to the wind power generation. Switched reluctance generator (SRG) is very suitable for wind power generation due to the low cost, reliability, fault-tolerant ability and high speed capability. This paper mainly focused on the application of SRG in wind power generation, and the maximum power point tracking control for wind power generation has been presented from simulation to experiment.

Firstly, the developing process and the present of wind power generation in the world were comprehensively introduced, its relative techniques were summarized, the advantages of SRG used in wind generation system were presented, and significance of developing SRG used in wind power system was pointed out.

Secondly, the structure and operating principle of the wind turbine based on DC motor were formulated and the control strategies were introduced. Also the construction and principle of SRG were represented and kinds of control method of SRG used in generation were introduced. Meanwhile the control principle and scheme of tracking maximum power point for SRG used in wind power generation system were discussed. In this control method, a constant resistance controlled circuit was set between SRG and converter.

Thirdly, the simulation models of the wind turbine and SRG system were built based on the finite element method (FEM) by using Ansoft/Simplorer. The characteristics of wind turbine system based on DC motor was simulated and analysed. By using the simulation model, the dynamic performances in both open loop control system and closed loop control system for the SRG, also that of changing loads, changing speeds in closed loop control system were simulated respectively. At last the control principle and scheme of tracking maximum power point for SRG used in wind energy conversion system were simulated and analysed. The results matched the theories well.

Fourthly, theory study and practice were combined and a set of experimental SRG system was developed, which based on DSP control technique. The design scheme of hardware and program principle of software also the control strategies of all the functional parts were fully discussed. Programs of control strategies such as maximum power point tracking control for the wind power generation has been done according to the existing hardware of the SRG system.

Finally, tests and experimental results of the whole system had been done. Compared with the simulation and the test results also the principle, the practicability of the system is testified and some

### **KEYWORDS**

Wind power generation, Switched reluctance generator (SRG), Maximum power point tracking control, Modeling and simulation

## 1 INTRODUCTION

As the problems of environment protection, energy sources shortage and conservation are being noticed gradually, people are paying more and more attention to the wind power generation. Wind power represents, in fact, a key component of available energy resources able to produce no greenhouse-gas emissions or waste products and to provide significant levels of renewable energy in world terms. In the past years, several types of generators such as induction generators, double fed induction generators (DFIG) or permanent magnet synchronous generators (PMSG) were used as wind generators. The speed of an induction generator is close to a constant value. Thus, the wind energy utilization factor cannot be maintained at the optimal value during wind speed variation. The DFIG can change its operating speed and has better utilization of wind energy. However, the structure of DFIG is complex and a gear box is required which results in reduced system reliability, extra energy losses and more maintenance works. The variable speed PMSG can be directly driven without gearbox, but its material cost is high and more efforts are required to further improve its performance and reliability, reduce its cost and size. Switched reluctance generator (SRG) is very suitable for wind power generation due to the low cost, reliability, fault-tolerant ability and high speed capability. These features make it very suitable for application to direct-driven wind turbines.

In the past researches, wind generator control methods have already been proposed to efficiently utilize the wind power which is prone to fluctuation every moment. The maximum power point tracking (MPPT) algorithm of wind turbine is one of the most important and key techniques. Several MPPT algorithms were presented, basically these algorithms depend on the characteristics of a wind turbine, which means the turbine characteristics have to be obtained either before or during the execution of these control algorithms, and sometimes an anemometer is needed.

This paper mainly focused on the application of SRG in wind power generation, and the maximum power point tracking control for wind power generation has been presented from simulation to experiment. The structure and operating principle of the wind turbine based on DC motor were formulated and the control strategies were introduced. Meanwhile the control principle and scheme of tracking maximum power point for SRG used in wind power generation system were discussed. The simulation models of the wind turbine and SRG system were built based on the finite element method (FEM) by using Ansoft/Simplorer. The characteristics of wind turbine system based on DC motor was simulated and analysed. By using the simulation model, the dynamic performances in both open loop control system and closed loop control system for the SRG, also that of changing loads, changing speeds in closed loop control system were simulated respectively. At last the control principle and scheme of tracking maximum power point for SRG used in wind energy conversion system were simulated and analysed. The results matched the theories well.

## 2 MPPT CONTROL METHOD

### 2.1 Wind turbine characteristics

Captured power of wind turbine generator depends on a shape of the blades and wind speed. It was found that the equations of  $P_{aw}$  and  $P_w$  are,

$$P_{aw} = \frac{1}{8} \rho \pi D_b^2 V_w^3 \quad (1)$$

$$P_w = \frac{1}{8} \rho \pi D_b^2 V_w^3 C_p \quad (2)$$

where  $P_{aw}$ : aerodynamic power(W),  $P_w$  : actual aerodynamic power captured by the wind turbine(W),  $\rho$  : Air density(kg/m<sup>3</sup>),  $D_b$  : Diameter of blade(m),  $C_p$  : Power coefficient,  $V_w$  : Wind speed(m/s).  $C_p$  can be characterized by TSR (and the typical  $C_p$  curve is shown in Fig.1), where TSR is the tip speed ratio; that is, the ratio between the angular velocity of the blades and wind speed(Eq.(3)).

$$TSR = \frac{1}{2} \frac{D_b \omega_b}{V_w} \quad (3)$$

where  $\omega_b$  : angular velocity of WTG (rad/s).

From Fig.1, it became clear that the blade of WTG has the optimum angular velocity for every wind speed, that is, more energy can be extracted from the wind energy by adjusting the angular velocity of the blade to the wind speed. This operation is maximum power point tracking (MPPT) for WTG.

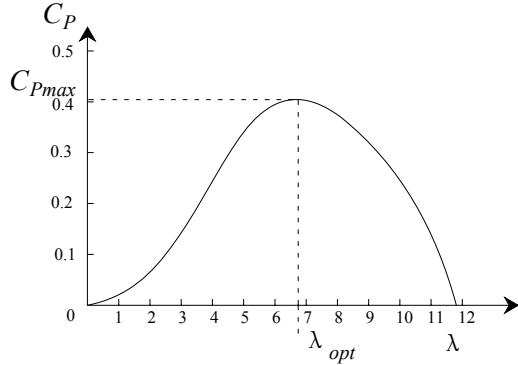


Fig.1 Power coefficient  $C_p$ , versus tip-speed ratio

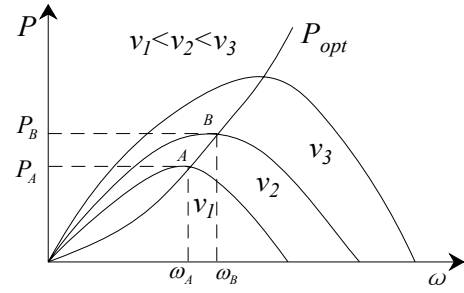


Fig.2 Power-speed characteristics of wind turbine

A wind turbine with a fix pitch angle has a fix  $C_p$ - $\lambda$  characteristic.  $C_p(\lambda)$  is a convex function. When  $\lambda$  is equated to the standard TSR ( $\lambda_n$ ),  $C_p$ , reaches its maximum value ( $C_{pmax}$ ).

As shown in Fig.2, when the wind speed varies, there is always a specific rotor speed for which the mechanical power of the wind turbine is maximized. For example, if the wind speed is  $v_1$  the maximum power could be captured when the rotor speed is  $A_n$ . If wind speed changes from  $v_1$  to  $v_2$ , the rotor speed should be increased from  $A_n$  to  $B_n$  to yield the maximum power. So in order to achieve maximum output power of wind turbine, the rotor speed should be operated in the curve of  $P_{opt}$ .

## 2.2 Maximum power point tracking algorithm

A control algorithm which is independent of wind turbine characteristics to track maximum output power of the wind turbine is developed. The algorithm regulates the SRG's phases current to achieve precise control of the SRG's torque and output power. The fundamental principle of the algorithm is to detect the change of SRG's output power  $\Delta p(k+1)$  and the change of shaft speed  $\Delta n(k+1)$  after an excitation current perturbation  $\Delta i(k)$  and decide the next current perturbation  $\Delta i(k+1)$  according to the variation of  $\Delta p(k+1)$  and  $\Delta n(k+1)$ . First the excitation current is perturbed by a step change  $\Delta i(k)$  and then the variations of output power and shaft speed are observed. If the output power or the shaft speed is increased after the perturbation of current, the same  $\Delta i(k)$  is further added for next perturbation as  $\Delta i(k+1)$ . If the output power and the shaft speed are decreased together after the current perturbation a current deviation with opposite sign should be added for next perturbation.

In order to get the maximum capture of wind energy, we use a speed feedback control strategy, which is based on Eq.(4) and Fig.2. The schematic diagram of this control strategy is shown as the Fig.3. In Fig.3,  $P_f$ , which is derived from the parameters of  $C_{pmax}$ ,  $\lambda_n$ , and the speed feedback is a given value of the output power. It represents the trajectory of the optimal power output in Fig.2.  $P_o$  is an observed quantity of the output power  $P_o$ . It is described as:

$$P_f = \bar{u}_{bus} \cdot \int_0^{\theta_r} \bar{i}_{bus}(\theta) d\theta = \bar{u}_{bus} \cdot \bar{i}_{bus} \quad (4)$$

where  $\bar{u}_{bus}$  is a mean of the bus voltage, and  $\bar{i}_{bus}$ , which is obtained from  $i_{bus}$  via a second order low-pass filter, is a mean of the bus current.

When the rotor speed of the wind turbine works in the operating range, the control system regulates the chopping current  $i_{cop}$  via PI controller so as to make the system state following the trajectory of the optimal power curve in Fig.3. If the working range of the rotor speed is so broad, the switch-on angle,  $\theta_1$ , must be changed according to different partitioned rotor speed. In this control system, there are two problems. One is that the observed quantity of the output power  $P_f$  does not exactly represent the output power  $P_o$ , which is written as:

$$P_o = \int_0^{\theta_r} u_{bus} \cdot i_{bus}(\theta) d\theta \quad (5)$$

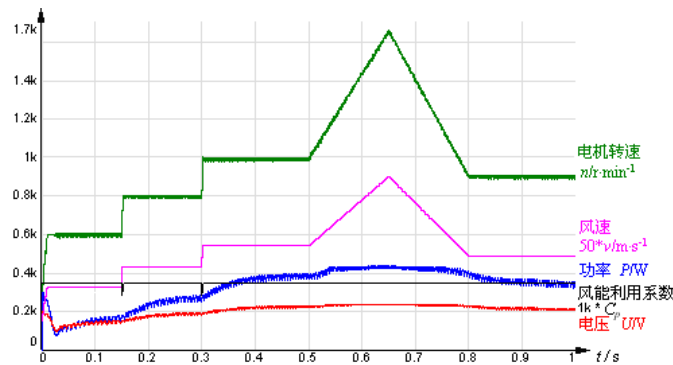


control with varied parameters, the angle position control (APC) and current chopping control are used in the power generation state.

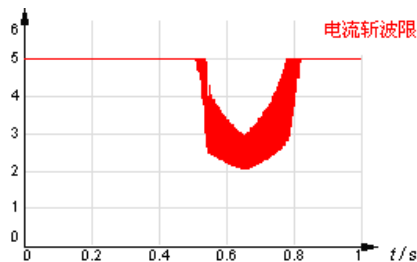
### 3.2 Simulation results

Fig.5 shows the simulation results of the SRG system based on the proposed MPPT algorithm. It should be pointed out that in Fig.5(a), the wind speed has been blown 50 times, and the wind power coefficient has been blown a thousand times. As shown in Fig.5(a), the starting wind speed is set as 3m/s. At 0.15s the output bus voltage reaches 151V, the output power reaches 172W, and the wind speed jumps to 8.7m/s, the machine speed reaches 800rpm at this time. At 0.25s the output bus voltage reaches 195V and the output power reaches 285W. Then the wind speed jumps to 10.8m/s at 0.3s, after amoment the machine speed reaches 990rpm, the output bus voltage reaches 225V and the output power reaches 390W at 0.37s. Then the wind speed reaches 18m/s at 0.5s, after amoment the machine speed reaches 1656rpm, the the output bus voltage stabilized at 230V and the output power stabilized at 400W. Then the wind speed drops to 9.8m/s at 0.8s, after amoment the machine speed stabilized at 900rpm, the the output bus voltage stabilized at 210V and the output power stabilized at 330W.

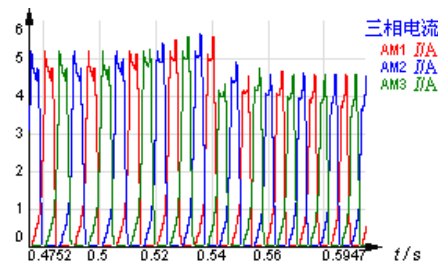
From Fig.5(a), wen can see that at the beginning, the SRG doesn't generate electricity because the shaft speed of the SRG is low. When the shaft speed reaches a preset value, the SRG begins to generate electricity and tracks the maximum power point. The other simulation results such as three phases currents and torque waveforms are shown in Figs.5(b)~(e) for the SRG operating under the proposed MPPT algorithm when the wind speed varies.



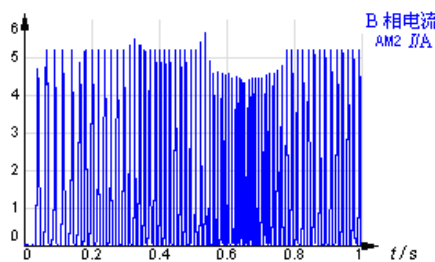
(a) Speed, voltage and power waveforms



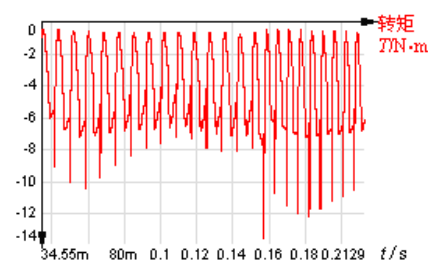
(b) Current chopping limit



(c) Three pahses currents



(d) Phase-B current

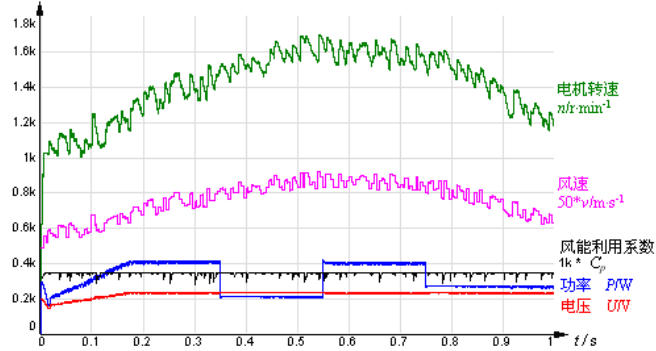


(e) Total torque

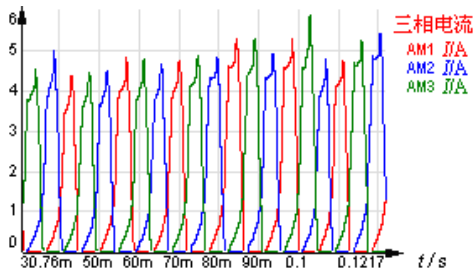
**Fig.5 Simulation results of proposed MPPT algorithm for SRG system**

In industrial applications, SRGs do not always run at constant load. Thus, it is necessary to analyze

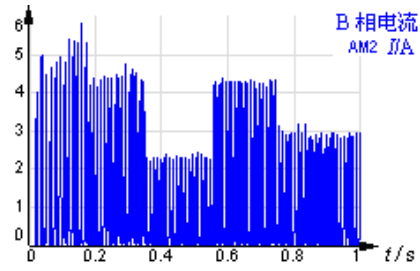
SRG system operations under the condition of sudden change of load. Fig.6 shows the different simulation results for the SRG system operated under the proposed MPPT algorithm when the wind speed varies smoothly and the load is suddenly changed. In these operations, the voltage feedback PI control, the angle position control and current chopping control are used. It should be pointed out that in Fig.6(a), the wind speed has been blown 50 times, and the wind power coefficient has been blown a thousand times. As shown in Fig.6(a), at the starting the resistance is set as  $132\Omega$ , at 0.17s the output bus voltage reaches the preset value 230V and the output power reaches 400W. At 0.35s, the resistance jumps to  $264\Omega$ , after a moment the output bus voltage still stabilized 230V but the output power drops to 200W. Then the resistance drops to  $132\Omega$  at 0.55s, the output bus voltage still stabilized 230V and the output power reaches 400W again. Then the resistance jumps to  $198\Omega$  at 0.75s, after a moment the output bus voltage still stabilized 230V and the output power still stabilized 400W. When the wind speed is lower 11.5m/s, the machine speed tracked the wind speed and the maximum output power point is tracked. The other simulation results such as three phases currents and torque waveforms are shown in Figs.6(b)~(e) for the SRG operating under the proposed MPPT algorithm when the wind speed varies.



(a) Speed, voltage and power waveforms



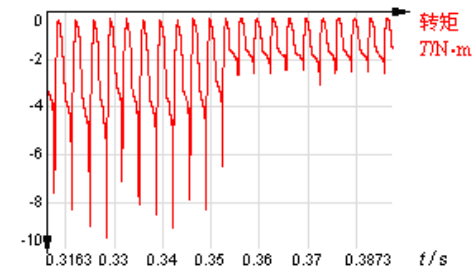
(b) Three phases currents



(c) Phase-B current



(d) Total torque



(e) Enlargement of torque

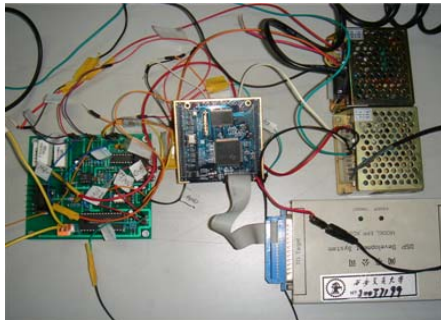
Fig.6 Simulation results of proposed MPPT algorithm for SRG system when the load is changed

3.3 Experimental results

In this section, a laboratory setup was built and the experimental results of proposed MPPT algorithm for SRG system are presented. The block diagram and the hardware arrangement of experimental SRG system setup are shown in Fig.7. The setup consists of a 0.55kW SRG, a resistance load, a dc power supply and the asymmetric three-phase half-bridge IGBT power converters, controller and drive

circuits which are used to switch the IGBT on and off, and the voltage and current sensors are used to sense the voltage and phase current.

Fig.8 shows the experimental results of the SRG system based on the proposed MPPT algorithm when the wind speed varies. At the starting, the wind speed is set as 12m/s and the voltage is set as 115V, after 10s the machine speed stabilized at 1140rpm, the the output bus voltage stabilized at 115V under the closed-loop control.

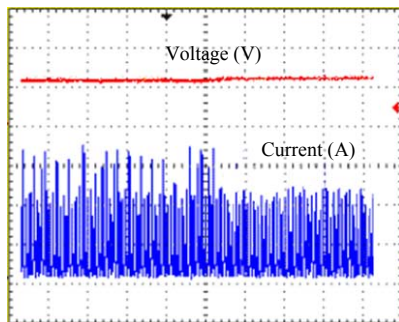


(a) Controller and driver circuits

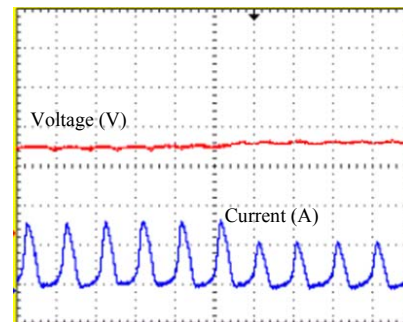


(b) experimental SRG machine

**Fig.7 Hardware of experimental system.**



(a) Bus voltage and phase current



(b) Enlargement of bus voltage and phase current

**Fig.8 Experimental results of MPPT algorithm for SRG system when the wind speed varies**

#### 4 CONCLUSION

This paper mainly focused on the application of SRG in wind power generation, and the MPPT control for wind power generation has been presented from simulation to experiment. The structure and operating principle of the wind turbine based on DC motor were formulated and the control strategies were introduced. Meanwhile the control principle and scheme of tracking maximum power point for SRG used in wind power generation system were discussed. The simulation models of the wind turbine and SRG system were built based on the FEM by using Ansoft/Simplorer. By using the simulation model, the dynamic performances in both open loop control system and closed loop control system for the SRG, also that of changing loads, changing speeds in closed loop control system were simulated respectively. At last the control principle and scheme of MPPT for SRG used in wind energy conversion system were simulated and analysed. The tests and experimental results of the whole system had been done.

#### BIBLIOGRAPHY

- [1] Chen H, Shao Z. Turn-on Angle Control for Switched Reluctance Wind Power Generator System[C]//The 30th Annual Conference of the IEEE Industrial Electronics Society. Busan, Korea ,November 2-6, 2004:2367-2370
- [2] Zhang Qe, Wang g, Zhu X, et al. A Small Single-phase Switched Reluctance Generator for Wind Power Generation. 2001 ICEMS:2001.Proceedings of the Fifth International Conference on, Aug

- 2001,2:1003-1006
- [3] Cardenas R, Pena R, Perez M, et al. Control of a Switched Reluctance Generator for Variable-Speed Wind Energy Applications. IEEE Transactions on Energy Conversion, December, 2005,20(4):781-791
  - [4] Datta R, Ranganathan V T. A Method of Tracking the Peak Power Points for a Variable Speed Wind Energy Conversion System. IEEE Transactions on Energy Conversion, March 2003,18(1):163-168
  - [5] Mademllis C, Kioskeridis I. Optimizing Performance in Current-Controlled Switched Reluctance Generators. IEEE Transactions on Energy Conversion, Sep 2005,20(3):556-565
  - [6] Mese E, Sozer Y, Kokernak, et al. Optimal Excitation of a High Speed Switched Reluctance Generator. Applied Power Electronics Conference and Exposition. APEC 2000:Fifteenth Annual IEEE, 2000, 2000

## **Design and Research of 10MW Large Wind Turbine Generator**

**Ning Yuquan**  
**The Huazhong Univ.of Sci. & Tech.**  
**China**

### **SUMMARY**

A novel variable speed salient pole synchronous generator is presented in this paper. It is applied for design of 10MW large wind generators base on the theory and characteristic of new type electric machines. A rough design for 10MW wind generators is made. It indicates that such a generator is feasible for large wind power. A 10MW wind generator with a single-stage planetary gearbox compares to PM generator system with a direct-drive. It indicates that research the wind turbine generator with a single-stage planetary gearbox is new direction for large wind power by using novel variable speed salient pole synchronous generator. The objectives of this paper are to investigate the feasibility of a 10MW generator for wind turbine with a single-stage planetary gearbox.

### **KEYWORDS**

Wind power , Variable speed, Constant frequency, Doubly fed , Variable speed synchronous machine

## 1 INTRODUCTION

Recently, a great attention has been paid to the pollution free renewable energy sources to be an alternative source for oil, gas, Uranium and coal sources that will last no longer than one century. Wind energy is considered as one of the most important types of renewable energy sources that have been used widely in electricity generation. The fact is that the cost of energy supplied by wind turbines is continuously decreasing.

Conventional generators are installed at the top of the towers and require step-up gearbox so that type of generator for this application needs tube compact and light. The gearbox of wind generator is expensive, subject to vibration, noise, and fatigue, and needs lubrications as well as maintenance at appreciable cost.

Many researches about design optimization and comparison of the different wind generator systems are reported in recent years. Some wind generator systems, which are the most widely application doubly-fed induction generator with 3-stage gearbox, the doubly-fed induction generator with 1-stage gearbox, the direct-drive synchronous generator with electrical excitation, the direct-drive PMSG(DDPMSG), and the PMSG with 1-stage gearbox(PMSGIG), were compared based on the annual emerge production(AEP) and cost-effective in paper[4,5]. With the increase of the power rating and decrease of the rotor speed, the PMSG is becoming larger and more expensive, especially for DDPMSG. Therefore, comprehensive study on the design characteristics and cost-effective of the different generator systems for wind turbines is essential.

Various concepts of wind turbines have been develop. Many researches about design optimization and comparison of the different wind generator systems are reported in recent years. Some wind generator systems, which are the most widely application, such as doubly-fed induction generator with 3-stage gearbox, the doubly-fed induction generator with 1-stage gearbox, the direct-drive synchronous generator with electrical excitation, the direct-drive PMSG(DDPMSG), and the PMSG with 1-stage gearbox(PMSGIG), were compared based on the annual emerge production(AEP) and cost-effective in paper[4,5]. With the increase of the power rating and decrease of the rotor speed, the PMSG is becoming larger and more expensive, especially for DDPMSG. Therefore, comprehensive study on the design characteristics and cost-effective of the different generator systems for wind turbines is essential. The objectives are to minimize the cost, and to improve the power quality. The direct-drive wind turbines have been to increase the emerge yield to reduce the gearbox failures, and to lower the maintenance problems. However it is difficult to conclude what generator system is the best for wind turbines.

According to comparisons of different generators systems, the direct-drive generators system is better in terms of the energy yield, reliability and maintenance problem compared to the geared generators system. Among different direct-drive systems, the permanent magnet (PM) type is superior compared to the electrically-excited type. For maximizing the energy yield, the direct-drive PM generators systems is better than both the gearbox generators system and the direct-drive electrically excited generation system. However, the direct-drive generators system has drawbacks such as a large diameter, a heavy weight, and a high cost to make high rated torque at low rotational speed.

In wind power, benefit of the Doubly Fed Induction Generator (DFIG) is the reduced size of converter and widely has been applied in the wind power. In fact, if the speed range of the turbine is depended on slip  $s$  of generators, then converter size is close to slip  $s$ . Current research on large direct-drive wind generator discusses generators and/or converters, and/or control, but researchers do not commonly consider DFIG.,

The direct-drive generators used in the wind turbines are large, heavy, and expensive when compared to the geared-wind turbines. Scaling them up will increase the size, the weight, and the cost rapidly, and the direct-drive generator requires full size converters and filters. In case of large direct-drive PM wind generator, the structural mass is dominant in the total mass of the generators.

Novel doubly fed variable speed salient pole synchronous machine (DFVSSPSM) is presented base on the patent. The novel salient pole synchronous machines possess the structure of salient pole electric

machines and the characteristic of the variable speed constant frequency. Therefore it establishes basis on large wind generator. Base on the DFVSSPSM, a novel wind generator unit for large wind power is presented.

The objectives of this paper are to investigate the feasibility of a 10MW wind generator systems with single-stage planetary gearbox and to compare the PM generator systems with direct-drive. To investigate the feasibility of a 10MW wind power, a rough electromagnetic design is made.

The paper starts with a section 2 about modeling of the wind turbine, the gearbox, the converter. Next section 3 is the introduction for the novel DFVSSPSM. The section 4 is rough electromagnetic design for 10MW wind generators; the resulting for rough design is given. The paper concludes 10MW wind generator system is feasibility.

## 2 MODELING OF THE WIND GENERATOR

Currently the wind PM generator system with direct-drive has been the develop direction for large wind power. The modeling of wind generator systems is presented in literature [4].

### 2.1 Wind Turbine Modeling

Base on essential theory of wind turbine it indicates that the available shaft power  $P_T$  from a wind turbine depended on the blade parameter  $C_p(\lambda, \beta)$  for wind turbine,  $D$  wind turbine rotor diameter. It is function of wind speed, and can be calculated as a function of the wind speed.

$$P_T = \frac{1}{8} \rho C_p(\lambda, \beta) \pi D^2 v^3$$

Where  $\rho$  is the air density,  $D$  is the wind turbine rotor diameter,  $v$  is the wind speed, and  $C_p(\lambda, \beta)$  is the power coefficient or aerodynamic efficiency, which is a function of the tip-speed ratio  $\lambda$  (the tip speed divided by wind speed) and the pitch angel of turbine blades  $\beta$ .

The typical power characteristic of a wind turbine clearly shows that the shaft power is assumed to be proportional to the cube of the wind speed at the maximum aerodynamic efficiency  $C_{p_{\max}}$  below the rated wind speed, and the blades are pitched to reduce the aerodynamic efficiency so that the shaft power is kept as a constant above the rated speed. It is shown as Fig 1.

The rated wind speed can be calculated as  $v_n = \sqrt[3]{\frac{8P_{Tn}}{\pi\rho C_{p_{\max}} D^2}}$

Where  $P_{Tn}$  is the rated shaft power, which can be calculated by design optimization of wind generator system,  $v_i$  is the cut-in wind speed,  $v_N$  is the rated wind speed, and  $v_c$  is the cut-out wind speed.

Base on the basis of the shaft power  $P_{Tn}$  of wind power, the wind turbine rotor diameter  $D$ , the rated wind speed  $v_N$ , and the blade parameter  $C_{p_{\max}}$ , the energy contribution can be estimated for wind turbine units. The calculating energy yield at each wind speed can be determined by the power output  $P_{grid}(v)$  of the wind generator system at a specific wind speed and the duration that the wind speed occurs annually. Therefore, the annual energy production (AEP) can be estimated by summing the incremental energy contributions at each wind speed, which can be expressed as

$$AEP = 8760 \int_{v_i}^{v_c} P_{grid}(v) f(v) dv = 8760 \sum_{j=1}^n P_{grid}(v_j) f(v_j) \Delta v$$

Where  $f(v)$  is Weibull density distribution, which is given as

$$f(v) = \frac{k}{c} \left(\frac{v}{c}\right)^{k-1} e^{-(v/c)^k}, \quad k > 0, \quad c > 1$$

Where  $k$  is the shape parameter and  $c$  is the scale parameter

Table I gives the main parameter of the 10MW wind generator systems.

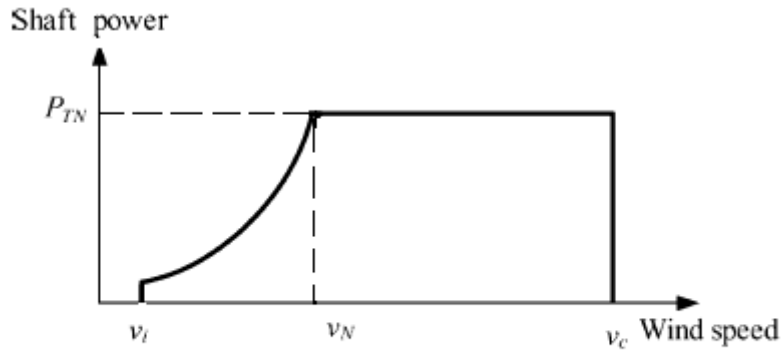


Fig 1 Power characteristic of a wind turbine.

The majority of wind farm sites around the world have the annual mean wind speeds in the range of 6~8m/s at 10m height. The hub height of wind turbine is approximately calculated with 1.2 times turbine blades diameter, Therefore a specific site with an average wind speed of 7m/s at 10m height ( $k = 2, c = 7.9$ ) is used. The AEP of different wind generator systems can be evaluated annual mean wind speeds at the hub height. The wind turbine modeling for 10MW wind power has been given in Table I [4].

Table I Modeling Parameters of PM Wind Generator System

Wind turbine modeling	
Rated power $P_N$ [MW]	10
Rated rotor speed $n_r$ [rpm]	10
Rotor diameter $D$ [m]	170
Sweep area [ $\times 10^3 m^2$ ]	22.7
Hub height [m]	204
Hub height mean wind speed	12.8
[ $m/s$ ]( for AEP estimates)	
Cut in wind speed $v_i$ [ $m/s$ ]	2.5
Cut out wind speed $v_c$ [ $m/s$ ]	25
Optimum tip speed ratio $\lambda_{opt}$	7
Maximum power coefficient[ $C_{p_{max}}$ ]	0.48
Air density[ $kg/m^3$ ]	1.225

## 2.2 Gearbox modeling

In the reference [4] the single-stage planetary gearbox modeling is given. It indicates that the gear trains of a gearbox can be of two distinct types: parallel shaft and planetary. Due to its compact and lightweight, a single-stage planetary gearbox is used in wind generator units. The weight of a single-stage gearbox depends upon the stage ratios chosen and the shaft torque level, which can be given as

$$G_{gear} = \frac{3.2T_m F_s F_w}{1000}$$

Where  $T_m$  is the output torque of gearbox (in Newton meters),  $F_s$  is the service factor considering surface damage and failure by metal fatigue.

The weight factor  $F_w$  is given as  $F_w = \frac{1}{Z} + \frac{1}{Zr_{rv}} + r_{rv} + r_{rv}^2 + 0.4 \frac{(1+r_{rv})}{Z} (r_{ratio} - 1)^2$

Where  $Z$  is the planet wheel number in a stage; the wheel ratio  $r_{rv} = (r_{ratio}/2) - 1$ ,  $r_{ratio}$  is the single-stage gear ratio.

The cost of a single-stage gearbox  $C_{gear}$  is roughly estimated by the weight  $C_{gear}$  and specific cost  $c_{gear}$  as  $C_{gear} = c_{gear} G_{gear}$

The large planet gear with a ratio of 3:1~15:1 is possible for a single-stage planetary gearbox to manufacturer and to ensure adequate lifetime. The weight and cost of the single-stage gearbox increase with increase of gear ratio and power ratings. According to the given turbines, the gearbox weight and cost with variable gear ration can be estimated by the presented gearbox modeling.

The losses in a gearbox can be divided into two different parts that is a gear teeth losses and bearing losses. It depends on input power, seal losses, and lubricant. In fact, It primary depend on input power and rotational speed of the gearbox. This means that the main losses in a gearbox are proportional to the shaft power and speed as

$$P_{gear} = k_g P_n \frac{n_r}{n_{rn}}$$

Where  $k_g$  is a constant for the speed-dependent losses (in the case, it is about 1.5% for a single-stage gearbox),  $P_n$  is the rated power of wind power,  $n_r$  is the rotor speed,  $n_{rn}$  is the rated rotor speed.

### 2.3 Power Electronic Converter Modeling

In the wind generator systems a back-back pulswidth modulation (PWM) power electronic converter has been widely used. The PM wind generator systems with direct-drive requires a full-scale power electronic convert, but the wind generator systems with 1-stage drive/3-stage drive requires slip power electronic convert. The convert power is  $P_{convN}$  as  $P_{convN} = sP_N$ .

Where  $P_{convN}$  is converter power,  $P_N$  is wind generator power, and  $s$  is slip.

The losses in the power electronic converter  $P_{conv}$  can be modeled as

$$P_{conv} = \frac{P_{convN}}{31} \left( 1 + 10 \frac{I_s}{I_{sN}} + 5 \frac{I_s^2}{I_{sN}^2} + 10 \frac{I_g}{I_{gN}} + 5 \frac{I_g^2}{I_{gN}^2} \right)$$

Where  $P_{convN} = k_c P_N$  is the dissipation in the converter at the rated power,  $I_s$  is the generator-side converter current,  $I_{sN}$  is the generator-side converter rated current,  $I_g$  is the grid-side converter current, and  $I_{gN}$  is the grid-side converter rated current.

## 3 THE NOVEL DOUBLY FED VARIABLE SPEED SALIENT POLE SYNCHRONOUS MACHINES

The Doubly Fed Variable Speed Salient Machine (DFVSSPSM) presented by patent (patent number: CN01128351.3) is a novel electrical machine which is possessed of originality innovation and self-determination intellectual asset. The novel DFVSSPSM was authorized and supported by the Hi-tech research and development program of China (863 programs) (863 program Number: 2001AA512050).

The patent has been validated by experiment through research. It carried out the theory and construction of novel electric machines. It successfully carries out a new technology on novel variable speed constant frequency of salient pole synchronous machine. It settles base on application for large water power station, pumped storage power plant, and wind power plant.

### **3.1 The theory on DFVSSPSM**

In the construction the stator of DFVSSPSM is as same as traditional ac electric machines, and its rotor also is type of salient pole. It breaks through the idea of traditional synchronous machines, and applies to ac excitation. It is key to separate synchronous rotate speed of air gap magnetic field from rotate speed of rotor. The rotate speed of electric machine can adjust using excitation of low frequency controlled by ac variable frequency power. The rotate speed of air gap magnetic field produced by winding of stator and rotor still comparatively are rest, but the synchronous rotational speed of air gap magnetic field separate from rotational speed of rotor. It can realize adjust speed of electric machines, and contradictorily can rotate. The theory and construction of Novel DFVSSPSM detail respect to literature [1, 2].

### **3.2 The construction of DFVSSPSM**

The stator of the DFVSSPSM has P-pairs of magnetic pole which is powered by normal rating frequency. The stator is as same as traditional ac electric machines. The rotor has a two phase's orthogonal winding. The rotor of the DFVSSPSM is applied to salient pole type, but it has 2P-pairs of magnetic pole which is powered by low frequency ac excite. The 2P-pairs of magnetic pole winding are formed p-pairs of magnetic pole winding. The two phases winding of rotor is located vertical each other on the space and time. Two windings are distributed by angle 90 electric degree located each other. The round rotational magnetic field of air gap has been produced by two phase's windings of rotor.

## **4 THE DFVSSPSM OF RATED 10MW WITH SINGLE-STAGE GEARBOX**

Base on wind power modeling a wind generator with single-stage gearbox is applied to rough design for 10MW wind generator. When the rated wind speed is 12m/s, and the rotor speed is 10 rpm, the single-stage gear ratio  $r_{ratio}$  is 10.7, and the magnetic pole number of salient pole synchronous machines is  $2P=56$ . The resulting indicates that the stator out diameter  $D_a$  is about 4.25m, stator core length  $L_t$  is about 1.8 m, and air gap is about 4~5mm, The optimal design results for the 10MW multibrid PM generator systems is given in [4], The optimal design shows that the generators air gap diameter  $D_{i1}=10m$ , stator length  $L_t = 1.81m$ , and the generator active material is 62.8 ton. The rough design shows clearly that the wind generator for rated power 10MW wind generator with a single-stage planetary gearbox is the feasibility by application to DFVSSPSM. When it be compared to PM generator systems with direct drive, the DFVSSPSM have lower cost and higher reliability. The large direct-drive PM generator systems have a large outer diameter. It produces many difficult such as manufacture, transport and assembly. This is easy and convenience to DFVSSPSM, It is obvious which the DFVSSPSM have a series advantage.

## **5 CONCLUSION**

This paper aims to present a new concept for wind power design by apply to DFVSSPSM with single-stage gearbox. The rough design for 10MW wind generator system with single-stage gearbox is feasibility. The design analysis and results of 10Mwind generator systems with single-stage gearbox indicate the new direction to develop and research wind power. The DFVSSPSM settles base on application for large water power station, pumped storage power plant, and wind power.

## **BIBLIOGRAPHY**

- [1] Ning Y. Doubly Fed Variable Speed Salient Pole Synchronous Machine[P]:CN,0112835 1.3

- [2] Ning Y. A Novel Variable Speed Constant Frequency Doubly Fed Salient Pole Synchronous .Machine Engineering Science of China, 2004, 6 (12):27-31
- [3] Ning Y.半驱是大型风电机组发展的新方向. 电气技术, 2009(8)
- [4] Li H, Chen Z, Polinder Henk.Optimization of Multibrid Permanent-Magnet Wind Generator Systems. IEEE Trans . Energy Convers, March 2009,24(1): 82-92
- [5] Polinder H, Pijl F, F A D Van, Vilder G J, Tavner P. Comparison of direct-drive and geared generator concepts for wind turbines. IEEE Trans. Energy Convers., Sep. 2006,21(3) :725–733

**Guide for On-line Monitoring of Turbo-generators**

**D. Zlatanovici**  
**Convener of WG A1.11 CIGRE**  
**Energy Research And Modernisation Institute - ICEMENERG**  
**Romania**

**SUMMARY**

In the report the definition and compenence of the on-line monitoring system and types of systems for monitoring and information interpretation are presented. Also, 20 parameters/components being monitored and the correspondent devices are presented. The benefit for using these systems with their advantages and disadvantages are presented and reasons for the future development of the on-line monitoring systems.

**KEYWORDS**

Turbo-generator, On-line monitoring, Partial discharge, Vibration, Cooling, Temperature, Failure

## 1 INTRODUCTION

The present report represents the upgrade of a report elaborated in 1999, “On-Line Condition Monitoring Tools for Large Turbine Generators”, prepared by WG Conveners Don Rose and Mal Park (AU) on behalf of SC A1.

The report has been based on the 13 answers received to the questionnaire elaborated and spread to all of the members and experts of SC A1. 8 countries have answered: Australia, Brazil, France, Japan (3 answers), Romania, Russia, Spain and United States (4 answers).

## 2 DEFINITION

The aim of an on-line monitoring system for electrical rotating machines is early detection and information about changing machine conditions during operation which later on may result in high wear or malfunctions.

An on-line monitoring system consists of: special measuring sensors, signal transducers to convert the sensor signal, data transmission systems, software acquisition and measurement, specialized software for monitoring, trending and analysing the measured parameters.

## 3 GENERAL COMMENTS

Generally, on-line monitoring systems are used mainly for larger generators with a power rating above 300 MVA having direct hydrogen or water cooled windings. But there is a tendency to extend on-line monitoring also for hydrogen or air cooled generators with ratings below 300 MVA. On-line monitoring is mainly applied to units with strategic importance in the utilities assets.

The most recognized benefit of early detection of incipient faults is the major savings that could be achieved in repair costs. The purpose of monitoring is to try to prevent major catastrophic failures and turn them instead into failures that can be repaired at a reduced cost during a planned outage.

## 4 PARAMETERS OR COMPONENTS TO BE MONITORED END DEVICES USED

### 4.1. Thermal decomposition of insulation materials in hydrogen or air cooled machines

*Generator Condition Monitor (GCM):* A device, which detects and analyses micro particles in hydrogen or air coolant to detect local thermal decomposition of insulation materials or special tagging compounds applied to machine components. It requires off-line analysis in a laboratory to identify the insulation materials or to differentiate the tagging compounds released into the coolant due to overheating.

### 4.2 Hydrogen leakage

- Leaking through housing, into sealing oil (bearings) or cooling water (H<sub>2</sub>-cooler)

*Hydrogen Make-Up Rate Monitor:* A device with a sensor system which determines the degree of hydrogen coolant loss corrected by operating parameter influence

- Leaking into stator winding cooling water

*Hydrogen-Into-Water Leakage Monitor:* A device to detect hydrogen in the stator winding water cooling system and measuring the rate of H<sub>2</sub>-leakage into stator winding water coolant.

### 4.3 Hydrogen gas purity

Efficiency of generator operation depends on hydrogen purity because a mixture of hydrogen with water vapour, oil dust or air will raise the gas density and therefore significantly increase windage losses.

*Hydrogen Purity Analyser:* A device for detecting the presence of impurity gases in hydrogen coolant and measuring hydrogen content in %.

### 4.4 Hydrogen dew point

Moisture content in cooling gas can result in creepage discharges or break down of high voltage stator winding insulation. It may also indicate water leakages at coolers or direct water cooled windings. To

control dew point temperature during start up after maintenance stand still is important because absorbed moisture may condense at cool parts of the machine and spread water droplets onto the stator winding.

*Hydrogen Dew-Point Monitor*: A device that measures moisture content in hydrogen coolant and expresses it as dew point. This is used as an operational / maintenance aid for ensuring hydrogen dryness and avoiding creepage discharges at wet insulation surfaces. Useful indicator for water leakages at direct water cooled rotor windings.

#### **4.5 Stator winding temperature monitoring (AU, JP2)**

The mean value of stator winding is controlled by a minimum of six slot RTD's acc. to IEC 60034. Additional slot RTD's often used at large machines due to the fact that failed sensors in the slot cannot be repaired without rewinding the stator. The temperature of all stator winding slot RTD's is monitored at the control room panel. (see also 4.7 c)

The temperature of direct hydrogen or water cooled stator windings may be controlled by measuring the individual stator bar temperature. (see 4.6)

#### **4.6 Direct hydrogen cooled stator winding**

In direct gas cooled stator windings the temperature rise of hydrogen cooling gas can be measured with fiber optic temperature sensors placed at the cooling duct outlet of stator bars. Prototype installations at direct hydrogen cooled stator windings of large turbine generators (850 MVA, 21 kV) have been running for several years to get monitoring experience.

#### **4.7 Stator winding cooling water condition**

To avoid clogging of hollow conductors on direct water cooled stator windings and to detect a leakage in the cooling water system the following parameters can be measured:

- a) Water conductivity (BR)

*Stator Cooling Water Conductivity Monitor*: A device for monitoring the purity of stator cooling water by measuring its electrical conductivity.

- b) Dissolved oxygen (US2)

*O<sub>2</sub>-Monitor / pH-Monitor*: Controls dissolved oxygen content and/or pH-value in cooling water as an indication of clogging risk or cooling water leakage.

- c) Individual stator bar temperature measurement (JP2)

*Generator Temperature Analyzer (GTA)*: Monitors the cooling water temperature at the warm side outlet of each stator bar and correlates it with generator load, temperature and H<sub>2</sub>-pressure to identify hollow conductor plugging. Same principle also used for direct hydrogen cooled stator windings.(see also 4.5).

#### **4.8 Partial discharge activity at stator winding**

Various monitoring systems are used to measure PD activity at stator windings and arcing effects at intermittent current connections (e.g. slot discharges, broken strands). They use different ways of detecting PD signals at the stator winding and different frequency ranges for PD measurement and analysis.

Measuring sensitivity depends on noise reduction strategies and on the capacitance value of the coupling capacitors. It can be said that the measuring sensitivity is improved, both in magnitude and number of pulses of partial discharge detected when the capacitance value of the coupling capacitors increase.

Fig.1 shows an example of a PD (at the white bands) occurring due to deterioration of the slot conductive coatings and/or the silicon carbide stress relief coatings.

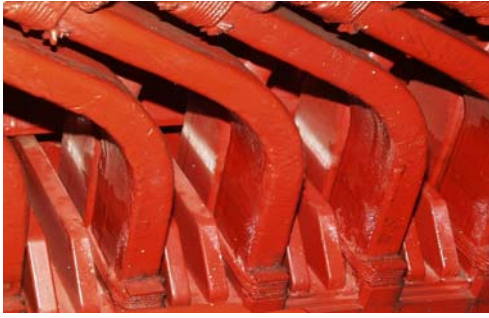


**Fig. 1** Example of a PD (at the white bands) occurring due to deterioration of slot conductive coatings and/or the silicon carbide stress relief coatings.



**Fig. 2** Coupling capacitors direct at the generator high voltage terminals

#### 4.8.1. Coupling devices / Sensors

- a) Using existing surge capacitors and a high frequency current transformer at grounding lead as coupling device (AU)
- b) Coupling capacitors at phase insulated bus bars – one or two couplers per phase
- c) Coupling capacitors direct at the generator high voltage (hv) terminals (Fig. 2)
- d) Coupling via transformer or additional capacitor at generator neutral connection
- e) Broad-band antenna in selected stator winding slots (Slot Coupler at line end or embedded RTD)
- f) Using insulated water manifolds of direct water cooled stator windings as an antenna for PD inside the generator

#### 4.8.2. PD monitoring systems

- a) Broad band PD monitor in the low frequency range of 10 kHz – 30 MHz
- b) Radio Frequency Monitor (RFM) in the MHz frequency range – narrow band or broad band system
- c) High Frequency Monitor up to a few hundred MHz
- d) Electro Magnetic Interference EMI PD spectrum measurement with a narrow band frequency analyzer

The monitor system to be used to measure the partial discharge activity depends on the capacitance of the coupling capacitors. With lower values of capacitance must be used a monitor system able to measure higher frequencies. However, as the stator winding may be considered as a long transmission line with resistance, inductance and capacitance, the attenuation of the signal increases at high frequencies making the measurement of the signals more difficult.

Thus, to establish the best coupling capacitor simulations must be done, considering some values of capacitance, and inserting signals of different frequencies at the beginning of a phase winding. These signals are captured at several points in the winding and their attenuations will allow to determine the best coupling capacitor.

#### 4.8.3. Noise suppression methods

Although PD data can be collected using many different techniques, the important criteria for any measurement made during normal generator operation is the ability to deal with electrical interference or noise. With the machine in operation and connected to the power system, many sources of noise are present including power system corona, slip ring sparking, poor electrical connections external to the stator winding, local power tool or arc welding equipment operation, etc. All of these can generate pulses with characteristics similar to PD, which can often be orders of magnitude larger than the actual PD levels in the winding. Without techniques to eliminate these noise sources, on-line PD measurements made by a non-expert can conclude the stator winding is deteriorated, when in fact it is not. Such false indications can reduce the credibility of PD testing. Thus, it is critical that any on line measurement technique include methods to separate noise from PD.

To this end, the following methods were developed to separate the noise found in on line measurements from the pure stator winding PD signals. Thus, it became possible for on-line PD testing for machines to be performed and interpreted by plant electrical staff with minimal training or detailed understanding of PD phenomena.

- a) Phase window gating with additional noise antenna input
- b) Digital filtering in time or frequency domain
- c) PD source identification by pulse traveling time measurement
- d) Phase separation by multi-channel measurement at two or three phases in parallel

#### 4.9 Stator end winding vibration (BR,CA)

*Stator End winding Vibration Monitor:* A device using piezoelectric or fiber optic accelerometers to measure and monitor end winding (overhang winding) vibration activity, which can occur as a result of loosening of the windings supports caused by operational overstressing events such as faults, switching surges and mal synchronization that could strain and relax the support structure . Most of the vibration related aging mechanisms are time dependent and are affected by the extensions of inspection periods.

The accelerometers are connected to an acoustical measurement system and a computer for analysis of the motion. Depending on the end winding parts to be monitored different sensors have to be used.

- a) Piezoelectric accelerometers: Placed at grounded bracings of end winding supports.
- b) Fiber optic sensors: Accelerometer without metal parts directly fixed to end winding coils, which may be on high potential. (Fig.3)

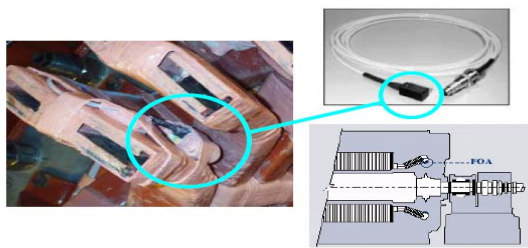


Fig. 3 Fiber optical accelerometer and details of its assembly at turbo-generator stator end winding

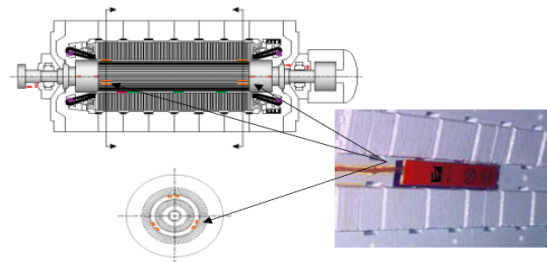


Fig. 4 Location of stator bar vibration sensors

#### 4.10. Stator frame and core vibration (BR)

*Stator Core/Frame (SCF) Vibration Monitor:* A measuring device with accelerometer sensors (or similar) connected to the stator core or/and frame for vibration measurement. For example, it may detect loosening of core/frame components or structural deterioration.

#### 4.11. Stator core lamination vibration (used only by FR)

*Audio Detector - Stator Core Lamination Vibration:* A device using audio frequency sensors for identifying vibration of stator core laminations caused by looseness of core pressing.

#### 4.12. Stator bar vibration (CA)

*Stator bar vibration Monitor:* This is a monitoring system that uses capacitive sensors to identify problems occurring in the stator wedges which radially fix the copper windings against electromagnetic forces caused by poles passage (Fig.4). If wedges loose their compression power, what usually occurs after some years, vibration amplitude of the bars will increase causing friction between bar and slot and as a consequence an abrasion on conductive component of the bar and its insulation which may lead to:

- a) Abrasion of semi-conductive painting and insulation drives to a drastic increase of partial discharges that destroy insulation from the inside.
- b) Partial discharges weaken insulation, causing more abrasion.

c) The increase of bars vibration decrease heat exchange between bar and slot, contributing to weaken the insulation.

#### **4.13. Brush condition of static excitation systems**

*Brush Condition Monitor:* A device to measure the voltage drop between slip rings and brushes for the purpose of monitoring low resistive brush/slip ring condition. Some types of monitor may measure a wider range of parameters such as brush temperature, brush movement, electrical sparking, slip-ring surface orbit together with ambient temperature and humidity.

#### **4.14. Diode failure at brushless excitation systems**

*Diode Breakdown Detector:* A device for detecting failure of diodes in a machine with brushless excitation by identifying irregularities in the field flux pattern. The system has the purpose of monitoring the integrity of the rotor winding particularly in regard to over-temperature as well as the diodes themselves.

*Diode Fuse Detector:* If a diode of rotating rectifier fails, a fuse in series will be released by short circuit current. The monitoring device identifies the destroyed diode fuse.

#### **4.15 Rotor winding shorted turns**

*Rotor Interturn Short-Circuit Monitor:* A device using a small coil sensor installed at the stator core inside surface in the air gap (flux probe) that detects the radial flux density of rotor windings and records of waveform pattern of magnetic flux density by rotation (Fig.5).

The purpose is to determine the presence of rotor winding faults (turn-to-turn shorts) from any irregularity in the induced voltage pattern at the air gap flux probe by digital comparison of flux pattern of both rotor poles. Must be used only one sensor assembled at the bottom part of the stator.

The short-circuit in the rotor can produce thermal unbalance, resulting in increased vibration levels that can be difficult to distinguish when compared to other mechanical problems. For an effective analysis, the results are combined with air gap measurements that allow correlation between flux and air gap for each pole allowing to detect if unbalance is caused by an electric failure as rotor winding faults (turn-to-turn shorts) in the pole or induced by a very small air gap.

#### **4.16. Shaft bearing vibration**

*Bearing Journal Vibration (ORBIT) Analyser:* A system of dual probes mounted on each bearing of a turbine generator set for the purpose of diagnosing vibration problems by observing the nature and magnitude of the shaft orbit and mean position.

#### **4.17. Rotor shaft vibration of turbo set (used only by ES )**

*Shaft Vibration Analyser:* A system of proximity probes axially mounted all over the turbine generator set for the purpose of diagnosing vibration problems by observing the nature and magnitude of the shaft orbit and mean position.

#### **4.18 Rotor shaft torsional oscillation (remaining life calculation) (used only by US4, FR, RU)**

*Shaft Torsional Oscillation Monitor:* A device to evaluate shaft fatigue of turbo generator set due to sudden load changes, out of phase synchronization, electrical faults in transmission network etc. Measuring principle: change of permeability due to magnetic-strictional effect at ferromagnetic shaft material under torsional forces.

#### **4.19 Retaining rings failures**

*Retaining rings failures Monitor:* This device uses proximity sensors to regularly monitor the retaining rings for detection of deformations or shape irregularities. The proximity sensors use the same capacitive technology of the stator bar vibration detectors, and are immune to all interferences existing in the area, such as dust, oil, humidity, radio-frequency and electromagnetic.

Retaining rings that are used to repress the centrifugal force at rotor windings end are the more stressed components of a generator and so require extreme care in the project as well as in

manufacturing and maintenance. In body-shaped rings can occur a high current circulation during unbalance conditions, driving to damages caused by heat excess. In spindle-mounted rings, they allow a flexibility between the rotor body and the ring, that can drive to insulation failures and cracking the coils in this area, resulting in a very dangerous condition in machines with frequent load cycles and run-up/run-down proceedings.

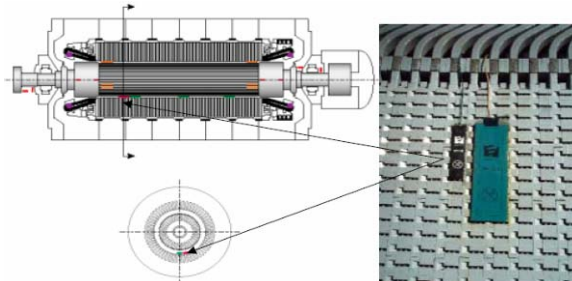


**Fig.5 Flux magnetic sensor assembled together with air gap sensor**

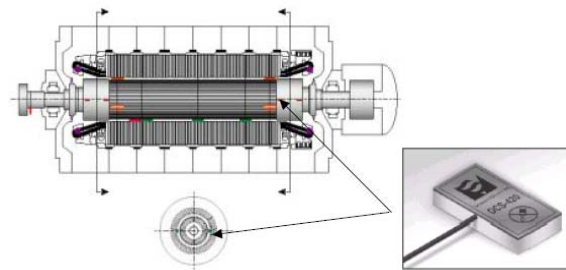


**Fig.6 Capacitive proximity sensor to measure retaining rings deformations**

#### **4.20 Shaft voltage / grounding (AU, ES, US4, FR, RU)**

The purpose is to detect any loss of permanent low resistive shaft grounding or loss of integrity in shaft insulation at bearings and exciter set, which can result in bearing babbitt damage due to discharge erosion in soft metals used in the bearing.

a) *Shaft Grounding Monitor* (US4, FR, RU): A instrument that measures shaft voltages and currents associated with the machine-grounding device.

b) *Shaft Voltage Monitor* (AU, ES): A device that controls shaft voltage only. Discharge spikes or reduction of voltage indicate bad shaft insulation.

Other devices that were suggested were:

I Rotor Earth Fault Monitor (AU). This is a generator protection device and not a monitoring system and should therefore be skipped

II Digital Fault Recording (CA). These systems collect data from many other systems and sensors and preserve data for evaluation in case of generator faults.

### **5 TYPES OF MONITORING SYSTEMS AND INTERPRETATION OF INFORMATION**

Depending on the monitoring device used for on-line measurement and depending on the amount of investment which correlates in most cases with the strategic importance of the unit the following types of monitoring systems are used:

- Individual devices or systems installed for each type of possible failure risk to be monitored
- Integrated monitoring systems, sometimes having a diagnostic shell, which combine different on-line monitoring modules for a number of different possible failures

The design concept of the on-line monitoring systems being used can be categorised as follows:

- *display* the values or the deviations of the surveyed parameters
- *analyse* the measured parameters using a technical rule base and generate warnings or alarms about the possibility of a failure to appear
- use a *diagnostic* knowledge base to perform a prediction of the condition generator or component and display it periodically

The information being recorded by data acquisition of the monitoring system is interpreted by:

- Experienced operator
- Specialized personnel like expert/advisory engineers at plant or headquarter
- Technical managers
- Dedicated diagnostic software based on artificial intelligence and knowledge based expert systems (majority)

## **6 OPERATIONAL VALUE AND ALARMS**

Information supplied by the monitoring systems is taken into account for adopting intervention decisions or for operational decisions (majority, except US 2,3)

When an alarm appears, decision is made taking into account the possible implications, by: exploitation operator, specialized personnel, technical managers, dedicated software (majority).

## **7 BENEFITS OF USING ON-LINE MONITORING SYSTEMS**

The following benefits of using on-line monitoring systems were mentioned:

- Reduction in off-line testing
- Change from time based maintenance to condition based maintenance
- Better management of maintenance
- Improvement in accuracy of diagnosis
- Increase in unit life
- Reduction in forced outages
- Prevention of failures
- Better evaluation of operational risk

## **8 FUTURE DEVELOPMENT OF ON-LINE MONITORING SYSTEMS**

### **8.1. Adapted on-line monitoring for all types of generators**

It is considered that on-line monitoring systems should be extended to all generators, depending on power, type or size . The selection of the sensors and monitored parameters have to be based upon value of the investment, in connection with generator size and type, as well as the operational scenario expected for the unit.

The extension of the on-line monitoring at the small machines has to be made depending on the performance, the costs, and the risk of the individual generator

### **8.2 Costs of on-line monitoring system versus benefit**

The costs can be justified for the on-line monitoring systems. Justification is dependent on criticality and risk for each case. Prevent one failure and the cost is returned .

Avoiding one failure can justify the monitoring costs for a whole fleet of generators.

Although the costs are justifiable, the generators owners consider they aren't .

These systems can protect the generators against operator's errors and can avoid the imminent problems of the generators .

Generally, at least the investment of monitoring instrumentation is recovered by the optimization of outages and by the reduction of failures and the damages.

### **8.3 Can on-line monitoring provide sufficient information for generator condition assessment**

Referring if the present systems provide sufficient information for generator condition assessment, the opinions are different. A part of answers considers the information is enough and other part considers that it is not enough. Problems such as looseness in the stator winding overhang, loose slot wedges, migration of rotor insulation can only be identified through visual inspection . Predicting final life of a component is still difficult with any accuracy

### **8.4 Open issues of existing on-line monitoring systems**

It is considered that individual generator components, some operational stresses or failure mechanisms are not covered by the actual on-line monitoring systems and improved systems have to be developed.

## 9 CONCLUSIONS

The questionnaire has once more proved the world wide opinion that on-line monitoring systems are very useful tool to increase availability of the generator and to reduce maintenance time. Under this view their installation and operational costs are justified.

On-line monitoring can be considered as a risk mitigation tool. It can give an inestimable knowledge about the machines, that allow utilities take the right decisions about maintenance based on the actual generation equipment conditions, instead of the traditional time based approach to maintenance.

Considerable experience from units with continuous monitoring shows that there can be significant benefits for the plant operator. One of the key benefits is that misinterpretation of the measurement data, which can lead to unnecessary and costly downtime of the unit, can be avoided.

All kinds of on-line monitoring systems will develop in the future and they will trend to integrated systems with a supervisory software shell including different monitoring modules individually chosen by the user

## BIBLIOGRAPHY

- [1] Stone, Fyles G C, Braun J F, et al. A Thermal Cycling Type Test for Generator Stator Winding Insulation. IEEE Transactions on Energy Conversion, Dec. 1991, 6(4):707 – 713
- [2] Zhu H, Green V, Sasic M, Halliburton S. Increased Sensitivity of Capacitive Couplers for In-service PD Measurement in Rotating Machines. IEEE Transactions on Energy Conversion, December 1999, 14(4)
- [3] Stone G C, Boulter E A, Culbert I, Dhirani H. Electrical Insulation for Rotating Machines – Design, Evaluation, Aging, Testing and Repair. John Wiley and Sons, Inc., 2004
- [4] Hudon C, Belec M. Partial Discharge Signal Interpretation for Generator Diagnostics. IEEE Trans. on Dielect. and Electr. Insul., April 2005, 12(2):297-319
- [5] A New Conception on on-Line Monitoring and Diagnose of Turbogenerators, Vibrosystem.
- [6] Helio P A ,Jr, Levy A F S, Carvalho A T. Estudo sobre a Influência dos Acopladores Capacitivos na Sensibilidade da Medição de Descargas Parciais em Máquinas Elétricas Rotativas. XX SNPTEE. Recife, Brasil, Novembro, 2009: 22-25

**This report is a result of WG.A1.11 members: Dan Zlatanovici, *Convener* (RO), Trevor Stokes (UK), Oscar Martinez (SP), Jürgen R. Weidner (DE), Robert Fenton (US), Erli F Figueiredo (BR), Kiyoshi Miyaike (JP), John Stein (US), Yury Vinitskij (RU), Michel Berlamont (FR), Carmo Gonçalves (BR), William McCown (US), John Linton (AU)**

## **Detailed On-Site Measurements to Validate Generator Numerical Modeling**

**Hudon, C., Chaaban, M., Belanger, S., Torriano, F. and Merkhouf, A.**  
**Institut de Recherche d'Hydro-Québec (IREQ)**  
**1800 Boul. Lionel-Boulet, Varennes, Québec, J3X 1S1**  
**Canada**

### **SUMMARY**

Over the last decade the arrival of powerful and affordable computers and improved numerical techniques has triggered several simulation studies of power generators and opened up entirely new research programs. However, although modeling offers a significant leap in the understanding of generator's behaviour, numerical results must always be validated before they can be used with confidence. At present, this is done by carrying out detailed on-site measurements (temperature, airflow velocity, magnetic field, vibration and strain) on generators operating at different load conditions. The true generator's behaviour will arise from the combination of the two partial sets of data: simulation and measurements. Instrumentation on generator is currently a huge task but should decrease with time as we can rely more on the models as they improve. This paper presents the extent of what is currently done at Hydro-Quebec to get the necessary information to validate numerical models. Example of temperature (optic fiber, thermocouples, thermistors) and flow rate measurements (from differential air pressure and indirect global cooling airflow) will be presented herein.

### **KEYWORDS**

Resistive thermal detector, Distributed temperature sensor, Thermistor, Stator, Rotor, Numerical modeling validation

## 1 INTRODUCTION

Availability of powerful and affordable computers have opened new opportunities to better understand the active physical phenomena in generators by using numerical modeling. However, these new numerical tools can lead to improved understanding or misleading results and the only way to discriminate between the two is to validate models with measurements before using them with confidence. In 2002, a major program has started at the research institute of Hydro-Quebec (IREQ) with the goal of building a complete numerical model of a generator. The current state of development of the project has been reported elsewhere [1]. The intent of this project is to increase nameplate rating of selected existing generators, but as generators are pushed closer to their true operation limit, comprehension of active physical phenomena must be refined so that the short term benefits are not detrimental of the equipment's life expectancy. One of the challenges is that complete measurements of a test object as large as a hydro-generator is impossible. Another challenge is that the prediction of behaviour based on numerical models has uncertainties due to simplification and missing data: material properties, geometric simplification and imposed boundary conditions. In addition, since the simple extrapolation of measured results to higher loads cannot be used when changes in behaviour occurs (magnetic saturation or mechanical interference between the core and frame), the use of a models is necessary to consider the correct change in physical phenomenon.

The ultimate goal of the project is to combine electromagnetic, thermal, mechanical and fluid dynamics simulations to replicate numerically the behaviour of hydro-generators. Although a fully integrated multi-physic model for generators including interactions between every field (electro, thermo-mechanical...) is years away, each aspect is currently being developed separately with exchanges between fields performed as weak coupling in a structured information flow, which will later be automated. Valuable information about generator losses and their distribution and its cooling is already being obtained. In parallel, validation by extensive field measurements is mostly done during standardize heat run test by operating the generator at different loads while measuring temperatures, airflow velocity, magnetic flux, vibrations, strain..., both feed the models and validate them. Several sensors are needed to make sure that the model's predictions do in fact correspond to reality. Without feedback from measurements, the generator model can only make general assumption such as using uniform air flow rate in every vent duct of the stator core, which is usually not true. This hypothesis may have minimal impact or greatly affect the calculation of the hot spot temperature, justifying performing air flow rate measurements to improve the model's predictions.

In addition to the measurement data used as input in models, it must be recognized that the models by themselves introduce uncertainty because calculations can depend on parametric settings. For instance, in Computational Fluid Dynamics (CFD), numerical settings can have a significant impact on the calculation of the windage losses and ventilation flow rate. Toussaint et al [2] have reported that with a steady state multiple frames of reference (MFR) solution, results were highly sensitive to the type of model (frozen rotor vs. mixing plane) and in settings such as the location in the air gap of the rotor-stator interface, which is an artificial boundary between the fix and the moving domain. They report that windage losses and global ventilation flow rate could vary by 10 - 20% only because of numerical settings, which clearly shows the need to calibrated models.

The main limits of a generator are thermal or mechanical and studying the actual performance of the generator model close to them provides a better understanding of interaction between physical phenomena. This paper will mainly focus on the thermal limitations of the generator, by presenting the strategic location where most of the sensors are installed and example of some results. Other related activities are air gap and magnetic flux measurements that will be used in the electromagnetic model to determine the magnetic and stray loss distributions more precisely. These losses are used with joule losses and in conjunction with the CFD calculating the machine's cooling and convection coefficients in order to evaluate the hot spot temperature and location in the thermal model. Analysis of mechanical limitation is also covered by the project but exceed the scope of the current paper.

## 2 INSTRUMENTATION OF A GENERATOR

### 2.1 Stator sensors

Temperature measurement over the entire stator is not possible, but the number of sensors should be sufficient and spread over strategic locations so that thermal models can be validated. Several sensors and types have been used. One of them was the Distributed Temperature Sensors (DTS) consisting in a single fiber measuring temperature all along its length using Raman backscattering. On the generator tested here, the fiber was installed in the vent ducts of four stator bars to measure the axial temperature profile of the cooling air in every duct along the length of the bars. The number of bars instrumented varies from one installation to the next, here four bar instrumented are shown in Fig. 1, either from the air gap or the core's back side.

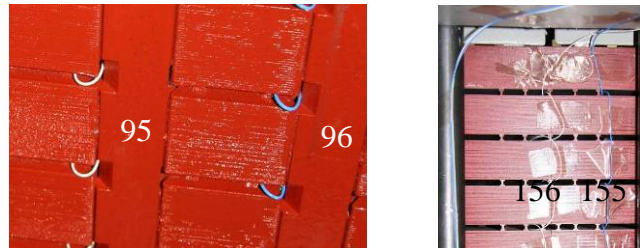


Fig. 1 Single DTS fiber loop from the gap side (left) and at the back of the core (right)

In addition, thermocouples were installed behind one slot at the back of the core, on the pressure fingers and on the frame as illustrated in Fig. 2 (left hand side). Additional tip sensing optic fibers were installed on the surface of energized bars and end caps (see Op-1 to Op-4 in Fig. 2). The air temperatures in specific location were also measured during the entire test period. These locations are shown in Fig. 2 (right hand side). Since the cooling system of the generator operates in closed circuit with heat exchangers, it is mandatory to monitor the air and water temperature at the input and output of the exchangers to determine total losses based on heat extraction. Four thermocouples were used to measure the warm air temperature and three were used for the cold air as illustrated in Fig. 2.

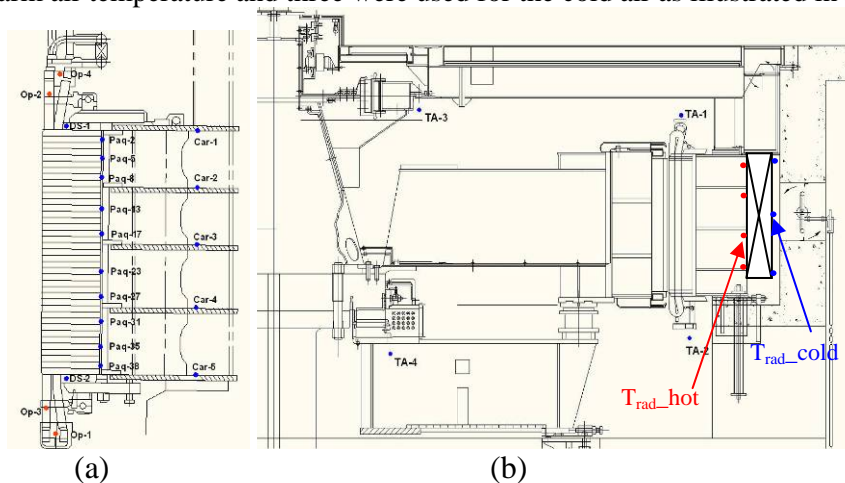
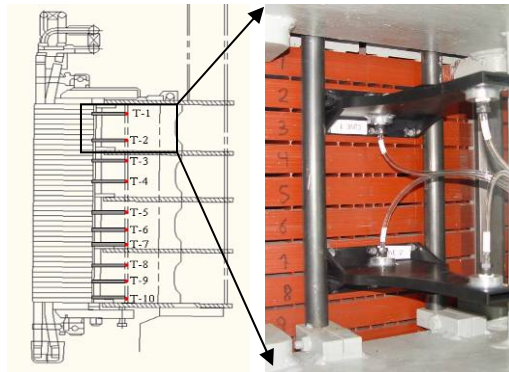


Fig. 2 Temperature sensors from (a) Thermocouples at the back of the stator core and on the frame and tip sensing fiber location and (b) thermocouples in the air in the cooling circuit.

Additional thermocouples were installed at the back of the core, at the output of converging conduits used for air pressure measurements at the exit of ten vent ducts. Each conduit has two pressure tap, as seen in Fig. 3, from which it is possible to calculate, with proper calibration, the air flow speed coming out of the stator. The axial profile of the air at the output of the stator is used as input to the thermal models to correct for any non-uniformity present.



**Fig. 3 Air temperature measurements at the output of convergent conduit (left) and two of conduits (right)**

Another critical input to the models is the air gap size. The design air gap under cold condition is usually easy to get, but as gap will change with the magnetic pull, the rotation and thermal expansion (rotor vs stator), true air gap must be measured in every condition in order to feed the different models. It will have an impact on the calculation of the excitation current and magnetic losses in the electromagnetic model, and on the estimated windage losses in the CFD model. The windage losses are expected to increase as the air gap dimension decreases because of the change in the air velocity gradients in the gap.

## 2.2 Rotor sensors

Detailed temperature measurements are required from pole faces, damper bars and field coil. Even if in some cases temperature could vary from one pole to the next, on the generator tested here only one pole was instrumented with several thermistors as illustrated in Fig. 4. As can be seen in the left hand side of this figure, rim and spider arm were also measured. Air temperatures at the entrance and the output of the rim ducts were recorded.

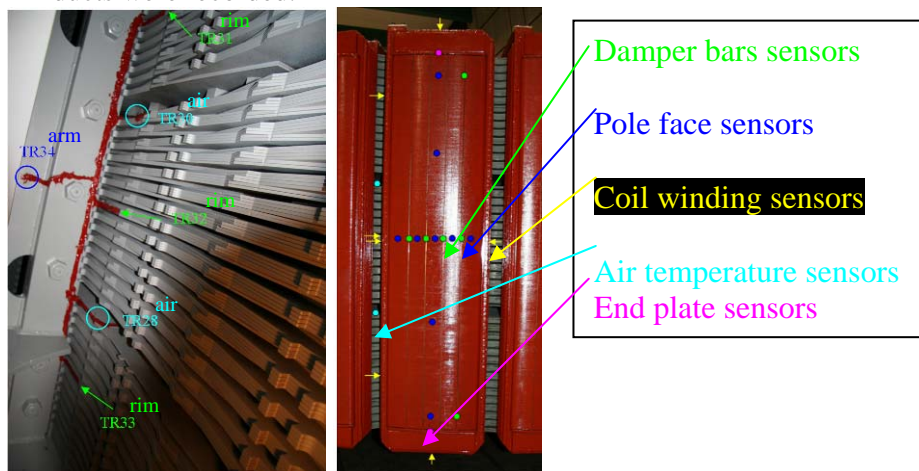


**Fig. 4 Thermistors installed on the rim and spider arm (left) and pole face, damper bar and field coil (right).**

## 3 RESULTS

Magnetic, stray losses and losses in the damper bars are obtained from the electromagnetic model in each test condition with the proper gap size. Once the results have been validated by the measured excitation current and magnetic flux, the calculated losses were transferred to the thermal model in accordance with the procedure reported in [3]. Examples of the ensuing thermal maps for a 2D slice of one pole when the test generator was running at 146.6 MVA and two slots with the stator bars and core are shown in Fig. 5. For thermal simulation to give the uneven axial temperature distribution in the right hand side in Fig. 5 (warmer temperature toward the bottom of the bars) the actual non uniform ventilation profile measured and illustrated in Fig. 6 had to be used in conjunction with the actual air temperature profile in Fig. 7.

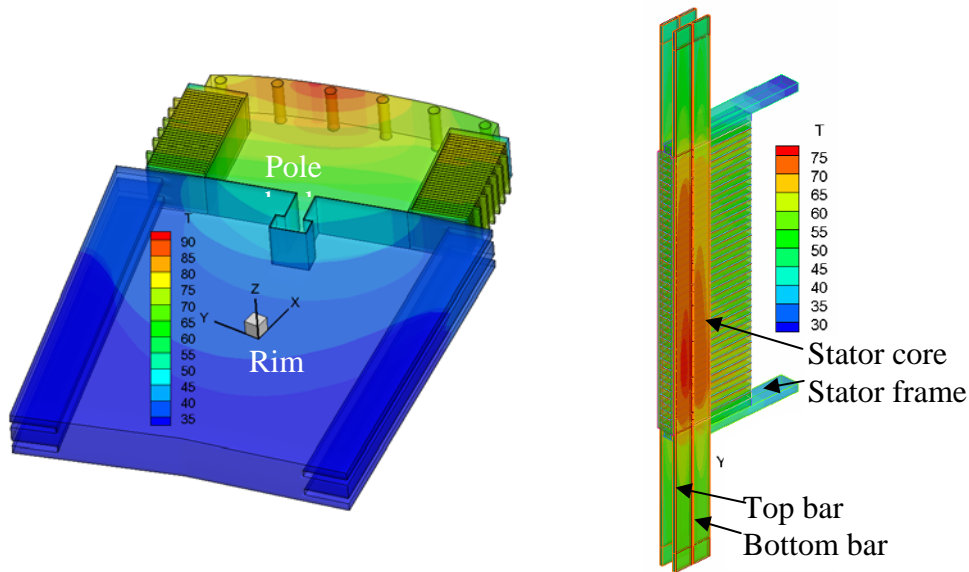


**Fig. 5 Simulation of temperature distribution in the rotor (left) and stator (right) at 146.6 MVA**

It was observed during test that the axial ventilation profile through the core stays almost constant being mainly affected by the speed of rotation and the structure of the machine, but also to a lesser extent by the air temperature. Under magnetization (at 13.8 kV) the average mass flow rate through the core was smaller but as soon as magnetic, joule and stray losses were introduced, the mass flow rate went up to about 56 kg/s and remained fairly constant for the three load conditions. The air speed at the exit of the ten ducts monitored (duct number one being on the connection end of the stator) is slower toward the end of the core and reaches a peak around duct number 23. This faster air speed does not translate to cooler temperature at this location in the model because air temperature must also be considered.

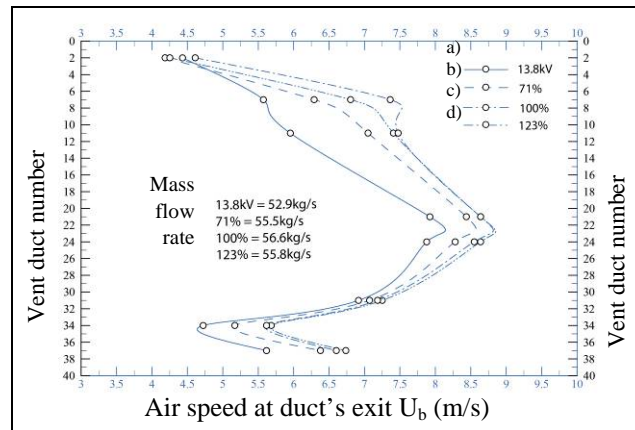


**Fig. 6 Axial ventilation profile measured at the exit of the convergent conduits at the back of the stator core for a) open circuit, b) 71% of nominal load, c) 100% and d) 123%.**

The temperatures measured at the output of the ten converging conduits are shown in the graph in the left hand side in Fig. 7 for the four test conditions. At 123% of the nominal load, there is 8°C of difference between the air coming out of duct number 7 vs. duct number 34. In addition to the air temperature at the duct's exit, lamination temperature at the back of the core, DTS fibers in the vent ducts and RTD all show a similar axial profile as depicted in the right hand side in Fig. 7, for the test done at 123% of the nominal summer load. It should be pointed out that the maximum load is dependent on the cooling water temperature and since the heat run test was carried out in November with water temperature of 6.2°C, the generator could be tested above nominal summer load. One special feature of this generator is that not all RTD were installed at mid length in the slot, as usually the case. Here, on third of the 12 RTD was centered around vent duct number 9, the second group of four were installed at mid-length in the slot and finally the last group was centered around vent duct

number 26. This arrangement made it possible to confirm that the axial temperature gradient from one end of the core to the other, with the bottom being warmer was also apparent in the RTD readings.

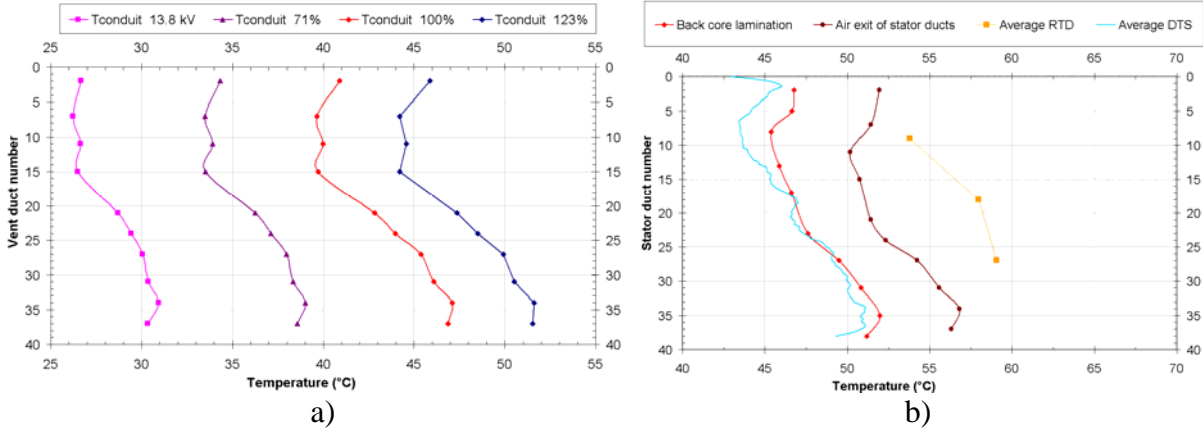


**Fig. 7 a) Air temperature at the exit of the stator vent ducts for the four test conditions  
b) Temperature of cooling air, DTS fiber, lamination at the back of the core and mean RTD at 123% of nominal load.**

Temperatures measured on the instrumented pole are used to validate the thermal model of the rotor and make sure that the total distribution of losses between the rotor and stator respects the overall energy balance as reported elsewhere [3]. During the heat run test, the average copper temperature calculated based on the current and average resistance of the field winding is used to determine the temperature rise, but this average value is not sufficient to validate spatial temperature distribution of our models. As can be seen in Fig. 8, for the temperature distribution at the back of the rim (right hand side), on the field winding, damper bars and on the pole face (left hand side), much more details are necessary for model validation. It can be seen in this figure that there is a temperature gradient of 15°C over the pole face from the leading to the trailing edge of the pole and of 13°C between the damper bars. The third turn (from the air gap) of the field winding at mid-height of the pole was at 77.5°C on the leading edge, whereas the same turn on the trailing edge was at 85.9°C. Because both ends of the pole are better cooled, the third turn of the coil at the top end and bottom end were 27 and 21 °C cooler, respectively. The 15<sup>th</sup> turn of the coil’s leading edge was also monitored and gave a radial temperature gradient of 2°C between those two points for the 123% condition. In comparison, the mean temperature of field coil conventionally calculated with the rotor current gave a value of 72°C, which is coherent with the measured values, but clearly underestimate the hot spot temperature.

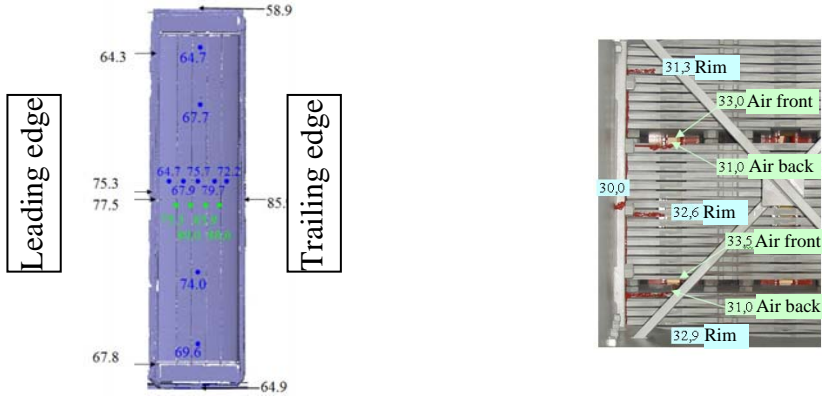


**Fig. 8 Temperatures (°C) of the pole face, damper bars, end plates and field windings (left) and at the back of the rim in blue (right) and of the air entering and exiting the 2 central vent duct (in green).**

The axial gradient on the pole face, the damper bar and the field coil all show that the pole temperature is higher in the middle and lower toward the end, with the top being cooler than the bottom. This temperature profile builds up through the poles because the temperature is fairly uniform axially ( $T = 1.6^\circ\text{C}$ ) at the back of the rim but somewhat warmer towards the bottom. The air at the entrance of each center ducts was equal and the rim’s output, the air temperature showed less than one degree of difference from one large duct to the other.

## 4 DISCUSSION

Numerical simulation offer exceptional generic insight about the physic active in generators, however as long a true multi-physics model are not available, validation by measurement data is mandatory to represent any specific machine. Simplifications in models and numerical choices in settings have to be compensated by some calibration based on field data. If the goal is to truly represent the behavior of a specific machine, each simulation results must be calibrated by measurement in different test conditions. The following discussion will only tackle some of these issues by presenting examples of a few step of the process used to validate specific aspect of the model.

The current thermal model is a two stages process coupling the stator and the rotor only through heat transfer in the air gap. The 2D model used in the rotor can be extruded as pseudo 3D, but does not yet includes the end cooling effects of the poles. The stator is a 3D model of the full axial length including winding, core and end arms. In this case, 3D effects such as higher losses from leakage flux or stray losses from circulating current will only be available in the next version of electromagnetic simulation. At present they are estimated from analytical calculation and experience. Once all rotor losses are transferred from the electromagnetic to the thermal model [3], an average air temperature at the air gap is calculated and this uniform value (41°C) can be imposed in the thermal model to calculate the air temperature at the stator output as depicted in left hand side in Fig. 9. As can be seen, this does not predict correctly the measured air temperature leaving the stator core. To circumvent this problem, the temperature profile in the air gap was adjusted to have the shape as the one measured at the stator's output, while respecting the air gap calculated average. The simulated curve in the right hand side in Fig.9 gives temperatures closer to the measured ones. The main difference is attributed to the fact that thermal stabilization was not reach during the test at 123%, whereas simulation are done in thermal equilibrium. It was estimated that 2°C should be added to the heat run test data at 123°C to represent equilibrium condition, which would give a good fit between measured and simulated values.

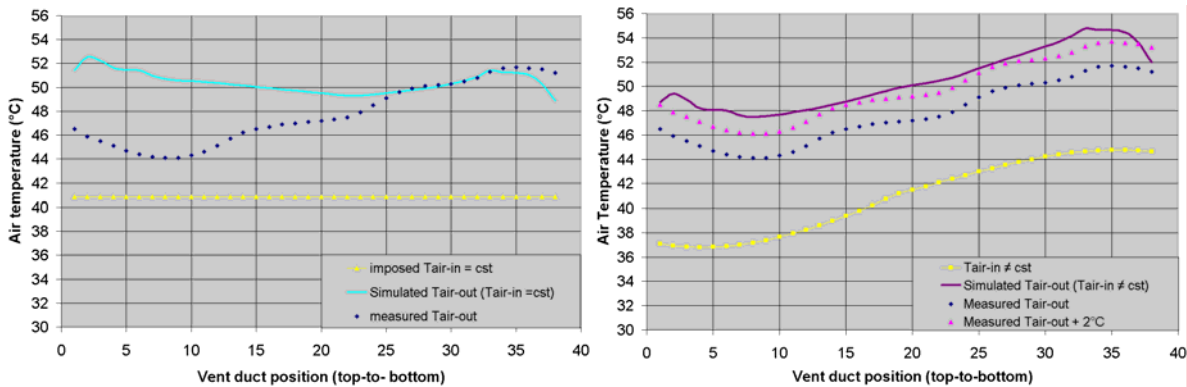


**Fig. 9 Stator output air temperature compared with measured values with constant air profile in the air gap (left) and with air gap temperature profile adjusted to the shape of the core exit temperatures at 123% of nominal load**

Once all the electromagnetic and joule losses are integrated in the thermal model, the ventilation losses and the convection coefficient must be distributed in both the rotor and stator to get a balanced model. As long as a full 3D CFD model is not functional, some details of the cooling are unavailable. In the stator, the convection coefficient in the vent ducts can be calculated analytically. However, this is not the case for the rotor where the problem is more complex because of the intricate interaction of the inter-pole and fan area and of the high tangential air speed at the air gap. Thus, results from CFD are needed to feed convection coefficients to the thermal model. Unfortunately, these coefficients cannot be measured in the machine and validation is only possible indirectly through temperature measurements on the pole face and field coil.

Our first approximation was to use uniform convection coefficients around the poles to estimate the temperature at the different pole sensor locations. The air temperature measured at exit of the rotor's rim (33.3°C in Fig. 8) was imposed as boundary condition in the model while temperature determined from the curve in Fig. 9 was imposed at the air gap. According to this curve, each 2D slice of the rotor model has its own air gap temperature but the same temperature on the rim side. By using these assumptions in the model could explain the radial temperature gradient from the back to the front of

the field coils (see Fig. 5), but not the asymmetry between the leading and trailing edge of the poles. To improve the model, convection coefficients had to be obtained by CFD modeling and used in the thermal model. The convection coefficients calculated with a transient CFD model of a 2D slice at mid-height of the pole and illustrated in Fig. 10, clearly show that they are far from being uniform.

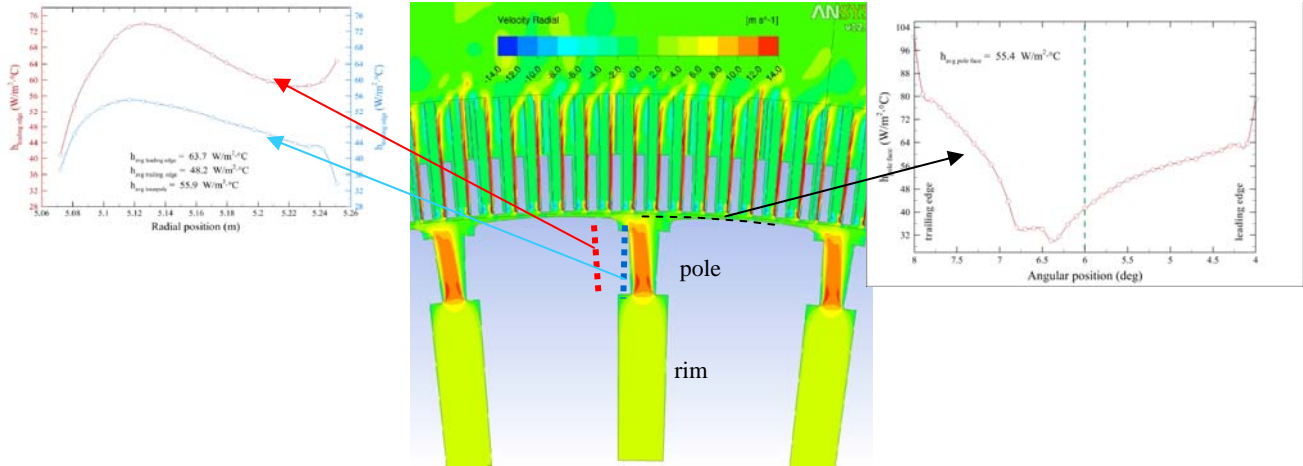


**Fig. 10** 2D air velocity around the poles of one time step (center), convection coefficient profile on the leading edge and trailing edge of the pole (left hand side) and on the pole face (right hand side).

The curves of the radial convection coefficient distribution can be transferred to the thermal model to introduce asymmetry effect between leading and trailing edges and explain the temperatures measured on the field coil (cf. Fig. 8). The temperature asymmetry on the pole face and damper bars is in part due to an uneven distribution of losses but also to the convection coefficient profile on the pole face (cf. right hand side curve in Fig. 10). The global thermal model must include all these inputs to adequately represent the actual response of a generator. In the future, data exchanges between electromagnetic simulation, CFD and thermal model will be automated, but in the meantime each step of the process will continue to be validated through measurements to lead to the best choices in building a global model.

**5 CONCLUSIONS**

Some examples were presented to show how detailed temperature measurements can be used both as inputs to numerical models and to validate them. These measurements will reveal any irregularity characteristic to a specific generator’s design, but most of the time cannot be used to predict the machine’s behavior beyond the range of test conditions. Simulation will provide this information, but to do it accurately it was shown that these models absolutely have to be coupled with measurements to avoid any misleading predictions.

**BIBLIOGRAPHY**

- [1] Hudon C, Merkhof A, Chaaban M, et al. Hydro-Generator Multi-Physic Modeling. European Journal of Electrical Engineering, 2010,13(5/6)
- [2] Toussaint K, Torriano F, Morrissette J F, et al. CFD Analysis of Ventilation Flow for a Scale Model Hydro-Generator[C]//Proceedings of the ASME 2011 Power Conference POWER. Denver, Colorado, USA, July 2011,12-14
- [3] Chaaban M, Leduc J, Hudon C. Thermal analysis of Large Hydro-Generator based on a multi-physic approach[C]// CIGRE Colloquium on Rotating Machine. Beijing, China, Sept. 11~13th, 2011

**Study of Quasi-synchronization Grid Connected  
1000MW Hydro-generator**

**Yang Mo**  
**Harbin University of Science  
and Technology**  
**Harbin, China**

**Ge Baojun**  
**Harbin University of Science  
and Technology**  
**Harbin, China**

**SUMMARY**

The study of giant hydro-generator unit and the grid connection of the system could provides a theoretical reference for the operation of 1000MW hydro-generator ,the choices of the other motors and electrical protection equipments which connected to it. In this paper, the quasi-synchronization grid connected of a 1000MW hydro-generator is studied. At the beginning, the mathematical models of 1000MW hydro-generator which is connected to the power system are established, the impact of voltage difference、 frequency difference and phase angle difference on the performance of 1000MW generator by quasi-synchronization grid connected is analyzed. Finally, the impulse current and torque are produced by phase angle difference are calculated for some special cases. The results show that the quasi-synchronization grid connected of 1000MW hydro-generator could excuted safely when voltage difference and frequency difference exist in a certain range.

**KEYWORDS**

1000MW hydro-generator ,Quasi-synchronization parallel in , Impulse current ,Impulse torque

# 1 INTRODUCTION

At present, power system in China has got access to a stage of being with extra-high voltage, large power and large units. Nowadays, there are nearly a hundred hydropower, firepower, nuclear power stations with a total installed capacity of more than one million kilowatts in China. They have formed an production system with efficient, high-capacity power generating units as the backbone.

Hydropower station usually located in the mountain gorge, the volume of hydro-generating unit is not increasing with the capacity increasing, operational efficiency and speed of construction is improved, unit cost and generation cost are retrenchment. Thereby the economic performance of projects are improved<sup>[1-3]</sup>. 1000MW hydro-generator is currently under development, there is no precedent in the world. The calculation of impulse current and electromagnetic torque of 1000MW hydro-generator when grid connect by quasi-synchronization can not only provide a reference design, but also provide a theory basis for the torsional vibration of generator<sup>[4]</sup>. In this paper, on the basis of conventional grid connect theory, the own characteristics of 1000MW hydro-generator is analyzed to provides a theoretical reference for assessing and establishing a design of the synchronization system of 1000MW hydro-generator.

# 2 THE MATHEMATICAL MODEL OF GRID CONNECTED OF 1000MW HYDRO-GENERATOR

During the operation of quasi-synchronization grid connected, the generator rotational speed should be adjusted to close to the synchronous speed. Due to the generator's model is linear, many transient processes, such as generator terminal short circuit, fault-synchronizing, the moment of grid connected could be analyzed by the principle of superposition.

The instantaneous electric motive force (EMF) of three phase generator and voltage of corresponding system bus are following<sup>[5]</sup>:

$$\begin{cases} e_A = -E \sin \gamma \\ e_B = -E \sin(\gamma - 120^\circ) \\ e_C = -E \sin(\gamma + 120^\circ) \end{cases} \quad (1)$$

$$\begin{cases} u_A = -U \sin(\gamma - \delta) \\ u_B = -U \sin(\gamma - \delta - 120^\circ) \\ u_C = -U \sin(\gamma - \delta + 120^\circ) \end{cases} \quad (2)$$

Where,  $E$  is generator EMF,  $U$  is bus voltage.  $\gamma$  is the angle between d-axis and A-axis,  $\theta = 90^\circ - \delta + \gamma$ ,  $\delta$  is the leading angle between generator EMF and bus voltage. Fig.1 is the vector graphics of generator EMF and bus voltage.

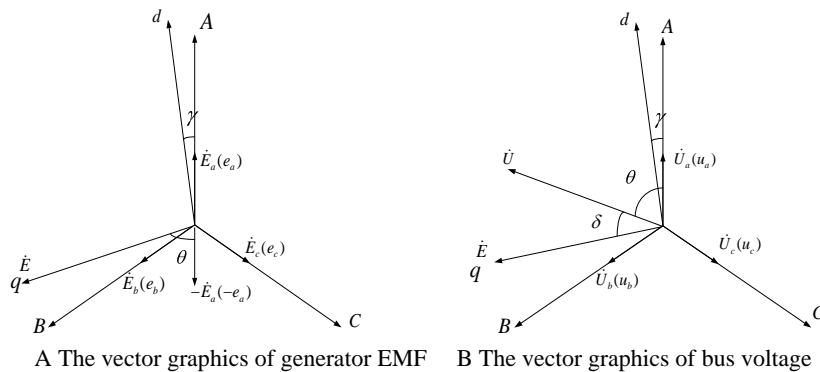


**Fig.1 The vector graphics of generator EMF and bus voltage**

Assume that the generator is no-load stably operating before grid connected, the progress of grid connected is non-ideal. And, the circuit breakers is attached considered by a sudden pulsant voltage with the following:

$$\begin{cases} u_{A0} = e_A - u_A = U \sin(\gamma - \delta) - E \sin \gamma \\ u_{B0} = e_B - u_B = U \sin(\gamma - \delta - 120^\circ) - E \sin(\gamma - 120^\circ) \\ u_{C0} = e_C - u_C = U \sin(\gamma - \delta + 120^\circ) - E \sin(\gamma + 120^\circ) \end{cases} \quad (3)$$

Where,  $u_{A0}$ ,  $u_{B0}$ ,  $u_{C0}$  is A,B,C phase of pulsant voltage.

### 3 THE ANALYSIS OF THE GRID CONNECTED CONDITIONS IMPACT ON HYDRO UNIT

With the ideal condition of grid connected, it is requested that voltage, frequency be equal to hydro-generator and power system, the phase angle different be zero<sup>[6]</sup>. In the circuit breaker closing moment, the stator current and the electromagnetic torque should be zero, so that there are no effect on the generator and power system<sup>[7]</sup>. But in the engineering practice, it is difficultly to achieve those conditions. When the rotor is rotating as invariable speed, the phase different is less than the allowed maximum of quasi-synchronization, the voltage of generator is approximate that of power system, the generator could be combined with the power system<sup>[8]</sup>. Table I is the parameters of 1000MW hydro-generator.

**Table I Parameters of 1000MW hydro-generator**

Parameter Name	P.U.	Parameter Name	P.U.
Armature reactance $r$	0.00155	System reactance $X_x$	0.25
Transient reactance d-axis non-saturated $x_d'$	0.317	Field winding reactance $r_f$	0.608
Synchronous reactance d-axis non-saturated $x_d$	1.118	Subtransient reactance d-axis non-saturated $x_d''$	0.22
Synchronous reactance q-axis non-saturated $x_q$	0.792	Subtransient reactance q-axis non-saturated $x_q''$	0.236

#### 3.1 The impact on the hydro-generator unit of the voltage amplitude difference

If the frequency and phase of generator and power system were same, but only both of the voltage amplitude was not equal in value, the instant impulse current could be brought about during the generator putting into operation. Due to the inductive impedance, the periodic component of impulse current at that moment is reactive current, which does not exist on the impact of active power.

$\dot{U}_x$  is the voltage of power system.  $\dot{U}_G$  is the voltage of generator.  $\Delta\dot{U}_s$  is the pulse voltage between generator and power system during the grid connected.  $\dot{I}_m$  is the impulse current occurred during the grid connection.

When  $\dot{U}_G < \dot{U}_x$ ,  $\dot{I}_m$  is lagging  $\Delta\dot{U}_s$   $90^\circ$ . For the grid connected generator,  $\dot{I}_m$  is to present capacitive current, with increasing magnetic capacity; For the operating generator,  $\dot{I}_m$  is showing capacitive character, with a demagnetization capability. When  $\dot{U}_G > \dot{U}_x$ ,  $\dot{I}_m$  is leading  $\Delta\dot{U}_s$   $90^\circ$ .  $\dot{I}_m$  is the magnetic effect on the generator, so that to make the voltage of generator drop to the voltage of power system, and then immediately send reactive power after grid connected<sup>[9]</sup>.

Here is  $\dot{I}_m$  reactive current, thus  $\dot{I}_m$  will not cause electromagnetic torque. From this point to consider that there is no risk at generator caused by  $\dot{I}_m$ . However,  $\dot{I}_m$  is too large to cause the generator stator windings heated, resulting in winding end damage. To avoid the damage occurred, the general provision of conventional generators is the maximum voltage amplitude different should not exceed 10 ~ 20% rated. It is better to control the range from 5 ~ 10% rated.

Fig.2, Fig.3 are separately shown the simulation results of  $\Delta\dot{U}_s$  and  $\dot{i}_m$  when the voltage amplitude difference of  $5\% U_N$ ,  $10\% U_N$  is existed of the grid connected of 1000MW hyndo-generator.  $t_N$  is the rated value of time.  $t_N = 2\pi f_N = 100\pi$ .

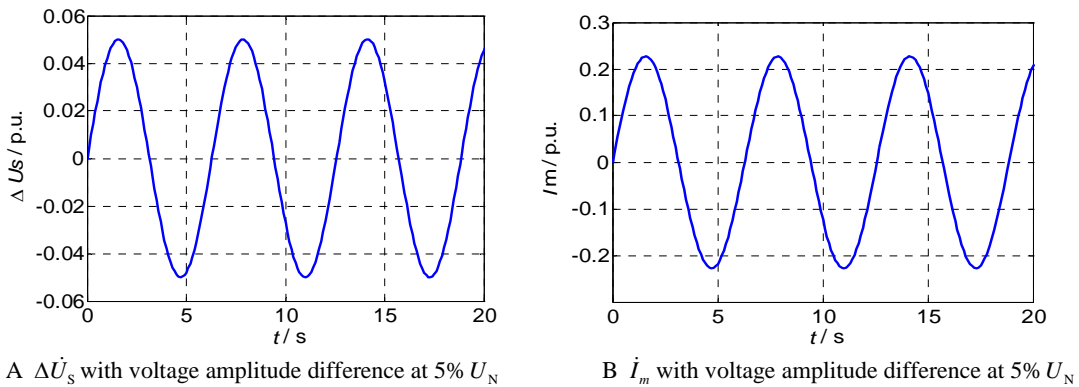


**Fig.2 The curve of  $\Delta\dot{U}_s$  and  $\dot{i}_m$  voltage amplitude difference at  $5\% U_N$**

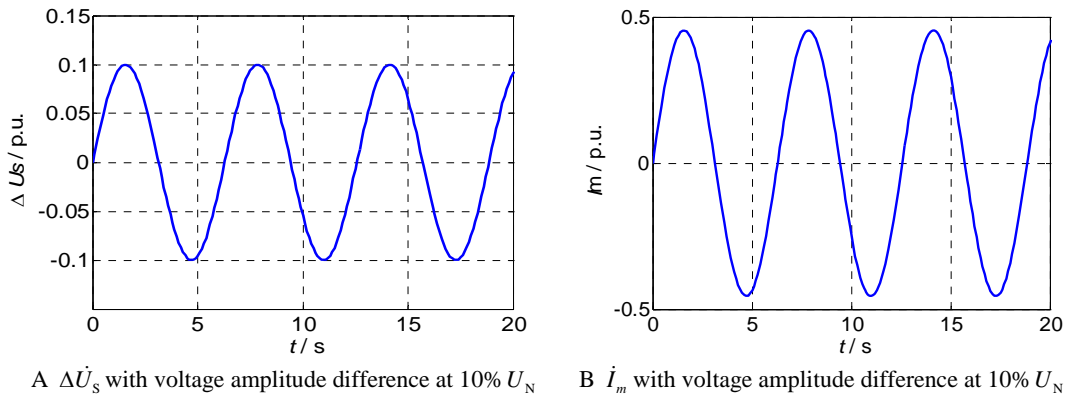


**Fig.3 The curve of  $\Delta\dot{U}_s$  and  $\dot{i}_m$  voltage amplitude difference at  $10\% U_N$**

The simulation results can be shown that: the curve of  $\Delta\dot{U}_s$  is changing as the sine curve. By the increasing of voltage amplitude difference, the magnitude of  $\Delta\dot{U}_s$  trends in direct proportion increasing. The cycle of  $\Delta\dot{U}_s$  does not vary with the changing of voltage amplitude difference. With the gradual increase of  $\Delta\dot{U}_s$ , the magnitude of  $\dot{i}_m$  also increases. It is shown that the unit could be put into the normal power system operation, when the voltage amplitude difference is no more than  $10\% U_N$ .

### 3.2 The impact on the hydro-generator unit of frequency difference

When frequency difference exists between the voltage power system and generator, it could cause the relative motion between the vectors. If  $\dot{U}_G$  is stationary,  $\dot{U}_X$  could be considered that it is separated with  $\dot{U}_G$  sometimes and sometimes as concurrent. So that  $\Delta\dot{U}_s$  becomes the varying pulsant voltage, the resulting is the pulsant current<sup>[10]</sup>. At that moment, the pulsant current might cause the generator which just puts into the power system is taken more positive or negative active power component, so that it will cause that the rotor axis vibrating. It is possible that the generator will be loss of synchronization for violently vibrating. Therefore, it is necessary to check of frequency difference. Make sure the frequency difference is nearly to 0 before grid connection.

The allowable frequency difference of conventional generators in the quasi-synchronization grid connected is  $0.1 \sim 0.5\% f_N$ , that  $f_N = 50\text{Hz}$ , the allowable frequency difference is range from 0.05Hz to 0.25Hz.

The simulation about the impacts of the frequency difference is separate  $0.1\% f_N$  and  $0.2\% f_N$  on  $\Delta \dot{U}_s$  in the quasi-synchronization grid connected of 1000MW hydro-generator is shown as Fig.4. The variation of  $\Delta \dot{U}_s$  is changing as the sine curve. The variation cycle of  $\Delta \dot{U}_s$  is gradually increasing as well as frequency difference decreasing. Meanwhile, the number of zero-crossing times is reduced. So that the frequency of the rotor axis vibration is reduced.

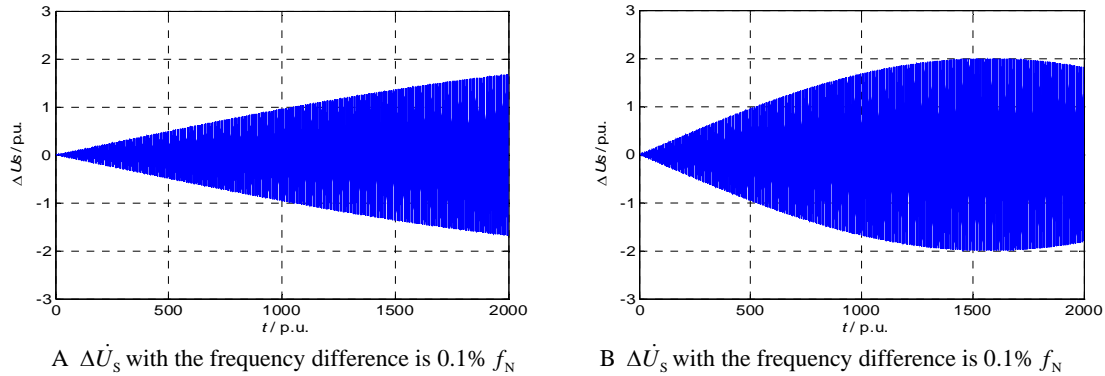


Fig.4 The curve of  $\Delta \dot{U}_s$  when the frequency difference is  $0.1\% f_N$  and  $0.2\% f_N$

### 3.3 The impact on the hydro-generator unit of phase angle difference

If voltage and frequency of the generator are the same as power system, meanwhile, phase angle difference between  $\dot{U}_G$  and  $\dot{U}_X$  is not 0 at the closing moment, it will cause the active of impulse current.  $\dot{I}_{mr}$  is the active component of  $\dot{I}_m$ . When  $\dot{U}_G$  is leading  $\dot{U}_X$ , the direction of  $\dot{I}_{mr}$  is the same as  $\dot{U}_G$ 's, the generator will output active power. When  $\dot{U}_G$  is lagging  $\dot{U}_X$ , the direction of  $\dot{I}_{mr}$  is opposite to  $\dot{U}_G$ 's, the generator will absorbed active power.

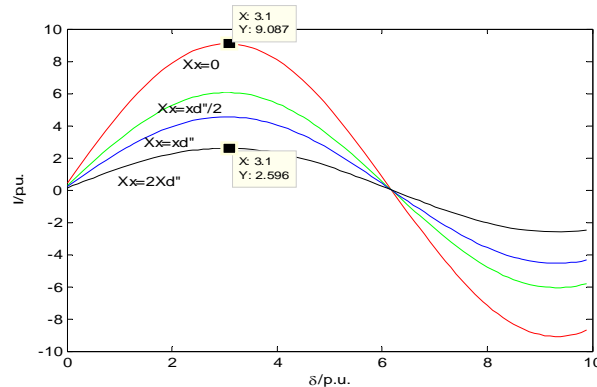


Fig.5 The curves of the impulse current variation with  $\delta$  and the sum of  $X_d''$  and  $X_x$

The curves of the impulse current variation with  $\delta$  and the sum of  $X_d''$  and  $X_x$  is shown as Fig.5. When the sum of  $X_d''$  and  $X_x$  is constant, the curve of impulse current is changing as the sine curve,  $2\pi$  for a cycle; When phase angle different is constant, with the increase of the sum of  $X_d''$  and  $X_x$ , the maximum amplitude of impulse current will be decreased at the same time. The amplitude of impulse current will be 9.087 times of rated, if the power system reactance is 0. The amplitude of impulse current will be 2.596 times of rated, if the power system reactance is two times of  $X_d''$ . Therefore, the impulse current and the impact of generator and power system will decrease a lot, if the reactances of transformer and transmission line were equal to or larger than  $X_d''$ .

The impact of phase angle difference on the current and its active component is shown as Fig.6. The impulse current is increasing phase angle difference, when the sub transient reactances of the d-axis and q-axis are approximate equal to each other, phase angle difference is changing from 0 to  $2\pi$ . If

$\delta = \pi/2$ , the amplitude of  $I_{mr}$  will achieve the maximum. When  $\delta = \pi$ , the amplitude of  $I_m$  will get the maximum, and this is the most serious impact on the generator. Therefore, it must be avoided to happen in practical operation.

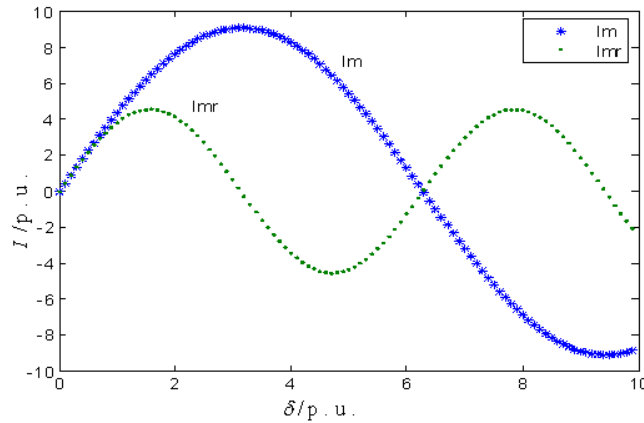


Fig.6 The impact of phase angle difference on the current and its active component

### 3.4 The impulse torque caused by grid connected

Above the comprehensive analysis, combined with the prototype parameters, the variation of the impulse torque of quasi-synchronization grid connected 1000MW hydro-generator is shown as Fig.7.

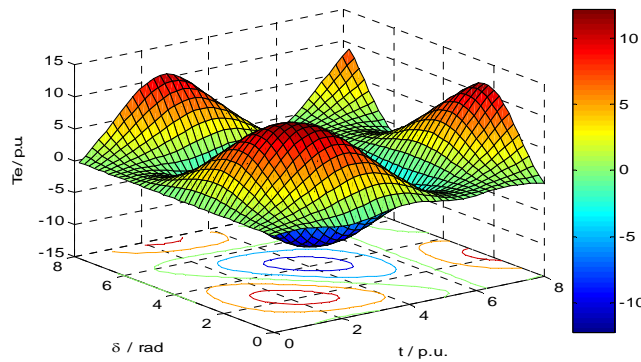


Fig.7 The curve of  $T_c$  variation with  $\delta$

In Fig.7, the peaks and troughs correspond to the maximum and minimum torque, the bottom contour lines correspond to the variation range of phase angle difference. It is shown that : the maximum value which is nearly 10 times of the rated value appears between  $\pi/2$  to  $\pi$  in the first cycle of phase angle difference. If the huge hydro-generator could bear this impulse, it will be operated safely.

## 4 CONCLUSION

Based on the analysis of the impulse current and torque of 1000MW hydro-generator when grid connect by quasi-synchronization, The conclusions are as followed: If the amplitude of the voltage difference was less than 10% of rated voltage and frequency difference was controlled in 0.1% to 0.5% (that 0.05Hz ~ 0.25Hz) of 1000MW hydro-generator , quasi-synchronization grid connected 1000MW hydro-generator by could be safe and reliable grid. When the sum of generator sub-transient reactance and the reactance of the system is constant, the impulse current will be max if the phase angle difference is  $\pi$ . When phase difference is constant, the impulse current will decrease with the sum of generator sub-transient reactance and the reactance of the system increasing. When phase angle difference is  $\pi$  as well as the reactance of the system is 0, the fundamental frequency alternating component of stator will be the maximum. When the phase difference is  $2\pi/3$ , the impulse torque which is nearly about 10 times of the rated will be the maximum. Therefore, it is better to avoid this situation occurred during practical operation.

## BIBLIOGRAPHY

- [1] Li S. Overview of China's hydropower development[J]. Station Electrical Technology, 2009, 32(3):105-107
- [2] Cheng Y. Rolling on the River Hydropower Development and the Launch of Million-Kilowatt Hydroelectric Generating Thinking[C]/Li J. Technical Proceedings Large Hydroelectric:China Society for Hydropower Engineering, 2008:3-7
- [3] Li X. Study on Setting of Protection for Huge Hydro-generator and Transformer Group[D]. Wuhan: Huazhong University of Science and Technology, 2008:1-22
- [4] Zhang Y, Huang J. Fault-synchronizing Electromagnetic Torque Analysis of synchronous Generator[J].Large Electric Machine and Hydraulic Turbine, 1998, (3):31-38
- [5] Chen H. The Basis Theory and Computer Algorithm of Synchronous Machine[M]. Beijing: China Water Power Press, 1992: 115-116
- [6] Gao Z. On-site Test and Research into the Application of Digital Auto Synchronization System[D]. Beijing: North China Electric Power University, 2006: 3-15
- [7] Zhang Z. The Influence of Parallel Operation on Torsional Osillation of Large Steam Generator Sets [J].Central China Electric Power, 2004, 17(1):15-17
- [8] Liu X, Tian J. Power System Analysis and Simulation with Matlab[J].Electric Power Automation Equipment, 2004, 24(3):43-46
- [9] SHIMA K, IDE K, TAKAHASHI M. Analysis of Leakage Flux Distributions in a Salient-pole Synchronous Machine Using Finite Elements[J]. IEEE TRANSACTIONS ON ENERGY CONVERSION,2003,18(1): 63~70
- [10] TAMKS,KUMARP. Application of Superconductive Magnetic Energy Storage in an Asynchronous Link between Power Systems[J].IEEE TRANSACTIONS ON ENERGY CONVERSION,1990,5(3):436-444



Yang Mo (1985-), Female. She is currently doing a master of power system and its automation. She mainly studies on the grid-connection operation analysis of large-capacity generator



Ge Bao-jun (1960-), Male. He received PH.D from Harbin Institute of Technology, Heilongjiang Province, China. Dr.Ge is now a professor of Harbin University of Science and Technology. He mainly studies on basis theory and application technology of large electromechanical energy conversion device.

**Experience with Acoustic Emission Monitoring of Stator Winding  
Delaminations During Thermal Cycling Testing**

**H. Zhu, D. Kung, M. Colwell**  
Powertech Labs  
Canada

**S. Cherukupalli**  
BC Hydro  
Canada

**SUMMARY**

This paper describes a novel technique for acoustic emission monitoring of insulation delaminations during thermal cycling (TC) testing on a stator bar. Acoustic signals emitted from insulation delaminations within the stator bar were continuously recorded during TC testing. An increase in measured acoustic signals indicates insulation delaminations within the stator bar under testing. To complement the acoustic detection method, several diagnostic tests, such as dissipation factor tests, partial discharge tests, tap tests and dissections, were performed. These diagnostic test results were compared with the acoustic test results to verify the insulation delamination process at various stages. It is concluded that acoustic monitoring is a useful tool to help establish the extent of insulation delamination during thermal cycling testing, the cycle in which delamination was most pronounced, and when delaminations occurred during the cooling or heating cycle. This technique could help refine the thermal cycling test program by optimising the number of test cycles required and achieving potential cost savings, and avoiding the need to disassemble and reassemble the test setup for the diagnostic tests currently used.

**KEYWORDS**

Stator winding, Thermal cycling testing, Insulation delamination, Menerator insulation, Acoustic monitoring of insulation defects.

## 1 INTRODUCTION

Frequent load changes and starts/stops in generator/motor operation result in rapid temperature changes which produce thermal cycling stress in the stator winding insulation. The thermal cycling stress can generate shear stress between the copper strands and the groundwall insulation as well as between the groundwall insulation layers. As a result, the thermal cycling stress with expansion and contraction cycles can cause de-bonding and delamination of the stator insulation system [1] [3] [4] [5] [6]. During the delamination process, delaminations emit acoustic signals which can be used to monitor the delamination process.

To evaluate the quality and performance of the new stator windings subjected to the thermally cycling stress during service, thermal cycling (TC) testing on stator bars and coils is performed according to IEEE 1310 [2]. The insulation system is tested under thermal cycling stress at a prescribed temperature range for 500 cycles. To monitor the progress of insulation delamination during the 500-cycle test, IEEE 1310 requires that diagnostic tests are carried out at periodic cycle intervals (e.g. at 50, 100, 250, 500 cycles). Some of the common diagnostic tests performed during TC testing to evaluate the winding condition are:

- Tap testing
- Dimension measurement
- Dissipation factor (DF) testing
- Partial discharge (PD) testing
- Capacitance testing

To perform these diagnostic tests, the thermal cycling test program has to be interrupted. The test set-up must be disassembled for the diagnostic tests and then reassembled after the diagnostic tests. This procedure is done for several times during the 500-cycle test. The disassembly and reassembly of the TC test setup and the associated diagnostic tests increase the total time and cost required for thermal cycling testing.

A novel technique has been developed which continuously monitors acoustic signals emitted from delaminations in the insulation system without interrupting TC testing. The acoustic monitoring technique and the test results are presented in this paper.

## 2 ACOUSTIC MONITORING SYSTEM

A thermal cycling (TC) test was performed on a 13.8 kV stator bar with epoxy-mica insulation. The TC test duration was 500 cycles with temperature cycled from 40 °C to 155 °C. The test was performed in accordance with IEEE Standard 1310.

Three acoustic sensors were installed on the narrow face of the bar under test. Sensors #1 and #3 were placed 25 cm away from the knuckles, as shown in Fig. 1. The detection sensitivity may be variable with the bars under test. The acoustic signals from insulation delamination were continuously recorded by a multi-channel acoustic analyzer. The acoustic data were then synchronized with the temperature data and the cycle numbers by a computer, so that the acoustic data matched the respective thermal cycle number. This system can determine:

- the cycle at which delaminations occur;
- the portion of the thermal cycle (heating or cooling cycle) at which delaminations occur;
- the number of the cycles at which delaminations occur;
- the severity of delamination;
- delamination locations by calculating the acoustic signals from the various sensors.

The diagnostic tests prescribed in IEEE1310 were performed at the various numbers of thermal cycles and the test results were compared with the acoustic test results.

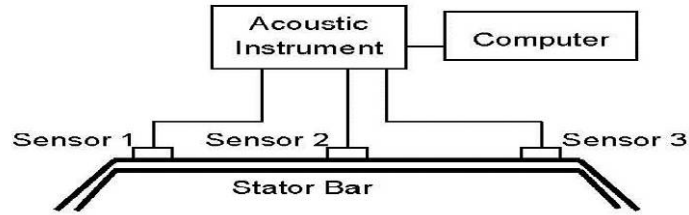


**Fig. 1 Set-Up of the Acoustic Monitoring System.**

### 3 ACOUSTIC TEST RESULTS

Acoustic energy is the area under the magnitude-time curve. The total energy recorded from all of the three acoustic sensors is presented in Fig. 2. Fig. 2 clearly shows that the acoustic energy significantly increased between the 14th–19th cycles during the 500-cycle test, indicating that the delamination was occurring.

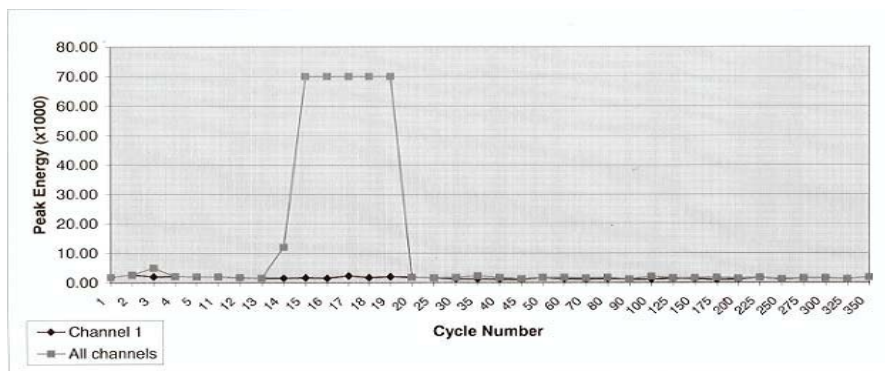


**Fig. 2 Acoustic Energy from Sensor #1.**

An acoustic count is defined as the number of times the acoustic signal crosses a detection threshold. The acoustic counts recorded from sensors #1 and #3 are presented in Fig. 3. There was a significant increase in the acoustic count between the 14th–19th cycles, indicating that the delamination was occurring. Fig. 3 shows that the acoustic count increased in sensor #3 and not in sensor #1, indicating that the delamination occurred at locations close to sensor #3. There was strong audible noise produced in the acoustic instrument speakers when the delamination was occurring between the 14th – 19th cycles.

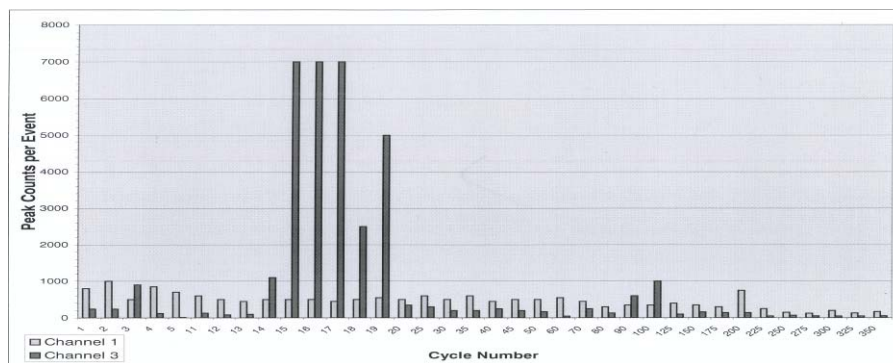


**Fig. 3 Acoustic Counts.**

An acoustic hit is defined as a detected acoustic signal. An acoustic hit can consist of several acoustic counts. The total acoustic hits recorded from the 3 sensors in the 14th cycle are presented in Fig. 4 which shows the number of acoustic hits against time. This is an initial stage of the severe delaminations. The delamination activity was concentrated in the middle of the heating cycle with the maximum of 4800 acoustic hits. In comparison with the delamination activity in the heating cycle, the delamination activity in the cooling cycle was spread over all of the cooling cycle with much lower

numbers of the acoustic hits. The maximum number of acoustic hits in the cooling cycle was 800. The delamination activities in the heating cycle were the discrete events while those in the cooling cycle were more continuous events.

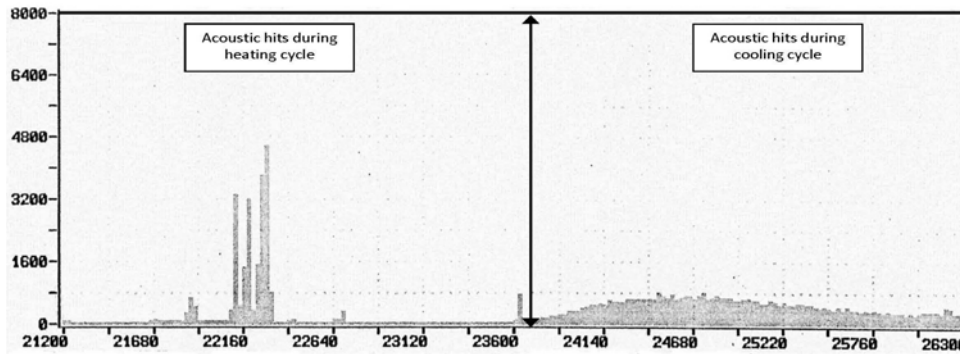


**Fig. 4 Acoustic Hits Recorded in the 14th Cycle.**  
(Left side of the arrow line: Heating Cycle; Right side of the arrow line: Cooling Cycle)

The total acoustic hits recorded from the 3 sensors in the 17th cycle are presented in Fig. 5. In comparing Fig. 4 and 5, it is clear that more acoustic activity in the heating cycle was occurring in the 17th cycle than in the 14th cycle. The maximum acoustic hits in the heating cycle of the 17th cycle increased to 7500, indicating the more delaminations in the heating cycle of the 17th cycle than those in the 14th cycle. In comparison of the heating and cooling cycles, the number of the delamination events in the heating cycle was much higher and the delamination events were occurring at the particular stages of the heating cycle, while the number of the delamination events in the cooling cycle was low and the delamination events were occurring in the whole cooling cycle.

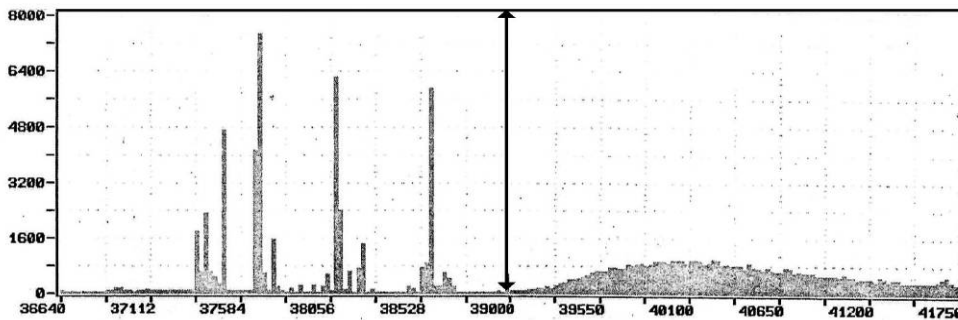


**Fig. 5 Acoustic Hits Recorded in the 17th Cycle.**  
(Left side of the arrow line: Heating Cycle; Right side of the arrow line: Cooling Cycle)

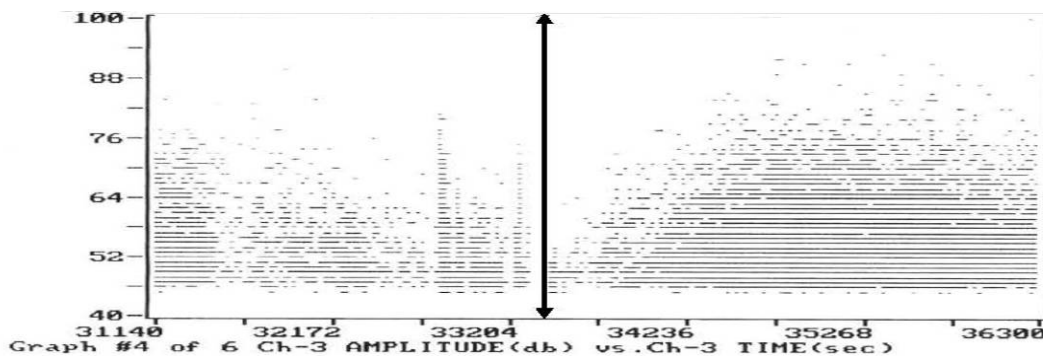


**Fig. 6 Acoustic Amplitude Recorded in the 17th Cycle.**  
(Left side of the arrow line: Heating Cycle; Right side of the arrow line: Cooling Cycle)

The acoustic signal amplitude is the peak voltage of the largest excursion attained by the signal waveform from an emission event. In comparison of the amplitude in the heating and cooling cycles in the 17th cycle as shown in Fig. 6, the acoustic signals with high amplitude were occurring in the middle of the cooling cycle. The amplitude of the acoustic signals in the beginning and end of the

cooling cycle was relatively smaller. The acoustic amplitude was higher in the cooling cycle than in the heating cycle. In general, it is expected that the higher amplitude of the acoustic signal is an indication of a higher degree of delamination.

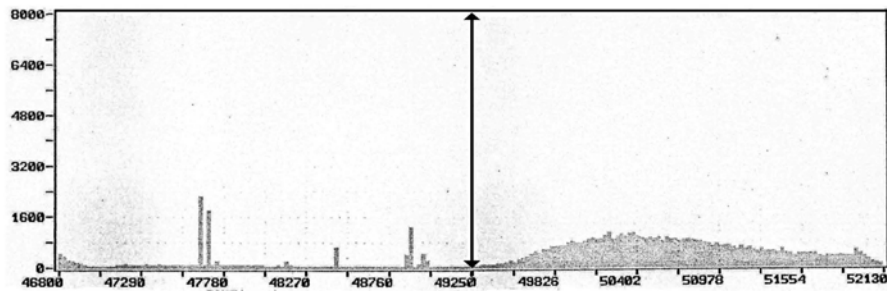


**Fig. 7 Acoustic Hits Recorded in the 19th Cycle.**  
(Left side of the arrow line: Heating Cycle; Right side of the arrow line: Cooling Cycle)

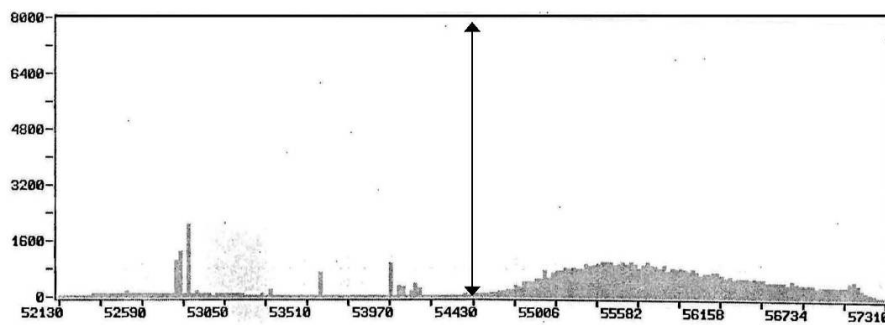


**Fig. 8 Acoustic Hits Recorded in the 20th Cycle.**  
(Left side of the arrow line: Heating Cycle; Right side of the arrow line: Cooling Cycle)

The acoustic hits recorded in the 19th and 20th cycle are presented in Fig. 7 and 8. Close to the end of the delamination process, the delamination activity in the heating cycle was decreasing while the delamination activity in the cooling cycle was almost the same as that in the 17th cycle.

#### 4 GUARDED DISSIPATION FACTOR (DF) AND PARTIAL DISCHARGE (PD) TEST RESULTS

Guarded DF tests were made from 2 kV to 16 kV in 2 kV intervals. The DF tip-up values were measured between the value at 8 kV and one at 2 kV. The DF and tip-up values are presented in Fig. 9 and 10. They increased significantly at the 50th cycle, supporting the finding that the major delaminations occurred between the 14th-19th cycles. Although no DF measurements were performed during the 14th-19th cycles but it suffices to note that that the effect of delaminations during the 14th-19th cycle were observed clearly during DF measurements at the end of the 50th thermal cycle.

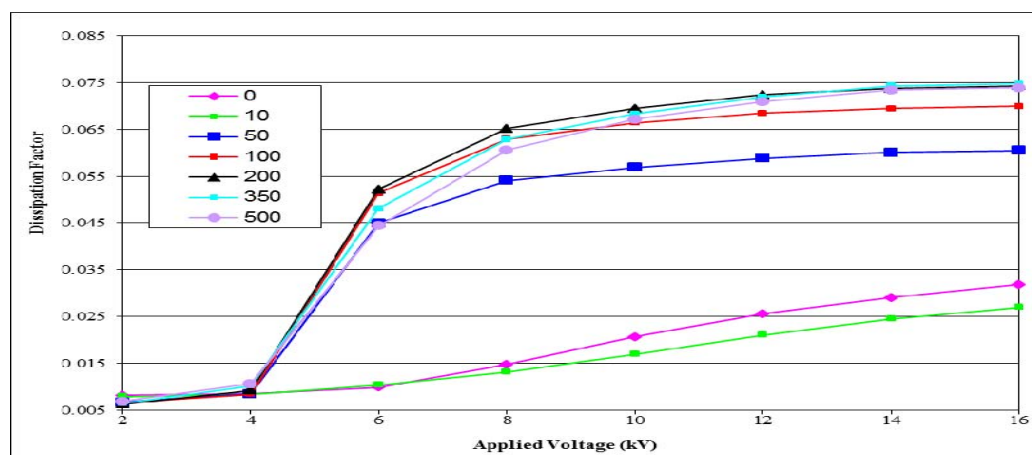


**Fig. 9 DF Test Results at Various Stages of the 500-cycle TC Test.**

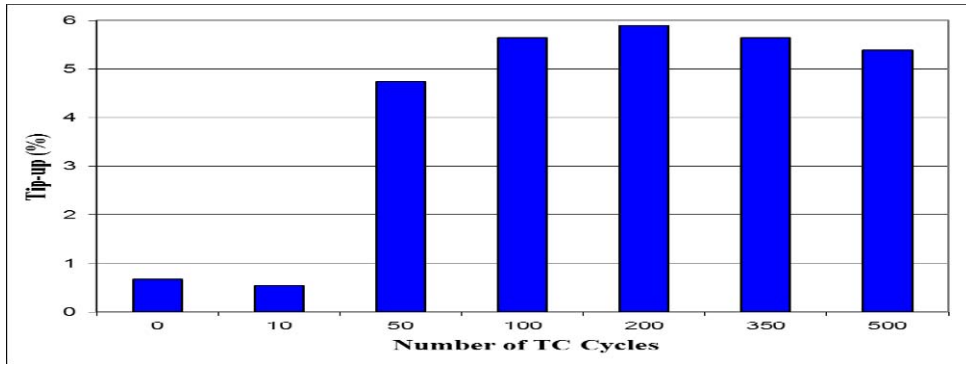


Fig. 10 DF Tip-Up Results at Various Stages of the 500-cycle TC Test.

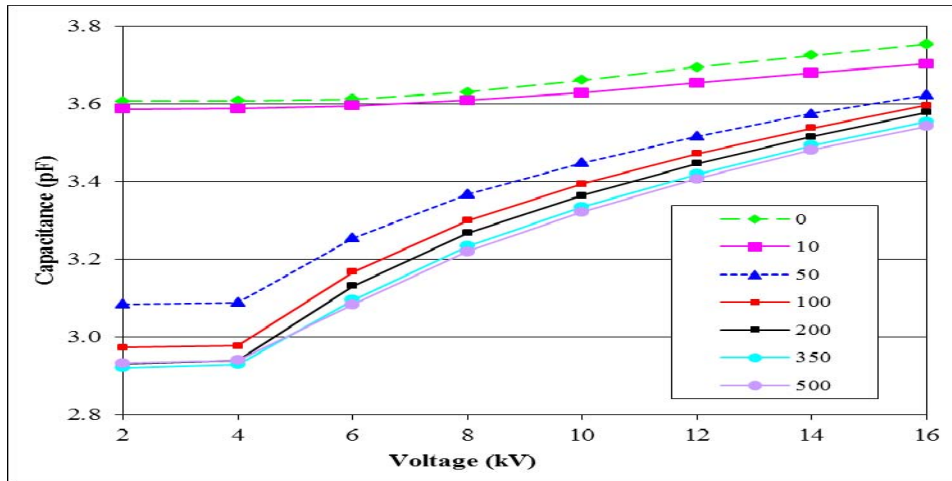


Fig. 11 Capacitance Values at Various Stages of the 500-cycle TC Test.

The capacitance values of the bar decreased significantly at the 50th cycle, as presented in Fig. 11. This is also an indication of the major delaminations occurring between the 14th – 19th cycles. The severe delamination can create air gaps between the insulation layers and de-bonding between the groundwall insulation and the copper. Hence the insulation system configuration was changed and therefore the capacitance was also changed.

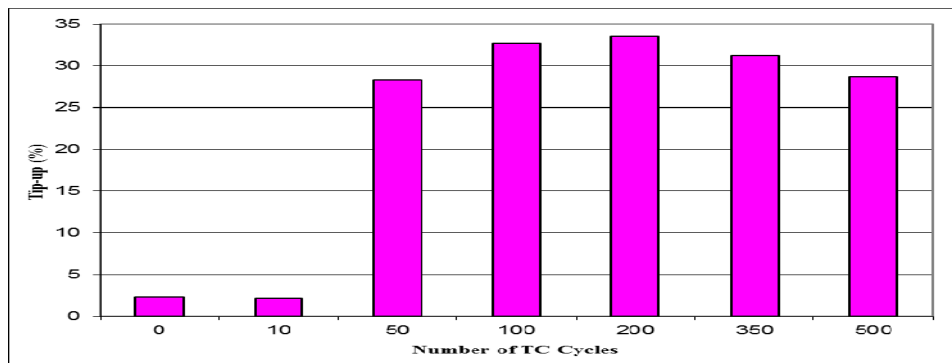


Fig. 12 Capacitance Tip-Up Results at Various Stages of the 500-cycle TC Test.

The capacitance tip-up values were calculated using the following formula:

$$\Delta C = (C_{8kV} - C_{2kV}) \times 100$$

The capacitance tip-up values are presented in Fig. 12. The considerably increased capacitance tip-up value at the 50th cycle indicates that severe delaminations were probably present.

The PD test results are presented in Fig. 13 and 14. The PD activity also considerably increased at the 50th cycle, indicating that the major delaminations occurred between the 14th–19th cycles. Decrease

in the PD activity in some cycles could be caused by thermal curing and thermal expansion which reduced the size of some voids.

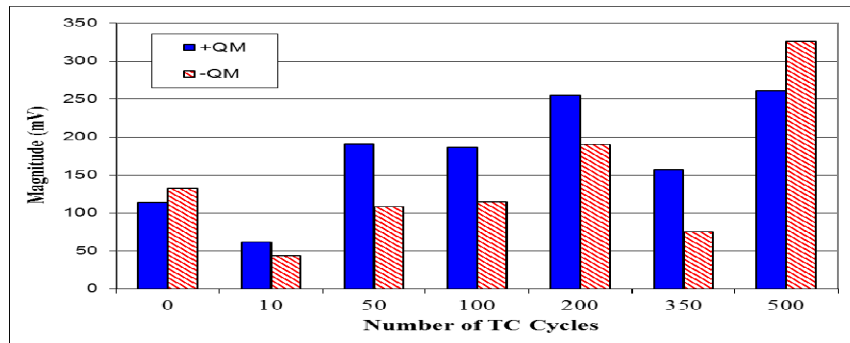


Fig. 13 Q<sub>max</sub> Values from PD Testing

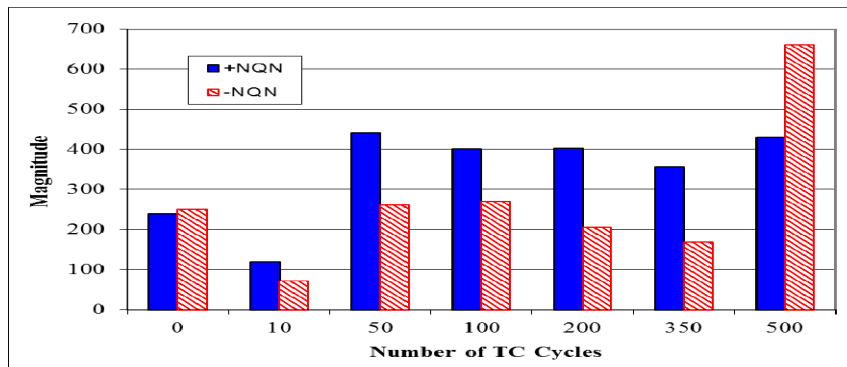


Fig. 14 NQN Values from PD Testing.

A tap test performed at the 50th cycle indicated the delamination locations. A calculation of the delamination locations from the acoustic signals received from the three sensors matched the result of the tap test. The DF, PD and tap test results were consistent with the acoustic test result.

## 5 DISSECTION AND MICROSCOPIC EXAMINATION

Dissection and microscopic examination are the useful tools to confirm delaminations in the insulation system. The delaminated sections identified by the acoustic test were dissected and examined under a microscope. Severe inter-layer delaminations on the groundwall insulation were found, as indicated by the arrows in Fig. 15.

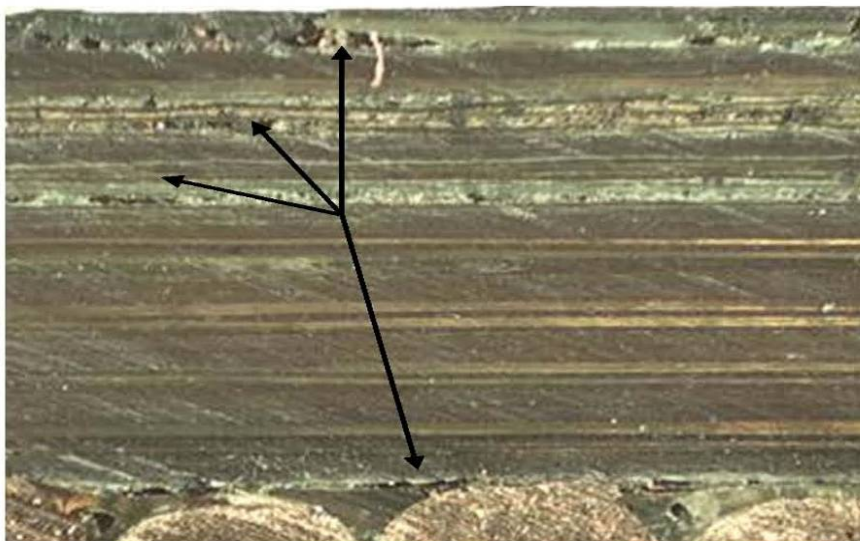


Fig. 15 Insulation Inter-layer Delaminations Under Microscopic Examination.

The length of the inert-layer delaminations is from a few mm to 10 mm. When the delaminations caused by thermal expansion and contraction were generated, the acoustic signals were produced. Under high voltage stress, the delaminations can produce high partial discharges which can eventually cause insulation failure.

## 6 CONCLUSIONS

A novel acoustic technique to monitor insulation delaminations during thermal cycling testing has been developed [1]. The dissipation factor tests, PD tests and tap tests performed at the various stages of the thermal cycling testing were used to compare the acoustic test results, thereby indicating that delaminations were occurring. Dissection and microscopic examination of the bar was used as a verification of the presence of insulation delaminations.

The acoustic monitoring technique offers the following benefits:

- The ability to continuously monitor insulation delaminations during thermal cycling testing in a non-destructive fashion;
- Undertaking condition assessment of insulation delamination without disassembly and reassembly of a TC test set-up with savings on test duration and cost;
- Identifying the cycle number at which significant delaminations occur;
- Identifying locations where such significant delaminations occurred;
- Identifying at what stages of the heating and cooling cycle delaminations occurred;
- Providing a better understanding of the delamination process during TC testing on stator bars and coils. The information may help to improve the winding design and manufacturing process, leading to improvements in overall quality.
- Providing an opportunity to examine the test duration requirements prescribed by IEEE 1310 and to explore any optimization opportunities to reduce test duration and costs.

Further work with different bar designs and coincident monitoring of electrical and acoustical diagnostics is needed to quantify the relationship between acoustic signals and the degree of delaminations.

## BIBLIOGRAPHY

- [1] Colwell M, Cherukupalli S E, Hannebutt D, Lee R, Pidcock R. Quality control of stator bars – An assessment of destructive and non-destructive testing techniques[R]/Internal Powertech Labs Report 5366-44, February 1996
- [2] IEEE Standard 1310-1996.Recommended Practice for Thermal Cycling Testing of Form Wound Stator Bars and Coils for Large Generators
- [3] Stone G C, Lyles J F, Braun J M, Kaul C L.A Thermal Cycling Type Test for Generator Stator Winding Insulation. IEEE Trans. Energy Conversion, December 1991, 6:707-713
- [4] Zhu H, Morton C. Quality Evaluation of Stator Coils and Bars under Thermal Cycling Stress. IEEE Intern. Sympos. Electr. Insul. (ISEI), Toronto, Canada, June 2006:384-387
- [5] Sedding H, Petit A. Experience with Electromechanical Testing of Stator Winding Insulation[C] 10th INSUCON, Birmingham, June 2006 :307-312
- [6] McDermid W. Experience with Thermal Cycling of Stator Coils and Bars.IEEE Intern. Sympos. Electr. Insul. (ISEI), Toronto, Canada, 2006 :344-345
- [7] Zhu H, Kung D. Acoustic Monitoring of Insulation Delaminations During Thermal Cycling Tests on a Stator Bar[C]/IEEE Electr. Insul. Conf., Montreal, Canada, June 2009:183-187

**A Novel Online Diagnosing Technique of Turn-to-Turn Short Circuit of Large Turbine Generator**

**Zhang Zhengping**  
Power Science Institute of Guangdong Power Grid, Guangzhou, Guangdong  
China

**SUMMARY**

As a typical fault that jeopardizes the safe operation of generator, rotor's turn-to-turn short circuit fault has long been a puzzle to be online diagnosed accurately in the fault diagnosing area of generator. A novel diagnosing method is presented in this paper to detect the rotor turn-to-turn fault based on correlation curve analysis of rotor vibration and field current. This method does not employ any extra instruments to conduct the detection, only uses the ready-made data or curves existing in the Distribution Control System (DCS) of the power plant, without any interference to the generator. Using this novel method can detect the rotor turn-to-turn fault easily, accurately and quickly, greatly enhancing the efficiency and the accuracy of the diagnosing job. Thus, it thoroughly changes the present difficult situation about online accurate diagnosis of the rotor turn-to-turn fault, exerting great importance on ensuring the safe operation of the turbine generator.

**KEYWORDS**

Turbine generator, Rotor, Turn-to-turn short circuit, Online diagnosis

# 1 INTRODUCTION

Turn-to-turn fault is very common for rotor of large generators, and it jeopardizes the safe operation of the generator. First, it causes the abnormal vibration of the rotor, even exceeding the limit value according to the relative norm, and the generator is often obliged to reduce its load amount. Longer this fault lasts, more electricity the power plant loses. Second, the high temperature at the short circuit point may probably harm the turn-to-turn insulation shim, causing more serious turn-to-turn fault, and even causing rotor windings to ground fault. Third, rotor turn-to-turn fault may magnetize the rotor shaft which worsens rotating vibration of the rotor, and then damages the bearing bush or the shaft neck. All of this may form a vicious cycle and endanger generator's safe operation<sup>[1-3]</sup>.

The exact online diagnosis of the rotor turn-to-turn fault has been a puzzle for long time. The main reasons of this state are not only the dimness of the turn-to-turn fault signature, but also the tremendous overhaul work and huge electricity loss that may be caused by misdiagnosis.

Presently, the common method to detect the rotor turn-to-turn fault depends on the gas magnetic field detecting coil which has been pre-installed in the generator stator core<sup>[4][5]</sup>. However, when the generator is working under actual load, the load current will exert a kind of effect to counteract the windings magnetic potential, and there exists some other effects of various disturbance, the actual waveform obtained from the detecting coil is not good enough, the waveform deformation is usually too serious to use for analyzing the rotor turn-to-turn fault exactly<sup>[6][7]</sup>. Actually, in order to acquire the perfect waveform from the detecting coil, the generator has to be taken off the line, and a thick copper bus is used to shorten the outlet of the three phase buses for three-phase short circuit test. The effect from the outer load will be eliminated this way and ideal gas magnetic field waveform can be obtained. Nevertheless, this is not strictly a real online meaning for rotor turn-to-turn fault diagnosis.

A novel diagnosing method is presented in this paper to detect the rotor turn-to-turn fault based on correlation curve analysis of rotor vibration and field current. This method does not employ any extra instruments to conduct the detection, only uses the ready-made data or curves existing in the Distribution Control System (DCS) of the power plant, without any interference to the generator. Using this novel method can detect the rotor turn-to-turn fault easily, accurately and quickly, greatly enhancing the efficiency and the accuracy of the diagnosing job. Thus, it thoroughly changes the present difficult situation about online accurate diagnosis of the rotor turn-to-turn fault, exerting great importance on ensuring the safe operation of the turbine generator.

## 2 RELATION OF THE ROTOR VIBRATION AND THE FIELD CURRENT

If the rotor is absent of the rotor windings turn-to-turn fault, the magnetic field produced by the rotor windings keeps perfectly symmetrical in space, as shown in Fig.1<sup>[8]</sup>. When a turn-to-turn fault occurs in a certain pole(e.g. pole S in Fig.1), the amount of the valid turns in this pole is less than that in pole N, so the amount of the valid turns in two poles will be different, thus an imbalance of the magnetic field in space will be inducted, as shown in the right figure in Fig.1. This directly leads to the distortion of the magnetic field distribution in space, shown as the real line in Fig. 2.

Distortion of the magnetic field distribution will exert imbalanced electron-magnetic force (EMF)

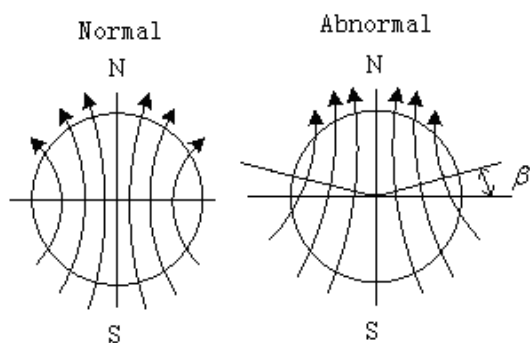


Fig.1 Distribution of the magnetic field for a sound rotor distribution.

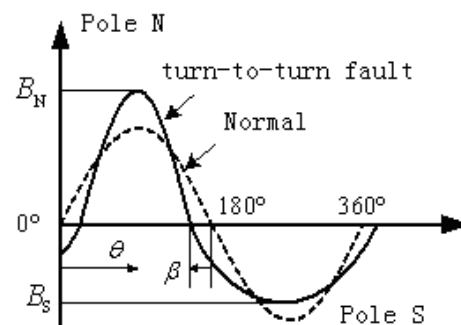


Fig.2 Deformation of the magnetic field for a faulty rotor windings.

upon the rotor in service. Then, what factors are in relation to this imbalanced electro-magnetic force?

As plotted in the right picture in Fig.1, since the magnetic flux through a same space is the same, an expression can be described as below<sup>[8]</sup>:

$$N_t \times (90^\circ - \beta) / 180 = (N_t - N_s) / (90^\circ + \beta) / 180 \quad (1)$$

$$\beta = 90^\circ \times N_s / (2N_t - N_s) \quad (2)$$

Where  $N_t$  is the total windings of each pole, and  $N_s$  is the number of the faulty turns.

Suppose the distribution of the magnetic field (even under kind of distortion) is still close to sinusoidal wave, the imbalanced EMF upon rotor is given as:

$$F = \left\{ \int_{\beta}^{\pi-\beta} B_N^2 \sin^2[(\theta - \beta)\pi / (\pi - 2\beta)] \times \sin \theta d\theta + \int_{\pi-\beta}^{2\pi+\beta} B_S^2 \sin^2[(\theta - \pi + \beta)\pi / (\pi + 2\beta)] \times \sin \theta d\theta \right\} LR / 2\mu_0 \quad (3)$$

Where  $F$  is the imbalanced EMF,  $B_N$  and  $B_s$  is respectively the intensity of magnetization of pole N and pole S,  $\mu_0$  is magnetic conductivity of air,  $\mu_0 = 4\pi \times 10^{-7} N/A^2$ ,  $L$  is the valid length of rotor bar, and  $R$  is the radius of the rotor forge piece.

$B_N$  and  $B_s$  in (3) can be given by

$$B_N = N_t \times I_f \times 4\pi \times 10^{-7} / (2 \times \delta) \quad (4)$$

$$B_S = (N_t - N_s) \times I_f \times 4\pi \times 10^{-7} / (2 \times \delta) \quad (5)$$

where  $I_f$  is the field current of the rotor windings,  $\delta$  is the gap width between the stator and the rotor.

Substitute (4) and (5) into (3), and except field current  $I_f$ , all the other variables like  $L$ 、 $R$ 、 $N_t$ 、 $\delta$  are constants, which are connected with the construction parameters of the rotor or the gap. Thus, the imbalanced EMF  $F$  given by (3) actually depends on  $I_f$ . So (3) can be simplified as

$$F = \lambda I_f^2 \quad (6)$$

where  $\lambda$  stands for the calculated value of the all the other parts excluding  $I_f^2$  in (3), and it is a fixed value.

As shown in (6), when a turn-to-turn fault occurs in the rotor windings, the imbalanced EMF upon the running rotor bears only relation with the field current  $I_f$ , and is proportional to square  $I_f$ .

So, what's the relation between the magnitude of the rotor vibration and the imbalanced EMF?

In actual service, the rotor is suspended on the bearing bush of the turbine end and the excitation end of the generator, Between the bearing bush and the shaft neck is a layer of very thin oil film, which not only has the functions of lubricating and sealing, but supporting the rotor as well. Armed with the tremendous pressure of the jacking oil system, this thin oil film can jack the rotor that weighs about 100 tons, so prevents the rotor from touching and damaging the bearing bush or the shaft neck. Thus, the rotor is actually suspended on the oil film, and can be regarded as a linear system<sup>[9]</sup>.

Relative researches show that in a linear system, the vibration magnitude of a part is proportional to the excited force upon it, and is inversely proportional to the dynamic stiffness, which can be given by<sup>[10]</sup>

$$A = P/K_d \quad (7)$$

where  $A$  is the magnitude,  $P$  is the excited force,  $K_d$  is the dynamic stiffness, and  $K_d$  is given by:

$$K_d = K_c/\mu \quad (8)$$

$$\mu = 1/\sqrt{[(1 - (\frac{\omega}{\omega_n})^2)]^2 + 4(\frac{\varepsilon\omega}{\omega_n})^2} \quad (9)$$

where  $K_c$  is the static stiffness,  $\mu$  is the dynamic amplification factor,  $\omega$  is the angular frequency of the excited force,  $\omega_n$  is the the natural frequency of the rotor, and  $\varepsilon$  is damping factor.

Usually  $\mu$  in (9) is very small value in normal service of the rotor. Since the rotating speed keeps a fixed value, i.e. 3000rpm,  $\mu$  is a fixed value by (9).

The EMF  $F$  in (6) is the excited force  $P$  in (7). Substitute (6), (8) and (9) into (7), we get the expression below:

$$A = \frac{\lambda}{K_c} \mu I_f^2 = K \mu I_f^2 \quad (10)$$

where  $K = \lambda/K_c$ , it is a factor.

Since  $K$  and  $\mu$  are fixed value, as shown in (10), the vibration of rotor is decided only by  $I_f^2$ , and be proportional to  $I_f^2$ .

So far, the positive correlation between the vibration magnitude and the field current has been explored theoretically for a generator rotor with turn-to-turn fault inside. However, this is a conclusion acquired from an ideal model. Actually, the rotor always runs in changing vibration, so  $\delta$  will fluctuate slightly, and so the same with  $B_N$  and  $B_S$  in (4) and (5), consequently, the imbalanced EMF upon the rotor will fluctuate with that. In addition, the mechanical construction for the rotor, oil and the bearing bush, after all, can not be a standard linear system in service, and is affected by different design, material, assembly technology and the oil pressure, etc. Therefore, the proportional relation of rotor vibration magnitude and the square field current is subjected to nonlinear factors from actual system. However, all of this can not change the inherent law that the vibration of the rotor will vary with the field current after a turn-to-turn fault occurs in the rotor windings. In other words, as long as the rotor windings has a turn-to-turn fault inside, the axis vibration of the rotor will vary with the field current. Therefore, a turn-to-turn fault can be quickly and accurately diagnosed for a rotor if an obvious positive correlation is detected between the rotor vibration and the field current.

### 3 ANALYSIS OF ACTUAL CASES

For a sound rotor in service, the axis vibration on both turbine and excitation ends keeps a steady vibration level and does not vary with the field current, shown in Fig.3 and Fig.4.

Fig.3 depicts the real-time relation curves of the axis vibration No.6 at the excitation end of the generator and the field current of No.1 generator in HY power plant. This is a faultless rotor, no turn-to-turn short circuit fault with the rotor windings. Fig.3 shows that the axis vibration No.6 including X direction and Y direction, i.e. 6X and 6Y, are relatively level and steady. Even though the field current shows a wide varying range, axis vibration No.6 shows no tracking with it. Fig.4 depicts the real-time relation curves of the axis vibration and the field current of No.3 generator in JW power plant. In Fig.4, the axis vibration No.7 at turbine end (7X and 7Y) and axis vibration No.8 at the excitation end (8X and 8Y) are quite level and steady. Though the field current varies dramatically and frequently, No.7 and No.8 axis vibrations don't any similar varying trend. So from Fig.3 and Fig.4 for sound rotors, no correlation can be detected between the axis vibration of the rotor and the field current.



Fig.3 Vibration and field current curves of sound rotor (Generator No.1, HY power plant)

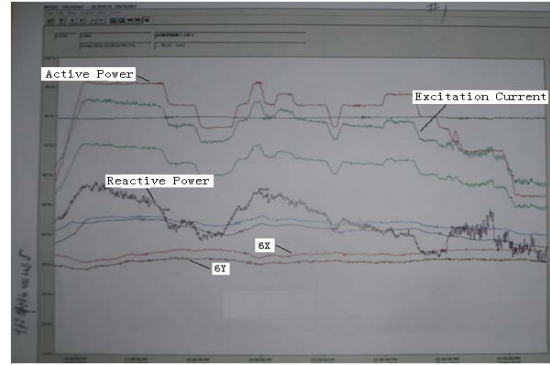


Fig.4 Vibration and field current curves of a sound rotor (Generator No.3, JW power plant).

However, this situation will be completely different when a turn-to-turn fault exists in the rotor windings. Fig.5 plots the relation curves of the rotor vibration and the field current of No.2 generator in SW power plant, which reported the abnormal rotor vibration in March, 2009. As shown in Fig.5, when the field current  $I_f$  varies its amplitude, the axis vibration 7Y at the turbine end and the axis vibration 8Y at the excitation end vary at the same time and shows the same trend, i.e., axis vibration 7Y and 8Y both keep a highly positive correlation with the field current. Based on this clear signature, the turn-to-turn fault was judged and the generator in operation was required to stop for a thoroughly check as soon as possible. After the generator was taken off the line, the rotor was drawn out of the stator. Electric tests were conducted to check the rotor windings and a steady metallic turn-to-turn short circuit fault in coil 5 of the inner slip ring, i.e., pole 2. After that, the rotor was shipped back to the generator manufactory and the windings were disassembled for a thorough repair. When the coil 5 was hung out of the rotor bar slot, the fault point was found to be at the corner between turn 2 and turn 3 at the excitation end on the left (seen from excitation end to turbine end), shown as Fig.6 and Fig.7. In this two figures, the turn-to-turn insulation shim can be seen clearly that the shim has been burned through and obvious burning marks were made on the bars, indicating a steady metallic short circuit fault at this point.



Fig.5 Vibration and field current Curves of a faulty rotor (Generator No.2, SW power plant)



**Fig.6 The burned-through turn-to-turn insulation shims between No.2 and No.3 turns.**



**Fig.7 The damaged condition on No.2 and No.3 rotor bars.**

In October, 2008, the rotor of No.2 generator in ZH power plant showed abnormal vibration in service, the curves of rotor axis vibration (No.5 and No.6 axis vibrations) and field current were acquired from DCS, as shown in Fig.8. It is obvious that the positive correlation can be seen between the rotor vibration curves (of 5X, 5Y, 6X and 6Y) and the field current. So this rotor was judged to be suffering the turn-to-turn fault.

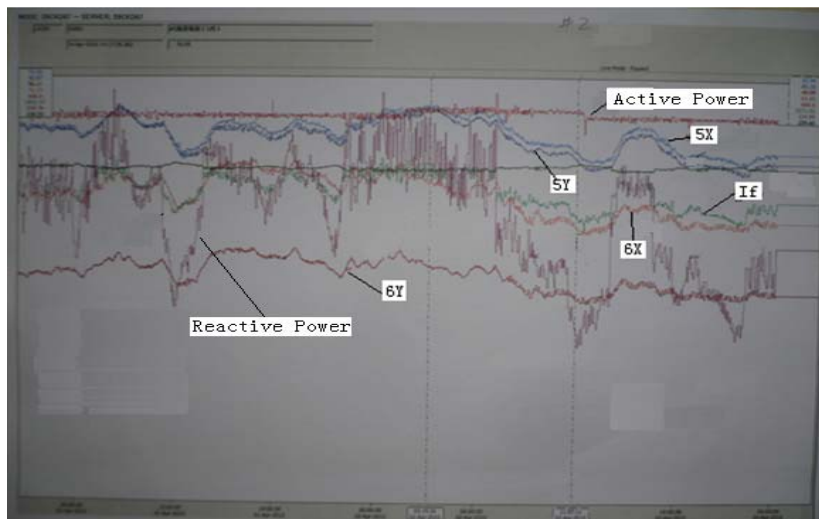


**Fig.8 Vibration and field current curves of a faulty rotor (Generator No.2, ZH power plant)**

In term of this judgment, the rotor was returned to the generator manufactory. After the rotor was disassembled, it was found that the insulation shim was jammed and crushed broken at the corner between turn1 and turn 2 in coil 8 of pole 1, so short circuit fault happened at this place, as shown in Fig.9. After the rotor has been repaired and re-installed into the generator, the correlation phenomenon shown in Fig.9 vanished completely, and the rotor vibration did not vary following the field current, as shown in Fig.10, and the rotor vibration recovered to normal operation.

It can be seen from all the cases above, the on-line diagnosing method of rotor turn-to-turn fault based on rotor vibration and field current is actually quite simple. Using this method does not need any extra instruments and equipments but the DCS now available in the power plant. Observing the relation between the rotor vibration and the field current curves, and determine whether the correlation exists or not, that is enough for an accurate judgment. This is quite easy but important for the power plant personnel to diagnose the rotor turn-to-turn fault by themselves.



**Fig.9** The turn-to-turn fault lies between turn 1 and turn 2, coil 8, pole 1.(Excitation end)

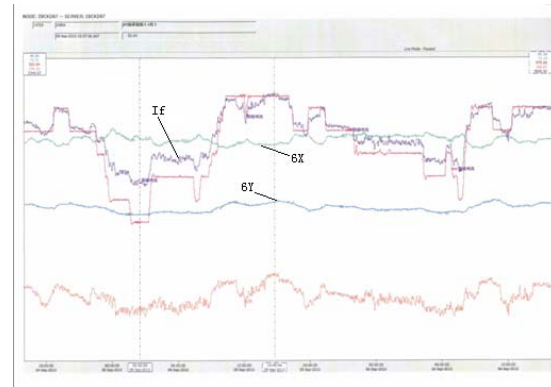


**Fig.10** The rotor vibration does not vary with the field current after the rotor has been repaired.

#### 4 CONCLUSION

(1) This paper presents a deep analysis about the relation between the rotor abnormal vibration and the field current of a rotor with turn-to-turn fault, and proves theoretically the positive correlation that definitely exists between them when a turn-to-turn fault occurs in the rotor windings. So according to this signature, the accurate on-line diagnosis can be performed to detect the turn-to-turn fault of a rotor with abnormal vibration;

(2) With this on-line diagnosing method based on the correlation of the rotor vibration and the field current, the complex fault analysis of the dynamic rotor turn-to-turn fault has been turned into a simple but accurate job, which is of great importance to instruct the power plant personnel to diagnose the rotor turn-to-turn fault by themselves;

(3) Traditionally the rotor turn-to-turn fault has long been puzzle to be diagnosed accurately because of the dimness of the fault signature and the complex analysis. The novel method put forward in this paper to diagnose the rotor turn-to-turn fault on-line is of simplicity but satisfied accuracy, and it will definitely change the difficult situation in large turbine generator domain to analyze and diagnose the rotor turn-to-turn fault accurately.

#### BIBLIOGRAPHY



Zhengping Zhang was born in Xiangxiang, Hunan province, China, on Oct.8, 1966. In 1996, He received the M.Eng. in power electronics technology from Wuhan University, China. In 2002, He received the Ph.D in Power system and Automation from South China University of Technology, Guangzhou, China. At present, He is a senior engineer with Power Science & Research Institute of Guangdong Power Grid, Guangdong Province, China. His main research interests are large-scale generator techniques, condition monitoring of electric machine, intelligent instruments design and HV test techniques.

#### REFERENCES

- [1] Li W. Fault Analysis And Prevention of Turbine Generator. Beijing: The Power Publish House of China, 2002
- [2] Wan S. Research On the Generator Rotor Fault Based On the Mechanic and Electric Combined Signatures[C]//Proceedings of North China Power University, June, 2007: 28~31
- [3] Zhang R. Diagnosis of the Bearing Vibration Caused By Generator Rotor Turn-To-Turn Fault. Thermal Power Generation, Sept. 1994: 49~51

- [4] Sottile J, Trutt F C, Leedy A W. Condition monitoring of brushless three phase synchronous generators with stator winding or rotor circuit deterioration. IEEE Transactions on Industry Applications, May, 2006: 1209~1215
- [5] Zhao Y, Li Y. Vibration Characteristic Analysis of The Turbine Generator Rotor With Turn-To-Turn Fault. Proceedings of North China Power University, Sept., 2008: 16~21
- [6] Wu Y, Li H. A Novel Method to Detect The Turn-to-turn Fault of The Generator Rotor. High Voltage Engineering, Nov., 2009: 2698~2703
- [7] Dorrell D G, Thomson W T, Roach S. Analysis of airgap flux current and vibration signals as a function of the combination of static and dynamic airgap eccentricity in 3 phase induction motors. IEEE Transactions on Industry Applications, Jan., 1997: 24~34
- [8] Du B. Thermal Vibration Balance Method of The Turbine Generator Rotor. Large Electric Machine Abroad, Jun., 1997: 14-21
- [9] Lu J. Dynamics of Machinery-Electricity Analysis. Beijing: Science Press, 1992
- [10] Shi W. Vibration and Fault of Turbine Generator Unit. Beijing: Higher Education Press, 1999

## **Online PD Monitoring System With Microstrip Antenna for Rotating Machines**

**H. Sako, Y. Kaneda, S. Tomita  
K. Mio, K. Suzuki  
Mitsubishi Electric Corporation  
Japan**

### **SUMMARY**

Online partial discharge (PD) monitoring for high voltage rotating machine is one of useful means from the view point of condition-based maintenance. Up to now, various on-line PD monitoring systems are developed and applied: for instance, using slot RTD wiring, stator slot coupler (SSC) or inductive sensors.

An online PD monitoring system using microstrip antenna (patch antenna) has been developed for high voltage rotating machines such as induction motors or synchronous generators. This system consists of microstrip antennas, PD detectors and a personal computer. Microstrip antenna is a small and flat antenna which detects electromagnetically radiated PD signals from stator or rotor windings. The frequency of electromagnetic wave detected with the antenna is normally ultra high frequency (UHF) range and depends on the structure of the antenna. It was designed to detect electromagnetic wave of 1.8 GHz around which background noise level is relatively low. Because of its small and flat shape, it is easily installed inside or outside of the machine housing without interfering with machine design, manufacturing or operation. It also means that microstrip antennas do not cause a failure of stator winding because they are completely insulated from high voltage stator windings.

This online PD monitoring system was applied to large turbine generators with rated voltage ranging from 13.5 to 27 kV, and it was confirmed to be sensitive enough to PD signals generated from generator windings. In case of online PD monitoring using near-field antennas, these antennas can detect PD signals very close to a PD source in the windings. On the other hand, the microstrip antenna designed for PD detection can detect attenuated PD signals sensitively beyond near field. This means that the microstrip antenna can cover large area of PD activities in the windings.

### **KEYWORDS**

Partial discharge, PD, Rotating machine, Microstrip antenna, Patch antenna, Online, Frequency, Generator, Motor, Electromagnetic

## 1 INTRODUCTION

High voltage rotating machines such as induction motors used in a factory or synchronous generators in a power plant are required to operate continuously without unexpected insulation failure. Hence, the importance of condition-based maintenance (CBM) has received considerable attention. Online partial discharge (PD) monitoring for high voltage rotating machine is one of useful means from the standpoint of condition-based maintenance. Up to now, various online PD monitoring systems are developed and applied to them: for instance, using slot RTD wiring, stator slot coupler (SSC) or inductive sensors.

An online PD monitoring system with microstrip antenna (patch antenna) has been developed for high voltage rotating machines. It was designed to detect electromagnetically radiated PD signals sensitively and to cover a large area of PD activities in the windings. In this paper, the characteristic of microstrip antenna, system configuration and PD data analyses obtained from high voltage synchronous generators are described.

## 2 SYSTEM CONFIGURATIONS AND MICROSTRIP ANTENNA

The configuration of the online PD monitoring system with microstrip antenna and the characteristic of microstrip antenna are described in this chapter.

### 2.1 System Configuration

This system consists of microstrip antennas, PD detectors and a personal computer. Fig.1 shows a schematic diagram of the system applied to a large turbine generator. Microstrip antennas are placed near generator windings, and PD detectors are placed outside the machine housing. A microstrip antenna and a PD detector are connected with a coaxial cable. The PD detectors are also connected to a monitoring PC with LAN cable via a HUB. The monitoring PC can be located in a central control room so that online PD monitoring is carried out in it. A number of antennas can be controlled simultaneously with a PC on this system.

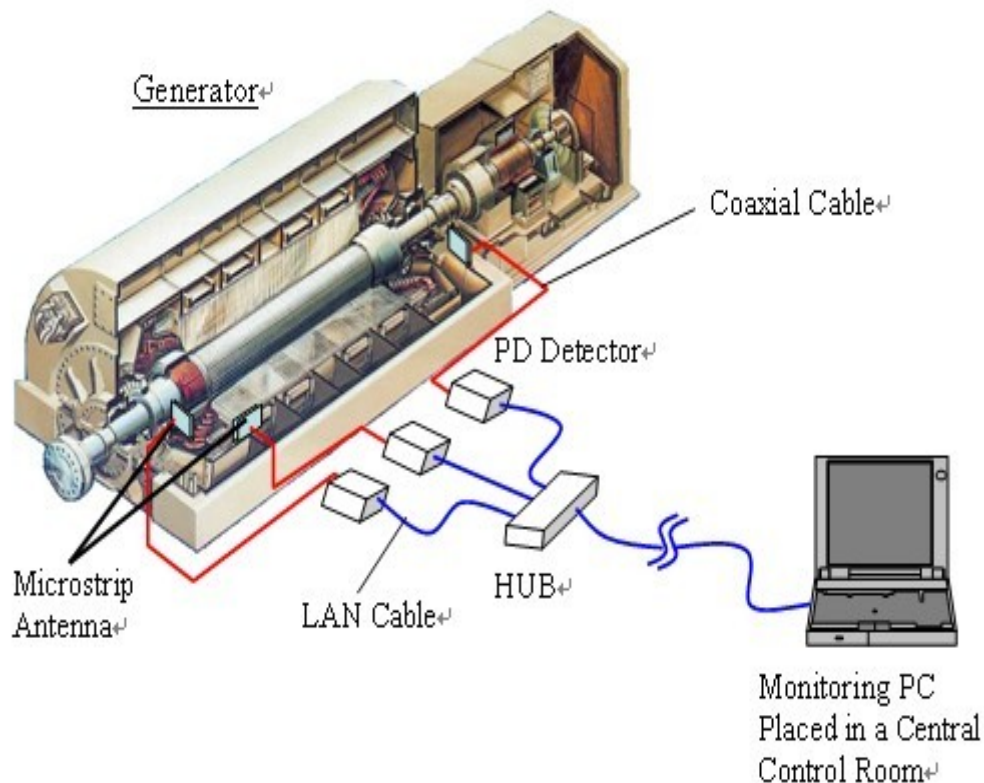


Fig. 1 System configuration applied to large turbine generator.

## 2.2 Microstrip Antenna

Microstrip antenna is a small and flat antenna which detects electromagnetically radiated PD signals from stator or rotor windings. The frequency of electromagnetic wave detected with the antenna is normally ultra high frequency (UHF) range and depends on the structure of the antenna.

### 2.2.1 Structure of Microstrip Antenna

A structure of a microstrip antenna is shown in Fig. 2. A dielectric substrate with dielectric constant  $\epsilon_r$  and thickness  $t$  is laid on a ground plate, and a patch conductor with length  $L$  and width  $W$  is placed on the dielectric substrate [1]. The resonance frequency  $f_r$  of the antenna is determined by  $\epsilon_r$  and  $L$ . The bandwidth of the antenna is also determined by  $t$ ,  $L$ ,  $W$ ,  $\epsilon_r$  and wave length of electromagnetic wave  $\lambda_0$ . Thus a microstrip antenna for PD detection can be designed to have narrow bandwidth. The length  $G$  shown in Fig. 2 relates to the peak gain of the antenna.

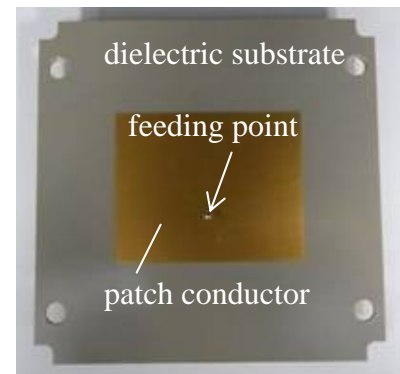
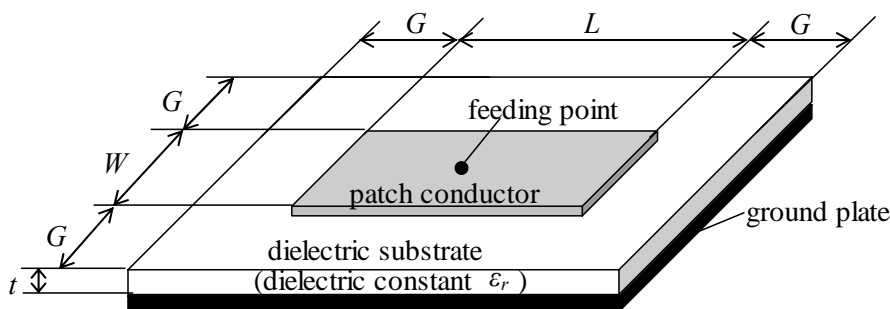


Fig. 2 Antenna structure.

### 2.2.2 Determination of Resonance Frequency [2]

On the antenna design, the determination of resonance frequency  $f_r$  is important. Hence, a PD frequency spectrum was measured with a wide band horn antenna on a 3.0 MW, 6.6 kV motor manufactured in 2002. Fig. 4 shows frequency spectra obtained from the motor under operation and shutdown. A comparison of both spectra demonstrates that the PDs have a wide frequency range, and appreciable PD magnitude still can be observed beyond 1.5 GHz. A lot of spikes considered as broadcasting or communication noises are observed, but the number of spikes around 1.8 GHz is relatively low. Thus the microstrip antenna was designed to have the resonance frequency  $f_r$  of 1.8 GHz. On PD measurements, noise must be suppressed or reduced so that the system can detect PD signals correctly. This antenna was designed to have narrow bandwidth in order not to be affected other than PD signals.

Fig.3 shows the microstrip antenna designed for PD detection. The length of each side is 116 mm, and the width including reinforcing material is 8 mm.

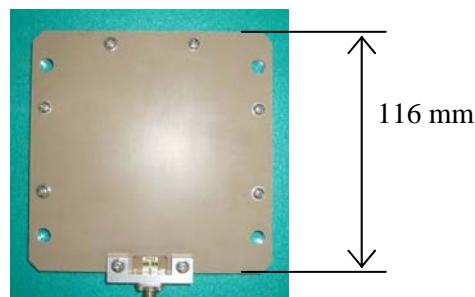
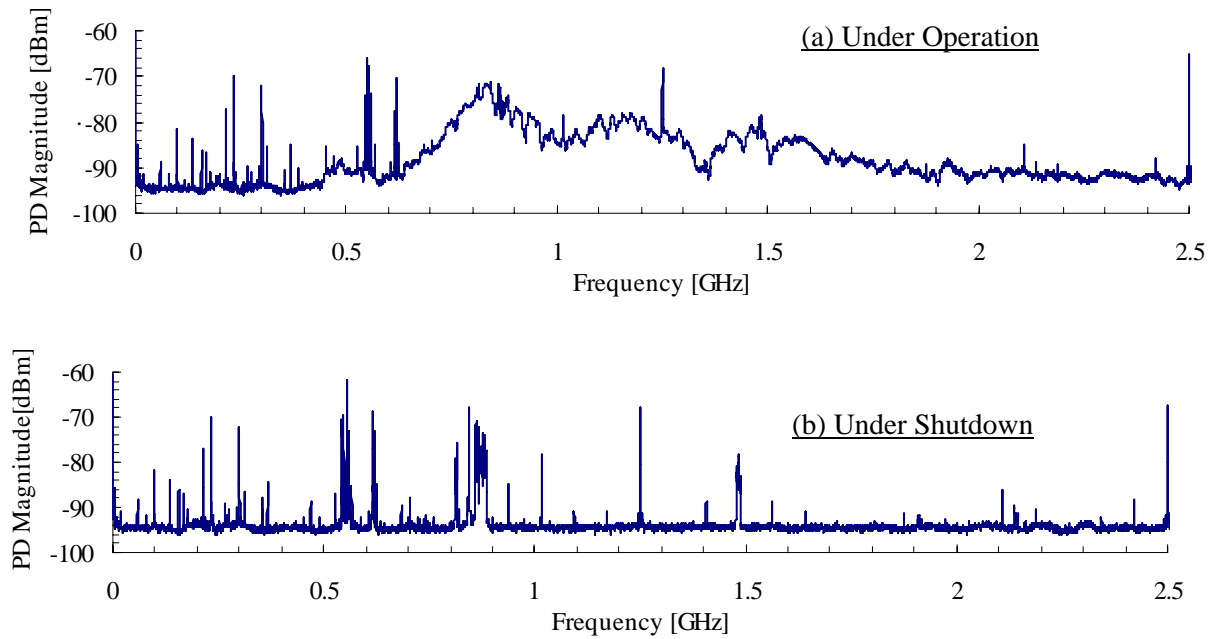


Fig. 3 Square microstrip antenna covered with resin.



**Fig. 4** Frequency spectra obtained with a wide band horn antenna on a 3.0 MW, 6.6 kV motor. (a) Under operation. (b) Under shutdown.

### 2.2.3 Frequency Characteristic of Microstrip Antenna [2]

The developed microstrip antenna was installed on a 1.3 MW, 6.6 kV motor manufactured in 1980 to check its frequency characteristic. Fig. 5 shows frequency spectra obtained with the microstrip antenna under operation and shutdown of the motor. Since PDs have a wide frequency range as described in section 2.2.2, Fig. 5 (a) demonstrates that the antenna has its peak frequency around 1.8 GHz and tens of megahertz of bandwidth.

The microstrip antenna has direction dependence with respect to perpendicularly incoming electromagnetic wave as shown in Fig. 6. Fig. 7 shows two frequency spectra obtained by rotating the antenna 90 degrees, but no significant difference is observed. It is probable that the electromagnetic wave repeats reflection inside the machine housing, and then the direction dependence diminishes.

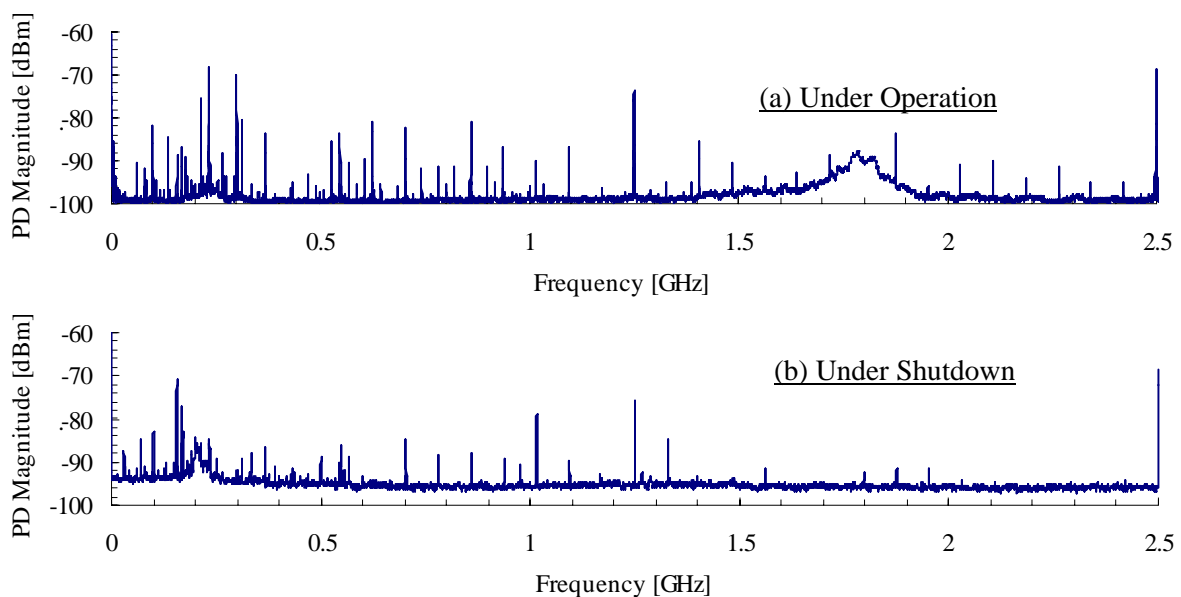


**Fig. 5** Frequency spectra obtained with the developed microstrip antenna on a 1.3 MW, 6.6 kV motor. (a) Under operation. A peak is observed around 1.8 GHz. (b) Under shutdown. No peak is observed around 1.8 GHz.

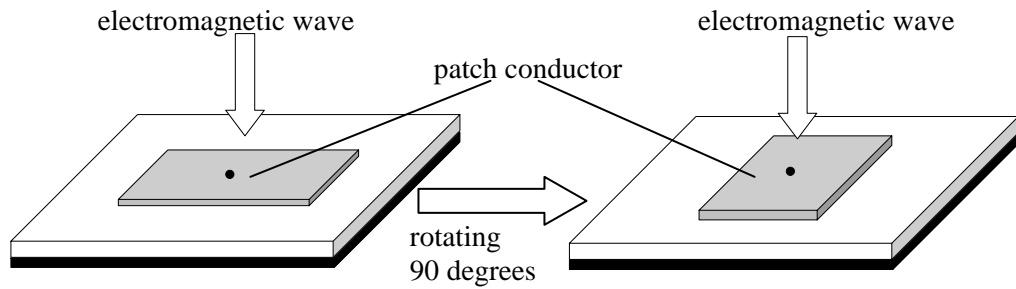


Fig. 6 Antenna direction with respect to perpendicularly incoming electromagnetic wave.

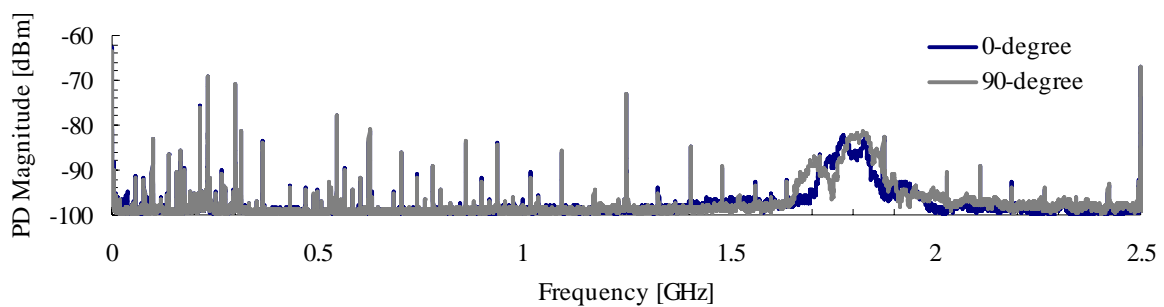


Fig. 7 Frequency spectra obtained by rotating the antenna 90 degrees.

### 2.3 PD Detector [2]

PD signals received with the microstrip antenna are sent to the PD detector and processed in it. Fig. 8 (a) illustrates the components of the detector. It consists of a band pass filter, logarithmic amplifier, peak hold circuit and A/D converter. The input PD signal ranging from -90 dBm to -30 dBm is transformed to the output voltage from 0 to 10 V through the detector. Fig. 8 (b) shows piled-up PD detectors.

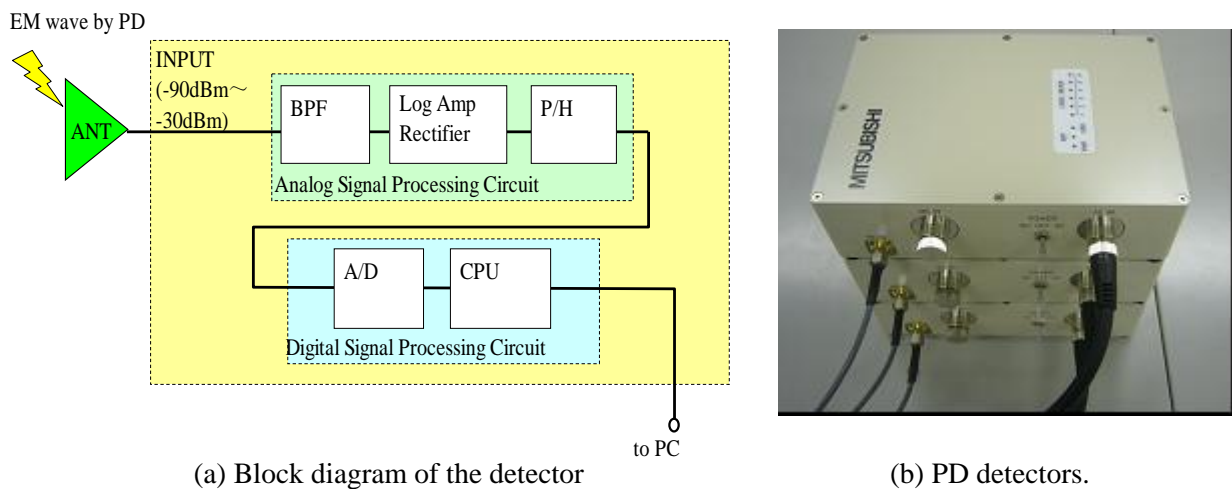


Fig. 8 PD detector.

### 3 PD MEASUREMENTS AND ANALYSES

This online PD monitoring system has been applied to a number of motors with rated voltage of 6.6 kV, and its availability as an online PD monitoring tool was confirmed [3]. This time, the system was also applied to large turbine generators. PD signals were measured online and offline.

#### 3.1 PD Measurement on Iron Loss Test

The online PD monitoring system with microstrip antenna was applied to large turbine generators with rated voltage ranging from 13.5 to 27 kV. Table I lists their specifications. PD signals were measured on iron loss tests on which rotor coil is excited to produce rated voltage at the open terminals.

**Table I Turbine Generator List for PD Measurement**

Generator Name	Rated Output	Rated Voltage	Frequency	Operation
	[MVA]	[kV]	[Hz]	
Generator A	200	13.5	50	before shipment
Generator B	315	21.0	50	before shipment
Generator C	1045	27.0	60	before shipment
Generator D	250	16.0	60	under operation

Microstrip antennas were placed near exciter side end windings and turbine side ones. They face stator end windings as shown in Fig. 9. Because of their small and flat shape, they are easily installed inside the machine housing without interfering with machine design, manufacturing or operation. It also means that the microstrip antennas do not cause a failure of stator windings because they are completely insulated from high voltage stator windings.

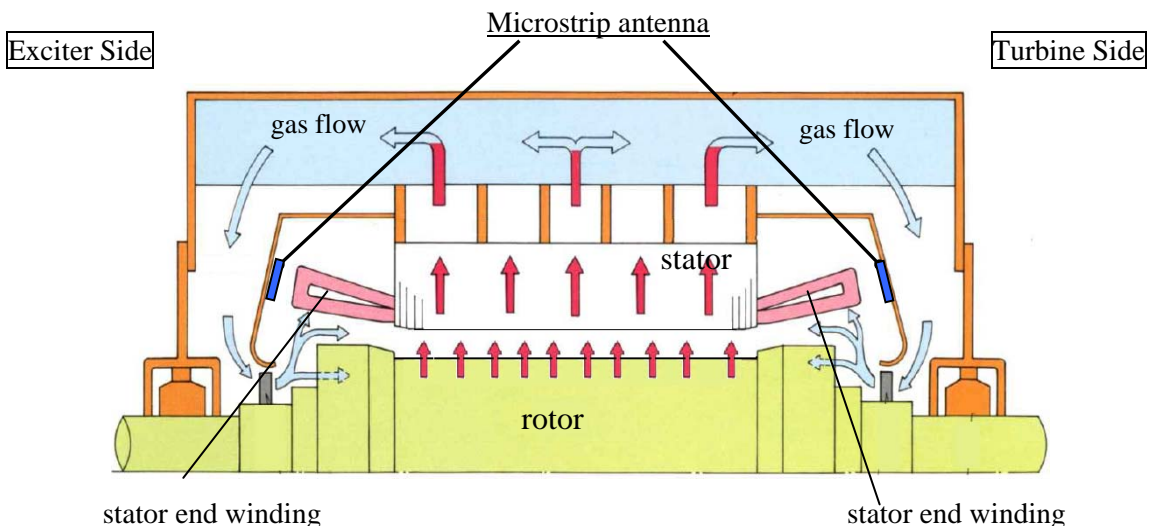


**Fig. 9 Cross-section of a large turbine generator.**

**Microstrip antennas are placed near stator end windings.**

Fig. 10 shows PD data observed on iron loss tests. The vertical axes show PD magnitude in volt [V] instead of [dBm]. 0 V and 10 V correspond to -90 dBm and -30 dBm respectively. PD magnitude used in Fig. 10 is 50 pps value for 50 Hz machine or 60 pps value for 60 Hz machine which are explained in section 3.2, so PD magnitude of 0 V does not necessarily mean no PD signals. Although these generators have different rated voltage, electric field and insulation design, PD signals were observed

on iron loss tests. It means that the microstrip antenna can cover large area of PD activities sensitively. PD magnitude tends to decrease with time on a iron loss test.

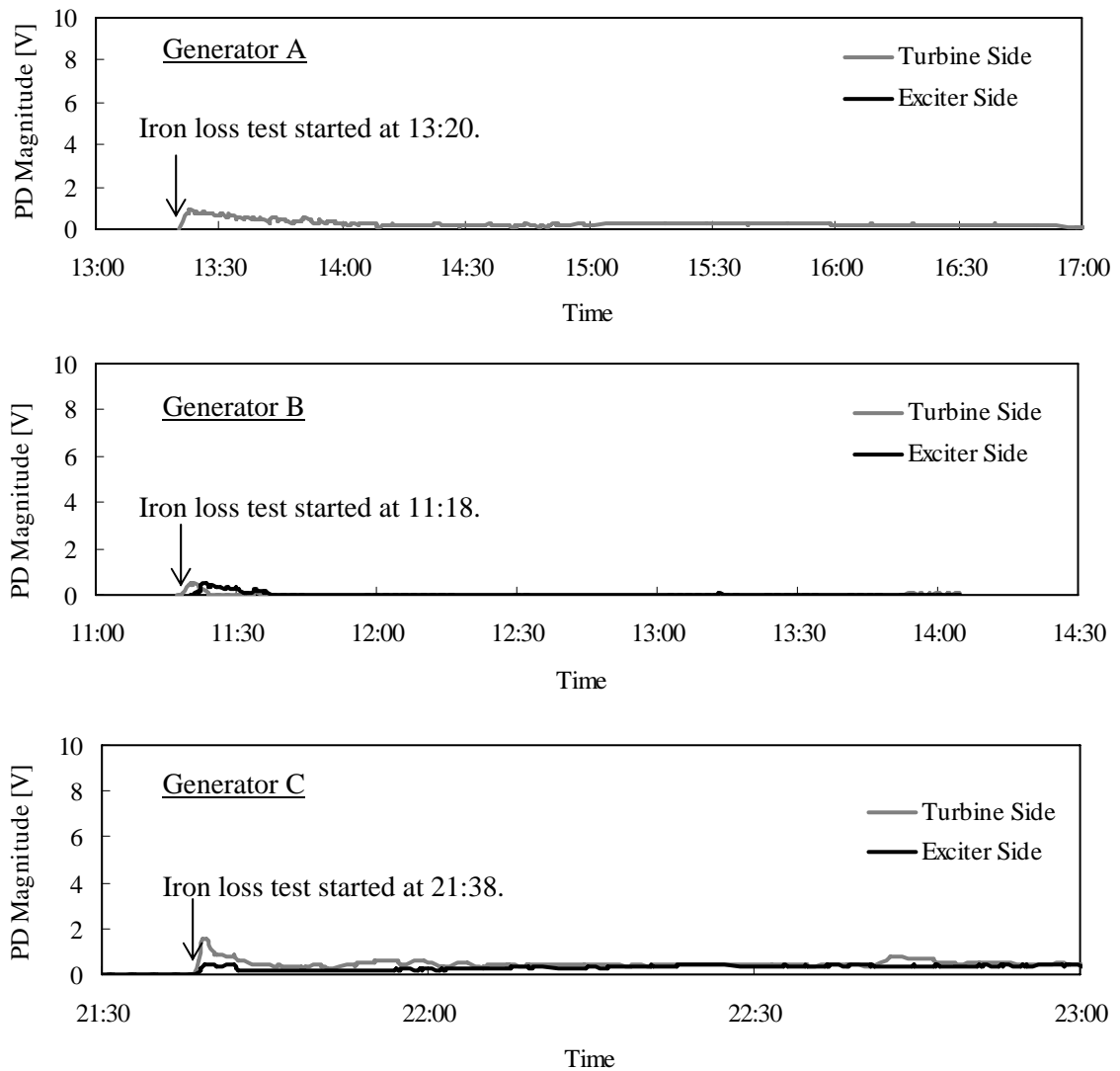


**Fig. 10 PD data observed on iron loss tests.**

Fig. 11 also shows PD data of Generator D which was manufactured in 1996. The stator windings are probably aged because of 15 years operation. The rated voltage is produced at the stator terminals, but they are open like iron loss test. Relatively high PD magnitude was measured at exciter side. Continuous online PD monitoring enables users to grasp the insulation condition.

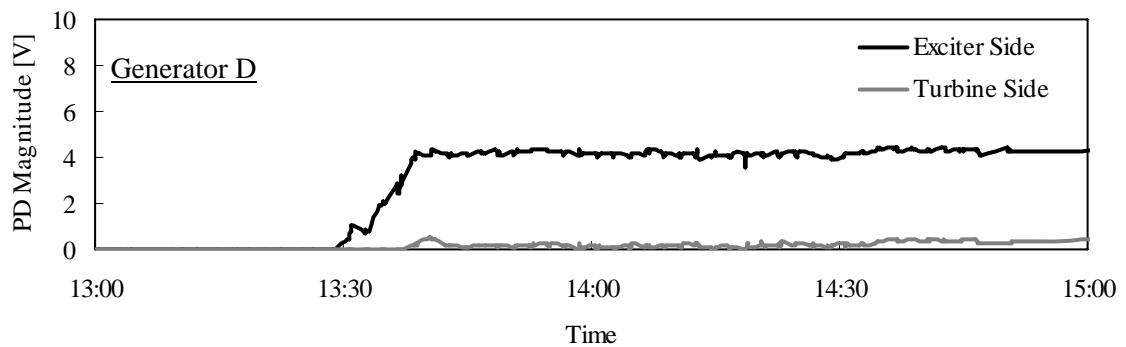
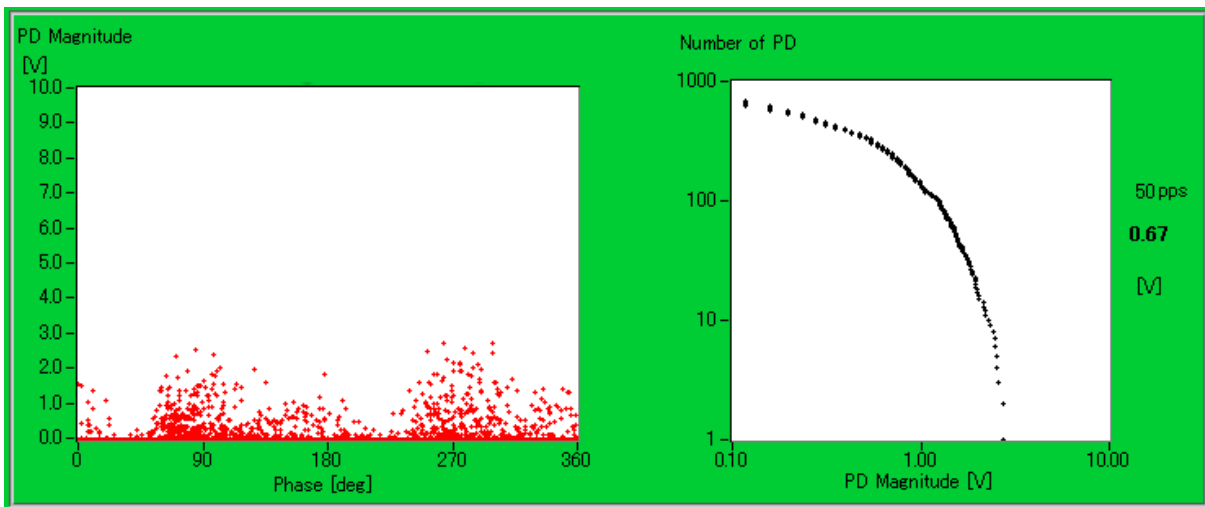


**Fig. 11 PD data of Generator D.**

### 3.2 PD Analysis on Iron Loss Test

Fig. 12 (a) is a PD phase characteristic and (b) is a cumulative PD one. They were measured at turbine side of Generator A at 13:32. The duration of the measurement is 5 seconds. In graph (a), every PD signal with magnitude is plotted against stator voltage phase. In graph (b), the PD magnitude at 50 pulses per second (pps) is displayed. Since the duration of measurement is 5 seconds, the PD magnitude at 50 pps equals the PD magnitude at 250 pulses in graph (b). The PD magnitude at 50 pps for 50 Hz machine and 60 pps for 60 Hz machine are used to evaluate the level of PD. The PD magnitude used in Fig. 10 and Fig. 11 is also 50 pps or 60 pps value.

Fig. 13 shows PD characteristics measured on Generator D which has relatively large PD signals. From Fig. 13 (a), it can be seen that one phase out of three has large PD signals. We can determine the phase by using the generator terminal voltage as trigger signals.

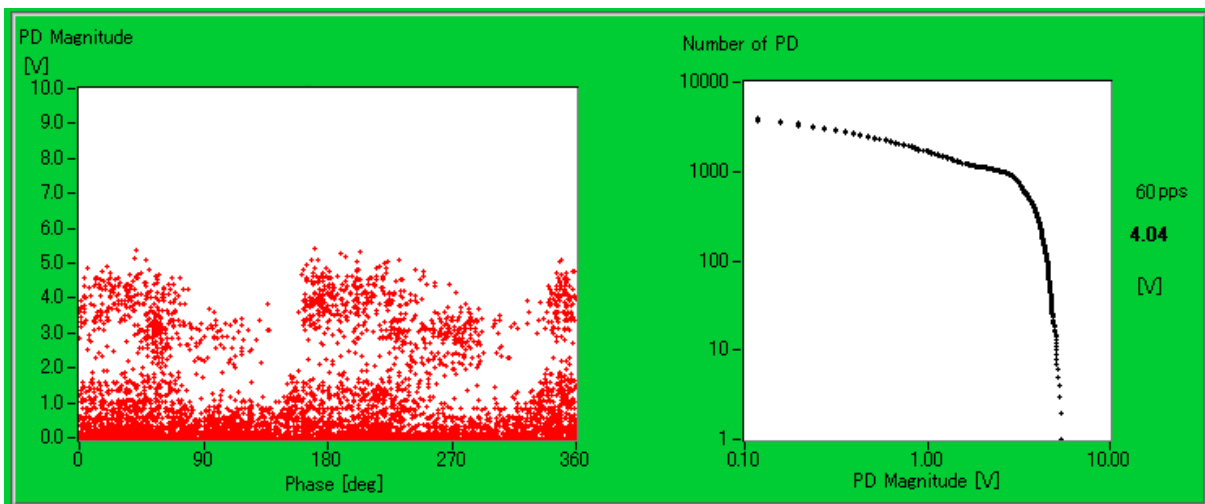


(a) PD phase characteristic

(b) Cumulative PD characteristic

Fig. 12 PD data measured on iron loss test at 13:32. (Generator A, turbine side)

(a) All PD events measured in 5 seconds were plotted against stator voltage phase.



(a) PD phase characteristic

(b) Cumulative PD characteristic

Fig. 13 PD data measured at 14:00 on Generator D. (Exciter side)

### 3.3 Correlation between PD Magnitude and Qmax

In addition to online PD measurement, offline PD measurements with the microstrip antenna were performed on Generator A. A PD characteristic shown in Fig. 14 (a) was obtained at turbine side by changing applied AC voltage externally on the phase U. PD magnitude increases with increasing applied AC voltage. It means high electric field causes large PD magnitude. If windings have localized high electric fields, large PD magnitude will be measured.

Fig. 14 (b) shows a relationship between PD magnitude obtained with the microstrip antenna and maximum partial discharge Qmax measured by conventional coupling capacitor method. Qmax values were measured on Generator A simultaneously. The correlation can be seen from Fig. 14 (b).

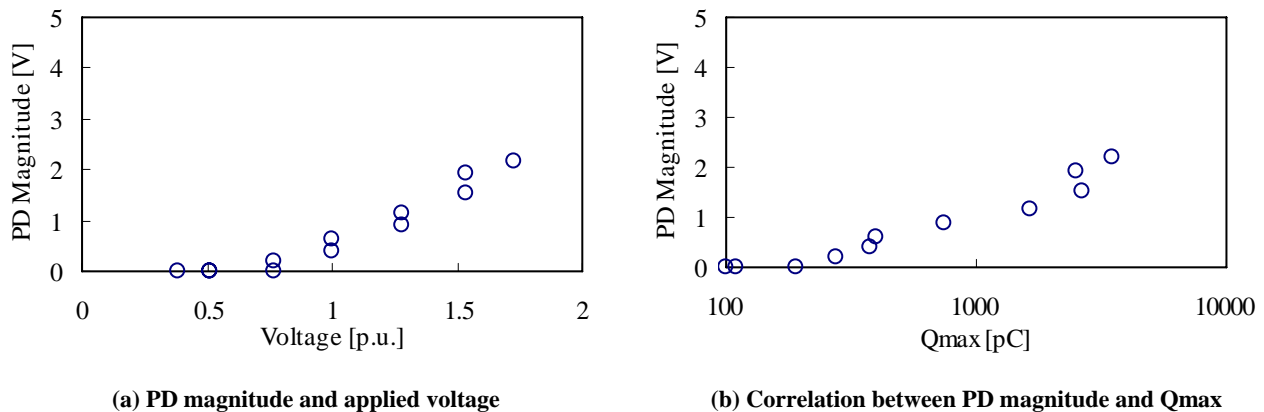


Fig. 14 PD characteristics obtained from voltage tests. (Generator A, turbine side, phase U)

## 4 CONCLUSIONS

The following conclusions were derived.

- (1) The online PD monitoring system with microstrip antenna has been developed. It consists of microstrip antennas, PD detectors and a PC. Microstrip antennas are easily installed inside the machine housing without interfering machine design, manufacturing or operation.
- (2) The resonance frequency of the microstrip antenna was determined to be 1.8 GHz around which back ground noise level is relatively low.
- (3) This system was applied to large turbine generators, and PD signals were measured online. High sensitivity was confirmed on iron loss tests.
- (4) The microstrip antenna can cover large area of PD activities.
- (5) Continuous online PD monitoring enables users to grasp the insulation condition.
- (6) The correlation between PD magnitude and Qmax can be seen.

## BIBLIOGRAPHY

- [1] Muto H, Kaneda Y, Aoki H, Hamamoto O. On-line PD monitoring system for rotating machines using narrow band detection of EM wave in GHz range[C]// International Conference on Condition Monitoring and Diagnosis, Beijing, China, 2008:1093-1096
- [2] Shibuya Y, Matsumoto S, Tanaka M, Muto H, Kaneda Y. Electromagnetic Waves from Partial Discharges and their Detection using Patch Antenna. IEEE Transactions on Dielectrics and Electrical Insulation, 2010, 17(3) :862-871
- [3] Sawada N, Yano S, Furuichi H, Hamamoto O, Iwanaga H, Kaneda Y. Application of On-line Partial Discharge Monitoring Technique for High-Voltage Motors[C]//The Technical Meeting of IEEJ, 2-006, 2010

**Necessity and Impendency of Online Monitoring the Vibration  
of 800MW Generator Stator End Winding in Suizhong Power Plant**

**Ni Zhiying**  
**Shenhua Guohua Suizhong Power Generation Co.,Ltd.**  
**Huludao, Liaoning, China**

**SUMMARY**

With the increase of generator unit capacity, more strict demands are put forward on the mechanical property of stator end winding support system. It is usually difficult to study these properties with calculating method, and the required precision can not be ensured. Moreover, calculation is sometimes hard to perform due to some unsteady parameters and many factors such as manufacturing technology, characteristics of the fixing materials, installation quality, inspection and repairing quality, operation and maintenance, and so on. Therefore, testing is the most popular and the only feasible method in the research of large generator mechanical property, i.e. the stability of its vibration characteristics. This paper demonstrates with a lot of facts and test data that the stator end winding structural design for the two 800MW generators manufactured in Russia are acceptable and it is not necessary to invest hundreds of million Yuan for its overall modernization by France Alstom company. Indeed, both generators had occurred some problems during the operation of more than a decade. Based on the operation experience of the worldwide large turbogenerators, we suggest that an optical on-line monitoring system for stator end winding vibration is installed in each of the generators, respectively, to realize real-time measuring of the vibration magnitude and thus giving early alarm for condition-based maintenance. In this way, huge economic losses resulted from emergent incidences and unnecessary retrofit due to mistake judgment can be avoided. This paper also stresses that the retrofit of generator stator end winding structure is very difficult. The existing technology can not ensure a hundred percent success. Therefore, vibration measurement before retrofit not only allows demonstrating the effectiveness of the retrofit, but is also indeed significant for reducing the risk of a failed retrofit.

**KEYWORDS**

Turbo-generator, Stator end winding, Static vibration characteristic, On-line monitoring, Vibration amplitude

# 1 INTRODUCTION

Suizhong Power Plant is equipped with two TBB-800-2EY3 generators manufactured by Russia. The No1 unit was commissioned in 1999, and its stator bars were completely replaced in 2004 due to burning of the end winding lead. The No2 unit was commissioned in 2000, because of water and hydrogen leakage resulted from crack of conductor strands at the end of the bars and other problems, some stator bars were replaced in 2003 and 2005, respectively, all the bars were completely replaced in 2008. The manager of the Power Plant concluded that the structural design of these two generators stator end winding was not acceptable and must be redesigned. In 2009, No1 generator was committed to France Alstom for complete modernization. But I have a different opinion. Practice is the only standard for proving the truth. Data will show everything.

## 2 TYPE TESTS AND VIBRATION ENDURANCE TESTS OF GENERATOR TBB-800-2

### 2.1 Results of type tests

#### 2.1.1 Results of Thermal Test <sup>[1]</sup>

Under nominal load, the temperature rise of stator winding was 30°C; Temperature rise for the active core was 35°C, temperature rise of stator core brim in the warm air region was 60°C, temperature rise at the end of press plate flange was 50°C; And less than 30°C at the other parts.

#### 2.1.2 Results of Mechanical Test <sup>[1]</sup>

Core vibration: 38µm under rated no load, 31µm at full load.

Frame vibration: 10µm under rated no load, 8µm at full load.

Vibration amplitude of stator end winding: under rated short circuit, nose end 20-40µm, involute 24µm; under full load, nose end 25-50µm, involute 35µm.

#### 2.1.3 Test of Impact Endurance Capacity <sup>[3]</sup>

Russia Electric Power Factory has carried out test of impact endurance capacity on generator TBB-800-2 for many times. Under the condition of sudden short-circuit on machine terminal, stator end winding vibrated in step with the core, no change of winding shape and end region vibration state caused by sudden short-circuit was observed.

### 2.2 Test results of vibration endurance during operation <sup>[2]</sup>

Vibration amplitude of stator end winding: nose end ≤70µm ; involute ≤96µm.

Vibration amplitude of the winding fixing component ≤85µm.

Radial vibration amplitude of stator core ≤25µm。

## 3 SUMMARY OF DATA LIST

3.1 Test results of vibration endurance during operation for generator tbb-800-2 are shown in table I <sup>[2]</sup>

3.2 Natural frequency for the stator end winding modal and lead of no1 & no2 generator in suizhong power plant <sup>[5]</sup>

(1) Natural frequency for the global modal of No1 generator stator end winding is shown in Table II. Natural frequency for the global modal of No2 generator stator end winding is shown in Table III.

Table I

Service Time of the Generator (h)	Operating Condition	Vibration Amplitude of Measuring Location and Direction (µm)									
		End region						Stator			
		Nose		Involute	Outer ring		Bracket	Core		Frame	
		P	T	P	P	T	P	T	P	T	
0	P = 75MW	16	20	67	32	14	19	15	28	3	8
	Q = 190MVar										
	I <sub>CT</sub> = 18KA	50	59		42	19					
3000	P = 805MW	22	28	84	35	18	17	21	27	4	8

	Q = 230MVar										
	I <sub>CT</sub> = 20.3KA										
	P = 720MW	15	20	65	28	17	14	15	30	4	10
	Q = 0MVar	42	55		45	25					
I <sub>CT</sub> = 21.4KA											
6000	P = 800MW	27	30	96	55	19	23	33	25	8	10
	Q = 420MVar	70	40		85	46					
	I <sub>CT</sub> = 21.4KA										
	P = 730MW	18	20	60	15	15	16	25	25	4	8
	Q = 180MVar	41	32		65	38					
I <sub>CT</sub> = 18.2KA											
9500	P = 800MW	30	19	82	48	12	23	25	23	5	7
	Q = 260MVar	68	70		77	43					
	I <sub>CT</sub> = 20KA										
	P = 730MW	18	24	60	40	12	25	23	30	5	10
	Q = 180MVar	63	56		74	38					
I <sub>CT</sub> = 18.2KA											

Table II

Year	Side	Test Location	Mode Frequency (Hz)	Mode Shape
2004	Global modal of exciter side	Nose end	114	ellipse
		Slot exit	113	ellipse
	Global modal of turbine side	Nose end	113	ellipse
		Slot exit	113	ellipse
2005	Global modal of exciter side	Nose end	98.6 ; 115	combined ; ellipse
		Slot exit	114	Approximate ellipse
	Global modal of turbine side	Nose end	114	ellipse
		Slot exit	114	ellipse
2006	Global modal of exciter side	Nose end	114	ellipse
		Slot exit	114	ellipse
	Global modal of turbine side	Nose end	114	ellipse
		Slot exit	114	ellipse

Table III

Year	Side	Test Location	Mode Frequency (Hz)	Mode Shape
2003	Global modal of exciter side	Nose end	92 ; 115	Approximate ellipse ; ellipse
		Slot exit	92.3 ; 115	Approximate ellipse ; ellipse
	Global modal of turbine side	Nose end	92 ; 115	Approximate ellipse ; ellipse
		Slot exit	93.1 ; 115	Approximate ellipse ; ellipse
2005	Global modal of exciter side	Nose end	90.4 ; 114	ellipse ; ellipse
		Slot exit	91.8 ; 114	sway ; ellipse
	Global modal of turbine side	Nose end	91.7 ; 115	ellipse ; ellipse
		Slot exit	91.8 ; 115	ellipse ; ellipse
2008	Global modal of exciter side	Nose end	118	ellipse
		Slot exit	118	ellipse
	Global modal of turbine side	Nose end	117	ellipse
		Slot exit	116	ellipse

Table IV

Lead Location	Natural Frequency (Hz)			Lead Location	Natural Frequency (Hz)		
	radial	axial	tangential		radial	axial	tangential
Top of 11 o'clock (H1)	—	112	112	Bottom of 11 o'clock (H2A)	112	112	—
Top of 1 o'clock (K3A)	112	—	113	Bottom of 1 o'clock (K1)	112	112	112
Top of 3 o'clock (H2)	112	111	—	Bottom of 3 o'clock (H3A)	113	112	—
Top of 5 o'clock (K1A)	112	—	114	Bottom of 5 o'clock (K2)	112	112	110
Top of 7 o'clock (H3)	113	—	—	Bottom of 7 o'clock (H1A)	112	112	—
Top of 9 o'clock (K2A)	112	—	—	Bottom of 9 o'clock (K3)	112	—	—

Table V

Lead Location	Natural Frequency (Hz)			Lead Location	Natural Frequency (Hz)		
	radial	axial	tangential		radial	axial	tangential
Top of 5 o'clock (H1)	119	115	120	Bottom of 5 o'clock (H2A)	118	118	120
Top of 7 o'clock (K3A)	108	109	108	Bottom of 7 o'clock (K1)	110	109	109

Top of 9 o'clock (H2)	118	113	111	Bottom of 9 o'clock (H3A)	118	113	112
Top of 11 o'clock (K1A)	121	113	112	Bottom of 11 o'clock (K2)	112	115	112
Top of 1 o'clock (H3)	114	113	114	Bottom of 1 o'clock (H1A)	119	111	110
Top of 3 o'clock (K2A)	118	108	108	Bottom of 3 o'clock (K3)	118	112	119

Table VI

Lead	Before Retrofit (Hz)						After Retrofit (Hz)						
	Axial			Tangential			Axial			Tangential			
K3A	86	126		86					191	201			
K1	60	65	110	60	65	110			128	189			224
H2	51			51	73		174	86		163			276
H3A	69		168	170	69		108			180	189		
K1A	44	74			61					158		158	222
K2	37				37	80				173			
H3	37	74			37	74				154	191		
H1A	66	97	109		66	97	109		123	128	131		204
K2A	75		135	148		75				166			
K3		98	129			94	129			169	193		
H1	54	69	81		54	69	94		88	146	168		
H2A	54	69	81	94	69	94	105		88		168	186	

(2) Natural frequency of the lead after complete replacement of the stator bars of No1 generator in 2004 is shown in Table IV. Natural frequency of the lead after complete replacement of the stator bars of No2 generator in 2008 is shown in Table V.

### 3.3 Natural frequency of stator end winding lead of generator tbb-1000-2y3 in lianyungang power plant ( table VI )<sup>[10]</sup>

### 3.4 Global modal and vibration amplitudes of generator stator end windings in douhe power plant<sup>[8]</sup>

The natural frequency for the global ellipse of No7 generator stator end winding in Douhe Power Plant is 107~108Hz, and the vibration amplitudes measured during operation are shown in Table VII.

Table VII

P (MW)	50	100	120	140	160	180	200
Q (Mavr)	20	30	35	25	30	30	30
I (kA)	2.0	4.4	4.9	5.5	6.1	6.8	7.5
No1 (μm)	37	41	41	41	45	41	51
No2 (μm)	27	22	25	25	29	22	29
No3 (μm)	57	47	47	35	35	32	41
No4 (μm)	75	186	79	73	91	95	83
No5 (μm)	119	143	146	149	149	140	149

### 3.5 Global modal and vibration amplitudes of two hitachi 600mw generators stator end windings in tuoketuo power plant<sup>[7]</sup>

The natural frequency for the global modal of Hitachi generator stator end windings is shown in Table VIII, and the maximum vibration amplitudes measured during operation are shown in Table IX.

### 3.6 Gb/t 20140—2006: avoiding range of natural frequency for the local and global ellipse of generator stator end windings (see table X)<sup>[4]</sup>

Table VIII

Test Location		Turbine Side			Exciter Side		
Modal Order		1	2	3	1	2	3
No 1	Mode frequency (Hz)	97.52	107.2	132.6	91.9	99.1	110.6
	Mode shape	ellipse	ellipse	irregular	ellipse	ellipse	3 parts
No 2	Mode frequency (Hz)	101.0	110.1		94.3	103.8	
	Mode shape	ellipse	ellipse		ellipse	ellipse	

Table IX

Unit Number	Test Condition	Test Location	Amplitude (peak-peak) $\mu\text{m}$	Time
1	Load 300MW	Bar No 8 at turbine side	120	2003.4.6~20
	Load 450MW	Bar No 8 at turbine side	155	2003.4.6~20
	Load 600MW	Bar No 8 at turbine side	188	2003.4.6~20
2	Load 280MW	Bar No 34 at turbine side	125	2003.7.3~20
	Load 450MW	Bar No 34 at turbine side	150	2003.7.3~20
	Load 600MW	Bar No 34 at turbine side	185	2003.7.3~20

Table X

Rated Speed / ( r/min )	Supporting	Natural Frequency of the Bars /Hz	Natural Frequency of the Leads /Hz	Natural Frequency for Global Ellipse /Hz
3000	stiff	$\leq 95, \geq 106$	$\leq 95, \geq 108$	$\leq 95, \geq 110$
	flexible	$\leq 95, \geq 106$	$\leq 95, \geq 108$	$\leq 95, \geq 112$

#### 4 DISCUSSION ON THE ACCEPTABILITY OF STRUCTURAL DESIGN OF TYPE TBB-800-2EY3 GENERATOR STATOR END WINDING

##### 4.1 The stator end winding support system of type tbb-800-2ey3 generator is acceptable

For type TBB-800-2 generator, test results such as type test<sup>[1]</sup>, in-service vibration endurance test<sup>[2]</sup> and impact endurance test<sup>[3]</sup> were all acceptable. While the two Russia TBB-800-2EY3 generators were manufactured after the first TBB-800-2 generator had put into operation for almost 30 years, and is improved for many times, hence the performance should be better than type TBB-800-2 generator. Therefore, the design of the stator end winding support system of type TBB-800-2EY3 generator is acceptable.

##### 4.2 Natural frequencies for the global modal and the lead of no1 and no2 generator stator end windings in suizhong power plant are acceptable

The natural frequency " $f \leq 93\text{Hz}, f \geq 113\text{Hz}$ " for the global ellipse and " $f \geq 108\text{Hz}$ " for the lead<sup>[5]</sup> of No1 and No2 generator stator end winding in Suizhong Power Plant can meet the demand of natural frequency " $f \leq 95\text{Hz}, f \geq 110\text{Hz}$ " for the global ellipse and " $f \geq 108\text{Hz}$ " for the lead<sup>[4]</sup> by national standard GB/T20140—2006. Therefore, neither of the two generators corresponds with the condition for structural retrofit of generator stator end winding.

##### 4.3 The problems with the stator end windings of no1 and no2 generator in suizhong power plant are not caused by unacceptable design

According to the operation experience of Power Plants in China and overseas, if natural frequency for the global ellipse of large generator stator end windings fall into 100Hz resonance area due to poor design, the problems would be fully exposed in several month or as long as one year, with looseness and erosion of the end winding during operation. But the problems for the stator end windings of TBB-800-2EY3 generator in Suizhong Power Plant appeared after two generators had put into operation for 3~4 years. Therefore the problems with the stator end winding were not due to design.

#### 5 NECESSITY AND IMPENDENCY OF ONLINE MONITORING THE VIBRATION OF 800MW GENERATOR STATOR END WINDING IN SUIZHONG POWER PLANT<sup>[6]</sup>

##### 5.1 Vibration is the criteria of evaluating the acceptability of the structural design of generator stator end winding

Practice proves that even if the stator end winding structure is acceptable in the factory test, the stiffness and strength will change after operating for a few years under a long term 100Hz alternating electromagnetic force, resulting in malignant faults such as insulation abrasion, conductor strands fatigue crack, water leakage, hydrogen leakage and phase-to-phase short-circuit. These faults may be resulted from imperfect design of the stator end winding or other uncertain factors. How to judge? According to theoretic analysis and practical experience, if the vibration amplitude during the operation of end winding is much large than  $250\mu\text{m}$ , and damage occurs in less than one year, and this situation also happened in other units of the same model, we can consider that it is caused by un-

qualified design. Otherwise, it may be caused by other uncertain factors. Therefore, it is very necessary to measure the vibration of the generator stator end winding.

### **5.2 Vibration measurement can avoid huge losses resulted from emergent incident**

Early in 20 years ago, many company such as ABB, GE, WH proposed requirements on the vibration amplitude of generator stator end winding during operation, carried out on-line monitoring and gained relatively successful operating experience. Since the criteria to determine the operation reliability of generator stator end winding is vibration amplitude, it is very crucial to perform on-line monitoring of the vibration amplitude for generators with evident end winding loose, abrasion or ellipse mode shape near 100Hz. Early alarm and condition-based maintenance can be achieved depending on the change of the vibration amplitude during operation, thus emergent fault of the end winding can be avoided and safe and economic operation of the generator can be ensured. The problems that had occurred in the two generators TBB-800-2EY3 in Suizhong Power Plant fully demonstrate the impendency of vibration measurement in the operation of the two generators.

### **5.3 Vibration measurement can avoid mistaken judge and useless retrofit**

In national standard GB/T 20140—2006, term 6.1.1 requires that natural frequency for global ellipse of generator stator end winding should be beyond 95Hz~110Hz for stiff support; term 6.1.2 requires that when natural frequency for global ellipse of a generator is not in the above required range, stator end winding vibration during operation should be measured. Judging from 6.1.1 alone often lead to mistake and useless retrofit of the stator end winding of a generator. Here is an example, in the two 600MW generators<sup>[7]</sup> of Tuoketuo Power Plant newly introduced from Hitachi company and a 200MW domestic generator<sup>[8]</sup> already operating 12 years with frequent trouble in Douhe Power Plant, approximately 100Hz natural frequency for global ellipse exist in the stator end winding. Determination was made based on the discussion of specialists, each generator is equipped with an optical vibration monitoring system by Hitachi and Douhe respectively. The measured vibration amplitudes for the three generators are 188 $\mu\text{m}$ , 185 $\mu\text{m}$  and 178 $\mu\text{m}$  respectively, all of them are less than 250 $\mu\text{m}$ . Therefore, they did not carry out retrofit on the end windings.

### **5.4 Vibration measurement can reduce the risk brought about by the retrofit of generator stator end winding**

Generator stator end winding is a complex, non-linear elastic system. Once design and manufacture are finished, it is very difficult to accomplish a rewind or remanufacturing of the end fixing structure, not only with an expensive cost, but also can not promise a hundred percent success in the existing technology. Therefore, I suggest inviting Russia specialists to reinforce the stator end winding structure by the opportunity of No1 generator maintenance in Suizhong Power Plant, and then measure the vibration by China and Russia specialists together. If the vibration amplitude is less than 250 $\mu\text{m}$  required by national standard GB/T20140—2006, I do not agree to retrofit its end winding structure; If the vibration amplitude is larger than 400 $\mu\text{m}$ , I agree to retrofit its end winding structure after verifying by China and Russia specialists that the vibration is indeed caused by unqualified design of stator end winding. Even if the retrofit is failed, there is no regret.

### **5.5 Vibration measurement can verify the effect of the generator stator end winding retrofit**

In my opinion, vibration measurement must be performed before the retrofit of No1 and No2 generator stator end winding in Suizhong Power Plant. Let us assume that the measured vibration amplitude during operation before retrofit is 100 $\mu\text{m}$ . After retrofit of the stator end winding by Alstom company, if the maximum vibration amplitude of the stator end winding measured during operation (at least one year) exceeded 40 $\mu\text{m}$ <sup>[9]</sup> required by companies such as ABB, we might ask the France for an explanation; If it exceeds Russia measured value 70 $\mu\text{m}$ , we might require the France to deal with it; If it exceeds 100 $\mu\text{m}$  measured before retrofit, we might demand the France to compensate for it. Otherwise, there would be nothing to support our demands.

## **6 ON-SITE TESTING RESULTS AND EXPERTS CONSULTATION REPORT FOR TECHNOLOGICAL RETROFIT OF NO1 GENERATOR STATOR IN SUIZHONG POWER PLANT**

From April to August in 2009, France Alstom carried out a complete retrofit on the No1 generator stator in Suizhong Power Plant. The information in this section comes from the on-site testing results obtained by the author in the process of retrofit of stator end winding of this generator and experts consultation reports<sup>[11]</sup>.

### **6.1 DC resistance of the stator winding**

Standard value: Measured under the cold state, deviation of DC resistance between any two phases which is eliminated influence caused of difference length of connector, shall not be more than 1.5% of least value. Measured after retrofit: 2.46%~2.81%. So it is unacceptable.

### **6.2 Insulation resistance and polarization index of the stator winding**

6.2.1 Insulation Resistance: Larger than 6000MΩ measured before retrofit under ambient temperature; Less than 500MΩ measured after retrofit under ambient temperature, if converting this value to operating temperature, it is less than 24MΩ, so it is unacceptable.

#### **6.2.2 Polarization Index**

Standard value: China 2.0; France 1.5.

Measured before retrofit:4.4; Measured after retrofit: phase A 1.39, phase B 1.56, phase C 1.44, so it is unacceptable.

### **6.3 DC leakage of the stator winding**

Test voltage:72kV; 1min leakage current measured: phase A 1372μA, phase B 903μA, phase C 1218μA. According to associated references and on-sited tests, the leakage current flowing through the winding insulation should be less than100μA. So it is unacceptable.

### **6.4 AC voltage withstanding test of the stator winding**

After retrofit, the insulation of the lead connection located at 9 o'clock position on the exciter side brokedown in the AC voltage withstanding test when the voltage was risen to 39kV. After treatment, when the voltage was risen to 49kV, corona occurred twice, but the position was uncertain. Before the retrofit, there was no this kind of phenomenon in the AC voltage withstanding test at same condition.

### **6.5 Potential of the slot corona protective coating of the stator to ground**

After retrofit, the measured value was larger than 6V; Before retrofit, the measured value was less than 1V.

### **6.6 Surface to ground potential of the hand-wrapped insulation of the stator end winding**

After retrofit, this test is impossible to perform; Before retrofit, this test could be performed.

### **6.7 Partial discharge test of the stator bar**

National standard GB/T 20833—2007 requires that largest apparent discharge quantity limit for single bar under phase voltage should not be larger than 200pC; In the factory test on the Alstom bars, the magnitude for single bar under phase voltage was 1200pC~2000pC. So it is unacceptable.

### **6.8 Quality checking test of large current through the brazing joint of the transition lead of stator winding**

Associated reference and documents in China: Test current (DC) 3000A; Test was performed under a condition without ventilation.

Suizhong-Alstom: Test current (DC) 1000A; Ambient temperature for the test:29°C, with good ventilation; Temperature rise of the brazing point after the test:1°C.

## **6.9 The tightening screw in the stator end winding insulation cracked frequently under static condition**

After retrofit, because the tightening screws in the insulation cracked frequently under static condition, they were entirely replaced on July 24<sup>th</sup>, 2009. But just six days after, one more screw was found to have cracked again. No cracking of tightening screw in the stator end winding had been observed before retrofit.

## **6.10 Installation position of vibration sensor for the stator end winding**

Alstom installed the vibration sensor on the press plate of end winding fixing system; While national standard GB/T 20140—2006 requires that the measuring point should be arranged in the position with largest vibration magnitude according to the test results of stator end winding vibration modal.

## **6.11 Natural frequency for the global ellipse and lead of stator end winding**

Before retrofit, the natural frequency for the global ellipse of stator end winding at both turbine and exciter side was larger than 113Hz, damping was larger than 1.5%; The natural frequency of the lead was larger than 110Hz.

After retrofit, there was 112Hz elliptical mode shape at nose end of turbine side, damping was 0.832; and there was 95.5Hz mode shape, damping was 0.621. The natural frequency of stator end winding was 102~103Hz for most bars at exciter side, and the natural frequency of the lead was 101~102Hz. So it is unacceptable.

## **6.12 Measurement of vibration amplitude of stator end winding during operation (under 100hz )**

Alarm value: Russia 125 $\mu$ m; France 150 $\mu$ m; China 250 $\mu$ m. Normal vibration level of the worldwide large turbogenerators during operation is typically less than 100 $\mu$ m, generally 40 $\mu$ m below.

(1) During no-load test and short circuit test, measured values after retrofit have exceeded the allowable value(100 $\mu$ m) of China factory standards. So it is unacceptable.

(2) With load: When active power is 761.31MW and reactive power is 179.06MVar, maximum amplitude:308.8 $\mu$ m. So it is unacceptable.

## **7 CONCLUSION**

Practice is the only standard to verify the truth. Only when the vibration amplitudes of the No1 and No2 generator stator end winding during operation are measured in Suizhong Power Plant, can we determine whether the end windings need complete retrofit.

## **BIBLIOGRAPHY**

- [1] Khutoretskii G M ,et al.TBB-800-2 Type 800MW Water Hydrogen Cooled Turbo-generator. Power Station, 1976(6):46-52
- [2] Baschkin A G,et al.Research Test on Vibration Endurance of 500MW and 800MW Turbo-generator during Operation.Power Station, 1975(7):31-35
- [3] Khutoretskii G M, et al.Solution on the Vibration Problems of Large Turbo-generator Stator. Electrical Engineering, 1989(2)
- [4] National Standards of Peoples Republic of China. GB/T 20140—2006 Test Method and Evaluation of Dynamic Characteristic and Vibration on stator winding of Turbine Generators ( Come into effect on August 1, 2006)
- [5] Northeast Electric Power Research Institute. Test Reports on the Static Vibration Characteristics of No1 and No2 Generator Stator End Winding in Suizhong Power Plant, 2003-2008
- [6] Bai Y.Practical Significance and Standards of Dynamic Characteristic Test for Generator Stator End Windings. Electrical Equipment, 2003, 4 (1)
- [7] BAI Y, GE H, ZENG F.Technical Measures of Preventing Failure from Stator End-Windings on Imported Two 600MW Turbo-generators.Large Electric Machine and Hydraulic Turbine, 2004, (Z1).

- [8] CHANG Y, ZHENG B, BAI Y, SHEN Li. Research Test of On-line Vibration Monitoring on 200MW Home Turbogenerator Stator End Winding. Large Electric Machine and Hydraulic Turbine, 2002(6)
- [9] Ji A. Testing and Study on the Static Characteristics of End Part Vibration of Generator's Stator Winding. Electrical Equipment, 2004, 5(9)
- [10] SHU X, CHENG F. Improvement of Stator End Windings for TBB-1000 Turbogenerator. Large Electric Machine and Hydraulic Turbine, 2006(1)
- [11] Chinese Society for Electrical Engineering .NanJing ZhongDianXueHui Evaluation of Electrical Safety. Ltd. Safety Consultation Reports of China Shenhua Energy Company Limited Guohua International Power Company Limited Suizhong Power Generation Co., Ltd., 2010.5.21

## **BIOGRAPHY**

Ni Zhiying (Presenting Author), female, born in 1967. Senior Engineer, insulation supervisor of China Shenhua Group Guohua Electric Power Suizhong Power Generation Co., Ltd.

**Impact of Auxiliaries Response on the Voltage Ride Through Capability of  
Synchronous Generator Power Plants**

**L. Díez-Maroto, F. Fernández-Bernal,  
L. Rouco And L. Sigrist  
Universidad Pontificia Comillas  
Spain**

**K. Chan  
Alstom  
Switzerland**

**SUMMARY**

Voltage Ride Through Capability (VRTC) refers to the ability of generators not to trip in case of a fault in the external network. VRTC requirements were firstly imposed to wind generators to cope with massive wind farm tripping following a fault in the external network. They have been subsequently extended to synchronous generators. VRTC has been incorporated to many grid codes worldwide as a voltage-time curve that generators must withstand without tripping. VRTC has been required either at the power plant high voltage bus or at the generator low voltage terminal bus.

A synchronous generator might disconnect from the grid due to either generator loss of synchronism or power plant auxiliaries tripping as a result of severe transmission system voltage transient variations. Power plant auxiliaries can be tripped either by minimum voltage protections to prevent that auxiliaries induction motors block or merely because of low voltage AC contactors drop out.

Assuming that the synchronous generator remains in synchronism after a fault, the paper addresses the problem of power plant tripping due to auxiliaries tripping. The relationship between the VRTC curve and the response of both the auxiliaries and the synchronous generator is studied. Sensitivity analysis with respect to relevant parameters of the auxiliaries is provided.

A fundamental simulation model of the power plant has been developed and is reported. The model includes a detailed representation of the synchronous generator and its controls. In addition, aggregated model of induction motor loads at the medium voltage bus bar of the power plant auxiliaries is considered.

**KEYWORDS**

Power plant auxiliaries, Synchronous generators, Induction motors, Critical clearing time, Grid code, Voltage ride through capability

## 1 INTRODUCTION

This paper studies the impact of auxiliaries' response in the VRTC of synchronous generator power plants assuming that auxiliaries are driven by induction motors. Voltage Ride Through Capability (VRTC) refers to the ability of generators not to trip in case of a fault in the external network. During the last 10 years, Transmission System Operators (TSOs) have incorporated VRTC requirements to grid codes. VRTC requirements were firstly imposed to wind generators to cope with massive wind farm tripping following a fault in the external network. They have been subsequently extended to synchronous generators. Hence, grid codes have added new requirements with respect to what IEC 0 and IEEE 0 standards demand to cylindrical rotor generators.

VRTC has been established as a time-voltage curve (rectangular or polygonal) which must be withstood by generators. VRTC is required either at the power plant high voltage bus or at the generator low voltage terminal bus. A number of studies have pointed out the wide variety of VRTC requirements found in grid codes worldwide and the need of grid code harmonization (0, 0). A very consistent formulation of the VRTC requirement can be found in the French grid code 0. It consists of assuming a solid fault at the power plant high voltage bus (rectangular time-voltage curve) and requiring that the voltage at the generator low voltage bus is above a polygonal time-voltage curve as approximate approach to ensure that the power plant does not trip because of auxiliaries tripping.

This paper discusses the accuracy of the VRTC requirement at the generator low voltage terminal bus to ensure that the power plant does not trip because of auxiliaries tripping. The paper assumes that auxiliaries will trip if the induction machines that drive the auxiliaries lose stability. The paper also studies the sensitivity of the power plant response to several parameters of the auxiliaries' model. The paper is organized as follows: section 0 discusses high voltage and low voltage formulations of VRTC requirements; section 3 assesses the impact of power plant components on the VRTC of power plant (auxiliaries, synchronous generator) and the plant as a whole; section 0 provides the results of a sensitivity study with respect to the several auxiliaries parameters; the conclusions of the study are summarized in section .

## 2 HIGH AND LOW VOLTAGE RIDE THROUGH CAPABILITY

VRTC is referred as the ability of generators to withstand a time-voltage variation without tripping from the network. The time-voltage curve can be either rectangular or polygonal. The recovery voltage is sharp in the rectangular time-voltage curves. English, Irish, French and Italian grid codes require a rectangular time-voltage curves. English and Irish grid codes incorporate a multi-dip requirement whereas French and Italian ones have a single-dip one. The multi-dip requirement of the English code results from the consideration of an explicit voltage-fault duration curve. The recovery voltage is smoother in polygonal time-voltage curves. The shape of recovery voltage in the polygonal time-voltage curves results from enveloping recovery voltages obtained from a number of simulations and measurements. German, Scandinavian, Spanish and American grid codes require polygonal time-voltage curves.

We have already shown that typical round rotor synchronous generators cannot withstand any of polygonal time-voltage variation at the high voltage bus required by grid codes 0. In other words, requiring High Voltage Ride Through Capability would not be feasible. Hence, we propose to consider the interpretation of the French grid code that considers a rectangular time-voltage variation at the high voltage bus and requires that the voltage of the generator low voltage bus to be above the polygonal time-voltage curve. We will call such interpretation Low Voltage Ride Through Capability. Fig. 1 compares high and low voltage ride through capability requirements.

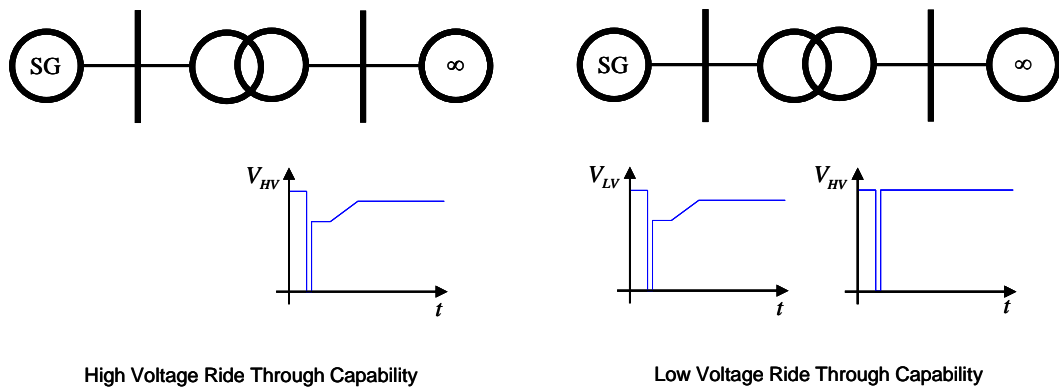


Fig. 1: High and low voltage ride through capability.

### 3 POWER PLANT RESPONSE TO A FAULT

This section studies the Low Voltage Ride Through Capability (LVRTC) of a synchronous generator power plant. The response of a power plant to a rectangular time-voltage variation at the power plant high voltage bus is determined and the voltage at the synchronous generator low voltage terminal is checked with respect to a polygonal time-voltage curve. In fact, the voltage at the synchronous generator low voltage bus will be checked with respect to the time-voltage required by the German grid code 0 as it is one of the most demanding ones.

A fundamental model of a power plant has been developed for this purpose. The single-line diagram of the power plant model is depicted in Fig. 2. The power plant comprises a synchronous generator connected to the grid through a step-up transformer and an induction motor connected to the synchronous generator terminal bus through a step-down transformer. The induction motor results from aggregating the large induction motors connected at medium voltage level (typically at 6 kV). We have neglected the effect of small induction motors connected at low voltage level (typically at 400 V).

A typical round rotor synchronous generator equipped with a bus fed static excitation system and a speed deviation power system stabilizer is considered. A turbine supplying constant mechanical power throughout the transient has been assumed. A typical induction motor has also been taken into consideration. We have considered that the rating of both the step-down transformer and the induction motor is 5% of the rating of the synchronous generator and the step-up transformer. The motor load torque has been assumed to be proportional to the square of the rotor speed. The start-up current of the induction motor is 5 pu.

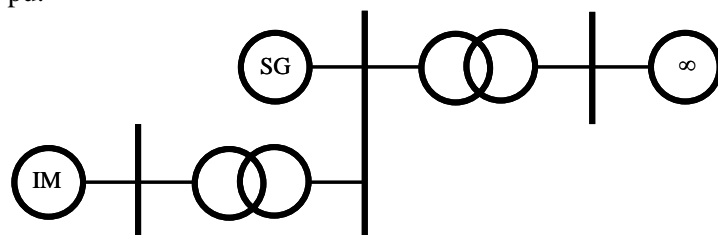


Fig. 2: Power plant model.

Three cases are explored when a rectangular time-voltage variation occurs at the power plant's high voltage bus to identify the influence of each power plant component on the voltage at synchronous generator low voltage bus recovers after the fault clearing. The first and the second cases study the response of the induction motor alone and the synchronous generator alone respectively. The third case analyzes the response of the power plant as a whole. All the cases investigated only the electromechanical response of the modeled components.

### Induction motor response

The response of the induction motor alone is studied firstly. If a fault occurs at the power plant high voltage bus, the rotor of the induction motor can block depending on the fault duration. During the fault, the induction motor rotor brakes and the slip increases. The longer the fault, the more the slip increases. If the slip is greater than the slip corresponding to the pull out torque, the current becomes the short circuit current. After the fault clearing, the short circuit current results in high voltage drops in the transformers and low voltages at the machine terminals. If the fault clearing time is smaller than the fault critical clearing time, the induction motor will be able to come back to pre-fault operating conditions.

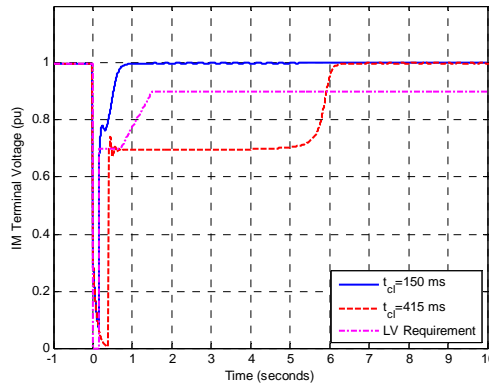


Fig. 3: IM response (terminal voltage) to a fault at power plant HV bus.

Fig. 3 displays the induction machine terminal voltage in case of the fault duration required by the German grid code (150 ms) and in case of the critical clearing time of the fault (415 ms). The time-voltage curve required of the German grid code is also displayed. If the fault clearing time is just 150 ms, the terminal voltage is above the time-voltage curve required. However, the power plant auxiliaries alone can theoretically withstand a fault of 415 ms despite the fact that the machine terminal voltage is below the time-voltage curve required. In practice, motors are specified to operate only for a short-time (1 to 2 s) below a certain voltage level.

A simple equivalent circuit can be considered to estimate the induction motor terminal voltage during the reacceleration process once the fault has been cleared. The detailed simulation informs that the induction motor terminal voltage during the reacceleration process is 0.696 pu. Taking into consideration that the voltage at high voltage bus in the pre-fault conditions is 1.046 pu, the equivalent circuit of Fig. 4 estimates that the induction motor terminal voltage during the reacceleration process is 0.655 pu.

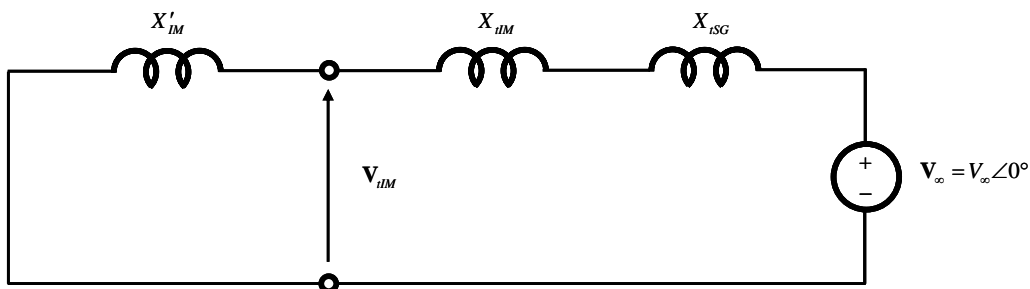


Fig. 4: Equivalent circuit to estimate the IM terminal voltage during IM reacceleration process.

### Synchronous generator response

The response of the synchronous generator alone is addressed secondly. If a fault occurs at the power plant high voltage bus, the rotor of the synchronous generator accelerates because the electromagnetic torque becomes very small whereas the mechanical torque remains constant. If the fault clearing time

is smaller than the fault critical time, the synchronous generator will be able to come back to pre-fault operating conditions.

Fig. 5-left depicts the synchronous generator terminal voltage in case of the fault duration required by the German grid code (150 ms) and in case of the critical clearing time of the fault (285 ms). The time-voltage curve required of the German grid code is also displayed. If the fault clearing time is just 150 ms, the terminal voltage is above the time-voltage curve required. However, the synchronous generator can withstand a fault of 285 ms despite the fact that the machine terminal voltage is below the time-voltage curve required.

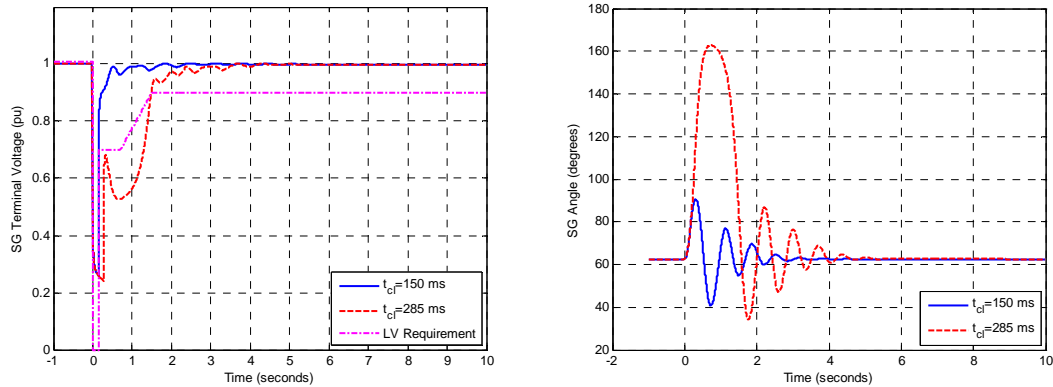


Fig. 5: SG response (left-terminal voltage and right-angle) to a solid fault at power plant HV bus.

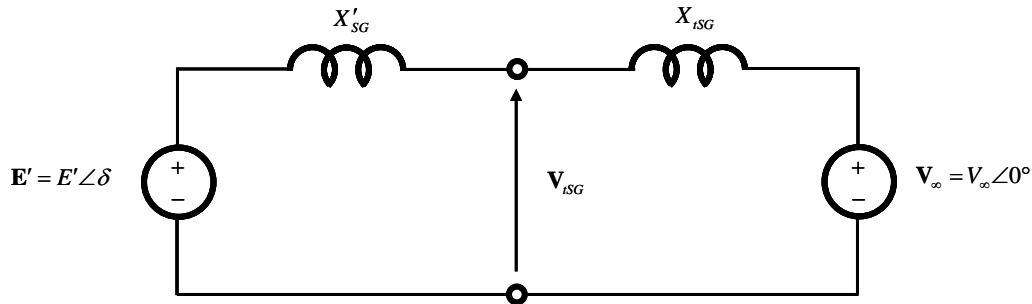
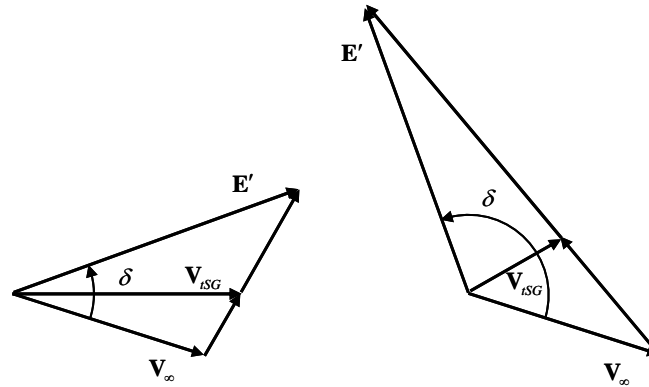


Fig. 6: Equivalent circuit to estimate the SG terminal voltage during SG deceleration process.

A simple equivalent circuit can also be considered in this case to estimate the synchronous terminal voltage during the deceleration process after the fault clearing. The detailed simulation informs that the maximum rotor angle is  $163^\circ$  (see Fig. 5-right). The equivalent circuit of Fig. 7 estimates that the synchronous generator terminal voltage at the maximum rotor angle is 0.358 pu whereas the detailed simulation informs that the minimum synchronous generator terminal voltage is 0.530 pu. The vector diagram Fig. 7 corresponding to the equivalent circuit shows that the synchronous terminal voltage variation is due to the rotor angle variation. In other words, the higher rotor angle, the lower terminal voltage.



**Fig. 7: Effect of the load angle variation on the terminal voltage variation. Left: vector diagram at  $t=0$  and right: vector diagram at  $t$ .**

### Power plant response

Terminal voltage variation after the fault clearing of induction motors and synchronous generators is dictated by different physical mechanisms. The response of power plant as a whole is determined and the dominant mechanism is investigated. A power plant is stable, from a theoretical point of view, if both the synchronous generator remains in synchronism and the induction motor does not block after a fault.

The critical clearing time of the power plant is 265 ms. It should be noted that if the clearing time were 285 ms, the synchronous machine would remain in synchronism while the induction motor would block. Auxiliaries modeling have resulted in lower power plant critical clearing time. Fig. 8-left shows the terminal voltage of both machines together with the time-voltage curve required of the German grid code. Fig. 8-right displays the speed deviation of the synchronous generator and the slip of the induction motor. The power plant is stable in case of a 265 ms fault despite the fact that terminal voltages are below the required time-voltage curve. In practice, operation of the power plant is much more complex and further constraints are imposed by plant processes (e.g. oil, water and gas pressures, etc) that further limit the stability of the power plant under fault conditions. These have not been considered in the analyses.

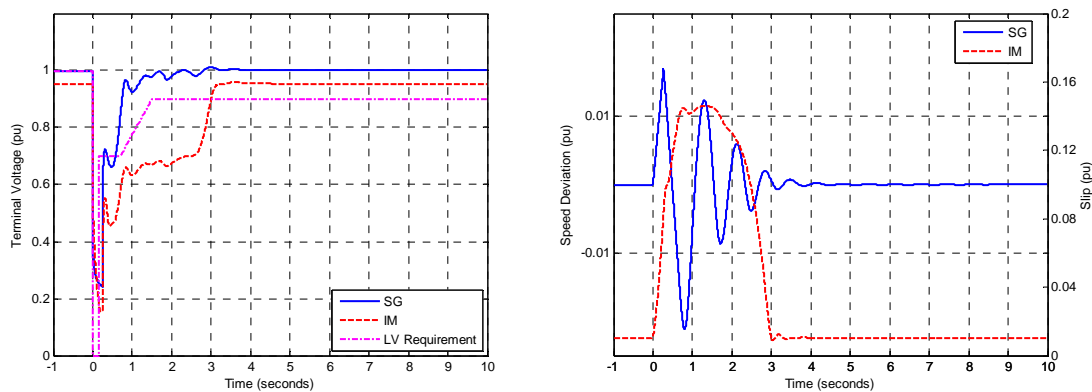


**Fig. 8: Power plant response (left-machine terminal voltages and right- machine speeds) to a 265 ms solid fault at power plant HV bus.**

## 4 SENSITIVITY STUDY

This section studies the sensitivity of the power plant response with respect to several parameters of the power plant auxiliaries. The sensitivity with respect to size of the auxiliaries, the induction motor start-up current and the load characteristic is provided.

### Sensitivity with respect to auxiliaries size

Depending on the technology, the power plants auxiliaries have different sizes. Typically the size of the auxiliaries, as a fraction of the power plant rating, varies from 2.5% in case of combined cycle gas turbine (CCGT) power plants to 7.5% in case of nuclear power plants. Three auxiliaries sizes have been checked: 2.5%, 5% and 7.5%. The critical clearing time of a solid fault at the power plant high voltage bus is not affected by the auxiliaries' size: it is 265 ms in all cases. Fig. 9 shows the synchronous machine terminal voltage. The synchronous machine terminal voltage is minimally affected by the auxiliaries' size.

### Sensitivity with respect to induction motor start-up current

The start-up current is a relevant parameter of induction motors. Hence, the sensitivity of the power plant critical clearing time with respect to the start-up current is determined. The case of an induction motor having a start-up current of 10 pu has been considered in addition to the case of an induction motor with start-up current of 5 pu as considered throughout the paper. Table I provides the sensitivity of the power plant critical clearing time in the considered cases. Higher induction motor start-up current has resulted in higher power plant critical clearing time.

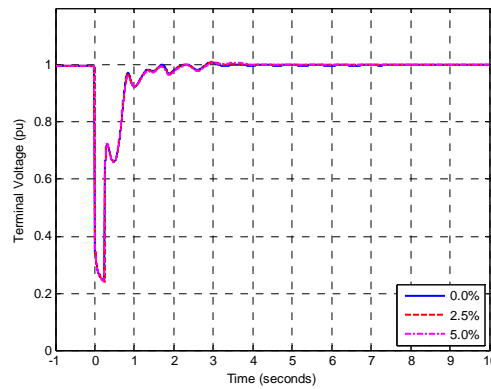


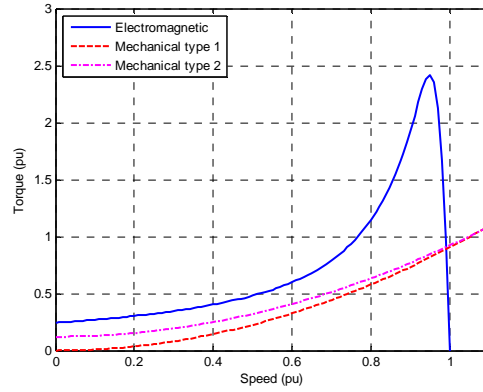
Fig. 9: Sensitivity of power plant response (synchronous generator terminal voltage) with respect to auxiliaries size in case of the power plant critical clearing time (265 ms).

Table I: Sensitivity of the critical clearing time with respect to auxiliaries size and start-up current.

Start-up current (pu)	Size (%)		
	2.5	5	7.5
5	265	265	265
10	285	285	285

### Sensitivity with respect to mechanical load characteristic

The induction motor mechanical load characteristic also affects the response of induction motors after a fault. The induction motor response has been evaluated assuming a mechanical torque proportional to the square of the speed and zero mechanical torque at zero speed. A more demanding mechanical load requires non-zero mechanical torque at zero speed. We have actually considered a mechanical load characteristic that requires half of the induction motor starting torque at zero speed. Fig. 10 displays the two mechanical load torque characteristics proposed together with the electromagnetic torque characteristic of the induction motor considered.



**Fig. 10: IM torque characteristics.**

Table II provides the sensitivity of the power plant critical clearing time in the considered cases. Non zero mechanical torque at zero speed load characteristic slightly affects the critical clearing time of a fault at the high voltage bus of the power plants.

**Table II: Sensitivity of the critical clearing time with respect to mechanical load characteristic.**

Mechanical load type	Size (%)		
	2.5	5	7.5
1	265	265	265
2	260	260	260

## 5 CONCLUSION

Low Voltage Ride Through Capability (LVRTC) of synchronous generator power plants requires that the synchronous generator terminal voltage is above a required time-voltage curve. The stability of a power plant as a whole requires that both the synchronous generator and the induction motors that drive the auxiliaries are stable in case of a fault at the power plant high voltage bus: the synchronous generator does not lose synchronism and induction motors do not block.

The synchronous generator may be stable despite the fact that the terminal voltage is below the required time-voltage curve. The modelling of auxiliaries affects the power plant critical clearing time. Several parameters of auxiliaries (start-up current and mechanical load characteristic) slightly affect the power plant critical clearing time.

LVRTC requirement in terms of a time-voltage curve is not suitable to assess the stability of a power plant. Power plant stability should be required in terms of the clearing time of a fault at the high voltage bus. Power plant response should be determined using detailed models of the power plant.

Finally, it must be pointed out that power plant operation is complex and the stability depends also to a large extent on the plant processes that impose constraints that are not only electromechanical in nature but a related to oil, water, gas pressures as well as temperatures. These additional constraints have not been considered in the paper.

## 6 REFERENCES

- [1] International Electrotechnical Commission. International Standard, Rotating electrical machines, Part 3: Specific requirements for synchronous generators driven by steam turbines or combustion gas turbines. IEC Standard 60034-3, Edition 6.0, 2007-11
- [2] IEEE. IEEE Standard for Cylindrical-Rotor 50 Hz and 60 Hz Synchronous Generators Rated 10 MVA and Above. IEEE Standard C50.13-2005

## 6 REFERENCES

- [1] International Electrotechnical Commission. International Standard, Rotating electrical machines, Part 3: Specific requirements for synchronous generators driven by steam turbines or combustion gas turbines. IEC Standard 60034-3, Edition 6.0, 2007-11
- [2] IEEE. IEEE Standard for Cylindrical-Rotor 50 Hz and 60 Hz Synchronous Generators Rated 10 MVA and Above. IEEE Standard C50.13-2005
- [3] Rouco L, Ginet C, Chan K, Major K, Malcher O, Díez-Maroto L, Cherkaoui R. Improvement of the voltage ride through capability of synchronous generators by excitation control[C] // 43 Cigré Session 43, Paper A1-106, Paris (France), 22-27 August 2010
- [4] Hulle F V, Christensen W, Seman S, Schulz V. European Grid Code Development – the Road towards Structural Harmonization. Proceedings of the 9th International Workshop on Large-Scale Integration of Wind Power into Power Systems as well as on Transmission Networks for Offshore Wind Power Plants, Québec City (Québec, Canada), 18 - 19 October 2010
- [5] EWEA Working Group on Grid Code Requirement. Position Paper on European Grid Code Requirements for Wind Power Generation”, Brussels, February 2008. [http://www.ewea.org/fileadmin/ewea\\_documents/documents/publications/position\\_papers/080307\\_WGGCR\\_final.pdf](http://www.ewea.org/fileadmin/ewea_documents/documents/publications/position_papers/080307_WGGCR_final.pdf).
- [6] RTE Gestionnaire du Réseau de Transport D'Electricité. Documentation technique du reference. 24 avril 2009. [http://clients.rte-france.com/htm/fr/mediatheque/telecharge/reftech/24-04-09\\_complet.pdf](http://clients.rte-france.com/htm/fr/mediatheque/telecharge/reftech/24-04-09_complet.pdf).
- [7] VDN. Transmission Code 2007 Network and System Rules of the German Transmission System Operators. August, 2007. [http://www.vde.de/de/fnn/dokumente/documents/transmissioncode%202007\\_engl.pdf](http://www.vde.de/de/fnn/dokumente/documents/transmissioncode%202007_engl.pdf). P. Kundur . Power System Stability and Control: Mc Graw Hill, 1994

## 7 ACKNOWLEDGEMENTS

The work reported in this paper has been developed in the context of a joint research project developed by Alstom and Universidad Pontificia Comillas. Several Alstom individuals have provided considerable support to that research effort. I. El-Merdaoui, O. Malcher and J. Menzel are gratefully acknowledged.

---

**The Conditional Diagrams Between the Electric Generator  
and the Electric Grid to Which it is Connected**

**R. Zlatanovici, D.Zlatanovici, C.Cicirone, S.Dumitrescu**  
**Energy Research And Modernisation Institute - ICEMENERG**  
**Romania**

**SUMMARY**

This article presents five types of important diagrams with the parameters of electric generators and the parameters of the electric grid to which they are connected. The PQ diagram (active power – reactive power) of electric generators is an important tool for the use of electric generators connected to an electric grid. The PQ diagram defines the operating region of a generator in the P – active power and Q- reactive power space, while connected to an electric grid. The space is conditioned on one side by the parameters of the generator and on the other side by the parameters of the transport grid. Also, secondary zones for the voltage regulation system service are outlined in this space. There is a theoretical PQ diagram, and on-line PQ diagram and a real PQ diagram. The  $Q_{\text{generator}} - U_{\text{grid}}$  diagram (generator reactive power – grid voltage) represents the power variation curves of the reactive power generated or absorbed by the generator as a function of the grid voltage in the connection point, for various constant parameters of the generator (rotor current, stator current, output voltage, internal angle). The entire family of curves defines the operating region of the generator as the reactive power as a function of the grid voltage. The  $U_{\text{grid}} - \cos\varphi_{\text{generator}}$  diagram (grid voltage – generator power factor) shows the operating region of the generator at nominal power or different power when the grid voltage and generator and network power factor are varied. This region is bounded by the minimum and maximum grid voltage, the inductive and capacitive power factor bounds, the maximum and minimum output voltage of the generator and the bounds of the stator and nominal excitation currents.

The  $U_{\text{generator}} - f_{\text{grid}}$  diagram (generator voltage – grid frequency) shows the operating condition of the generator in the rated frequency domain of the grid to which it is connected. The domain is bounded by the rated normalized generator voltage and grid frequency at the connection point. The  $P_{\text{generator}} - f_{\text{grid}}$  diagram (generator power – grid frequency) is an availability curve for a generator to reduce its output power when operating with an already low grid frequency. This diagram represents the operating condition of the generators in the extended domain of the frequency of the network.

The article presents the theoretical fundamentals for each diagram, as well as an example for a 210MW turbogenerator connected to a 220kV grid through a 250MW transformer.

**KEYWORDS**

Diagrams, Electrical generator, Grid, Power, Voltage, Frequency

# 1 THE P-Q DIAGRAM

The P-Q active – reactive power diagram of the synchronous generators is a synthetic diagram that delimits the admissible operational field of the machines.

The diagram has been developed in the P – active power and Q – reactive power coordinates and is valid for the rated values of the active power, voltage at the generator terminals, stator current, field current, frequency and parameters of the cooling agent (temperature, pressure). The modification of one of these parameters leads to the modification of the PQ diagram, by increasing or diminishing the admissible operational field.

Operation in an inductive regime is conditioned by the field current limit and the stator current limit determined from the condition of non-surpassing the admissible temperatures. The inductive limit is obtained through a calculation where the rated parameters, including the synchronous reactances of the generator, are included.

Operation in a capacitive regime is conditioned by the supplementary electrical losses in the frontal zone of the stator, the stator teeth respectively (the first sheets packs with retracted steps). The capacitive limit is determined experimentally or is replaced by the natural static stability curve (the  $dP/d\theta$  criterion) of the generator, in general with a 10% reserve and by the limit of the minimum field current. But a safe limit, not dangerous for the generator, is the one determined experimentally.

The electromagnetic and thermal phenomena that occur in the generator during operation in a capacitive regime influence exclusively the frontal zone of the stator. In the conditions of a capacitive regime, the magnetic reaction, being a magnetizing one, produces an increase in the leakage flux in the end zone area of the machine and, therefore, an important axial magnetic flux component occurs. This flux gets into the terminal stator teeth where it generates eddy currents that, in the end, produce a high heating of these teeth. Due to saturation, only the stator teeth at the stator ends are affected.

There are several types of PQ diagrams: the theoretical PQ diagram, determined for the rated parameters defining it, the on-line PQ diagram whose defining parameters are taken over directly from the process, the actual PQ diagram, whose defining quantities are the temperatures.

## 1.1 The theoretical PQ diagram

The theoretical PQ diagram is a synthetic electric diagram which delimits the admissible operating field of the generator, determined by its rated parameters (terminal voltage, active power, power factor) and by its designed constructive parameters (geometrical dimensions, specific loads etc).

The theoretical PQ diagram derives from the phasor diagrams of the synchronous machine with cylindrical rotor – turbo generators (Fig.1) and of the machine with salient poles – hydro generators (Fig.2) where the RI voltage drop is neglected.

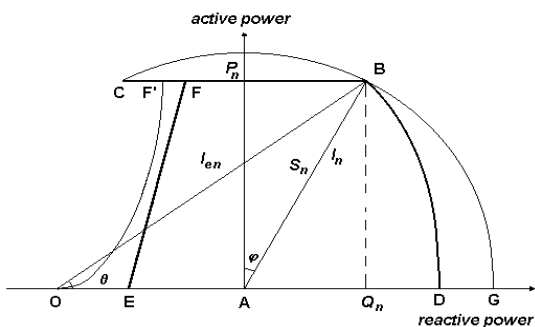


Fig. 1 Theoretical PQ diagram of a turbo-generator

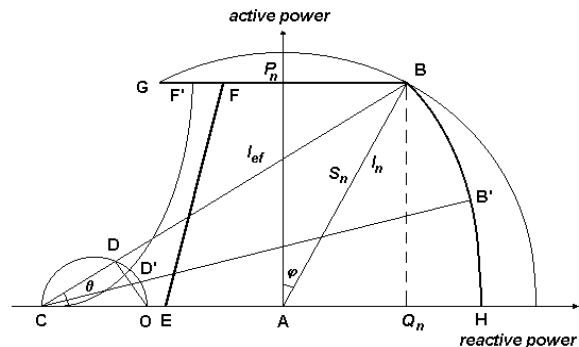


Fig. 2 Theoretical PQ diagram of a hydro-generator

The basic equations of the PQ diagram for the generator are obtained starting from the phasor diagram:

$$P = \frac{U E_d}{x_d} \sin \theta + \frac{U^2}{2} \left( \frac{1}{x_q} - \frac{1}{x_d} \right) \sin 2\theta \quad Q = \frac{U E_d}{x_d} \cos \theta + U^2 \left( \frac{1}{x_q} - \frac{1}{x_d} \right) \cos^2 \theta - \frac{U^2}{x_d} \quad (1)$$

where:

$E_d$  - longitudinal electromotive force

$\theta$  - generator internal angle

$x_d, x_q$  - synchronous longitudinal and transversal reactance

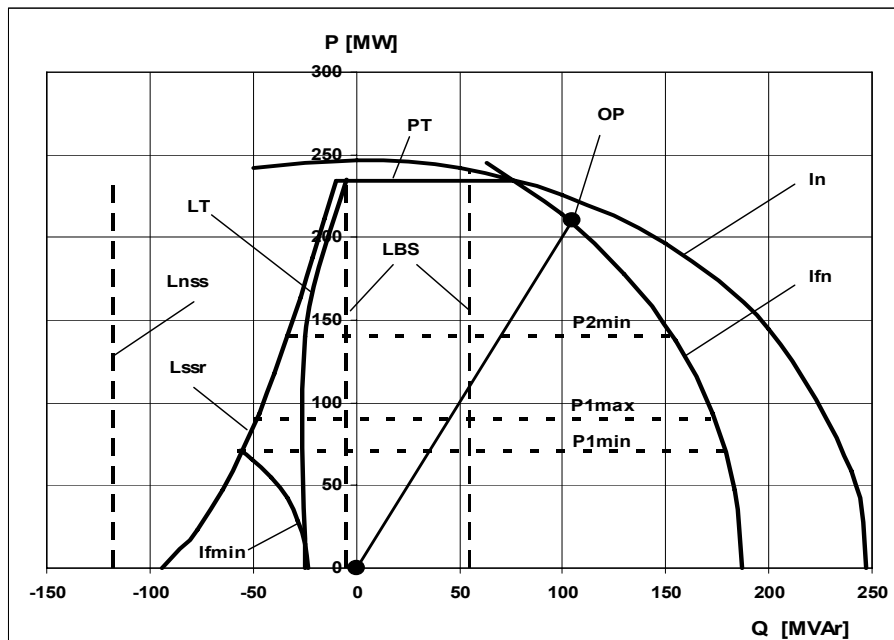
### 1.2 The actual PQ diagram

The actual PQ diagram is, in fact, a thermal diagram where the main theoretical curves represent isotherms of maximum admissible temperatures of different active parts of the electric generator. Thus, the limit of the stator current represents the stator isotherm, the limit of the field current represents the rotor isotherm, the limit under capacitive regime conditions represents the isotherm of the frontal teeth and the limit of the turbine power represents the rated power isotherm. In the ideal case, that of the new generators or that of those that have operated under easier operating conditions, the two diagrams are practically identical. The only difference that must be mentioned may occur in the capacitive regime, where, in the case of hydro-generators, the thermal limit of the frontal zone is in general more restrictive than the natural static stability limit with reserve and vice versa, for turbo-generators.

In the case of the generators that have operated for long time (great number of operation hours) and especially in the case of those functioning under hard operating conditions (only peak load operation, or operation under frequency-power regulation conditions), the two diagrams are no longer identical. The actual PQ diagram becomes more restrictive due to the ageing of the sensitive elements of the generator: the stator winding, rotor winding, stator core, coolers, etc. Thus, loosening the winding consolidation, contact between the rotor turns, loosening of the stator core, cooler clogging, increase in the vibration level, cavitation phenomena, etc may appear. The actual diagram can be determined only experimentally.

### 1.3 The on-line PQ diagram

The on-line PQ diagram is the PQ actual diagram where all the defining parameters are directly acquired from the process and the current position of the operation point at every time is also shown (Fig.3). The parameters acquired from the process that vary during operation are: the active and reactive powers, the field current, the terminal voltage, the value of temperature and pressure (there where necessary) of the cooling agent required by the generator and the frequency of the grid.



$L_{nss}$ - natural static stability limit;  $L_{ssr}$ - static stability limit with 10% reserve; LT-thermal limit in capacitive mode; LBS-secondary bands limit; PT- turbine power;  $I_n$ - nominal stator current;  $I_{fn}$ - nominal field current;  $P_{min}, P_{max}$  - minimum, maximum generator power

**Fig. 3 The actual on-line PQ diagram for the 235 MW turbo-generator**

## 1.4 The voltage control ancillary service

One of the important ancillary services is voltage control of the transport grid. This control is performed by means of the production or absorption of reactive power by the generators connected to the respective grid according to their PQ diagrams. The National Energy Regulatory Agency imposed the delimitation of two types of bands in the PQ diagram of the electric generators:

- The primary band of the voltage control, defined as the zone in the PQ diagram of a synchronous generator where the produced or absorbed reactive energy is not paid for;
- The secondary bands of the voltage control, defined as the zones in the PQ diagram where the production and absorption of reactive energy is made at high costs and great generator stress and where the reactive energy, produced or absorbed at the express request of the TSO is paid for.

In Europe, the issue has not been unitary regulated yet and each country applies its own system.

In some countries there are imposed inductive and capacitive power factors, delimiting the field in the PQ diagram inside which the produced /absorbed reactive energy is not paid for; outside this field, up to the PQ diagram limits, the produced /absorbed reactive energy is paid for. The value of the inductive power factor varies between 0.85 – 0.928, and the capacitive one between 0.95 – 0.989.

## 2 THE $Q_g U_r$ DIAGRAM

The  $Q_g U_r$  diagram (generator reactive power – grid voltage) represents the variation curves of the reactive power produced or absorbed by the generator versus the electric grid voltage in the transformer connection point for certain constant parameters of the generator ( $I_r, U_g, I_g, \theta$ ). The entire curve family defines the operation range of the generator from the point of view of the reactive power versus the grid voltage.

The determination of this diagram is made on the basis of an equivalent electric scheme in  $\Pi$  of the transformer (Fig. 4).

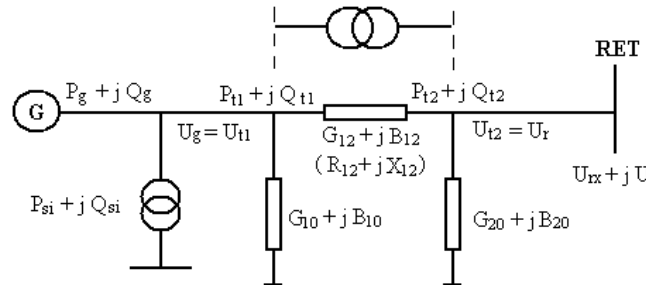


Fig. 4 Equivalent scheme in  $\Pi$  for the calculation of the QU diagrams

Taking into account the powers generated by the generator at the terminals, the primary voltage of the transformer (equal to the voltage at the generator terminals and considered as phase origin in the following calculations), the powers absorbed by the internal services transformer  $P_{si}$  and  $Q_{si}$  and on the basis of the above given equivalent scheme of the transformer, there result the following relationships:

$$\begin{aligned}
 \overline{U_r} &= U_{rx} + j U_{ry} & \overline{U_g} &= U_{gx} + j U_{gy} \\
 U_{rx} &= U_g (1 + R_{12} G_{10} + X_{12} B_{10}) - \frac{P_{t1} R_{12} + Q_{t2} X_{12}}{U_g} & U_{gx} &= U_r (1 + R_{12} G_{20} + X_{12} B_{20}) + \frac{P_{t2} R_{12} + Q_{t2} X_{12}}{U_r} \\
 U_{ry} &= U_g (X_{12} G_{10} - R_{12} B_{10}) + \frac{-P_{t1} X_{12} + Q_{t2} R_{12}}{U_g} & U_{gy} &= U_r (X_{12} G_{20} - R_{12} B_{20}) - \frac{-P_{t2} X_{12} + Q_{t2} R_{12}}{U_r} \\
 P_{t1} &= P_g - P_{si} & Q_{t1} &= Q_g - Q_{si} \\
 P_{t2} &= U_g (U_{rx} G_{12} - U_{ry} B_{12}) - U_r^2 (G_{12} + G_{20}) & Q_{t2} &= U_g (U_{rx} B_{12} + U_{ry} G_{12}) - U_r^2 (B_{12} + B_{20}) \\
 P_{t1} &= U_r (X_{12} G_{12} - U_{gy} B_{12}) + U_g^2 (G_{12} + G_{10}) & Q_{t1} &= -U_r U_{gx} B_{12} + U_{gy} G_{12} - U_g^2 (B_{12} + B_{10})
 \end{aligned} \tag{2}$$

where :

- RET- electricity transmission network
- r , g - network, generator value index
- B, G, X, R - equivalent susceptance, conductance, reactance, resistance
- P, Q – active, reactive power

Besides these relationships, the relationships (1) expressing the active and reactive powers of the generator versus the internal angle and the electromotive force under steady state regime are also considered.

Fig. 5 presents the  $Q_g U_r$  diagram for the 235 MW turbo-generator connected to the 220 kV grid.

By means of the relationships (2) the following types of curves can be developed in the  $Q_g - U_r$  plane:

- the curves  $U_r = f(Q_g)$  for  $U_g = \text{const}$  and for the extreme levels of the delivered active power ( $P_{\text{max}}$  and  $P_{\text{min.technic}}$ ), delimiting on the ordinate  $U_r$  the generator admissible operating zone, required by the admissible range for the voltage at the generator terminals ( $U_{gn} \pm 5\%$ ).
- The curve  $U_r = f(Q_g)$  for the stator current  $I_g = I_{gn} = \text{const}$ . delimiting a range from the point of view of the stator winding heating, if it is considered that  $P_{t1} = P_{gn}$ . For each value of the delivered reactive power  $Q_g$  on the diagram the terminal voltage is calculated.
- The curve  $U_r = f(Q_g)$  for the internal angle of the generator  $\theta = \text{const}$  and for the maximum level of the generator active power  $P_g = P_{g,\text{max}}$  that delimits the maximum admissible range for the generator, both from the point of view of static stability and stator frontal side heating in underexcited regime.. The maximum theoretical value for  $\theta$  from the point of view of static stability is 90 electrical degrees. Though, the maximum admissible value for the internal angle  $\theta$  is of about  $60^\circ - 80^\circ$ .

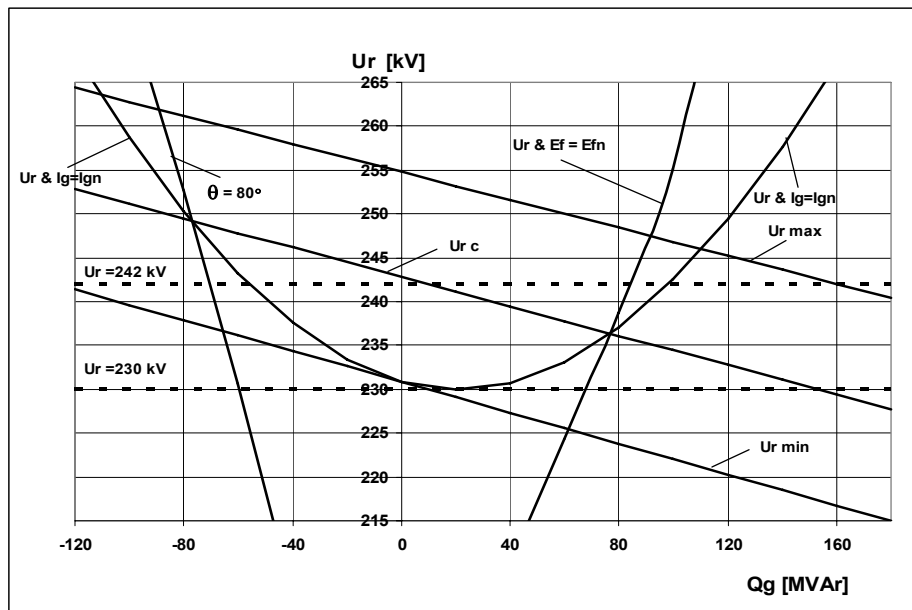


Fig. 5  $Q_g U_r$  diagram for the 235 MW turbo-generator

The curve  $U_r = f(Q_g)$  for a constant value of the generator field current, namely the rated current  $I_f = I_{fn} = \text{const}$ , corresponding to the rated value of the internal electromotive force of the generator  $E_d = E_{dn}$  and for the maximum level of the generated active power  $P_g = P_{gn}$ . This curve delimits the maximum operating range of the generator in the overexcited regime zone, imposed by the rotor winding heating reasons. From formulas 1 there results the relationship for the calculation of electromotive force  $E_d$ , a parameter which is directly proportional to the generator field current  $I_f$

The  $U_{rc}$  line represents the line corresponding to the current terminal voltage. This line translates upwards and downwards according to the terminal voltage. The operation point in coordinates  $(Q_g U_{ri})$

can move along this curve within the network admissible voltage range of  $230 \div 242$  kV, marked with dot lines in the diagram.

### 3 THE $U_r \cos \phi|_g$ DIAGRAM

Usually, the generators are connected to the network through a transformer. The generators standards require a  $\pm 5\%$  voltage range on the low voltage side. The grid codes include requirements for the grid voltage in the connection point. Some transformers are not provided with tap changers for the modification of the transformer ratio. In these cases the transformer ratio is constant and it is not possible to adapt the generator voltage to the grid voltage during long time operation. Other transformers are provided with taps that can be changed only in the absence of voltage or under load.

In these cases it is possible to regulate the generator voltage according to the grid voltage during long time operation. In order to underline the on-load dependence between the generator power factor and the grid voltage, the  $U_r \cos \phi|_g$  diagram is used (Fig.6).

For the calculations, the same relationships written for the scheme in Fig. 6 are used. In fact, the points in these diagrams can be calculated simultaneously with those in diagrams  $Q_g U_r$ . There will result the same types of curves in the same conditions:  $U_r = f(\cos \phi|_g)$  for  $U_g = \text{const}$ , for  $I_g = I_{gn} = \text{const}$ , for  $\theta = \text{const}$  and for  $I_f = I_{fn} = \text{const}$ .

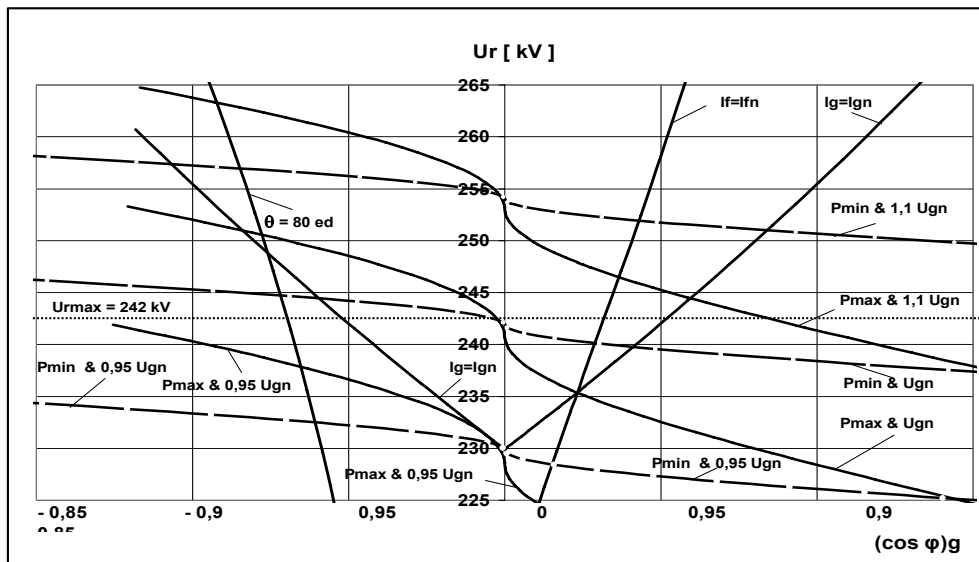


Fig. 6  $U_r = f(\cos \phi|_g)$  diagram of the 235 MW turbo-generator connected to the 220 kV grid

### 4 THE $U_g f_r$ DIAGRAM

The diagram  $U_g f_r$  (generator voltage - grid frequency) is a general diagram, valid for all the electric generators. This diagram represents the operating conditions of the generators in the frequency standardized range of the grid to which it is connected to.

Thus, each generator should be able to supply the rated active power at the rated power factor under continuous operation conditions, within  $\pm 5\%$  ( $0,95$  and  $1,05$ )  $U_N$  voltage limits and  $\pm 2\%$ , ( $49$  and  $51$  Hz) frequency limits as they are defined by the interior polygon  $S_n$  area in figure 11. The maximum admissible overheating limits should be applied only for rated voltage and frequency.

When the operating point deviates from the voltage and frequency rated values, the overheating may increase progressively. The uninterrupted operation at rated power in the neighborhood of the interior polygon sides leads to overheating up to about 10 K.

The machines should also operate at the nominal power and nominal power factor within the  $\pm 5\%$  range for voltage and  $\pm 5\%$  for frequency, defined by the exterior border  $S_{red}$  in Fig.7, but the overheating will attain even greater values. Consequently, in order to minimize the decrease of the machine life duration due to temperature effects or temperature differences, it is recommended that the

operation outside the interior polygon be limited in duration and frequency of occurrence. In such situations, it is recommended to reduce the machine load or to take other corrective measures as quickly as possible.

The mathematical model of this diagram is described by the equations of certain lines.

The upper branch:

$$U_g = \begin{cases} f_r + 0.1 & f_r \in (0.95 - 1.0) \\ 1.1 & f_r \in (1.0 - 1.02) \\ -3.3333 f_r + 4.45 & f_r \in (1.02 - 1.05) \\ 0.95 & f_r = 1.05 \end{cases}$$

The lower branch:

$$U_g = \begin{cases} 1.05 & f_r = 0.95 \\ -3.3333 f_r + 4.1167 & f_r \in (0.95 - 0.98) \\ 0.85 & f_r \in (0.98 - 1.0) \\ 2 f_r - 1 & f_r \in (1.0 - 1.05) \end{cases} \quad (3)$$

The diagram is a fixed diagram, only the position of the operation point moves according to the terminal voltage and the frequency of the respective grid.

In the  $U_g f_r$  diagram (Fig.7), the generator can operate at the rated apparent power inside the polygon  $S_n$ . When the operation point OP is outside the  $S_n$  polygon, the generator power should be diminished in order to protect it against overheating. The  $S_{red}$  polygon sets the limits of the zone where the generator can operate for a long time at maximum 80% of the rated power.

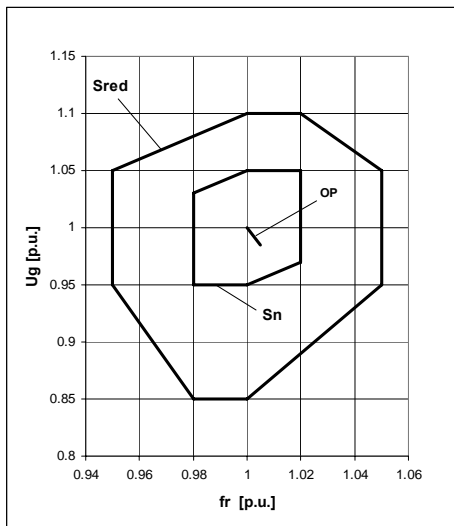


Fig. 7  $U_g f_r$  diagram

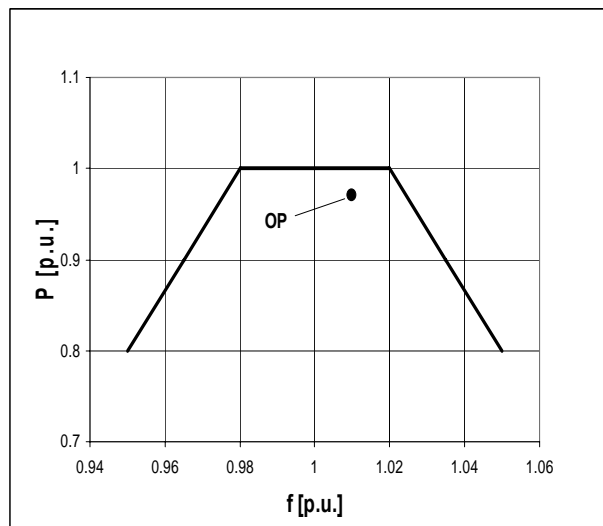


Fig. 8  $P_g f_r$  diagram

## 5 THE $P_g f_r$ DIAGRAM

The  $P_g f_r$  diagram (generator power – grid frequency) is a general diagram, valid for all the electric generators. The  $P_g f_r$  diagram represents an availability curve of a generator to reduce the generated power below  $P_n$  when the frequency is beyond the range of  $\pm 2\%$ . In fact, this diagram represents the requirement for generators to operate in the expanded field of the electricity transport grid frequency.

Thus, each generator should be able to simultaneously produce active and reactive power according to its actual PQ diagram in the 49.5 – 50.5 Hz frequency band and for the entire range of standardized voltages in the connection point to the grid.

Another important requirement is that each generator be able to supply continuously the active power scheduled or demanded by TSO in the 50.5 Hz and 52 Hz frequency range. Outside the network frequency range of 47 Hz and 52 Hz, the generators should be disconnected from the grid by their own protections or, intentionally, by the operator.

The mathematical model of this diagram is described by the equations of the straight lines:

$$P_g = \begin{cases} 6.6667 f_r - 5.5333 & f_r \in (0.95 - 0.98) \\ 1 & f_r \in (0.98 - 1.02) \\ -6.6667 f_r + 7.8 & f_r \in (1.02 - 1.05) \end{cases} \quad (4)$$

Fig. 8 presents the  $P_g f_r$  diagram for the 235 MW turbo-generator connected to the 220 kV grid. The same conditions as in the case of the  $U_g f_r$  have been considered. The operation point OP can move under the  $P_g=f(f_r)$  curve, but its movement outside this curve is not allowed.

Fig. 7 presents the  $U_g f_r$  diagram for the 235 MW turbo-generator connected to the 220 kV grid.

The conditions imposed by the grid code and the turbo-generator technical book are considered:

- For  $U_n \pm 5\%$  the rated active power is maintained.
- For the supplementary interval  $U +10\%$ ,  $U -15\%$ , the apparent rated power are established between  $0.88 S_n$  and  $S_n$  and the rated stator current are established between  $0.8 I_n$  and  $1.05 I_n$
- for  $f_r \pm 2\%$  the rated power is maintained.
- in the supplementary interval  $f_r \pm 5\%$  the power should be reduced to 80% of the rated power

## 6 APPLICATION

The presented diagrams have been particularized for a 235 MW turbo-generator with two boilers,  $U_n = 15,75$  kV,  $I_n = 9060$  A,  $\cos \varphi = 0,95$ ,  $I_{fn} = 2164$  A,  $n = 3000$  rpm,  $x_d = 2,2$  p.u. connected to a 220 kV grid through a 250 MVA transformer having  $r = 15,75/242$  kV,  $x_k = 10,5$  %, and an off load tap changer. A monitoring system has been realized; it can display each diagram separately, or all of the 6 diagrams at once. The system consists of power transducers, a communication and data acquisition system and a computer with the respective software programs. The application has been mounted at the generator no. 3 and the data have been transmitted wireless. The system offered on-line information about the operating capacity of the generator, taking into account of the own condition of the generator and of the grid. The system has given satisfaction and it will be implemented at all of the 6 generators, being integrated in the already existent monitoring system of the powerplant.

A picture of the control room with the experimental system is presented in fig. 13, and the 6 displayed diagrams are shown in Fig. 9 and Fig. 10.



Fig.9 Control room of the powerplant and the experimental monitoring system



Fig.10 The 5 diagrams displayed on the display

## BIBLIOGRAPHY

- [1] Walker J H. Operating characteristics of salient-pole machines IEEE 1952 ,100, (II)
- [2] Sedlazeck K. IEEE C50.13, IEC 34 and CIGRE Grid-Code Questionnaire - Comparison from the viewpoint of IEC 34, Report to Group A1 Rotating Electrical Machines , Set of papers CIGRE 2004
- [3] Zlatanovici D, Budulan P, Zlatanovici R, *Determination of the actual PQ diagram of the hydro-generators being in service, in order to establish their maximum operating domains and their capacity to provide system services.* CIGRE 2004, Raport A1 203
- [4] Gott B. Grid Code Comparison Study . Report to Working Group A1.01 , Set of papers CIGRE 2004
- [5] Zlatanovici D, Zlatanovici R. Considerations on the PQ diagram (active power – reactive power) of the synchronous electric generators. Roumanian Rev. Energies Technologies, 2009(4) :21-27

## **Study on Asynchronous Self-excitation and Its Protection Measures in Generator**

**Zheng Wei, Wang Xiaofeng, Wang Yingying, Liu Quan, Wang Shanshan, Jiao Shaohua  
Beijing Sifang Automation Co.,Ltd.,China**

### **SUMMARY**

Series compensation transmission technology will cause SSR, mounting block filters in the power plant is a solution to avoid SSR. In China, A power plant adopted block filters has been found asynchronous self-excitation phenomenon in synchronous generators. Self-excitation in synchronous generator can be divided into synchronous self-excitation and asynchronous self-excitation, when the generator is in a state of excessive capacitive loads, the current and voltage will grow, it is an abnormal operation mode, and it has threatened the safety operation of the generator and power system. This paper analyzes the cause of asynchronous self-excitation and introduces the study of asynchronous self-excitation, also this paper proposes protection technology and its applications.

As the modeling shows: asynchronous self-excitation is a kind of resonance, it is only related with electrical parameters of the system. In A power plant which installed block filters, asynchronous resonance self-excitation of sub synchronous frequency range occurred because of the matching of the power system parameters and the block filter parameters. As the impedance of block filters is non-linear, it performs strongly capacitive characteristics around the resonant frequency, matching with the power system parameters, a series resonant circuit is formed and asynchronous self-excitation is inspired. So, to avoid asynchronous self-excitation, the easier way is to improve the damping of generator and the power system, and adjust quality factor of the resonant circuit to inhibit asynchronous self-excitation. In order to prevent the system from the asynchronous self-excitation effectively, this paper proposes a protection measure, if the asynchronous self-excitation happens, the device will disconnect the generator from system to protect the unit from harm.

According to analysis of this paper: asynchronous self-excitation is a current resonance. After studying the asynchronous current trend, this paper puts forward the following three protection criteria: criterion of divergence protection judges the asynchronous current trend and then exports the control signals; criterion of inverse-time over current protection starts to cumulate if asynchronous current is oscillating or diverging, when integrated value exceeds the set value, it acts; criterion of definite time over current protection works as backup protection, once asynchronous current value is greater than set value, it trips. Based on the above ideas, this paper designs an asynchronous self-excitation protection device. At present, the study results - asynchronous self-excitation protection device has been applied to practice for monitoring and protecting the system from asynchronous self-excitation. Since the device was put into operation, the device has not only monitored multiple asynchronous self-excitation phenomena, but also recorded valuable experimental data for the system. In the meantime, it also proves this study is reliable and practical.

### **KEYWORDS**

Subsynchronous oscillation , Asynchronous self-excitation, Mode current

## 1 INTRODUCTION

Induction generator effect is one of the core issues of the SSO. When the synchronous generator stator circuit connects with a capacitor, and the transmission lines run with a large series or parallel capacitor compensation device or the generator run with a no-load long transmission line, the stator current amplitude may be increased spontaneously because of the additional magnetic effect of the armature reaction, and the over-voltages which are disproportionate with the generator excitation current will generate. The over-voltages and over-currents will cause serious consequences [1] [2] and damage the generators, the exciters, the lines and the transformers, etc.,

On June 21, 1976, China Danjiangkou Hydropower Station, the unit self-excitation caused by accident of electric power system, resulting in an over-voltage of 364kV, lead to a fire explosion accident of the current transformer of Makou 220kV substation. Manitoba in Canada, the self-excitation caused by a load rejection of the hydroelectric system has greatly damaged an exciter by a high reverse phase excitation voltage. So understanding and analysis the self-excitation of synchronous motor, and taking the corresponding control measures, has an important guiding significance for the safe and stable operation of power system [3].

In this paper, we start from the actual demands of the asynchronous self-excitation problem in Tuketuo power plant, adopt the frequency domain analysis method to analyze the asynchronous self-excitation formation conditions and explain the formation principles, this paper also put forward the principles and the criterions of asynchronous self-excitation. At last, we introduce the application of asynchronous self-excitation protection devices CSC-812C who adopt these principles.

## 2 ANALYSIS OF GENERATOR ASYNCHRONOUS SELF-EXCITATION

Synchronous generator self-excitation can be divided into synchronous self-excitation and asynchronous self-excitation. If the resonant frequency decided by the stator inductance, capacitance is equal to synchronous frequency, it is called synchronous self-excitation, otherwise is asynchronous self-excitation. In power system of China, series compensation technology gets more and more application, the power system parameters is growing complexity, when the parameters are unsuitable, the possibility of self-excitation phenomenon will greatly increased[4][5].

For improving the transmission capacity, Inner Mongolia Tuoketuo power plant installed series compensation devices on the four circuits of 500V lines of Tuoketuo-Huiyuan. It is shown as Fig.1.

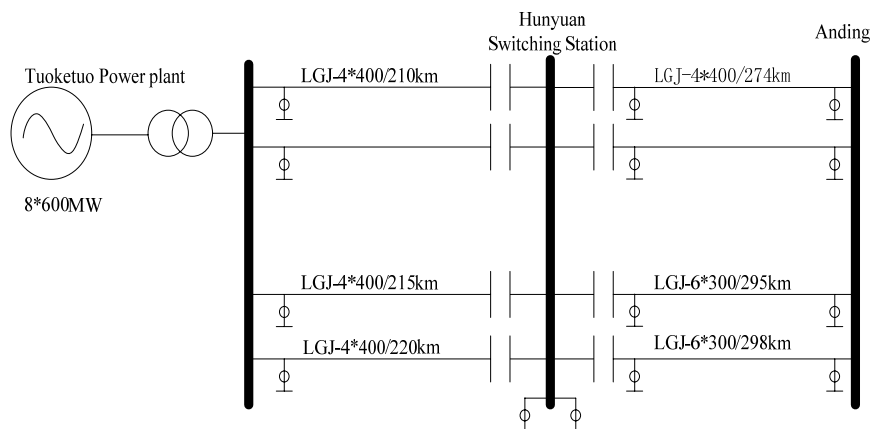


**Fig.1 Send power system in Tuoketuo power plant**

Tuoketuo power plant output system exist the risks of sub-synchronous resonance (i.e. SSR). For solving the SSR, the power plant used a complete solution that was made up by a blocked filter (i.e. BF) and a torsional vibration protection device (i.e. TSR). The figure of BF connected to the power grid is shown as Fig.2: open the central point of the main transformer HV side, connect the three phases with the combinational circuit corresponding which is constituted by several parallel resonant circuits and one similar series resonant circuit, and then ground [9].

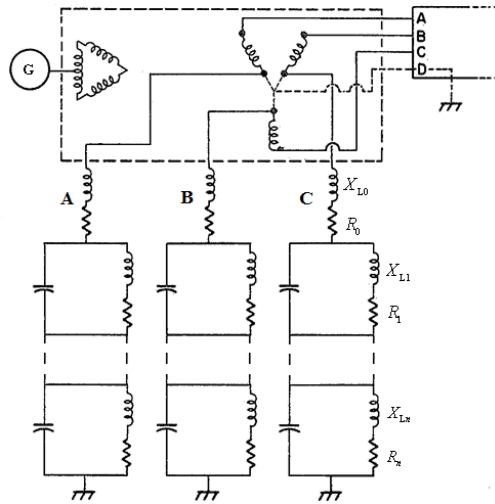


**Fig.2 BF connected to the power grid**

In 2009, Tuoketuo power plant appeared asynchronous self-excitation phenomenon after #1 generator parallel, when the BF of unit 1# was first put into operation and the BF of unit 3# and 8# were putted into operation test. That made the unit appearing vibration sharply, and the power grid current rises sharply. After the analysis of data of Tuoketuo asynchronous self-excitation phenomenon, we can obtain a typical resistance-frequency characteristics figure of three-order BF, such as Fig. 3. BF is frequency domain non-linear impedance. Its parallel resonant frequency is normally slightly higher than the complement frequency of torsional vibration needed. That means its complement frequency of torsional vibration can be shown as an impedance of high reactance and high resistance. It can offset the effect of series compensation capacitor in the grid near the complement frequency in order to improve the electrical damping of torsional mode corresponding and reduce the transient torque caused by the system disturbance. The BF is shown as a very small capacitance value nearby the frequency (50HZ), and it has no effect on the frequency of machine nets. The BF is shown as a very high capacitance and a very small resistance near the slightly higher frequency of parallel resonant. That is the hidden danger of causing asynchronous self-excitation.

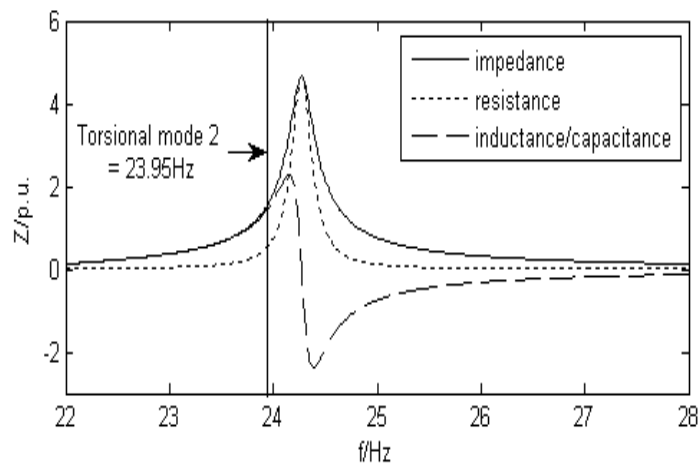


**Fig.3 Impedance-frequency characteristics of Tuoketuo 8# unit**

Make equivalent resistance on units and power grid besides BF and construct a total equivalent circle by series connection with BF, shown as Fig. 4. The total resistance characteristics of changing with frequency are shown as Fig. 5. In Fig. 5, there are three small resistance series resonances. Since the lower series resonance frequency than power frequency, generator is equivalent to an asynchronous motor with negative slip in this frequency. When the total resistance of the armature and the grid side is not enough to offset negative resistance effect of the rotor caused by negative slip, it leads to divergence asynchronous self-excitation phenomenon.

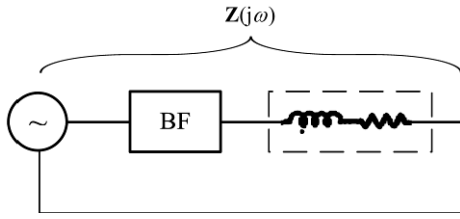


Fig.4 Equivalent circuit with BF

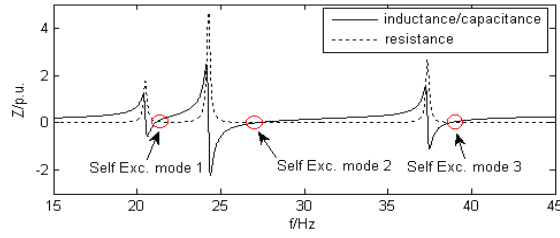


Fig.5 Impedance-frequency characteristics on line side

According to the asynchronous generator / motor theory, the self-excitation circuit produced conditions can be simple generalization as follow:

(1) Frequency conditions:  $\omega_s L = \frac{1}{\omega_s C}$ ,  $\omega_s = \sqrt{\frac{X_C}{X_L}} \omega_0$ ,  $\omega_s$  is self-excitation frequency,  $L, C$  is the total inductance and capacitance of equivalent circuit of the frequency corresponding.

(2) Impedance conditions:  $R_N + \frac{R_r}{s} \leq 0$ ,  $s = \frac{\omega_s - \omega_0}{\omega_s} < 0$ ,  $R_N, R_r$  are the stator side total resistance and the rotor side equivalent resistance of the equivalent circuit on the self-excitation frequency,  $s$  is slip frequency.

So, we can get the conclusions as follow:

- (1) Asynchronous self-excitation modal frequency is decided by blocked filter parameters and machine nets parameters. That means the modal frequency is determined.
- (2) Asynchronous self-excitation ever happened, and how it goes on, that is concerned with the stator resistance (include grid side resistance) and the rotor resistance. The stator equivalent larger, the possibility of asynchronous self-excitation is smaller.

### 3 INTRODUCTION ASYNCHRONOUS SELF-EXCITATION PROTECTION PRINCIPLES AND CRITERION

Because asynchronous self-excitation is a kind of pure electric parameter resonance, when the machine network parameters match the blocking filter parameters, namely, when the above frequency conditions and damping conditions are meet, the asynchronous resonance of secondary synchronous frequency range will be excited so that asynchronous self-exciting can be inhibited by destroying the forming conditions of the self-excitation. For this asynchronous self-excitation caused by bringing in the blocking filter, study showing, asynchronous self-excitation can be inhibited from happening by Stringing into resistance in the blocking filter circuit to destroy the damping conditions of the resonance formation. The suppression resistance  $R$  matched with the resonant frequency can be obtained by modeling the system sent by Tuoketuo power plant.

However, due to the modeling inaccuracy and the complex varied nature of the power grid operation, the choice of the suppression resistor  $R$  has a multi-valued nature. In order to fundamentally eliminate the asynchronous self-excitation phenomenon and ensure the machine network security, the security measures to the asynchronous self-excitation are raised to protect the generators.

Through the analysis of the asynchronous self-excitation of TuoKeTuo power plant, we can see:

(1) The asynchronous self-excitation is the current resonance within the sub-synchronous scope, the inner current is very great when the resonance occurring and the exchange of the resonant energy is maintained by the current changes.

(2) When an asynchronous self-excitation happen, the stator current, except the normal frequency current, is mixed with the asynchronous self-excitation mode current. The modal current features are obvious. Therefore, the monitoring of the asynchronous self-excitation can be achieved by monitoring the stator current changes.

In summary, if the stator current and modal current are used as the core fault electrical quantities of the asynchronous self-excitation protection, no asynchronous self-excitation is produced when the machine network is in a normal operation and the modal amplitude of the asynchronous current by the side of the stator is 0. When the machine network parameters have the resonance condition and the asynchronous self-excitation is caused because of investment return series compensation or blocked filter, unit load rejection or black starting, etc., asynchronous current will be brought about and the performance of the asynchronous current shows the three forms as follows:

- (a) Showing a divergent trend gradually revealing
  - (b) Showing oscillation amplitude gradually revealing
  - (c) Gradually revealing then gradually damping to zero
- (a) and (b) of the three forms are the most serious, needing real-time monitoring and judgment.

According to the development trend of the asynchronous current, the three criteria of the asynchronous self-excitation protection are as follows:

(1) Divergence criterion

Divergent criterion extracts each modal characteristic quantity by real-time measuring the generator stator current and distinguishes the change trend of the modal characteristic quantity. Protection goes out when the identification is divergent trend and the criterion is the main core criterion of the asynchronous self-excitation protection.

Modal extraction uses the technology of combined filters, it shows in Fig. 6. Simulation based on the function module of digital filters constructed by Simulink

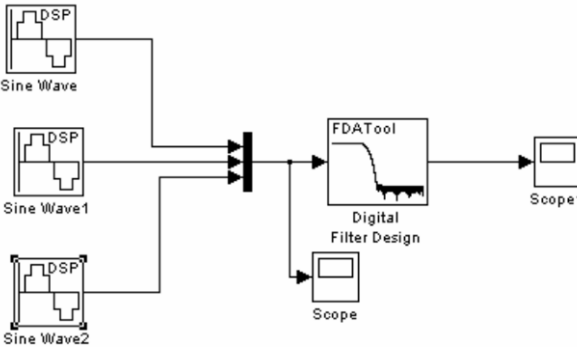


Fig.6 Simulation based on the function module of digital filters constructed by Simulink

The band filter which adopted Butterworth filter original design will generate filter parameters automatically according to the setting modal frequency. The center frequency of modal filter can be set flexibly, the bandwidth can be adapted to changes the shaft modal frequency, that will make good filtering in range of 3.0HZ and achieve the best columnar filtering effect.

(2) The over-current inverse-time protection criterion

The basic forms of the common mathematic models of the inverse time protection commonly used at

$$t = \frac{KM}{\left(\frac{I}{I_P}\right)^n - a} \tag{3-1}$$

home and abroad are [10][11][12][13]:

In the formula , $t$  for the action time,  $K$  for design constant,  $M$  for user setting time constant,  $I$  for measuring current,  $I_P$  for the benchmark current,  $a$  for curve level moving constants, response the able action current of the inverse time protection relative to the  $I_P$  multiples. According to the

characteristic of the asynchronous self-excitation, combined with the above formula, the inverse time

$$t = \frac{K}{\sum_{i=1}^n I_i^2} \quad (3-2)$$

innovative computation formula proposed in this article is as follows:

$K$  ——Inverse time coefficient setting value ;

$I_i$  ——Modal current value,  $i=1,2$  ;

$t$  ——The time of inverse time action

This criterion is real-time monitoring the asynchronous self-excitation modal current trends, if the modal current trends is divergent or constant, the device will calculate the inverse time accumulation value of this mode. when the modal current accumulates and reaches the limitation of the inverse time set value, the device will trip.

### (3) The over-current time limit set protection criterion

When the mode current value is greater than the limited current value of the over current time set, the device of protecting discriminating corresponding time limited value will trip.

According to the above theory research and protection criterion, study design measures are done via the continuous monitoring and analysis of the generator stator current. According to the characteristics of modal current, modal current divergent, amplitude or convergence are judged. When the judgment quantity reaches the limited value, or the greater modal current may constitute a threat to the safety of the unit, protection tripping, alarm and linkage are executed in order to protect the safe operation of local networks.

## 4 PROJECT APPLICATION OF ASYNCHRONOUS SELF-EXCITATION PROTECTION

The CSC-812C asynchronous self-excitation protection devices using the self-excited generator protection technology described in this paper have been applied 8\*600MW units in Tuoketuo power plant. According to the asynchronous self-excitation problem researching result of Tuoketuo power plant, there are two self-excitation frequencies at Tuoketuo units, the first frequency 38Hz named by current mode1, the second frequency 27HZ named current mode2.

### 4.1 Real-time digital simulation (RTDS) experiments

Tuoketuo power plant operating conditions were selected: There was no series compensation capacitor from Tuoketuo power plant to HunYuan transformer substation, 300MW (50%) units output, no mode suppression resistor, three-phase Bf was applied, wave recorder of devices are shown as Fig.7, when A, B, C three-phase BF switched on, there were generator terminal current change suddenly, the input of BF phase C excited a typical asynchronous self-excitation, generator terminal current shows a divergent trend, the current mode1 diverged to 0.74A rapidly (It was 3700A conversion to the primary side), the divergence lasted for 8.1s until the excitation devices started asynchronous protection action.

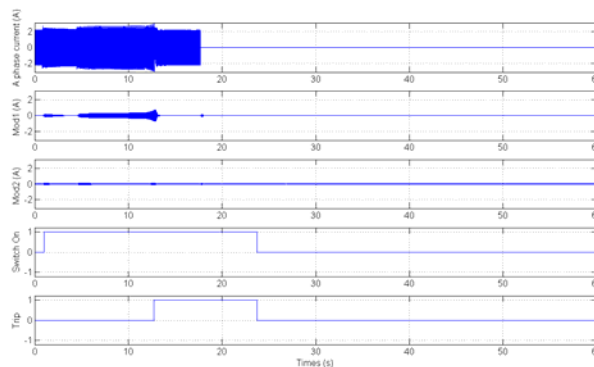


Fig.7 RTDS wave record from CSC-812C

The meaning of each wave in Fig.7 is as follows:

- (1) The stator current  $I_a$ , vertical axis unit: A, horizontal axis unit: s.
- (2) The current mode 1, frequency: 38Hz, vertical axis unit: A, horizontal axis unit: s.
- (3) The current mode 2, frequency: 27Hz, vertical axis unit: A, horizontal axis unit: s.
- (4) The start signal of asynchronous self-excitation protection devices.
- (5) The trip signal of asynchronous self-excitation protection devices.

#### 4.2 A typical instance of field

The field experiment chose the conditions which easily excited asynchronous self-excitation. In this test, the main transformer high voltage side of generator was shorted, when the generator rotor rotated, the rotor circuit was shorted and a certain remanent magnetism was retained, then the blocking filter was put into operation. At this time, the typical asynchronous self-excitation was excited, generator terminal current mode showed divergent trends, the current mode 1 excitation value which was extracted from the generator terminal current was large, it showed an equal amplitude because of the MOV role, current mode2 diverged rapidly on 26s, as shown in Fig.8.

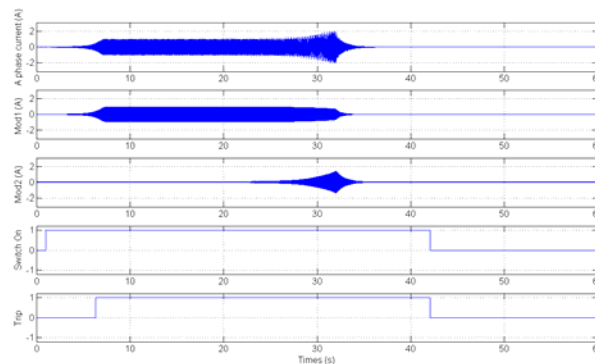


**Fig.8 Field experiment wave recorder**

The meaning of the waves in Fig.8 is same as waves in Fig.7

It can be seen that devices determine the occurrence of asynchronous self-excitation quickly and accurately. According to the standards of 1200MVA and below capacity generator allows stator windings overload in a short time and the research and analysis of the impact on equipment from asynchronous current, the protection start value is set on 0.02A, in this experiment, when three phases blocking filter was applied, mode 1 appears, the maximum value is 0.923A (it's 4615A conversion to the primary side), 26 seconds later, mode 2 appears and divergence occurs, the maximum value is 1.3992A (it's 6996A conversion to the primary side), devices act in 6.3s under the protection criterion. Because trip export does not access in field experiment, the figure shows that the current mode still exists after trip, until the blocked filter exits.

The experiment above verifies asynchronous self-excitation protection devices can trip timely when asynchronous self-excitation occurred on generator.

#### 5 CONCLUSIONS

In this paper, we begin with the asynchronous self-excitation problem in TuoKeTuo power station, study and propose the frequency and damping conditions that an asynchronous self-excitation occurred. Asynchronous Self-excitation is a serious instable phenomenon in generator and power grid, which we should pay more attention to. For protecting the security of units, asynchronous self-excitation protection devices are strongly recommended to install. This paper focuses on the protection technology of asynchronous self-excitation generator, describes the protection principle, criteria and operating characteristics. This paper also applied the technology into real projects and give effective protection on safe operation, establish the technical route and direction for solutions of generator induction effect caused by SSR

## BIBLIOGRAPHY

- [1] WAGNER C F. Self excitation of induction motors with series capacitors. AIEE Trans., 1941, 60:1241-1247
- [2] BARKLE J E, FERGUSON R W. Induction generator theory and application. AIEE Trans., 1954, 73, (III A):12-19
- [3] Alolah A I. A Simple Iterative Method For Steady State Analysis of Three Phase Self-Excited Induction Generator[C]// International Conf. on Electrical Machine (ICEM), Istanbul, Turkey, 1998:1550-1553
- [4] LIMEBEER D J N, HARLEY R G. Subsynchronous resonance of single-cage induction motors. IEEProc. B, Electr. Power Appi, 1981, 128 (1) : 33-42
- [5] Aljabr A K, Alolah A I. Capacitance requirement for isolated self-excited induction generator. Proc. of IEE.pt.B, 1990137(3):154-159
- [6] Chan T F. Performance analysis of a three-phase induction generator self-excited with a single capacitance[J]. IEEE Trans on Energy Conversion, 1999, 14(4):894-900
- [7] Alolah A L, Alkanhal M A. Optimization-based steady state analysis of three phase self-excited induction generator[J]. IEEE Trans on Energy Conversion, 2000, 15(1):61-65
- [8] Chan T F. A novel single-phase self-regulated self-excited induction generator using a three-phase machine[J]. IEEE Trans on Energy Conversion, 2001, 16(2):204-208
- [9] Cui W, Lu C, Xia Zu, et al. Simulation of self—excitation of generators connected to long transmission lines)I-J. Journal of Tsinghua University(Science and Technology), 2002, 42(9):1154—1157
- [10] Murthy S S, Singh B, Gupta S, et al. General steady state analysis of three-phase self-excited induction generator feeding three-phase unbalanced load/single-phase load for stand-alone stations[J]. IEE Proceedings C-Generation, Transmission and Distribution, 2003, 150(1)L49-55
- [11] Singh G K. Self-excited induction generator research: a survey [J]. Electric Power Systems Research, 2004(69):107-114
- [12] Bansal R C. Three-Phase Self-Excited Induction Generators: An Overview. IEEE Trans., 2005, EC-20(2):292-299
- [13] XU Z, ZHANG F. SSR analysis of series compensation transmission scheme for Tuoketuo Power Plant. ELECTRIC POWER, 2006, 39(11)
- [14] WANG Y, ZHENG W, LI L, LIU Q. CSC-812C Generator Asynchronous Self-Excitation Protection Specification. V2.0, 2010

**The Simulation and Discussion on SSR of TCSC Transmission System in a Power Station**

**Li Guifen, Sun Yutian, Fan Jisong**  
**Harbin Research Institute of Large Electric Machinery**  
**China**

**SUMMARY**

Thyristor controlled series compensation (TCSC) transmission system may inadvertently increase the risk of SSR<sup>[1]</sup>. In recent years, the SSR phenomenon has occurred in several series compensation transmission system in China. In this paper, the SSR phenomenon for TCSC transmission system of a power station (called as Y Power Station below) in China is simulated and analysed. The damage in the generator due to SSR is represented, the waveforms are recorded and the SSR stability is analysed with the combination of complex torque coefficient method and time-domain simulation method. First, electrical damping-frequency characteristics of generator unit for different series compensation degrees, which are calculated with the complex torque coefficient method realised by time-domain simulation-the test signal method, is compared with the measured mechanical damping of generator. According to the comparison, the SSR stabilities for different series compensation degrees of the power station are discussed. Then the time-domain simulation is carried out with the software package SIMSEN, the simulation results verified the conclusion obtained by the test signal method. In addition, the comparison between simulation results and waveforms recorded validate the model set up in this paper.

**KEYWORDS**

TCSC, SSR, The test signal method, Electrical damping

## 1 INTRODUCTION

The phenomenon of SSR on AC power system was first discussed in technical literature in 1937. The SSR phenomenon originally resulted in the destruction of two generator shafts at the Mohave Power Station in southern Nevada on December 9, 1970 and again in October 26, 1971 in USA [2]. After that, an upsurge of the SSR study emerged all over the world. Since 1980's, some failures for torsional oscillations are often reported in China. The in-depth researches of SSR including mechanism, study method, monitoring and control have been carried out by many experts and scholars, and many fruitful productions have been achieved at the same time. Several methods for analysing SSR are proposed such as the eigenvalue method, the complex torque coefficient method and the time-domain simulation method etc. which are widely used now. These methods can be used to analyse the SSR problem resulted from the fixed series capacitive compensation (FSCC) [3-5]. But if the HVDC or Flexible Alternating Current Transmission System (FACTS) device is included in the transmission system, the eigenvalue method is very difficult to realise. So the complex torque coefficient method is often combined with the time-domain simulation method to analyse and calculate the SSR problem in power system including HVDC and FACTS in engineering [6].

The SSR phenomenon has occurred in several series compensation transmission system in China. In this paper, the SSR phenomenon of Y Power Station in China is represented, the waveforms recorded such as speed deviations of each Torsional Mode, the terminal voltages and currents are given. Then the detailed simulation models of the system for the test signal method and the time-domain simulation method are set up by means of SIMSEN to calculate and analyse the SSR problem of the power station. The comparison of the results obtained by the two methods gives the consistent conclusion. In addition, the comparison between the simulation results and waveforms recorded validates the model by SIMSEN.

## 2 THE SSR CASE IN Y POWER STATION

### 2.1 Equivalent system

The equivalent transmission system of Y Power Station is depicted in Fig. 1. Units #1 and #2 are completely same, 2 poles and 500MW. Units #3 and #4 are completely same, 2 poles and 600MW. The mechanical shaft of units #1 and #2 consist of 6 lumped masses and units #3 and #4 consist of 4 lumped masses. The power is transmitted through the two lines where the FSCC (the line-frequency capacitance of capacitor is 30% of the line reactance) and TCSC (the compensation capacitance produced by capacitor with thyristors OFF is 15% of the line reactance) are respectively equipped in. In great way of the system, the short-circuit currents of 500kV bus of substation 1 and substation 2 are respectively 15.53kA and 17.77kA. Units #3 and #4 are mainly studied in this paper.

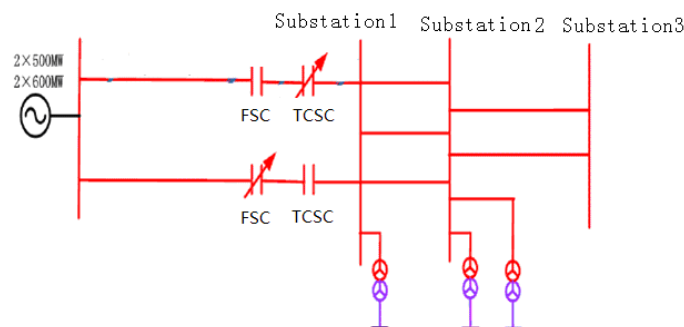


Fig. 1 Equivalent Transmission System of Y Power Station

### 2.2 The damage of unit #3 for SSR

The vibration of bearing pad #7 of unit #3 increased rapidly since May 2 to 5, 2008, and the shaft vibration amplitude increased from 0.03mm to 0.14mm. After the rotor was removed, 8 significant cracks are found on the flange in the generator side, in which 6 cracks are located near the round keys, the more serious cases are shown in Fig. 2-5. The further examination for the generator rotor by

Manufacturer is performed, two linear cracks in the generator rotor shaft shoulder, the length are respectively about 250mm and 65mm, are found again, as shown in Fig. 5.

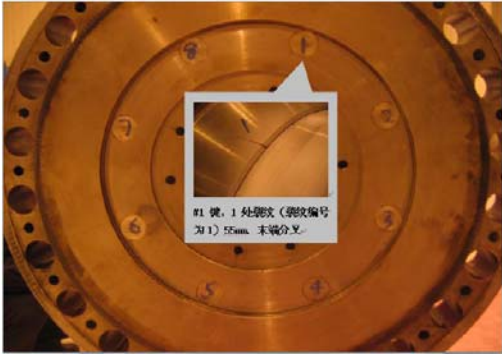


Fig. 2 Crack Near Round Keys #1 on the Flange

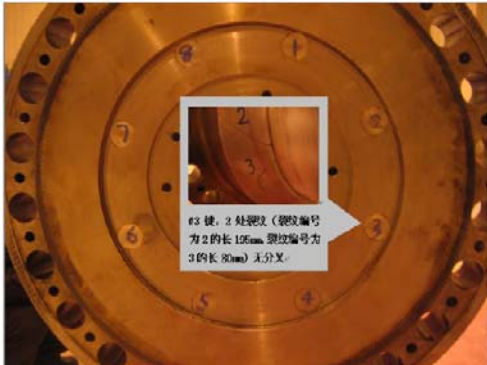


Fig. 3 Crack Near Round Keys #3 on the Flange



Fig. 4 Crack Near Round Keys #5 on the Flange

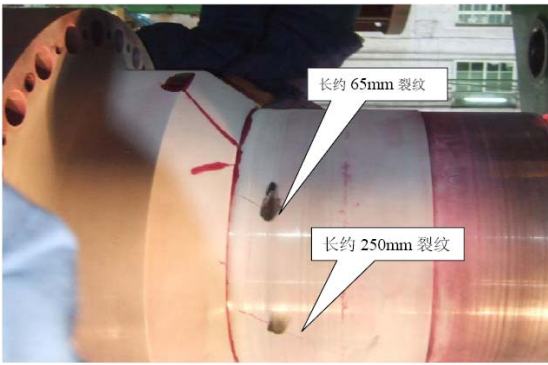


Fig. 5 Crack in the Shaft on the Turbine Side

**2.3 The waveforms recorded of SSR**

The torque oscillation of shaft system was monitored for units #3 and #4 in Y Power Station on March 5, 2008, the waveforms recorded of speed deviations of each Torsional Mode, the terminal voltages and currents are given in Fig. 6 and Fig. 7. The speed deviations of Torsional Mode1-3 and its local enlarged map are shown in Fig. 6(a) and Fig. 6(b). From these two figures, we can see the speed deviation of Torsional Mode 2 (21.28Hz) oscillates sharply in equal amplitude while the other two modes responses are quite small. The terminal voltages and currents and its local enlarged map are shown in Fig. 7(a) and Fig. 7(b). According to Fig. 7(a), spectrum of currents is analysed by the correlative department, the obvious 28.7Hz signal in the currents was found, which is complementary with Torsional Mode 2 frequency (21.28 Hz) —the sum of them equals 49.98Hz.

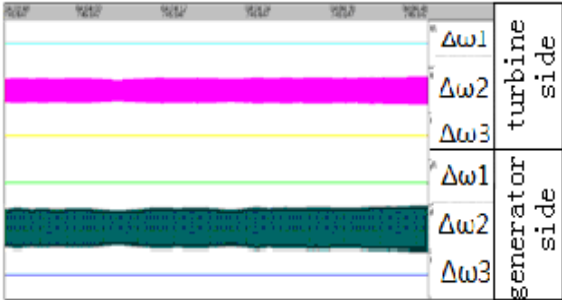


Fig. 6(a) Speed Deviations of Torsional Mode1~3

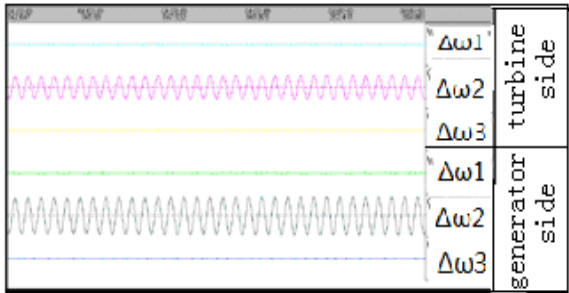


Fig. 6(b) Local Enlarged Map of Fig. 6(a)

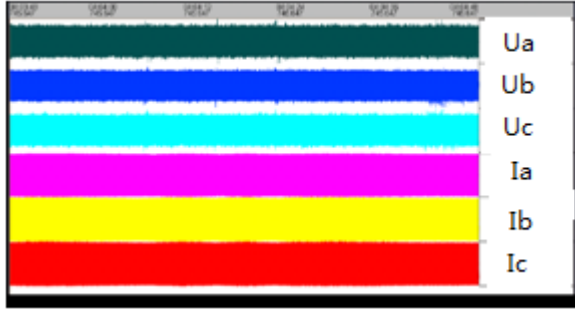


Fig. 7(a) The Terminal Voltages and Currents

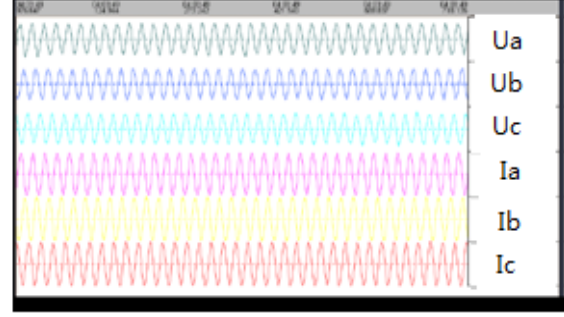


Fig. 7(b) Local Enlarged Map of Fig. 7(a)

### 3 STUDY METHOD

There are several study methods to analyse SSR problem such as the eigenvalue method, the complex torque coefficient method, frequency scanning method and the time-domain simulation method etc. as mentioned above. As TCSC is equipped in the transmission system except FSCC in Y Power Station, the study steps adopted in this paper are as follows: (1) the electrical damping in the range of sub-synchronous frequencies of the unit are calculated with the complex torque coefficient method realised by time-domain simulation-the test signal method, (2) the calculated electrical damping is compared with the measured modal damping, the system is stable to SSR if the algebraic sum of electrical damping and mechanical damping is positive otherwise SSR is not convergent, (3) the time-domain simulation results by SIMSEN verifies the conclusion obtained by the test signal method.

#### 3.1 The complex torque coefficient method

For a generator to be studied, the basic premise for complex torque coefficient method is that the increment of electromagnetic torque of generator can be expressed as follows,

$$\Delta T_e = K_e \Delta \delta + D_e \Delta \omega \quad (1)$$

where,  $K_e \Delta \delta$  is the synchronous torque,  $D_e \Delta \omega$  is the damping torque,  $K_e$  and  $D_e$  are respectively synchronous and damping torque coefficient,  $\Delta \delta$  and  $\Delta \omega$  are respectively power angle and angular speed increment based on the synchronous rotating coordinate system. In above equation  $\Delta T_e$ ,  $K_e$ ,  $D_e$  and  $\Delta \omega$  are all in p.u., and  $\Delta \delta$  is in rad. The relation between  $\Delta \delta$  and  $\Delta \omega$  is

$$\Delta \omega = \frac{1}{\omega_0} \frac{d\Delta \delta}{dt} \quad (2)$$

here, the synchronous speed  $\omega_0$  is in rad/s, the time  $t$  is in s. To assume that the generator rotor has a small value oscillation with the frequency  $\lambda \omega_0$  ( $\lambda < 1$ ), the expression of synchronous torque coefficient and damping torque coefficient corresponding to the complex torque coefficient method can be educed.

All variables can be expressed in vector when generator rotor has the steady state small value oscillation. And according to equation (2),

$$\Delta \dot{\omega} = \frac{1}{\omega_0} (j\lambda \omega_0) \Delta \dot{\delta} = j\lambda \Delta \dot{\delta} \quad (3)$$

According to equation (1),

$$\Delta \dot{T}_e = K_e(\lambda) \Delta \dot{\delta} + D_e(\lambda) \Delta \dot{\omega} \quad (4)$$

therefore

$$\frac{\Delta \dot{T}_e}{\Delta \dot{\delta}} = K_e(\lambda) + j\lambda D_e(\lambda) \quad (5)$$

or

$$\frac{\Delta \dot{T}_e}{\Delta \dot{\omega}} = D_e(\lambda) - j\frac{1}{\lambda} K_e(\lambda) \quad (6)$$

According to equation (5) or (6), the value of electrical damping torque coefficient  $D_e$  can easily be obtained [6].

Because complex torque coefficient method is only applicable to a system of single-machine to fixed frequency power supply but not to multi-machine system [3-6], multi-machine system should be equivalent to single-machine. And as mechanical and electrical part can be calculated respectively, mechanical shaft is modelled with equivalent single cylinder while the complete mathematic model is adopted for electrical part of generator to calculate the electrical damping-frequency characteristic with the test signal method [6].

#### 4 CALCULATIONS OF ELECTRICAL DAMPING AND ANALYSIS OF SSR STABILITY

Analysis and discussion are carried out from electrical and mechanical damping aspect to determine SSR stability of the system in Fig. 1. The criteria to estimate the stability of shaft torsional oscillation is that any Torsional Mode  $j$  of mechanical shaft system should meet the follow equation

$$D_{ej} + D_j^{(m)} > 0 \quad (7)$$

where,  $D_{ej}$  and  $D_j^{(m)}$  are respectively electrical and mechanical damping torque coefficient corresponding to Torsional Mode  $j$  frequency, p.u..

The stability of system in a certain condition can easily be estimated according to the equation (7) as long as  $D_{ej}$  and  $D_j^{(m)}$  are obtained [6].

The series compensation transmission system depicted in Fig. 1 is modeled and simulated by SIMSEN with the test signal method. 1 equivalent unit, described with equivalent circuit of q and d axes, is adopted as a substitute for 4 units, and mechanical shaft is modelled with equivalent single cylinder. TCSC is modelled as real model and control mode (open-loop constant impedance control). Moreover, the equivalent reactance of the TCSC as a function of the firing angle ( $\alpha$ ) in p.u. ( $X_c$  is based value) is

$$X_{pu} = 1 - \frac{K^2 [2(\pi - \alpha) + \sin 2(\pi - \alpha)]}{\pi(K^2 - 1)} + \frac{4K^2 \cos^2(\pi - \alpha)}{\pi(K^2 - 1)^2} [K \tan K(\pi - \alpha) - \tan(\pi - \alpha)] \quad (8)$$

where,  $K = \frac{\omega_r}{\omega} = \sqrt{\frac{X_c}{X_L}}$ ,  $\omega_r = \frac{1}{\sqrt{LC}}$ ,  $\omega$  is the fundamental wave angle frequency of the plant.

The simulation conditions are that 4 units are all at rated load and all lines are operating online. Electrical damping - frequency characteristics of the system with  $X_{pu}$  changing from 1.0 to 1.4 are calculated and analyzed, the results calculated are shown in Fig. 8. With  $X_{pu}$  increasing the resonant frequency (converted to the rotor side) gradually move to higher frequencies, and the electrical damping characteristics of system are gradually improved. When  $X_{pu} \geq 1.2$ , the electrical damping characteristics has little change. TCSC can improve the electrical damping characteristics of the system, electrical damping was increased to -2.15 p.u. corresponding to  $X_{pu}=1.4$  from -4.75 p.u. corresponding to  $X_{pu}=1.0$ . But electrical damping within subsynchronous frequency is still negative, which provides instability preconditions for SSR.

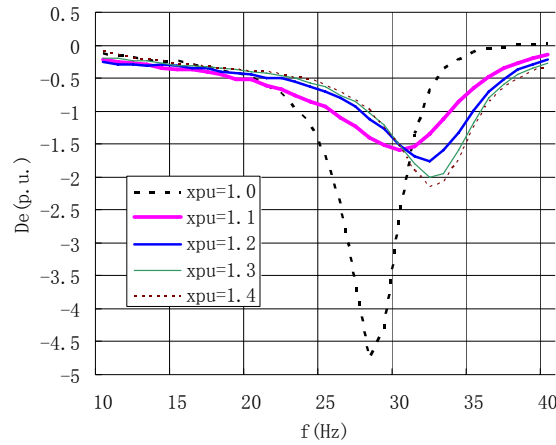


**Fig. 8 Electrical Damping-Frequency Characteristics of the System**

The measured values of mechanical damping decrement factor  $\sigma_j$  for units #3 and #4 are shown in table I. The measured values of mechanical damping of Torsional Mode 3 at rated load are not obtained. According to the experience mechanical damping logarithmic decrement  $\delta$  is 0.05% at no-load and 0.5% at rated load in calculation process for Torsional Mode 3. Mechanical damping torque coefficient can be calculated from the equation  $D_j^{(m)} = 2M_j^{(m)}\sigma_j$ ,  $M_j^{(m)}$  is modal inertia constant time, and  $\sigma_j = f_j\delta$ . The calculated results of  $D_j^{(m)}$  according to the measured values of  $\sigma_j$  shown as in table I are listed in table II in order to compare conveniently with  $D_{ej}$ . The values of  $D_j^{(m)}$  at rated load can be regarded as limitation. If the absolute value of negative electrical damping torque coefficient exceeds this limited value, the SSR will not be stable otherwise it will.

The measured values of modal frequency  $f_j$  are given in table II, 12.5Hz, 21.28Hz and 25Hz respectively, and the values of  $D_{ej}$  at different Xpu values corresponding to Torsional Mode 1-3 frequency obtained from the curves in Fig. 8 are also listed in the table. From the comparison between  $D_{ej}$  and  $D_j^{(m)}$  it is not difficult to estimate the stability of the system depending on the criteria provided by equation (7). From the table II, when Xpu changes from 1.0 to 1.4, the  $D_{ej}$  corresponding to Torsional Mode 2 increases from -0.66 to -0.4 and all the absolute values corresponding to Torsional Mode 2 almost exceed or close the values of  $D_j^{(m)}$ . It indicates that Torsional Mode 2 is liable to be instable for SSR although the electrical damping is improved with Xpu increasing. However the Torsional Mode 1 and Torsional Mode 3 are stable in all conditions.

**Table I Measured Values of Mechanical Damping Decrement Factor  $\sigma_j$  for units #3 and #4**

$\sigma_j$ (1/s)	Mode1	Mode2	Mode3
no load	0.044	0.044	0.026
half rated load	0.084	0.041	-
rated load	0.114	0.069	-

**Table II Comparison of Electrical and Mechanical Damping of Torsional Mode 1-3 at Rated Load**

Mode	$f_j$ (Hz)	$M_j^{(m)}$ (s)	$D_j^{(m)}$	$D_{ej}$				
				Xpu=1.0	Xpu=1.1	Xpu=1.2	Xpu=1.3	Xpu=1.4
1	12.51	4.4434	1.013	-0.18	-0.27	-0.29	-0.25	-0.18
2	21.28	3.0318	0.4184	-0.66	-0.68	-0.45	-0.42	-0.4
3	25.0	132.65	33.16	-1.4	-0.8	-0.67	-0.6	-0.55

## 5 TIME-DOMAIN SIMULATION

The above conclusions obtained by the test signal method give the general estimate information and general trend of each Torsional Mode for SSR to the transmission system. But the limitation of this method is that a lot of equivalence and simplification has been done in the calculation process and results obtained are a bit rough. Therefore, in engineering the test signal method are often combined with time-domain simulation method, which can provide detailed curves of variables versus time. The results obtained by time-domain method can further verify the conclusion by test signal method.

The simulation model (see Fig. 9) is set up by SIMSEN for the studied transmission system as depicted in Fig. 1. 4 generators are respectively modelled with equivalent circuit of q and d axes, the mechanical system is represented by a multi-mass spring-dashpot system and TCSC is considered as real model and control mode (open-loop constant impedance control). The modal damping decrement factor  $\sigma_j$  given in table I is changed to mutual damping coefficients used in time-domain simulation model [7].

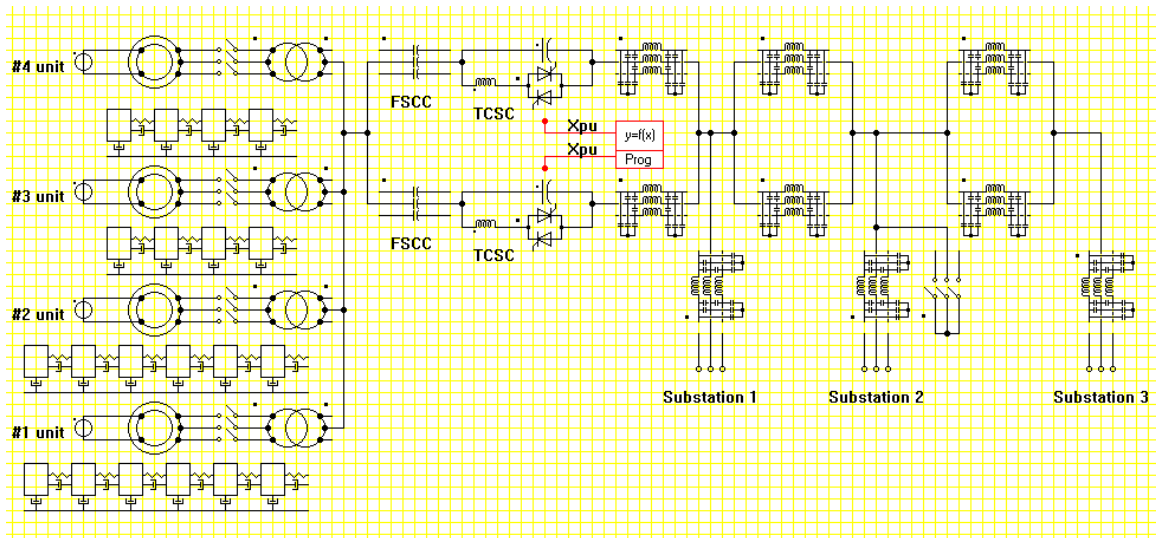


Fig. 9 Simulation Model in SIMSEN

### 5.1 Time-domain simulation

The simulation condition is that 4 units are all at rated load and all transmission lines are operating online. The units operate in specified condition, a three-phase fault (the duration is 0.05s) was applied at 500kV bus of substation 2 (see Fig. 9) at a certain time to excite the torsion modes of the system. The speed deviations of each Torsional Mode for units #3 and #4 are obtained after the fault was rid of and the main simulation results are given in Fig.10-14.

As shown in Fig.10-14, the torsion oscillation of Torsional Mode1 and 3 always decrement when Xpu change from 1.0 to 1.4. But Torsional Mode 2 is not decrement with relative small values of Xpu, SSR is instable. With Xpu increasing Torsional Mode 2 decrement gradually, but the decrement speed is slower than Torsional Mode 1 and 3. This conclusion accords with that obtained by test signal method. It is indicated that Torsional Mode 2 of units #3 and #4 is exactly instable for SSR. In addition, from Fig. 11 and Fig. 12 it is concluded that there must be a condition which make Torsional Mode2 resonate in equal amplitude when  $1.1 < Xpu < 1.2$ . This conclusion accord with waveforms recorded (see Fig. 6), and the model is validated.

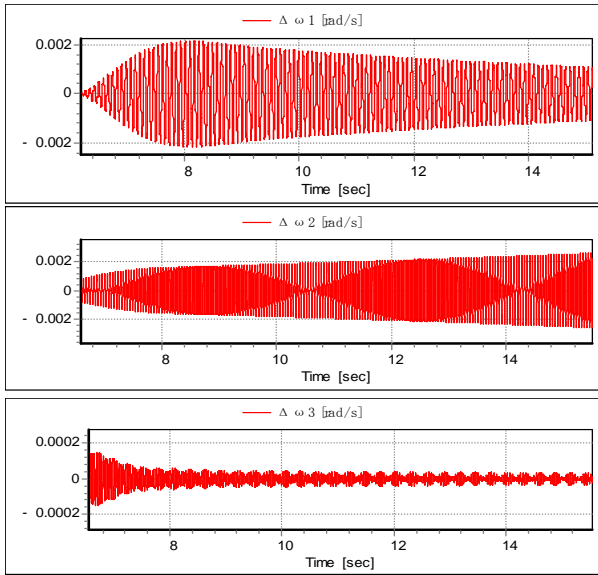


Fig. 10 The Speed Deviations of Model1-3 with Xpu=1.0

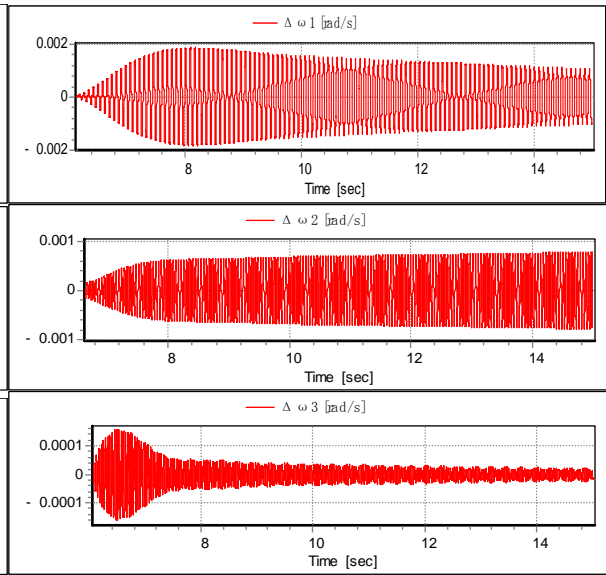


Fig. 11 The Speed Deviations of Model1-3 with Xpu=1.1

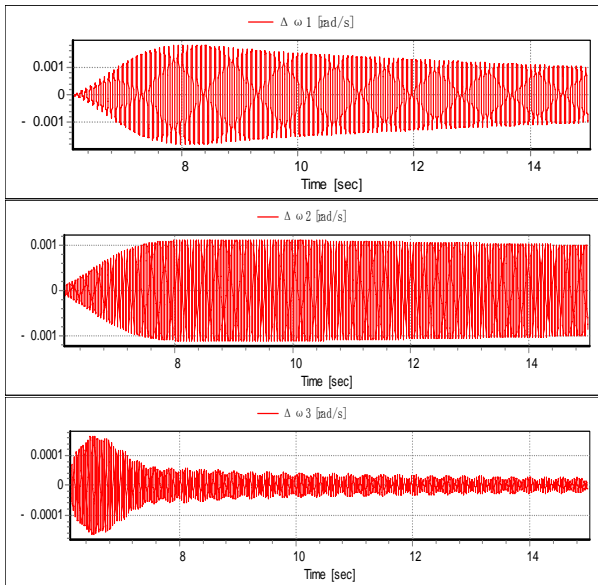


Fig. 12 The Speed Deviations of Model1-3 with Xpu=1.2

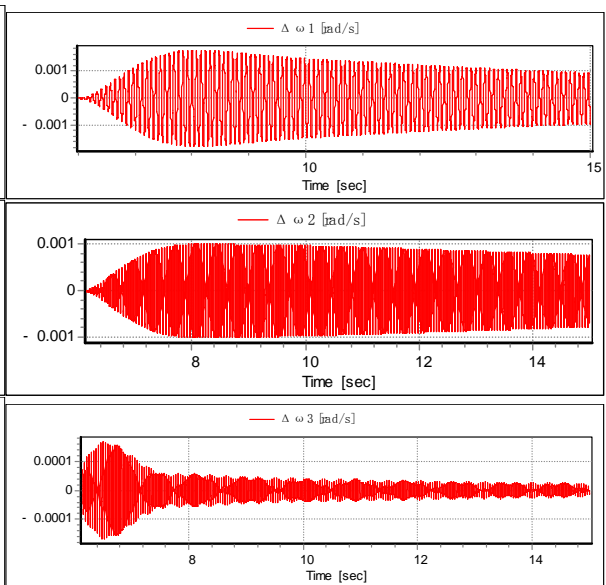
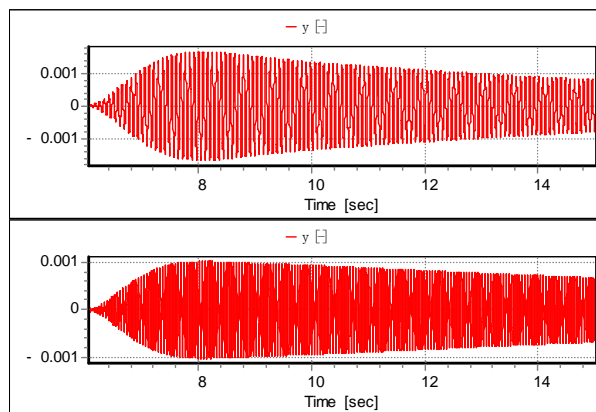
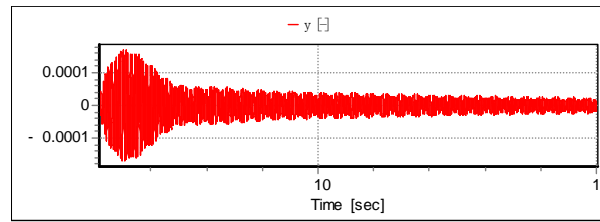


Fig. 13 The Speed Deviations of Model1-3 with Xpu=1.3





**Fig. 14 The Speed Deviations of Mode1-3 with  $X_{pu}=1.4$**

## 6 CONCLUSIONS

In this paper, the detailed simulation models for the test signal method and the time-domain simulation method are set up by means of software SIMSEN to calculate and analyse the SSR problem of transmission system with TCSC equipped in. In the model TCSC is considered as real model and control mode (open-loop constant impedance control). Then the SSR phenomenon of Y Power Station in China is simulated and analysed with the models. The comparison of calculated results and waveforms recorded validate the models.

In addition, the detailed simulation of the SSR problem for units #3 and #4 of Y Power Station gives the conclusions as follows,

(1) The electrical damping of the system is negative in the range of subsynchronous frequency when TCSC adopt open-loop constant impedance control. If the absolute values of negative electrical damping are more than mechanical damping, the system will be liable instable for the SSR.

(2) The electrical damping of the system can be improved in the range of subsynchronous frequency by TCSC, and TCSC can make the electrical damping increasing.

(3) The Torsional Mode 2 of units #3 and #4 is liable to be instable for SSR although the electrical damping is improved with  $X_{pu}$  increasing. However the Torsional Model 1 and Torsional Mode 3 is stable in all operating conditions

## BIBLIOGRAPHY

- [1] Pilotto L A S, Bianco A, Long W F, Edris A. Impact of TCSC Control Methodologies on Subsynchronous Oscillations. IEEE Transactions on Power Delivery, January 2003, 18(1)
- [2] Walker D N, et al. Results of subsynchronous resonance test at Mohave. IEEE Transactions on Power Apparatus and Systems, September/October 1975, PAS-94(5)
- [3] XU Z. The complex torque coefficient approach's applicability analysis and its realization by time domain simulation [J]. Proceedings of the CSEE, 2002, 20(6):1-4
- [4] Zhan F, XU Z. SSR damping study on a generator connected to TCSC [J]. High Voltage Engineering, 2005, 31(3):68-70
- [5] Chen C, Yang Y. Discussion of several analytical approaches and tools about subsynchronous resonance (SSR). Power System Technology, 1998, 22(8):10-13
- [6] Xu Z, Dynamic analysis of AC/DC power systems [M]. Beijing China Machine Press, 2004
- [7] Qiu P, Xu Z. Shaft Damping Modeling for Turbine-Generator in Electromagnetic Transient Simulation. Southern Power System Technology, Dec. 2008, 2(6)

**Effect of Automatic Reclosing on the Torsional Fatigue Life Expenditure of Turbine-Generator Shafts**

**Xitian Wang**  
Shanghai Jiao Tong University  
China

**Xue Yang**  
Shanghai Jiao Tong University  
China

**Chen Chen**  
Shanghai Jiao Tong University  
China

**SUMMARY**

The electrical disturbances in the large complex power grid, causing severe transient torque impacts and high stresses on the shafts of turbine-generator, can have an adverse effect on accumulative fatigue life expenditure (FLE) of the machine shafts. The automatic reclosing procedure following some short faults is one of the most typical electrical disturbances. There are some literatures which have evaluated the effect of automatic reclosing on the machine shafts. However, the studied results have some limitation owing to the case number restriction and calculation tool restriction up to now.

For 600 MW turbine-generator units equipped with blocking filters in one series compensated transmission system in North China, torsional fatigue life expenditure of shafts is evaluated in numerous cases, in consideration of different system conditions, different types and locations of faults. The results show that unsuccessful circuit breaker reclosing due to a permanent single-phase fault occurring on the transmission line terminal close to the power plant can cause significant fatigue life expenditure, which may be beyond the endurable strength of the turbine-generator shafts. In this paper, the reason of significant fatigue life expenditure caused by the unsuccessful single-phase reclosing procedure is discussed and validated.

The effect of single-phase reclosing time sequence on the machine shaft fatigue life expenditure is investigated with enough cases, by using the Multiple Run Component of PSCAD/EMTDC to carry out simulation of numerous cases automatically. The cases are dealt with a large number of different moments for single-phase reclosing and the timing of three-phase tripping off for unsuccessful reclosure. Torsional fatigue life expenditure of machine shafts is evaluated for each case. The results have revealed that single-phase reclosing time sequence and three-phase tripping time sequence after single-phase reclosure failure have nonlinear influence on fatigue life expenditure of the machine shafts. In addition, the distance between the fault location and the power plant has certain effect as well.

**KEYWORDS**

Turbine-generator, Torsional oscillation, Fatigue life expenditure, Automatic reclosing, single-phase reclosure

## 1 INTRODUCTION

Some electrical system faults and switching operations can cause the accumulation of the torsional fatigue life expenditure of turbine-generator shafts and lead to the adverse impact on the machine security. Until the mid-seventies, a short circuit between terminals of a turbine-generator was the only evaluation criterion for maximum torsional stressing of the turbine-generator shaft system. However, comprehensive investigations on the effects of electrical system faults conducted since 1970s have revealed that short-circuits between terminals do not impose the highest stresses possible on the turbine-generator, a great number of other disturbances have to be taken into consideration. The subject of torsional stresses being induced in the shafts of turbine-generators by electrical system faults and switching operations is rather complicated, hence it is involved with multiple discipline knowledge both of electrical and mechanical engineering, and together with multiple businesses of the power generation and transmission as well as the machine manufacture and power system planning. Although there were a number of studies reported in the literature during the 1970s and 1980s<sup>[1-9]</sup>, there are few recent reports of simulation studies that describe stress levels for transient events or provide guidelines for system design and operation to minimize possible damage<sup>[10]</sup>.

Typically, there are specific attributes of a turbine-generator and its surrounding transmission network that increase the risk for torsional damage. Torsional interaction phenomena fall into three main categories<sup>[10,11]</sup>:

1. Interactions with system transient disturbances, including faults, reclosing etc.
2. Subsynchronous resonance (SSR) interactions.
3. Device Dependent Subsynchronous Oscillation (DDSO).

With the development of series compensation transmission, the issues have been gotten more attention in recent years in China. It is recognized that SSR can be controlled, thus making it possible to benefit from the distinct advantages of series capacitors<sup>[12]</sup>. But there are the most severe SSR problems which are great challenges to get appropriate solutions, because of China's actual conditions. On the one hand turbine-generators are connected directly to the series compensated 500 kV system. On the other hand the plant owners are generally asked to be responsible for the solution of the SSR problems.

For 600MW turbine-generator units equipped with blocking filters in one series compensated transmission system in North China, torsional fatigue life expenditure of shafts is evaluated in numerous cases, in consideration of different system conditions, different types and locations of faults. The results show that unsuccessful circuit breaker reclosing due to a permanent single-phase fault occurring on the transmission line terminal close to the power plant can cause significant fatigue life expenditure, which may be beyond the endurable strength of the turbine-generator shafts. There are some literatures which have evaluated the effect of automatic reclosing on the machine shafts<sup>[4,7]</sup>. However, the studied results have some limitation owing to the case number restriction and calculation tool restriction up to now.

In this paper, the reason of significant fatigue life expenditure caused by the unsuccessful single-phase reclosing procedure is discussed and validated in details. The effect of single-phase reclosing time sequence on the machine shaft fatigue life expenditure is investigated with enough cases, by using the Multiple Run Component of PSCAD/EMTDC to carry out simulation of numerous cases automatically<sup>[13]</sup>. The cases are dealt with a large number of different moments for single-phase reclosing and the timing of three-phase tripping off for unsuccessful reclosure. Torsional fatigue life expenditure of machine shafts is evaluated for each case. The conclusions are summarized based on the evaluated results.

## 2 INVESTIGATED SYSTEM

The investigated system is based on TKT Plant Project in North China. TKT plant is with eight turbine-generators rated 600MW. All electrical power is transported directly to the receiving network about 500km away through quadruple transmission lines that includes series capacitors, as shown in Fig. 1. The mode shapes and frequencies of the three subsynchronous modes are calculated versus the simple concentrated mass as shown in Fig. 2. This transmission scheme is a typical radial transfer

corridor, which has been identified as highly exposed to SSR risk. It seems that TKT case is a good example for SSR study except well-known IEEE benchmarked cases<sup>[14]</sup>.

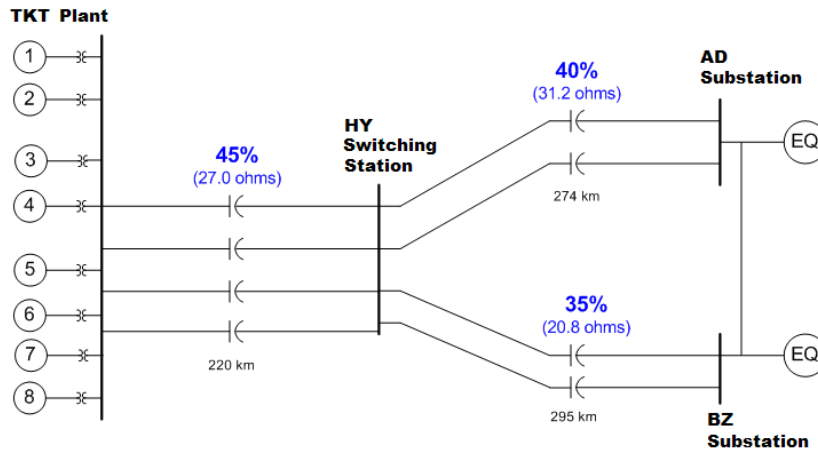


Fig. 1 Diagram of the Investigated System

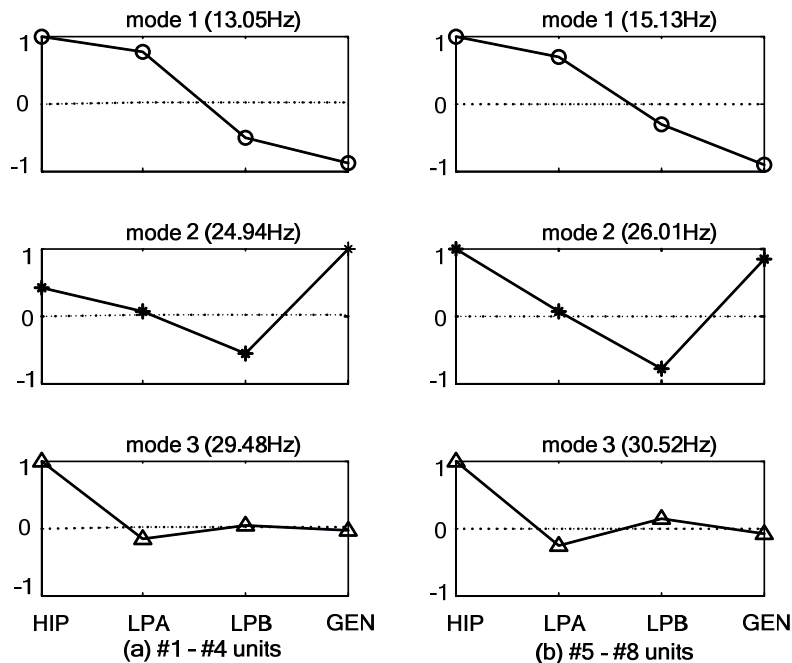


Fig. 2 Mode Shapes and Frequencies of the Three Subsynchronous Modes

The overall philosophy for mitigating SSR is to apply blocking filters in series with the generator connection to the grid, and torsional stress relays (TSR) to trip the generators in case of excessive torsional oscillation. The relays prevent damage to the machine, while the blocking filters prevent excessive torsional oscillation for important operating conditions<sup>[15]</sup>.

### 3 VALIDATION OF THE MOST SEVERE CASE

In order to confirm effectiveness of the solution of SSR problem in the TKT Plant Project, torsional fatigue life expenditure of shafts is evaluated in consideration of all available and extreme conditions. The evaluated conditions include the following aspects.

1. Generation dispatch conditions (GDC): (1) 100% load or rated MW; (2) 40% load or the minimum load for continuous operation; (3) about 0.0% load or slight load just after synchronization; (4) unit off line. In addition, Units 1 and 2 are identical, units 3 and 4 are identical, and units 5 through 8 are identical.
2. Line service conditions (LSC): (1) all lines in service; (2) one of lines TKT-HY out of service (N-1); (3) one of lines HY-AD out of service (N-1); (4) one of lines HY-BZ out of service (N-1).

3. Capacitor service conditions (CSC): (1) all capacitors in service; (2) capacitors of lines TKT-HY out of service; (3) capacitors of lines HY-AD out of service; (4) capacitors of lines HY-BZ out of service.
4. Fault type conditions (FTC): (1) temporary single-phase fault; (2) permanent single-phase fault; (3) temporary two-phase fault; (4) permanent two-phase fault; (5) temporary three-phase fault; (6) permanent three-phase fault.
5. Fault location conditions (FLC): (1) TKT Plant bus bar; (2) start of one of lines TKT-HY; (3) end of one of lines TKT-HY; (4) HY Switching Station bus bar; (5) start of one of lines HY-AD; (6) end of one of lines HY-AD; (7) AD Substation; (8) start of one of lines HY-BZ; (9) end of one of lines HY-BZ; (10) BZ Substation.

In fact, a few of almost impossible conditions combined by the above aspects, e.g. more than two units are in slight load, are out of account.

For the single-phase fault, automatic reclosure is adopted to enhance the stability and overall system reliability. Nowadays in China, the practical automatic reclosing is single-phase reclosing, since two-phase or three-phase reclosing may consequentially cause unallowable mechanical and electromagnetic impacts upon the machines and the power grid. In electromagnetic transient simulation of the investigated system, the default reclosing sequence is set as follows: the fault single-phase is tripped off 90ms later than the fault occurrence moment, then the fault single-phase is reclosed 1.0s later; if the fault has been removed the reclosure is successful, and if the fault has not been removed then three-phases are tripped off 110ms later.

Numerous evaluated results have been shown that the most severe case is as follows: six units in service with 40% load, all of the lines and capacitors are in service, a permanent single-phase fault occurring on the start of one of lines TKT-HY. The maximum FLE induced in the case of the permanent single-phase fault and unsuccessful reclosure is reached to 8.3%, as shown in Table I. But the maximum FLE induced in the case of the temporary single-phase fault and successful reclosure is just 0.0014%, small enough to ignore. And the maximum FLE induced in the case of the temporary three-phase fault with the same GDC, LSC, CSC and FLC conditions is 1.7%.

**Table I Maximum FLE Induced in the most severe case and the other two contrastive cases**

Fault type	Case 1: permanent single-phase fault and unsuccessful reclosure	Case 2: temporary single-phase fault and successful reclosure	Case 3: temporary three-phase fault
Maximum FLE	8.3%	0.0014%	1.7%

The results show that unsuccessful circuit breaker reclosing due to permanent single-phase fault can cause significant fatigue life expenditure, even larger than the maximum FLE induced in the case of three-phase fault. And there are a few possibilities to occur single-phase fault in practical systems. It is probable that the maximum FLE induced in the most severe case would be beyond the endurable strength of the turbine-generator shafts. Therefore, it is necessary to validate whether the most severe case is involved with permanent single-phase fault. For this reason, time waveform of the electromagnetic torque,  $T_e$  and mechanical torque between LPB and GEN,  $T_{BG}$  in three contrastive cases are illustrated, as shown in Fig. 3 (a) - (c).

There are two obvious transient torque impacts on the machines in the case of permanent single-phase fault and unsuccessful reclosure, as shown in Fig. 3 (a). By drawing a comparison between Fig. 3 (a) and Fig. 3 (b), it is indicated there is a same large transient torque impact during the initial period both of permanent and temporary single-phase fault. There is difference during the later period between permanent and temporary single-phase fault. There is more obvious transient torque impact once again with respect to permanent single-phase fault. And there is no longer obvious transient torque impact with respect to temporary single-phase fault. The maximum FLE induced in the case of permanent single-phase fault and unsuccessful reclosure is much greater than that of temporary single-phase fault and successful reclosure. Therefore, the transient torque impact occurred once again during the later period has played a dominant role in the accumulation of torsional fatigue life expenditure of turbine-generator shafts. By drawing a comparison between Fig. 3 (a) and Fig. 3 (c), it is shown that the peak

of the mechanical torque during the later period of permanent single-phase fault is approaching to that of the mechanical torque during the initial period of temporary three-phase fault. However, time waveform of the mechanical torque of the former one is decayed much slower than that of the latter one. So the maximum FLE induced in the case of permanent single-phase fault and unsuccessful reclosure is greater than that of temporary three-phase fault. It can be concluded that the most severe case is validated as permanent single-phase fault.

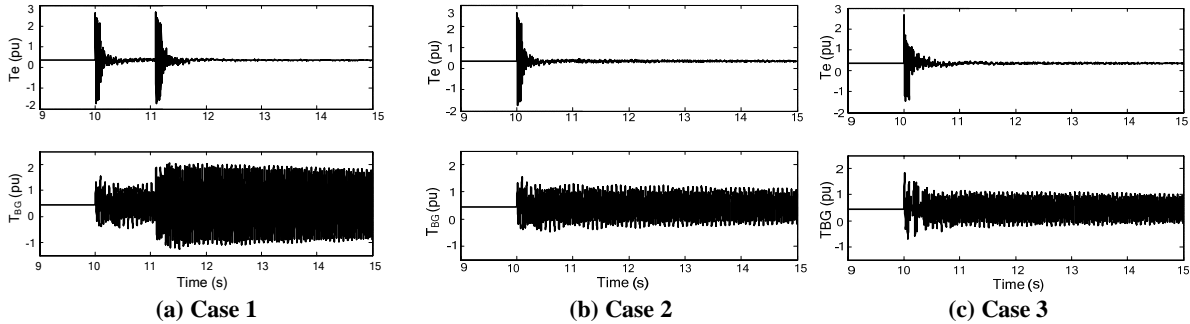


Fig. 3 Time Waveform of the Electromagnetic Torque,  $T_e$  and Torque between LPB and GEN,  $T_{BG}$  in three contrastive cases

#### 4 IMPACTS OF RECLOSING SEQUENCE ON MAXIMUM FLE

As mentioned above, the transient torque impact occurred once again during the later period of permanent single-phase fault has played a dominant role in the accumulation of torsional fatigue life expenditure of turbine-generator shafts. There are twice disturbances during the later period, one is fault phase closing and the other is three phases trip off. The twice disturbances may be superposed positively on the former disturbances to enhance the later transient torque impact. Obviously, time to the twice disturbances occurring is closed related to impact enhancement and fatigue life expenditure. Therefore, it is necessary to carry out simulation of numerous cases with different single-phase reclosing time sequence to obtain more particular results.

A powerful tool to carry out simulation of numerous cases automatically is provided by software PSCAD/EMTDC<sup>[13]</sup>. There is Multiple Run Component in the master library of PSCAD/EMTDC, which can be used to control a multiple run, while manipulating variables from one run to the next. These variables are output from the component (up to six outputs) and can be connected to any other PSCAD/EMTDC components. Some examples of the use of multiple run are: (1) Changing the time or angle of faults; (2) Changing the type or location of faults ; (3) Modifying gains of a controller to find the best response to a disturbance; (4) Stepping through a range of RLC or system parameters to determine an optimum. Output Channel Component can also be used to save the complete time waveform for each run.

##### 4.1 Time span between single-phase trip off and reclosing

Reclosure time span between the fault single-phase trip off and reclosing is set from 1.0s to 30.0s with interval 1.0s by Multiple Run Component. The other time sequence is kept the default setting. Total of 30 cases are simulated and the mechanical torque time waveforms are saved one by one run automatically. Then the mechanical torque time waveforms data are used to evaluate the maximum FLE. The curves of the evaluated maximum FLE versus reclosure time span with interval 1.0s are as shown in Fig. 4 (a). It is shown that with increase of reclosure time span, the maximum FLE is decreased on the whole.

Moreover, the curves of the evaluated maximum FLE versus reclosure time span with interval 0.5s are as shown in Fig. 4 (b). It is shown that the relative high points and the relative low points alternate each other. The relative low points are missed out with interval 1.0s in Fig. 4 (a). The default reclosure time span is 1.0s, just corresponding to a relative large maximum FLE.

Overall, it is also shown that the maximum FLE may be relatively large (more than 1.0%) with reclosure time span less than 20.0s. The maximum FLE may be rather small with reclosure time span great than 30.0s.

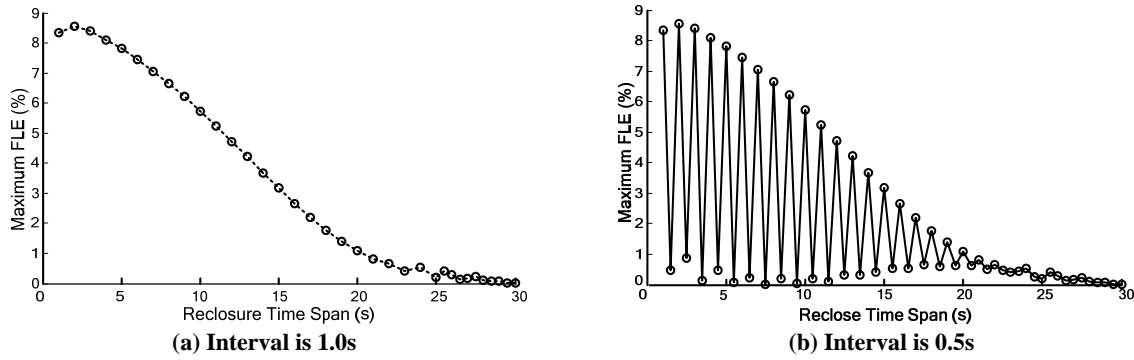


Fig. 4 Curves of Maximum FLE versus Reclosure Time Span with Different Interval

The interval of reclosure time span deviation is further decreased to 0.005s. Reclosure time span is set from 0.9s to 1.8s and 30.0s to 30.1s. It is totalled to over 200 cases. The curves of the evaluated maximum FLE versus reclosure time span with interval 0.005s are as shown in Fig. 5. It is indicated there is a group of relative high points (FLE more than 8.0%, the other less than 3.0%) with reclosure time span varying between 0.9s and .8s. Time interval of the nearby two relative high points is about 0.04s, approximate to the period of torsional mode 2. Furthermore, the maximum FLE may be close to 0 with reclosure time span great than 30.0s. It can be explained that the mode oscillations excited by the former transient torque impact would be almost decayed off and not to enhance the later transient torque impact at all.

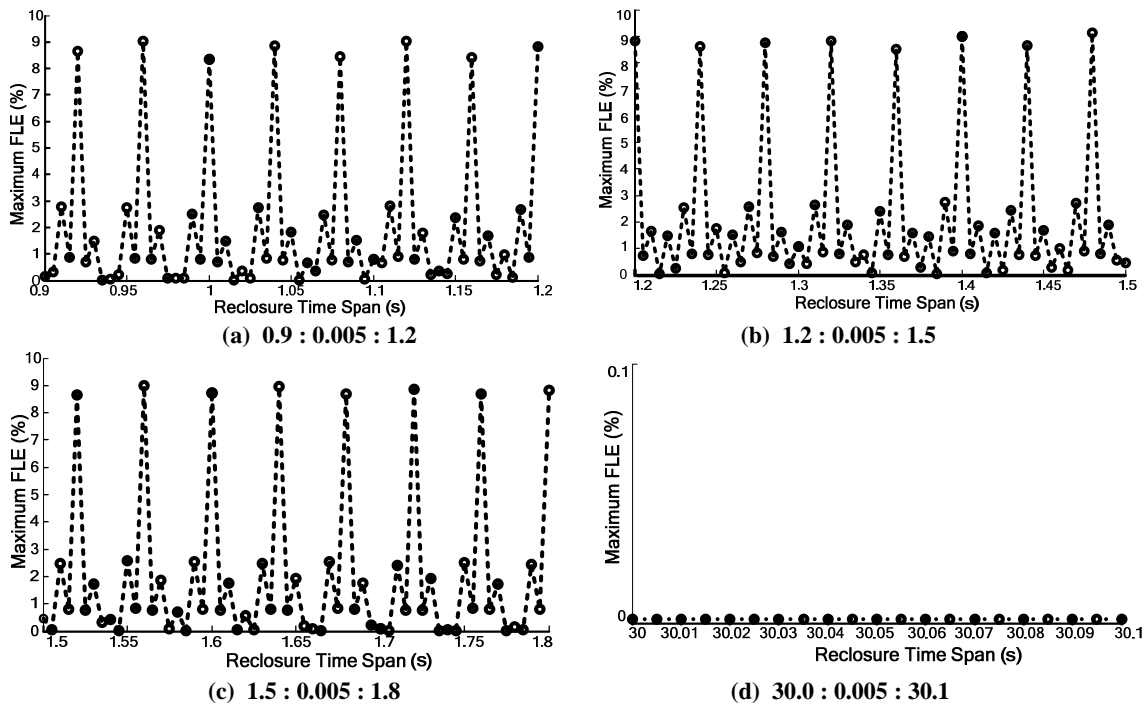


Fig. 5 Curves of Maximum FLE versus Reclosure Time Span with Interval 0.005s

#### 4.2 Time span between single-phase reclosing and three-phases tripping off

Trip-off time span between single-phase reclosing and three-phases tripping off is set from 60ms to 150ms with interval 2ms by Multiple Run Component. The other time sequence is kept the default setting. It is totalled to 46 cases. The curves of the evaluated maximum FLE versus trip-off time span with interval 2ms are as shown in Fig. 6.

It is shown that the maximum FLE is relatively large when trip-off time span is as about 70ms, 110ms or 150ms, but the maximum FLE is relatively small when trip-off time span is varied between 90ms and 110ms or between 130ms and 140ms. The maximum FLE is varied between 8.6% and 0.92%. Difference is almost close to one order of magnitude. The default trip-off time span is 110ms, just corresponding to a relative large maximum FLE. Furthermore, time interval of the nearby two relative large maximum FLE is about 0.04s, approximate to the period of torsional mode 2.

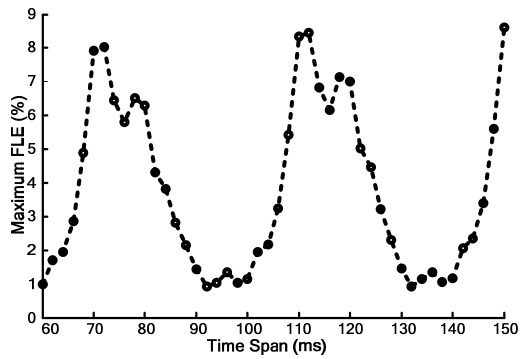


Fig. 6 Curves of Maximum FLE versus Trip-off Time Span

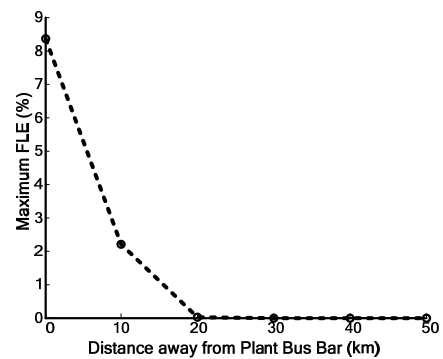


Fig. 7 Curves of Maximum FLE versus Fault Location Distance

## 5 IMPACTS OF FAULT LOCATION ON MAXIMUM FLE

It is revealed that the maximum FLE induced in the case of permanent single-phase fault and unsuccessful reclosure is related with the distance between fault location and the plant bus bar. Fault location distance between the plant bus bar and the fault location on the start of one of lines TKT-HY is set from 0km to 50km with interval 10km. The curves of the evaluated maximum FLE versus fault location distance with interval 10km are as shown in Fig. 7. It is shown that the maximum FLE is larger, as fault location is closer to the plant bus bar or the machines. The maximum FLE induced in the case of permanent single-phase fault occurring on the start of one of lines TKT-HY is reached to 8.3%. However, the maximum FLE induced in the case of the same type of fault occurring at the location 20km away from the plant bus bar is too small to ignore.

## 6 CONCLUSIONS

The procedure of permanent single-phase fault and unsuccessful reclosure is included multiple disturbances, which may be superposed positively to enhance transient torque impact. There are twice of obvious transient torque impacts in the typical procedure of permanent single-phase fault. The later more obvious transient torque impact has played a dominant role in the accumulation of torsional fatigue life expenditure of turbine-generator shafts. Reclosure time sequence and fault location have an obvious effect on the maximum FLE induced in the case of permanent single-phase fault. Sometimes the maximum FLE induced in the case of permanent single-phase fault and unsuccessful reclosure is greater than that of three-phase fault.

Numerous evaluated results of the investigated system have been shown that the most severe case is permanent single-phase fault and unsuccessful reclosure with few distances between fault location and machines. The maximum FLE induced in the most severe is much great than 0.1%. And there are a few possibilities to occur single-phase fault in practical system. It is probable that the maximum FLE induced in the most severe case would be beyond the endurable strength of the turbine-generator shafts. It is suggested to improve the scheme of single-phase reclosure.

Moreover, it is provided a feasible and effective tool to investigate the impact of fault time sequence on the related turbine-generator shafts, by using the multiple run component of PSCAD/EMTDC to carry out simulation of numerous cases automatically.

## BIBLIOGRAPHY

- [1] Joyce J S, Kulig T, Lambrecht D. Torsional Fatigue of Turbine-Generator Shafts Caused by Different Electrical System Faults and Switching Operations. IEEE Transactions on Power Apparatus and Systems, 1978, PAS-97(5): 1965-1977
- [2] Joyce J S, Lambrecht D. Status of Evaluating the Fatigue of Large Steam Turbine-Generators Caused by Electrical Disturbances. IEEE Transactions on Power Apparatus and Systems, 1980, PAS-99(1): 11-119

- [3] Jackson M C, Umans S D, Dunlop R D, Horowitz S H, Parikh A C. Turbine-Generator Shaft Torques and Fatigue: Part I - Simulation Methods and Fatigue Analysis. IEEE Transactions on Power Apparatus and Systems, 1979, PAS-98(6): 2299 -2307
- [4] Dunlop R D, Horowitz S H, Parikh A C, Jackson M C, Umans S D. Turbine-Generator Shaft Torques and Fatigue: Part II - Impact of System Disturbances and High Speed Reclosure. IEEE Transactions on Power Apparatus and Systems, 1979, PAS-98(6): 2308-2328
- [5] Jackson M C, Umans S D. Turbine-Generator Shaft Torques and Fatigue: Part III - Refinements to Fatigue Model and Test Results. IEEE Transactions on Power Apparatus and Systems, 1980, PAS-99(3): 1259-1268
- [6] Walker D N, Adams S L, Placek R J. Torsional Vibration and Fatigue of Turbine-Generator shafts. IEEE Transactions on Power Apparatus and Systems, 1981, PAS-100(1): 4373 - 4380
- [7] Aspragathos N, Dimarogonas A D. Fatigue damage of turbine-generator shafts due to fast reclosing. IEE Proceedings C: Generation, Transmission and Distribution, 1982, 129(1): 1 - 9
- [8] Hammons T J. Electrical Damping and its Effect on Accumulate Fatigue Life Expenditure of Turbine-Generator Shafts Following Worst-Case Supply System Disturbances. IEEE Transactions on Power Apparatus and Systems, 1983, PAS-102(6): 1552 - 1565
- [9] Lambrecht D, Kulig T, Berchthold W, Hoorn J V, Fick H. Evaluation of the Torsional Impact of accumulated Failure Combination on Turbine Generator Shaft as basis of Design Guidelines. CIGRE Session 1984, August 29 – September, 1984: 11-06
- [10] Pourbeik P, Ramey D G, Abi-Samra N, Brooks D, Gaikwad A. Vulnerability of Large Steam Turbine Generators to Torsional Interactions During Electrical Grid Disturbances. IEEE Transactions on Power Systems, 2007, 22(3): 1250 - 1258
- [11] IEEE Committee Report. Reader's guide to subsynchronous resonance. IEEE Transactions on Power Systems, 1992, 7(1): 150 - 157
- [12] Anderson P M, Farmer R G. Series Compensation of Power Systems. Encinitas. CA: PBLSH!, 1996
- [13] Manitoba HVDC Research Centre. PSCAD User's Guide. Manitoba: Manitoba HVDC Research Centre, 2006
- [14] Liu Q, Zhou C, Angquist L, Rehtanz C. A novel active damping control of TCSC for SSR suppression in a radial corridor. Third International Conference on Electric Utility Deregulation and Restructuring and Power Technologies, DRPT 2008, 2008: 136 - 142
- [15] GE Energy Technical Report. Tuoketuo SSR Filter Project SSR Blocking Filter Design Study. GE Energy, 2007

**Methods for Inter Coil Short Circuit Detection in Excitation Winding Coils of Turbo Generator in Operation and in Standstill Condition**

**J. Polak**  
KONČAR – Institut za elektrotehniku d.d.  
Croatia

**J. Študir**  
KONČAR – Generatori i motori d.d.  
Croatia

**M. Šašić**  
IRIS Power LP  
Canada

**A. Elez**  
KONČAR – Institut za elektrotehniku d.d.  
Croatia

**N. Bulaić**  
KONČAR – Generatori i motori d.d.  
Croatia

**SUMMARY**

Detection of inter-coil short circuits has a significant importance in nowadays diagnostics of rotating electrical machines. In this paper two modern, reliable and economically viable methods for such detection in excitation windings of turbo generator have been described. One can be applied in operation and the other in standstill condition. First method for detection of excitation winding insulation state at standstill condition is based on impulse voltage test. Test impulse passes through the winding turns and in the case of weak or faulty point in insulation, directly continues through this weak point to the next winding coil turn, coil, group, phase, or if possible to the ground. Inter-coil short circuit between turns reduces inductance of the faulty winding coil, which results with higher oscillating frequency. In that case voltage stress response curves have oscillations that are not identical i.e. fault is present in winding. By combining winding connections and analysis of response characteristics, inter-coil short circuit extent and its approximate location ( $\pm 0,5$  m) can be determined.

Second presented method for detection of inter-coil short circuits in excitation winding during generator operation is based on magnetic field measurement in the air gap of the machine. Magnetic field can be measured using Hall sensors or measuring coils fitted on the stator tooth. If an inter-coil short circuit appears in excitation winding, it will cause disturbance of magnetic field in the machine. This change will be seen as localized disturbance in measured magnetic field or flux density waveform. Signal from measuring sensors are collected via analog input modules of adequate monitoring system and process measuring data using algorithm specifically developed for this purpose, based on mathematical model using FEM (finite element method). Monitoring system can provide information whether inter-coil short circuit is present in excitation winding coils and number of shorted turns per coil.

**KEYWORDS**

Electrical machine, Turbo generator, Rotor windings, Diagnostic, Inter-coil short circuit, Impulse voltage, Finite element method (FEM).

## 1 INTRODUCTION

Testing of turbo generator rotor insulation system is performed during manufacturing of the generator, during generator installation, repair or planned controls in operation. On the rotor winding and insulation system a complex stress is present during generator startup and operation. This stress is manifested by high values of static and dynamic forces, thermal forces due to temperature differences between rotor winding and the iron, voltage stress between winding and rotor iron and voltage stress between turns in each coil. Due to this complex effects of stress, rotor winding insulation system ages faster than other turbo generator parts. Cooling medium, air or hydrogen, in spite of the closed circulation and filtered ventilation, to a certain extent is polluting winding through dust, metallographic dust from sliding brushes and oil vapour what is reducing the level of isolation between winding and the ground and between turns in coils. Although the voltage between coil turns, depending on the turbo generator winding design is only a few volts and the excitation voltage is usually 100-380 V, one or more shorted turns are known to occur during generator operation. Appearance of shorted turns can cause the magnetic unbalance which can cause increase of generator vibration level and the necessity for more excitation for all operating conditions. Usually at the beginning only one shorted turn occurs which is not stable. That means that shorted turn is not present during generator standstill and is present during generator operation or vice versa. This shorted turn strengths over time and usually expands what can result in more shorted turns in the same coil. There may be shorted turns in different coils of the same pole and even a breach on the rotor ground as a result of shorted turn temperature effects.

## 2 METHOD FOR INTER-COIL SHORT CIRCUIT DETECTION IN STANDSTILL CONDITION

Today, usage of the pulse voltage as a method for detection of shorted turns is spread worldwide and its usage is constantly increasing. Impulse voltage tests are not destructive and they can detect weak spots in the insulation between turns or between winding and ground at early stage of development. The main difference between AC and impulse voltage testing is that with the AC voltage test all parts of the winding are under the same voltage (this test determines the dielectric strength of insulation between winding and ground - lateral insulation), while with impulse voltage test a voltage difference, between turns in the coil and between each coil which are electrically connected, is applied. Only with this test, beside the insulation dielectric strength between winding and the ground (lateral insulation), insulation dielectric strength between electrically connected parts of the winding (the longitudinal isolation) can be determined.

Testing device produces voltage pulse which emerges from a capacitor into the tested winding. Test impulse passes through the winding turns and in the case of weak or faulty point in insulation, directly continues through this weak point to the next winding coil turn, coil, group, phase, or if possible to the ground. When such a voltage pulse is presented on the oscilloscope screen, typical oscillatory waveform of a damped LC oscillatory circuit can be detected.

By using two pulse voltage generators, simultaneously both characteristic oscillation curves can be seen on the screen. If both windings are equal and without fault, then both oscillation curves are identical and only one curve is visible on the screen. If a winding has a breakdown in isolation, oscillation curves are not identical and two curves can be seen on the screen.

A short circuit between turns reduces the inductance of faulty windings and leads to a higher oscillation frequency. Insulation is tested with impulse voltage that is higher than the winding operating voltage, so that the weak spots in isolation can be easily detected. Impulse voltage wave spreads through the coil and creates a potential difference in the winding. For example, impulse voltage of 3000 V reaches a turn number X, while the other turns are still unloaded or at a lower voltage. If the potential difference is higher than the dielectric strength of insulation between turns, one or more turns can be shorted. When such a shorted turn is compared with a good turn, their images on the screen differ. Faulty turn provides additionally unstable image due to sparks skipping. If the current is held low, that short-term shorted turn will not further damage the insulation.

### 3 TESTING METHODS WITH IMPULS VOLTAGE APPLICATION

The test methods that are applied during testing of turbo generator rotor winding, by applying the pulse voltage are: Single-sided and Comparative method. Single-sided method is applied when the midpoint of rotor winding is not available for connection. This is in the most cases because it is covered by the rotor cap which is removed only in the case of failure or by the planed schedule. Impulse voltage is applied to a sliding ring (no. 1) and goes across the rotor winding to another sliding ring (no. 2). By oscilloscope response is recorded with a defined amplitude and time base. Then impulse voltage is applied to the second slip ring (no. 2) and goes across rotor winding to the first sliding ring (no. 1), and again response is recorded by oscilloscope with same amplitude and the time base as in the first case. By comparing images of recorded voltage responses, defects in the coil can be very easily detected.

Comparison method is applied when the winding mid-point is available for connection. This is in the case when the rotor caps are removed. The essence of this method is comparison of two impulse voltages that are simultaneously sent over a sliding ring no. 1 and sliding ring no. 2, in one and the other half of the rotor winding, and return through the middle point of the winding. Simultaneously comparing the voltage responses on the oscilloscope screen we can determine the type of failure. Fig. 1 presents voltage responses of the turbo generator winding with permanent shorted turns inside pole coil.

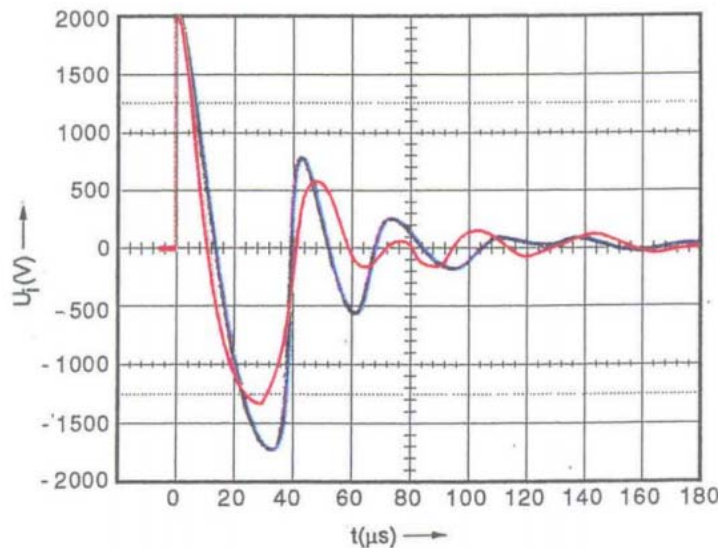


Fig. 1  $U_u = 2000 \text{ V}$ ,  $u_u = 500 \text{ V/d.s.}$ ,  $t = 20 \text{ μs/d.s.}$

Based on analysis of impulse voltage response characteristics, using a combination of connections, known geometry of the coil and knowing the speed of a traveling pulse voltage wave through the test coil (Equation 1) we can determine the extent and approximate location ( $\pm 0.5 \text{ m}$ ) of shorted turn.

$$v = \frac{l_n}{\sqrt{L_n C_n}} \quad (1)$$

Where  $v$  is the speed of wave traveling through the winding,  $l_n$  length of the tested winding,  $L_n$  inductance of the tested winding and  $C_n$  is he capacity of the tested winding.

### 4 METHOD FOR INTER-COIL SHORT CIRCUIT DETECTION DURING OPERATION

On-line air gap flux monitoring is a proven method, which has been used for detection of turn-to-turn short circuits in rotor winding of the synchronous machines for many years. The condition of the rotor winding insulation sometimes is difficult to assess during a shutdown due to limited access and absence of centrifugal forces on coils, which are present during generator operation. As a result, on-line detection of shorted turns has some advantages in comparison with testing while generator is at standstill. Usually, flux measurements have been performed using flux probes (measuring coils) installed on a stator tooth or wedge connected to portable or permanently installed instrument that

provide measuring signal analysis. Traditionally, to achieve a reliable diagnostic, the signal from the flux probe has to be measured under different load conditions, ranging from no load to full load. This requirement presents a serious obstacle when applying this method on base load generators. So, in order to test this requirement for generator load change, extensive study based on Finite Element Models (FEM) has been performed. With FEM models shorted turns in rotor winding coils have been simulated for different generator load conditions. Results of study presented in this paper, and confirmed by measurements on a real generator, shows that shorted turns in any of rotor winding coils can be detected even without changing of the generator load.

FEM models are made on the basis of actual generator technical documentation in which measurements were performed. Voltage waveform induced in measuring coil, installed on the stator tooth, where calculated with more than fifty models. With these models the impact of turn-to-turn short circuits in the excitation winding for all rotor slots, has been calculated at different loads in a range from idling to full load in 7 steps. FEM model, finite element meshes and the distribution of the magnetic field lines for one of the solutions are presented in Fig. 2.

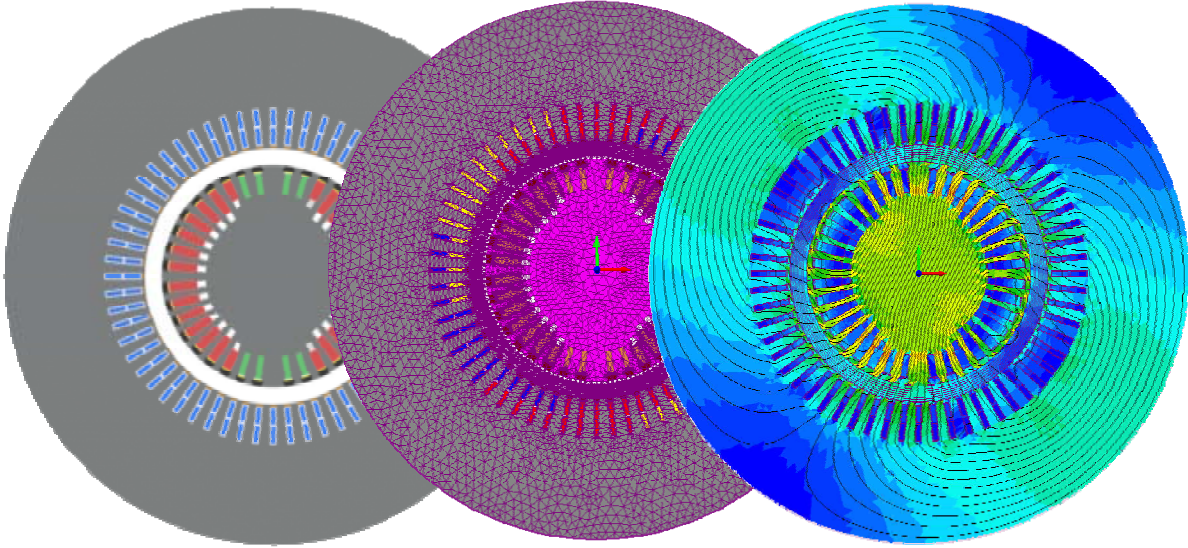


**Fig. 2 FEM model, finite elements network and magnetic field lines for one solution.**

Calculated voltage waveform induced in the measuring coil installed on the stator tooth and integrated voltage waveforms are presented in Fig. 3. Numbers from 1 to 7 in Fig. 3 represent the rotor slots, the vertical red dashed line indicates the q axis and the vertical dashed blue line marks the passage of the integrated voltage waveform through zero or FDZC axis.

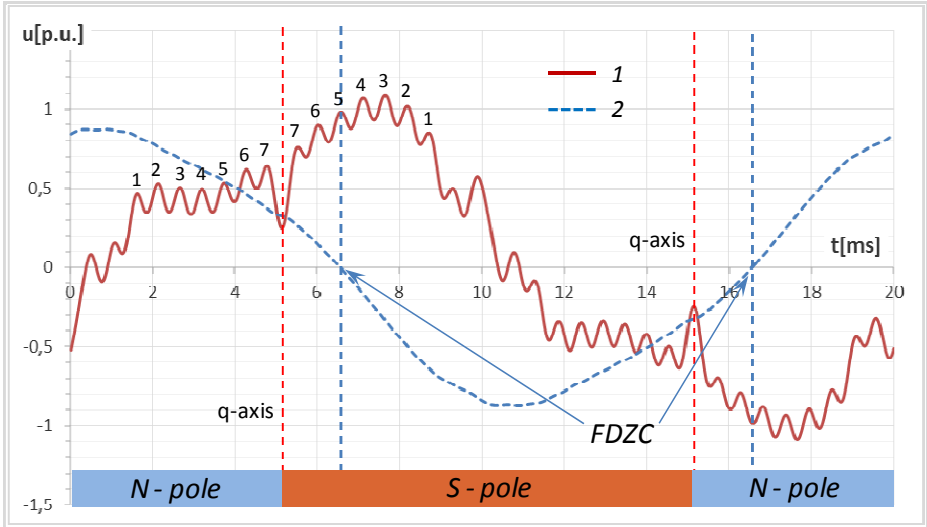


**Fig. 3 Calculated waveform: Curve 1- voltage induced in measuring coil, Curve 2 – integrated voltage**

Method for detection of turn-to-turn shorted circuits is based on comparison of voltage waveform across one pole to the voltage waveform across another pole. Due to the occurrence of shorted turns in one of the rotor slots, induced voltage for that slot will decrease in comparison to the induced voltage for the same slot on another pole. This change of voltage amplitude depends on the number of turns involved in short circuit, the position of FDZC axis and the short circuit contact resistance. The highest sensitivity for detection of shorted turns in any of the rotor slots can be achieved if FDZC axis coincides with the same slot (in Fig. 3 FDZC axis coincides with the slot number 5). In this case, 1 shorted turn of a total of 10 turns in the coil, theoretically will result in reduction of the induced voltage amplitude, for that particularly slot, by 10%. In practice this amount is less.

On Fig. 4 results of calculations and measurements, for loaded generator without shorted turns in rotor windings, are presented. Deviation between the measurements on a real generator and the calculation is negligible, from which it can be concluded that the models used for calculation give sufficiently accurate results.

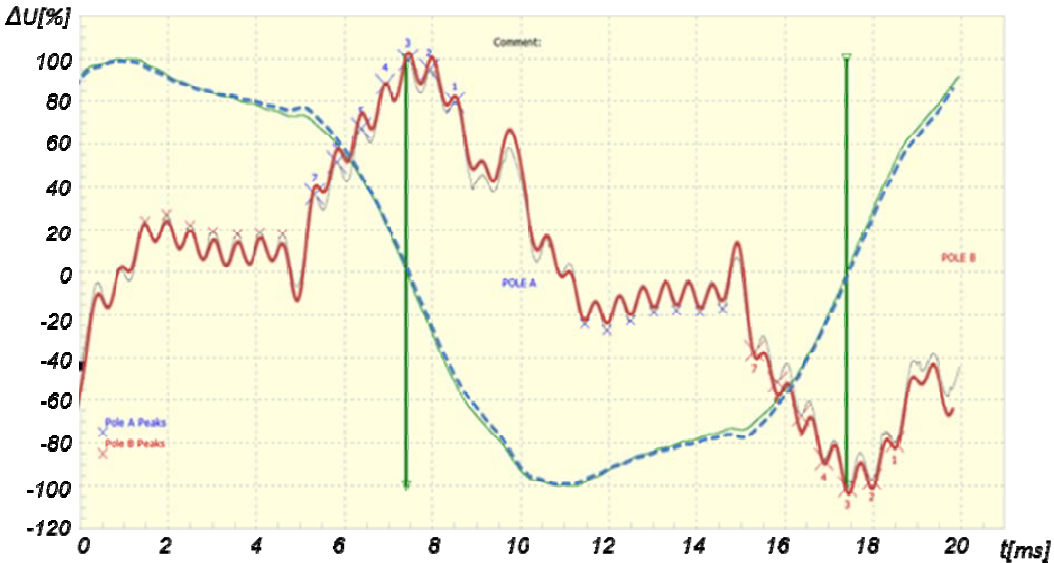


Fig. 4 Measured and calculated induced voltage waveform and integrated voltage waveform

The next step included a simulation of shorted turns in each of the rotor slots. Fig. 5 presents the processed calculation results for one shorted turn in slot number 5, for 7 different generator loads.

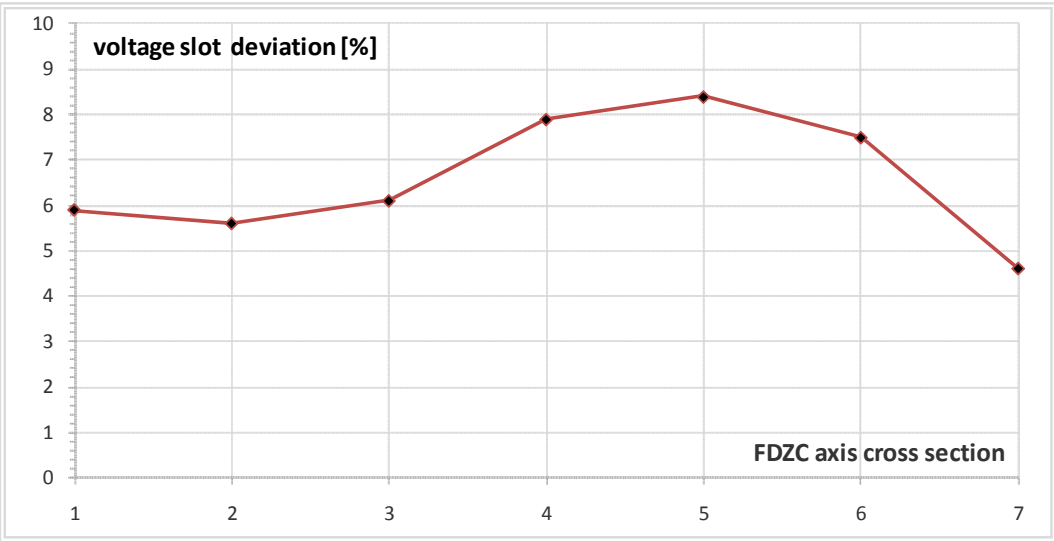


Fig. 5 Voltage amplitude slot deviation for shorted turn in the excitation winding coil number 5 for 7 different generator loads.

The highest sensitivity for the detection of shorted turns in slot number 5 is achieved for the generator load at which FDZC axis coincides with the slot number 5, as shown in Fig. 5. In this case voltage slot deviation, in comparison with the voltage for the slot number 5 under other pole, is 8.4%. For the remaining generator loads, detection sensitivity is slightly smaller but sufficient for a positive detection of shorted turns.

Fig. 6, 7 and 8 present the results of flux measurements on the generator in which shorted turns have been detected in the slot number 6, with different method during regular testing at generator standstill. By measuring the magnetic flux in the air gap with the measuring coil, and comparing the induced voltage waveform for booth poles, voltage deviation that indicate shorted turns have been detected and presented in Fig. 6 and 7. As can be seen in Fig. 6, FDZC axis coincides with the slot number 6, however in the Fig. 7 FDZC axis coincides with the slot number 3 and shorted turn is still obvious in the waveforms.

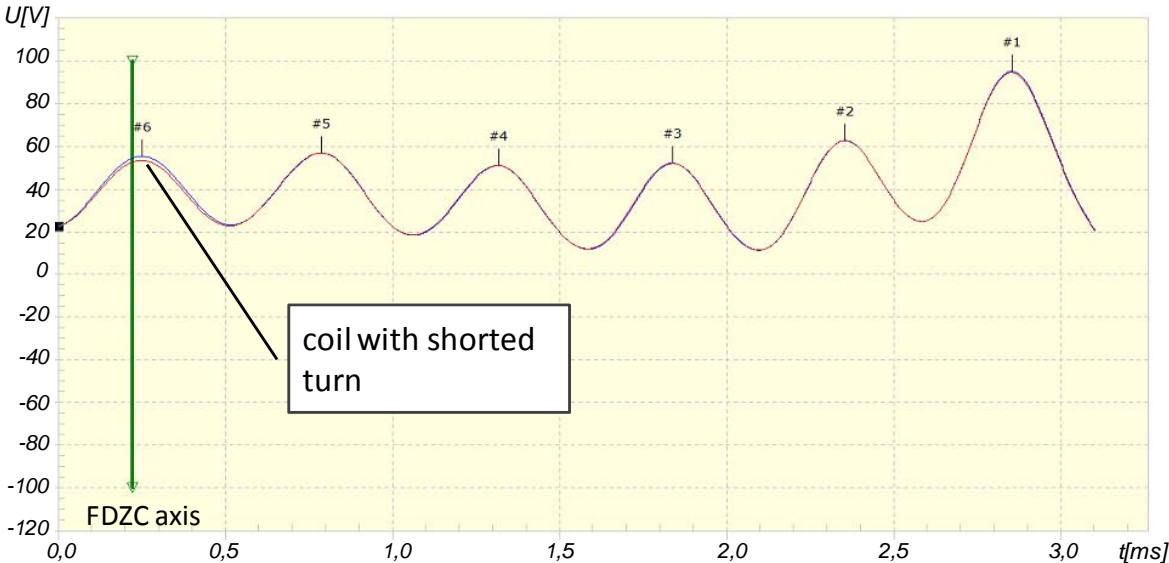


Fig. 6 Comparison of the induced voltage waveform for booth poles at the generator load for which FDZC axis coincides with the slot number 6.

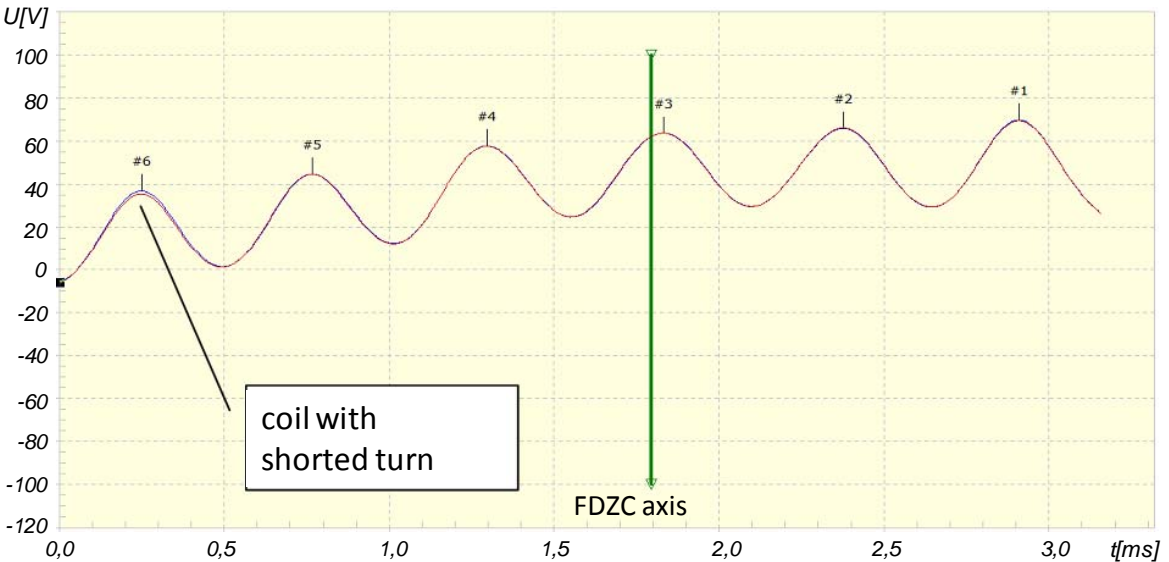
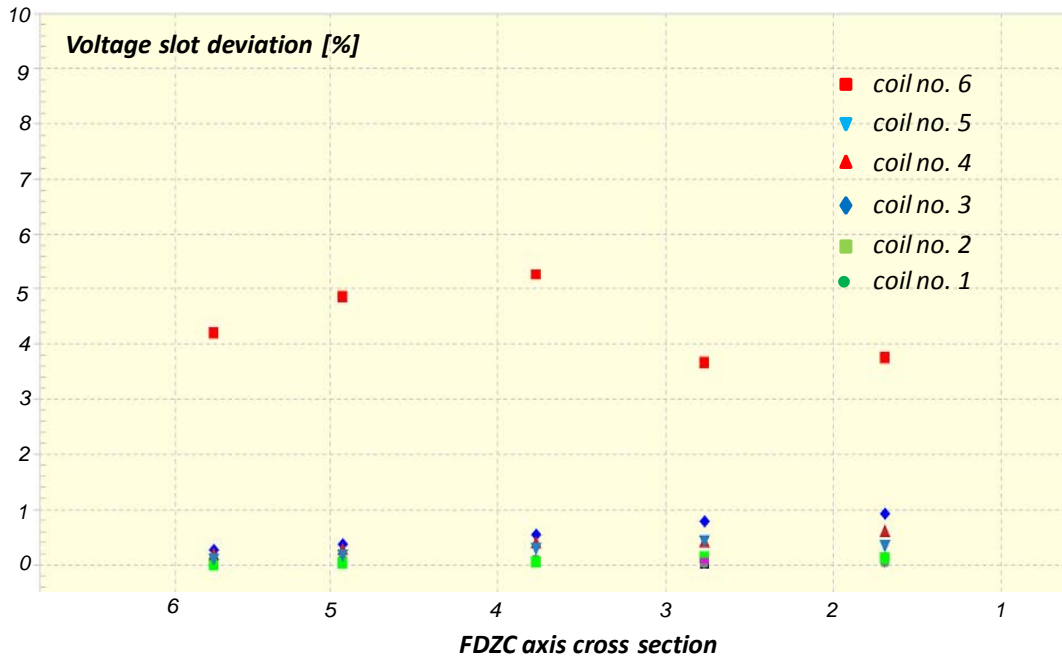


Fig. 7 Comparison of the induced voltage waveform for booth poles at the generator load for which FDZC axis coincides with the slot number 3.



**Fig. 8 Measured induced voltage slot deviations for all slots under pole and different generator loads with shorted turn present in the slot number 6.**

From the data presented in Fig. 8, it can be concluded that the induced voltage deviations under the slot number 6, through all generator loads, is between 3.5 % and 5.3 %. For the remaining slots, in which shorted turn is not present, this deviation is in the range from 0 % to 1 %.

Thus it can be concluded from measurements and calculations presented in this work that shorted turns in the excitation winding can be clearly detected using the presented method without the need for generator load change.

### 5 SHORTED TURNS CONSEQUENCE

Consequences of shorted turns in turbo generator rotor windings can result in following:

1. Shorted turns result in the reduction of flux density because part of the coil is excluded and not contributing to the creation of generator flux. With the same excitation current, flux density distribution over pole will differ between poles. Reduction of flux density will be present over the pole with shorted turns. That will result in uneven magnetic flux distribution in the generator air gap. Magnetic forces between stator and rotor are proportional to the square of the flux density in air gap, so shorted turns causes disbalance between attraction forces for all poles. The lowest attraction force will act on the pole with shorted turns, and the highest on the pole that is located on opposite side of rotor. The difference between these two forces is the force of unilateral magnetic attraction, which rotates with the rotor speed, causing magnetic unbalance. Observed from the stator side, this force can cause increase of generator vibration.

2. Exclusion of excitation winding shorted turns from magnetic flux creation, leads to reduction of the induced voltage in the stator winding, which corresponds to the reduction of the excitation current in the rotor which does not have shorted turns. This means that the generator with shorted turns will need more excitation current for all operating conditions in comparison with the same generator without shorted turns.

3. For generator operating on the grid, reactive power i.e. power factor  $\cos\phi$ , is regulated by the excitation current. There by, for overexcited area of PQ generator diagram, with the same values of generator voltage, current and excitation current ( $u, i, i_f$ ), a generator with a shorted turns will produce less reactive power (power factor  $\cos\phi_{ind}$  will increase). In the capacitive working area, for the same values of  $u, i$  and  $i_f$ , generator will be under excited in the greater extent in comparison with the period before the appearance of shorted turns (power factor  $\cos\phi_{cap}$  will

decrease). Reduction of the generator induced voltage, the due to shorted turns in excitation winding, can be compensated by corresponding increase in excitation current, and thus reactive power i.e. power factor  $\cos\phi$  adjusted to the desired value.

Based on the above stated, it follows that there is no reliability of rotor winding insulation system if shorted turns are present.

## 6 CONCLUSION

From the long term experience working with turbo generators, in the case of the shorted turn presence in the rotor winding, the reliability of generator insulation system is low and thereby availability of the machine itself is reduced. That is the main reason why it is necessary to develop methods for shorted turn detection, both at standstill and at generator operation, in order to detect presence of the potential malfunctions, monitor it and take the necessary preventive measures. Both methods are reliable and economically viable, and it should be noted that the shorted turns in the rotor winding of turbo generator in operation can be detected, with presented method, without the need for generator load change.

## BIBLIOGRAPHY

- [1] Albright D R. Interturn Short-circuit Detector for Turbine-Generator Rotor Windings. IEEE Transactions on Power Apparatus and Systems, March/April 1971, PAS-90 (2)
- [2] Jenkins, M P, Wallis D J. Rotor Shorted Turns: Description and Utility Evaluation of a Continuous On-line Monitor[C]//EPRI Predictive Maintenance and Refurbishment Conference, December 1993
- [3] Polak J. Dijagnostika međuzavojnih spojeva namota rotora turbogeneratorskog impulsnim naponom. 2 Seminar EDZ , Dijagnostika i održavanje električnih strojeva, Stubičke Toplice 1997
- [4] Albright D R, Albright D J, Albright J, D. Generator Fields Winding Shorted Turn Detection Technology. IRMC, May 1999
- [5] Klemperer G. Rotor Shorted Turns-Detection and Diagnostics[C]//EPRI Generator Predictive Maintenance and Refurbishment Conference, December 2003
- [6] Whittle A. Continuous Rotor Flux Monitoring. EPRI Generator Workshop, August 2007
- [7] Šašić M, Lloyd B, Elez A. Finite elements analysis of rotor shorted turns. EPRI Generator Workshop, 2011